

# DOTTORATO DI RICERCA IN CHIMICA

Ciclo 37

**Settore Concorsuale:** 03/C1 - CHIMICA ORGANICA

Settore Scientifico Disciplinare: CHIM/06 - CHIMICA ORGANICA

ALTERNATIVE METHODS AND CROSS-COUPLING REACTIONS, HECK-CASSAR-SONOGASHIRA/SUZUKI/CATELLANI, FOR THE SYNTHESIS OF BIOACTIVE MOLECULES AND THE DEVELOPMENT OF SUSTAINABLE APPROACHES FOR NEW PEPTIDE SYNTHESIS

Presentata da: Chiara Palladino

Coordinatore Dottorato Supervisore

Cristina Puzzarini Walter Cabri

**Co-supervisore** 

Paola Galletti

It will always be like dancing with you,
waiting for the trains with you,
being with you.
To You with love.



#### **Abstract**

My PhD research focused on investigating novel strategies to achieve faster, costeffective and sustainable synthesis of bioactive molecules, driven by the strong interest in this area shared by academia and industry.

The first part is dedicated to palladium-catalysed cross-coupling reactions, as these represent an important tool to face the increasing complexity of active pharmaceutical ingredients (APIs) and the need for rapid processes. In particular, since it is possible to develop efficient processes by fine-tuning the conditions for a specific Pd-catalysed reaction, we have investigated in detail the copper free Heck-Cassar-Sonogashira (HCS) reaction mechanism. In fact, despite its wide application and huge success, the mechanism was still under discussion. Experimental results and theoretical calculations were helpful in shedding light on the preferred pathway. In addition, a complete guide to the efficient in situ activation of the L2PdX2 pre-catalyst was presented, as this was not yet available. The study was driven by the need to thoroughly understand the Pd(II) pre-catalyst reduction process in order to avoid excess reagents, save precious ligands, use lower temperatures and make the reduction faster. Pd(OAc)2 and Pd(ACN)2Cl2 were chosen as pre-catalysts and the reduction process was monitored by <sup>31</sup>P NMR in the presence of different ligands such as PPh<sub>3</sub>, dppf, dppp, Xantphos and SPhos in different solvents and temperatures. Finally, a sustainable approach was described for Heck-Cassar and Suzuki-Miyaura reactions in the presence of aryl chlorides, which are the less expensive and available aryl halides. The strategy developed was also applied to the synthesis of two fungicides such as Boscalid and Fluxapyroxad.

The second part describes the development of green methodologies for peptide synthesis and the design of potential new antimicrobial peptides for intestinal diseases.

The peptide therapeutics market is estimated to be worth \$43.30 billion in 2024 and is expected to reach \$60.90 billion by 2029. These data are representative of the significant success of peptides. Specifically, the peptide-based drugs rank third behind small molecules and monoclonal antibodies. For this reason, the availability of efficient and environmentally friendly protocols for peptide synthesis is required.

In this scenario, we have investigated cyclic propylphosphonic anhydride (T3P®) and demonstrated its ability to replace the classical and hazardous coupling reagents in LPPS and SolPPS. In addition, these new protocols have been applied to the synthesis of potential new antimicrobial peptides (AMPs). Since most antibiotics on the market affect both harmful and beneficial bacteria, such as *bifidobacteria*, our goal was to design an antimicrobial peptide capable of selectively acting on pathogenic bacteria to treat intestinal diseases. In pursuit of this goal, a small library was generated and biological data were collected.

The third part of the research was carried out at the University of Oxford under the supervision of Professor Véronique Gouverneur.

Fluorinated compounds are widely used in the agrochemical and pharmaceutical sectors as the incorporation of fluorine modifies the physicochemical and biological properties of bioactive molecules. In particular, I focused on the development of catalytic enantioselective fluorination strategies of neutral electrophiles with KF, allowing the avoidance of expensive reagents.

## Contents

GENERAL INTRODUCTION	1
1.1. OVERVIEW OF BIOACTIVE MOLECULE SYNTHESIS	1
1.2. PALLADIUM CATALYSED CROSS-COUPLING REACTIONS	7
1.3. PEPTIDES	5
1.4. FLUORINATED COMPOUNDS	3
1.5. AIM OF THE PROJECT	3
THE MECHANISTIC INVESTIGATION AND SUSTAINABLE APPROACH OF PALLADIUM CATALYSED CROSS-	
COUPLING REACTION	Э
2.1. New mechanistic insights into the copper-free Heck-Cassar-Sonogashira cross-coupling reaction29	Э
2.1.1. Introduction	9
2.1.2. Results and Discussion33	3
2.1.3. Conclusion	9
2.1.4. Experimental Section50	)
2.1.4.1. General Information50	)
2.1.4.2. Palladium species5	1
2.1.4.3. Synthesis of palladium complexes58	3
2.1.4.4. Pd(II) reduction with base and PPh363	3
2.1.4.5. Pd(II) reduction in presence of phenylacetylene, with and without PPh₃64	4
2.1.4.6. Heck-Cassar reaction with Palladium (II) and Palladium (0)6	5
2.1.4.7. Direct coordination versus transmetalation68	3
2.1.4.8. Evaluation of the reaction rate75	5
2.1.4.9. The stability of complex M70	5
2.1.4.10. Simultaneous competition reaction77	7
2.1.4.11. Base effect on AO-complex By <sup>x</sup> 79	9
2.1.4.12. Evaluation of the kinetic constants8	1
2.1.4.13. The Addition of phenylacetylene and Scope82	2
2.1.4.14. Computational studies89	5
2.2. THE CRITICAL ROLE OF IN SITU PD(II) PRE-CATALYST REDUCTION DESIGN	7
2.2.1. Introduction	7

2.2.2. Results and Discussion	88
2.2.3. Conclusion	101
2.2.4. Experimental Section	102
2.2.4.1. General Information	102
2.2.4.2. Palladium pre-catalyst reduction with PPh <sub>3</sub>	103
2.2.4.3. Palladium pre-catalyst reduction with dppf	112
2.2.4.4. Palladium pre-catalyst reduction with dppp	119
2.2.4.5. Palladium pre-catalyst reduction with Xantphos	126
2.2.4.6. Palladium pre-catalyst reduction with SPhos	134
2.2.4.7. Investigation of Pd-NPs	139
2.2.4.8. Kinetic Isotope Effect (KIE)	141
2.2.4.9. Pd reduction with different nucleophiles	141
2.2.4.10. Pd reduction with different ligands and green solvents	141
2.2.4.11. Selectivity studies	142
2.2.4.12. DFT calculations	142
2.3. COPPER-FREE HECK-CASSAR-SONOGASHIRA AND SUZUKI-MIYAURA REACTIONS OF ARYL CHLORIDE:	a Sustainable
Approach	143
2.3.1. Introduction	143
2.3.2. Results and Discussion	143
2.3.3. Conclusion	153
2.3.4. Experimental Section	154
2.3.4.1. General Information	154
2.3.4.2. General procedures	154
2.3.4.3. Calculation of TON, PMI and PMIr	158
2.3.4.4. Recovery of HEP, and Pd in the HCS cross-coupling with 2 mol%	
2.3.4.5. Recovery of HEP and Pd in the SM cross-coupling with 0.05 mol%	160
2.3.4.6. Base Screening in the SM coupling	
2.3.4.7. PdCl <sub>2</sub> (sSPhos) <sub>2</sub> reduction	163
2.3.4.8. Compound characterisation	165
2.3.4.9. Calculation of Relative Response Factor (RRF)	171
2.3.4.10. Computational methods	
DIGA STILLE DEDTIDE SVALTUESIS AND ALTERNATIVE STRATEGIES	475
BIOACTIVE PEPTIDE SYNTHESIS AND ALTERNATIVE STRATEGIES	175
3.1. T3P® AS ALTERNATIVE COUPLING REAGENT	175
3.1.1. Introduction	175
3.1.2. Results and Discussion	176
3.1.3. Conclusion	182
3.1.4. Experimental Section	182
3.1.4.1. General Information and Analytical Methods	182
3.1.4.2. General procedure of coupling step for the solvent screening and su	ubstrate scope:
	183
3.1.4.3. Full SoIPPS of Leu-Enkephalin via Boc chemistry	183
3.1.4.4. General Procedure for the Synthesis of 2,5-Polycarbon Substituted I	Hydrophobic
Benzyl Alcohols (HBA) Tag	184
3.1.4.5. Full LPPS of Leu-Enkephaline via Fmoc Chemistry	185
3.2. SYNTHESIS OF BIOACTIVE PEPTIDE PRODUCTS	188
3.2.1. Introduction	188
2.2.2 Pacults and Discussion	102

3.2.3. Conclusion and Future Prospective	199
3.2.4. Experimental Section	199
3.2.4.1. General Information	199
3.2.4.2. Synthesis of Boc-NH-Trp-OEt (1)	200
3.2.4.3. Synthesis procedure for 3a-c	201
3.2.4.4. Synthetic procedure for 10a-b	202
3.2.4.5. Synthesis of dipeptide 4a-c and 11a-b	205
3.2.4.6. Synthesis of compounds 5a-c and 12a-b by removal of the ethyl ester	207
3.2.4.7. Synthesis of compound 16	209
3.2.4.8. Synthesis of tripeptides 6a-c and 13a-b	
3.2.4.9. Synthesis of final products 7a-c and 14 a-b	211
3.2.4.10. Procedure for late-stage functionalisation of Boc-NH-Trp-Leu-O <sup>t</sup> Bu	213
ENANTIOSELECTIVE NUCLEOPHILIC FLUORINATION VIA SYNERGISTIC PHASE TRANSFER CATALY	SIS WITH
KF	
	245
4.1. Introduction	_
4.2. RESULTS AND DISCUSSION	
4.3. CONCLUSION	
4.4. EXPERIMENTAL SECTION	
4.4.1. General Information	
4.4.2. Optimisation of reaction conditions	
4.4.3. Control experiments	
4.4.4. Time course experiments	
4.4.5. Substrate synthesis and Characterisation	
4.4.6. General procedure for enantioselective fluorination and Characterisation	222
	232

CHAPTER 1

### **General Introduction**

## 1.1. Overview of bioactive molecule synthesis

Bioactive molecules are chemical substances that interact with biological systems to elicit specific biological responses. With a focus on pharmaceuticals, they are mainly small molecules, monoclonal antibodies (mAbs), peptides and proteins, oligonucleotides and natural products. A total of 370 new drugs were approved by the U.S. Food and Drug Administration (FDA) between 2016 and 2023. As shown in Figure 1, small molecules account for the largest share (45.7%), followed by mAbs and peptides. Therefore, focusing on the development of effective and alternative strategies for the synthesis of small molecules and peptides can have a significant impact on the pharmaceutical outlook.

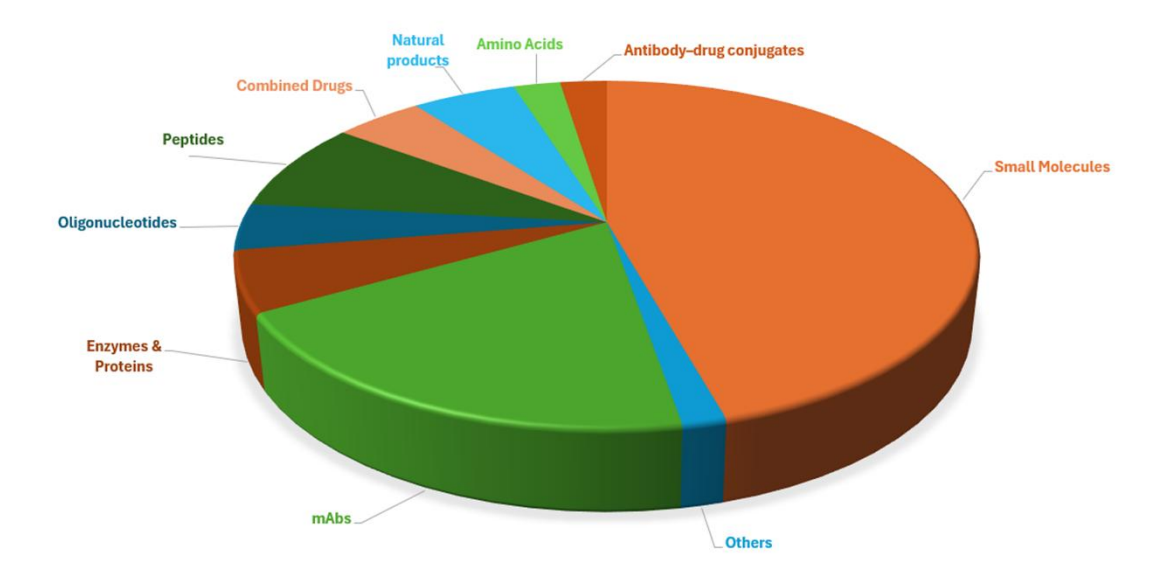


Figure 1. A total of 370 new drugs were approved by the FDA between 2016 and  $2023^{[1]}$ .

Active pharmaceutical ingredients (APIs) are characterised by increasing complexity, and palladium-catalysed cross-coupling reactions are key reactions for the synthesis of complex architectures. On the other hand, fluorine is widely used in medicinal to improve the pharmacological profile in terms of metabolic stability, permeation and biological activity. These technologies need to be sustainable and, in this context, we have studied cross-coupling reactions, fluorochemistry and peptide synthesis.

Transition metal-catalysed cross-couplings have become a reliable and indispensable tool in the synthesis of pharmaceuticals and agrochemicals. In particular, palladium has become the metal of choice because it allows low loadings compared to other metals such as Cu, Ni and Fe, promotes reactions with less reactive substrates (*e.g.* aryl chlorides) and often provides high turnover numbers (TONs), which is essential for large-scale applications<sup>[2,3]</sup> (Figure 2).

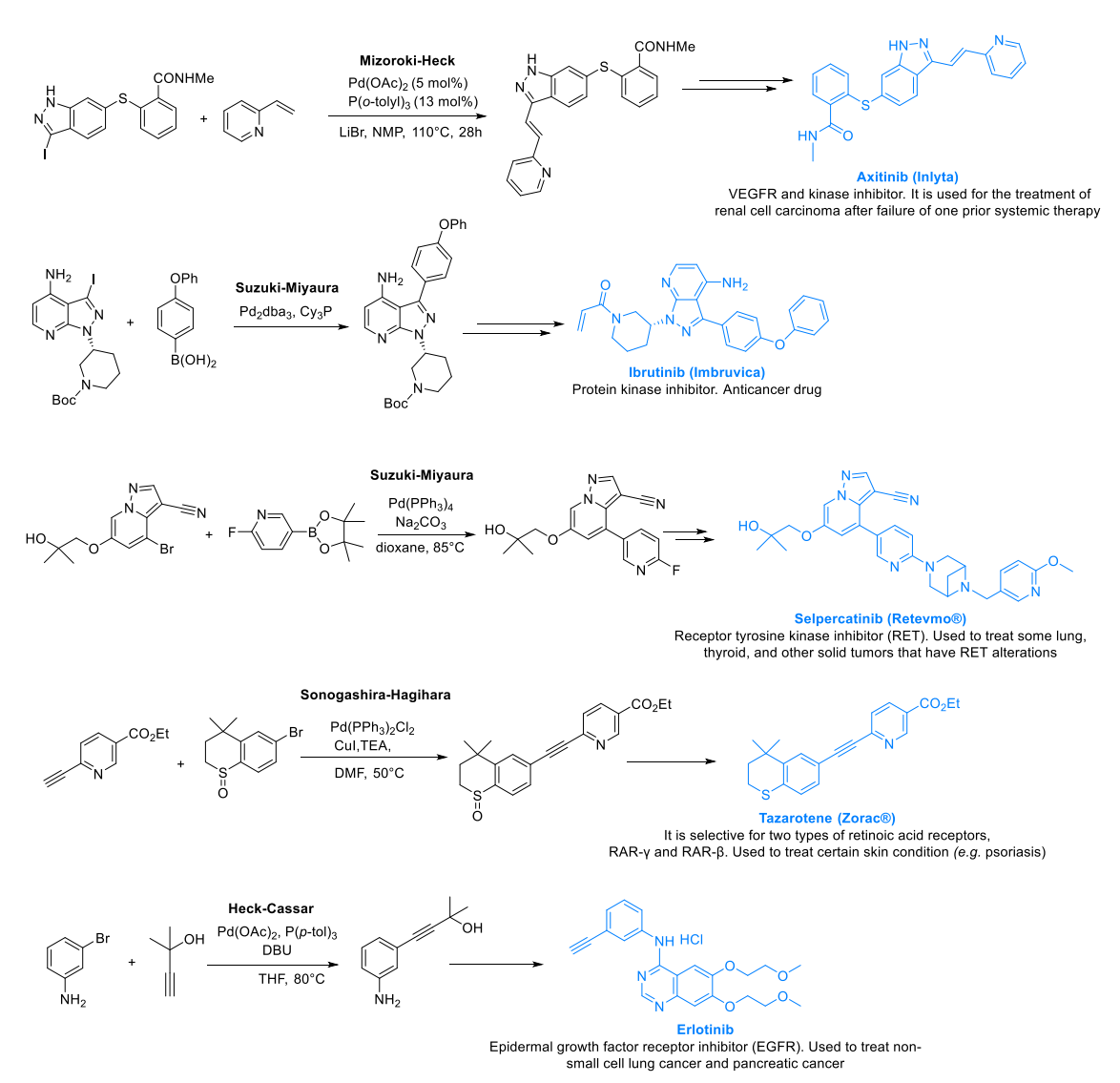


Figure 2. Examples of palladium-catalysed cross-coupling reactions in API synthesis from the literature<sup>[2-8]</sup>.

Although small molecules represent the majority of protein-targeting agents for therapeutic purposes, amino acids and peptides represents a promising area of investigation. Indeed, protein-protein interactions (PPIs) are critical mediators of signalling and play a key role in the progression of several pathological conditions. As large protein surfaces are challenging as therapeutic targets, peptide-based drugs have attracted increasing attention[9]. The site-selective derivatisation of amino acids and peptides represents an attractive field with potential applications in the establishment of structure-activity relationships and the labelling of bioactive compounds. In this respect, Pd-catalysed reactions provide valuable tools for the synthesis of peptide-based therapeutics and pharmacological probes by incorporation of unnatural amino acids or late-stage modification[10]. Many efforts have been made in this field, among which Liu et al.[11] reported a palladium(II)-catalysed selective C(sp3)-H alkynylation of inactivated side-chains oligopeptides with alkyne coupling partners. Ketones, including biologically active coprostanol, estradiol and fatty acids, can be covalently attached to peptides using this approach (Figure 3a). Ali et al.[12] conjugated the phtalocyanines as fluorescent and/or positron emission tomography (PET) probes to peptides moieties using Sonogashira, Buchwald-Hartwig and Suzuki-Miyaura reactions (Figure 3b). In 2015, Buchwald and Pentelute's groups documented that palladium(II) oxidative addition (OA) complexes can be used for efficient and highly selective cysteine bioconjugation reaction<sup>[13]</sup>. More recently, in 2022, they also demonstrated a complementary approach in which a palladium-peptide OA complex can bind a wide range of external nucleophiles<sup>[14]</sup> (Figure 3c).

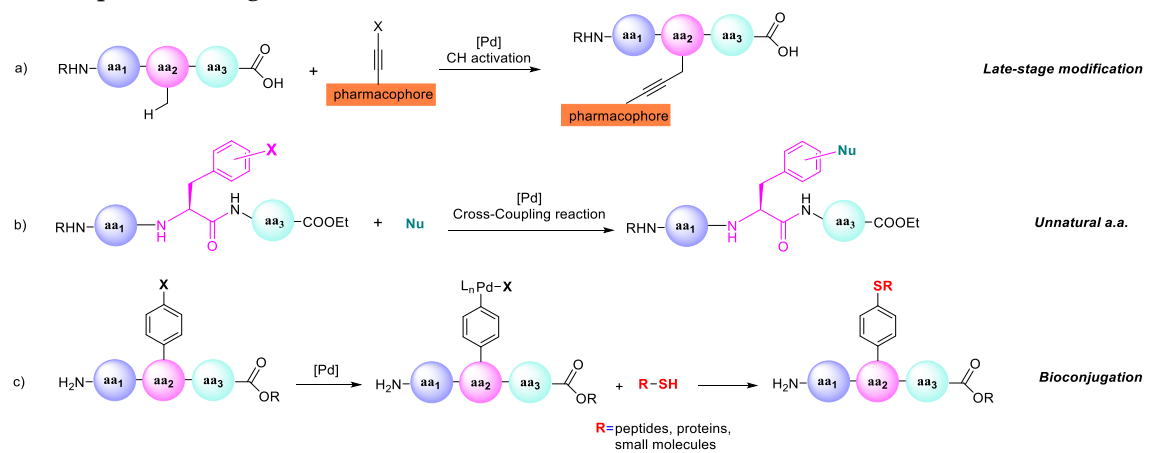


Figure 3. General examples of the use of Pd catalysis as a tool for peptide modification.

Furthermore, fluorination chemistry is a useful approach to change physicochemical and biological properties of bioactive molecules. There has also been a significant increase in interest in the synthesis of <sup>18</sup>F-labelled molecules as tracers in PET<sup>[15]</sup>. Many efforts have been made to develop new fluorination strategies, and in

particular the fluorination of peptides and proteins has received increasing attention (Figure 4)<sup>[16]</sup>.

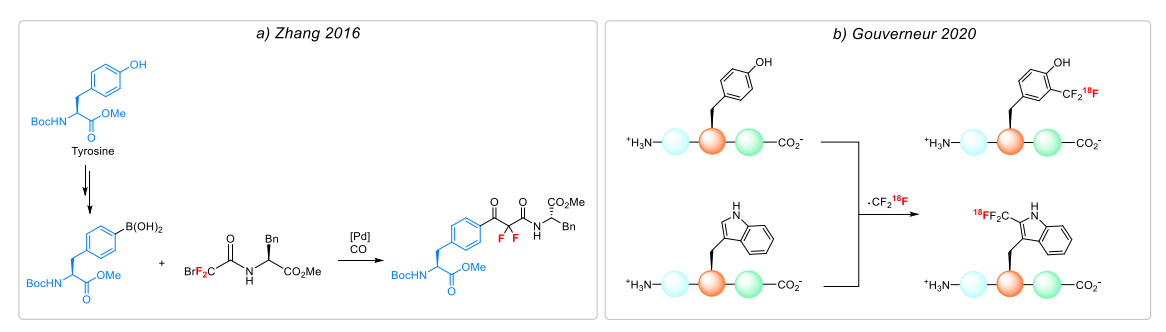


Figure 4. Examples of difluoro dipeptide synthesis[17] (a) and direct 18F-trifluoromethylation of peptide[18] (b).

As companies increasingly prioritise sustainability in their products and supply chains, the environmental impact of pharmaceutical manufacturing has become a focus of the scientific community. However, there are still significant economic, regulatory and technical barriers to the full adoption of green chemistry practices in the pharmaceutical industry. In addition, there are specific limitations in the pharmaceutical sector due to the fact that any change to the synthesis process for an active pharmaceutical ingredient becomes more complex as the drug progresses through development, with more stringent regulatory requirements at each stage. In addition, process changes closer to the final stages of manufacture have a greater potential impact on the quality of the API<sup>[19]</sup>.

As a result, the API processes developed by pharmaceutical companies to date, do not always reflect the best possible molecular assembly strategies. In this scenario, it is therefore crucial to explore alternative approaches, taking into account multiple factors and finding the right balance to make these processes viable for industrial application.

## 1.2. Palladium catalysed cross-coupling reactions

Palladium catalysed cross-coupling reactions, as mentioned above, have become a central tool for the synthesis of bioactive compounds both in academia and industry field<sup>[3,8,20]</sup>. The main reasons for the success of these reactions are that they are very flexible and selective in terms of substrates, solvents, catalysts and reaction conditions<sup>[21]</sup>. These reactions were first discovered in the 1970s and reached their peak in 2010 when Richard Heck, Ei-ichi Negishi<sup>[22]</sup> and Akira Suzuki<sup>[23]</sup> were awarded the Nobel Prize for their work in this field.

These reactions are distinguished on the basis of the nucleophile used, but it is possible to define a generally accepted mechanism (Figure 5). The catalytic cycle begins with the oxidative addition (OA) of the aryl halide to the active L<sub>n</sub>Pd(0) species, which is

usually obtained by reduction of a more stable pre-catalyst. In C-C cross couplings involving a metallic reagent, the transmetalation (TM) step occurs, leading to the reductive elimination complex  $R^1Pd(II)L_nR^2$  which produces the final product (Figure 5, *left cycle*). Instead, the Mizoroki-Heck coupling<sup>[24]</sup> goes through the alkene coordination to the Pd(II) species followed by a *syn*-migratory insertion. *Syn*  $\beta$ -hydride elimination then occurs to form the alkene product and, in the presence of a base, the active  $L_nPd(0)$  species is regenerated (Figure 5, *right cycle*). A review of the literature on the most important cross-coupling reactions shows how the interest in palladium-catalysed cross-coupling reactions has grown over time (Figure 6).

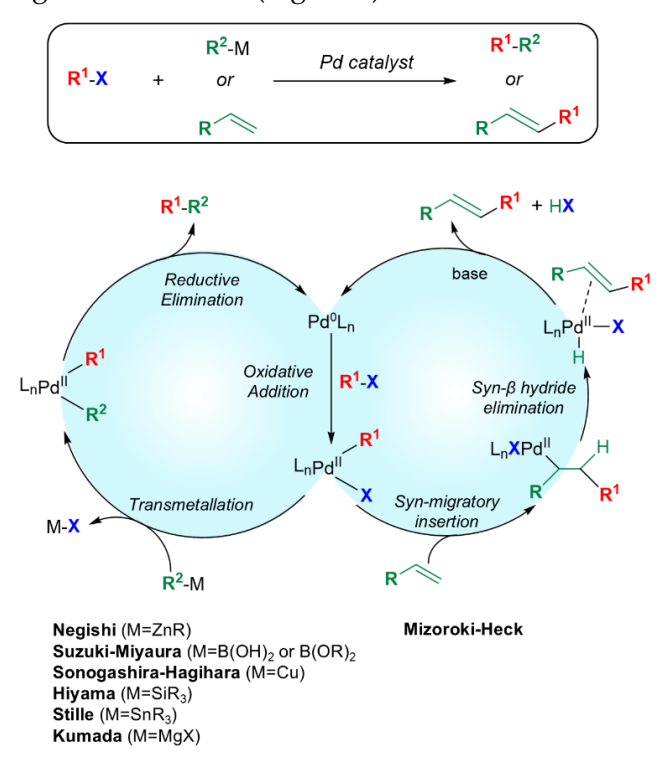


Figure 5. General catalytic cycles for C-C bond forming process palladium-catalysed.

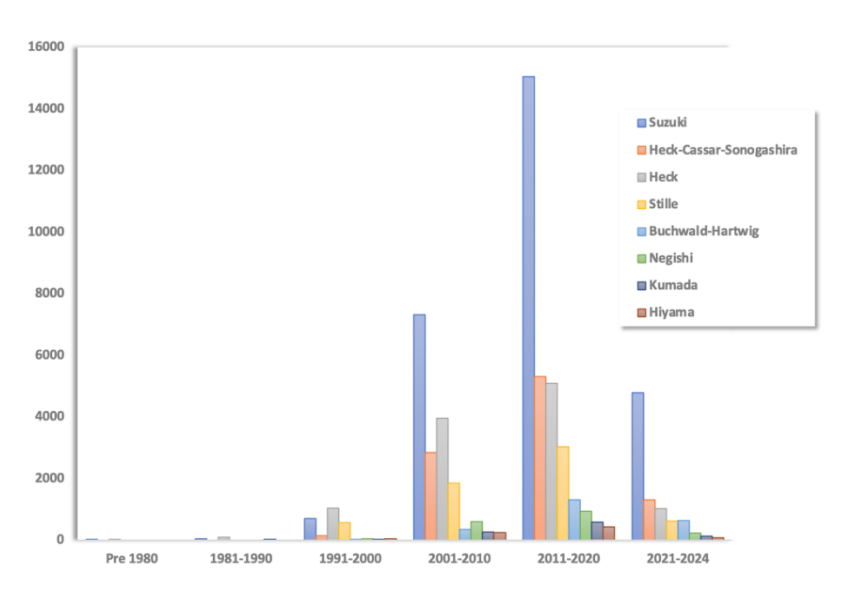


Figure 6. Growth in publications and patents related to cross-coupling reactions.

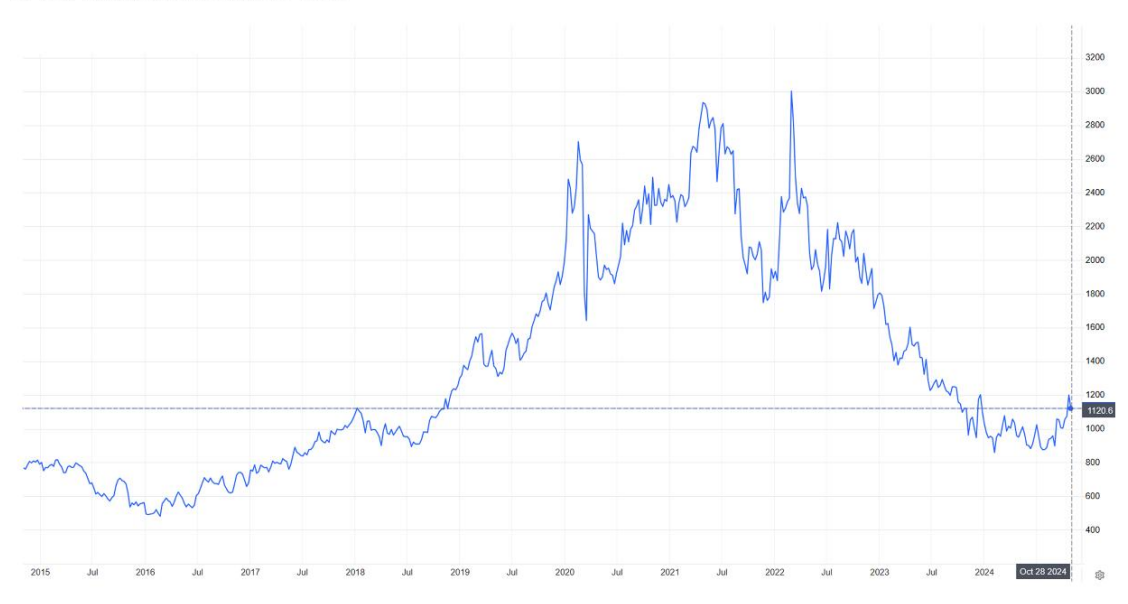
In this context, the study and the application of new sustainable approaches has become even and even more important. To pursuit this goal, the reaction design must be guided by the 12 principles of green chemistry<sup>[25]</sup>, which highlight the need for safe, simple, and environmentally friendly methods. However, even though catalysis is the number 9 on the list, it would be a mistake to think that all catalysis is green<sup>[26]</sup>. In fact, it is necessary to take a more holistic view of the whole process considering the metal, the ligands, the solvent, the reduction process, the reagents and the reaction conditions.

Palladium is the most widely used and studied metal in cross-coupling reactions due to its high reactivity, selectivity and versatility in terms of ligand compatibility. It is one of the ninth rarest metals and is an expensive metal (price updated on 28th October 2024 is 1120 USD/t.oz<sup>[27]</sup> or 36 USD/g). Demand in the palladium market is dominated by its extensive use in automotive emission control for catalytic converters[28], but as our society is moving away from the fossil fuel, it is possible to forecast a decline in palladium demand and cost in the next decade (Figure 7). However, to avoid being to dependant on this expansive and rare metal, many works have been published promoting the use of earth-abundant metals (EAMs), such as Ni<sup>[29–31]</sup>, Cu<sup>[32–34]</sup> and Co<sup>[35–34]</sup> <sup>37]</sup>. In addition, these metals are considered as valid alternatives to the heavy metals, which are typically considered to be more toxic. Seemingly, these reasons should be enough to justify the move towards EAMs and away from the widely used palladium. However, the cost and the earth metal abundance are not the only parameters to take into account[38]. In fact, many parameters need to be considered to have a general overview, including catalyst loading, catalyst recycle, functional group tolerance and the selectivity. Compared to nickel, palladium allows lower catalyst loadings, higher functional group tolerance and is more selective[39]. In addition, a deeper analysis of what is meant by "toxicity" is needed. Egorova et al.[40] have shown that there is no single parameter to describe the general toxicity of a metal, but it is a result of multi-parameter effects that strongly depend on the route of exposure, bioavailability, solubility, valence state, dose, etc. Comparison of the toxicological data indicates that light metals do not always have obvious advantages over heavy metals. Furthermore, in terms of cost, it has been pointed out that the use of cheap catalysts can be associated with the use of toxic waste, which can have a significant impact on overall cost effectiveness.

The metal and ligands contamination is another important parameter that has to be considered, especially for pharmaceutical applications, since the International Conference of Harmonization Guidelines Q3D (ICH Q3D) set very low limits for elemental impurities in medicines (*e.g.* 10 ppm per day per dose is allowable for Pd<sup>[28]</sup>). Contamination of APIs from palladium-catalysed reactions can result not only from API-metal and API-adsorbent binding, but also from the strong interactions of palladium with its ligands. As a result of these stabilising effects, it is possible for the Pd to remain in the solution rather than being adsorbed<sup>[41]</sup>. To overcome this problem, 'ligand-less' palladium systems have been developed<sup>[42]</sup>, although the main drawbacks of these

processes are the formation of inactive 'Pd black' and the need for ligands, particularly bulky and electron-rich monophosphines, for challenging substrates<sup>[8]</sup>.

#### a. Ten-year palladium price trend



#### b. Palladium market demand

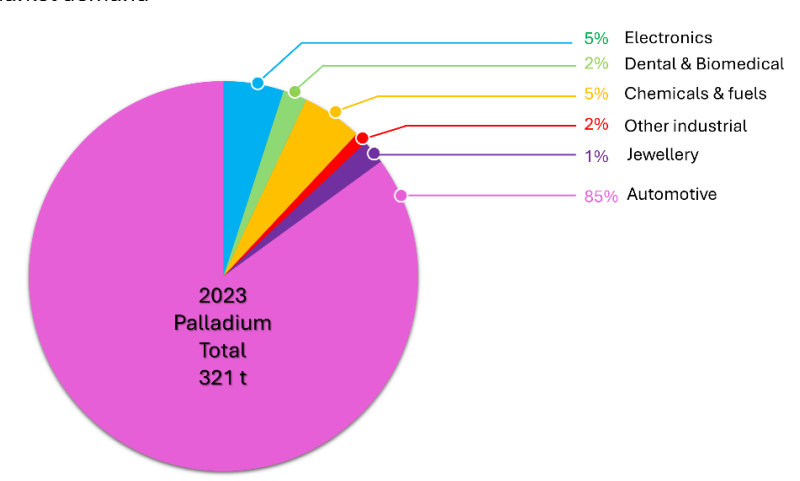
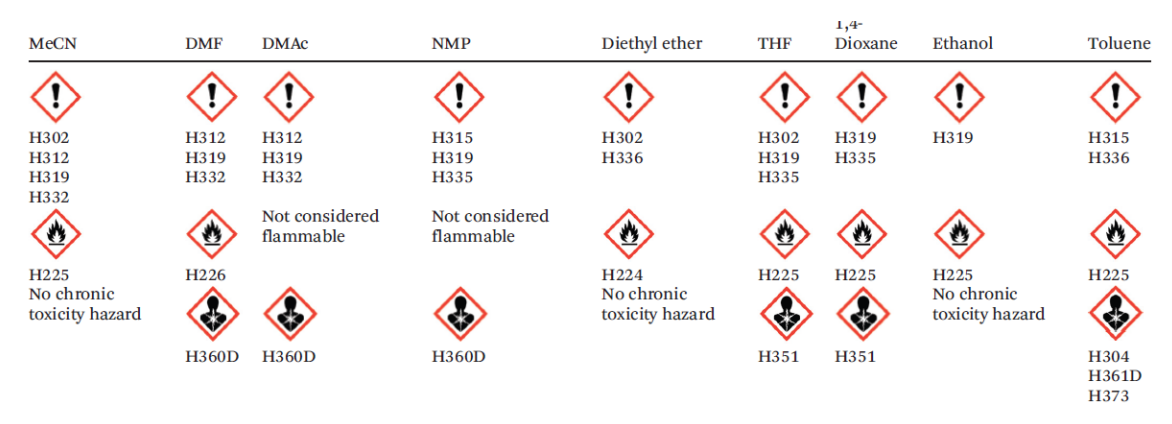


Figure 7. a) Palladium price trend over ten years. b) Palladium market demand (values taken from Johnson Matthey website<sup>[28]</sup>).

Many efforts have been made to develop alternative protocols with low palladium loadings and that allow the metal separation/removal from the final product. Lipshutz and co-workers<sup>[43]</sup> reported Suzuki-Miyaura reactions using a micellar method with water and tetrahydrofuran (THF) as co-solvent and TPGS-750-M as surfactant. These micelles, with a hydrophilic exterior and a hydrophobic interior<sup>[44]</sup>, with the development of suitable ligands such as HandaPhos, allowed Pd loadings often as low as 300 ppm. These significantly reduced loadings translate into much lower residual palladium levels in the final product. This method also simplifies product purification, as the products, which are often solids, precipitate from the aqueous solution as they

form. This "self-recrystallisation" process eliminates the need for extraction and simplifies purification to simple filtration. Our group has also developed a strategy to reduce the metal contamination in Heck-Cassar-Sonogashira reactions. Fantoni et al. [45] performed the couplings in N-hydroxyethylpyrrolidone (HEP)/water mixture as solvent with N,N,N',N'-tetramethyl guanidine (TMG) as base and sulfonated phosphine ligand, such as sodium 2'-dicyclohexylphosphino-2,6-dimethoxy-1,1'-biphenyl-3-sulfonate (sSPhos)[45]. This protocol ensured no metal contamination, as HEP has a very high affinity for water and the HEP/water ratio of 8/2 allows efficient extraction of the final product with an immiscible solvent, leaving metal residues in the HEP/water mixture.

To develop greener protocols for palladium catalysed reactions, the solvents must be considered since they represent c.a. 80-90% of waste in the pharmaceutical industry<sup>[19,46]</sup>. N,N-Dimethylformamide (DMF) is widely used in Pd cross-coupling reactions as it can dissolve most organic compounds and many inorganic salts to some extent. The boiling point of DMF is 153°C, which is high enough to enhance reaction rates, but also recoverable by distillation. However, DMF with also N,N-dimethyl acetamide (DMAc) and N-methyl pyrrolidone (NMP) are reprotoxic solvents and they are under restriction<sup>[47–49]</sup>. In particular, the use of DMF in industry has been severely restricted since December 2023[49] and its replacement has therefore been considered "advisable or requested" by the ACS Green Chemistry Institute® Pharmaceutical Round Table (GCIPR), which defined this goal as one of the hot topics in the list of 12 Green Chemistry Key Research Areas (KRAs)[50]. In Figure 8 are shown the main solvents used in palladium cross-coupling reactions reporting their hazards. In this context, the investigation of alternative solvents becomes mandatory, and GSK has developed a solvent selection guide based on waste, health, safety, environmental and life cycle impacts to guide solvent selection<sup>[51]</sup>.



H224: Extremely flammable liquid and vapour; H225: Highly flammable liquid and vapour; H226: Flammable liquid and vapour; H302: Harmful if swallowed; H304: May be fatal if swallowed and enters airways; H312: Harmful in contact with skin; H315: Causes skin irritation; H319: Causes serious eye irritation; H332: Harmful if inhaled; H335: May cause respiratory irritation; H336: May cause drowsiness or dizziness; H351: Suspected of causing cancer; H360D: May damage the unborn child; H361D: Suspected of damaging the unborn child; H373: May cause damage to organs through prolonged or repeated exposure.

Figure 8. The hazards of solvents commonly used in cross-coupling reactions from the literature<sup>[52]</sup>.

The alternative solvent should ideally be non-toxic and non-hazardous and should not be released into the environment. Removal of residual solvents from products is usually by evaporation or distillation, so commonly used solvents tend to be highly volatile. However, spillage and evaporation contribute to air pollution, a significant global environmental problem, and worker exposure to volatile organic compounds (VOCs) poses serious health risks<sup>[53]</sup>.

Many efforts have been made to find more environmentally friendly solvents, some of which are shown in Figure 9. Among them, γ-valerolactone (GVL), which is a bio-based cyclic ester, was used by Vaccaro and co-workers<sup>[54]</sup> to perform a Sonogashira coupling with DABCO as base using 0.5 mol% of palladium on charcoal. Dihydrolevoglucosenone (Cyrene<sup>TM</sup>) has also been studied as a bio-based solvent in Sonogashira reaction with 2 mol% of Pd(PPh<sub>3</sub>)<sub>2</sub>Cl<sub>2</sub>, 4 mol% CuI and triethylamine (TEA)<sup>[55]</sup> as base and in Suzuki-Miyaura coupling in water mixture with 4 mol% of Pd(dppf)Cl<sub>2</sub> or Pd(OAc)<sub>2</sub>, SPhos and Cs<sub>2</sub>CO<sub>3</sub> as base<sup>[55]</sup>. Capriati et al.<sup>[56]</sup> developed a protocol to perform direct and fast Pd-catalysed C-C cross-coupling reactions between organolithium and various (hetero)aryl halides at rt, with NaCl as an additive in water. Considering properties of NMP, our group investigated the capability of longer *N*-alkylpyrrolidones since they are safe solvents also used as surfactants in cosmetic formulations<sup>[57]</sup>. Ferrazzano et al.<sup>[58]</sup> found that HEP was the best among this category of solvents to perform the Sonogashira reactions using 2 mol% of Pd(PPh<sub>3</sub>)<sub>2</sub>Cl<sub>2</sub>, 1 mol% CuI and TMG as base<sup>[28]</sup>.

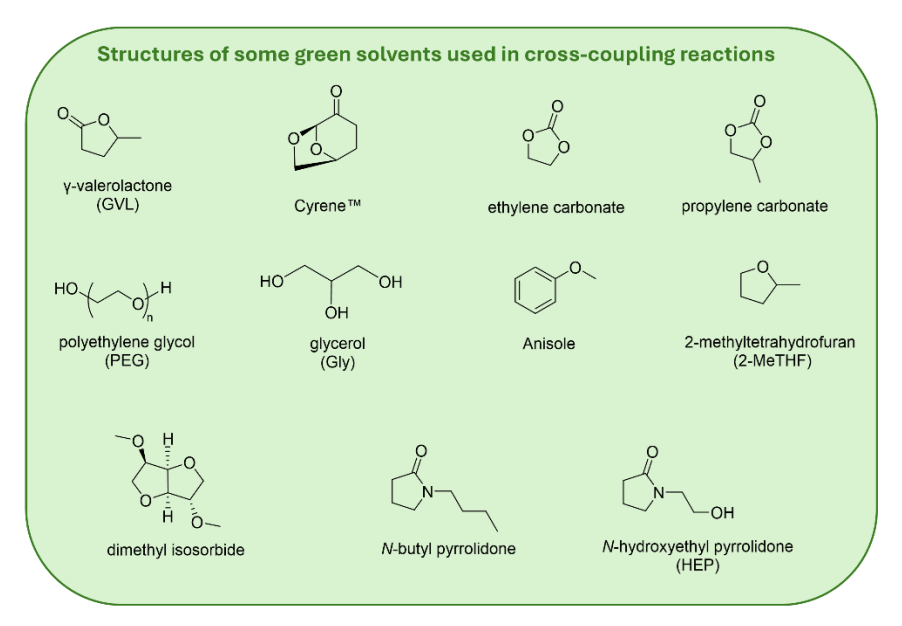


Figure 9. Structures of some green solvents used in cross-coupling reactions

Another important tool to avoid hazardous and VOCs solvents are the Deep Eutectic Solvents (DESs)<sup>[59]</sup>. DESs typically consist of two or three safe, bio-based and

cost-effective components that interact through hydrogen-bond interactions to form an eutectic mixture. This mixture has a melting point lower than that of the individual components as a result of self-association between them. Those are typically prepared by mixing and gently heating a quaternary ammonium salt, such as choline chloride (ChCl), with a neutral hydrogen-bond donor, such as glycerol (Gly), in a specific molar ratio. DESs have also attractive properties, such as non-flammability, recyclability, low vapour pressure and are environmentally friendly [60,61]. In 2018, Capriati and coworkers[62] documented the use of Gly/ChCl (2:1) to perform a ligand-free Suzuki-Miyaura reaction with up to 1 mol% of Pd(OAc)2 and Na2CO3 as base at 60°C with aryl iodides and bromides and at 100°C with chlorides in 5 hours. In 2020, the same group also provided a strategy to carry out a ligand-free Sonogashira-Hagihara reaction of electron-poor and electron-rich (hetero)aryl at 60°C within 3 hours in the eutectic mixture Gly/ChCl (2:1) with 2 mol% Pd/C, and TEA as base<sup>[63]</sup>. In addition, in 2021 they also explored the Negishi reaction in ChCl/urea at 60°C, with reactions completed in 20 seconds and yields up to 91%[64]. Marset et al.[65] also developed cationic pyridiniophosphine as DES-compatible phosphine ligands for Suzuki-Miyaura, Sonogashira-Hagihara and Mizoroki-Heck coupling with PdCl2 as pre-catalyst in ChCl/Gly (1:2), Ph<sub>3</sub>PMeBr/Gly (1:2) and ChCl/Gly (1:2) respectively.

Focusing on the aryl halides, the chlorides are arguably the most useful single class because of they are cheaper and more widely available than the parental aryl iodides and bromides, making chlorides a more economical choice for large-scale or industrial applications. In addition, chlorides are generally less toxic and environmentally harmful than others, thus they are more favourable from a green chemistry and industrial scale process perspective. However, they are the less reactive substrates in cross-coupling reactions, due to the strength of C-Cl bond (bond dissociation energies for Ph-X: Cl: 96 kcal mol<sup>-1</sup>; Br: 81 kcal mol<sup>-1</sup>; I: 65 kcal mol<sup>-1</sup>)<sup>[66]</sup> which makes the oxidative addition step more difficult<sup>[67]</sup>. Several research groups investigated green protocols with aryl chlorides. Among them, Orecchia et al.[68] developed a SM reaction in water using electron-poor chlorides with 0.005 mol% of Pd(OAc)2, P(t-Bu)Cy2 as ligand and Na<sub>2</sub>CO<sub>3</sub> as base at 100°C. They also applied this protocol for the synthesis of the fungicides Boscalid, Fluxapyroxad and Bixafen on large scale (290.0 mmol). Takale et al.<sup>[69]</sup> described a 1-pot synthesis of Boscalid performing the SM coupling with 0.07 mol% of Pd(OAc)2 and SPhos as ligand under aqueous micellar conditions with 10% THF as cosolvent and K<sub>3</sub>PO<sub>4</sub>·H<sub>2</sub>O as base at 55°C. Peng et al.<sup>[70]</sup> documented the Sonogashira coupling with aryl and heteroaryl chlorides in water/acetonitrile (0.5/0.5) with 1 mol% of PdCl2 and sulfonated (2-mesitylindenyl)dicyclohexylphosphine as ligand at 100°C.

In this context, it is also worth mentioning some green metrics that have been introduced to guide the development of greener strategies<sup>[19]</sup> (Table 1). These include the Environmental Impact Factor, or *E factor*, and the *Process Mass Intensity* (PMI), which are

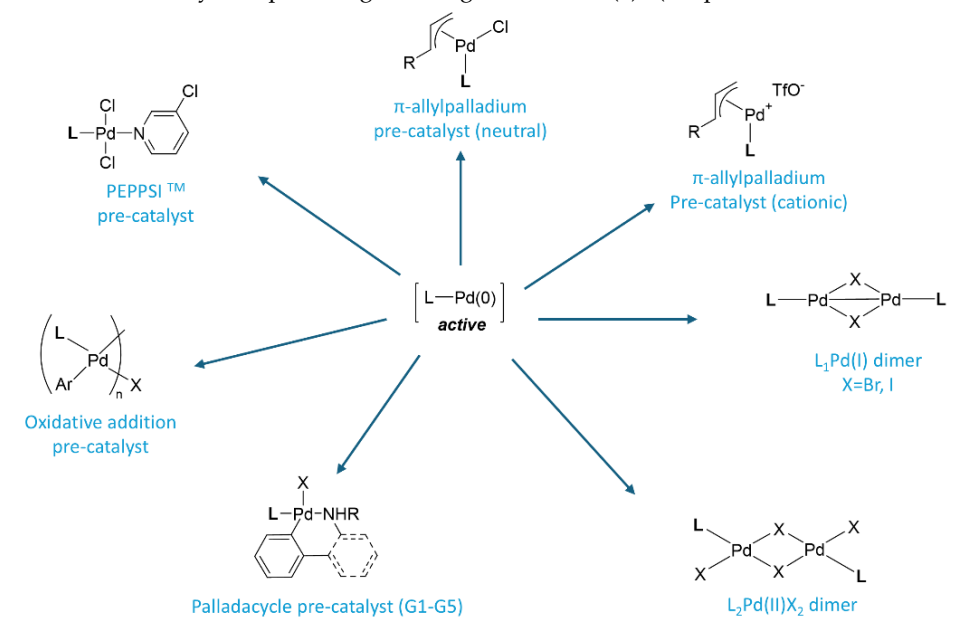
two of the most widely used. The *E factor* was introduced by Sheldon in 1992<sup>[71]</sup> and it assesses the efficiency of a step or process by measuring the total amount of chemical waste generated per kg of product isolated, taking into account yield, spent reagents and solvent losses, excluding water. The ideal *E factor* is 0. The PMI was introduced by the Environmental Protection Agency (EPA) and the American Chemical Society Green Chemistry Institute (ACS GCI) in 2006, and it evaluates efficiency by considering all materials and water used in a step or process, inclusive of workup chemicals.

Table 1. Common green metrics

Green metric	Abbr.	Formula	Unit of measure	Consideration for				Best	
				Waste	Yield	Stoichiometry	Solvent	Water	Value
Chemical Yield	CY	$\frac{m(\textit{Product}) \times \textit{MW} \; (\textit{Raw Material}) \times 100}{m(\textit{Raw Material}) \times \textit{MW} \; (\textit{Product})}$	%	yes	yes	no	no	no	100%
Atom economy	AE	$\frac{\textit{MW (Product)} \times 100}{\Sigma \textit{MW (Raw materials)} + \Sigma \textit{MW (Reagents)}}$	%	yes	no	no	no	no	100%
Environmental impact factor	E- factor	$\frac{\Sigma m(Input\ materials) - m(Product)}{m\ (Product)}$	Kg Kg <sup>-1</sup>	yes	yes	yes	yes	no	0
Process Mass Intensity	PMI	$\frac{\Sigma m  (Input  materials  with  water)}{m (Product)}$	Kg Kg <sup>-1</sup>	yes	yes	yes	yes	yes	1
Reaction Mass efficiency	RME	$\frac{m(product) \times 100}{\sum m(Raw\ materials)}$	%	yes	yes	yes	yes	yes	100%
Reaction Mass Intensity	RMI	$\frac{\Sigma m(\textit{Raw materials}) + \Sigma m(\textit{Reagents})}{m(\textit{Product})}$	Kg Kg <sup>-1</sup>	yes	yes	yes	no	no	1

The development of new strategies that can be viably applied at both academic and industrial levels must be guided by knowledge of green metrics, but a deep understanding of reaction mechanisms is mandatory to control each step and parameter. Mechanistic studies allow chemists to identify the rate-determining step and modify specific conditions to speed up the reaction. Furthermore, by studying the mechanism, it is possible to find the best parameters and conditions to obtain the formation of the desired product over unwanted by-products. Indeed, understanding how the precatalyst, the ligands, the reagents, the solvent and the temperature affect the reaction outcome, is fundamental to planning the reaction protocol. By fine-tuning the conditions for a specific palladium-catalysed reaction, it is possible to develop processes that are less time consuming and costly, as well as improving efficiency and safety. In particular, the formation of the active catalyst is the first step common to all Pd-catalysed crosscoupling reactions, and by precisely controlling this process it is possible to avoid excess reagents, save precious ligands, use lower temperatures and make the reduction faster. The active species of palladium is a Pd(0) species, usually 14-electron based L<sub>2</sub>Pd(0) complexes that are directly used, such as Pd(PtBu3)2, or generated in situ from a precursor. The monoligated L<sub>1</sub>Pd(0) species, although impossible to synthesise and isolate, are highly reactive due to the unsaturated coordination sphere. Indeed, Fu and co-workers[72] showed that Suzuki-Miyaura couplings, with less reactive aryl chlorides, go through the monoligated Pd(PtBu3) specie rather than Pd(PtBu3)2. It has also been shown that bulky and electron-rich phosphines are able to favour the formation of L<sub>1</sub>Pd(0)<sup>[73]</sup>, which promotes more difficult reactions. For this reason, Buchwald incorporated the -P('Bu)2 moiety into the biaryl scaffold to generate P('Bu3)2R (R=biphenyl) JonhPhos and many other biaryl ligands (e.g. Sphos, RuPhos, Xphos)[74,75]. In this scenario, various pre-catalysts have been synthesised to produce the air sensitive and highly reactive "L<sub>1</sub>Pd(0)" in situ. Hartwig and co-workers<sup>[76]</sup> disclosed the superior catalyst activity of the dimer  $[(P^tBu_3)Pd(\mu-Br)]_2^{[77]}$ , which is an air-sensitive and dark green 16-electron complex able to act in situ as a reservoir of the highly reactive 12electron Pd(PtBu3). In this field, it is also worth mentioning the remarkable studies carried out by Schoenebeck's group, such as the synthesis of the corresponding and airstable iodo-bridged dimers[78] and the potential activation mechanism[79]. Shaughnessy and co-workers[80] also suggested the use of the air stable Pd(II) dimers [(PR3)PdCl2]2 ditert-butylneopentylphosphine (DTBNpP) or trineopentylphosphine Alternative Pd(II) pre-catalyst to generate L<sub>1</sub>Pd(0) in situ are the palladacycle and PEPPSI type after activation by a suitable base. The first category has been extensively studied by Buchwald and co-workers[81-83], who developed five generations (G1-G5) of biphenylamine-based palladacycles. While, Organ and co-workers[84] first reported the class of N-heterocyclic carbene (NHC) based air- and moisture-stable Pd catalyst called Pyridine-Enhanced Pre-catalyst Preparation Stabilization and Initiation (PEPPSI) (Scheme 1).

Scheme 1. Pre-catalysts capable of generating active "L<sub>1</sub>Pd(0)" (adapted from the literature<sup>[85]</sup>).



The reduction of the pre-catalyst L<sub>2</sub>PdX<sub>2</sub> has been extensively studied by various scientists. Important contributions have been made by Amatore and Jutand, who demonstrated that Pd(OAc)<sub>2</sub> in THF and in DMF reacts with 3 equivalents of triphenylphosphine to initially form Pd(OAc)<sub>2</sub>(PPh<sub>3</sub>)<sub>2</sub>, which then spontaneously evolves into triphenylphosphine oxide (OPPh<sub>3</sub>) and a zerovalent palladium complex<sup>[86]</sup>.

They also studied the reduction of  $Pd(OAc)_2$  with 2 equivalents of the bidentate 1,3-bis(diphenylphosphino)propane (dppp)<sup>[87]</sup> (Figure 10a). In addition, Blanc and co-workers<sup>[88]</sup> demonstrated the ability of *n*-butanol to promote the reduction of  $Pd(XPhos)_2Cl_2$  (Figure 10b).

However, a comprehensive understanding of the most effective modes of  $L_2PdX_2$  pre-catalyst activation for specific conditions has not yet been fully achieved.

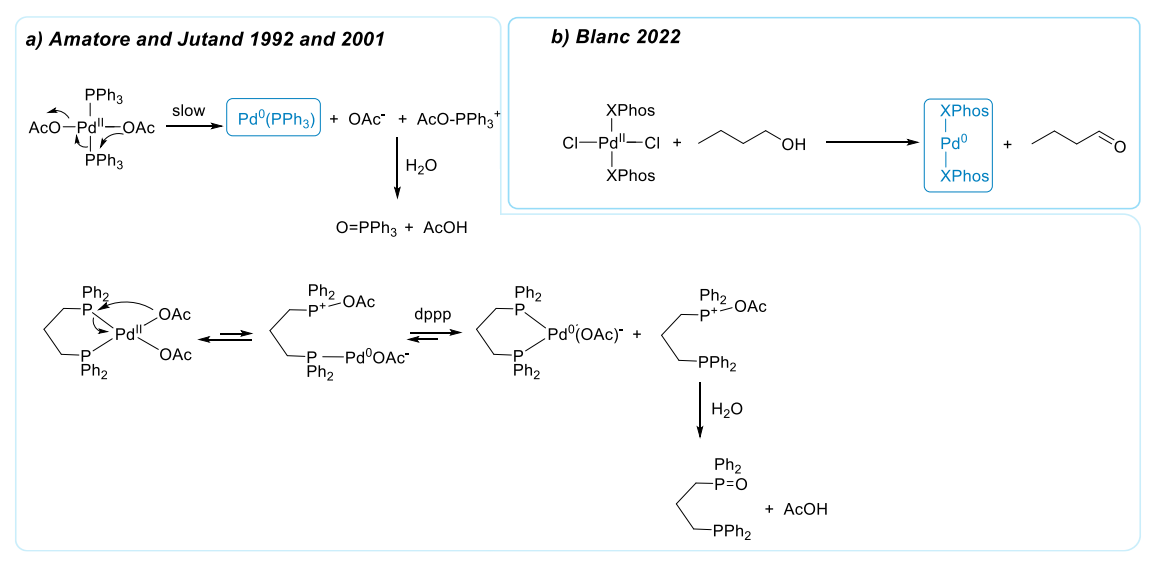


Figure 10. a) Pd(OAc)<sub>2</sub>(PPh<sub>3</sub>)<sub>2</sub> and Pd(OAc)<sub>2</sub>dppp reduction by acetate, b) PdCl<sub>2</sub>(Xphos)<sub>2</sub> reduction by *n*-butanol.

### 1.3. Peptides

Peptide-based drug discovery is attractive because peptides are smaller than proteins, allowing them to target both extracellular and intracellular sites. Over the past two decades, peptides have attracted increasing attention, largely due to advances in peptide synthesis and purification techniques. These developments have made pharmaceutical-grade peptides more accessible, even when they have a high number of amino acids. As a result, approximately 80 peptide-based therapeutics (PbTs) have been approved and launched on the market. In addition, more than 150 peptides are in clinical development and 400-600 are in preclinical studies<sup>[89]</sup>.

However, although peptides have demonstrated significant success as pharmacological agents, their native forms are often unsuitable for treating many diseases. Various structural modifications have been developed to improve their pharmaceutical properties. These include the incorporation of unnatural amino acids, cyclization techniques, the design of stapled peptides and conjugation with stabilising components such as lipids or pegylated chains. A review of the major milestones in the discovery and development of peptide-based therapeutics highlights their importance in modern drug development (Figure 11). From a commercial perspective, the peptide

therapeutics market size is estimated at USD 43.30 billion in 2024, and is expected to reach USD 60.90 billion by 2029, growing at a Compound Average Growth Rate (CAGR) of 7.06% during the forecast period (2024-2029)<sup>[90]</sup>. CAGR is a business, economic and investment term used to describe the average annualised growth rate of compounded values over a period of time (CAGR= [(ending value / starting value)^(1 / number of years)] – 1) (Figure 12).

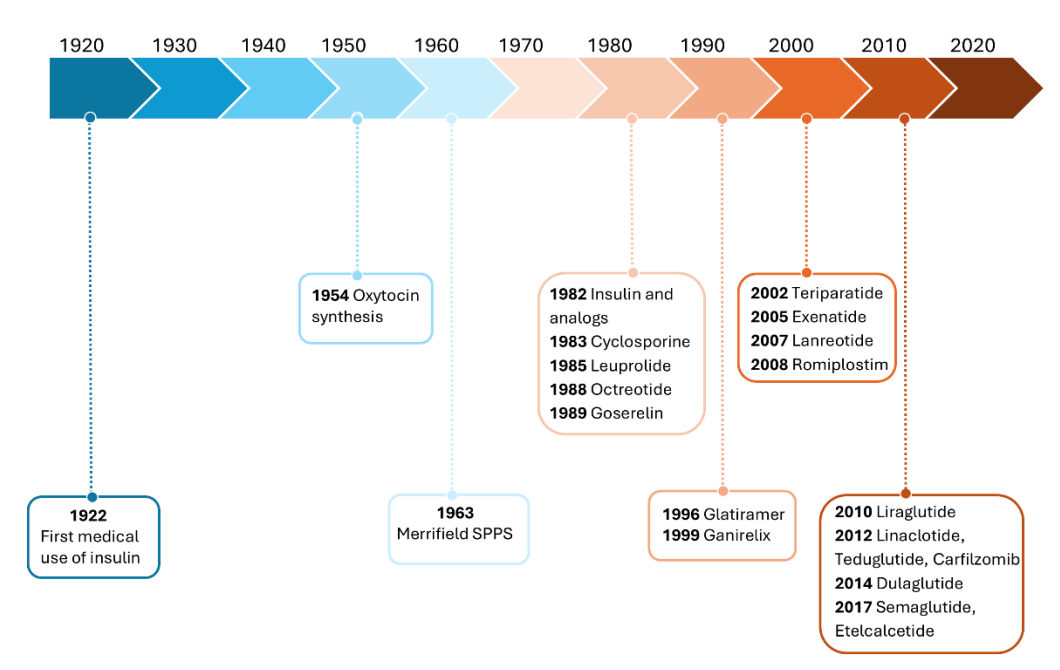


Figure 11. Timeline of key milestones, developments and approvals in the field of peptide therapeutics[91].

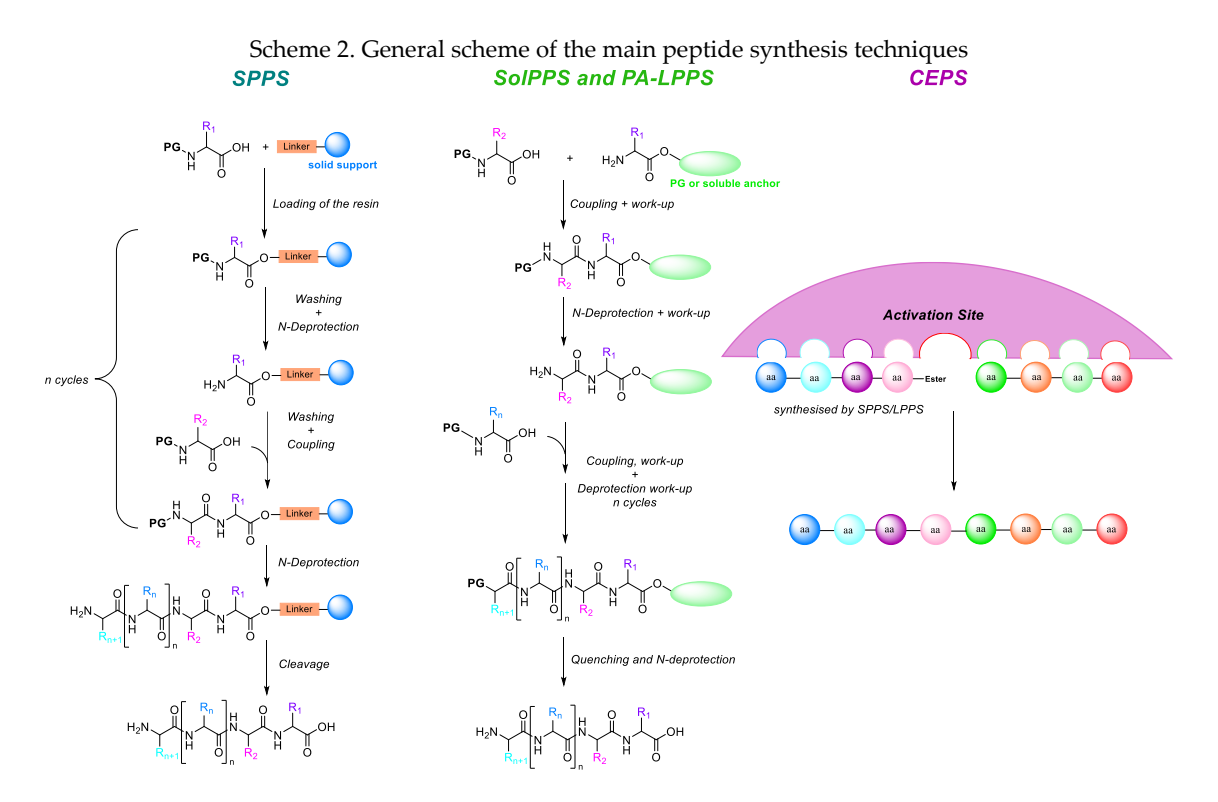
# 

#### Peptide Therapeutics Market Size Growth Trends and Forecast (2024-2029)

Figure 12. Peptide therapeutics market sales in USD million for the period 2024-2029[90].

Peptides can be synthesised by a variety of methods, including solid-phase peptide synthesis (SPPS), solution-phase peptide synthesis (SolPPS), peptide-anchored liquid-phase peptide synthesis (PA-LPPS), chemo-enzymatic peptide synthesis (CEPS),

mechanochemical peptide synthesis and recombinant production via fusion proteins. Of these, the recombinant approach is primarily suitable for the synthesis of long peptides composed of natural amino acids, which limits its applicability in modern drug discovery. SPPS introduced by Merrifield in 1963[92] (see Figure 11), revolutionised peptide synthesis by allowing the fully automated incorporation of over ten amino acid residues per day. This method is based on the stepwise assembly of a peptide sequence onto an insoluble polymer-based solid support. The process begins by anchoring the first amino acid, protected at its amino group, to the resin through its acidic terminal. Peptide extension proceeds through an iterative sequence of reactions involving deprotection, washing, coupling and additional washing steps. Once the desired peptide sequence is complete, the peptide is cleaved from the solid support and isolated by precipitation with an anti-solvent. In contrast, SolPPS operates in a monophasic system where the growing peptide chain is attached to a soluble tag, requiring the isolation of intermediates at each step. The soluble tags, such as a benzylic ester (-OBz) or methyl ester (-OMe), act as protecting groups. Instead, the PA-LPPS uses longer anchors, such as polyethylene glycol (PEG)-based supports, to facilitate peptide synthesis. CEPS is particularly valuable for the construction of long-chain peptides, as it uses enzymes to ligate two chemically synthesised peptide segments (Scheme 2).



Finally, mechanochemical peptide synthesis is based on the use of ball milling techniques, which allow the reaction to be carried out without solvents.

As peptide drugs continue to grow in economic and technological importance, the development of greener synthesis methods has become increasingly important. One of the most pressing challenges in peptide synthesis is the significant amount of solvent required, with washes accounting for 80-90% of the total process waste. For peptides with an average molecular mass of 1000 to 5000 Da, the waste generated during synthesis is significant, resulting in a PMI of approximately 3000 to 15,000 kg of waste per kilogram of API<sup>[93]</sup>. The environmental impact is compounded by the reliance on hazardous solvents and reagents, further emphasising the need for sustainable alternatives. Mechanochemical peptide synthesis is a valuable tool to move towards greener strategies, but it is limited to short Boc-protected peptides requiring the use of HCl gas<sup>[94,95]</sup>. The chemo-enzymatic approach is also a greener option and allows excellent regio- and chemoselectivity under mild reaction conditions, avoiding highly reactive and toxic stoichiometric amounts of coupling reagents. However, it is used for fragment coupling and must be performed with green LPPS or SPPS protocols<sup>[96]</sup>.

DMF is the best solvent for peptide synthesis, both in the solid and solution phase, due to its high performance in solubilising reagents and by-products. However, as mentioned above, it is reprotoxic and classified as a hazardous solvent. Several solvents have been investigated with the common goal of finding an alternative. Pioneers in this field, the Albericio group first proposed the use of ACN and THF for SPPS[97], despite being listed as solvents of moderate to high concern in the GSK Solvent Sustainability Guide<sup>[51]</sup>. They also investigated the use of *N*-formylmorpholine (NFM), isosorbide dimethyl ether, cyclopentyl methyl ether (CPME)[98] and dimethyl carbonate (DMC)[99]. The research groups of Albericio[100] and Rasmussen[101] also suggested ethyl-5-(dimethylamino)-2-methyl-5-oxopentanoate (Rhodiasolv® PolarClean, marketed by Solvay)[102] as a green solvent for SPPS. N-alkylpyrrolidones, which have a similar structure to NMP, have also been found to be valid alternatives. In 2018, Gallou and coworkers proposed the N-butylpyrrolidone (NBP)[103] and three years later, our group showed the high performance of N-octyl pyrrolidone (NOP) as a solvent for SPPS<sup>[104]</sup>. Green mixtures have also been investigated, such as Cyrene©/diethyl carbonate (3/7), sulfolane/diethyl carbonate (7/3) and anisole/DMC (7/3) by our group<sup>[105]</sup> (Figure 13).

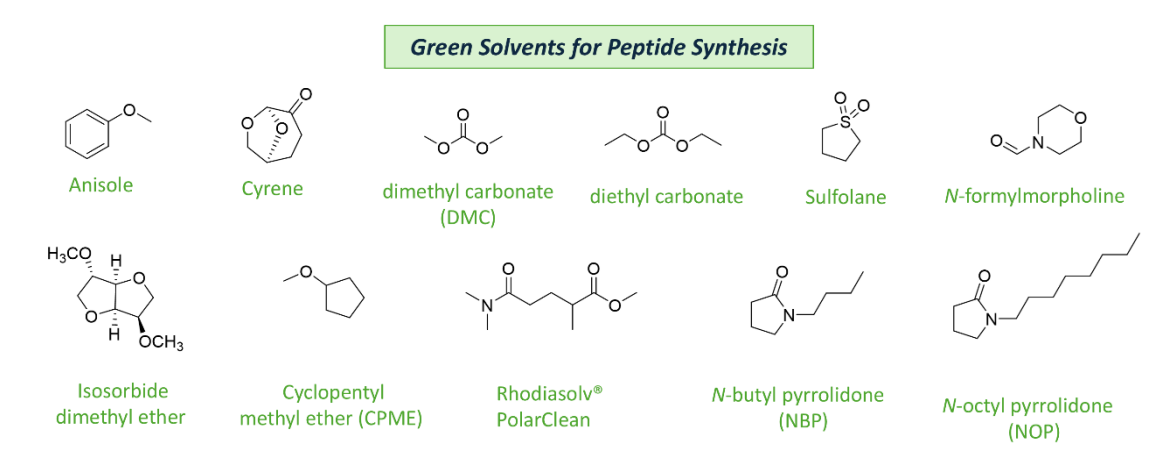


Figure 13. Green solvents used in green peptide synthesis.

However, other key components must be considered to achieve the goal of a fully green approach, such as the base to remove the *N*-protecting group and the coupling reagent.

In SPPS, fluorenylmethoxycarbonyl (Fmoc) was introduced by Carpino<sup>[106]</sup> as a base-labile protecting group for the amino terminal. Fmoc groups can be cleaved under mildly basic conditions via an E1cB  $\beta$ -elimination mechanism (Figure 14a). According to the mechanism, dibenzofulvene (DBF) is formed in the first step and, as a highly reactive electrophile, can promote side reactions.

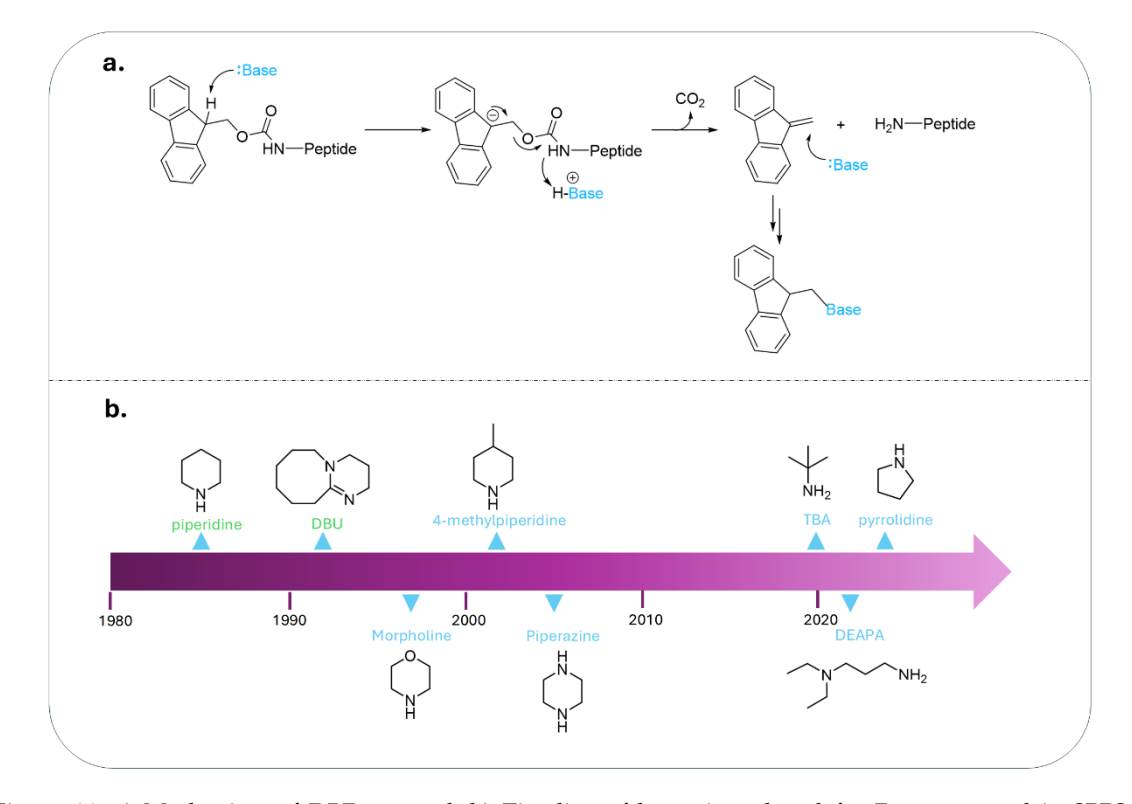


Figure 14. a) Mechanism of DBF removal. b) Timeline of bases introduced for Fmoc removal in SPPS (adapted from literature<sup>[107]</sup>).

Piperidine is very efficient in this context, being both a strong base and a good nucleophile, so a solution of 20% piperidine in DMF at room temperature is typically used in both SPPS and PA-LPPS<sup>[108]</sup>. However, it is a highly regulated substance used in the illegal manufacture of phenylcyclohexylpiperidine (PCP), also known as "angel dust", a powerful hallucinogen.

In this context, several alternative deprotecting bases have been investigated, including piperazine<sup>[109]</sup>, morpholine<sup>[110]</sup>, methylpiperidines, 4-methylpiperazine<sup>[111]</sup>, pyrrolidine<sup>[112]</sup> and 1,8-diazabicyclo<sup>[5,4,0]</sup>undec-7-ene (DBU)<sup>[109]</sup>. With the aim of investigating a complete green protocol, several research groups have also studied the use of safe and not controlled deprotecting bases in sustainable solvents. Gallou and coworkers<sup>[103]</sup> proposed the use of 4-methylpiperidine in several green solvents such as NBP and Rasmussen et al.<sup>[101]</sup> in a green solvent mixture. The group of Tolomelli and Cabri reported the use of tert-butylamine (TBA)<sup>[113]</sup> and 3-diethylaminopropylamine (DEAPA)<sup>[114]</sup> in NOP and NOP/DMC mixtures (Figure 14b).

The current state-of-the-art methodology for peptide bond formation in SPPS is predominantly based on the carbodiimide/additive approach, with diisopropylcarbodiimide (DIC) being the most commonly used carbodiimide[115]. Among the additives used in combination with carbodiimides, benzotriazoles and oximes are the primary choices. Although the benzotriazole family was the first coupling reagent introduced for SPPS (HOBt, HOAt, HBTU are prime examples, see Figure 15), these additives carry a risk of explosion and are therefore regulated as "class 1 explosives" [116-<sup>118]</sup> and can cause skin sensitisation after long-term exposure<sup>[119]</sup>. This category also includes more stable derivatives that are stand-alone coupling reagents with improved stability, enhanced coupling efficiency and reduced racemisation. Despite these advantages, safety concerns drove the search for alternatives. In this context, oximes emerged as a safe and efficient option when Albericio and co-workers introduced this class of additives in 2009[120]. In particular, their work highlighted OxymaPure® (ethyl 2cyano-2-(hydroxyimino)acetate), which showed excellent performance in terms of yield, low racemisation and improved safety compared to hydroxybenzotriazole-based additives. Since then, several oxime derivatives have been developed, including K-Oxyma<sup>[121]</sup>, PyOxyma<sup>[122]</sup>, OxymaB<sup>[123]</sup> and COMU<sup>[124,125]</sup> (Figure 15).

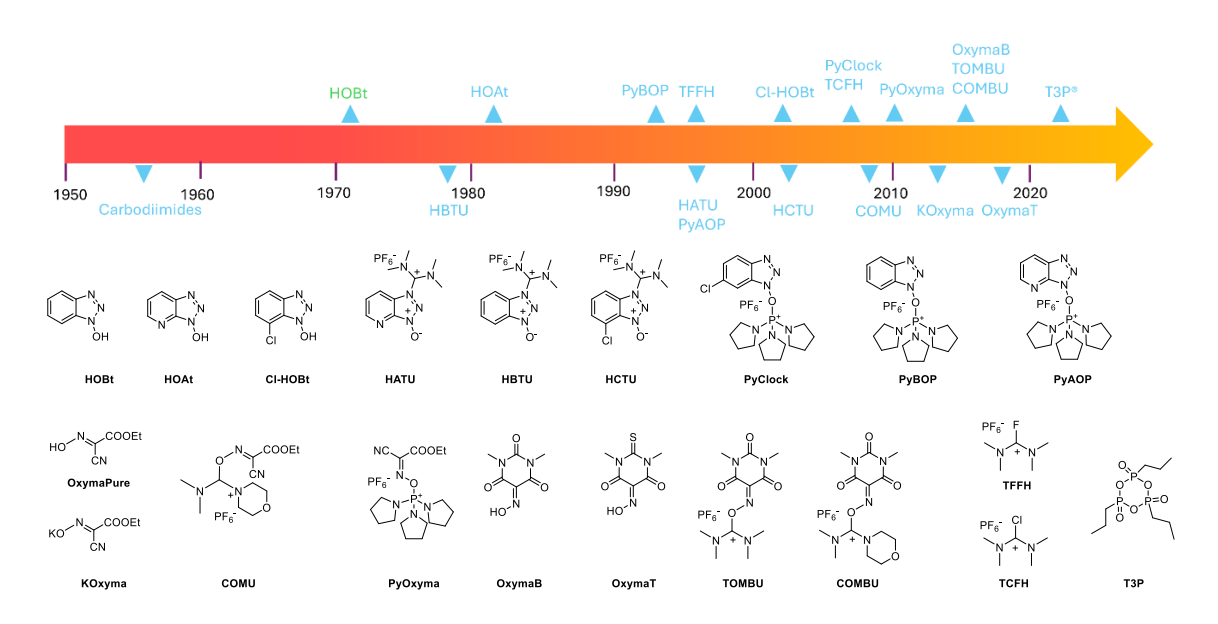


Figure 15. Timeline of introducing coupling reagents and additives in SPPS and relative structures (adapted from the literature<sup>[107]</sup>).

DIC/OxymaPure® has become the gold standard in peptide synthesis due to its exceptional efficacy, safety profile, thermal stability, low cost and the good solubility of its diisopropylurea (DIU) by-product in organic solvents. In particular, its compatibility with green solvents for SPPS is well established, as first demonstrated by Albericio's group in 2015 during coupling reactions in 2-MeTHF and ACN<sup>[97]</sup>. However, researchers from Eli Lilly have recently identified a significant drawback to this protocol by observing the formation of hydrogen cyanide (HCN) during amino acid activation<sup>[126]</sup>. The proposed mechanism for HCN formation is shown in Figure 16. To address this challenge, Albericio's group conducted a study in 2021 to evaluate the influence of carbodiimides on HCN production when used with OxymaPure®. Their results showed that steric hindrance of the *N*-substituents on carbodiimides plays a key role in promoting HCN release<sup>[127]</sup>. In 2019, Isidro-Llobet and colleagues introduced tetramethylfluoroformamidinium hexafluorophosphate (TFFH) and propylphosphonic anhydride (T3P®) as more sustainable alternatives for coupling reagents<sup>[128]</sup>. Although these reagents exhibit promising properties, their application in SPPS remains limited.

Despite the excellent results already achieved for more sustainable peptide synthesis, it is still necessary to investigate other approaches that are environmentally friendly and affordable to convince the industry to change protocols that have been consolidated for decades.

Figure 16. Peptide coupling mechanism with DIC/OxymaPure® and proposed mechanism for HCN formation.

### 1.4. Fluorinated compounds

Fluorinated compounds are the least abundant natural halides<sup>[129]</sup>, but organofluorine compounds have been widely used in bioactive agents, such as pharmaceuticals and agrochemicals. The number of approved fluoro-pharmaceuticals has increased steadily over the last 50 years. Worldwide, more than 300 fluoro-drugs have been registered, including the best-selling fluorinated drugs: Prozac, Lipitor and Ciprobay (Figure 17).

Figure 17. Structures of Prozac, Lipitor and Ciprobay.

In particular, 23 new molecular entities (NMEs) were approved by the FDA in 2024, of which 7 (30%) were fluorinated, with an average of 34% fluorinated NMEs over the last nine years (Figure 18).

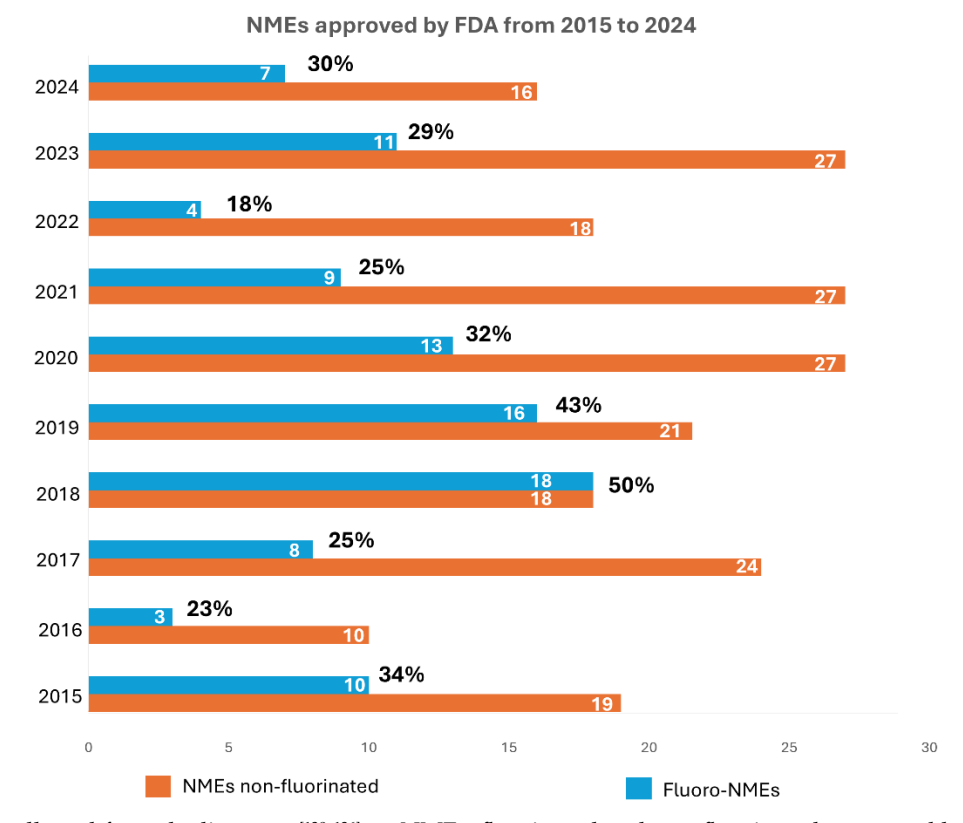


Figure 18. Data collected from the literature<sup>[130–136]</sup> on NMEs, fluorinated and non-fluorinated, approved by the FDA in the period 2015-2024.

The continued success of fluoro-pharmaceuticals strongly suggests to medicinal chemists that the selection of fluoro-organic molecules is a potential strategy to significantly minimise the risk of unsuccessful trial-and-error attempts during the drug discovery process<sup>[136]</sup>. There are several reasons for the widespread use of fluorinated organic compounds in pharmaceuticals. Firstly, fluorine is the second smallest atom in the periodic table after hydrogen, so replacing an H atom in a drug candidate with fluorine does not significantly alter the parent structure<sup>[137]</sup>. The bond length of C-F (1.41 Å) is also very similar to that of C-O (1.43 Å), and structures such as C=CHF can be used to replace peptide bonds[138]. These properties are fundamental because bioisosterism, the substitution of atoms or functional groups of comparable size or shape to achieve similar biological effects, is essential for lead optimisation. In particular, the ability of fluorine to alter the properties of a molecule can be drastic, it is enough to consider acetic acid and fluoroacetic acid. The former is completely harmless, being an essential component of vinegar, whereas the latter, found in more than 40 plants, is highly toxic, inhibiting the Krebs cycle and leading to the death of the organism. In addition, the Fsubstitution is also useful to change the conformational preferences of a small molecule due to size and stereochemical effect, and it can be useful to stabilise a precise conformation of a bioactive molecule to improve site-specific binding. It is also important to consider that the ionisation state and the balance between lipophilicity and

hydrophilicity, significantly influence the biological absorption and distribution of a drug molecule. The incorporation of fluorine into a drug can increase its bioavailability. Lipophilicity is quantified by logD, a logarithmic coefficient that indicates how a compound distributes between octanol and water. A higher logD value corresponds to greater lipophilicity, and replacing a hydrogen atom with fluorine typically increases the logD value by about 0.25[139]. Fluorine has also a strong electron-withdrawing inductive effect, which gives the C-F bond a "polar-hydrophobic" character, as F reduces the polarizability and increases the hydrophobicity of molecules. This property improves the membrane permeability of fluorinated molecules compared to non-F analogues[137]. In addition, a sufficient number of nearby F atoms can leave an amine unprotonated at physiological pH, affecting the membrane permeability<sup>[140]</sup>. The H/F substitution is also helpful in enhancing the protein-ligand interaction due to the capability of C-F to participate in multipolar interactions. For example, Diederich's group found that fluorinated tricyclic thrombin inhibitors had a better affinity for the active site due to the multipolar interactions C-F···H-C $\alpha$  and C-F···C=O in the binding pocket<sup>[141,142]</sup> (Figure 19). Finally, the fluorination of natural bioactive molecules also makes them more resistant to metabolic degradation[137].

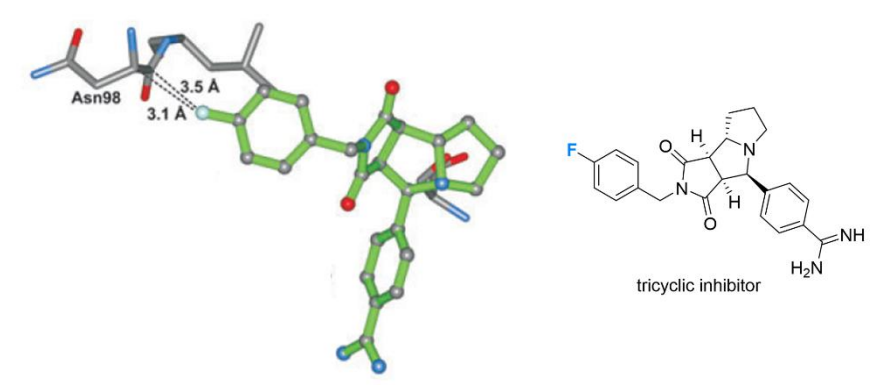


Figure 19. X-ray crystal structure taken by the literature<sup>[143]</sup> to show multipolar interaction C-F···C=O in the binding pocket. Colour code: inhibitor skeleton: green; C: grey; O: red; N: blue; F: cyan.

Incorporation of fluorine atoms has been shown to influence several critical properties, including metabolic pathways, pharmacokinetics and permeability. Unfortunately, the most commonly used synthetic methods for fluorination often have poor green chemistry metrics or are impractical for complex molecules with multiple functional groups. There is a pressing need within the synthetic community for fluorination methods that are both practical and environmentally sustainable<sup>[144]</sup>.

Fluorine is the 13<sup>th</sup> most abundant terrestrial element and occurs almost exclusively as fluoride salts<sup>[145]</sup> of which calcium fluoride (also known as fluorite or fluorspar), found mainly in Mexico, China and South Africa, is the only resource exploited. The purest fraction, known as Acidspar, is treated with sulphuric acid (first reported by Scheele in 1771<sup>[146]</sup>) to produce over one million tons of anhydrous HF gas

per year, which is used directly or indirectly in the synthesis of all the fluorinated organic compounds[147] (Figure 20).

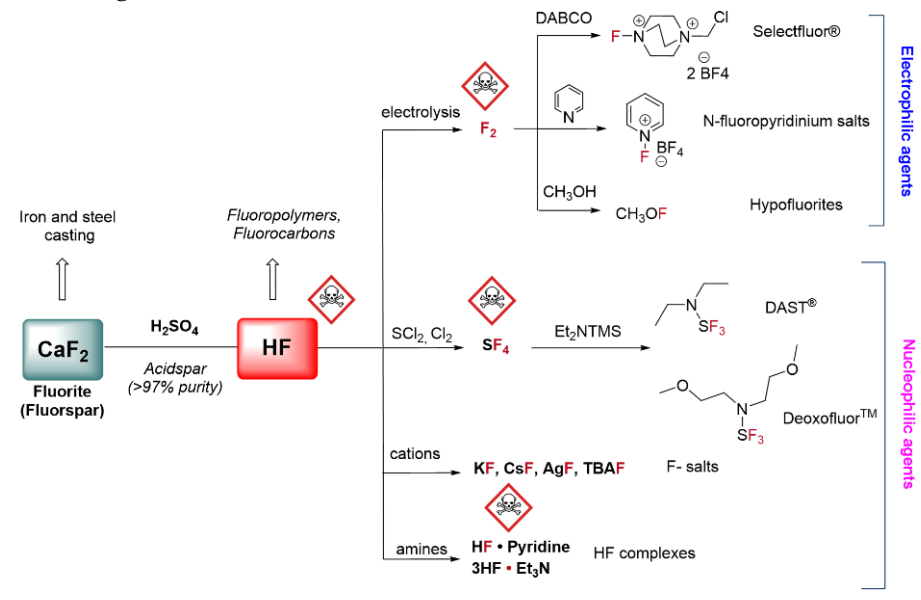


Figure 20. The main sources of fluorine atoms used in the chemistry of organofluorine compounds (adapted from the literature<sup>[144]</sup>).

HF is not a laboratory friendly reagent due to its ability to dissolve glass by reacting with silicon. It is highly corrosive and must be handled with care as it can penetrate the skin causing severe burns and toxicity. This is because the fluoride ion interacts with calcium in the body, posing significant health risks<sup>[148]</sup>. The news reported in 2019 a catastrophic accident in Philadelphia (USA) in which 300,000 kg of hydrofluoric acid was released due to corroded pipes. HF, a common acid catalyst used in the refining of low molecular weight hydrocarbons, was released into the atmosphere during a 24-hour fire. The accident miraculously caused no fatalities, but the company responsible for the plant filed for bankruptcy<sup>[149]</sup>.

Fluorination can occur by electrophilic, nucleophilic or radical reactions. 1-Chloromethyl-4-fluoro-1,4-diazoniabicyclo[2.2.2]octane bis(tetrafluoroborate) (Selectfluor®), *N*-fluoropyridinium salts and *N*-fluorosulfonimides, such as *N*-fluorobenzenesulfonimide (NFSI) are widely used in modern organic synthesis<sup>[150–156]</sup>. However, electrophilic F<sup>+</sup> reagents have several disadvantaged. They are expensive and dangerous to synthesise as they rely on the F<sub>2</sub> gas storage and, being highly reactive, their oxidising properties can be incompatible with some substrates. They also have a high molecular weight, which makes them a poor choice in terms of atom economy. The N-F reagents, such as NFSI and Selectfluor, have also been employed for radical fluorination due to the low N-F bond strength<sup>[147]</sup>. Regarding nucleophilic F-sources, alkali metal fluoride salts are the best choice because they are safe, available and inexpensive.

Fluorine also plays a key role in PET through the synthesis of <sup>18</sup>F-labelled radiotracers. PET is a highly sensitive imaging technique that enables non-invasive in vivo characterisation of biochemical processes at a molecular level. It is an indispensable tool in drug discovery, disease diagnosis, therapeutic evaluation and patient stratification, thereby facilitating the treatment of various diseases[157]. The radioisotope <sup>18</sup>F is commonly used due to its excellent decay properties (t<sub>1/2</sub>=109.8 min, 97% β<sup>+</sup> decay, 0.63 MeV positron energy)[158]. Specifically, the low positron energy results in highresolution images and the long half-life of <sup>18</sup>F (the t<sub>1/2</sub> of <sup>11</sup>C is 20 min) allows multiple patients to be imaged from a single radiotracer production, as well as off-site delivery of the <sup>18</sup>F-radiotracers<sup>[159]</sup>. Innovative methods for late-stage <sup>19</sup>F-fluorination and the important role of fluorinated compounds in the pharmaceutical sector, have guided the progress of <sup>18</sup>F- radiolabelled molecules for PET<sup>[160]</sup>, with particular relevance to the development of "[18F]N-F" reagents, such as [18F]-NFSI[161] and [18F]-Selectfluor bis(triflate)[162] described by the Gouverneur group. The <sup>18</sup>F-labelling of biomolecules, such as peptides and proteins, has been carried out by attaching a prosthetic group or via late-stage, some examples are shown in Figure 21.

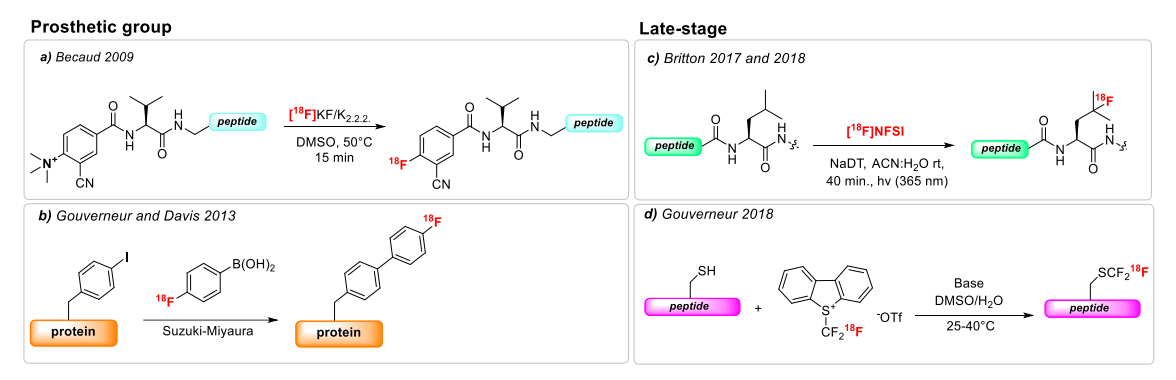


Figure 21. Examples of prosthetic groups in <sup>18</sup>F-radiolabelling of peptide-protein: a) Becaud in 2009<sup>[163]</sup> and b) Gouverneur and Davis in 2013<sup>[164]</sup>. Examples of late-stage modification on <sup>18</sup>F-radiolabelling of peptide-protein: c) Britton in 2017 and 2018<sup>[165,166]</sup>, d) Gouverneur in 2018<sup>[167]</sup>.

Despite the great success of fluorinated molecules in the pharmaceuticals and agrochemical sectors, safety concerns regarding the supply chain to prepare the starting materials, poor green chemistry metrics and high costs are major drawbacks. In this context, the recent study published by Gouverneur's group showing a new way of using fluorspar as a direct source of fluoride, bypassing HF production, is noteworthy<sup>[168]</sup>. However, the need to develop other alternative strategies for fluorination continues to grow in parallel with the number of fluorinated molecules approved on the market each year.

#### 1.5. Aim of the Project

The aim of this project is to explore alternative strategies for the synthesis of biologically active compounds. The thesis is divided into three sections, each addressing a different area of research.

The first part focuses on palladium-catalysed reactions. In particular, we have elucidated the mechanism of the Heck-Cassar-Sonogashira reaction, investigated the process of Pd(II) pre-catalyst reduction, and developed a sustainable approach for Heck-Cassar and Suzuki-Miyaura reactions using aryl chlorides.

The second part is dedicated to peptide synthesis. Specifically, we evaluated the applicability of safe and environmentally friendly coupling reagent for SolPPS and PA-LPPS methods and synthesised a small library of potential antimicrobial peptides.

The third section describes the development of novel enantioselective fluorination protocols based on a nucleophilic approach. This part of the research was carried out at the University of Oxford under the supervision of Professor Véronique Gouverneur.

CHAPTER 2

## The Mechanistic Investigation and Sustainable Approach of Palladium Catalysed Cross-Coupling Reaction

# 2.1. New mechanistic insights into the copper-free Heck-Cassar-Sonogashira cross-coupling reaction

#### 2.1.1. Introduction

The palladium-catalysed cross-coupling of a terminal alkyne with a vinyl or aryl halide is a powerful reaction in organic synthesis because it provides a direct route to sp-sp<sup>2</sup> carbon-carbon bonds. For this reason, since its discovery in 1975, it has found wide application in diverse areas, including pharmaceuticals and natural products<sup>[169,170]</sup>. In the presence of cuprous iodide (CuI) the reaction is known as Sonogashira reaction while, without the metal additive, as Heck-Cassar reaction (Scheme 3).

Scheme 3. General Scheme of the HCS Reaction.

```
Heck-Cassar Pd(0)
Sonogashira Pd(0)/Cu(l)

R — H + Ar — X

solvent / base

X= I, Br, Cl, OTf, N<sub>2</sub>
```

In the beginning of 1975, Heck<sup>[171]</sup> and Cassar<sup>[172]</sup> independently published methods for the palladium-catalysed coupling of aryl halides, or pseudohalides, with alkynes, using different bases, solvents, and temperatures. Cassar used sodium

methoxide in DMF at 50°C, while Heck neat triethylamine at 100°C. Shortly thereafter, Sonogashira<sup>[173]</sup> introduced a similar protocol but under milder conditions, using neat diethylamine at room temperature, with CuI as a cocatalyst. The presence of copper(I) allowed the reaction to achieve complete conversion of aryl iodides even at room temperature.

Despite improved reactivity with copper as a cocatalyst, it also presents challenges. The use of copper requires stringent exclusion of oxygen to prevent alkyne homocoupling, a side reaction mediated by the copper-catalysed Glaser–Hay reaction<sup>[174]</sup>. This is a major problem when the supply of acetylene is limited or expensive and represent a problem in terms of selectivity. Furthermore, copper itself is environmentally harmful<sup>[40]</sup> and complicates catalyst recovery, as it is difficult to separate from palladium at the end of the reaction. In addition, the reagents may be sensitive to the presence of copper and require alternative variants of the coupling procedure<sup>[175]</sup>. To overcome these problems, the interest in studying copper-free protocols became increasingly significantly.

The Pd/Cu-catalysed Sonogashira mechanism is generally understood to proceed via two independent catalytic cycles<sup>[176–178]</sup> (Figure 22a).

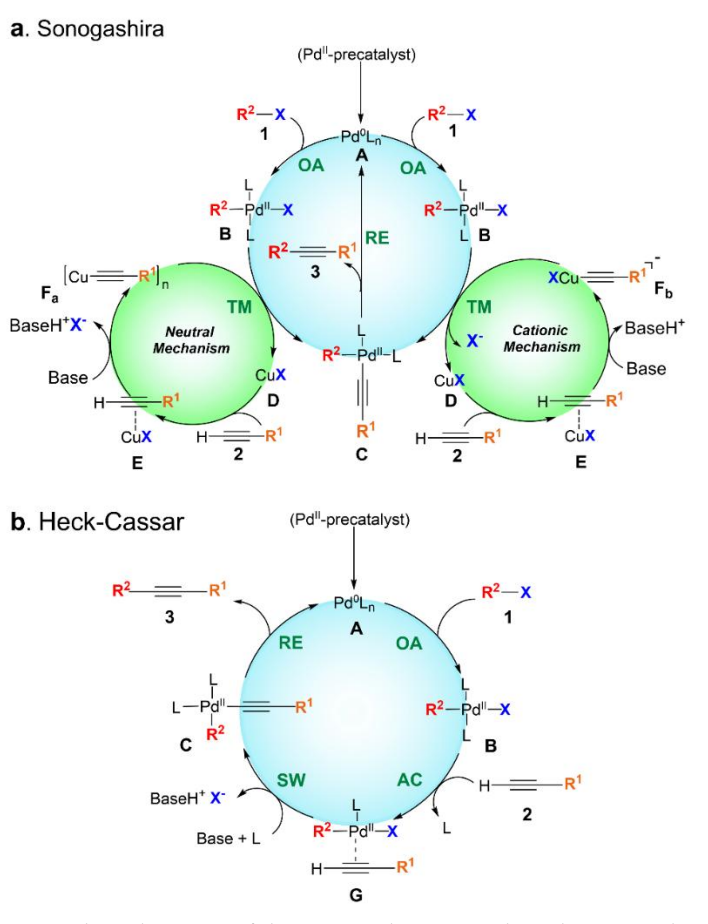


Figure 22. General mechanisms of the Sonogashira (a) and Heck-Cassar (b) protocols.

The catalytic cycle goes through the classic C–C bond cross-coupling pathway, where the initial step involves the oxidative addition (OA) of an aryl or alkyl halide to a Pd(0) complex. The efficiency of this step depends significantly on the nature of the Ar–X substrate, with reactivity increasing in the order ArCl < ArBr < ArI<sup>[179]</sup>. After the formation of the complex **B** R²Pd(II)L<sub>n</sub>X, the transmetalation occurs with a copper acetylide ( $\mathbf{F}_{a/b}$ ) generated in the copper catalytic cycle. The mechanism can proceed via a neutral or anionic mechanism<sup>[178,180,181]</sup>, where the main role of the copper is in both cases to make the terminal alkyne proton more acidic by forming a  $\pi$ -complex **E** and forming the Cu-complex  $\mathbf{F}_{a/b}$ . Even if certain aspects of the transmetalation process and the copper cycle are not completely defined, the overall mechanism of the Pd/Cu-catalysed Sonogashira reaction is widely accepted in the scientific community. Regarding the general mechanism for the copper-free Heck–Cassar, described in Figure 22b, the coordination of the alkyne is still a matter of investigation for several research groups.

The mechanism of the Heck-Cassar protocol has been extensively studied by several researchers over the years. In 1975, Heck proposed a mechanism where the oxidative addition complex reacts directly with deprotonated acetylene to form a σcomplex C[171]. However, this hypothesis was questioned due to the high pKa of acetylenes (e.g. phenylacetylene has a pKa >20), which is inconsistent with the basicity of the reagents typically used in these reactions<sup>[182,183]</sup>. In 2003, Soheili<sup>[184]</sup> proposed an alternative mechanism, suggesting that acetylene first enters the metal coordination sphere to form a  $\pi$ -complex G. This  $\pi$ -complex undergoes  $\pi/\sigma$  switching (from G to C), promoted by the base, leading to the efficient formation of the coupling product. This proposal offered a more plausible explanation of the reaction mechanism, and a few years later Mårtensson's studies supported the deprotonation mechanism proposed by Soheili, ruling out the possibility of carbopalladation. Mårtensson et al.[175,185] proposed that the process likely involves either anionic or cationic coordination, rather than the previously suggested pathways. Later, scientific efforts to elucidate the mechanism of the Heck-Cassar protocol have focused mainly on the nature of the  $\pi/\sigma$  switching, and an ionic pathway has also been proposed (Figure 23)[186].

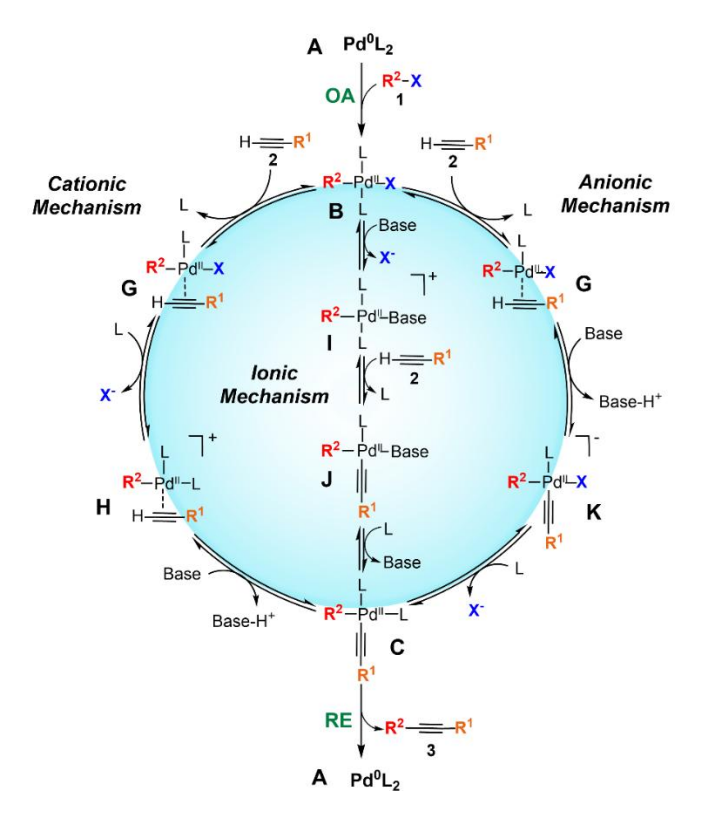


Figure 23. Heck-Cassar protocol based on direct coordination of the alkyne, via cationic, anionic, and ionic routes.

In 2018, Košmrlj and co-workers proposed a general mechanism for the Heck–Cassar protocol based on a second cycle of palladium, as shown in Figure 24a<sup>[187]</sup>. The mechanism was supported by density functional theory (DFT) calculations, kinetic studies and <sup>31</sup>P NMR analysis of intermediate complexes. The suggested model consists of two distinct palladium cycles and assumes a Pd(II)–Pd(II) transmetalation (TM) process, similar to that of the Sonogashira coupling between the oxidative addition complex **B** and the copper(I) alkyne complex **F** (comparison between Figure 22a and Figure 24a). Based on the Pd(II)–Pd(II) transmetalation pathway, the main side product should be the homodimer **4** formed from complex **M** by a simple reductive elimination (RE) process. However, this hypothesis was not consistent with the results previously published by our group where the formation of the homodimer **4** was never detected<sup>[45,58,188]</sup>. In fact, they observed the enyne as byproduct, originating from self-hydroalkynylation (Figure 24b), when the oxidative addition step to generate **B** was inefficient<sup>[45]</sup>.

# 

Figure 24. Heck-Cassar protocol based on the Pd(II)-Pd(II) transmetalation mechanism (a); Self-hydroalkynylation mechanism (b).

These observations led to a more detailed investigation of the Heck-Cassar protocol, focusing in particular on the behaviour of the alkyne under both stoichiometric and catalytic conditions. To effectively control the reaction, several key parameters were considered, including ligand, base, solvent, leaving group, concentration and temperature. Using techniques such as <sup>31</sup>P NMR, HPLC, GC and DFT calculations, this study aimed to elucidate the detailed mechanism of the Heck-Cassar protocol under operational conditions. I focused on the experimental part related to the synthesis of palladium complexes and mechanistic investigations using NMR.

### 2.1.2. Results and Discussion

Since rapid and complete pre-catalyst reduction is critical for an efficient process, we initiated this study to investigate the effects of base, ligand, and solvent effects on the reduction of (PPh<sub>3</sub>)<sub>2</sub>PdCl<sub>2</sub>. We chose three bases used in the HCS reaction, namely *N*,*N*,*N*′,*N*′-tetramethylguanidine (TMG), pyrrolidine (PYR) and triethylamine (TEA), and deuterate chloroform (CDCl<sub>3</sub>) and dimethylformamide (DMF-d<sub>7</sub>) as solvents. PYR and TEA are standard bases for the HCS reaction, while TMG was introduced by Cabri et al. only in 1998<sup>[189]</sup>. The results shown in Table 2 clearly indicate that the nature of the base influences the reduction process. Indeed, TMG and PYR were able to reduce the pre-catalyst in 10 minutes at 25°C, with a complete conversion in the presence of an excess of PPh<sub>3</sub> (entries 1-4, Table 2). In particular, TMG, with a higher pKa (23.3 in acetonitrile)<sup>[190]</sup>, was more efficient than PYR. On the contrary, TEA was not able to reduce the pre-catalyst via phosphine oxidation at room temperature (entries 5 and 6,

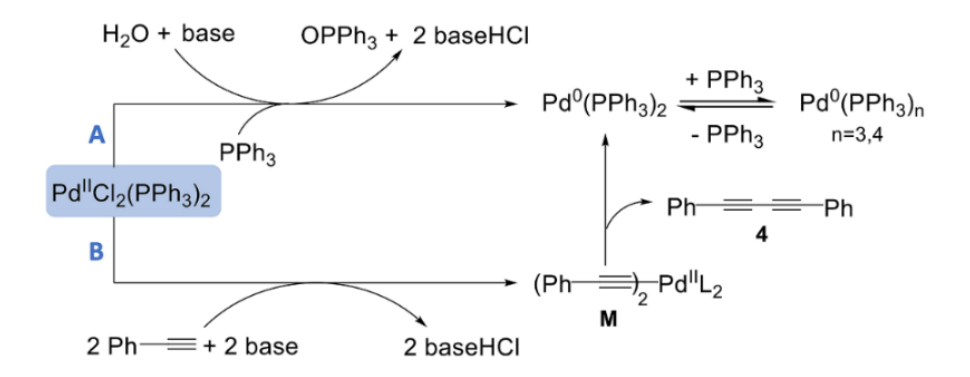
Table 2). In fact, TMG and PYR can enter the palladium coordination sphere and displace the ligand, favouring its oxidation (route A, Scheme 4), and when extra quantities of ligand are present, the reduction is complete. This process does not occur with tertiary amines, such as TEA, because they are ineffective in coordinating the metal. For this reason, when we carried out the reactions with secondary amines (e.g. TMG) and an excess of ligand, we did not detect the formation of complex **M** (Figure 25), whereas in the presence of TEA and phenylacetylene, the formation of complex **M** occurred quantitatively (Figure 26), in accordance with route B in Scheme 4.

Table 2. Evaluation of Base and Ligand Effects on (PPh<sub>3</sub>)<sub>2</sub>PdCl<sub>2</sub> Reduction to Pd(0)<sup>a</sup>

Entry	Base	Solvent	Conv(%)	+ PPh <sub>3</sub> (% conv) <sup>b</sup>
1	TMG	DMF-d <sub>7</sub>	64	100
2	TMG	CDCI <sub>3</sub>	85	100
3	Pyr	DMF-d <sub>7</sub>	31	100
4	Pyr	CDCI <sub>3</sub>	65	100
5°	TEA	DMF-d <sub>7</sub>	0	0
6°	TEA	CDCI <sub>3</sub>	0	0

<sup>&</sup>lt;sup>a</sup>Reactions were carried out at room temperature with 0.013 mmol of pre-catalyst and 0.026 mmol of base in 600 μL of solvent for 10 min. Conversions of Pd(II) into Pd(0) were calculated by <sup>31</sup>P NMR. <sup>b</sup>Two equivalents of triphenylphosphine were added. <sup>c</sup>The quantitative formation of **M** was observed.

Scheme 4. Pathway for Pd(II) pre-catalyst reduction.



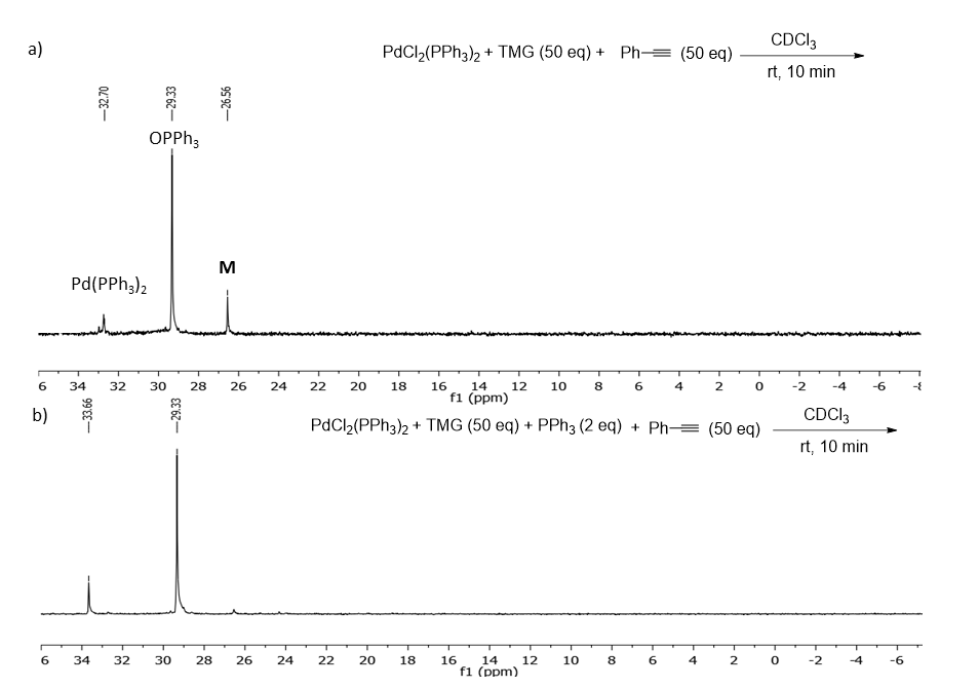


Figure 25.  $^{31}P$  NMR spectra of  $PdCl_2(PPh_3)_2$  in CDCl<sub>3</sub> with a) TMG (50 equiv) and phenylacetylene (50 equiv) and b) with  $PPh_3$  (2 equiv).

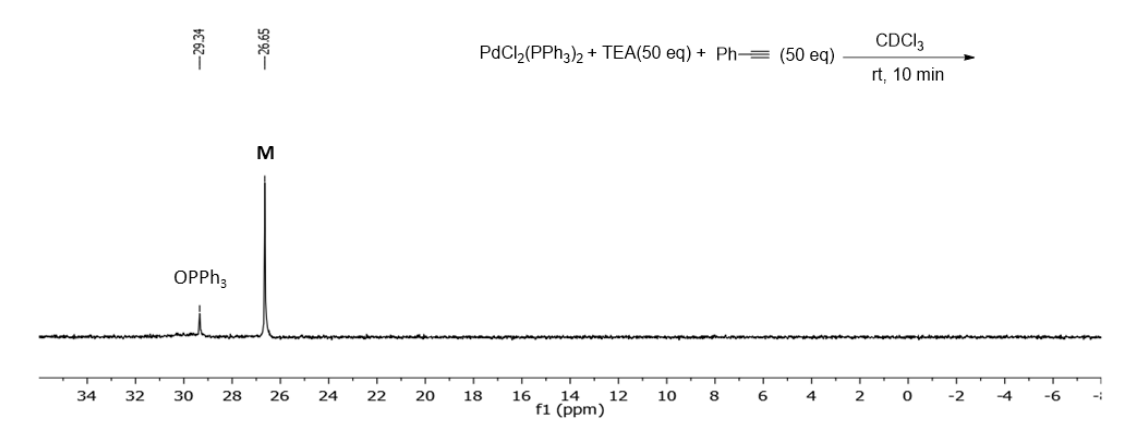


Figure 26. <sup>31</sup>P NMR spectra of PdCl<sub>2</sub>(PPh<sub>3</sub>)<sub>2</sub> in CDCl<sub>3</sub> with TEA (50 equiv) and phenylacetylene (50 equiv).

The mechanism of the reaction was investigated using a standard protocol, involving the reaction of 4-nitrophenyl iodide  $\mathbf{1}_{NO_2}$  with 1.1 equivalents of phenylacetylene (2a), 2 equivalents of the base, and 20 mol% pre-catalyst (PPh<sub>3</sub>)<sub>2</sub>PdCl<sub>2</sub> to obtain good quality spectra. The presence of the nitro substituent on the aromatic ring of aryl iodide  $\mathbf{1}_{NO_2}$  is able to slow down the RE step and increase the chances of detecting intermediate complex  $\mathbf{C}$ . The Pd(II) complexes  $\mathbf{B}_{NO_2}^{\mathbf{I}}$ ,  $\mathbf{C}$ ,  $\mathbf{M}$ , and  $\mathbf{L}$  (Figure 27a) were individually previously synthetised (see *Experimental Section 2.1.4.2.*)<sup>[187]</sup>. For this purpose, only TMG and PYR were screened as the base, while TEA was not tested, due to its inefficiency in generating Pd(0) species at room temperature. Independent of the bases or solvents used, it was possible to observe the formation of a small amount of  $\mathbf{M}$ . However, with the addition of PPh<sub>3</sub>, which accelerates the Pd(II) reduction, the complex

**M** was not detected by <sup>31</sup>P NMR, regardless of the base (TMG, PYR) and solvent (DMF-d<sub>7</sub>, CDCl<sub>3</sub>) used. As an example, the <sup>31</sup>P NMR spectrum of the reaction using TMG as the base, both with and without additional PPh<sub>3</sub>, is reported in Figure 27. The evidence shows that complex **M** was formed and detected only when the reduction of the Pd(II) pre-catalyst was inefficient. This suggests that the formation of complex **M** is not essential for the HCS reaction to proceed, but rather represents an alternative pathway for the palladium reduction process. Consistently, when palladium tetrakis triphenylphosphine [Pd(PPh<sub>3</sub>)<sub>4</sub>] was used as the catalyst, **M** was never detected (for details, see *Experimental Section 2.1.4.6.*).

Moreover, we evaluated the potential formation of palladium nanoparticles during the reduction of the pre-catalyst or the cross-coupling process, which could theoretically interfere with the experiments, and we demonstrated that nanoparticles did not form during the processes.

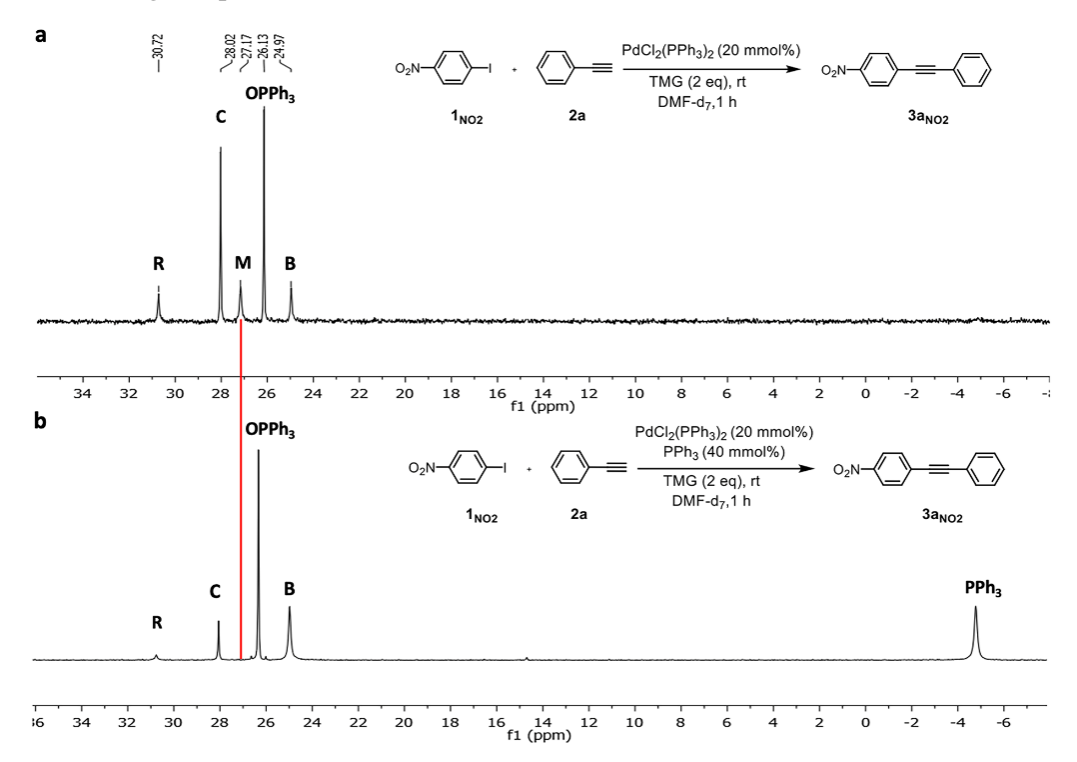


Figure 27.  $^{31}P$  NMR of the HCS reaction carried out with  $1_{NO2}$  (0.5 mmol), 2a (1.1 equiv), and TMG (2 equiv) as base in DMF-d<sub>7</sub> (0.5 M) at  $25^{\circ}$  C without additional quantities of PPh<sub>3</sub> (a) and with the addition 2 equiv of PPh<sub>3</sub> (b). Complex **R** is the OA complex with the TMG coordinated to palladium.

We also wanted to evaluate the stability of critical Pd(II) complexes at different temperatures in CDCl<sub>3</sub> and DMF-d<sub>7</sub> monitoring the formation of the desired coupling product **3a** and the homocoupling **4a**, within a 30 min timeframe. Complex **M** remained stable at 25°C in CDCl<sub>3</sub> and in DMF-d<sub>7</sub> (entries 1–2, Table 3), while in CDCl<sub>3</sub> at 60°C, 30% of complex **M** was converted into the reductive elimination product **4a** (entry 3, Table 3). In DMF-d<sub>7</sub>, the conversion into **4a** was even faster; in fact the conversion was

completed already at 40°C (entry 4, Table 3). The OA complex 4-NO<sub>2</sub>-Pd(PPh<sub>3</sub>)<sub>2</sub>I  $B_{NO_2}^{I}$  in the presence of M in CDCl<sub>3</sub> at 25°C generated only a small amount of the cross-coupling product 3a (entry 5, Table 3), while at 60°C in DMF-d<sub>7</sub>, M generated mainly 4a and only 21% of the coupling product 3a (entry 6, Table 3). These results show that the formation of the homocoupling product 4a is diagnostic for the presence of the complex M. As expected, the cross-coupling between the oxidative addition complex  $B_{NO_2}^{I}$  and 2a generated exclusively the target product 3a (entries 7 and 8, Table 3).

Table 3. Pd(II) Complex M stability studies<sup>a</sup>

Entry	Solvent	T (°C)	В	2a	М	Conv (%)	3a/4a <sup>b</sup>
1	CDCl₃	25	-	-	1	<b>M</b> (0) <sup>b</sup>	0/0
2	DMF-d <sub>7</sub>	25	-	-	1	<b>M</b> (0) <sup>b</sup>	0/0
3	CDCI <sub>3</sub>	60	-	-	1	<b>M</b> (30) <sup>b</sup>	0/100
4	DMF-d <sub>7</sub>	40	-	-	1	<b>M</b> (100) <sup>c</sup>	0/100
5	CDCl <sub>3</sub>	25	1	-	1	<b>B</b> (5) <sup>b</sup>	100/0
6	DMF-d <sub>7</sub>	60	1	-	1	<b>M</b> (100) <sup>c</sup>	21/79 <sup>d</sup>
7	CDCl <sub>3</sub>	25	1	1	-	<b>B</b> (36) <sup>b</sup>	100/0
8	DMF-d <sub>7</sub>	60	1	1	-	<b>B</b> (42) <sup>b</sup>	100/0

<sup>&</sup>lt;sup>a</sup>All reactions were carried out for 30 min with [C]=0.024 M. For entries 7 and 8, 1.1 equiv of TMG was added. <sup>b</sup>The mixture was analysed after 30 min by <sup>1</sup>H NMR. <sup>c</sup>The mixture was analysed after 30 min, and the conversion was calculated using <sup>31</sup>P NMR. <sup>a</sup>The ratio **3a/4a** was determined by HPLC.

These experiments further demonstrated that the HCS coupling did not require the formation of **M** and that the oxidative addition complex **B** was stable in CDCl<sub>3</sub> or DMF and did not generate, as described by Košmrlj et al.<sup>[187]</sup>, the Ar<sub>2</sub>Pdl<sub>2</sub> and Ar<sub>2</sub>Pd(PPh<sub>3</sub>)<sub>2</sub>. This last complex is the intermediate of a palladium-catalysed Ullman-type reaction that follows a completely different path<sup>[191,192]</sup>. Furthermore, the complex Ar<sub>2</sub>Pd(PPh<sub>3</sub>)<sub>2</sub>, if formed, should also have produced the Ar–Ar homocoupling product by reductive elimination and was consistently never detected.

In order to compare the alkyne direct coordination and the transmetalation step, we independently synthesised complex **B** and **M** to react as shown in Figure 28, according to the Košmrlj's experiments<sup>[187]</sup>. The reactions were performed in CDCl<sub>3</sub> because of the low solubility of **M** in other solvents. It is possible to observe that the reaction carried out between complex  $\mathbf{B}_{NO_2}^{\mathbf{I}}$  and **M** at room temperature in CDCl<sub>3</sub> with 1.1 equivalents of TMG, was slower than the coupling  $\mathbf{B}_{NO_2}^{\mathbf{I}}$  and 2a (Figure 28a). The reaction with PYR and 4-Me-PhPd(PPh<sub>3</sub>)<sub>2</sub>I ( $\mathbf{B}_{Me}^{\mathbf{I}}$ ) was also carried out in order to replicate

the identical conditions of Košmrlj et al.<sup>[187]</sup>, and we obtained similar results to the previous one (Figure 28b). Furthermore, since in the compared study they claimed that the maximum rate corresponds to the initial rate only in the  $\bf B+M$  reaction, due to the absence of an induction period to form  $\bf M^{[187]}$ , we calculated the  $V_{max}$  and we found that the maximum value is at the starting point in both cases.

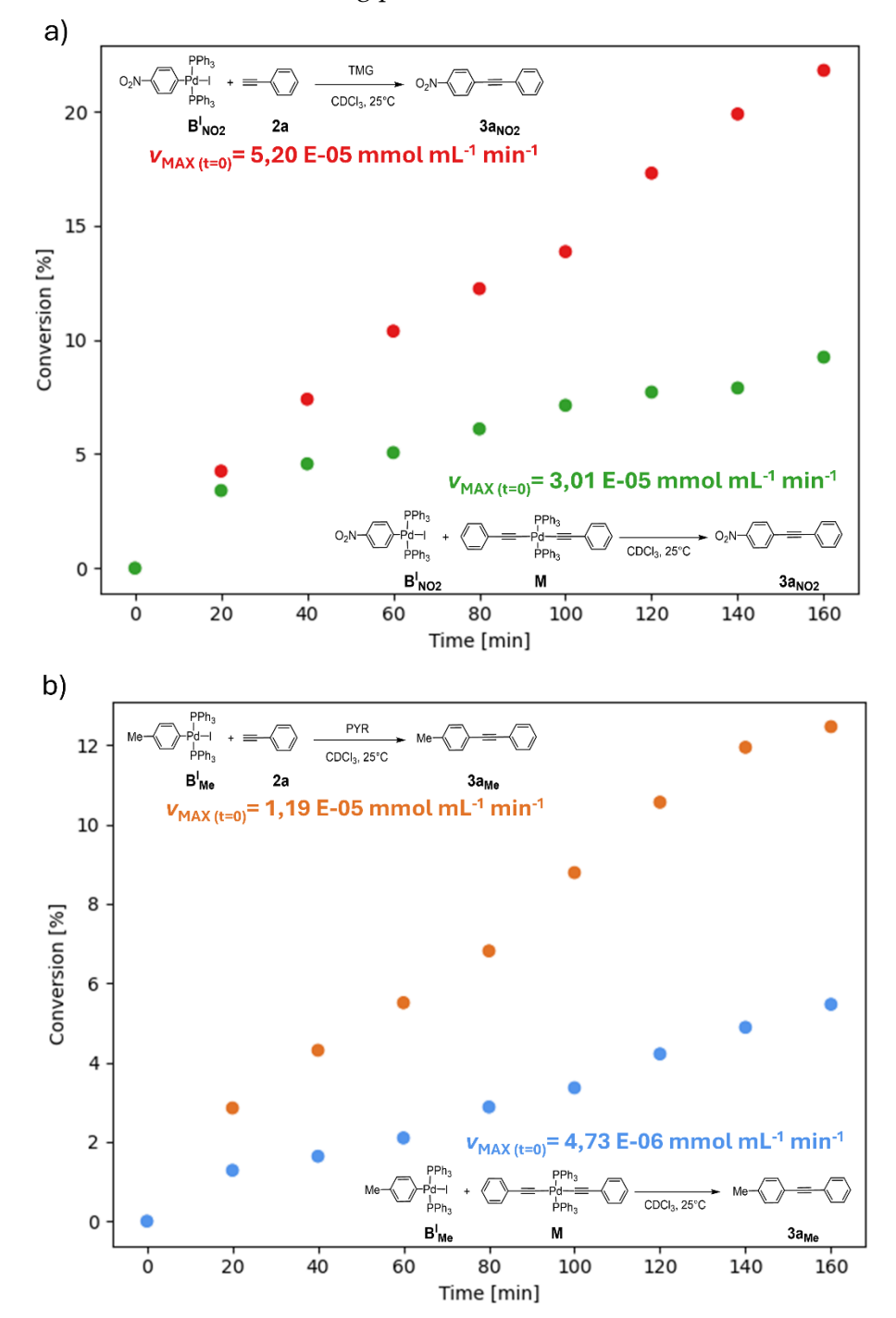


Figure 28. HCS reaction between the oxidative addition complex  $B^I_{NO_2}$  (0.018 mmol) with 2a (1 equiv) and TMG (1.1 equiv) and with M (1 equiv) in CDCl3 (0.024 M) at 25°C (a). HCS reaction between the oxidative addition complex  $B^I_{Me}$  (0.0095 mmol) with 2a (1.2 equiv) and Pyr (5 equiv) and with M (1.2 equiv) in CDCl3 (0.013 M) at 25°C (b). All experiments were performed in triplicate and the values reported are the average of the three measurements.

These experiments highlighted that, even if complex **M** is able to promote the cross-coupling, the direct coordination is faster than the Pd(II)–Pd(II) transmetalation and it is significantly the most efficient one. In the study under comparison, Košmrlj and co-workers observed a different result<sup>[187]</sup>, however, it is important to notice that the outcome of the stoichiometric reaction can be affected by the solubility of the complexes and the quality of the CDCl<sub>3</sub>. In all the experiments described above, the palladium complexes were freshly prepared, the phenylacetylene was brand new and CDCl<sub>3</sub> was passed over alumina to remove any trace of acidity. In fact, chlorides can easily exchange the iodide in the oxidative addition complex<sup>[193]</sup>. In addition, these reactions produce Pd(0) species, which can react with CDCl<sub>3</sub> to produce other by-products<sup>[194,195]</sup>, or with **2a**, further reducing the available alkyne<sup>[45]</sup>.

In order to avoid any variability or interference of solvent, reagents and conditions, a direct competition between M and 2b in reaction with the OA complex B was carried out. Therefore, the simultaneous competition between the direct coordination and the Pd(II)-Pd(II) transmetalation step, was studied under different reaction conditions with an equimolecular amount of the complexes  $B_R^I$ , M, and 1-ethynyl-3-methylbenzene (2b) (Scheme 5). The use of 2b allowed us to distinguish the products resulting from the different reaction mechanisms.

Scheme 5. Competition between M and 2b in reacting with Oxidative Addition Complex  $B_{NO_2}^{I}$  and  $B_{Me}^{I}$ .

With the use of a 1/1/1 ratio of  $\mathbf{B_R^I}/\mathbf{M}/2\mathbf{b}$ , preferential formation of  $3\mathbf{b}$  was observed after 1 h in CDCl<sub>3</sub> at 25°C independent of the substitution on the aromatic ring of  $\mathbf{B_R^I}$  and the base (entries 1–4, Table 4). The use of 10 equivalents of  $2\mathbf{b}$ , which mimics the excess of the alkyne in a catalytic reaction, completely suppresses the formation of  $3\mathbf{a}$  (entries 5–6, Table 4). To perform the reaction under completely homogeneous conditions and to demonstrate the flexibility of the system, CDCl<sub>3</sub>, DMF, NMP, NBP, HEP, THF, ethanol and toluene were screened at 60°C. The competition reactions selectively gave the alkyne cross-coupling product  $3\mathbf{b}$  independent of the solvent used (entries 8–15, Table 4). Since the product  $3\mathbf{b}$  can only be generated by the direct coordination mechanism, the Pd(II)–Pd(II) transmetalation process was definitively ruled out. In all of the reactions, the only side product detected was the homocoupling

product **4a** coming from the reductive elimination RE of **M** and compounds **4b**, **4c**, **5a**, and **5b** were never detected.

Table 4. HCS cross-coupling competition studies, direct coordination versus Pd(II)/Pd(II) transmetalation process<sup>a</sup>

Entry	В	Solvent	Base	T(°C)	%Conv (1h) <sup>b</sup>	3a/3b (1h) <sup>c</sup>
1	$B_{NO_2}^I$	CDCI <sub>3</sub>	TMG	25	73	0/100
2	$B_{NO_2}^I\\$	CDCI <sub>3</sub>	PYR	25	60	0/100
3	$B_{Me}^{I} \\$	CDCI <sub>3</sub>	TMG	25	66	2/98 <sup>b</sup>
4	$B_{Me}^{I} \\$	CDCI <sub>3</sub>	PYR	25	41	3/97 <sup>b</sup>
5 <sup>d</sup>	$B_{Me}^{I} \\$	CDCI <sub>3</sub>	TMG	25	60	0/100
6 <sup>d</sup>	$B_{Me}^{I} \\$	CDCI <sub>3</sub>	PYR	25	59	0/100
7	$B_{NO_2}^I\\$	DMF	TMG	40	100	0/100
8	$B_{NO_2}^I\\$	DMF	TMG	60	100	0/100
9	$B_{NO_2}^I\\$	CDCI <sub>3</sub>	TMG	60	100	0/100
10	$B_{NO_2}^I\\$	NMP	TMG	60	100	0/100
11	$B_{NO_2}^I$	NBP	TMG	60	100	0/100
12	$B_{NO_2}^I$	HEP	TMG	60	100	0/100
13	$B_{NO_2}^I\\$	THF	TMG	60	100	0/100
14	$B_{NO_2}^I\\$	EtOH	TMG	60	100	0/100
15	$B_{NO_2}^I\\$	Toluene	TMG	60	100	0/100

<sup>&</sup>lt;sup>a</sup>Reactions were carried out with  $\mathbf{B_R^I}$  /M/2b in a 1/1/1 ratio, 1,1 equiv of base with a concentration of 0.13 M under nitrogen for 1 h. <sup>b</sup>Determined by HPLC-MS. <sup>c</sup>Determined by GC-MS. In entries 7–15, the conversion of **M** into **4a** was completed. <sup>d</sup>10 equiv of **2b** were added.

To gain a deeper understanding of the step following oxidative addition, we investigated various Pd(II) complexes under operative conditions. We performed  $^{31}$ P NMR analysis on the oxidative addition complexes  $\mathbf{B}_{NO_2}^{\mathbf{X}}$ , with different leaving groups (X = I, Br, Cl, or OTf), in the presence of bases such as TMG, PYR, or TEA in DMF-d<sub>7</sub>. Subsequently, we introduced the alkyne to the system.

The base effect was studied using 50, 20, and 10 equivalents of base relative to the Pd(II) complex  $\mathbf{B_{NO_2}^X}$  to replicate the operative conditions. In fact, when using a 1 mol% catalyst, the data showed the impact of 1.1 equiv of the base on the oxidative addition catalyst at different conversions (60, 90, and 99%). <sup>31</sup>P NMR spectra revealed that complexes **R** were the predominant Pd(II) species with TMG and PYR (entries 1–6, Table

5), regardless of base excess. Interestingly, with the exception of the chloride complex, TMG consistently outperformed PYR in replacing PPh<sub>3</sub> within the Pd(II) coordination sphere. As previously mentioned, the tertiary base TEA was unable to coordinate with the metal centre (entries 7–9, Table 5) and no coordination was detected. The equilibrium constant k was generally low, consistent with the findings of Jutand and co-workers<sup>[196]</sup>.

Scheme 6. Oxidative addition complexes  $\mathbf{B}_{NO_2}^{\mathbf{X}}$  with X = I, Br, I, OTf in presence of a coordinating base

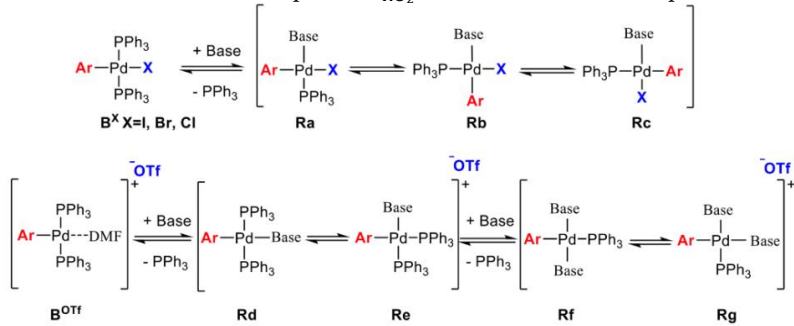


Table 5. Base Effect on the Oxidative Addition Complexes  $\mathbf{B}_{NO}^{X}$ , with X = I, Br, I, OTf a

	Base / B <sub>R</sub> ratio						
Entry	Х	$B_R^X$	Base	50 equiv	20 equiv	10 equiv	keq <sup>b</sup>
1	I	$B_{NO_2}^I\\$	Pyr	93/7	85/15	68/32	0.182
2	Br	$B_{NO_2}^{Br} \\$	Pyr	91/9	78/22	68/32	0.099
3	CI	$B_{NO_2}^{Cl} \\$	Pyr	93/7	82/18	70/30	0.134
4	1	$B_{NO_2}^I$	TMG	100/0	97/3	93/7	0.910
5	Br	$B^{Br}_{NO_2} \\$	TMG	96/4	85/15	74/26	0.122
6	CI	$B_{NO_2}^{Cl}$	TMG	87/13	71/29	63/37	0.074
7	1	$B_{NO_2}^I$	TEA	0/100	0/100	0/100	-
8	Br	$B_{NO_2}^{Br} \\$	TEA	0/100	0/100	0/100	-
9	CI	$B_{NO_2}^{Cl} \\$	TEA	0/100	0/100	0/100	-
10	OTf	$B_{NO_2}^{OTf} \\$	TMG	100/0	100/0	100/0	С

<sup>&</sup>lt;sup>a</sup>The reaction was performed with  $\mathbf{B_{No_2}^X}$  (0.026 mmol) dissolved in DMF-d<sub>7</sub> (600 μL). <sup>b</sup>Ratios of the complexes and equilibrium constants were calculated using <sup>31</sup>P NMR). <sup>c</sup>It was not possible to calculate k since the formation of the  $\mathbf{R}$  complex is efficient even with a low amount of base.

Moreover, as expected, the presence of a large excess of base shifted the equilibrium toward the formation of R complexes. It is important to note that no exchange occurred between the base and halide due to the strong Pd(II)–I, Br, and CI

bonds. Indeed, the formation of complexes **R** was perfectly balanced by the release of free PPh<sub>3</sub> into the solution (Figure 29). With oxidative addition complexes coming from aryl halides, the triphenylphosphine release begins upon the addition of the first equivalent of TMG or PYR into the mixture.

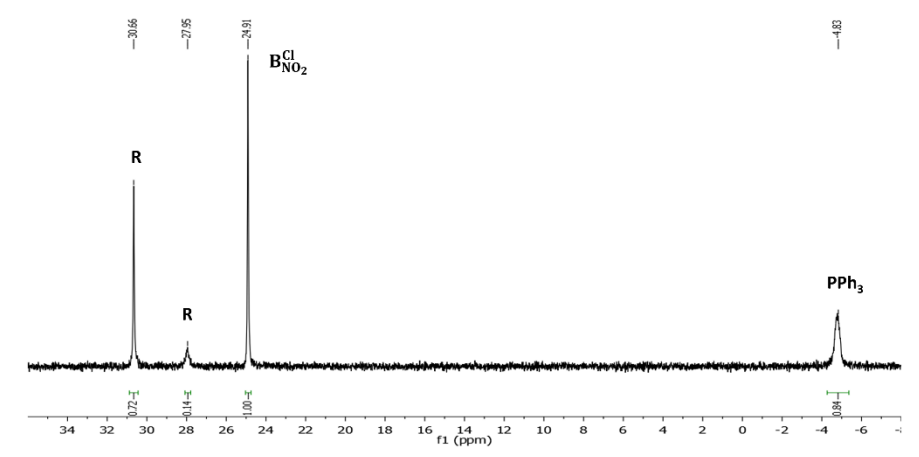


Figure 29.  $^{31}P$  NMR spectrum in DMF-d<sub>7</sub> of  $B_{NO_2}^{Cl}$  after the addition of TMG 10 equiv as an example.

Three different complexes **Ra–c** can be formed after the PPh<sub>3</sub> replacing, as shown in Scheme 6. To evaluate their stability, DFT calculations with TMG as the base, X=I, Br, Cl have been carried out by the group. The data supported the hypothesis that **Ra** was the most stable (Figure 30).

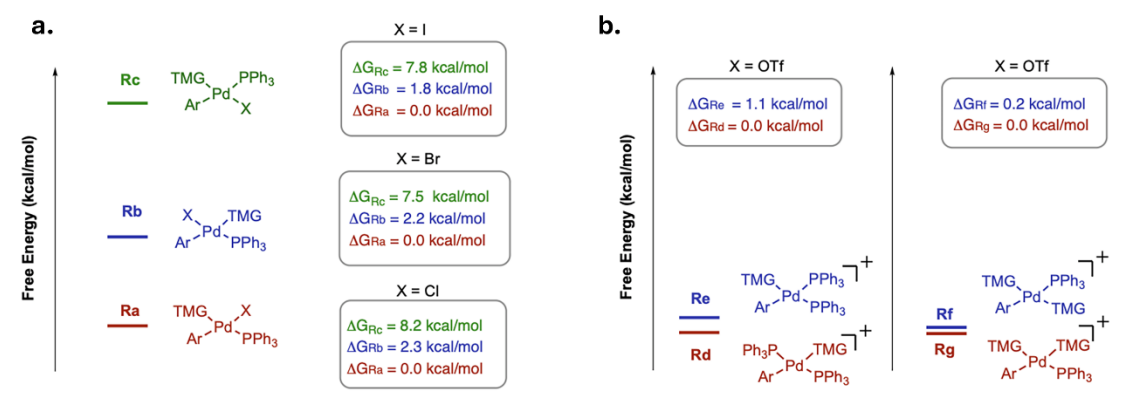


Figure 30. Gibbs energies in DMF ( $\Delta$  GDMF, kcal mol<sup>-1</sup>) at 298 K for isomers of complexes **R** with counterion halide (a) and a triflate (b).

Regarding the oxidative addition complex with triflate, after the addition of a second equivalent of TMG, the complex *cis-trans* ArPdPPh<sub>3</sub>(TMG)<sub>2</sub> was formed because **B**<sub>NO<sub>2</sub></sub><sup>OTf</sup> is completely dissociated in DMF<sup>[197]</sup>. Indeed, two peaks were observed at 27.78 and 19.32 ppm in the <sup>31</sup>P NMR spectrum after the addition of 2 equivalents of PPh<sub>3</sub> (Figure 31b).

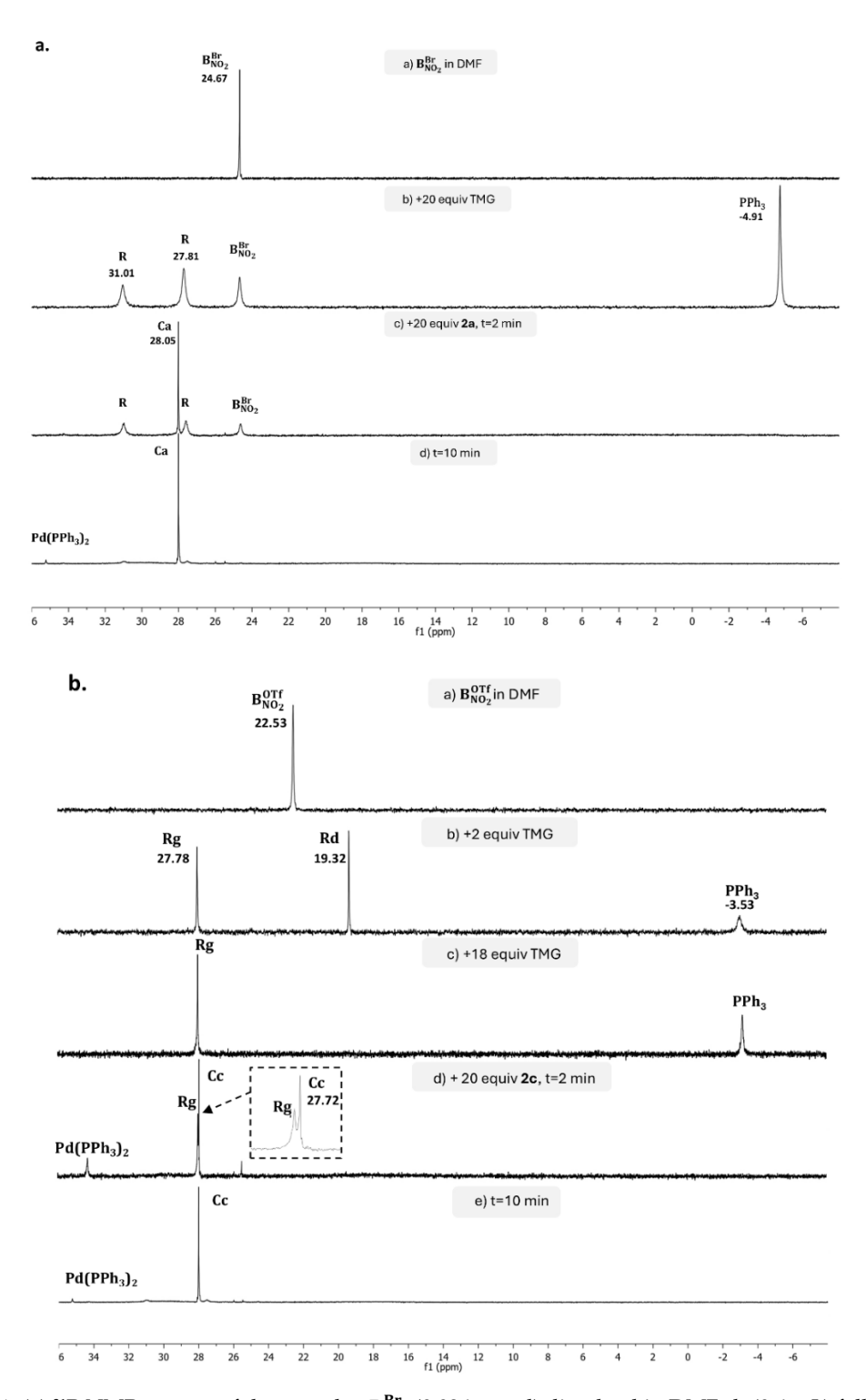


Figure 31. (a) <sup>31</sup>P NMR spectra of the complex  $\mathbf{B_{NO_2}^{Br}}(0.026 \text{ mmol})$  dissolved in DMF-d7 (0.6 mL) followed by the addition of TMG and  $\mathbf{2a}$  at 25°C. (b) <sup>31</sup>P NMR spectra of the complex  $\mathbf{B_{NO_2}^{OTf}}(0.013 \text{ mmol})$  dissolved in DMF-d7 (0.6 mL) followed by the addition of TMG and  $\mathbf{2c}$  at 25°C.

Since with the excess of base, only the peak at 27.78 ppm was observed with the corresponding amount of PPh<sub>3</sub>, it is reasonable to assume that the peak at 19.32 ppm is related to *trans-cis* ArPd(PPh<sub>3</sub>)<sub>2</sub>TMG (**Rd,e**) and at 27.78 ppm to *trans-cis* ArPdPPh<sub>3</sub>

(TMG)<sub>2</sub> (**Rf,g**). The cationic complexes **Rd,e** and **Rf,g**, formed from one and two molecules of TMG respectively in the palladium coordination sphere, have almost the same energy (Figure 30b). However, the slightly more stable complexes are those that result from the first substitution of one molecule of TMG in *trans* (**Rd**), and so, these are the ones that are likely to react in the mechanism and gives the **Rg** rather than **Rf** complexes.

In Figure 32, the mechanisms and energies for the interconversion among the intermediates  $\mathbf{Ra}$ ,  $\mathbf{Rb}$ , and  $\mathbf{Rc}$  starting from complex  $\mathit{trans-B^I_{NO_2}}$  are reported. The only  $\mathbf{R}$  isomer that can be formed from  $\mathit{trans-B^I_{NO_2}}$  is  $\mathbf{Ra}$ , which is the most stable complex.  $\mathbf{Ra}$  can isomerize to give first  $\mathbf{Rb}$  and then  $\mathbf{Rc}$ . The total energy required to go from  $\mathbf{Ra}$  to  $\mathbf{Rb}$  is 17.5 kcal/ mol, while the energy needed to form complex  $\mathbf{Rc}$  from  $\mathbf{Rb}$  is 25.9 kcal. These calculations are in line with the <sup>31</sup>P NMR, which shows the presence of a largely predominant  $\mathbf{R}$  isomer and small amounts of the other two when just 10 equivalents of base are used (see Figure 29). On the other hand, when a large excess of base is present, mimicking the reaction conditions, the isomerization is completely inhibited and only the most stable isomer, presumably  $\mathbf{Ra}$ , is detected.

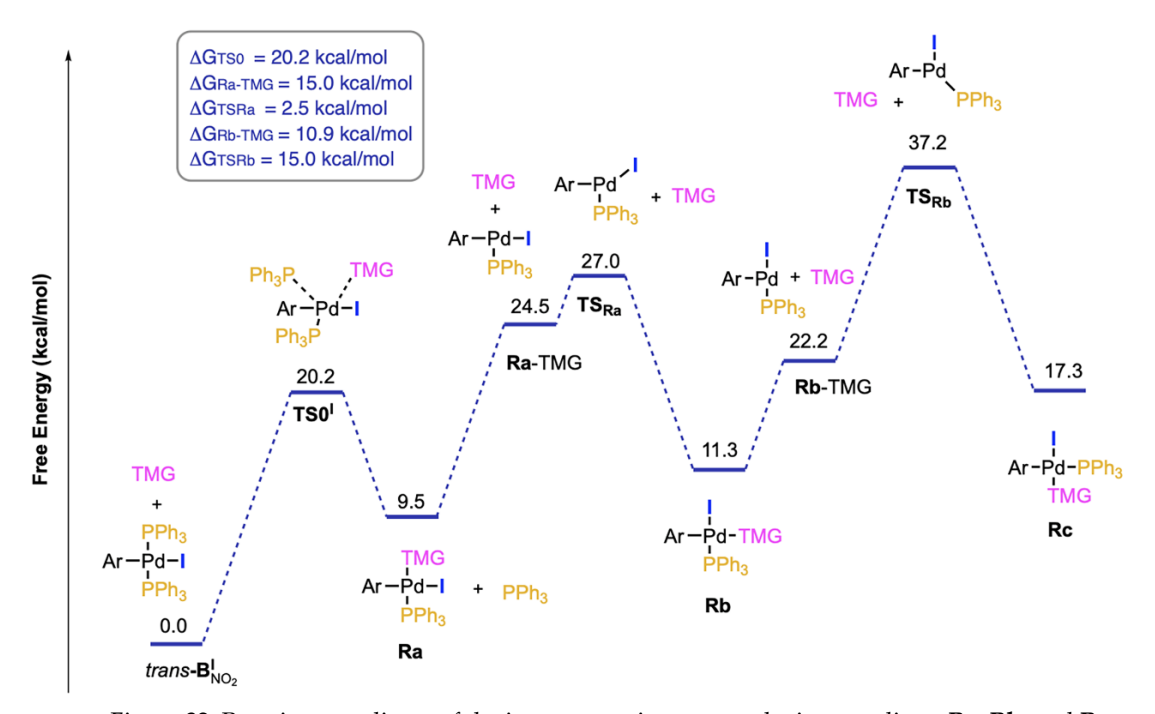


Figure 32. Reaction coordinate of the interconversion among the intermediates Ra, Rb, and Rc.

The reaction mechanism via neutral (**Ra-c**) or cationic (**Rd-g**) complexes is mainly related to the nature of the counterion in the oxidative addition Pd(II) complex **B**. We have investigated the effects of alkyne **2a** incorporation in the catalytic cycle using both experimental and theoretical approaches.

<sup>31</sup>P NMR analysis showed that after the addition of 20 equivalents of **2a**, regardless of the counterion, the formation of complex **C**, which precedes the RE step, is

a fast process. Indeed, after 2 min we observed the formation of the reductive elimination complex C at 28.03 ppm and after 10 min the complete disappearance of complexes  $\mathbf{R}_y$  (Figure 31a-b). We also studied the effect of the alkyne on the reaction outcome using the  $\mathbf{B}_{NO_2}^{\mathbf{Br}}$  complex. Complex C was rapidly formed after 10 min at room temperature and was absent after 5 hours independently from the alkyne typology (Figure 33). The complete conversion to the corresponding HCS products 3a-1 was demonstrated by HPLC analysis. These results further support the observation that the different excess of alkyne required to achieve complete conversions under standard conditions is not determined by the alkyne reactivity in the HCS coupling. The alkyne coordination and  $\pi/\sigma$  switching required to generate C is very fast and we were unable to detect any intermediate. Density functional theory calculations were performed to further confirm these experimental results and to understand this step in more detail.

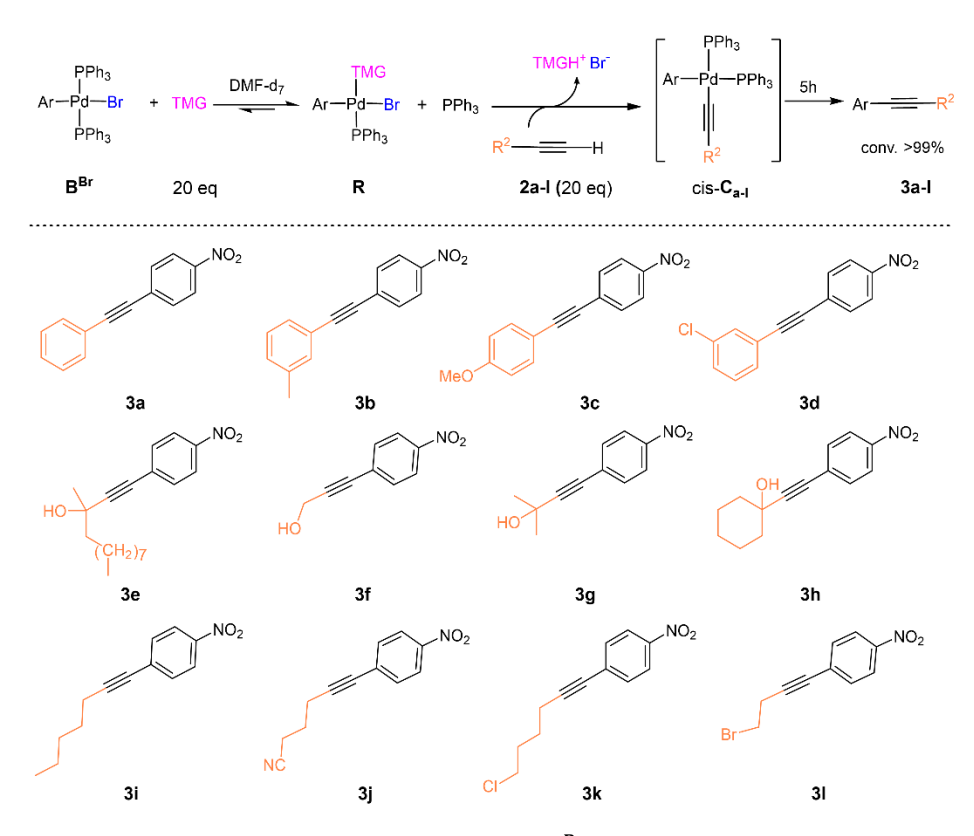


Figure 33. Alkyne carbopalladation into complex  $B_{NO_2}^{Br}(0.026 \text{ mmol})$  in  $600\mu\text{L}$  of DMF-d<sub>7</sub>.

DFT calculations of the HCS reaction have been performed by the group to further investigate and validate these experimental results. The calculations have been performed with the PBE/def2-TZVP level of theory<sup>[198]</sup> starting from the oxidative addition complexes, namely,  $B_{NO_2}^{I}$  and  $B_{NO_2}^{OTf}$ , phenylacetylene 2a, and TMG as a model system. According to the experimental data on the effect of the TMG base, two different mechanisms were investigated using the iodide and the triflate as counterions: the neutral/anionic pathway via Ra-c for the halide species and the cationic/neutral pathway

via Rd-g for the triflate as the leaving group. Ra and Rg were chosen among the different isomers on the basis of the data described in Figure 30. The computed Gibbs energy profile for the copper-free HCS reaction starting from the oxidative addition complex  $\mathbf{B_{NO_2}^l}$  is shown in Figure 34a. The energy of the transition state of the direct carbopalladation of the acetylene on complex  $B_{NO_2}^I$ , without passing through  $TSO^I$ , was found to be 32.0 kcal/mol (TS1PPh3). This is the energy required for the mechanism involving tertiary amines. With secondary amines, such as TMG, the key step of the process is the transformation of  $B_{N0}^{I}$ , into intermediate Ra by displacement of one equivalent of PPh<sub>3</sub> by the base. Our calculations found a barrier of 20.2 kcal/mol (TSOI), a difference in energy offset by the excess base that is used in the process. The reaction coordinate was based on Ra because it was the most stable isomer (Figure 30a). The ability of the secondary amine to enter the palladium coordination sphere is critical because it lowers the energy required for the acetylene carbopalladation step. The energy required to go from Ra to G through TS11 is only 22.9 kcal/ mol, a process favoured by 7.1 kcal over the direct passage from TS1PPh3. The calculations therefore reinforce the concept that the carbopalladation step is much faster when it passes through the complex **Ra**, rather than directly from complex **B**<sup>I</sup>. The step from **Ra** to **G** via **TS1**<sup>I</sup> is the rate-determining step of the alkyne carbopalladation process. All subsequent energy barriers from G to C are lower than the previous transition state from R to G. The deprotonation of the acetylene is also favoured because of the base, which has just left the complex to make room for the alkyne, remains close to the intermediate, facilitating the formation of the anionic complex N with an energy barrier of 9.8 kcal/mol. The rupture of the Pd-I bond from the anionic complex N requires a low activation energy, and the replacement with PPh<sub>3</sub> is therefore very efficient. Indeed, the  $\Delta G$  between N and TS31 is only 12.6 kcal/mol, affording the neutral complex C, which undergoes reductive elimination with a free energy of 10.8 kcal/mol, giving rise to the coupling product 3 and regenerating the catalyst. In contrast to the neutral/anionic mechanism that occurs with halides as leaving groups, the HCS reaction with triflates is characterised by a cationic/neutral mechanism (Figure 34b). There are currently no DFT data available in the literature calculations for any aryl triflates.

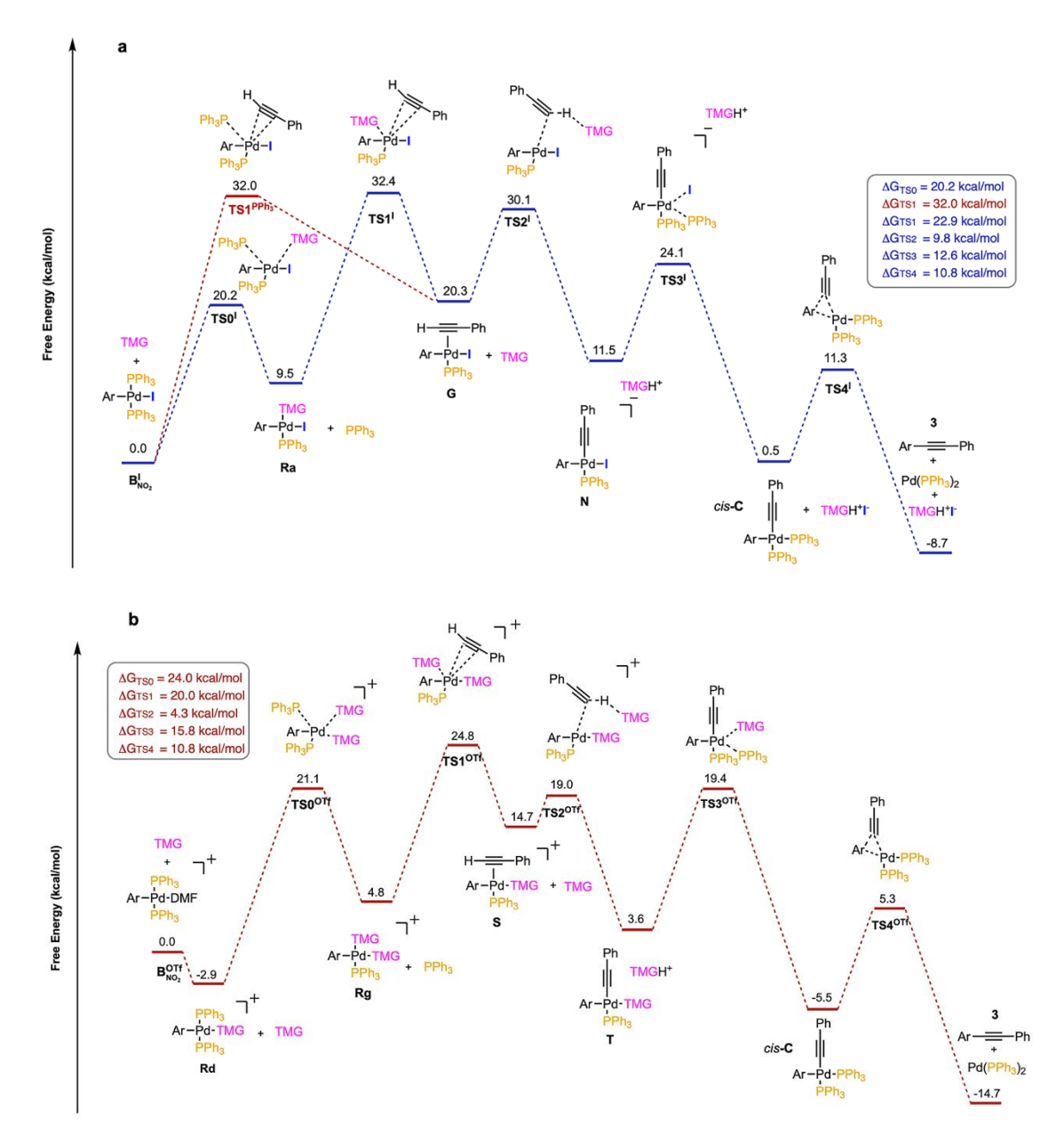


Figure 34. DFT-calculation-computed reaction profile and solution-state Gibbs free energies in the DMF ( $\Delta$  GDMF, kcal mol<sup>-1</sup>) PBE/def2-TZVP level of theory at 298 K for stationary points of the Heck–Cassar protocol mechanism. (a) Energy profile with iodide as the counterion. (b) Energy profile with triflate as the counterion.

The Pd–OTf bond is weaker than the Pd–I bond and easily dissociates even in the presence of a ligand such as DMF. For this reason, we started the Gibbs energy profile of the mechanism from  ${\bf B_{NO_2}^{OTf}}$  with DMF instead of TfO as the Pd(II) ligand. Based on experimental <sup>31</sup>P NMR data, the key initial step was the formation of the complex **Rg** with two TMGs coordinated to the metal. Coordination of the first TMG stabilised the cationic complex by –2.9 kcal/ mol ( $\Delta G$  between  ${\bf B_{NO_2}^{OTf}}$  and **Rd**). Similar to the previous mechanism, the second TMG replaces one of the PPh<sub>3</sub> ligands, with a Gibbs free energy

of 24.0 kcal/mol, to give the isomer Rg, corresponding to the rate-determining step of the process (TS0otf). The carbopalladation of the acetylene into Rg takes place with an energy barrier of 20.0 kcal/mol. This transition state energy barrier from Rg to TS1<sup>OTf</sup> is lower than the one previously calculated for the corresponding mechanism step from the iodide complex Ra. Interestingly, the average distance between the sp carbons of the alkyne and the palladium complex in TS1<sup>I</sup> was 2.40–2.47 A, while for TS1<sup>OTf</sup>, a distance of 2.62–2.92 A was sufficient to activate the C-H bond, creating a lower stressful steric interaction. Analogous to the mechanism outlined for the iodide, after TS1<sup>OTf</sup>, all of the other reaction steps required lower activation energies: the TMG base, which had just come out of the coordination sphere in TS1OTf, deprotonates the acetylene, favouring the switch from the  $\pi$  complex **S** to the  $\sigma$  complex **T** with an activation energy of only 4.3 kcal/mol. This process is highly favoured because it leads to the more stable complex T and subsequently to the intermediate C through the displacement of TMG by the phosphine with a  $\Delta G$  energy of 15.8 kcal/mol. The cis/trans isomerization of complex C was not discussed since it is not relevant for the reaction mechanism and can only affect the kinetic of the RE being the trans isomer more stable and unable to generate the final product. With both halide and triflate, the DFT calculation showed that the phenylacetylene insertion to the complex R is thermodynamically favoured over the direct coordination to B. This result is consistent with the experimental data described in Figure 31. The formation of complex **R** and **C** is accelerated by the excess of reagents being both bimolecular processes. In fact, the base and the alkyne are always present in large excess with respect to the Pd(II) complexes in a catalytic reaction. The proposed reaction mechanism is described in Figure 35. In the presence of a halide as a counterion, the direct coordination of the alkyne took place in a neutral complex G (Figure 35a), while with triflate, the coordination took place in a cationic complex S (Figure 35b). Concerning the overall reaction rate-determining step, with iodides, the oxidative addition and the coordination of the alkyne transition states have similar energy requirements, around 17-20 kcal/mol<sup>[186,199]</sup>. On the contrary, for bromides, chlorides, and triflates, the oxidative addition is by far the most demanding step, with an energy higher than 30 kcal/mol<sup>[200]</sup> and higher than that of the acetylene carbopalladation TS1<sup>Br,Cl,OTf</sup>, which in our calculations turns out to be just 20–23 kcal/mol.

# a. Neutral Mechanism (X=I, Br, CI) b. Cationic Mechanism (X=Off) (Pd"-precatalyst) (Pd"-precatalyst) R2-Off + Base R2-Pd"-X Base R2-Pd"-X Base R2-Pd"-X Base R2-Pd"-X Base R2-Pd"-Base R2-Pd"-Base R2-Pd"-Base R3-Pd"-Base R3-Pd"-Base

Figure 35. HCS copper-free reaction mechanisms according to the neutral (a) or cationic (b) route.

### 2.1.3. Conclusion

The investigation of the fate of palladium complexes mimicking operative catalytic conditions was crucial to understand the copper-free HCS reaction mechanism. Palladium species are highly reactive and can undergo side reactions that have the potential to significantly influence the outcome of the reaction and affect data interpretation. In this study, we demonstrated that the bis acetylene Pd(II) complex M, suggested by Košmrlj and co-workers as a key intermediate in the catalytic cycle<sup>[187]</sup>, is not involved in a standard HCS copper-free reaction. In fact, this complex is unstable and cannot compete with the direct coordination process of the alkyne, which is faster and more efficient than the Pd(II)-Pd(II) transmetalation mechanism. The complex M can be formed and participate in the formation of Pd(0) if the pre-catalyst reduction process is not efficient, forming the homocoupling species as a by-product. The result is independent of the leaving group, solvent, alkyne or temperature used. Furthermore, we have investigated the presence of secondary organic amines in the copper-free Heck-Cassar-Songashira protocol to understand their fundamental role in promoting precatalyst reduction and entering the coordination sphere of the metal. Experimental results showed that under catalytic conditions, the large excess of secondary amines with respect to the palladium metal and the phosphine ligand influences the Pd(II) complexes and their fate. Theoretical calculations and experimental results showed that there are two different catalytic cycles depending on the type of counterion involved: (i) with the halide as counterion, the mechanism involves the coordination of the alkyne in a neutral Pd(II) complex; (ii) with the triflate, which is completely dissociated from the metal, two molecules of the secondary amine enter the palladium coordination sphere, promoting the coordination of the alkyne in a cationic Pd(II) complex.

This study has identified the role of each component (*e.g.* ligand, base, leaving group, alkyne, temperature) in the HCS reaction and will hopefully guide chemists in developing optimised protocols to minimise reagent excess, by-product formation and palladium loading.

### Acknowledgments:

DFT calculations for this work were performed by Dr. Tommaso Fantoni. Nanoparticles have been analysed and evaluated by Beatrice Muzzi (ICCOM-CNR).

### Published work:

The full version can be found in "C. Palladino and T. Fantoni, L. Ferrazzano, B. Muzzi, A. Ricci, A. Tolomelli, W. Cabri, ACS Catal. 2023, 13, 12048–12061".

# 2.1.4. Experimental Section

# 2.1.4.1. General Information

Commercially available reagents (reagent grade, >99%) were purchased from Sigma Aldrich, Fluorochem and TCI Chemicals and used without any further purification. Solvents (dichloromethane (DCM), tetrahydrofuran (THF), toluene, deuterated N,N-Dimethylformamide (DMF-d<sub>7</sub>), deuterated chloroform (CDCl<sub>3</sub>), ethyl acetate (EtOAc), cyclohexane (Cy), N-Methyl-2-pyrrolidone (NMP), N-Butyl-2-pyrrolidone (NBP), 1-(2-Hydroxyethyl)-2-pyrrolidone (HEP), Ethanol (EtOH), acetonitrile (ACN) commercially available and solvent for reaction were used after degassing. Tetrakis(triphenylphosphine)palladium Pd(PPh<sub>3</sub>)<sub>4</sub>, bis(triphenylphosphine)palladium chloride(II) PdCl<sub>2</sub>(PPh<sub>3</sub>)<sub>2</sub> 1,1'-Bis(diphenylphosphino)ferrocene] palladio(II)dichloride PdCl<sub>2</sub>(dppf), Bis(acetonitrile)dichloropalladium(II) PdCl<sub>2</sub>(ACN)<sub>2</sub>, triphenylphospine (PPh3), 3-Bis(diphenylphosphino)propane and 1,1'-(dppp) Bis(diphenylphosphino)ferrocene (dppf) from FaggiEnrico (Italy).

 $^{1}$ H NMR,  $^{13}$ C NMR and  $^{31}$ P NMR spectra were recorded on Varian 400-MR (400 MHz) (equipped with autoswitchable PFG probe) and Bruker Avance Neo 600 MHz (equipped with CryoProbe Prodigy Broadband 5mm) spectrometers. NMR multiplicities are abbreviated as follows: s = singlet, d = doublet, t = triplet, q = quartet, spt = septet, m = multiplet, bs = broad signal. Coupling constants J are given in Hz. All  $^{1}$ H and  $^{13}$ C chemical shifts are calibrated to residual protic-solvents and all  $^{31}$ P chemical shifts are referenced to external 85% phosphoric acid ( $\delta = 0$  ppm). HPLC-UV analysis were recorded with an Agilent 1260 InfinityLab instrument. Column: Zorbax® SB-C18; particle size 5 μm; pore size 100 Å; length 250 mm, internal diameter: 4.6 mm. Mobile phase A: H<sub>2</sub>O, mobile phase B: ACN. Gradient (Time(min), %B): 0, 80; 25, 80; 28, 10; 30, 10; flow 0.5 mL min-1 column temperature 30°C; injection volume: 10 μL. GC-MS analysis were recorded with

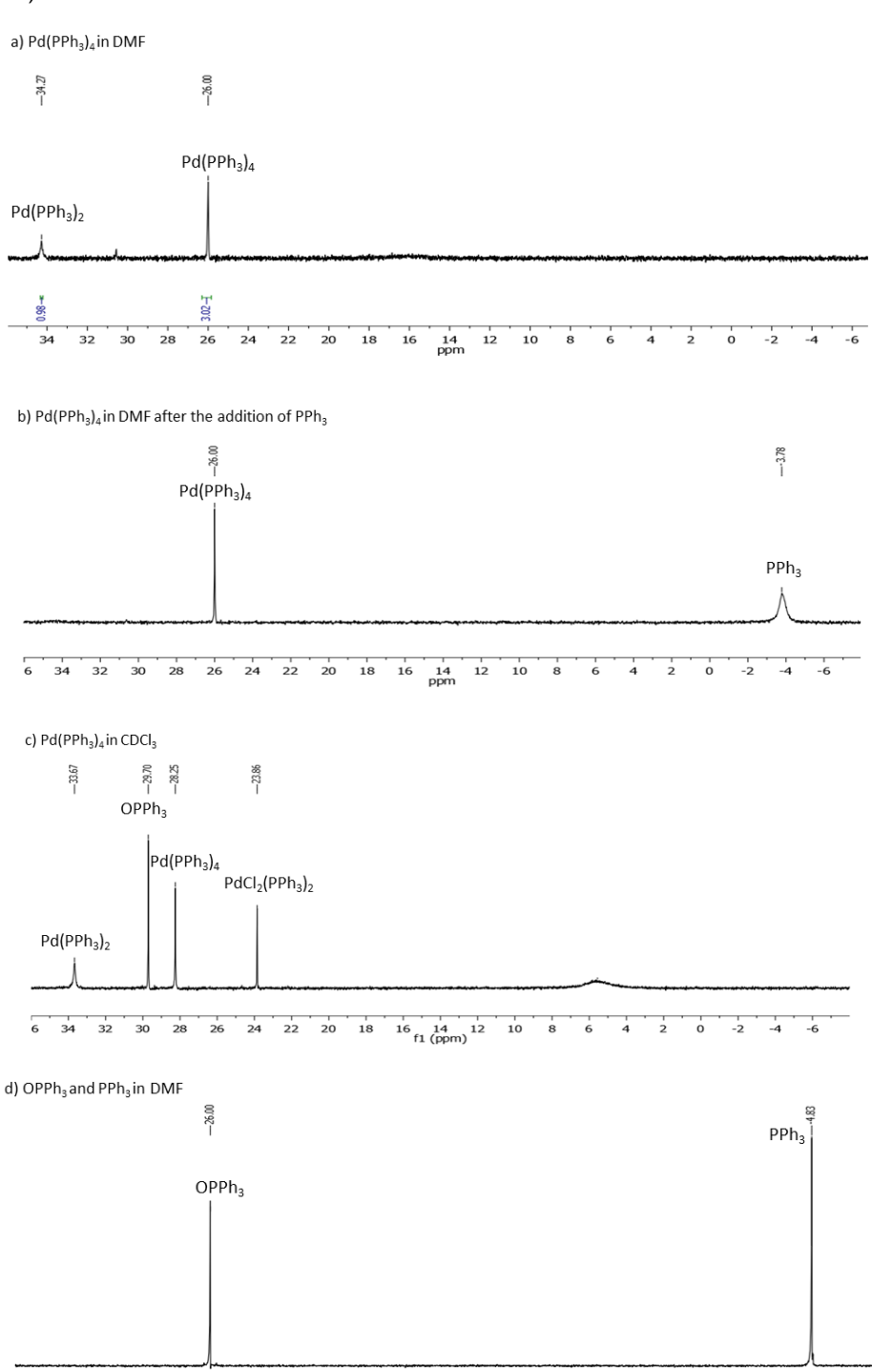
a Hewlett-Packard 5971 spectrometer with GC injection and EI ionization at 70 eV coupled with an Agilent Technologies MSD1100 single-quadrupole mass spectrometer, reported as: m/z (rel. intensity). High-Resolution transmission electron microscopy (HR-TEM) images were acquired on a ThermoFischer Talos F200X operated at 200 kV, which is equipped with an extreme field emission gun (FEG) electron source and Super-X Energy Dispersive X-ray Spectroscopy (EDS) system for chemical analysis. HRMS spectra were obtained with a G2XS QTof mass spectrometer using either ESI. Room temperature (rt) refers to the ambient temperature of the laboratory, ranging from 22 °C to 26 °C.

### 2.1.4.2. Palladium species

Table 6. <sup>31</sup>P NMR chemical shift in DMF-d<sub>7</sub> and CDCl<sub>3</sub> of palladium species.

	MR chemical shift in DMF-α7 and CDCl3 of palladium spec δ (ppm)		
Entry	Compound	DMF-d <sub>7</sub>	CDCI <sub>3</sub>
1	Pd(PPh <sub>3</sub> ) <sub>4</sub>	26.00	28.25
2	Pd(PPh <sub>3</sub> ) <sub>3</sub>	24.84	23.85
3	Pd(PPh <sub>3</sub> ) <sub>2</sub>	34.33	33.78
4	PPh <sub>3</sub>	-4.83	-5.46
5	OPPh <sub>3</sub>	26.00	29.70
6	PdCl <sub>2</sub> (PPh <sub>3</sub> ) <sub>2</sub>	24.85	23.86
7	complex L	24.06	23.43
8	complex M	27.19	26.56
9	complex $C_{NO_2}$	28.05	27.53
10	complex $B_{NO_2}^{I}$	23.43	23.17
11	$\text{complex } B_{Me}^{I}$	22.81	22.53
12	$\text{complex } B^{Br}_{NO_2}$	24.67	24.08
13	complex $\mathbf{B}_{\mathrm{NO_{2}}}^{\mathrm{Cl}}$	24.93	24.18
14	complex $\mathbf{B}_{\mathbf{N0}_{2}}^{\mathbf{OTf}}$	22.53	-
15	complex $B_{0Me}^{I}$	23.79	24.15

# Entries 1-6, Table 6



6 34 32 30 28 26 24 22 20 18 16 14 12 10 8 6 4 2 0 -2 -4 -6 ppm

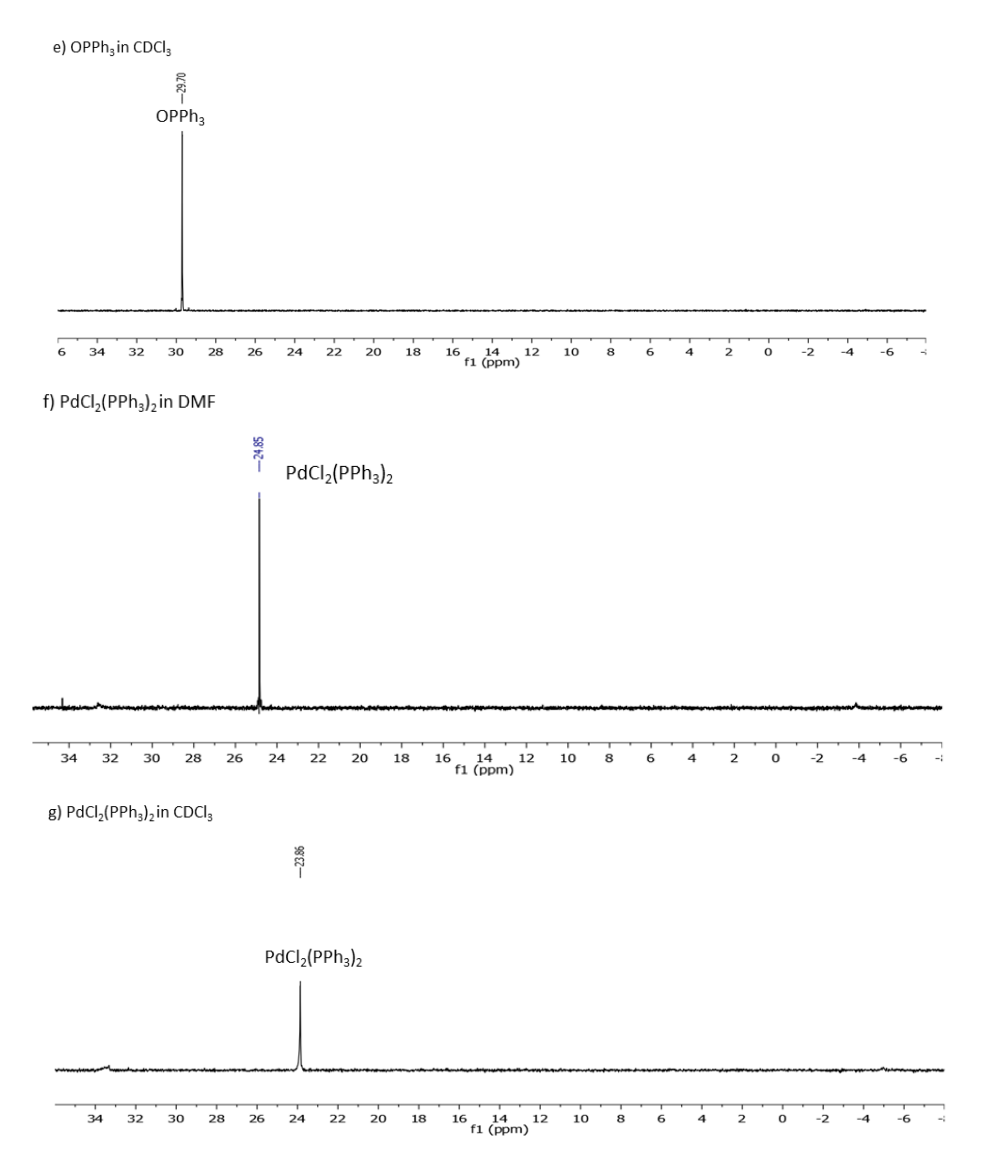
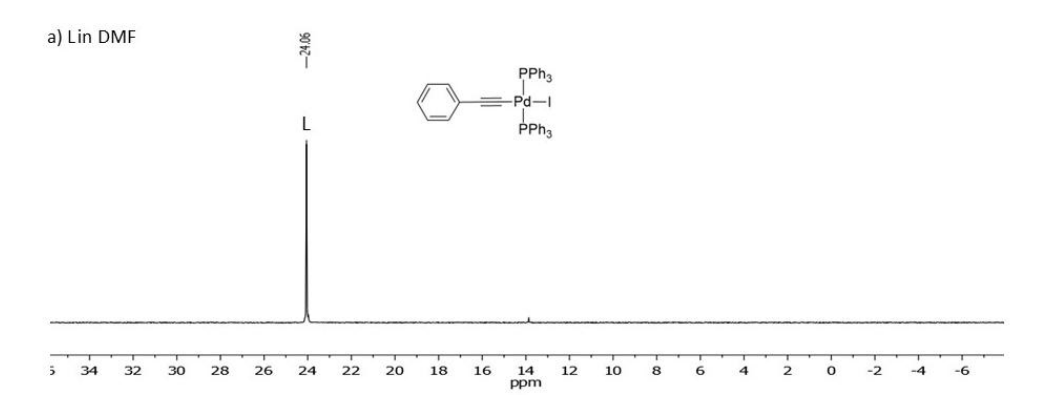


Figure 36. <sup>31</sup>P NMR spectra of: a) Pd(PPh<sub>3</sub>)<sub>4</sub> in DMF-d<sub>7</sub>, b) Pd(PPh<sub>3</sub>)<sub>4</sub> with the addition of PPh<sub>3</sub>, c) Pd(PPh<sub>3</sub>)<sub>4</sub> in CDCl<sub>3</sub>, d) Triphenylphosphine oxide (OPPh<sub>3</sub>) and Triphenylphosphine (PPh<sub>3</sub>) in DMF-d<sub>7</sub>, e) OPPh<sub>3</sub> in CDCl<sub>3</sub>, f) PdCl<sub>2</sub>(PPh<sub>3</sub>)<sub>2</sub> in DMF-d<sub>7</sub>, g) PdCl<sub>2</sub>(PPh<sub>3</sub>)<sub>2</sub> in CDCl<sub>3</sub>

# Entry 7, Table 6



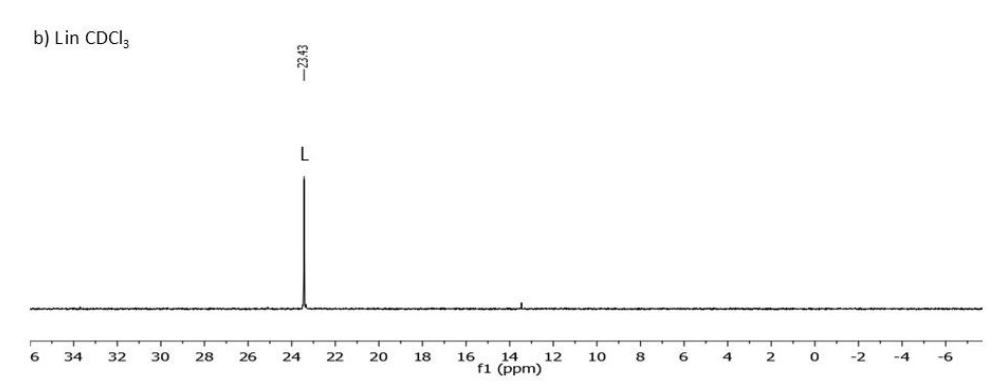


Figure 37. <sup>31</sup>P NMR spectra of the complex L in DMF-d<sub>7</sub> (a) and in CDCl<sub>3</sub> (b).

# Entry 8, Table 6

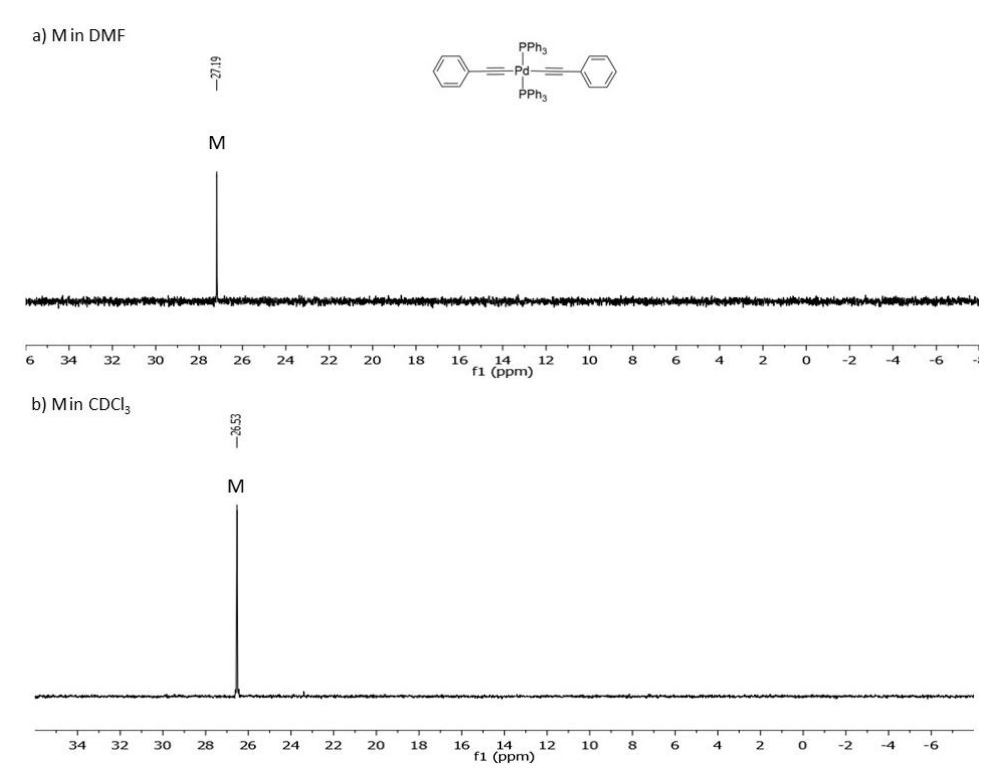
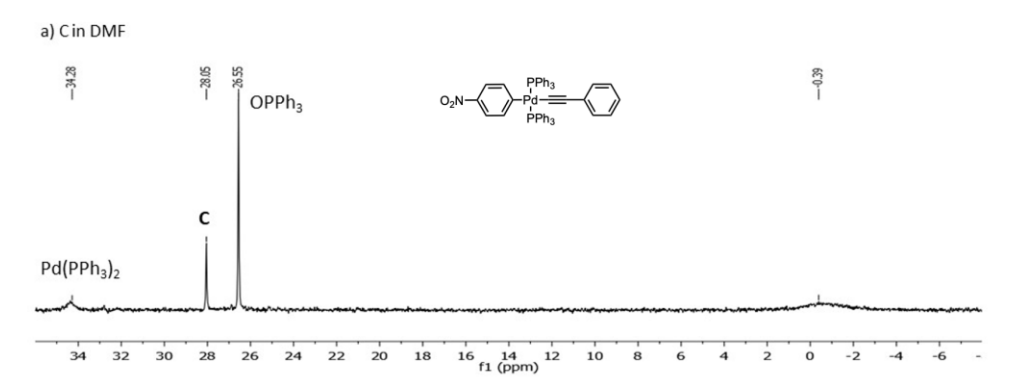


Figure 38.  $^{31}P$  NMR spectra of the complex **M** in DMF-d<sub>7</sub> (a) and in CDCl<sub>3</sub> (b).

# Entry 9, Table 6



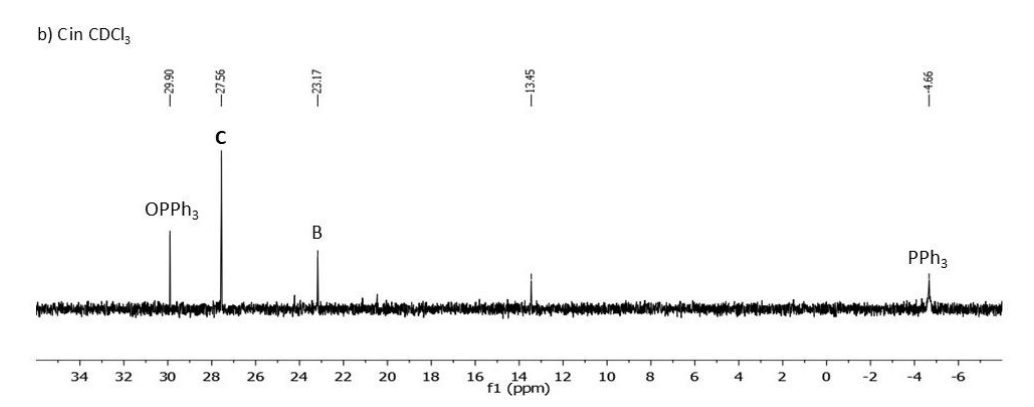


Figure 39.  $^{31}P$  NMR spectra of the complex {trans-C in DMF-d7 (a) and in CDCl3 (b)}

# Entry 10, Table 6

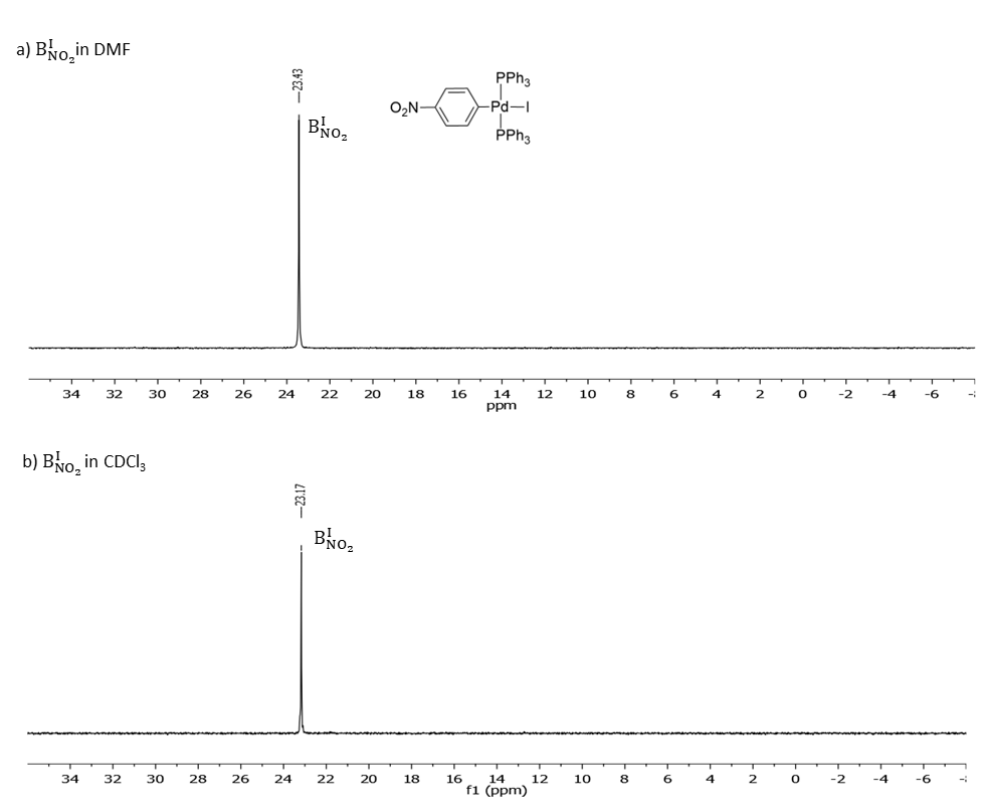


Figure 40.  $^{31}P$  NMR spectra of the complex  $\mathbf{B_{NO_2}^I}$  in DMF-d7 (a) and in CDCl3 (b).

# Entry 11, Table 6

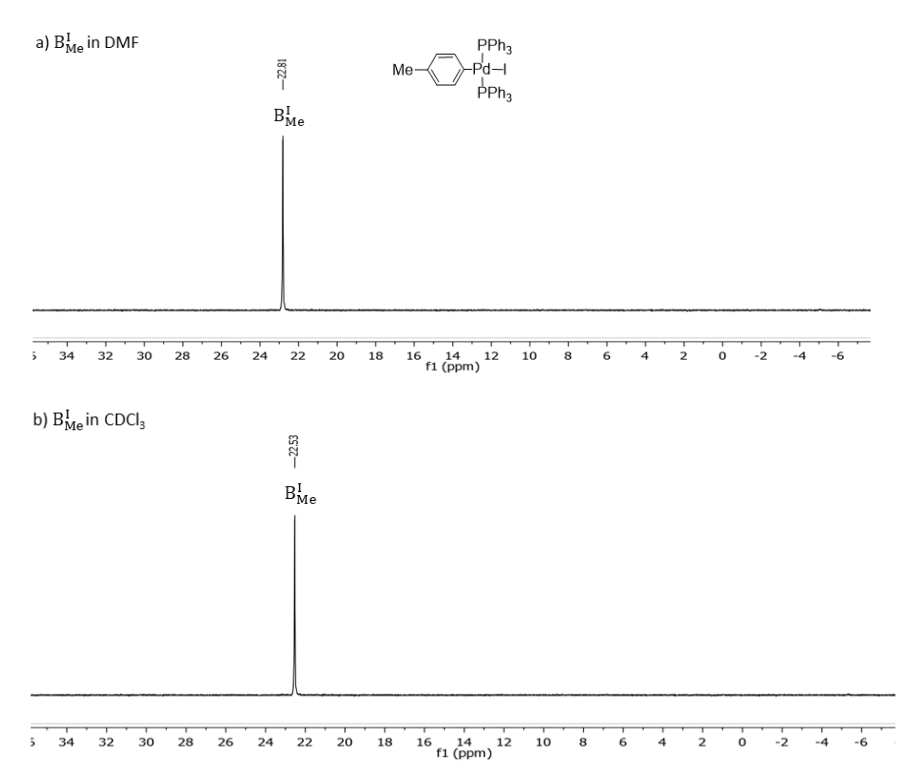
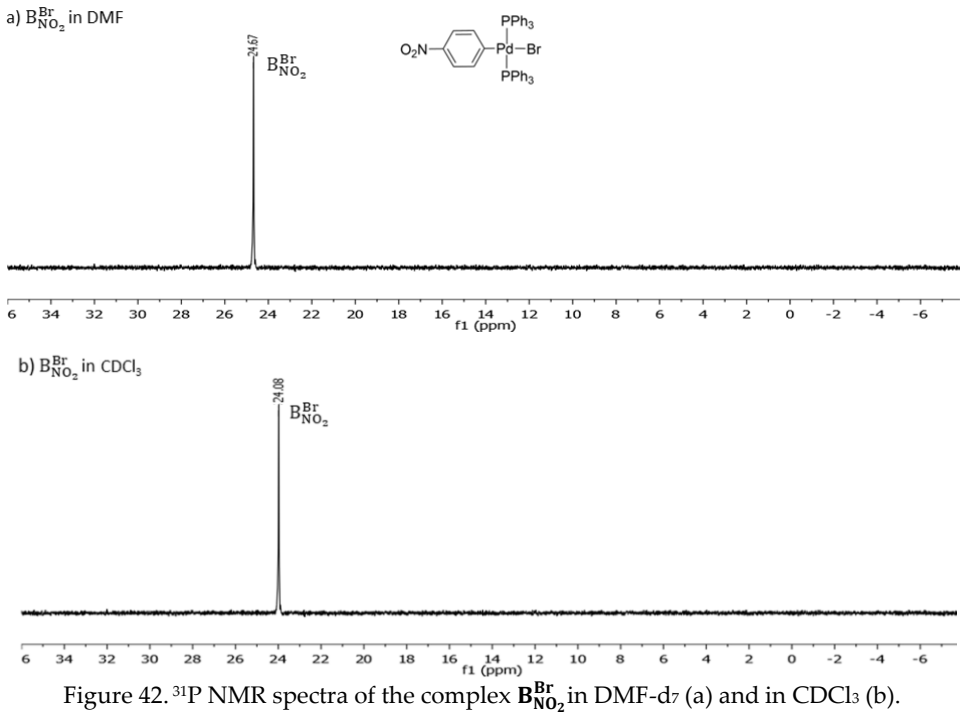


Figure 41.  $^{31}P$  NMR spectra of the complex  $B^{I}_{Me}\mbox{in DMF-dz}$  (a) and in CDCl3 (b).

# Entry 12, Table 6



# Entry 13, Table 6

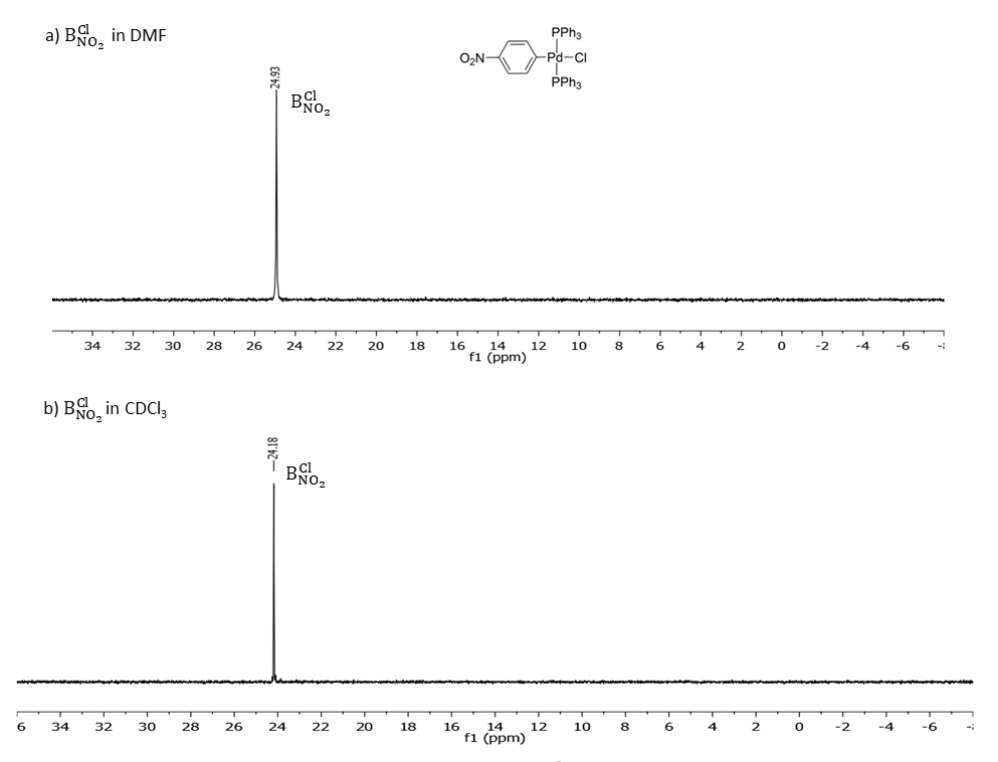


Figure 43.  $^{31}P$  NMR spectra of the complex  $B^{Cl}_{NO_2}\mbox{in DMF-dz}$  (a) and in CDCl3 (b).

# Entry 14, Table 6

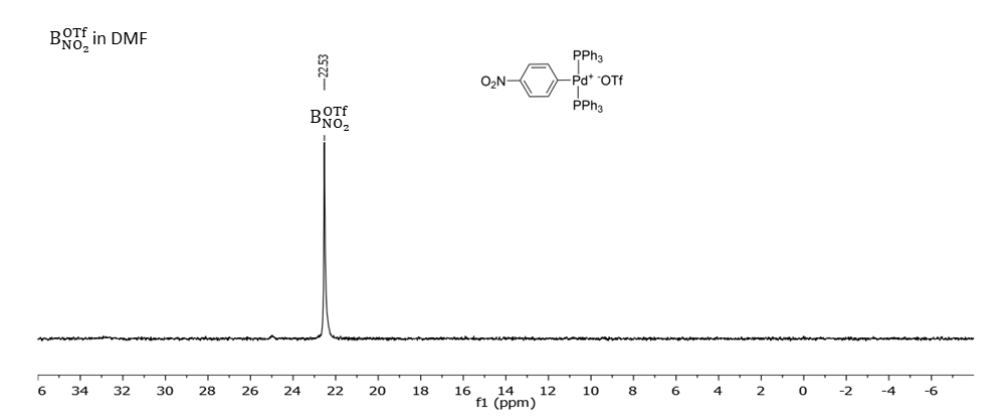


Figure 44.  $^{31}\text{P}$  NMR spectra of the complex  $B_{NO_2}^{OTf}$  in DMF-d7 (a) and in CDCl3 (b).

# Entry 15, Table 6

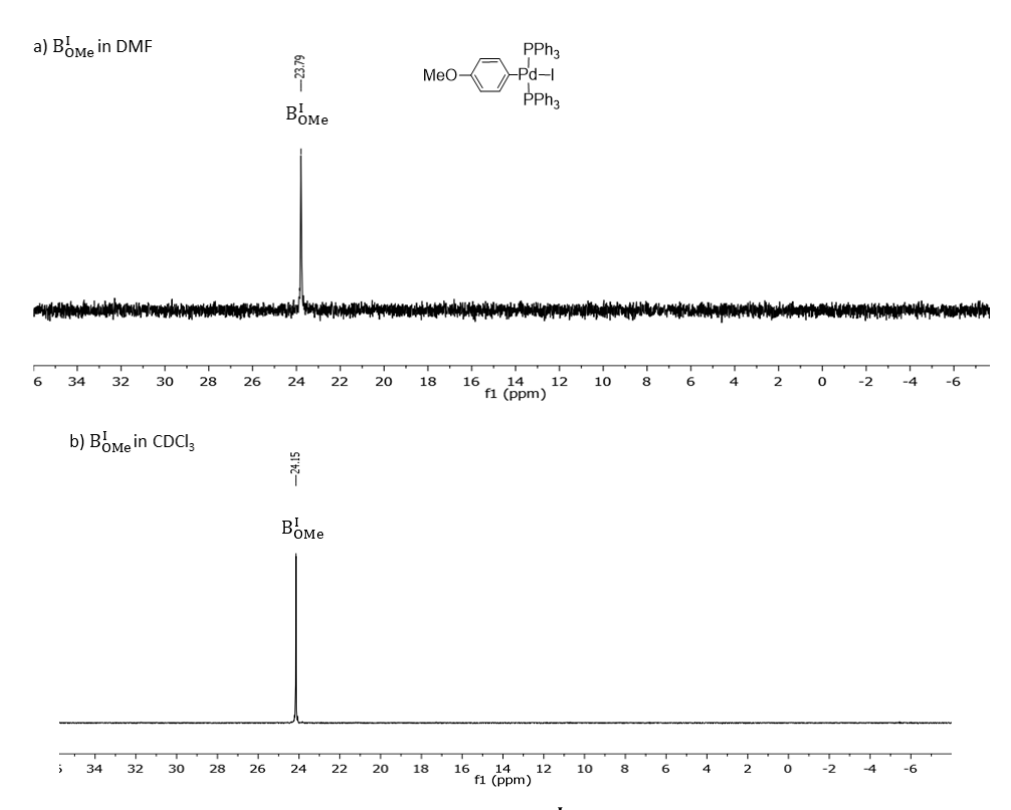


Figure 45.  $^{31}P$  NMR spectra of the complex  $\mathbf{B_{0Me}^{I}}$  in DMF-d<sub>7</sub> (a) and in CDCl<sub>3</sub> (b).

### 2.1.4.3. Synthesis of palladium complexes

• Synthesis of OA complex **B**<sub>NO<sub>2</sub></sub> [194]

$$O_2N$$
  $\longrightarrow$   $I$  +  $Pd(PPh_3)_4$   $\longrightarrow$   $O_2N$   $\longrightarrow$   $O_2N$ 

To an oven-dried 20 mL Schlenk purged under argon atmosphere, a mixture of 1-Iodo-4-nitrobenzene  $1_{NO2}$  (423 mg, 1.7 mmol, 2.46 equiv) and Pd(PPh<sub>3</sub>)<sub>4</sub> (798 mg, 0.69 mmol, 1 equiv) was stirred in degassed toluene (13 mL), in the dark for 1 h at room temperature. The reaction mixture was filtered and the crude was washed with diethyl ether (Et<sub>2</sub>O) to obtain the pure product (564 mg, 93 %) as a white solid.

<sup>1</sup>H NMR (600 MHz, CDCl<sub>3</sub>): δ 7.56-7.53 (m, 12H, Hb-Hf); 7.36-7.33 (m, 6H, Hd); 7.27-7.25 (m, 12H, Hc-He); 7.02-7.01 (d, J=6 Hz 2H, Hc'-He'); 6.85-6.84 (m, 2H, Hb'-Hf')

<sup>13</sup>C NMR (151.2 MHz, CDCl<sub>3</sub>): δ 177.07 (s, Cd'); 143.84 (t, J=1.51 Hz, Ca'); 135.96 (t, J=4.53 Hz, Cb'-Cf'), 134.94 (t, 6.05 Hz, Cb-Cf), 131.49 (t, J=24.2 Hz, Ca), 130.37 (s, Cd), 128.10 (t, J=4.53, Cc-Ce), 120.95 (t, Cc'-Ce').

<sup>31</sup> P NMR (242.4 MHz, CDCl<sub>3</sub>): δ +23.17 (s)

# • Synthesis of OA complex $\mathbf{B}_{Me}^{\mathbf{I}}$

Me 
$$\longrightarrow$$
 I + Pd(PPh<sub>3</sub>)<sub>4</sub>  $\longrightarrow$  Toluene, rt  $\longrightarrow$  H<sub>3</sub>C  $\longrightarrow$  Pd  $\longrightarrow$  PPh<sub>3</sub>  $\longrightarrow$  Pbh<sub>3</sub>

To an oven-dried 20 mL Schlenk purged under argon atmosphere, a mixture of 4-Iodotoluene  $1_{\text{Me}}$  (457 mg, 2.09 mmol, 2.46 equiv) and Pd(PPh<sub>3</sub>)<sub>4</sub> (982 mg, 0.85 mmol, 1 equiv) was stirred in degassed toluene (11.5 mL), in the dark for 2 h at room temperature. The reaction mixture was filtered, and the crude was washed with diethyl ether to obtain the pure product (671 mg, 93 %) as a white solid.

<sup>1</sup>H NMR (600 MHz, CDCl<sub>3</sub>): δ 7.50-7.19 (m, 12H, Hb-Hf); 7.31-7.18 (m, 6H, Hd); 7.23-7.19 (m, 12H, Hc-He); 6.40-6.38 (d, J=4 Hz 2H, Hb'-Hf'); 6.06-6.05 (m, 2H, Hc'-He'); 1.92 (s, 3H, Hg').

<sup>13</sup>C NMR (151.2 MHz, CDCl3):  $\delta$  152.7 (t, J=1.51 Hz, Ca'), 135.5 (t, J=4.53 Hz, Cb'-Cf'), 134.9 (t, 6.05 Hz, Cb-Cf), 132.2 (t, J=1.51 Hz, Ca'), 129.6 (s, Cd), 130.9 (s, Cd'), 128.9 (t, Cc'-Ce'),127.7 (t, J = 5.0 Hz, (t, J=4.53, Cc-Ce), 20.1 (Cg');

<sup>31</sup> P NMR (242.4 MHz, CDCl<sub>3</sub>): δ +22.53 (s)

# • Synthesis of OA complex $B_{NO_2}^{Br}$ [194]

$$O_2N$$
—Br + Pd(PPh<sub>3</sub>)<sub>4</sub> Toluene,  $60^{\circ}C$ 
 $O_2N$ — $O_2N$ 

To an oven-dried 20 mL Schlenk purged under argon atmosphere, a mixture of 1-Bromo-4-nitrobenzene  $\mathbf{1}_{NO_2}^{Br}$  (274 mg, 1.35 mmol, 2.46 equiv) and Pd(PPh<sub>3</sub>)<sub>4</sub> (634 mg, 0.55 mmol, 1 equiv) was stirred in degassed toluene (13 mL). The reaction mixture was heated to 60°C with an oil bath and stirred for 5 h. The reaction mixture was filtered, and the crude was washed with diethyl ether to obtain pure product (411 mg, 90 %) as a white solid. <sup>1</sup>H NMR (600 MHz, CDCl<sub>3</sub>):  $\delta$  7.56-7.53 (m, 12H, Hb-Hf); 7.36-7.34 (m, 6H, Hd); 7.28-7.25 (m, 12H, Hc-He); 7.02-7.00 (d, J=12 Hz, 2H, Hc'-He'); 6.87-6.86 (m, 2H, Hb'-Hf') <sup>13</sup>C NMR (151.2 MHz, CDCl<sub>3</sub>):  $\delta$  174.27 (s, Cd'); 143.67 (t, J=1.51 Hz, Ca'); 136.06 (t, J=4.54 Hz, Cb'-Cf'), 134.66 (t, 6.05 Hz, Cb-Cf), 130.69 (t, J=24.2 Hz, Ca), 130.26 (s, Cd), 128.07 (t, J=4.54, Cc-Ce), 120.80 (t, Cc'-Ce').

<sup>31</sup> P NMR (242.4 MHz, CDCl<sub>3</sub>): δ +24.08 (s)

• Synthesis of OA complex  $B_{NO_2}^{Cl}$  [201]

$$O_{2}N \xrightarrow{PPh_{3}} Pd-I + Et_{4}NCI \xrightarrow{DCM, rt, PPh_{3}} DcM, rt, 12 h$$

$$B^{I}_{NO2}$$

$$B^{C}_{NO2}$$

$$B^{C}_{NO2}$$

$$B^{C}_{NO2}$$

To an oven-dried 20 mL Schlenk purged under argon atmosphere, a mixture of  $Pd(PPh_3)_2(PhNO_2)I$   $B_{NO_2}^I$  (105 mg, 0.12 mmol, 1 equiv) and  $Et_4NCl$  (40 mg, 0.24 mmol, 2 equiv) was stirred in DCM (1.2 mL) for 12 h at room temperature. The reaction mixture was filtered, washed with toluene (1 mL) and concentrated to 1 mL under reduced pressure. Hexane (1 mL) was added dropwise and the precipitated was filtered. In order to obtain  $B_{NO_2}^{Cl}$  as white solid, the precipitate was washed with hexane and ethanol and dried under vacuum (94 mg, 80%).

 $^{1}$ H NMR (600 MHz, CDCl<sub>3</sub>):  $\delta$  7.55-7.52 (m, 12H, Hb-Hf); 7.36-7.34 (m, 6H, Hd); 7.27-7.25 (m, 12H, Hc-He); 7.01-6.99 (d, J=12 Hz, 2H, Hc'-He'); 6.87-6.86 (m, 2H, Hb'-Hf')

<sup>13</sup>C NMR (151.2 MHz, CDCl<sub>3</sub>): δ 172.56 (s, Cd'); 143.77 (t, J=1.51 Hz, Ca'); 136.40 (t, J=4.53 Hz, Cb'-Cf'), 134.68 (t, 6.05 Hz, Cb-Cf), 130.52 (t, J=24.2 Hz, Ca), 130.41 (s, Cd), 128.27 (t, J=4.53, Cc-Ce), 120.85 (t, Cc'-Ce').

<sup>31</sup> P NMR (242.4 MHz, CDCl<sub>3</sub>): δ +24.18 (s)

• Synthesis of OA complex **B**<sup>I</sup><sub>OMe</sub><sup>[194]</sup>

MeO 
$$\longrightarrow$$
 I + Pd(PPh<sub>3</sub>)<sub>4</sub>  $\xrightarrow{\text{Toluene, rt}}$   $\xrightarrow{\text{H}_3CO}$   $\xrightarrow{\text{d}}$   $\xrightarrow{\text{Pd}}$   $\xrightarrow{\text{Pl}}$   $\xrightarrow{\text{Ph}_3}$   $\xrightarrow{\text{Pl}}$   $\xrightarrow{\text{Ph}_3}$   $\xrightarrow{\text{Pl}}$   $\xrightarrow$ 

To an oven-dried 20 mL Schlenk purged under argon atmosphere, a mixture of 4-iodoanisole  $\mathbf{1_{0Me}^{l}}$  (397 mg, 1.7 mmol, 2.46 equiv) and Pd(PPh<sub>3</sub>)<sub>4</sub> (798 mg, 0.69 mmol, 1 equiv was stirred in degassed toluene (13 mL), in the dark for 2 h at room temperature. The reaction mixture was filtered, and the crude was washed with diethyl ether to obtain the pure product (543 mg, 91 %) as a white solid.

<sup>1</sup>H NMR (400 MHz, CDCl<sub>3</sub>): δ 7.52-7.48 (m, 12H, Hb-Hf); 7.33-7.30 (m, 6H, Hd); 7.26-7.21 (m, 12H, Hc-He); 6.42-6.40 (d, J=4 Hz 2H, Hb'-Hf'); 6.08-6.07 (m, 2H, Hc'-He'); 1.92 (s, 3H, Hg').

 $^{13}$  C NMR (100.8 MHz, CDCl<sub>3</sub>):  $\delta$  152.90 (s, Ca'); 135.59 (t, J=5.04 MHz, Cb'-Cf'); 135.04 (t, J=7.06 MHz, Cb-Cf); 132.33 (t, J=23.18 MHz, Ca); 131.08 (s, Cd'); 129.74 (s, Cd); 129.07 (s, Cc'-Ce'); 127.82 (t, J=5.04 MHz, Cc-Ce); 22.24 (s, Cg').

<sup>31</sup> P NMR (161.6 MHz, CDCl<sub>3</sub>): δ +23.43 (s)

# • Synthesis of OA complex $B_{NO_2}^{OTf[202]}$

$$O_{2}N \xrightarrow{PPh_{3}} Pd - I + AgOTf \xrightarrow{THF, 1 h,} O_{2}N \xrightarrow{e^{\circ}} Pd^{+}OTf + AgI$$

$$B^{I}_{NO2}$$

$$B^{OTf}_{NO2}$$

To an oven-dried 20 mL Schlenk purged under argon atmosphere, a mixture of  $Pd(PPh_3)_2(PhNO_2)I$   $B_{NO_2}^I$  (60 mg, 0.068 mmol, 1 equiv) and Silver trifluoromethanesulfonate (AgOTf) (18 mg, 0.072 mmol, 1.06 equiv) was stirred in THF (2 mL) for 1 h at room temperature in the dark. The reaction mixture was filtered through a pad of celite, washed with THF and concentrated to 0.5 mL of solvent under reduced pressure. The THF solution was layered with hexane and allowed to rest at -24° C overnight. The precipitated was filtered to obtain the pure product as white solid (13 mg, 20%).

 $^{1}$ H NMR (400 MHz, DMF-d<sub>7</sub>):  $\delta$  7.60-7.53 (m, 30H, Hb-Hc-Hd-He-Hf); 7.32-7.30 (m, 6H, Hd); 7.32-7.15 (m, 4H, Hb'-Hc'-He'-Hf'). Spectroscopic data matches with the literature [197]

 $^{31}P$  NMR (161.6 MHz, DMF-d<sub>7</sub>):  $\delta$  +22.53 (s). Spectroscopic data matches with the literature[197]

<sup>19</sup>F NMR (377 MHz, DMF-d<sub>7</sub>): δ -74.37

### • Synthesis of Complex L<sup>[187]</sup>

$$I_{2} \stackrel{+}{\overset{O}{\underset{H}{\longrightarrow}}} \underbrace{\begin{array}{c} O\\ \\ N\\ \end{array}} \xrightarrow{\text{Toluene,}} \underbrace{\begin{array}{c} O\\ \\ N^{+}\\ \end{array}} \underbrace{\begin{array}{c} Pd(PPh_{3})_{4}\\ \\ C \stackrel{b'}{\longrightarrow} \end{array}} \xrightarrow{\begin{array}{c} e^{-} \\ V \stackrel{b'}{\longrightarrow} \end{array}} \underbrace{\begin{array}{c} Pd(PPh_{3})_{4}\\ \\ Toluene\\ \\ rt, 24h \end{array}} \xrightarrow{\begin{array}{c} e^{-} \\ V \stackrel{b'}{\longrightarrow} \end{array}} \underbrace{\begin{array}{c} Pd(PPh_{3})_{4}\\ \\ PPh_{3} \\ \end{array}} + \underbrace{\begin{array}{c} Et_{4}NI\\ \\ PPh_{3} \\ \end{array}}$$

The reaction was performed in presence of  $I_2$  (2.80 g, 11 mmol, 1.1 equiv) and morpholine (2.62 mL, 30 mmol, 3 equiv) in toluene (12 mL) for 30 min at room temperature. After the formation of an orange solution, phenylacetylene 2a (1.10 mL, 10 mmol, 1 equiv) diluted in toluene (18 mL) was added dropwise and the mixture was stirred at 45°C for 24 h. After the filtration and washing with diethyl ether, the organic phase was washed with NH<sub>4</sub>Cl<sub>(aq)</sub>, NaHCO<sub>3(aq)</sub> and water. After drying with Na<sub>2</sub>SO<sub>4</sub>, the solvent was removed under reduce pressure to obtain 6 (1.35 g, 60%) as a brown oil.

<sup>1</sup>H NMR (600 MHz, CDCl<sub>3</sub>): δ 7.47-7.46 (m, 2H, Hb'-Hf'); 7.35-7.32 (m, 3H, Hc'-Hd'-He').

<sup>13</sup> C NMR (151.2 MHz, CDCl<sub>3</sub>): δ 132.39 (s, Cb'-Cf'); 128.88 (s, Cd'); 128.32 (s, Cc'-Ce'); 127.48 (s, Ca'), 123.43 (s, Cg'); 94.23 (s, Ch')

To an oven-dried 20 mL Schlenk purged under argon atmosphere, a mixture of 6 (675 mg, 2.96 mmol, 1.1 equiv) and tetrakis(triphenylphosphine)palladium(0) (3.11 mg, 2.69 mmol, 1 equiv) was stirred in degassed toluene (25 mL), in the darkness for 24h at room temperature. The reaction mixture was filtered, and the crude was washed with diethyl ether to obtain pure product (2.15 mg, 80 %) as a white solid.

<sup>1</sup>H NMR (600 MHz, CDCl<sub>3</sub>): δ 7.78-7.76 (m, 12H, Hb-Hf); 7.41-7.35 (m, 18H, Hc-Hd-He); 6.91-6.89 (m, 1H, Hd'); 6.86-6.83 (m, 2H, Hc'-He'); 6.09-6.08 (m, 2H, Hb'-Hf').

<sup>13</sup> C NMR (151.2 MHz, CDCl<sub>3</sub>): δ 135.16 (t, J= 6.05 Hz, Cb-Cf); 132.79 (t, J=24.2 Hz, Ca); 130.66 (t, J=1.51 Hz, Cb'-Cf'); 130.27 (s, Cd); 127.97 (t, J= 4.53, Cc-Ce); 127.34 (s, Ca'); 127.17 (s, Cc'-Ce'); 125.27 (s, Cd'); 109.67 (t, J=6.05 Hz, Cg'); 101.57 (t, J=13.61 Hz, Ch').

<sup>31</sup> P NMR (242.4 MHz, CDCl<sub>3</sub>): δ +23.43 (s)

# • Synthesis of Complex M<sup>[187]</sup>

To an oven-dried 20 mL Schlenk purged under argon atmosphere, a mixture of complex L (240 mg, 0.28 mmol, 1 equiv) and phenylacetylene 2a (396  $\mu$ L, 3.57 mmol, 12.78 equiv) and 0.2 M NaOH in methanol (7 mL) was stirred for 16 h at room temperature. The reaction mixture was filtered, and the crude was washed with water and methanol to obtain pure product (207 mg, 89 %) as a white solid.

<sup>1</sup>H NMR (600 MHz, CDCl<sub>3</sub>): δ 7.84-7.81 (m, 12H, Hb-Hf); 7.41-7.38 (m, 6H, Hd); 7.36-7.33 (m, 12H, Hc-He); 6.92-6.91 (m, 6H, Hc'-Hd'-He'); 6.34-6.32 (m, 4H, Hb'-Hf')

<sup>13</sup>C NMR (151.2 MHz, CDCl<sub>3</sub>): δ 135.14 (t, J= 6.05 Hz, Cb-Cf); 132.66 (t, J=24.2 Hz, Ca); 130.91 (s, Cb'-Cf'); 130.09 (s, Cd); 128.23 (t, J= 1.51 Hz, Ca'); 128.02 (t, J=4.54 Hz, Cc-Ce); 127.20 (s, Cc'-Ce'); 124.86 (s, Cd'); 114.90 (t, J=4.53 Hz, Cg'); 113.74 (t, J=16.63 Hz, Ch')

<sup>31</sup>P NMR (242.4 MHz, CDCl<sub>3</sub>): δ +26.56 (s)

### Synthesis of Complex trans-C

To an oven-dried 20 mL Schlenk purged under argon atmosphere,  $Pd(PPh_3)_4$  (578 mg, 0.5 mmol, 1 equiv) was dissolved in degassed DMF-d<sub>7</sub>. The other reagents were added in the following order: 1-Iodo-4-nitrobenzene 1 (249 mg, 1 mmol, 2 equiv), phenylacetylene 2a (142.8  $\mu$ L, 1.3 mmol, 2.6 equiv) and sodium methoxide (70 mg, 1.3 mmol, 2.6 equiv). After 3 minutes, an aliquot was collected and immediately analyzed by <sup>31</sup>P NMR. The isolation of complex *trans*-C was not possible, according to the data reported in literature<sup>5</sup>.

<sup>31</sup>P NMR (242.4 MHz, CDCl<sub>3</sub>): δ +27.56 (s)

### 2.1.4.4. Pd(II) reduction with base and PPh<sub>3</sub>

To an oven-dried 20 mL Schlenk purged under argon atmosphere, the pre-catalyst PdCl<sub>2</sub>(PPh<sub>3</sub>)<sub>2</sub> (9.12 mg, 0.013 mmol, 1 equiv.) was dissolved in degassed solvent (0.6 mL). The base (0.026 mmol, 2 equiv.), triphenylphosphine (6.81 mg, 0.026 mmol, 2 equiv.) and triethyl phosphonoacetate as internal standard (0.0065 mmol, 0.5 equiv) were added. The reaction was stirred at room temperature and after 10 minutes, the <sup>31</sup>P NMR spectra were collected (see Table 2).

The  $PdCl_2(PPh_3)_2$  reduction with TMG (2 equiv.) with and without 2 equiv. of  $PPh_3$  in DMF-d<sub>7</sub> at 25°C is taken as an example.

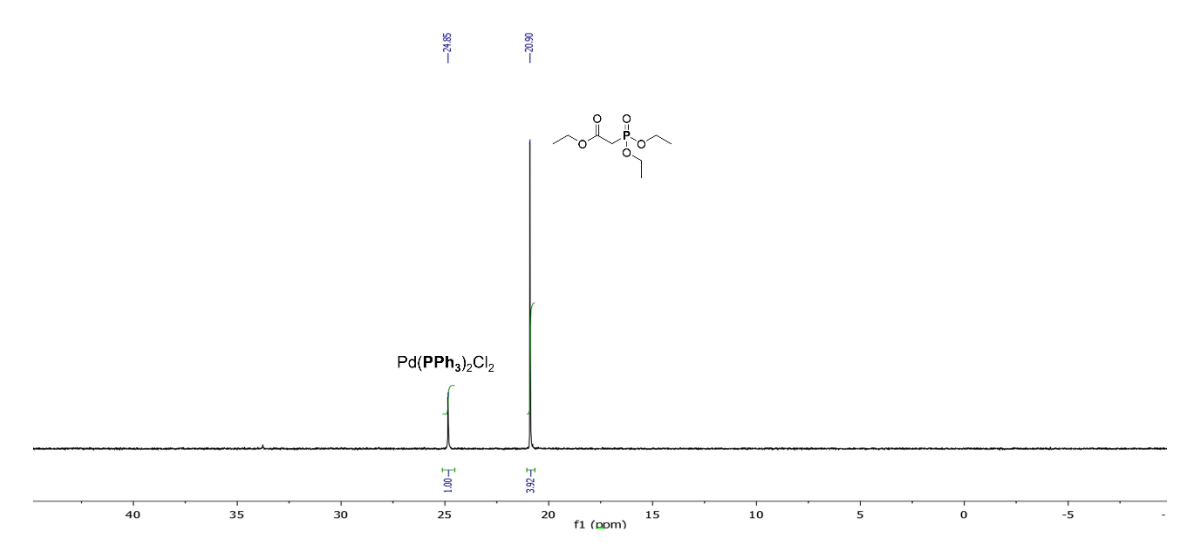


Figure 46.  $^{31}P$  nmr spectrum of Pd(PPh<sub>3</sub>)<sub>2</sub>Cl<sub>2</sub> (1 equiv) and the internal standard IS triethyl phosphonoacetate (1 equiv) to know their integration ratio under the same setting used for all the experiments (d<sub>1</sub>=1, nt=256).

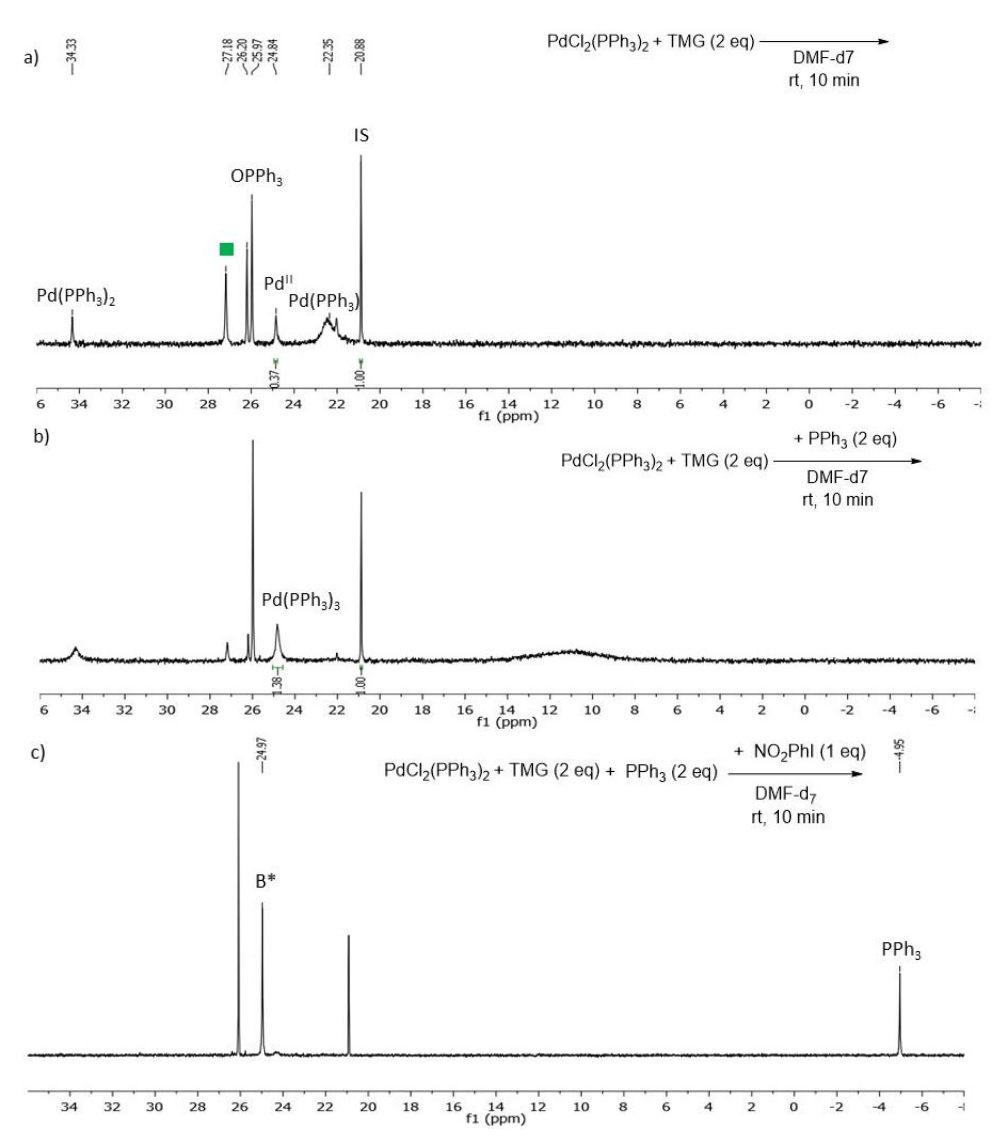


Figure 47.  $^{31}P$  NMR spectra of the reduction of  $PdCl_2(PPh_3)_2$  in DMF-d<sub>7</sub> with TMG 2 equiv. The peak labelled in green is supposed to be (TMG) $Pd^0(PPh_3)$ , but the complex is not isolable. (a); with TMG (2 equiv) and PPh<sub>3</sub> (2 equiv) (b); with TMG 2 eq, PPh<sub>3</sub> (2 equiv) and the reagent 4-NO<sub>2</sub>PhI (1 equiv) to show that the reduction of Pd(II) was complete, (c).

### 2.1.4.5. Pd(II) reduction in presence of phenylacetylene, with and without PPh<sub>3</sub>

To an oven-dried 20 mL Schlenk purged under argon atmosphere, the pre-catalyst  $PdCl_2(PPh_3)_2$  (9.12 mg, 0.013 mmol, 1 equiv) was dissolved in degassed CDCl<sub>3</sub> (0.6 mL). Base (0.65 mmol, 50 equiv), phenylacetylene **2a** (71.38  $\mu$ L, 0.65 mmol, 50 equiv) and triphenylphosphine (6.81 mg, 0.026 mmol, 2 equiv) were added. The reaction was stirred at room temperature and <sup>31</sup>P NMR spectra were collected after 10 minutes. (see Figure 25 and Figure 26).

### 2.1.4.6. Heck-Cassar reaction with Palladium (II) and Palladium (0)

# General procedure for the HCS reaction with Palladium (II)

$$O_2N \longrightarrow I + \bigcirc Pd^{II}Cl_2(PPh_3)_2$$

$$(Ligand)$$

$$Base$$

$$Solvent, rt$$

$$1 \qquad 2a \qquad 3a$$

To an oven-dried 10 mL Schlenk purged under  $N_2$  atmosphere,  $PdCl_2(PPh_3)_2$  (20% mmol) and  $PPh_3$  (40% mmol) were dissolved in the degassed solvent (1 ml). After the addition of 1-Iodo-4-nitrobenzene **1** (124.5 mg, 0.5 mmol, 1 equiv), phenylacetylene **2a** (60  $\mu$ L, 0.55, 1.1 equiv) and the base (2 equiv), the reaction mixture was stirred at room temperature. After a given time, the  $^{31}P$  NMR spectra were collected to detect which species were formed. The reactions were performed in DMF-d<sub>7</sub> and in CDCl<sub>3</sub> with TMG and pyrrolidine. The reaction performed in DMF-d<sub>7</sub> with TMG is shown in Figure 27.

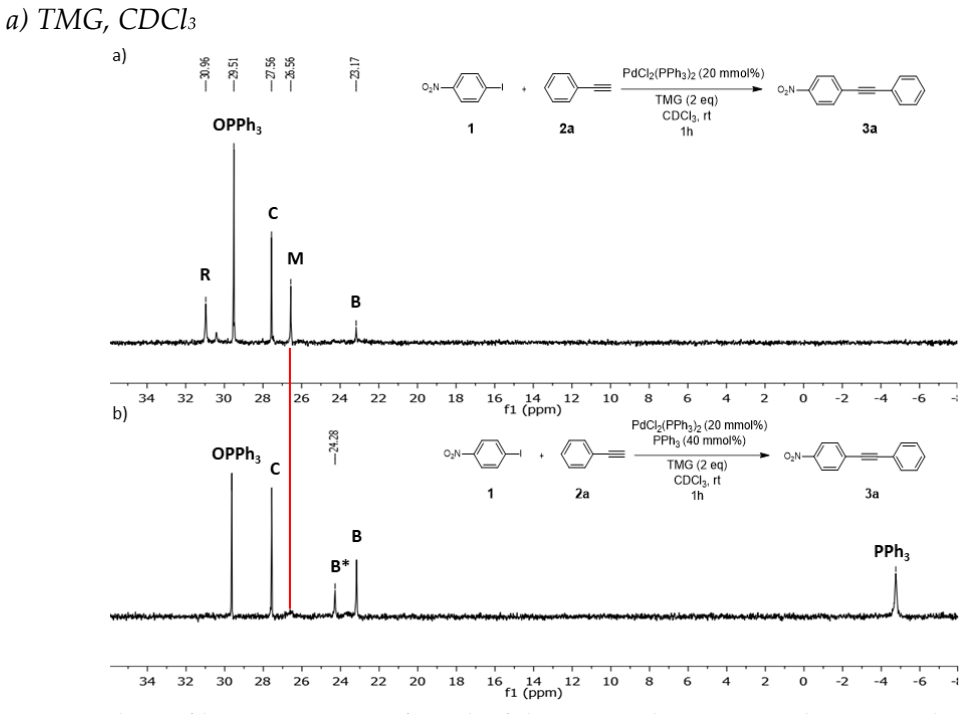


Figure 48. Stacking of  $^{31}P$  NMR spectra after 1 h of the reaction between **1** and **2a** in CDCl<sub>3</sub>, with TMG 2 equiv (a); with TMG 2 equiv and 40 mmol% of PPh<sub>3</sub> (b).

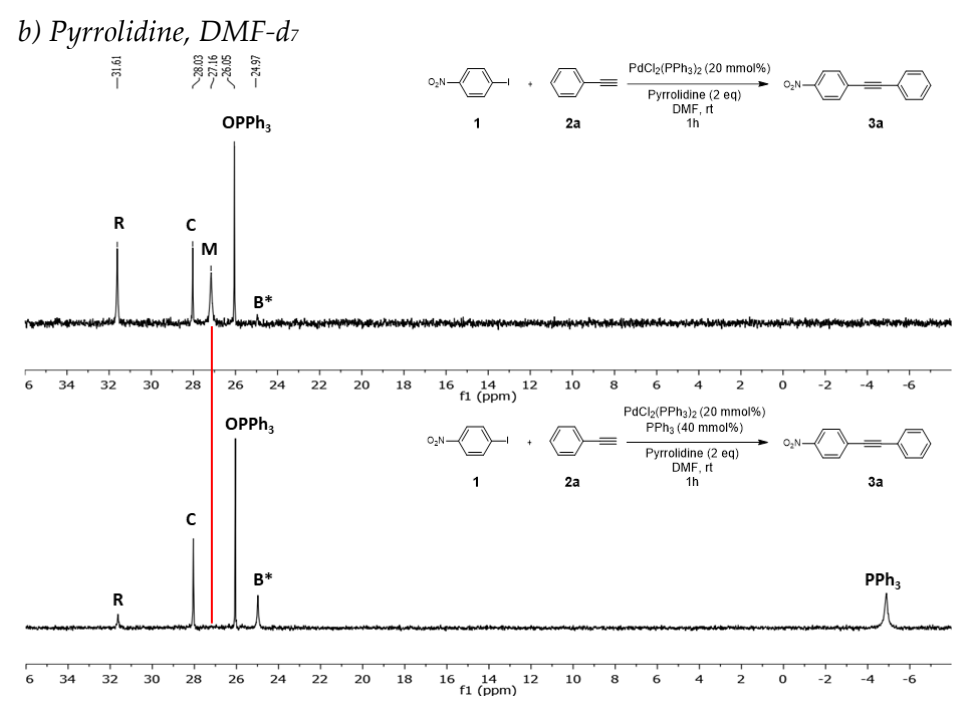


Figure 49. Stacking of <sup>31</sup>P NMR spectra after 1 h of the reaction between **1** and **2a** in DMF-d<sub>7</sub>, with PYR 2 equiv (a); with PYR 2 equiv and 40 mmol% of PPh<sub>3</sub> (b).

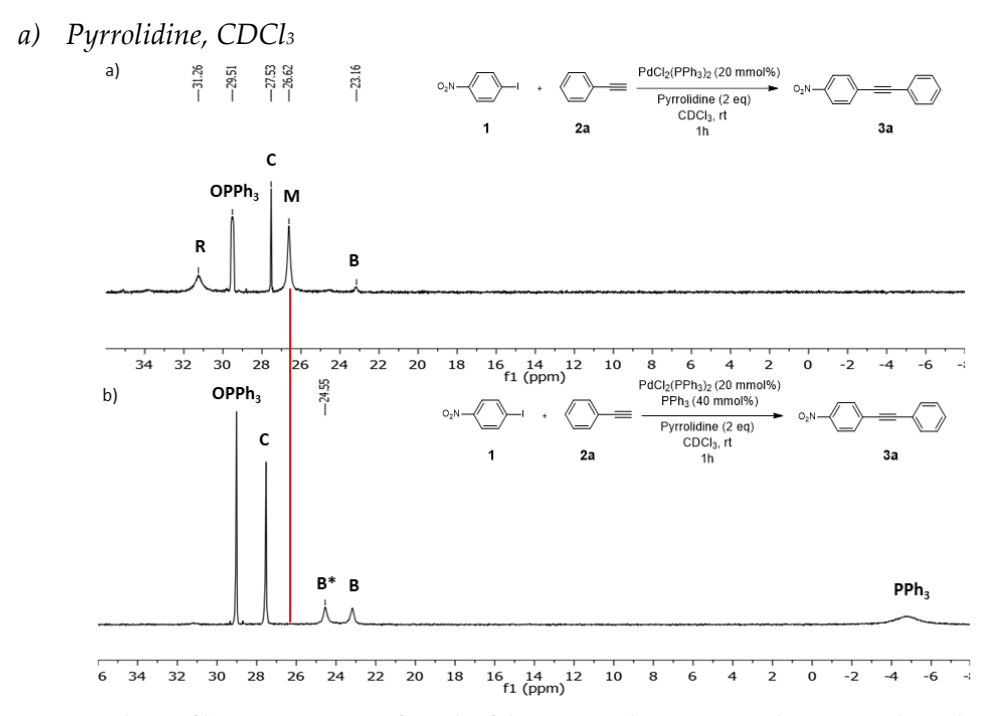


Figure 50. Stacking of  $^{31}$ P NMR spectra after 1 h of the reaction between **1** and **2a** in CDCl<sub>3</sub>, with PYR 2 equiv (a); with PYR 2 equiv and 40 mmol% of PPh<sub>3</sub> (b).

# General procedure for the HCS reaction with Palladium (0)

To an oven-dried 10 mL Schlenk purged under  $N_2$  atmosphere, Tetrakis(triphenylphosphine)palladium(0) (20% mmol) was dissolved in degassed DMF-d<sub>7</sub>. After the addition of 1-Iodo-4-nitrobenzene 1 (124.5 mg, 0.5 mmol, 1 equiv), phenylacetylene 2a (60  $\mu$ L, 0.55, 1.1 equiv) and the base, the reaction mixture was stirred at room temperature. After a given time, the <sup>31</sup>P NMR spectra were collected to detect which species were formed.

### a) TMG, DMF-d7

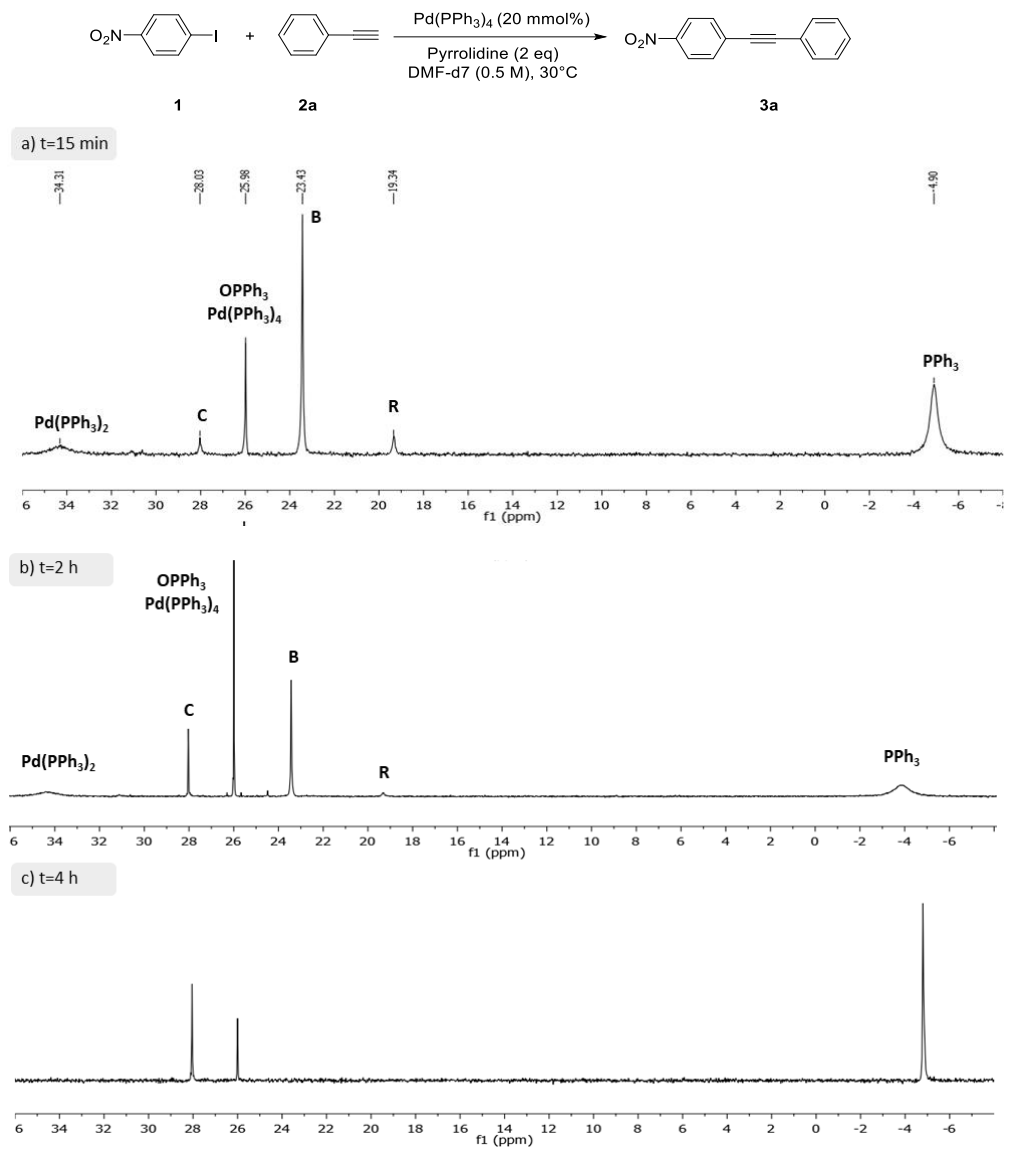


Figure 51. Stacking of <sup>31</sup>P NMR spectra of the reaction between **1** and **2a** in DMF-d<sup>7</sup> using TMG after 15 min (a); 1 h (b); 4 h (c).

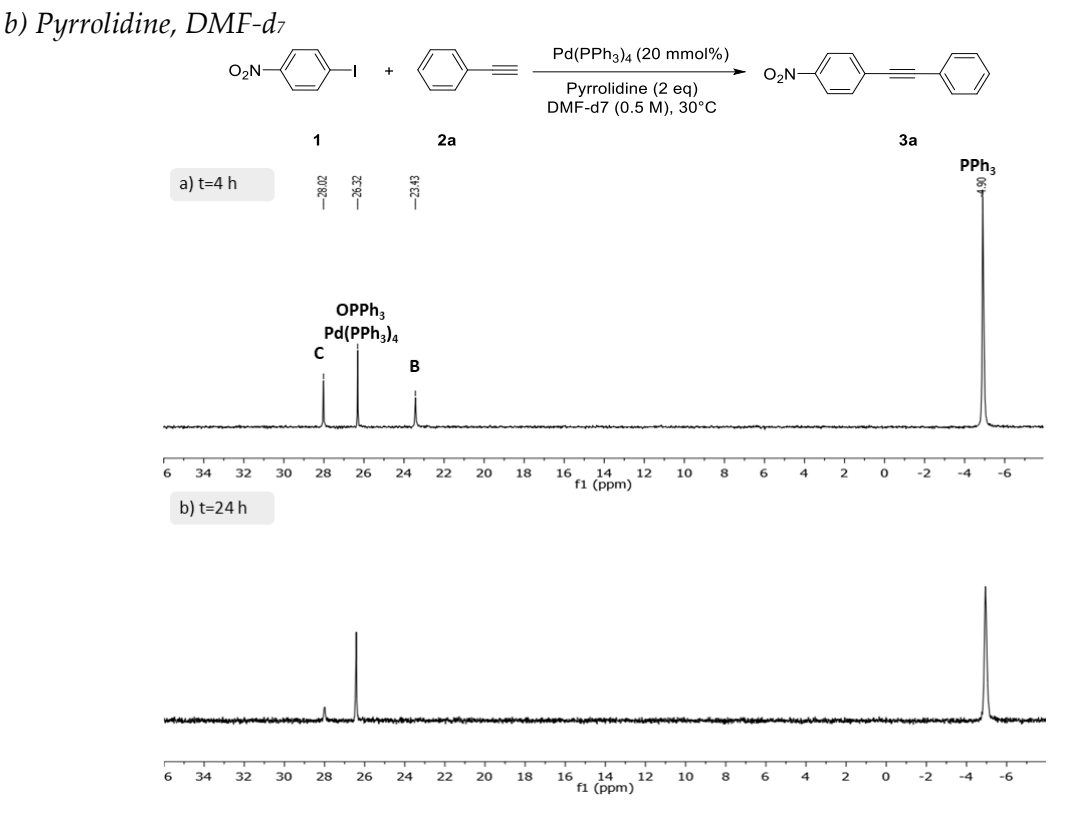


Figure 52. Stacking of  $^{31}P$  NMR spectra of the reaction between 1 and 2a in DMF-d7 using PYR after 4 h (a) and 24 h (b).

#### 2.1.4.7. Direct coordination versus transmetalation

## Procedure for the Transmetalation step:

The reaction was performed in an oven-dried NMR tube purged under nitrogen atmosphere. The complexes  $B_{NO_2}^{I}$  (15.8 mg, 0.018 mmol, 1 equiv) and M (15 mg, 0.0.18 mmol, 1 equiv) were dissolved in CDCl<sub>3</sub> (0.750 mL). The mixture was let at room temperature and monitored by  $^{1}H$  and  $^{31}P$  NMR spectroscopy at intervals of 20 minutes for 7 hours using tert-butyl methyl ether (TBME) as internal standard. The reaction was repeated three times with consistent results. The following NMR spectra belong to one experiment and are given as examples.

$$O_{2}N \xrightarrow{PPh_{3}} P_{0}^{PPh_{3}} + \bigvee_{PPh_{3}} P_{0}^{PPh_{3}} \xrightarrow{TBME} O_{2}N \xrightarrow{PPh_{3}} O_{2}N$$

$$B^{I}_{NO2} M 3_{NO2}$$

# <sup>1</sup>H NMR spectra:

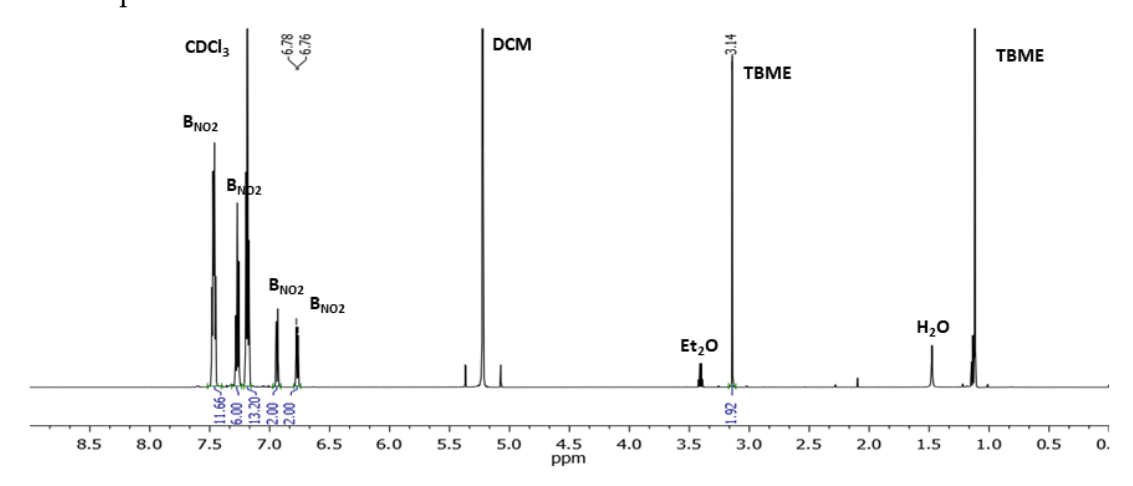


Figure 53.  $^{1}$ H NMR spectrum before the addition of **M** (t=0).

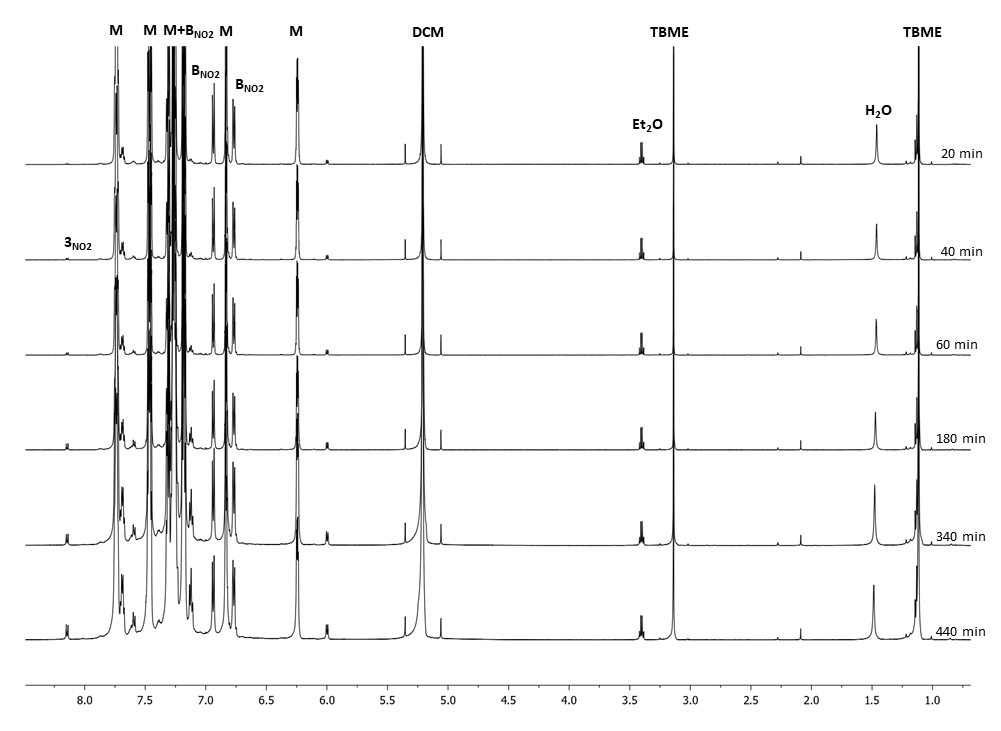


Figure 54. Stacking of  $^1H$  NMR spectra of the stoichiometric reaction between  $B_{NO_2}^{I}$  and M in CDCl $_3$  at several times.

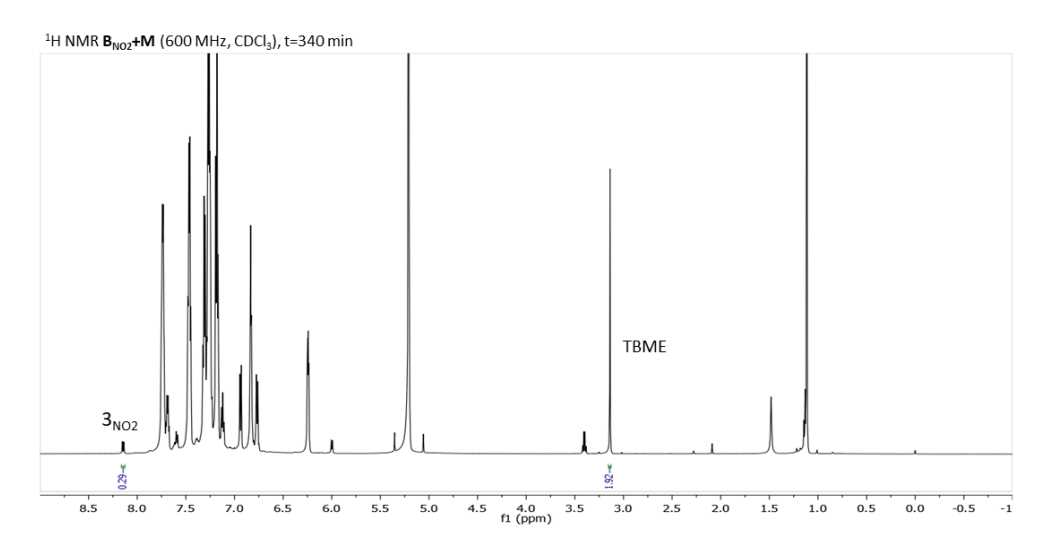


Figure 55.  $^1$ H NMR spectrum of the stoichiometric reaction between  $B_{NO_2}^I$  and M in CDCl3 after 340 min as an example

# <sup>31</sup>P NMR spectra

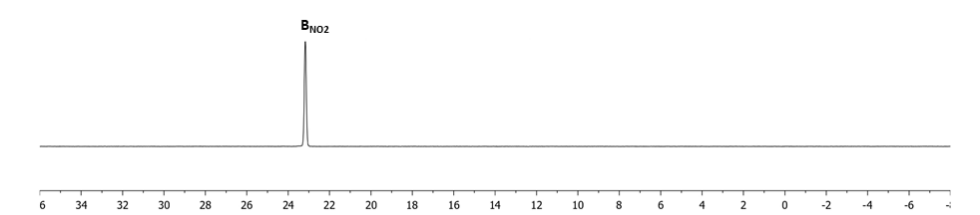


Figure 56. <sup>31</sup>P NMR spectrum before the addition of **M** (t=0).

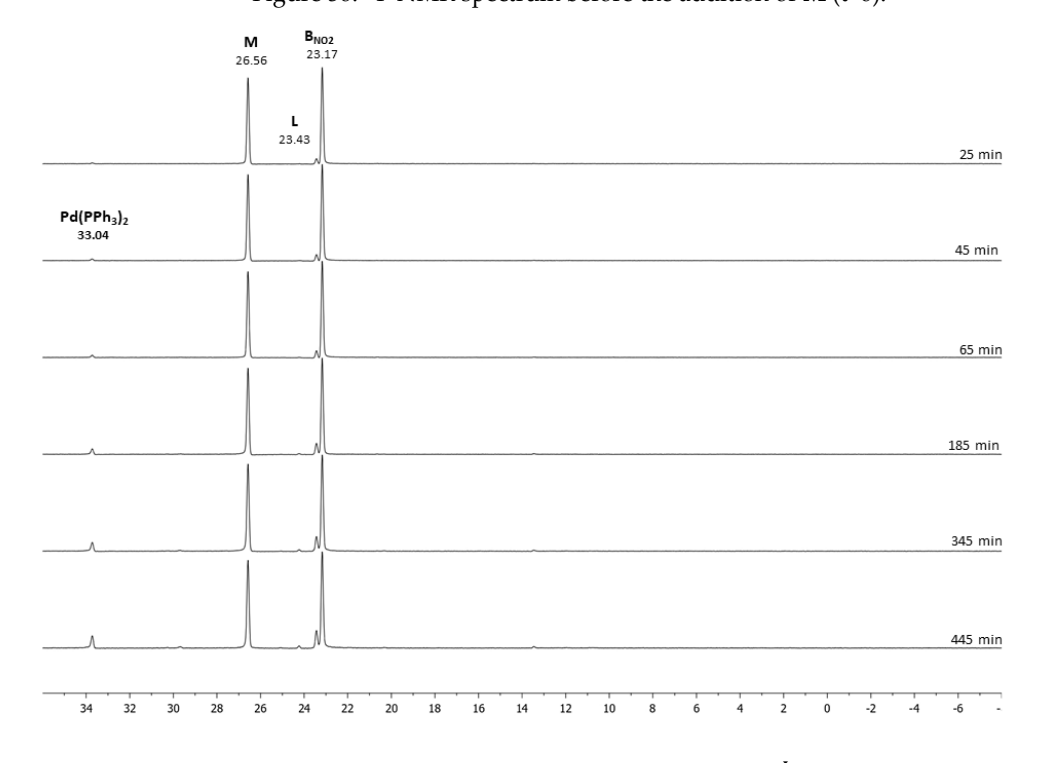


Figure 57. Stacking of  $^{31}P$  NMR spectra of the stoichiometric reaction between  $B^{l}_{NO_{2}}$  and M in CDCl3 at several times

### Procedure for the Direct Coordination step:

The reaction was performed in an oven-dried NMR tube purged under nitrogen atmosphere. The complex  $B^{I}_{NO_2}$  (15.8 mg, 0.018 mmol, 1 equiv) was dissolved in CDCl<sub>3</sub> (0.750 mL), followed by the addition of 2a (29  $\mu$ L from a stock solution of 0.66 M, 0.018 mmol, 1 equiv) and TMG (32.5  $\mu$ L from a stock solution of 0.66 M, 0.02 mmol, 1.1 equiv). TBME (1 equiv) was used as internal standard. The mixture was let at room temperature and monitored by  $^{1}$ H and  $^{31}$ P NMR spectroscopy at intervals of 20 minutes for 7 hours. The reaction was repeated three times with consistent results. The following NMR spectra belong to one experiment and are given as examples.

### <sup>1</sup>H NMR spectra:

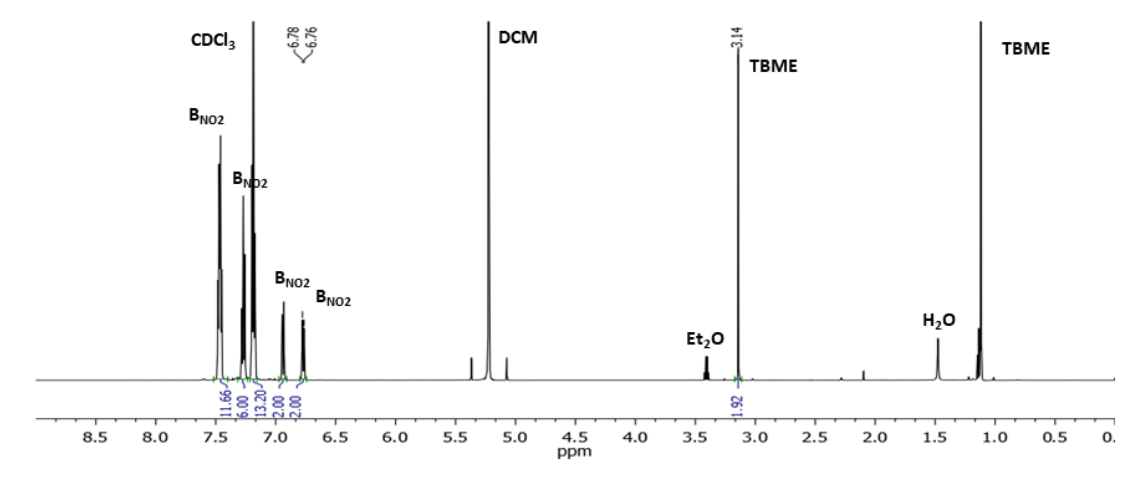


Figure 58. <sup>1</sup>H NMR spectrum before the addition of 2a and TMG (t=0).

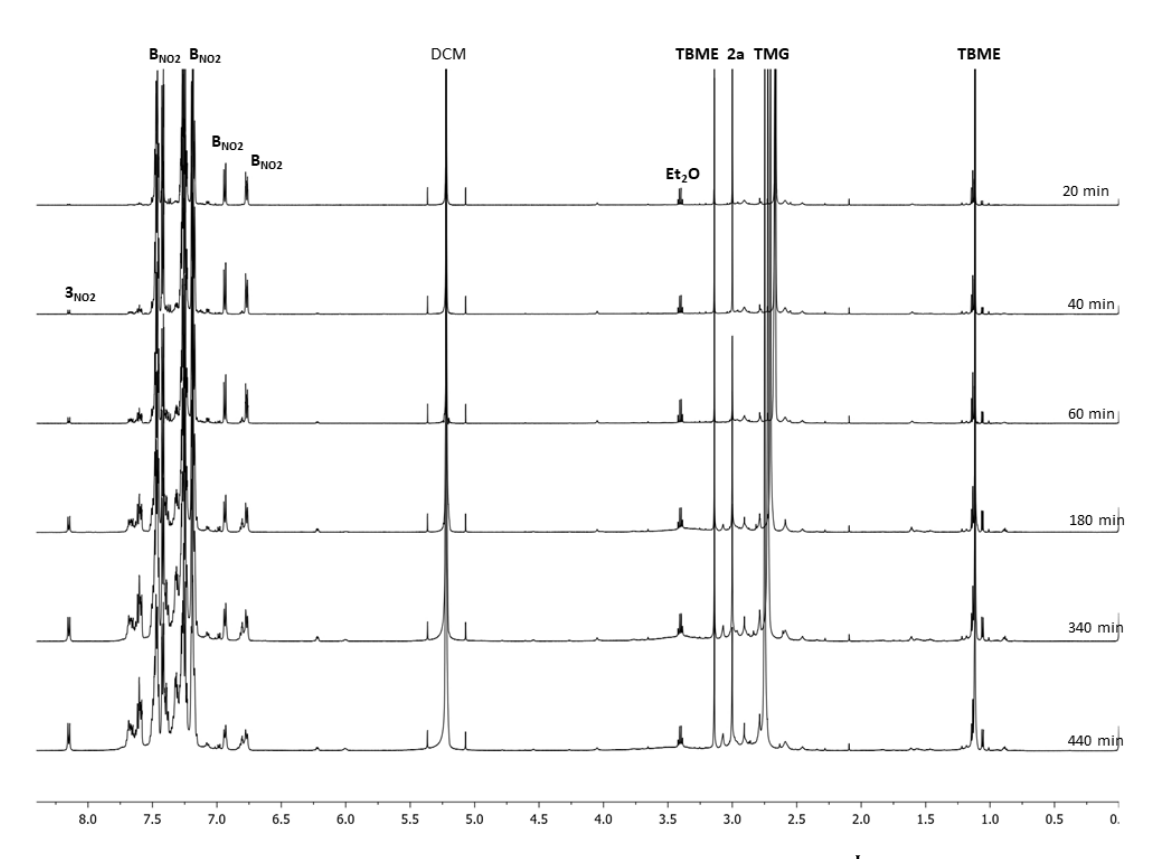


Figure 59. Stacking of  ${}^{1}H$  NMR spectra of the stoichiometric reaction between  $B_{NO_{2}}^{I}$  and 2a with TMG in CDCl $_{3}$  at several times.

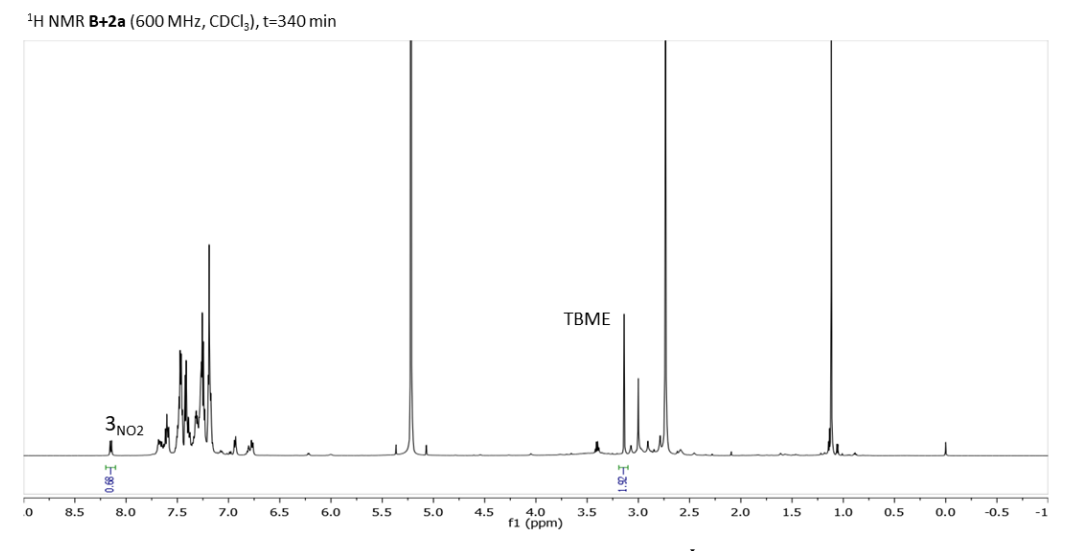


Figure 60.  $^1$ H NMR spectrum of the stoichiometric reaction between  $B_{NO_2}^I$  and 2a in CDCl $_3$  after 340 min as an example.

# <sup>31</sup>P NMR spectra:

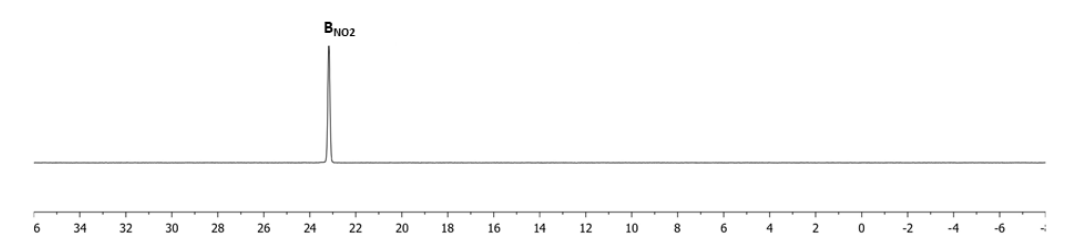


Figure 61. <sup>31</sup>P NMR spectrum before the addition of **2a** and TMG (t=0).

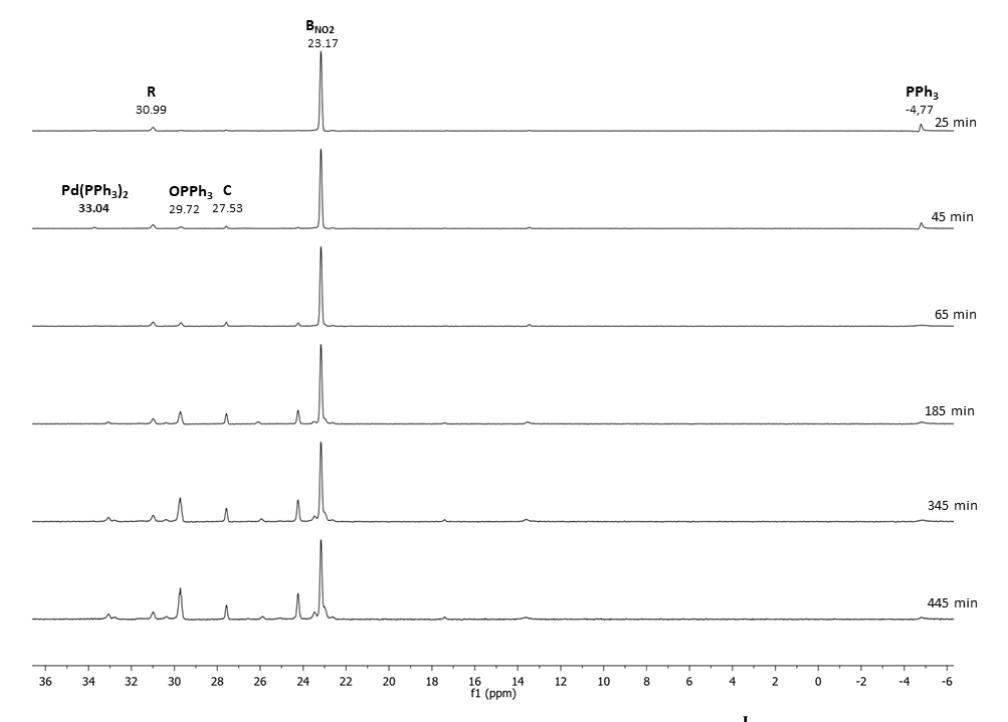


Figure 62. Stacking of  $^{31}P$  NMR spectra of the stoichiometric reaction between  $B_{NO_2}^{I}$  and 2a with TMG in CDCl $_3$  at several times.

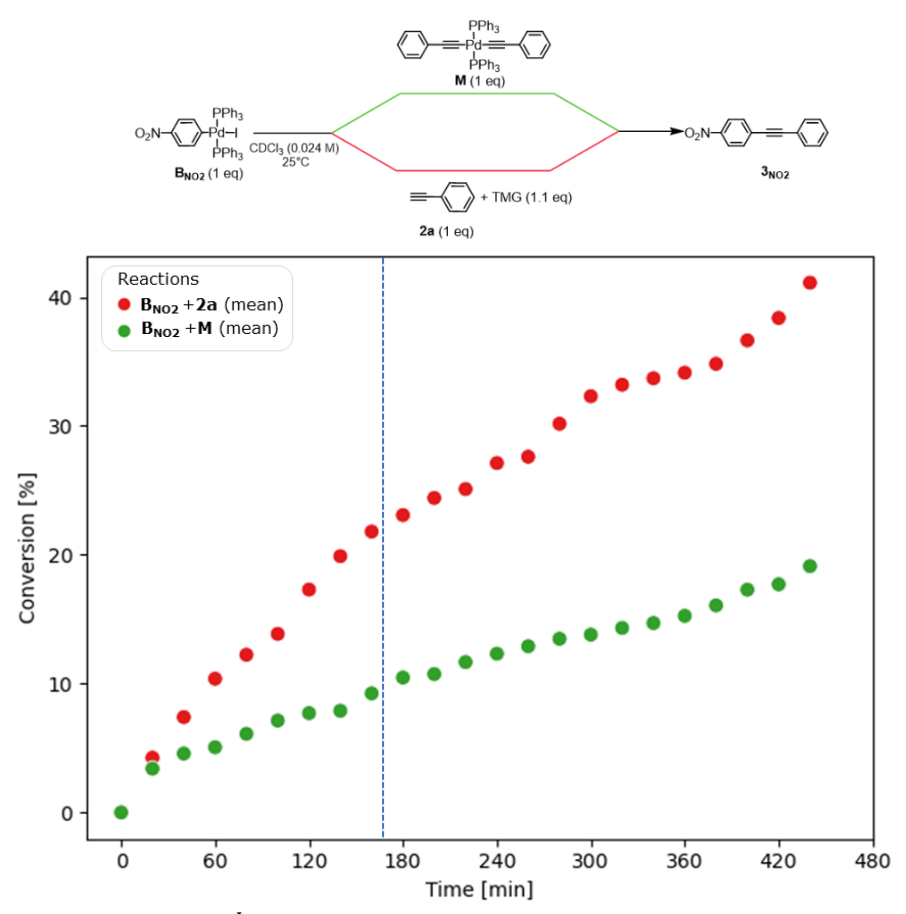


Figure 63. Conversions (%) of  $B_{NO_2}^I$  in product  $3_{NO_2}$  averaged over three experiments every 20 minutes. Reactions between  $B_{NO_2}^I$  and M (green) and  $B_{NO_2}^I$  and 2a (red).

Time [min]	BNO2+M*	BNO2+M**	BNO2+M***	BNO2+M (mean)	error*	emor**	error***	BNO2+2a*	BNO2+2a**	BNO2+2a***	BNO2+2a (mean)	error*	error**	error***
20	3,25	3,19	3,76	3,40	-0,15	-0,21	0,36	4,55	4,11	4,10	4,25	0,30	-0,14	-0,16
40	4,11	4,64	4,97	4,57	-0,46	0,07	0,40	7,68	7,09	7,44	7,40	0,28	-0,31	0,03
60	5,00	4,98	5,21	5,06	-0,06	-0,09	0,15	10,41	9,99	10,76	10,38	0,03	-0,40	0,37
80	6,06	6,09	6,16	6,10	-0,04	-0,02	0,06	12,45	11,86	12,42	12,24	0,20	-0,38	0,18
100	7,17	7,15	7,07	7,13	0,04	0,02	-0,06	13,19	12,82	13,77	13,26	-0,07	-0,44	0,51
120	7,57	7,90	7,66	7,71	-0,14	0,19	-0,05	17,54	17,43	16,94	17,30	0,24	0,13	-0,37
140	7,92	7,88	7,89	7,89	0,02	-0,02	0,00	20,36	19,82	19,49	19,89	0,47	-0,07	-0,40
160	9,37	9,21	9,13	9,24	0,13	-0,03	-0,11	21,94	21,79	21,69	21,80	0,13	-0,01	-0,12
180	10,95	10,49	9,97	10,47	0,48	0,02	-0,50	23,10	23,02	23,12	23,08	0,02	-0,06	0,04
200	10,87	10,63	10,73	10,74	0,13	-0,12	-0,01	24,72	24,21	24,30	24,41	0,31	-0,20	-0,11
220	11,71	11,75	11,57	11,67	0,03	0,08	-0,11	25,25	25,08	24,98	25,10	0,15	-0,03	-0,13
240	12,37	12,34	12,24	12,32	0,05	0,02	-0,07	27,20	27,47	26,71	27,12	0,07	0,34	-0,41
260	12,71	13,14	12,84	12,90	-0,19	0,24	-0,06	27,50	27,92	27,43	27,61	-0,12	0,31	-0,19
280	13,59	13,50	13,36	13,48	0,11	0,02	-0,12	30,20	30,29	30,02	30,17	0,03	0,12	-0,15
300	13,75	13,94	13,70	13,80	-0,05	0,14	-0,10	32,08	32,94	31,91	32,31	-0,23	0,63	-0,40
320	14,33	14,36	14,27	14,32	0,01	0,04	-0,05	33,35	33,12	33,15	33,20	0,15	-0,09	-0,06
340	14,76	14,62	14,73	14,70	0,06	-0,09	0,02	33,64	33,58	33,89	33,70	-0,06	-0,12	0,18
360	15,16	15,44	15,18	15,26	-0,10	0,18	-0,08	34,19	33,99	34,21	34,13	0,06	-0,14	0,08
380	16,16	16,21	15,85	16,07	0,09	0,13	-0,22	35,12	34,82	34,53	34,82	0,30	0,00	-0,30
400	17,31	17,28	17,28	17,29	0,02	-0,01	-0,01	36,96	36,64	36,33	36,64	0,32	0,00	-0,32
420	17,80	17,65	17,68	17,71	0,09	-0,06	-0,03	38,23	38,44	38,47	38,38	-0,15	0,06	0,09
440	19,30	19,10	18,95	19,12	0,18	-0,02	-0,17	40,45	41,67	41,23	41,12	-0,66	0,55	0.11

Figure 64. Errors of each measurement calculated by the difference between the average and calculated value of the conversion at the same time. Reactions between  $B^I_{NO_2}$  and M (green) and  $B^I_{NO_2}$  and 2a (red).

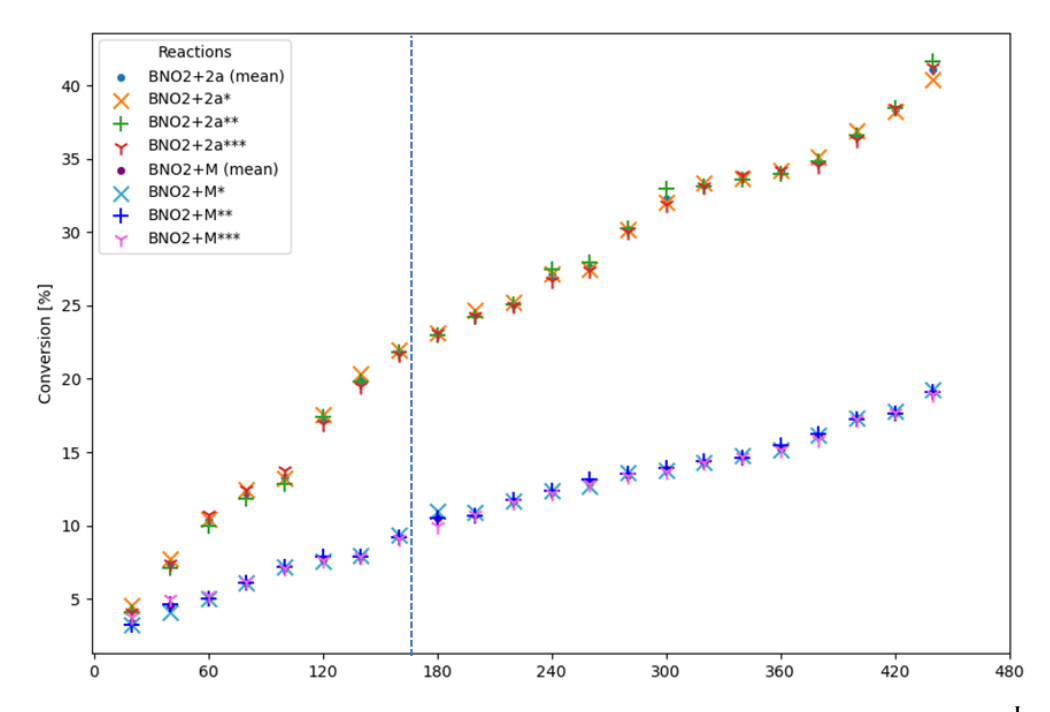
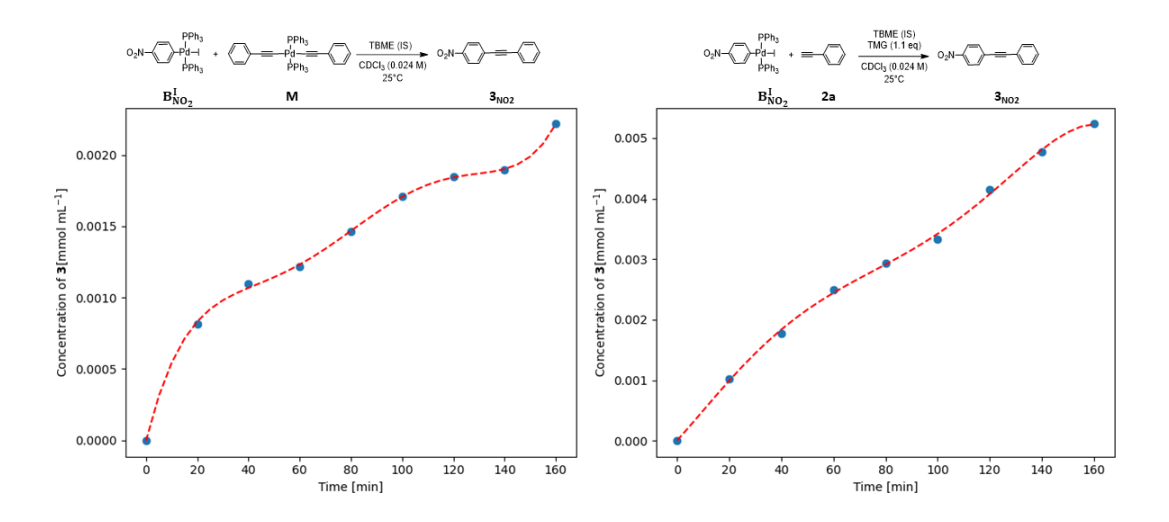


Figure 65. Values of conversions (%) every 20 minutes of reactions repeated three times between  $B_{NO_2}^I + M$  and  $B_{NO_2}^I + 2a$ .

### 2.1.4.8. Evaluation of the reaction rate

The concentration of the product **3** was calculated was calculated from the average conversion (%) obtained by the <sup>31</sup>P nmr spectra reported above. The value of maximum rate was determined by considering the range 0-160 min., because after this time side reactions start to occur. Experimental data were fitted using the curve\_fit function of the free and open-source Python library SciPy. The reaction rates were calculated in each point obtaining the derivative with the polymer function of the open-source Python library NumPy.



c(3 <sub>NO2</sub> )= A <sub>0</sub> + A <sub>1</sub>	$t^{1} + A_{2} t^{2} + A_{3} t^{3} + A_{4} t^{4} + A_{5} t^{5}$	Time [min]	B+M	B+2a	$c(3_{NO2}) = A_0 + A_1 t^1 + A_2 t^2 + A_3 t^3 + A_4 t^4 + A_5 t^5$
$A_0 = 0.000125$				5,20E-05	$A_0 = 1,99 E-05$
0 ,				4,32E-05	
A <sub>1</sub> = 3,01 E-05				3,66E-05	A <sub>1</sub> = 5,20 E-05
A <sub>2</sub> =-2,44 E-07				3,19E-05 2,85E-05	A <sub>2</sub> = -2,53 E-07
A <sub>3</sub> = 1,29 E-09				2,61E-05	A <sub>3</sub> = 1,16 E-09
J ,				2,44E-05	· ,
A <sub>4</sub> = -3,17 E-12		140	8,47E-06	2,31E-05	A <sub>4</sub> = -2,88 E-12
A <sub>5</sub> = 2,87 E-15	ν <sub>MAX (t=0)</sub> = 3,01 E-05 mmol mL <sup>-1</sup> min <sup>-1</sup>	160	8,71E-06	2,20E-05	$A_5 = 2,72 \text{ E-}15$ $v_{\text{MAX (t=0)}} = 5,20 \text{ E-}05 \text{ mmol}$
		fast		slow	

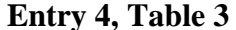
Figure 66. Concentration of  $3_{N0_2}$  calculated at several times within 160 minutes in the reaction between  $B_{N0_2}^I$  + M (left) and  $B_{N0_2}^I$  + 2a (right). The maximum rate and the point at which the rate is highest were obtained by fitting the values and finding the derivatives.

The same experiments and calculations were carried out for kinetic study for the reactions  $B_{Me}^{I} + M$  and  $B_{Me}^{I} + 2a$  with pyrrolidine as base in CDCl<sub>3</sub>, in order to reproduce exactly the experiments performed by Košmrlj et al<sup>[187]</sup>. The results are presented in Figure 28.

### 2.1.4.9. The stability of complex M

To an oven-dried NMR tube purged under nitrogen atmosphere, complex **M** was dissolved in CDCl<sub>3</sub> and DMF-d<sub>7</sub>(0.75 mL) at room temperature and at 60° C. TBME was used as internal standards. After 30 minutes of stirring, the samples were analysed using <sup>1</sup>H NMR, <sup>31</sup>P NMR, HPLC-UV or GC-MS techniques. The results have already been reported in *Results and Discussion* in Table 3.

The evaluation of the complex  $\mathbf{M}$  stability in DMF-d<sub>7</sub> at 40°C after 30 minutes is reported below as an example.



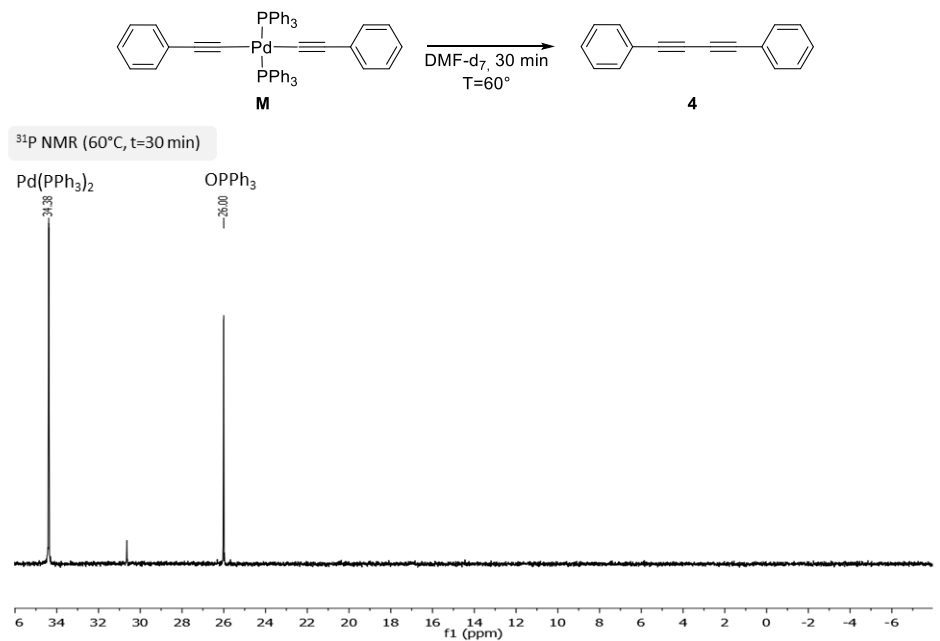


Figure 67. <sup>31</sup>P NMR spectrum of M in DMF-d<sub>7</sub> at t=60°C after 30 minutes.

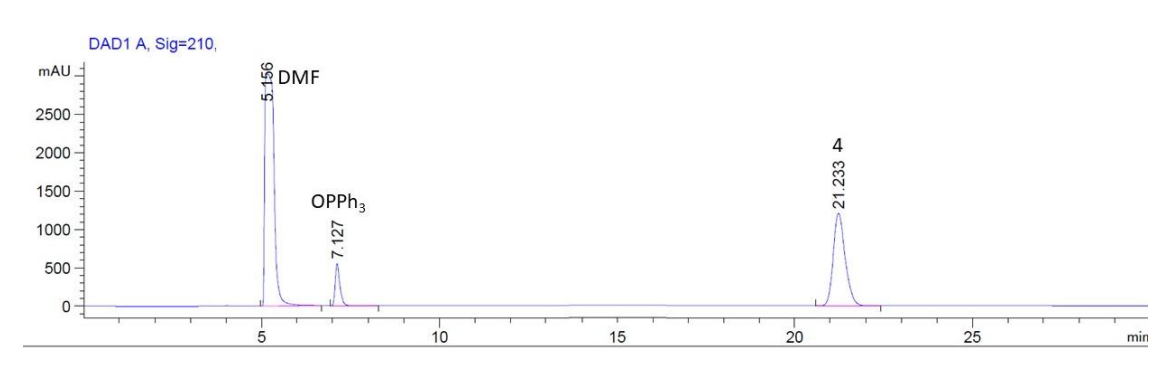


Figure 68. HPLC chromatogram of complex M at 60°C in DMF-d<sub>7</sub> after 30 minutes; peak at 5.156 min = DMF; peak at 7.127 min = OPPh<sub>3</sub>; peak at 21.233 min = 4

### 2.1.4.10. Simultaneous competition reaction

#### General Procedure:

To an oven-dried 10 mL Schlenk purged under N<sub>2</sub> atmosphere, AO-complex (0.05 mmol, 1 equiv), **M** (43.9 mg, 0.05 mmol, 1 equiv), and **2b** were dissolved in the solvent (0.375 mL). After the addition of the base (0.1 mmol, 2 equiv), the reaction was stirred for 1 h and monitored by HPLC-MS and GC-MS technique. The results have been previously reported in *Results and Discussion* in Table 4.

The reaction between  $B_{NO_2}^I + M + 2b$  in CDCl<sub>3</sub> at 25°C with TMG (entry 1, Table 4) and  $B_{NO_2}^I + M + 2b$  in DMF-d<sub>7</sub> at 40°C with TMG (entry 7, Table 4) are reported below as examples.

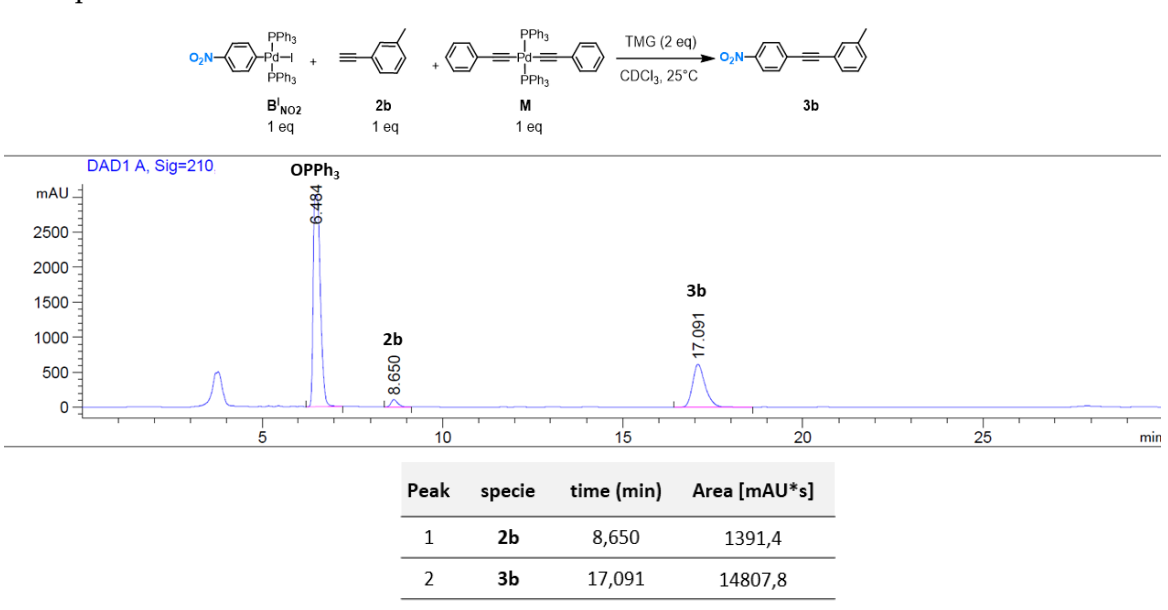


Figure 69. HPLC chromatogram of  $\mathbf{B_{NO_2}^l}$  (1 equiv) +  $\mathbf{2b}$  (1 equiv) +  $\mathbf{M}$  (1eq) with TMG in CDCl<sub>3</sub> at 25°C. Peak at 6.484 min = OPPh<sub>3</sub>, peak at 8.650 min =  $\mathbf{2b}$ ; peak at 17.091 min =  $\mathbf{3b}$ . Calculated conversion (RRF=3.96) of  $\mathbf{2b}$  into  $\mathbf{3b}$  = 73%.

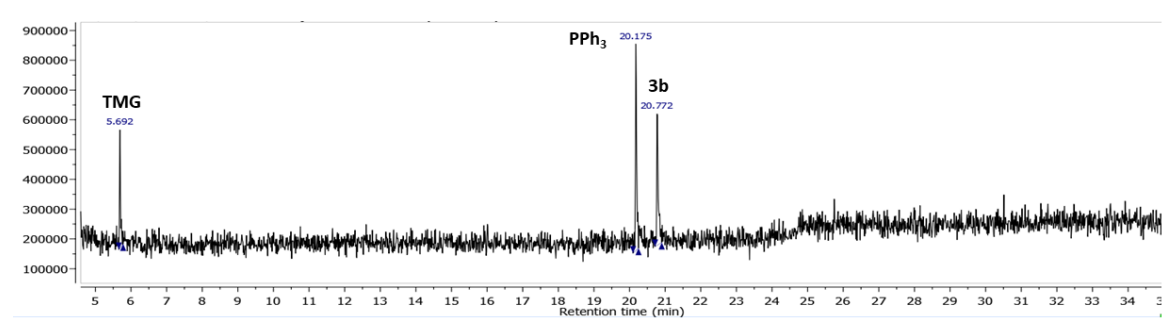


Figure 70. GC chromatogram of  $\mathbf{B_{NO_2}^I}$  (1 equiv) +  $\mathbf{2b}$  (1 equiv) +  $\mathbf{M}$  (1 equiv) with TMG in CDCl<sub>3</sub> at 25°C. Peak at 5.692 min = TMG, peak at 20.175 min PPh<sub>3</sub> and peak at 20.772 min =  $\mathbf{3b}$ .

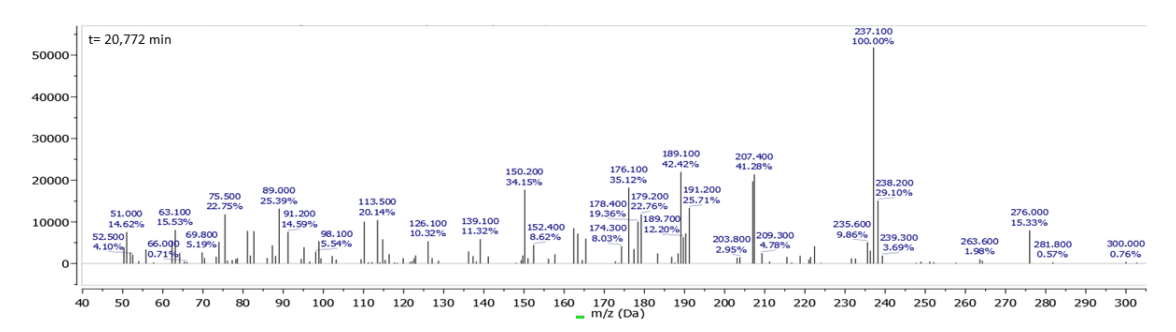


Figure 71. Mass spectrum of 3b (Exact Mass= 237.08 g mol-1 t=21.26 min)

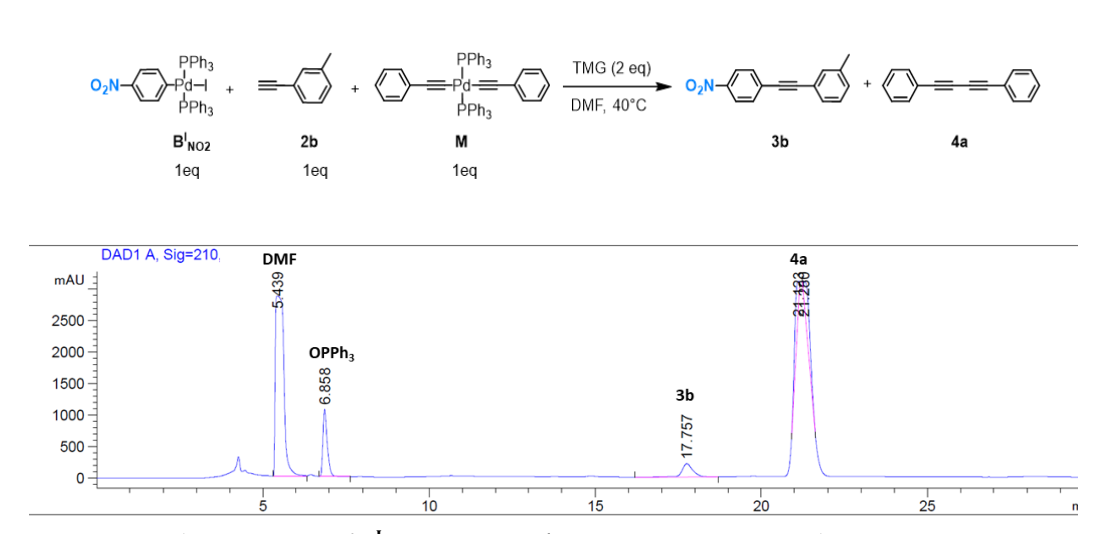


Figure 72. HPLC chromatogram of  $\mathbf{B_{NO_2}^I}$  (1 equiv) +  $\mathbf{2b}$  (10 equiv) +  $\mathbf{M}$  (1eq) with TMG in DMF at 40°C. Peak at 5.439 min = DMF, peak at 6.858 min = OPPh<sub>3</sub>, peak at 17.757 min=  $\mathbf{2b}$  and peak at 21.268 min =  $\mathbf{4a}$ .

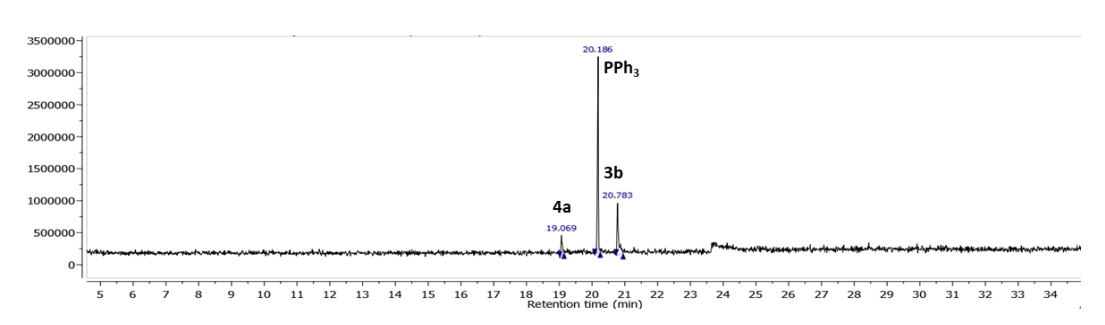


Figure 73. GC chromatogram of  $\mathbf{B_{NO_2}^I}$  (1 equiv) +  $\mathbf{2b}$  (1 equiv) +  $\mathbf{M}$  (1eq) with TMG in DMF at 40°C. Peak at 19.069 min =  $\mathbf{4a}$ , peak at 20.186 min =  $\mathbf{PPh_3}$  and peak at 20.783 min =  $\mathbf{3b}$ 

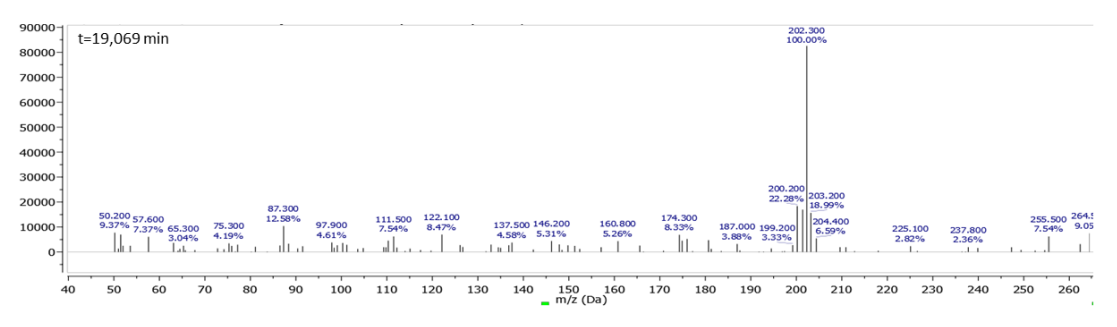


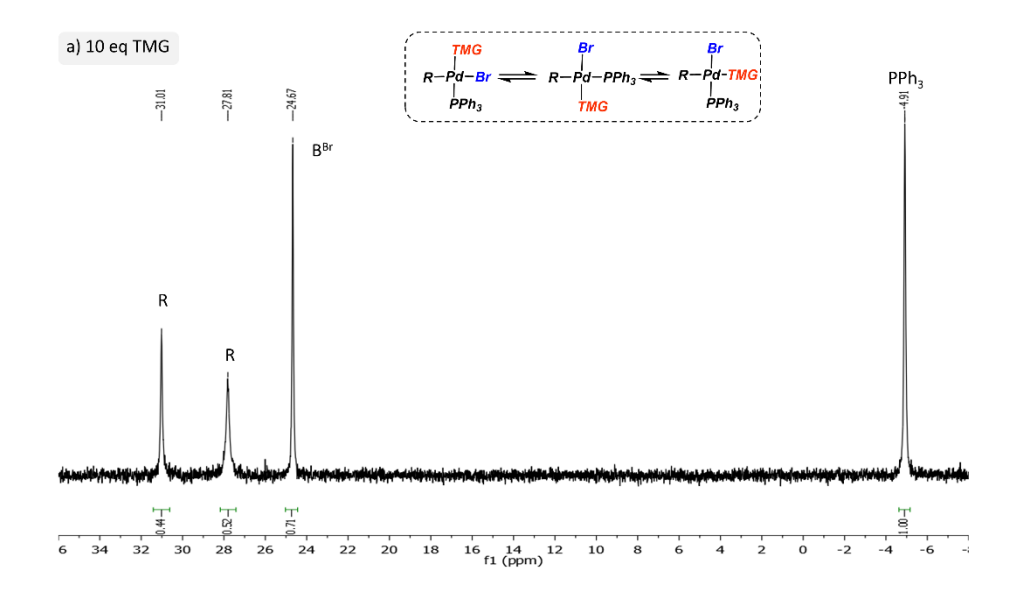
Figure 74. Mass spectrum of 4a (Exact Mass= 202.08 g mol<sup>-1</sup>t=19.069 min)

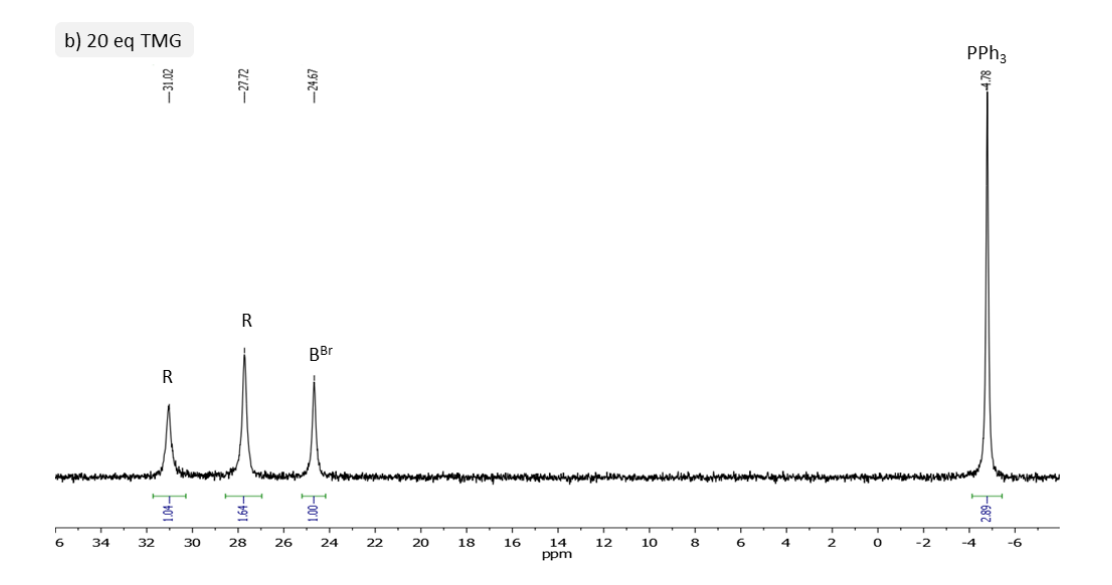
### 2.1.4.11. Base effect on AO-complex Byx

#### General Procedure:

The reaction was performed in an oven-dried NMR tube purged under nitrogen atmosphere. The complex  $\mathbf{B_y^x}$  (0.026 mmol, 1 equiv) was dissolved in DMF-d<sub>7</sub> (0.60 mL) followed by the addition of the TMG, PYR and TEA (10-20-50 equiv). The base effect was evaluated using <sup>31</sup>P NMR technique. The spectra were collected as soon as after the addition and after 30 minutes, but the provided the same results.  $\mathbf{B_y^x}$  stands for X=I, Br, Cl, OTf and y=NO<sub>2</sub>, Me. The results have been reported above in *Results and Discussion* in Table 5.

The TMG (10-20-50 equiv) effect on  $\mathbf{B_{NO_2}^I}$  in DMF-d<sub>7</sub> is reported below as an example to show the formation of complexes  $\mathbf{R}$ . After the addition of TEA, the spectrum was the same before and after the addition of the base.





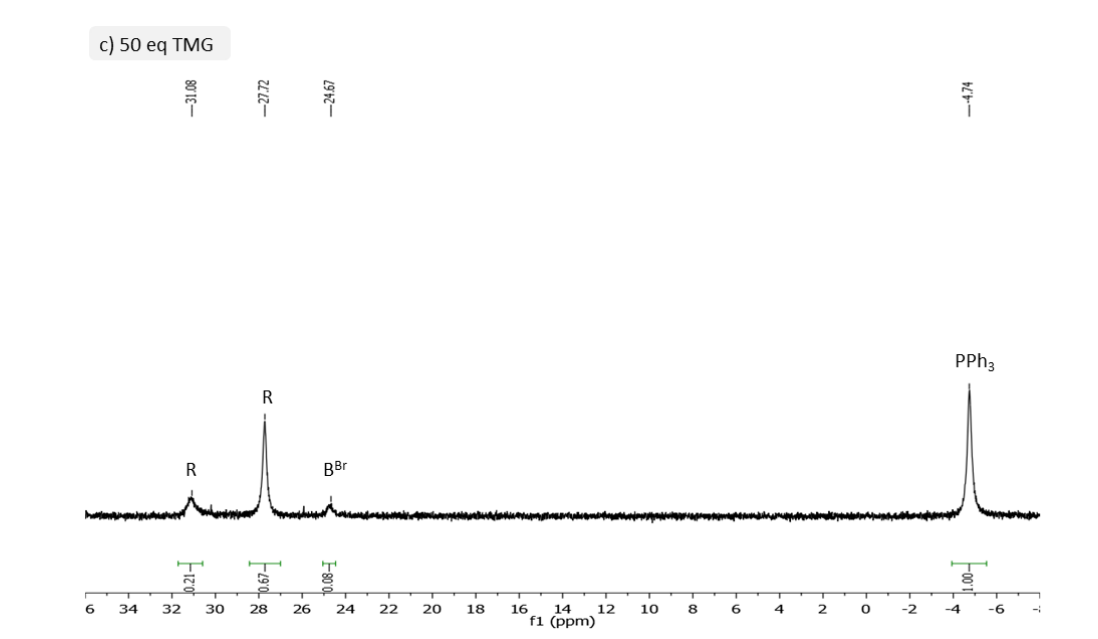


Figure 75.  $^{31}$ P NMR spectra in DMF-d<sub>7</sub> of  $\mathbf{B_{NO_2}^{Br}}$  with TMG 10 equiv (a); TMG 20 equiv (b) and TMG 50 equiv (c).

#### 2.1.4.12. Evaluation of the kinetic constants

# General procedure<sup>[196]</sup>

The equilibrium constant Keq=[Ligand ][ $\Sigma R$ ]/[B][base] was determined in DMF-d<sub>7</sub> by <sup>31</sup>P NMR spectroscopy.

To evaluate Keq for the compounds  $\mathbf{B}_{\mathbf{y}}^{\mathbf{Br}}$  and  $\mathbf{B}_{\mathbf{y}}^{\mathbf{Cl}}$ , the amine was added in the range of 10-50 equivalents, whereas the amount of base was lowered in case of  $\mathbf{B}_{\mathbf{y}}^{\mathbf{l}}$ , due to the high tendency to produce  $\mathbf{R}$ . By considering [Ligand]=[ $\Sigma \mathbf{R}$ ], the formula becomes  $Keq = x^2/(1-x)(n-x)$  where n is the number of equivalents of base added to  $\mathbf{B}$ , x is the molar fraction of  $\mathbf{R}$  in the equilibrium  $x=2z_{\rm L}/(z_{\rm B}+2z_{\rm L})$  and  $z_{\rm L}$  and  $z_{\rm B}$  are the magnitude of the ligand and  $\mathbf{B}$  respectively. Keq was determined from the slope of the straight line obtained by the plot of  $x^2$  versus (1-x)(n-x). All experiments were repeated three times and carried out with  $\mathbf{B}_{\mathbf{y}}^{\mathbf{x}}$  with  $x=\mathbf{I}$ ,  $\mathbf{Cl}$ ,  $\mathbf{Br}$ ,  $\mathbf{OTf}$ ,  $\mathbf{y}=\mathbf{NO}_2$ ,  $\mathbf{Me}$  and  $\mathbf{PYR}$  and  $\mathbf{TMG}$  as bases (Table 5). Determination of the equilibrium constant between  $\mathbf{ArPdBr}(\mathbf{PPh}_3)\mathbf{2}$  and  $\mathbf{ArPdBr}(\mathbf{PPh}_3)\mathbf{TMG}$  is reported below as an example.

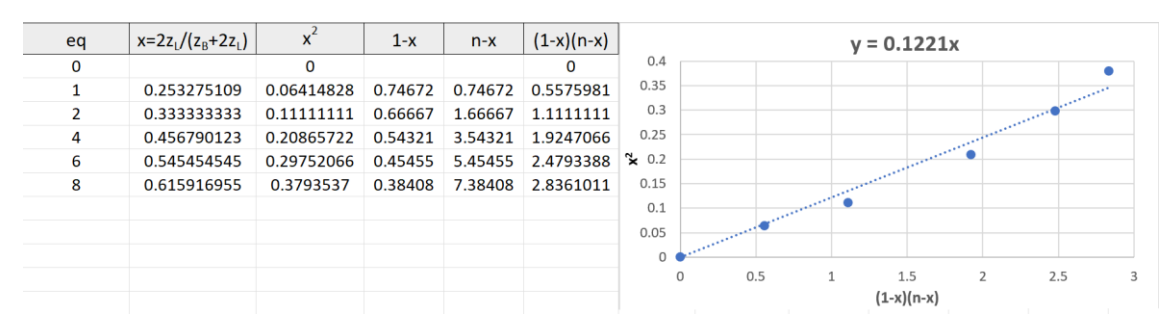


Figure 76. Determination of the equilibrium constant between ArPdBr(PPh3)2 and ArPdBr(PPh3)TMG (Entry 5, Table 5). Keq=0.122

### 2.1.4.13. The Addition of phenylacetylene and Scope

### General procedure 1:

The reaction was performed in an oven-dried NMR tube purged under nitrogen atmosphere. The complex  $\mathbf{B_{NO_2}^X}$  (0.026 mmol, 1 equiv) was dissolved in DMF-d<sub>7</sub> (0.60 mL) followed by the addition of the base (20-50 equiv). The <sup>31</sup>P NMR were collected as soon as after the addition of **2a** (20-50 equiv) and after 10 minutes. The investigation was performed with Pyr, TMG and TEA as bases. The addition of the alkyne (20 equiv) to  $\mathbf{B_{NO_2}^{Br}}$  and  $\mathbf{B_{NO_2}^{OTf}}$  have already been reported as an example in *Results and Discussion* in Figure 31a-b respectively.

*General Procedure 2:* The reaction was performed in an oven-dried Schlenk purged under  $N_2$  atmosphere. The complex  $B_{NO_2}^{Br}$  (21.6 mg, 0.026 mmol, 1 equiv) was dissolved in DMF-d<sub>7</sub> (0.60 mL) followed by the addition of TMG (65 μL, 0.52 mmol, 20 equiv). The <sup>31</sup>P NMR were collected as soon as after the addition of **2a-l** (0.052 mmol, 20 equiv). After **24h** of stirring, the mixture was quenched with H<sub>2</sub>O (1 mL) and extracted with cyclohexane or ethyl acetate (3x1 mL, ethyl acetate was used to extract product with hydroxyl group). Then, the collected organic phases were washed with brine, dried over anhydrous sodium sulfate (Na<sub>2</sub>SO<sub>4</sub>) and concentrated under reduced pressure. Finally, the crude was purified by flash chromatography (Figure 33).

### 1-nitro-4-(phenylethynyl)benzene (3a)

Yellow solid; Purification by flash chromatography (Cy 100%)

<sup>1</sup>H NMR (400 MHz, CDCl<sub>3</sub>): 
$$\delta$$
 (ppm) 8.19 – 8.17 (d, J = 9.0 Hz, 2H), 7.64 – 7.62 (d, J = 9.0 Hz, 2H), 7.56 – 7.53 (m, 2H), 7.38 – 7.36 (m, 3H).

<sup>13</sup>C NMR (100.8 MHz, CDCl<sub>3</sub>): δ (ppm) 146.95, 132.27, 131.84, 130.22, 129.28, 128.57, 123.58, 122.10, 94.75, 87.59.

### 1-Methyl-3-(4-nitrophenyl)benzene (3b)

Yellow solid; Purification by flash chromatography (Cy 100%)

<sup>1</sup>H NMR (400 MHz, CDCl<sub>3</sub>): 
$$\delta$$
 (ppm) 8.23-8.20 (d, J= 9 Hz, 2H);

7.66-7.64 (d, J= 9 Hz, 2H); 7.39-7.36 (m, 1H); 7.30-7.28 (m, 1H);

7.22-7.20 (m, 1H), 2.38 (s, 3H).

<sup>13</sup>C NMR (100.8 MHz, CDCl<sub>3</sub>): δ (ppm)147.02, 138.42, 132.52, 132.36, 130.33, 129.07, 128.57, 125.92, 123.76, 122.54, 122.01, 95.12, 87.38, 21.38.

### 1-Methoxy-4-((4-nitrophenyl)ethynyl)benzene (3c)

O<sub>2</sub>N—OMe Yellow solid; Purification by flash chromatography (Cy/EtOAc 95/5)

3c ¹H NMR (400 MHz, CDCl₃): δ (ppm) 8.22-8.20 (d, J= 9 Hz, 2H); 7.64-7.62 (d, J= 9 Hz, 2H); 7.51-7.49 (d, J=8.9 Hz, 2H), 6.92-6.90 (d, J=8.9 Hz, 2H); 3.85 (s, 3H)

<sup>13</sup>C NMR (100.8 MHz, CDCl<sub>3</sub>): δ (ppm) 160.54, 146.81, 133.59, 132.13, 130.84, 123.78, 114.35, 95.28, 86.78, 55.52.

### 1-Chloro-3-((4-nitrophenyl)ethynyl)benzene (3d)

Yellow solid; Purification by flash chromatography (Cy/EtOAc 90/10)

3d <sup>Cl</sup> <sup>1</sup>H NMR (400 MHz, CDCl<sub>3</sub>): δ (ppm) 8.24-8.22 (d, J= 8.8 Hz, 2H); 7.67-6.65 (d, J= 8.8 Hz, 2H); 7.54 (s, 1H); 7.45-7.43 (m, 2H) 7.38-7.30 (m, 2H).

<sup>13</sup>C NMR (100.8 MHz, CDCl<sub>3</sub>): δ (ppm) 147.33, 134.54, 132.51, 131.78, 130.07, 129.91, 129.77, 129.65, 123.92, 123.82, 93.09, 88.61

### 3-methyl-1-(4-nitrophenyl)dodec-1-yn-3-ol (3e)

Orange oil; Purification by flash chromatography (Cy/EtOAc 90/10)

<sup>1</sup>H NMR (400 MHz, CDCl<sub>3</sub>)  $\delta$  (ppm) 8.20 – 8.18 (d, J = 9.0

Hz, 2H), 7.57 - 7.55 (d, J = 9.0 Hz, 2H), 1.80 - 2.75 (m, 2H),

1.50 (s, 3H), 1.32 – 1.28 (m, 14H), 0.90 – 0.87 (m, 3H).

<sup>13</sup>C NMR (100.8 MHz, CDCl<sub>3</sub>) δ (ppm) 146.99, 132.36, 129.78, 123.50, 98.51, 83.12, 81.49, 68.67, 67.37, 43.53, 29.65, 29.53, 29.42, 29.27, 24.69, 22.64, 14.08

#### 1-(hept-1-yn-1-yl)-4-nitrobenzene (3f)

<sup>13</sup>C NMR (100.8 MHz, CDCl<sub>3</sub>) δ (ppm) 147.25, 132.39, 129.41, 123.57, 92.46, 83.81, 51.49.

### 2-methyl-4-(4-nitrophenyl)but-3-yn-2-ol (3g)

 $O_2N$  Yellow solid; Purification by flash chromatography (Cy/EtOAc 90/10)

 $_{3g}$   $^{1}H$  NMR (400 MHz, CDCl<sub>3</sub>)  $\delta$  (ppm) 8.20 – 8.18 (d, J = 9.0 Hz, 2H), 7.58 – 7.56 (d, J = 9.0 Hz, 2H), 1.65 (s, 3H).

<sup>13</sup>C NMR (100.8 MHz, CDCl<sub>3</sub>) δ (ppm) 147.02, 132.34, 129.70, 123.46, 99.08, 80.38, 65.61, 31.20.

**CHAPTER 2** 

## 1-((4-nitrophenyl)ethynyl)cyclohexan-1-ol (3h)

$$O_2N$$

White solid; Purification by flash chromatography (Cy/EtOAc 90/10)

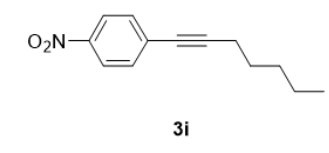
3h

<sup>1</sup>H NMR (400 MHz, CDCl<sub>3</sub>)  $\delta$  (ppm) 8.19 – 8.17 (d, J = 9.0 Hz, 2H), 7.58 – 7.56 (d, J = 9.0 Hz, 2H) 2.19 (s, 1H), 2.04 – 2.03 (m, 2H), 1.78

-1.55 (m, 8H).

<sup>13</sup>C NMR (100 MHz, CDCl<sub>3</sub>) δ (ppm) 147.02, 132.70, 129.81, 123.55, 98.29, 82.54, 69.12, 39.74, 25.04, 23.25

### 1-(hept-1-yn-1-yl)-4-nitrobenzene (3i)

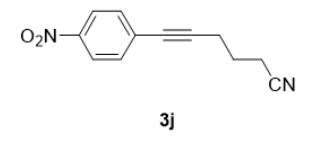


Yellow oil; Purification by flash chromatography (Cy 100%).  $^{1}$ H NMR (400 MHz, CDCl<sub>3</sub>)  $\delta$  (ppm) 8.16 – 8.14 (d, J = 9.0 Hz, 2H), 7.52 – 7.50 (d, J = 9.0 Hz, 2H), 2.46 – 2.43 (t, J = 12.0 Hz, 2H), 1.66 – 1.60 (m, 2H), 1.48 – 1.34 (m, 4H), 0.95 – 0.91 (t, J =

12.0 Hz, 3H).

<sup>13</sup>C NMR (100.8 MHz, CDCl<sub>3</sub>) δ (ppm) 146.53, 132.19, 131.20, 123.43, 96.79, 79.25, 31.08, 28.08, 22.16, 19.50, 13.93.

### 6-(4-nitrophenyl)hex-5-ynenitrile (3j)



Yellow oil; Purification by flash chromatography (Cy/EtOAc 95/5)

<sup>1</sup>H NMR (400 MHz, CDCl<sub>3</sub>)  $\delta$  (ppm) 8.19 – 8.17 (d, J = 9.0 Hz, 2H), 7.55 – 7.53 (d, J = 9.0 Hz, 2H), 2.69 – 2.66 (t, J = 6.8 Hz, 2H),

2.59 - 2.56 (t, J = 7.1 Hz, 2H), 2.04 - 1.97 (p, J = 7.0 Hz, 2H).

<sup>13</sup>C NMR (100.8 MHz, CDCl<sub>3</sub>) δ (ppm) 146.87, 132.32, 130.12, 123.52, 118.88, 92.84, 80.82, 24.21, 18.63, 16.30.

### 1-(6-chlorohex-1-yn-1-yl)-4-nitrobenzene (3k)

 $O_2N$ 

Yellow solid; Purification by flash chromatography (Cy/EtOAc 95/5)

<sup>3k</sup> <sup>1</sup>H NMR (400 MHz, CDCl<sub>3</sub>): δ (ppm) 8.16-8.14 (d, J= 8.9 Hz, 2H); 7.52-7.50 (d, J= 8.89 Hz, 2H); 3.62-3.59 (J=6.5 Hz, 2H); 2.52-2.49 (7 Hz, 2H); 1.99-1.92 (m, 2H); 1.83-1.76 (m, 2H).

<sup>13</sup>C NMR (100.8 MHz, CDCl<sub>3</sub>): δ (ppm) 146.80, 132.39, 130.95, 123.63, 95.61, 44.55, 31.73, 25.71, 19.03

### 1-(4-bromobut-1-yn-1-yl)-4-nitrobenzene (3l)

Yellow solid; Purification by flash chromatography (Cy/EtOAc 95/5)

<sup>1</sup>H NMR (400 MHz, CDCl<sub>3</sub>)  $\delta$  (ppm) 8.21 – 8.18 (d, J = 9.0 Hz, 2H), 7.60 – 7.57 (d, J = 9.0 Hz, 2H), 6.08 – 6.01 (dd, J = 17.5, 11.2 Hz, 1H), 5.87 – 5.82 (dd, J = 17.6, 2.0 Hz, 1H), 5.70 – 5.66 (dd, J = 11.2, 2.0 Hz, 1H).

<sup>13</sup>C NMR (100.8 MHz, CDCl<sub>3</sub>) δ (ppm) 132.24, 130.06, 129.09, 123.57, 116.45, 93.15, 87.97.

#### 2.1.4.14. Computational studies

#### *Methods:*

DFT calculations were conducted through the Molecular Graphics and Computation Facility (MGCF) at the University of California, Berkeley using the Gaussian 16 software package<sup>[203]</sup>

Geometry optimizations for all reported structures were performed using the PBE0 functional (the hybrid functional based on the Perdew-Burke-Ernzerhof functional [PBE][204,205]) with Grimme's D3 dispersion correction with Becke Johnson damping (GD3-BJ)[206] and the basis sets def2-TZVP[207] (with effective core potential) for Pd, I, Br, Cl and def2-SVP for all the other atoms. Frequency calculations were performed on all optimized structures to ensure that each local minimum lacked imaginary frequencies and that each transition state contained exactly one imaginary frequency. Solvation in DMF were introduced through single point calculations at optimised gas-phase geometries for all the minima and transition state using the dispersion corrected PBE0 with def2-TZVP for all atoms and the SMD implicit solvation model.[208] The reported Gibbs free energies were corrected considering the thermal correction computed at 298.15 K.

The Gibbs energies for isomers of complexes **R** with halide and triflate, the reaction coordinate of the interconversion between **Ra**, **Rb**, **Rc** and the calculations for the HCS protocol mechanism have already been reported in *Results and Discussion* in Figure 30, Figure 32 and Figure 34 respectively.

# Alternative pathways:

# Dissociation of PPh3 from $B^{I}_{NO_{2}}\,$

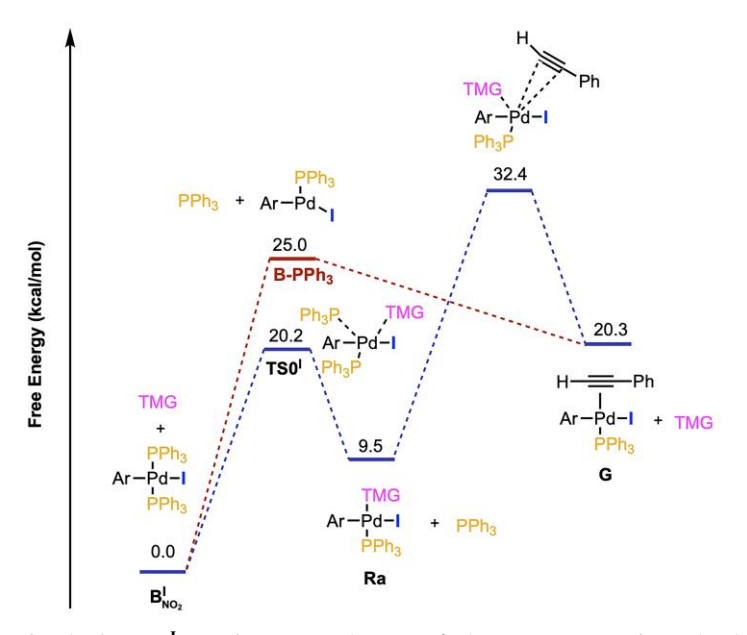


Figure 77. Dissociation of PPh<sub>3</sub> from  $B_{NO_2}^I$  to form complex **B-PPh**<sub>3</sub> has an energy of 25.0 kcal/mol, therefore unfavoured over the formation of  $TSO^I$  where the TMG displaces the phosphine giving intermediate.

# Equilibrium between cis-C and trans-C

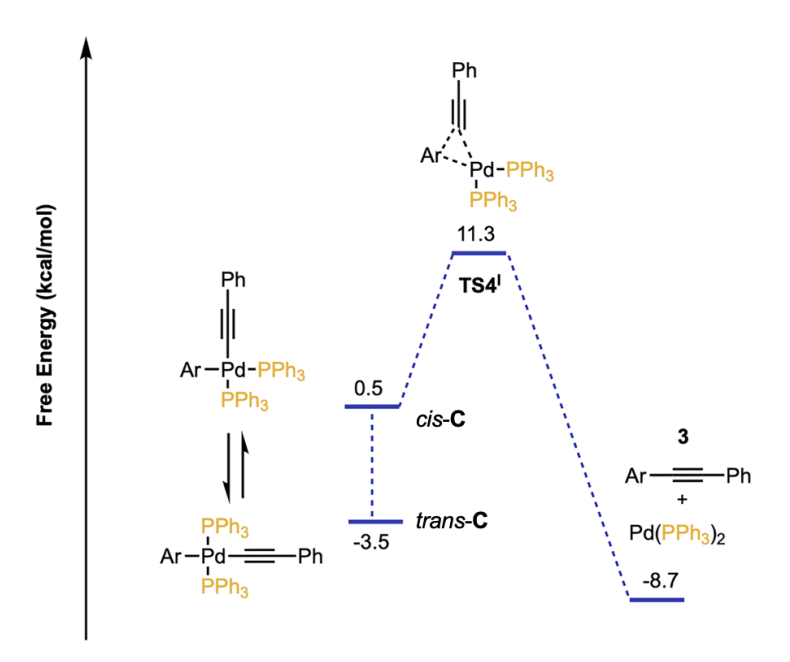


Figure 78. The equilibrium between *cis*-**C** and *trans*-**C** (4.0 kcal/mol more stable than *cis*-**C**) could slow down the reductive elimination step.

# 2.2. The critical role of in situ Pd(II) pre-catalyst reduction design

#### 2.2.1. Introduction

The preferred approach to managing Pd(0)-catalysed reactions involves the use of Pd(II) salts, such as palladium(II) acetate (Pd(OAc)2) or palladium(II) chloride (PdCl<sub>2</sub>/Pd(ACN)<sub>2</sub>Cl<sub>2</sub>), combined with the appropriate ligand to form the pre-catalysts. They are commercially available Pd(II) complexes, stable at room temperature and cost effective compared to preformed pre-catalysts or stable Pd(0) complexes, making them a practical choice for both academic and industrial applications. For example, the use of Pd<sub>2</sub>(dba)<sub>3</sub> allows the Pd(0)phosphine complex to be generated by a simple ligand exchange. However, the manipulation of palladium increases the cost and the presence of nanoparticles, already present in the Pd2(dba)3 complex, is a serious problem<sup>[209]</sup>. On the other hand, well-defined Pd(II) pre-catalysts have been designed to undergo rapid reductive elimination[210], facilitating the formation of the target Pd(0) complex. Although these approaches minimise side reactions and ensure a smoother transition into the catalytic cycle, they have drawbacks that limit their industrial application. For example, the Pd(II) catalysts may be protected by intellectual property rights[211] and/or the synthesis requires further manipulation of the ligand and the expensive metal, reducing the overall efficiency and increasing the cost.

The simple mixing of Pd(II) salts, ligands, auxiliaries and substrates under standard reaction conditions does not guarantee the efficient formation of the active Pd(0)L<sub>n</sub> species necessary to initiate and maintain catalytic cycles in cross-coupling reactions. Figure 79 generally describes the first step of the Pd(II) reduction process, where suitable solvent, reactant and base enter the palladium coordination sphere.

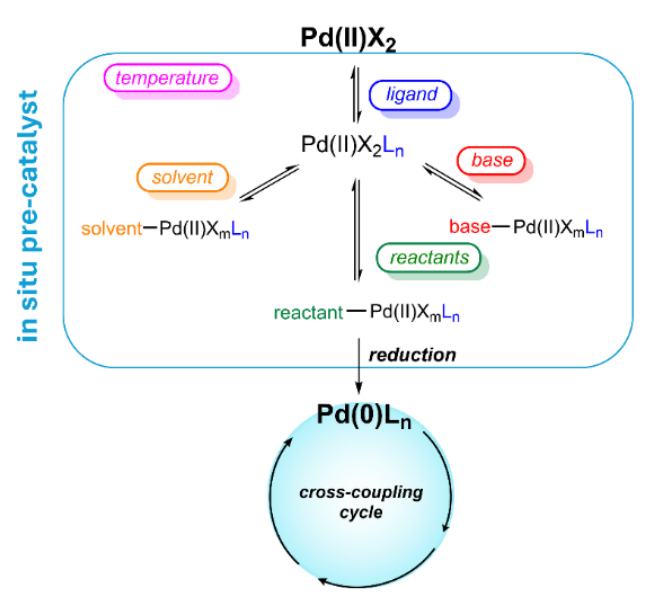


Figure 79. Pd(II) pre-catalyst reduction.

Efficient in situ reduction of Pd(II) to Pd(0) is essential to optimise reaction performance, such as: (i) reducing palladium and ligand consumption, (ii) decreasing costs, (iii) improving sustainability.

Typically, the reduction of the metal occurs at the expense of the phosphine ligand or some reagents. However, while Amatore and Jutand and many other scientists, have studied metal reduction at the expense of the phosphine ligands, it has not been clearly described how to avoid the scenario where the phosphine ligand undergoes oxidation to form phosphine oxide, altering the ligand-to-metal ratio. Indeed, this oxidative pathway can affect the structure and stability of the desired catalysts. In addition, the main risk is the formation of mixed catalysts or nanoparticles<sup>[212]</sup> with a significantly different reactivity compared to the intended catalysts. Using a large excess of ligand can overcome the oxidation problem, but this approach can influence the reaction outcome. It may stabilise unreactive complexes or inhibit certain steps of the catalytic cycle that require ligand dissociation. Careful consideration and balance are therefore required to optimise ligand usage without compromising the desired catalytic activity.

Pre-catalyst reduction can also be carried out at the expense of reagents, with the concomitant formation of impurities. On an industrial level, especially in the pharmaceutical and agrochemical segments, this can be an efficiency issue, as most of the expensive fragments can be consumed over time. In addition, using, for example, a 0.1-1 mol% catalyst loading to produce 1000 tonnes of a product, as in the case of the fungicide Boscalid<sup>[8]</sup>, generates a quantity of waste in the boronate-palladium reduction step equivalent to 1-10 tonnes of by-product. The combination of the above factors, based on an uncontrolled equilibrium between the palladium and the ligand, can lead to a complete misinterpretation of the reaction data, which is not based on the formation of the desired Pd(0) catalyst. Although several strategies have been developed, a complete guide to the efficient in situ activation of the L<sub>2</sub>PdX<sub>2</sub> pre-catalyst reduction is still not available. In this context, we have studied the Pd(II) pre-catalyst reduction in detail by investigating the effect of ligands, salts, bases and substrates. By precisely controlling the process, maximising the rapid formation of the active Pd(0) catalyst and avoiding the formation of nanoparticles, the efficiency of palladium cross-coupling reactions can be improved. In particular, we have focused on HCS,

### 2.2.2. Results and Discussion

We have considered the stable and widely available Pd(OAc)<sub>2</sub>, PdCl<sub>2</sub>(ACN)<sub>2</sub> (instead of the commonly used PdCl<sub>2</sub>) and, in the case of dppf as ligand, PdCl<sub>2</sub>(dppf) as palladium sources. The two counter ions, acetate and chloride, show completely

Suzuki-Miyaura (SM), Mizoroki-Heck (MH) and Stille reactions.

different behaviour, which is directly related to the strength of the Pd-X bond. Therefore, the effects of ligands, bases and reaction conditions had to be studied with both salts. Phosphine ligands are widely used in coordination chemistry<sup>[213]</sup>. Among them, we decided to investigate: (i) the monodentate triphenylphosphine (PPh<sub>3</sub>) being popular thanks to its low cost and availability; (ii) bidentate phosphine ligands, namely 1,1'bis(diphenylphosphino)ferrocene (dppf), 1,3-bis(diphenylphosphino)propane (dppp), and van Leuween's large bite angle phosphine 4,5-Bis(diphenylphosphino)-9,9dimethyl-xanthene (Xantphos)[214]; (iii) basic monodentate Buchwald's phosphine as 2dicyclohexylphosphino-2',6'-dimethoxybiphenyl (SPhos)[215]. The reduction process was evaluated using <sup>31</sup>P NMR, DFT calculations<sup>[216]</sup> and for selected reduction processes, the detection of nanoparticles was also investigated. The Pd(II) reduction was studied in DMF, a polar aprotic solvent capable of solubilising all the pre-catalysts except Pd(OAc)<sub>2</sub>/Xantphos, which required the use of THF. In DMF or THF, the reaction was also carried out with 30% HEP as cosolvent to reduce the Pd(II) by oxidation of the primary alcohol moiety (Figure 80, mechanism A)[88,217]. The effect of HEP is similar to that of primary alcohol with the difference that the products extraction does not require extensive quantities of organic solvents[45]. The reduction was carried out in the presence of several bases, such as TMG, TEA, Cs2CO3, K2CO3 and pyrrolidine.

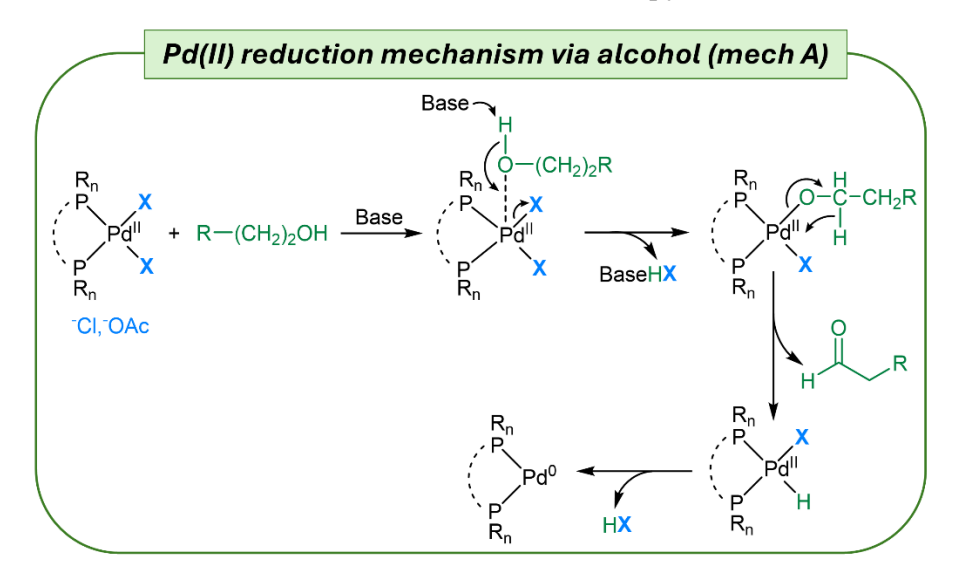


Figure 80. Reduction mechanism A via oxidation of a primary alcohol.

In order to understand which partner of the different cross-coupling reactions could be consumed in the presence of a pre-catalyst, we used as a model the pre-catalyst generated in situ from Pd(ACN)<sub>2</sub>Cl<sub>2</sub> and two equivalents of SPhos. Indeed, under these conditions, the stable complex PdCl<sub>2</sub>(SPhos)<sub>2</sub> is rapidly formed (Table 7, entry 1).

Table 7. PdCl<sub>2</sub>(SPhos)<sub>2</sub> reduction promoted by the cross-coupling reactants<sup>a</sup>

Pd<sup>II</sup>Cl<sub>2</sub>(SPhos)<sub>2</sub> 
$$K_2$$
CO<sub>3</sub> (5.0 equiv)

Pd<sup>OSPhos + SPhos + side products

DMF, 20 min</sup>

Entry	Reactant	T (°C)	Reaction	Pd(0)/Pd(II) <sup>b</sup>
1	-	25	-	0/100
2	Styrene	25	МН	0/100
3	Styrene	60	МН	0/100
4	PhSnBu <sub>3</sub>	25	Stille	0/100
5	PhSnBu <sub>3</sub>	60	Stille	0/100
6	PhB(OH) <sub>2</sub>	25	SM	0/100
7	PhB(OH) <sub>2</sub>	60	SM	100/0
8	PhC≡CH	25	HCS	0/100
9	PhC≡CH	60	HCS	100/0

 $<sup>^</sup>a$ Reactions were carried out with 0.013 mmol in 600  $\mu$ L of DMF for 20 minutes.  $^b$  Conversion of Pd(II) into Pd(0) was calculated by  $^{31}$ P NMR with internal standard after 20 minutes from the addition of the reactant.

The effect of the excess of reactant on the reduction of the metal, producing a monoligated Pd<sup>0</sup>SPhos and free SPhos, which can be evaluated by <sup>31</sup>P NMR. We chose to limit the monitoring to 20 minutes after the addition of 5 equivalents of the reactant at 25°C or 60°C, as the catalyst reduction is rapidly completed. The reagents studied were styrene for the Mizoroki-Heck reaction, tributylphenylstannane for the Stille reaction, phenylboronic acid for the Suzuki-Miyaura reaction and phenylacetylene for the Heck-Cassar-Sonogashira reaction. All experiments were carried out in DMF with K2CO3 as the base. The pre-catalyst proved to be stable under MH and Stille conditions (entries 2-5, Table 7) and no traces of Pd<sup>o</sup>SPhos or free SPhos were observed. On the other hand, while the pre-catalyst was stable at room temperature in the presence of phenylboronate and phenylacetylene (entries 6 and 8, Table 7), it was quantitatively reduced to Pd<sup>o</sup>SPhos by both reagents at 60°C (entries 7 and 9, Table 7). These experiments highlighted that the risk of consuming the pre-catalyst by reducing the reagent, needs to be considered only for Suzuki or HCS reactions. In this case, in addition to performing low-palladium cross-coupling reactions according to green chemistry principles, efficient pre-catalyst reduction can avoid excess reagents or the formation of by-products that affect both yield and product purification (Figure 81, mechanisms B and C).

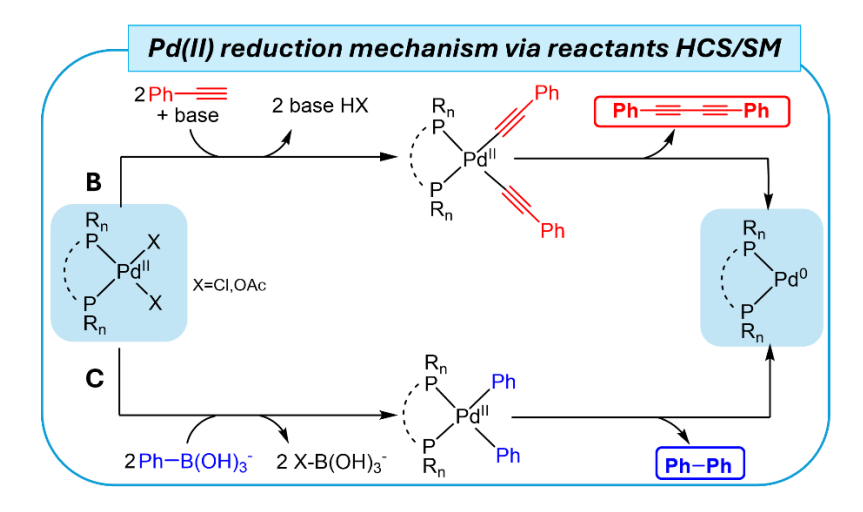


Figure 81. Reduction mechanism B and C, via alkyne and boronate, respectively.

Regarding the investigation of PPh3, the proper ligand/Pd(II) ratio was established to be 3/1, to avoid the formation of palladium nanoparticles and also to compensate the reduced amount of available phosphine due to oxidation. PdCl<sub>2</sub>(PPh<sub>3</sub>)<sub>2</sub> complex was stable in DMF (entry 1, Table 8) and it was reduced to Pd(0) only after addition of TMG with concomitant formation of OPPh<sub>3</sub> (entry 2, Table 8). TMG and secondary amines can coordinate with palladium, displacing 1 equivalent of PPh<sub>3</sub>. This mechanism facilitates the oxidation of the PPh<sub>3</sub> (Figure 82, mechanism D and see also 2.1.4. Experimental Section). On the contrary, nothing happened in the presence of TEA even at 80°C (entry 3, Table 8). With inorganic bases, the pre-catalyst reduction was slower than that promoted by TMG. Only at 60°C (entries 4-6, Table 8) was a partial conversion observed in 20 minutes according to mechanism E (Figure 82). By adding HEP in 1/2 ratio with DMF, complete pre-catalyst reduction was obtained at 25°C with TMG and Cs<sub>2</sub>CO<sub>3</sub> (entries 7 and 8, Table 8), while complete reduction with K<sub>2</sub>CO<sub>3</sub> was only observed at 60°C (entry 10). As expected, the reduction of Pd(OAc)2 was much faster than that of PdCl<sub>2</sub> In fact, in DMF, even in the absence of a base, Pd(0) was partially formed already at 25°C and it was completely obtained at 60°C (entries 11 and 12, Table 8). With TMG, the reduction was completed at 25°C (entry 13, Table 8). These data indicate that the base plays a key role in accelerating the reduction process with Pd(OAc)<sub>2</sub>. With the inorganic bases and Pd(OAc)<sub>2</sub>, complete reduction at 25°C was only achieved in the presence of HEP (entries 15-16, Table 8). While the preferred pathways could be envisaged for the experiments described above, in a few cases (entries 7, 10, 15 and 16, Table 8) it was not possible to clearly determine the predominant reduction mechanism. In general, the acetate can easily dissociate from the metal, producing a cationic palladium species, which is stabilised by the excess of inorganic salts according to mechanism E. These results suggest that it is difficult to avoid phosphine oxidation

with PPh<sub>3</sub>, the only exceptions being the reaction with chloride as counterion and  $Cs_2CO_3$  or  $K_2CO_3$  as base at 25°C (entries 8 and 9, Table 8).

Table 8. Base, temperature and solvent effect on Pd(II) reduction from PdX2 and 3 PPh3.a

$$PdX_2$$
 +  $3PPh_3$  Base (5.0 equiv)  $Pd^0(PPh_{3)2}$  +  $PPh_3/OPPh_3$  Solvent, 20 min

Entry	Х	Solvent	Base	T (°C)	Mech	Pd(0)/Pd(II)b	P/OH°
1	CI	DMF	-	60	-	0/100	-
2	CI	DMF	TMG	25	D	100/0	100/0
3	CI	DMF	TEA	80	-	0/100	-
4	CI	DMF	Cs <sub>2</sub> CO <sub>3</sub>	25	-	0/100	-
5	CI	DMF	Cs <sub>2</sub> CO <sub>3</sub>	60	Е	34/66	100/0
6	CI	DMF	K <sub>2</sub> CO <sub>3</sub>	60	Е	12/88	100/0
7	CI	DMF/HEP <sup>d</sup>	TMG	25	A/D	100/0	nd
8	CI	DMF/HEP	Cs <sub>2</sub> CO <sub>3</sub>	25	Α	100/0	0/100
9	CI	DMF/HEP	K <sub>2</sub> CO <sub>3</sub>	25	Α	28/72	0/100
10	CI	DMF/HEP	K <sub>2</sub> CO <sub>3</sub>	60	A/D	100/0	nd
11	AcO	DMF	-	25	Е	42/58	100/0
12	AcO	DMF	-	60	Е	100/0	100/0
13	AcO	DMF	TMG	25	D/E	100/0	100/0
14	AcO	DMF	Cs <sub>2</sub> CO <sub>3</sub>	25	E	43/57	100/0
15	AcO	DMF/HEP	Cs <sub>2</sub> CO <sub>3</sub>	25	A/E	100/0	nd
16	AcO	DMF/HEP	K <sub>2</sub> CO <sub>3</sub>	25	A/E	100/0	nd

 $<sup>^{</sup>a}$ Reactions were carried out with 0.013 mmol in 600  $\mu$ L solvent for 20 minutes.  $^{b}$  Conversion of Pd(II) into Pd(0) was calculated by  $^{31}$ P NMR with internal standard after 20 minutes from the addition of the base.  $^{c}$ P/OH is the ratio between the reduction via phosphine (P) or alcohol (OH) and "nd" = not determined.  $^{d}$  DMF/HEP were used in 2/1 ratio.

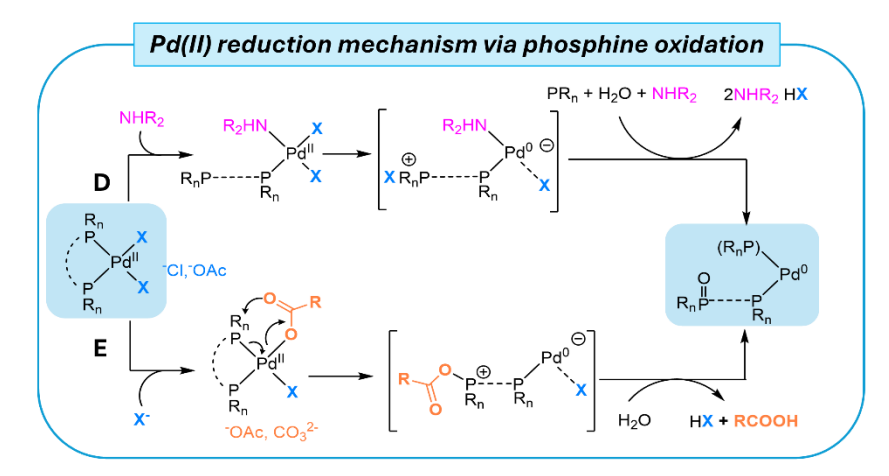


Figure 82. Reduction mechanism D and E, via displacement of the ligand and counterion respectively.

Bidentate ligands are widely used in palladium cross-coupling reactions and for this reason dppf, dppp and Xantphos were also investigated. These ligands are characterised by a different bite angle, respectively of 91° for dppp, 96° for dppf and 112° for Xantphos, with that of dppp being close to the perfect angle for a square planar complex<sup>[218]</sup>. The three phosphines also differ in terms of basicity, with dppp being more basic than the others due to the presence of an alkyl moiety. The use of only 1 equivalent of bidentate ligand can produce nanoparticles (see 2.2.4.7. Experimental Section) and less stable catalysts, and for this reason all experiments were carried out using 2 equivalents of phosphine. There are several papers describing the beneficial effect in cross-coupling reactions that occur when the bidentate phosphine is oxidised to the corresponding monophosphine oxide<sup>[219]</sup>. We therefore investigated whether the combination of base and solvent could produce one of the target catalysts shown in Figure 83.

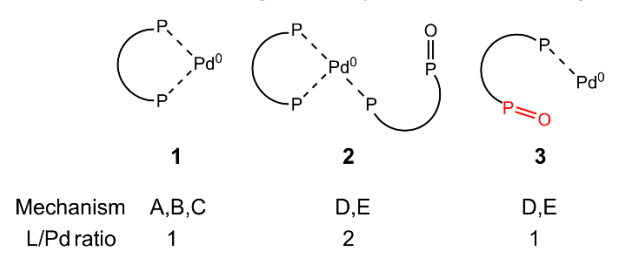
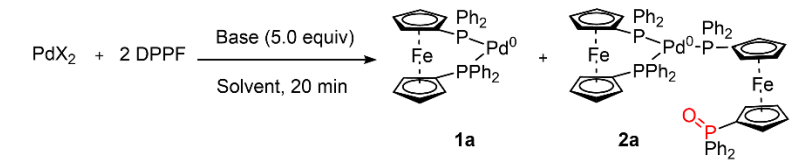


Figure 83. Potential Pd(0) species with dppf and dppp in function of the pre-catalyst reduction mechanism and ligand excess.

With Pd(dppf)X<sub>2</sub> it was possible to discriminate between the reduction mechanism A and D/E by <sup>31</sup>P NMR, comparing Pd<sup>0</sup>(dppf) **1a** and Pd<sup>0</sup>(dppf)dppf(O) **2a**. Pd(dppf)Cl<sub>2</sub> is stable in DMF at 60°C (entry 1, Table 9) and can be efficiently and rapidly reduced in the presence of a base (entries 2-4, Table 9) as TMG via mechanism D or the inorganic ones via mechanism E. The presence of HEP favours the reduction (entries 5-8, Table 9). However, only with K<sub>2</sub>CO<sub>3</sub> at 25°C the reduction was achieved selectively via mechanism A (entry 7, Table 9).

With Pd(OAc)<sub>2</sub> the pre-catalyst reduction was efficient even in the absence of the base (entries 9-10, Table 9), while in the presence of any base the reduction was completed within 20 minutes at 25°C (entries 11-13, Table 9).

Table 9. Base, temperature and solvent effect on Pd(II) reduction with PdX2 and 2 dppf.a



Entry	Х	Solvent	Base	T (°C)	Mech.	Pd(0)/Pd(II)b	P/OH°
1	CI	DMF	-	60	-	0/100	-
2	CI	DMF	TMG	25	D	100/0	100/0
3	CI	DMF	Cs <sub>2</sub> CO <sub>3</sub>	60	Е	100/0	100/0
4	CI	DMF	K₂CO₃	60	E	100/0	100/0
5	CI	DMF/HEP <sup>d</sup>	TMG	25	A/D	100/0	91/9
6	CI	DMF/HEP	Cs <sub>2</sub> CO <sub>3</sub>	25	A/E	100/0	23/77
7	CI	DMF/HEP	K₂CO₃	25	Α	100/0	0/100
8	CI	DMF/HEP	K₂CO₃	60	A/E	100/0	84/16
9	AcO	DMF	-	25	E	20/80	100/0
10	AcO	DMF	-	60	E	100/0	100/0
11	AcO	DMF	TMG	25	D	100/0	100/0
12	AcO	DMF/HEP	K <sub>2</sub> CO <sub>3</sub>	25	Α	100/0	0/100
13	AcO	DMF/HEP	Cs <sub>2</sub> CO <sub>3</sub>	25	A/E	100/0	55/45

 $<sup>^{</sup>a}$ Reactions were carried out with 0.013 mmol in 600  $\mu$ L solvent for 20 minutes.  $^{b}$ Conversion of Pd(II) into Pd(0) was calculated by  $^{31}$ P NMR with internal standard after 20 minutes from the addition of the base.  $^{c}$ P/OH is the ratio between the reduction via phosphine (P) or alcohol (OH),  $^{d}$  DMF/HEP were used in 2/1 ratio.

These data shown that, as with PPh<sub>3</sub>, it is possible to avoid ligand oxidation by using  $K_2CO_3$  at 25°C in the presence of HEP with chloride as counterion (entry 7, Table 9). In addition, different from PPh<sub>3</sub>, under the same conditions, the formation of Pd<sup>0</sup>(dppf) occurs by mechanism A (Figure 80) only, also with Pd(OAc)<sub>2</sub>dppf as precatalyst (entry 12, Table 9).

The dppp pre-catalyst prepared with  $Pd(ACN)_2Cl_2$  was perfectly stable at  $60^{\circ}C$  in DMF (entry 1, Table 10).

Table 10. Base, temperature and solvent effect on Pd(II) reduction with PdX2 and 2 dppp.a

Entry	Х	Solvent	Base	T (°C)	Mech.b	Pd(0)/Pd(II) <sup>b</sup>	P/OH <sup>c</sup>
1	CI	DMF	-	60	-	0/100	-
2	CI	DMF	TMG	60	-	0/100	-
3	CI	DMF	Cs <sub>2</sub> CO <sub>3</sub>	60	E	100/0	100/0
4	CI	DMF	K <sub>2</sub> CO <sub>3</sub>	60	E	100/0	100/0
5	CI	DMF/HEP <sup>d</sup>	Cs <sub>2</sub> CO <sub>3</sub>	25	Α	100/0	0/100
6	CI	DMF/HEP	K <sub>2</sub> CO <sub>3</sub>	25	Α	55/45	0/100
7	AcO	DMF	-	25	E	11/89	100/0
8	AcO	DMF	-	60	Е	100/0	100/0
9	AcO	DMF/HEP	Cs <sub>2</sub> CO <sub>3</sub>	25	A/E	100/0	nd
10	AcO	DMF/HEP	K <sub>2</sub> CO <sub>3</sub>	25	A/E	100/0	nd

<sup>a</sup>Reactions were carried out with 0.013 mmol in 600  $\mu$ L solvent for 20 minutes. <sup>b</sup>Conversion of Pd(II) into Pd(0) was calculated by <sup>31</sup>P NMR with internal standard after 20 minutes from the addition of the base. <sup>c</sup>P/OH is the ratio between the reduction via phosphine (P) or alcohol (OH) and "nd" = not determined. <sup>d</sup>DMF/HEP were used in 2/1 ratio.

Interestingly, the addition of TMG did not promote metal reduction (entry 2, Table 10). While TMG is able to compete with dppf in coordinating PdCl<sub>2</sub> to promote mechanism D (see entry 2, Table 9), in the case of the more basic dppp, TMG was not able to compete with the phosphine in coordinating Pd(II) and mechanism D was completely inhibited even at 60°C (entry 2, Table 10). Only by moving to inorganic bases such as Cs<sub>2</sub>CO<sub>3</sub> and K<sub>2</sub>CO<sub>3</sub> at 60°C was the reduction via mechanism E complete (entries 3-4, Table 10). The addition of HEP allowed a switch to the alcohol-based mechanism A at 25°C (Figure 80), selectively generating **2b** (entries 5-6, Table 10). Switching to acetate as counterion, the trend was identical to that of dppf, with reduction occurring even in the absence of a base via mechanism E (entries 7-8, Table 10) and accelerated at 25°C by the addition of inorganic bases and HEP as cosolvent (entries 9-10, Table 10). Only the use of PdCl<sub>2</sub> in the presence of HEP and inorganic bases (K<sub>2</sub>CO<sub>3</sub> or Cs<sub>2</sub>CO<sub>3</sub>) at 25°C could avoid ligand oxidation (entries 5-6 Table 10).

The results of the experiments carried out with the bidentate ligand Xantophos are quite different from the trend shown for dppf and dppp (Table 11).

Table 11. Base, temperature and solvent effect on Pd(II) reduction with PdX2 and 2 Xantphos.a

Entry	Х	Solvent	Base	T (°C)	Mech.	Pd(0)/Pd(II) <sup>b</sup>	P/OH°
1	CI	DMF	-	60	-	0/100	-
2	CI	DMF	TMG	60	-	0/100	-
3	CI	DMF	Cs <sub>2</sub> CO <sub>3</sub>	60	-	0/100	-
4	CI	DMF	K₂CO₃	60	-	0/100	-
5	CI	DMF	NaOAc	60	E	100/0	100/0
6	CI	DMF/HEP <sup>d</sup>	Cs <sub>2</sub> CO <sub>3</sub>	60	Α	100/0	0/100
7	CI	DMF/HEP	K <sub>2</sub> CO <sub>3</sub>	60	А	100/0	0/100
8	AcO	THF	-	25	-	0/100	_
9	AcO	THF	-	60	E	100/0	100/0
10	AcO	THF	TMG	25	-	0/100	-
11	AcO	THF	K₂CO₃	25	-	0/100	_
12	AcO	THF	Cs <sub>2</sub> CO <sub>3</sub>	25	E	40/60	100/0
13	AcO	THF/HEP <sup>e</sup>	Cs <sub>2</sub> CO <sub>3</sub>	25	A/E	100/0	47/53
14	AcO	THF/HEP	K <sub>2</sub> CO <sub>3</sub>	25	Α	100/0	0/100

 $^a$ Reactions were carried out with 0.013 mmol in 600  $\mu$ L solvent for 20 minutes.  $^b$ Conversion of Pd(II) into Pd(0) was calculated by  $^{31}$ P NMR with internal standard after 20 minutes from the addition of the base.  $^c$ P/OH is the ratio between the reduction via phosphine (P) or alcohol (OH).  $^d$ DMF/HEP were used in 2/1 ratio.  $^c$ THF/HEP were used in 2/1 ratio.

The pre-catalyst with chloride as counterion was stable even in the presence of bases at 60°C (entries 1-4, Table 11). With the addition of NaOAc, a rapid exchange with chloride promoted the palladium reduction via mechanism E (entry 5, Table 11). Eastgate and Blackmond, in an interesting paper coming from the collaboration between academia and industry, highlighted the role of Xanthphos monophosphine oxide in a CH activation reaction as a "hemilabile" efficient ligand **2c**<sup>[219]</sup>. The catalyst (4 mol %) was generated using dimethyl acetamide and conditions very similar to entry 5 in Table 11. The role of the acetate was crucial not only for the cross-coupling step, but also for obtaining the palladium reduction via mechanism E and the selective formation of the

monophosphine oxide. In the presence of HEP, the inorganic salts allowed the reduction of the pre-catalyst via mechanism A (entries 6 and 7, Table 11). Since the combination Pd(OAc)<sub>2</sub>/Xantphos is not soluble in DMF, it was studied in THF. Under these conditions, complete catalyst reduction occurred at 60°C (entry 9, Table 11). At 25°C, the reduction did not occur with TMG and K<sub>2</sub>CO<sub>3</sub> (entries 10-11, Table 11), while was accelerated in the presence of Cs<sub>2</sub>CO<sub>3</sub> (entry 12, Table 11). The addition of HEP was able to favour Pd(II) reduction via mechanism A at 25°C (entries 13-14, Table 11). Again, K<sub>2</sub>CO<sub>3</sub> as a base was able to favour the selective formation of Pd<sup>0</sup> at 25°C when it was paired with Pd(OAc)<sub>2</sub> (entry 14, Table 11), whereas at 60°C with PdCl<sub>2</sub>, both Cs<sub>2</sub>CO<sub>3</sub> and K<sub>2</sub>CO<sub>3</sub> were able to avoid the ligand oxidation (entries 6-7, Table 11).

Table 12. Base, temperature and solvent effect on Pd(II) reduction with PdX2 and 2 SPhos.a

PdX<sub>2</sub> + 2 SPhos Base (5.0 equiv) Pd<sup>0</sup>SPhos + SPhos + OSPhos Solvent, 20 min

Entry	Х	Solvent	Base	T (°C)	Mech.	Pd(0)/Pd(II)b	P/OH <sup>c</sup>
1	CI	DMF	-	25	-	0/100	-
2	CI	DMF	TMG	60	-	0/100	-
3	CI	DMF	Cs <sub>2</sub> CO <sub>3</sub>	60	-	0/100	-
4	CI	DMF	K₂CO₃	60	<u>-</u>	0/100	-
5	CI	DMF/HEP <sup>d</sup>	Cs <sub>2</sub> CO <sub>3</sub>	25	Α	56/44	0/100
6	CI	DMF/HEP	Cs <sub>2</sub> CO <sub>3</sub>	60	Α	100/0	0/100
7	CI	DMF/HEP	K₂CO₃	60	Α	100/0	0/100
8	CI	DMF/HEP	TMG	60	Α	15/85	0/100
9	AcO	DMF	-	60	E	29/71	100/0
10	AcO	DMF	Cs <sub>2</sub> CO <sub>3</sub>	25	E	71/29	100/0
11	AcO	DMF	K₂CO₃	25	E	54/46	100/0
12	AcO	DMF	Cs <sub>2</sub> CO <sub>3</sub>	60	E	100/0	100/0
13	AcO	DMF	K₂CO₃	60	E	100/0	100/0
14	AcO	DMF/HEP <sup>d</sup>	Cs <sub>2</sub> CO <sub>3</sub>	25	A/E	100/0	42/58
15	AcO	DMF/HEP <sup>d</sup>	K <sub>2</sub> CO <sub>3</sub>	25	Α	100/0	0/100
16	AcO	DMF/HEPd	TMG	60	A/E	31/69	nd

 $<sup>^</sup>a$ Reactions were carried out with 0.013 mmol in 600  $\mu$ L solvent for 20 minutes.  $^b$ Conversion of Pd(II) into Pd(0) was calculated by  $^{31}$ P NMR with internal standard after 20 minutes from the addition of the base.  $^c$ P/OH is the ratio between the reduction via phosphine (P) or alcohol (OH) and "nd" = not determined.  $^d$ DMF/HEP were used in 2/1 ratio.

We were also interested in SPhos, both because it is frequently used in Suzuki-Miyaura<sup>[215]</sup> and because we have carried out extensive catalytic studies with the corresponding water-soluble sulfonate ligand sSPhos<sup>[45]</sup>. The main characteristic of this ligand is that the Pd(II) complex coordinates two SPhos ligands, whereas Pd(0) coordinates only one in the 12-electron complex<sup>[73,85,88]</sup>. Therefore, we decided to use 2 equivalents to stabilise the complexes in the case of phosphine oxidation (Table 12). The reduction via phosphorous oxidation using PdCl<sub>2</sub> did not occur even in the presence of bases at 60°C (entries 1-4, Table 12). However, the addition of HEP enabled reduction by primary alcohol oxidation of the pre-catalyst in the presence of bases, with inorganic bases being more efficient (entries 5-8, Table 12). Pd(OAc)<sub>2</sub> was reduced in DMF both with and without bases with a complete reduction only with inorganic bases at 60°C (entries 9-13, Table 12). In the presence of HEP, Pd<sup>0</sup> was selectively generated by mechanism A using only K<sub>2</sub>CO<sub>3</sub> at 25°C (entry 15, Table 12).

With the aim of demonstrating that the reduction of Pd(SPhos)<sub>2</sub>Cl<sub>2</sub> with K<sub>2</sub>CO<sub>3</sub> at 25°C in the presence of HEP allows to avoid pre-catalyst reduction at the expense of alkynes or boronates, we investigated HCS and SM cross-coupling under these conditions. Pd(SPhos)<sub>2</sub>Cl<sub>2</sub> generated with PdCl<sub>2</sub>(ACN)<sub>2</sub> and SPhos was rapidly reduced to the corresponding Pd<sup>0</sup>SPhos in the presence of phenylacetylene or phenyl boronic acid, respectively. Under these stressed conditions, with 20 mol% of palladium and a 1/1 ratio of PhI to reactants, no homocoupling products were formed via the pre-catalyst reduction (mechanism B or C, Figure 81). The HCS and SM gave only the expected products, 1,2-bisphenylacetylene and 4-methyl-1,1-biphenyl respectively (Figure 84).

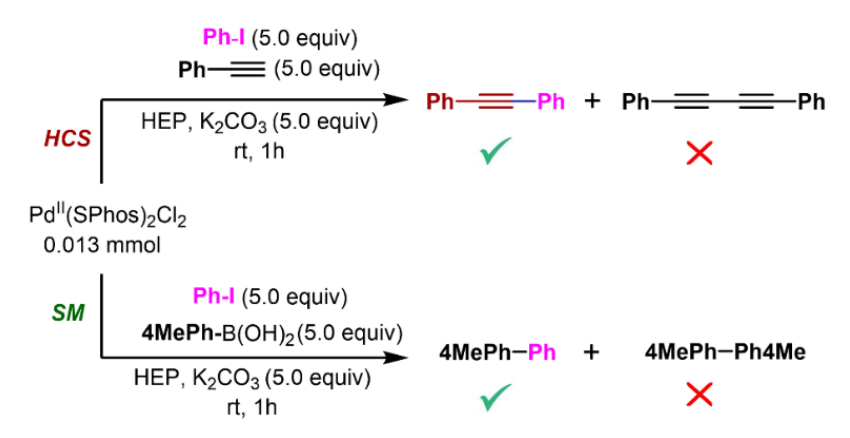


Figure 84. Heck-Cassar-Sonogashira and Suzuki-Miyaura cross-coupling effect of the present of the reactants in HEP.

We also investigated the The PdCl<sub>2</sub>(ACN)<sub>2</sub>/ligand/alcohols/base protocol in several green solvents (Table 13).

Table 13. Pre-catalysts reduction generated with  $PdCl_2$  and Buchwald's ligands with a base at  $60^{\circ}C$  in the presence of alcohols. <sup>a</sup>

Entry	Ligand	Base	Solvent	Pd(0)/Pd(II)b
1	SPhos	K <sub>2</sub> CO <sub>3</sub>	Anisole/EtOH 2/1	100/0
2	SPhos	K <sub>2</sub> CO <sub>3</sub>	CPME/EtOH 2/1	100/0
3	SPhos	K <sub>2</sub> CO <sub>3</sub>	MeTHF/EtOH 2/1	100/0
4	SPhos	K <sub>2</sub> CO <sub>3</sub>	Anisole/MeOH 2/1	100/0
5	SPhos	K <sub>2</sub> CO <sub>3</sub>	Anisole/HEP 2/1	100/0
6	RuPhos	K <sub>2</sub> CO <sub>3</sub>	Anisole/EtOH 2/1	100/0
7	XPhos	K <sub>2</sub> CO <sub>3</sub>	Toluene/EtOH 2/1	100/0
8	SPhos	PYR	Anisole/EtOH 2/1	25/75
9	SPhos	TMG	Anisole/EtOH 2/1	28/72
10	sSPhos	K <sub>2</sub> CO <sub>3</sub>	HEP/H <sub>2</sub> O 4/1	100/0
11	sSPhos	K <sub>2</sub> CO <sub>3</sub>	EtOH/H <sub>2</sub> O 4/1	100/0
12	sSPhos	PYR	EtOH/H <sub>2</sub> O 4/1	52/48
13	sSPhos	K <sub>2</sub> CO <sub>3</sub>	IPA/H <sub>2</sub> O 4/1	0/100

 $<sup>^</sup>a$ Reactions were carried out with 0.013 mmol in 600  $\mu$ L solvent for 20 minutes.  $^b$ Conversion of Pd(II) into Pd(0) was calculated by  $^{31}$ P NMR with internal standard after 20 minutes from the addition of the base.

In the presence of SPhos, the protocol worked perfectly in several green solvent combinations via mechanism A (entries 1-5, Table 13). The protocol was successfully applied to 2-dicyclohexylphosphino-2',6'-diisopropoxy-1,1'-biphenyl (RuPhos)[220], and 2-dicyclohexylphosphino-2',4',6'-triisopropylbiphenyl (XPhos). With XPhos it was necessary to use toluene as cosolvent due to the solubility of the ligand. As expected, the complex reduction was less efficient with organic bases such as TMG and PYR. The presence of these bases, which enter the coordination sphere of Pd(II), destabilised the Pd(SPhos)2Cl2 and the formation of PdoSPhos was less efficient (entries 8-9, Table 13). The amount of PdoSPhos did not increase with time and macroscopically we observed the formation of palladium black after 1 hour. The formation of palladium black indicates catalyst decomposition, probably due to ligand loss. In addition, the experiment was carried out using a conservative approach of 5 equivalents of base. This is because typical

reactions often require >100 times the stoichiometry of base to phosphine ligand to stabilise intermediates. The use of sSPhos allowed the introduction of water as a cosolvent in the green protocol (entries 10-11, Table 13)[221-223]. Again, the use of PYR generated only 52% of the expected Pd<sup>0</sup>sSPhos complex within 20 min (entry 12, Table 13). Secondary alcohols such as isopropanol (IPA), used to replace HEP or EtOH, were not able to reduce the pre-catalyst (entry 13, Table 13). The solvent mixture described in Table 13 was not optimised and only showed the generality of the approach to use alcohols for Pd(II) pre-catalyst reduction, provided the pre-catalyst was soluble at these concentrations and the preference for inorganic bases.

DFT calculations were performed by the group for mechanism A using the B3LYP/DEF2-TZVP level of theory<sup>[198]</sup>, focusing on the cationic Pd(II) complex.

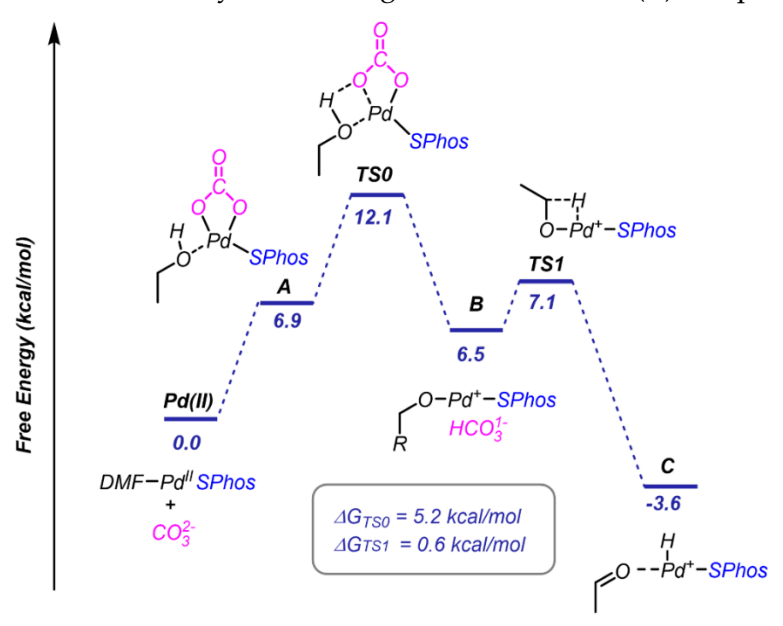


Figure 85. DFT-calculation-computed reaction profile and solution-state Gibbs free energies ( $\Delta$ GDMF, kcal mol-1) B3LYP/DEF2-TZVP level of theory at 298 K for stationary points of Mechanism A.

We excluded the counterion and the second SPhos in the Pd(II) pre-catalyst to avoid calculation inaccuracies due to their presence. Therefore, a simplified Pd(II)-SPhos complex with DMF as ligand was chosen as a reference model to evaluate the reduction process (Figure 85). This approach generalises the model to a variety of palladium systems. The initial step in mechanism A involves coordination of the carbonates and the alcohol to form complex **A** with an energy of 6.9 kcal/mol. This coordination makes the proton of the alcohol more acidic, allowing deprotonation by a base to give **B** via the **TS0** transition state, which has an energy barrier of 5.2 kcal/mol. The total activation energy required for alcohol deprotonation is calculated to be 12.1 kcal/mol, with the transition state influenced by the specific coordination of the carbonate to the palladium centre. Our calculations revealed that the most stable configuration involves both oxygen atoms of the carbonate coordinating to the palladium complex. The reaction pathway

proceeds via beta-hydride elimination at **TS1**, with a very low energy barrier of 0.6 kcal/mol, leading to the formation of intermediate **C**, which is by far the more stable complex. The DFT studied with PYR as the base showed a similar trend with higher transition energies. In fact, the total energy to reach the corresponding **TS0** is 15.2 kcal, confirming that the reduction with PYR was less efficient (see *Experimental Section* 2.2.4.12.).

DFT studies identified the deprotonation process as the rate-determining step of mechanism A. This observation was confirmed by a kinetic isotope effect (KIE) study using <sup>31</sup>P NMR (Figure 86). Indeed, the reaction with CH<sub>3</sub>OH was consistently faster than the one in CD<sub>3</sub>OD, with a KIE of 1.6.

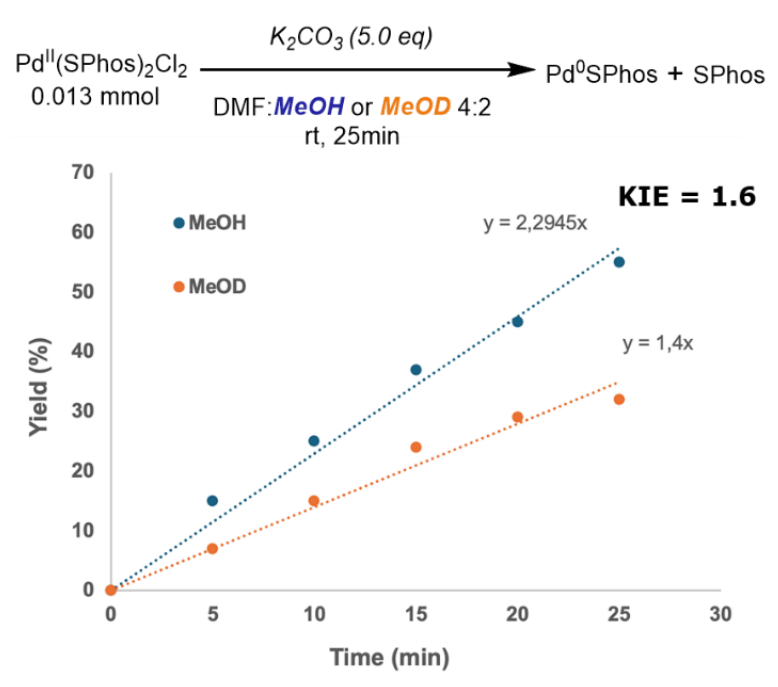


Figure 86. Kinetic isotopic effect CH<sub>3</sub>OH versus CD<sub>3</sub>OD.

#### 2.2.3. Conclusion

This study has shed light on the X<sub>2</sub>Pd(II)L<sub>n</sub> pre-catalytic reduction, where the counterion is acetate or chloride, using PPh<sub>3</sub>, dppf, dppp, Xantphos and SPhos in DMF/THF also in the presence of a green primary alcohol as well as HEP.

These results led to the development of efficient protocols for the synthesis of Pd(0)L<sub>n</sub> complexes by simply mixing Pd(II) salts with phosphine ligands. The effect of different combinations of PdX<sub>2</sub>/phosphine ligands/bases/temperature/solvent on the reduction process has been investigated in detail. It has been shown that it is possible to prevent the oxidation of the ligand and to avoid the formation of by-products *via* unwanted palladium reduction pathways in the HCS and SM cross-coupling reactions. Density functional theory studies were used to investigate the mechanism of the process, revealing that deprotonation, which generates the oxygen-palladium sigma bond in the

Pd(II) complex, is the rate-determining step. Different classes of ligands were found to require specific reaction conditions to ensure high catalyst efficiency and optimal reaction performance. Furthermore, the best protocol developed for the ligand SPhos was successfully extended to other Buchwald ligands, demonstrating its versatility in different organic solvent mixtures, as long as a primary alcohol is present, and the catalyst is soluble.

With this information in hand, it will be possible to generate Pd<sup>0</sup> active species in a most efficient way, saving time, metal and ligands, and avoiding the unwanted consumption of reactants.

### Acknowledgments:

DFT calculations for this work were performed by Dr. Tommaso Fantoni. Nanoparticles have been analysed and evaluated by Beatrice Muzzi (ICCOM-CNR).

#### Published work:

The full version can be found in "T. Fantoni and **C. Palladino**, R. Grigolato, B. Muzzi, L. Ferrazzano, A. Tolomelli, W. Cabri, *Org. Chem. Front.* 2025, DOI: 10.1039/d4qo02335h"

# 2.2.4. Experimental Section

#### 2.2.4.1. General Information

Commercially available reagents (reagent grade, >99%) were purchased from Sigma Aldrich, Fluorochem and TCI Chemicals and used without any further purification. Solvents (deuterated N,N-Dimethylformamide (DMF-d7), deuterated chloroform (CDCl<sub>3</sub>), 1-(2-Hydroxyethyl)-2-pyrrolidone (HEP), Ethanol (EtOH), dichloromethane (DCM) are commercially available and solvent for reaction were used after degassing. bis(triphenylphosphine)palladium PdCl<sub>2</sub>(PPh<sub>3</sub>)<sub>2</sub> chloride(II) 1,1'-Bis(diphenylphosphino)ferrocene] palladio(II)dichloride PdCl2(dppf), Bis(acetonitrile)dichloropalladium(II) PdCl<sub>2</sub>(ACN)<sub>2</sub>, Bis(dibenzylideneacetone)palladium(0) Pd(dba)2, triphenylphospine (PPh<sub>3</sub>), Bis(diphenylphosphino)propane (dppp) and 1,1'-Bis(diphenylphosphino)ferrocene Dicyclohexyl(2',6'-dimethoxy[1,1'-biphenyl]-2-yl)phosphane Bis(diphenylphosphino)-9,9-dimethylxanthene (Xantphos) from FaggiEnrico (Italy). <sup>1</sup>H NMR, <sup>13</sup>C NMR and <sup>31</sup>P NMR spectra were recorded on Varian 400-MR (400 MHz) (equipped with autoswitchable PFG probe) and Bruker Avance Neo 600 MHz (equipped with CryoProbe Prodigy Broadband 5mm) spectrometers. NMR multiplicities are abbreviated as follows: s = singlet, d = doublet, t =triplet, q = quartet, spt = septet, m = multiplet, bs = broad signal. Coupling constants J are given in Hz. All <sup>1</sup>H and <sup>13</sup>C chemical shifts are calibrated to residual protic-solvents and all  $^{31}$ P chemical shifts are referenced to external 85% phosphoric acid ( $\delta$  = 0 ppm). HPLC-UV analysis were recorded with an Agilent 1260 InfinityLab instrument. Column: Zorbax® SB-C18; particle size 5 µm; pore size 100 Å; length 250 mm, internal diameter: 4.6 mm. Mobile phase A: H<sub>2</sub>O, mobile phase B: ACN. Gradient (Time(min), %B): 0, 80; 25, 80; 28, 10; 30, 10; flow 0.5 mL min¹-column temperature 30°C; injection volume: 10 µL. GC-MS analysis were recorded with a Hewlett-Packard 5971 spectrometer with GC injection and EI ionization at 70 eV coupled with an Agilent Technologies MSD1100 single-quadrupole mass spectrometer, reported as: m/z (rel. intensity). High-Resolution transmission electron microscopy (HR-TEM) images were acquired on a ThermoFischer Talos F200X operated at 200 kV, which is equipped with an extreme field emission gun (FEG) electron source and Super-X Energy Dispersive X-ray Spectroscopy (EDS) system for chemical analysis. HRMS spectra were obtained with a G2XS QTof mass spectrometer using either ESI. Room temperature (rt) refers to the ambient temperature of the laboratory, ranging from 22 °C to 26 °C.

#### 2.2.4.2. Palladium pre-catalyst reduction with PPh<sub>3</sub>

Table 14. <sup>31</sup>P NMR chemical shift in DMF-d<sub>7</sub> and HEP/DMF-d<sub>7</sub> (2:4) of palladium species with PPh<sub>3</sub>

entry	Compound	DMF-d <sub>7</sub>	HEP/DMF-d <sub>7</sub> (2:4)
1	PPh <sub>3</sub>	-4.94	-5.08
2	Pd(OAc) <sub>2</sub> (PPh <sub>3</sub> ) <sub>2</sub>	15.69	15.60
3	3NO <sub>2</sub> Ar(OAc)Pd(PPh <sub>3</sub> ) <sub>2</sub>	22.50	22.34
4	Pd <sup>0</sup> (PPh <sub>3</sub> )	23.37	23.30
5	3NO <sub>2</sub> ArPdI(PPh <sub>3</sub> ) <sub>2</sub>	24.10	23.98
6	Pd(PPh <sub>3</sub> ) <sub>2</sub> Cl <sub>2</sub>	24.85	24.64
7	OPPh₃	26.15	27.57
8	3NO <sub>2</sub> ArPdl(PPh <sub>3</sub> )	25.10	25.37
9	3NO <sub>2</sub> Ar(OAc)Pd(PPh <sub>3</sub> )TMG	29.61	29.19
10	Pd(PPh <sub>3</sub> ) <sub>2</sub> Cl(CO <sub>3</sub> <sup>2-</sup> )M	30.58	
11	3NO <sub>2</sub> Ar(PdI(PPh <sub>3</sub> )TMG	30.86	28.32
12	Pd(PPh <sub>3</sub> ) <sub>2</sub> (OAc)(CO <sub>3</sub> <sup>2-</sup> )M <sup>+</sup>		31.06
13	Pd <sup>0</sup> (PPh <sub>3</sub> ) <sub>2</sub>	34.29	34.03

### Synthesis of palladium species with PPh<sub>3</sub>

a) Entry 5, Table 14: 3NO<sub>2</sub>ArPdI(PPh<sub>3</sub>)<sub>2</sub>

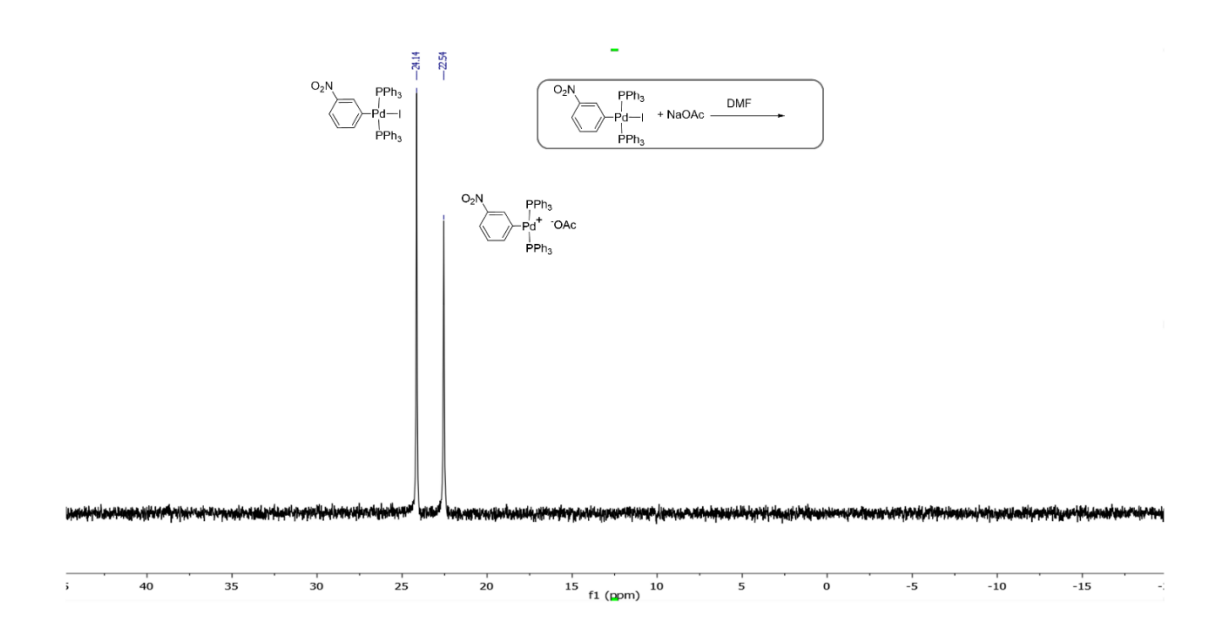
To an oven-dried 20 mL Schlenk purged under argon atmosphere, a mixture of 1-Iodo-3-nitrobenzene 3NO<sub>2</sub>ArI (423 mg, 1.7 mmol, 2.46 equiv) and tetrakis(triphenylphosphine)palladium(0) (798 mg, 0.69 mmol, 1 equiv) was stirred in degassed toluene (13 mL), in the dark for 1 h at room temperature. The reaction mixture was filtered, and the crude was washed with diethyl ether (Et<sub>2</sub>O) to obtain the pure product (534 mg, 88%) as a white solid.

<sup>1</sup>H NMR (600 MHz, CDCl<sub>3</sub>): δ 7.55-7.50 (m, 12H, Hb-Hf); 7.33-7.29 (m, 6H, Hd); 7.26-7.22 (m, 13H, Hc-He, -Hd'); 7.15-7.11 (m, 3H, Hb'-Hc'-He').

<sup>13</sup>C NMR (151.2 MHz, CDCl<sub>3</sub>): δ 178.07 (s, Cd'); 143.86 (t, J=1.51 Hz, Ca'); 135.89 (t, J=4.53 Hz, Cb'-Cf'), 134.92 (t, 6.05 Hz, Cb-Cf), 131.21 (t, J=24.2 Hz, Ca), 130.40 (s, Cd), 128.00 (t, J=4.53, Cc-Ce), 120.95 (t, Cc'-Ce').

<sup>31</sup>P NMR (242.4 MHz,)  $\delta$  +24.14 (s) DMF-d<sub>7</sub>;  $\delta$  +24.02 (HEP/DMF-d<sub>7</sub> 2/4)

### b) Entries 9 and 11, Table 14: 3NO<sub>2</sub>Ar(OAc)Pd(PPh<sub>3</sub>)TMG, 3NO<sub>2</sub>Ar(PdI(PPh<sub>3</sub>)TMG



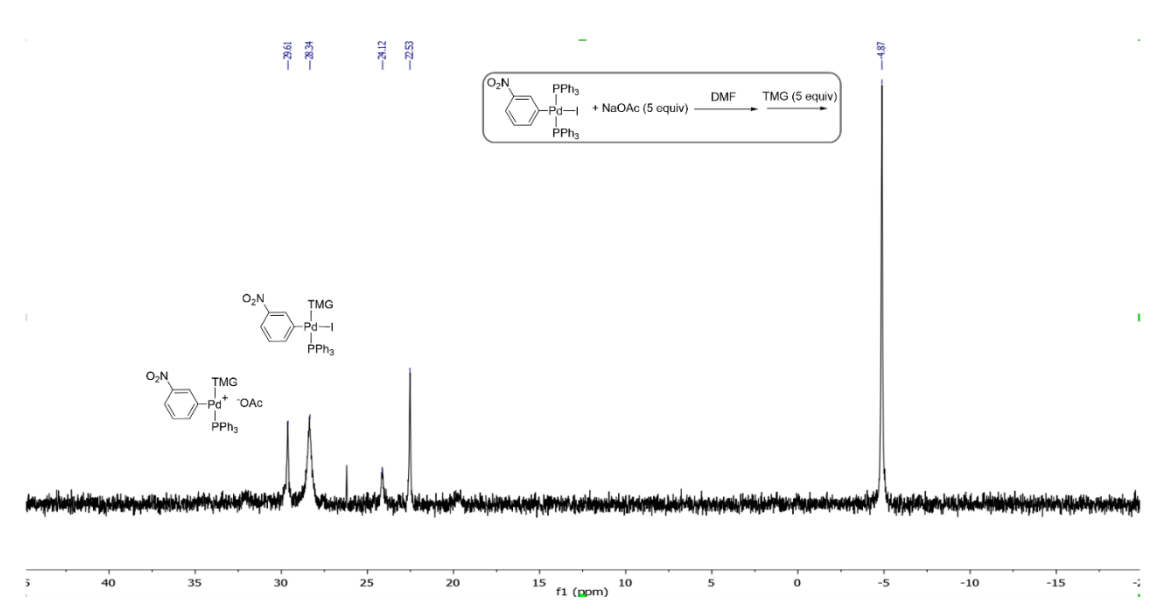


Figure 87.  $^{31}$ P NMR spectra of 3NO<sub>2</sub>ArPd(PPh<sub>3</sub>)<sub>2</sub> (11.40 mg, 0.013 mmol, 1 equiv) previously synthesized + NaOAc (5 mg, 0.065, 5 equiv) in DMF-d<sub>7</sub> (0.6 ml) (above); and after the addition of TMG (10 $\mu$ L, 0.065 mmol, 5 equiv) (below).

#### Pd(OAc)<sub>2</sub>

#### General Procedure 1:

$$Pd(OAc)_2 + 3 PPh_3 \xrightarrow{\text{Base (5 equiv)}} Pd(PPh_3)_n + n-1 OPPh_3/PPh_3$$

$$Solvent$$

$$T (°C)$$

To an oven-dried 20 mL Schlenk purged under argon atmosphere, the precatalyst Pd(OAc)<sub>2</sub> (2.91 mg, 0.013 mmol, 1 equiv) was dissolved in the degassed solvent (0.6 mL). Triphenylphosphine (10.21 mg, 0.039 mmol, 3 equiv) and base (0.065 mmol, 5 equiv) were added. The reaction was stirred for 20 minutes at the desired temperature and analyzed by <sup>31</sup>P NMR analysis. To calculate the conversion of the uncompleted reduction, the triethyl phosphonoacetate (0.13 mmol, 1 equiv) was added as internal standard (IS).

To further demonstrate that the formation of Pd(0) specie occurred, 3NO<sub>2</sub>ArI (16.2 mg, 0.065 mmol, 5 equiv) was added to detect the formation of the oxidative addition (OA) complex. The OA complex was previously synthesized according to *Experimental Section* 2.1.4.3.

Table 15. All experiments carried out to study the  $Pd(PPh_3)_2(OAc)_2$  reduction in both DMF-d<sub>7</sub> and HEP/DMF-d<sub>7</sub> a. Rows underlined in grey have already been reported in Table 8.

Entry	Solvent	Base	T (°C)	Mech	Pd(0)/Pd(II) <sup>b</sup>	P/OH°
1	DMF	-	25	D	42/58	100/0
2	DMF	-	60	D	100/0	100/0
3	DMF	TMG	25	D/E	100/0	100/0
4	DMF	cyclohexylamine	25	D/E	100/0	100/0
5	DMF	pyrrolidine	25	D/E	100/0	100/0
6	DMF	Cs <sub>2</sub> CO <sub>3</sub>	25	E	43/57	100/0
7	DMF	K <sub>2</sub> CO <sub>3</sub>	25	Е	46/54	100/0
8	DMF	TEA	25	Е	42/58	100/0
9	DMF	Cs <sub>2</sub> CO <sub>3</sub>	60	Е	100/0	100/0
10	DMF	K <sub>2</sub> CO <sub>3</sub>	60	Е	100/0	100/0
11	DMF	TMG	60	D/E	100/0	100/0
12	DMF	TEA	80	E	100/0	100/0
13	DMF/HEPd	-	60	Α	100/0	100/0
14	DMF/HEP	TMG	25	A/D	100/0	nd
15	DMF/HEP	Cs <sub>2</sub> CO <sub>3</sub>	25	A/E	100/0	nd
16	DMF/HEP	K <sub>2</sub> CO <sub>3</sub>	25	A/E	100/0	nd
17	TEA	DMF/HEP	25	Α	42/58	100/0
18	Cs <sub>2</sub> CO <sub>3</sub>	DMF/HEP	60	A/E	100/0	nd
19	K <sub>2</sub> CO <sub>3</sub>	DMF/HEP	60	A/E	100/0	nd
20	TMG	DMF/HEP	60	A/E	A/E	nd

 $<sup>\</sup>ensuremath{^{\text{a}}}$  The reactions were carried out according to the  $General\ Procedure\ 1$ 

 $<sup>^{\</sup>rm b}$  The conversion was calculated by  $^{\rm 31}P$  NMR comparing the signals of the IS signal and Pd(OAc)2(PPh3)2

 $<sup>^{\</sup>rm c}$ P/OH represents the ratio between the oxidation of phosphine (P) or alcohol (OH) to form Pd(0) and "nd" means not determined.

 $<sup>^{</sup>d}\,600\mu L$  of DMF-d7

 $<sup>^</sup>e The \ solvent \ is \ a \ mixture \ of HEP \ 200 \mu L$  and DMF-d7  $400 \mu L$ 

# <sup>31</sup>P NMR spectra of complete reduction as an example in both DMF and HEP/DMF a) Entry 2, Table 15:

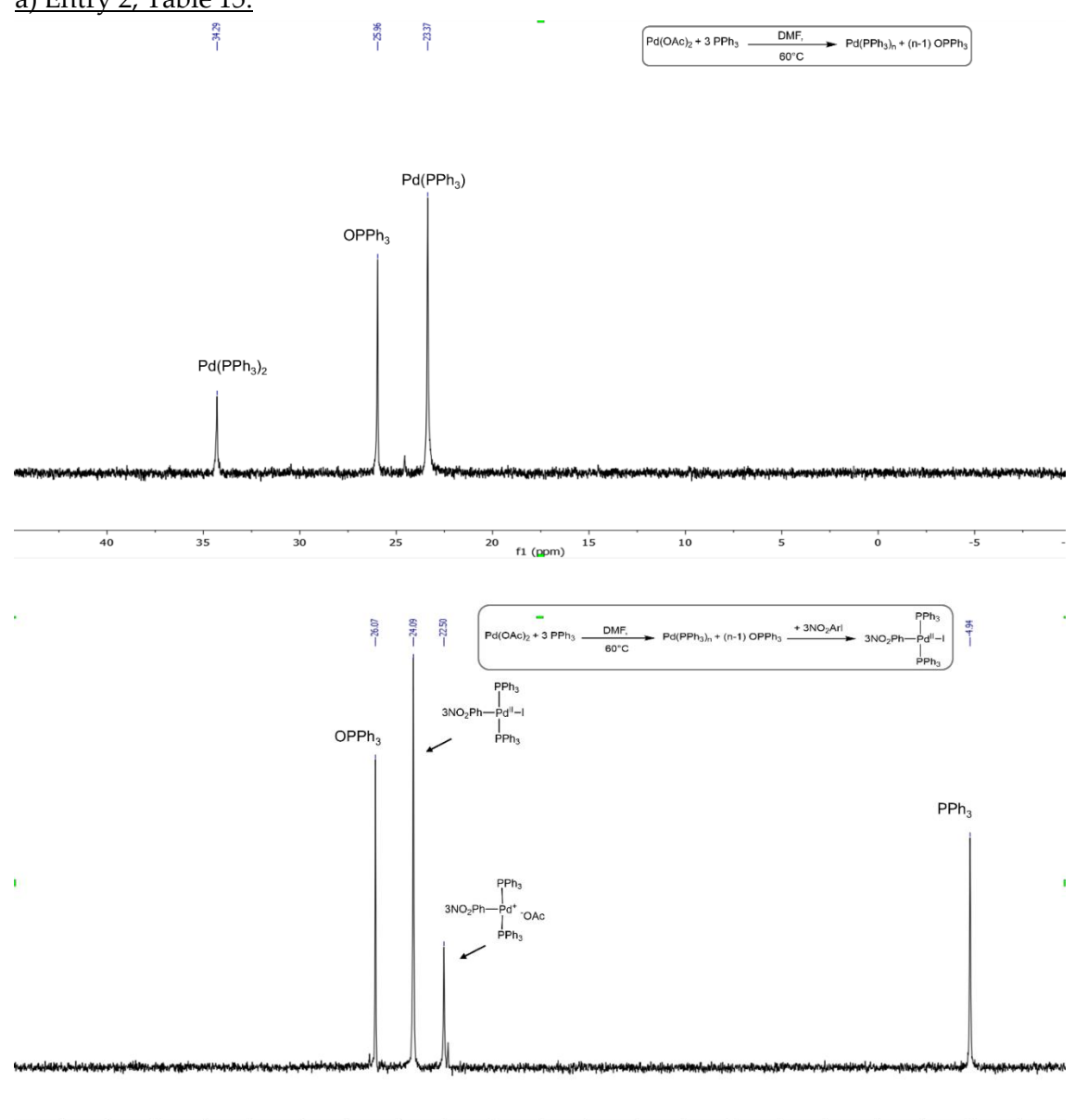


Figure 88.  $Pd(OAc)_2 + 3PPh_3$  in DMF-d<sub>7</sub> at 60°C for 20 min (top); after the addition of  $3NO_2ArI$  to confirm the disappearance of the Pd(0) species (bottom).

20 15 f1 (ppm)

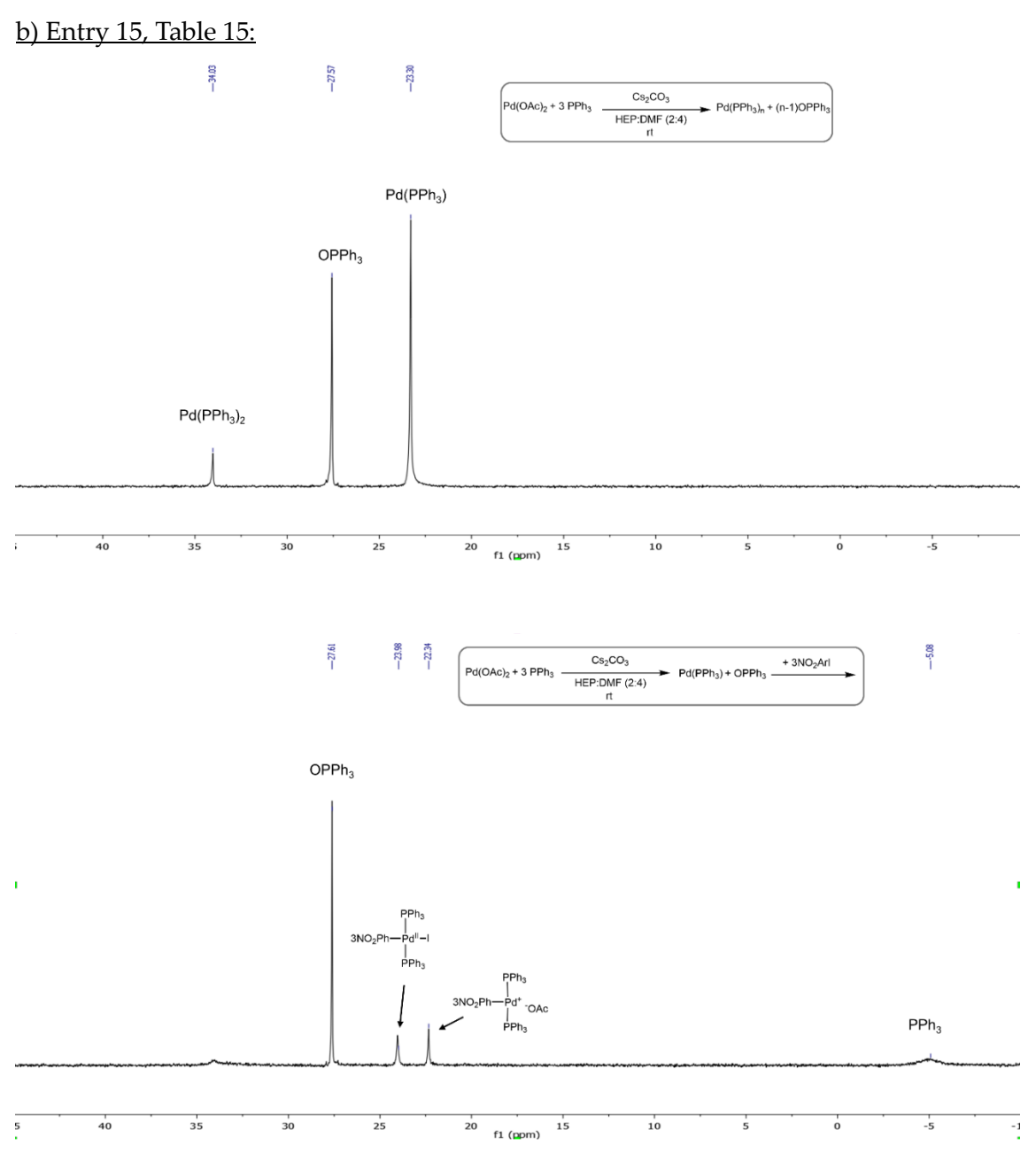


Figure 89.  $Pd(OAc)_2 + 3PPh_3 + Cs_2CO_3$  (5 equiv) in HEP/DMF-d<sub>7</sub> (2/4) at rt for 20 min (top); after the addition of 3NO<sub>2</sub>ArI to confirm the disappearance of the Pd(0) species (bottom).

#### PdCl<sub>2</sub>

#### **General Procedure 2:**

To an oven-dried 20 mL Schlenk purged under argon atmosphere, the pre-catalyst Pd(PPh<sub>3</sub>)<sub>2</sub>Cl<sub>2</sub> (9.12 mg, 0.013 mmol, 1 equiv) was dissolved in the degassed solvent (0.6 mL). Triphenylphosphine (3.41 mg, 0.013 mmol, 1 equiv) and base (0.065 mmol, 5 equiv) were added. The reaction was stirred for 20 minutes at the desired temperature and

analysed by <sup>31</sup>P NMR analysis. To calculate the conversion of the uncompleted reduction, the triethyl phosphonoacetate (0.013 mmol, 1 equiv) was added as internal standard (IS).

To further demonstrate that the formation of Pd(0) specie occurred, 3NO<sub>2</sub>ArI (16.2 mg, 0.065 mmol, 5 equiv) was added to detect the formation of the oxidative addition (OA) complex.

Table 16. All experiments carried out to study the Pd(PPh<sub>3</sub>)<sub>2</sub>Cl<sub>2</sub> reduction in both DMF-d<sub>7</sub> and HEP/DMF-d<sub>7</sub><sup>a</sup>. Rows underlined in grey have already been reported in Table 8

Entry	Solvent	Base	T (°C)	Mech	Pd(0)/Pd(II) <sup>b</sup>	P/OH <sup>c</sup>
1	DMF	-	60	-	0/100	-
2	DMF	TMG	25	D	100/0	100/0
3	DMF	cyclohexylamine	25	D	100/0	100/0
4	DMF	Pyrrolidine	25	D	100/0	100/0
5	DMF	Cs <sub>2</sub> CO <sub>3</sub>	25	-	0/100	-
6	DMF	TEA	25	-	0/100	-
7	DMF	Cs <sub>2</sub> CO <sub>3</sub>	60	Е	34/66	100/0
8	DMF	K₂CO₃	60	E	12/88	100/0
9	DMF	TEA	80	-	0/100	-
10	DMF/HEPd	Cs <sub>2</sub> CO <sub>3</sub>	25	Α	100/0	0/100
11	DMF/HEP	K₂CO₃	25	Α	28/72	0/100
12	DMF/HEP	TMG	25	A/D	100/0	nd
13	DMF/HEP	TEA	25		0/100	-
14	DMF/HEP	Cs <sub>2</sub> CO <sub>3</sub>	60	A/D	100/0	nd
15	DMF/HEP	K <sub>2</sub> CO <sub>3</sub>	60	A/D	100/0	nd

 $<sup>\</sup>ensuremath{^{\text{a}}}$  The reactions were carried out according to the  $General\ Procedure\ 2$ 

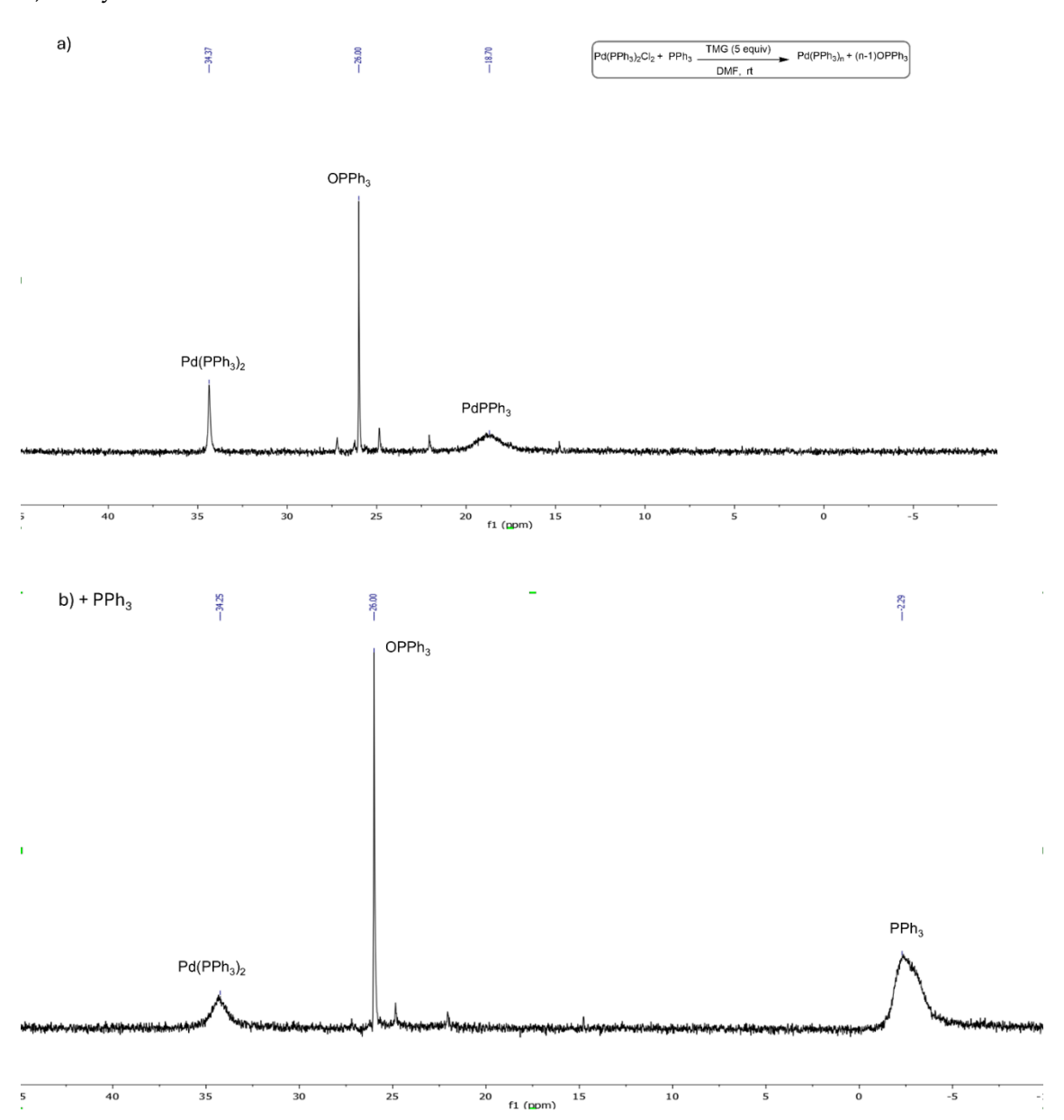
<sup>&</sup>lt;sup>b</sup> The conversion was calculated by <sup>31</sup>P NMR comparing the signals of the IS signal and Pd(PPh<sub>3</sub>)<sub>2</sub>Cl<sub>2</sub>

 $<sup>^{\</sup>rm c}$ P/OH represents the ratio between the oxidation of phosphine (P) or alcohol (OH) to form Pd(0) and "nd" means not determined.

 $<sup>^{</sup>d}\,600\mu L$  of DMF-d7

 $<sup>^</sup>e$  The solvent is a mixture of HEP 200  $\mu L$  and DMF-d7 400  $\mu L$ 

# <sup>31</sup>P NMR spectra of complete reduction as an example in both DMF and HEP/DMF a) Entry 2, Table 16:



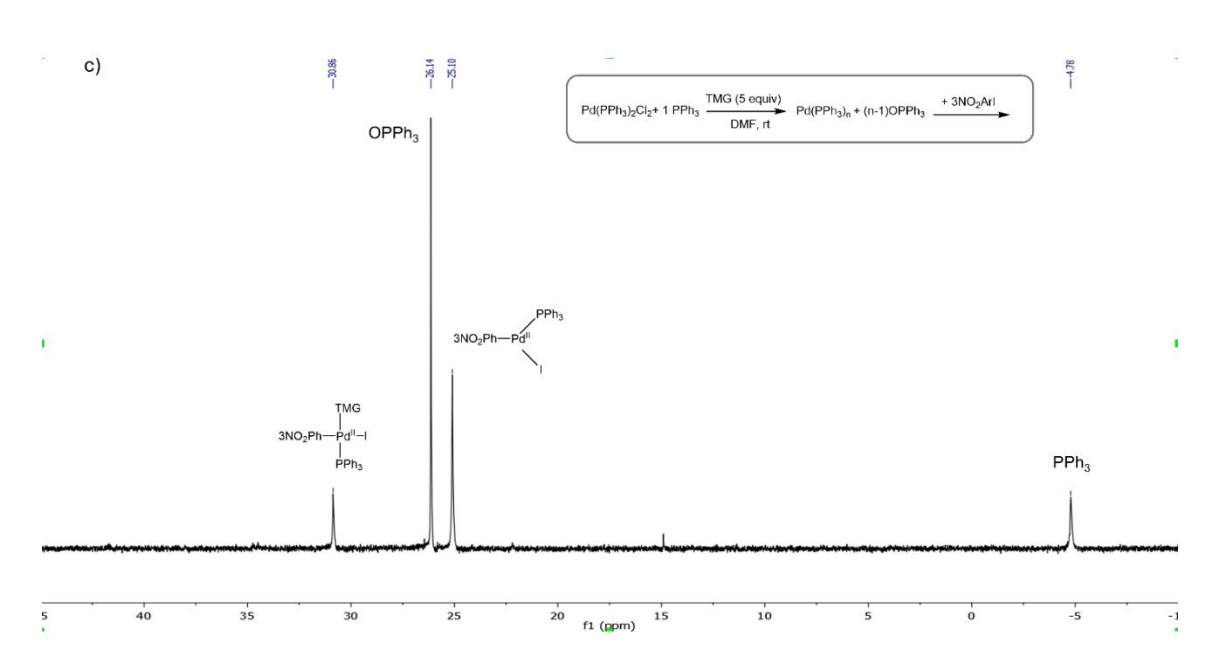
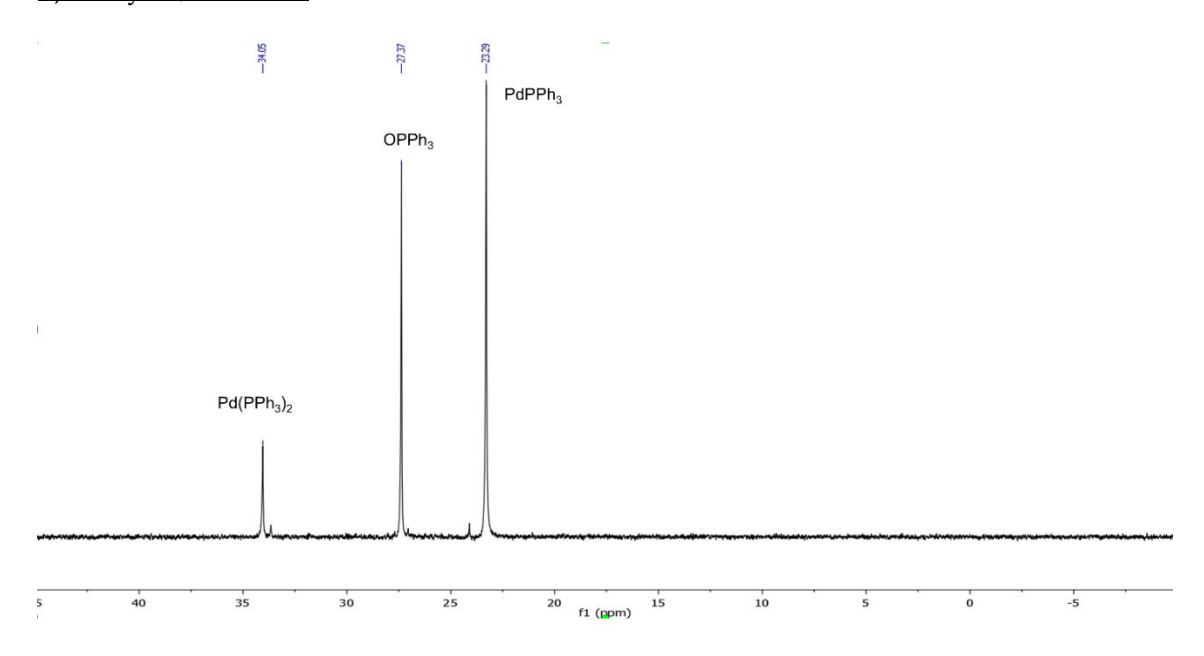


Figure 90.  $Pd(PPh_3)_2Cl_2 + PPh_3$  (1 equiv) + TMG (5 equiv) in DMF-d<sub>7</sub> at rt in 20 min. The resonance at 18.70 ppm has been assigned to a Pd(0) specie and this was confirmed by adding  $PPh_3$  (spectrum **a**). After the addition, the peak at +18.70 disappeared (spectrum **b**). Spectrum **c** shows the disappearance of the Pd(0) species in the presence of  $3NO_2ArI$ 

# b) Entry 10, Table 16:



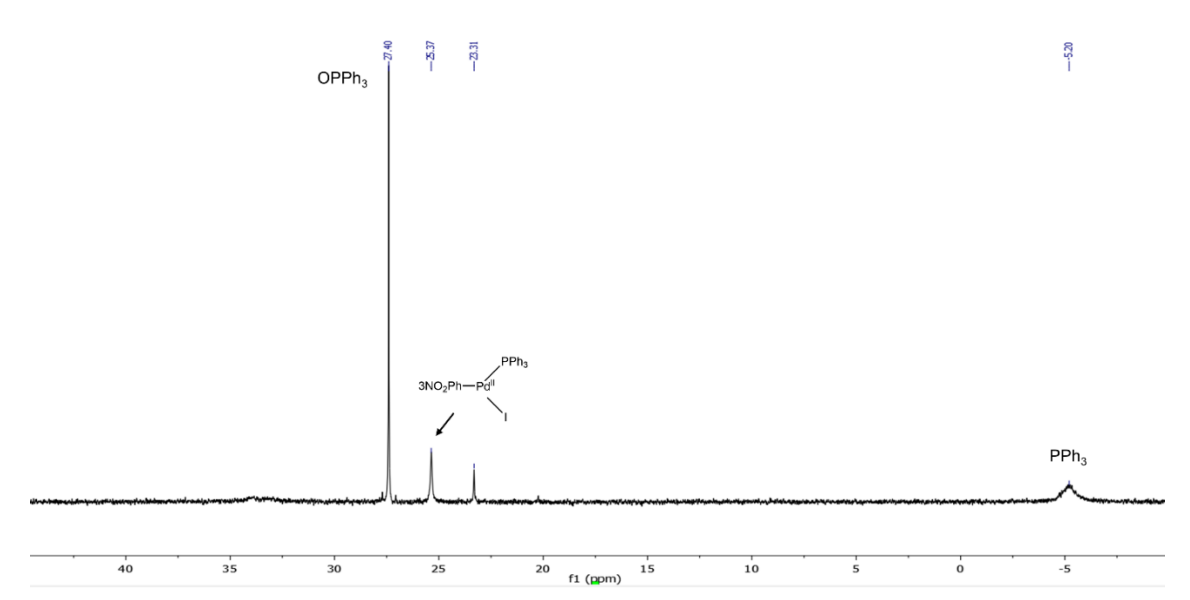


Figure 91.  $Pd(PPh_3)_2Cl_2 + 1$   $PPh_3 + Cs_2CO_3$  (5 equiv) in DMF-d7/HEP at rt for 20 min (top); after the addition of 3NO<sub>2</sub>ArI to confirm the disappearance of the Pd(0) species, although a small amount remains, probably because the oxidative addition was not complete when the spectrum was acquired (bottom).

### 2.2.4.3. Palladium pre-catalyst reduction with dppf

Table 17. 31P NMR chemical shift in DMF-d7 and HEP/DMF-d7 (2:4) of palladium species with dppf

entry	Compound	DMF-d <sub>7</sub>	HEP/DMF-d <sub>7</sub> (2:4)
1	dppf	-17.12	-17.16
2	dppf(O) <sup>a</sup>	-17.43; 25.95	-17.58; 27.30
3	Pd <sup>0</sup> (dppf)	6.91; 33.83	34.25
4	Pd <sup>0</sup> dppf(O)dppf	9.3 (m); 16.60 (m)	9.18 (m); 16.56 (m)
5	3NO <sub>2</sub> ArPd(dppf)I	12.83 (d); 32.62 (d)	12.83(d); 32.72 (d)
6	Odppf	26.04	27.76
7	Pd(OAc)₂dppf	31.69	32.14
8	PdCl <sub>2</sub> (dppf)	34.94	34.97
9	Pd(OAc) <sub>2</sub> (dppf)	31.66	32.18

<sup>&</sup>lt;sup>a</sup> dppf(O) is the label for the dppf mono-oxide

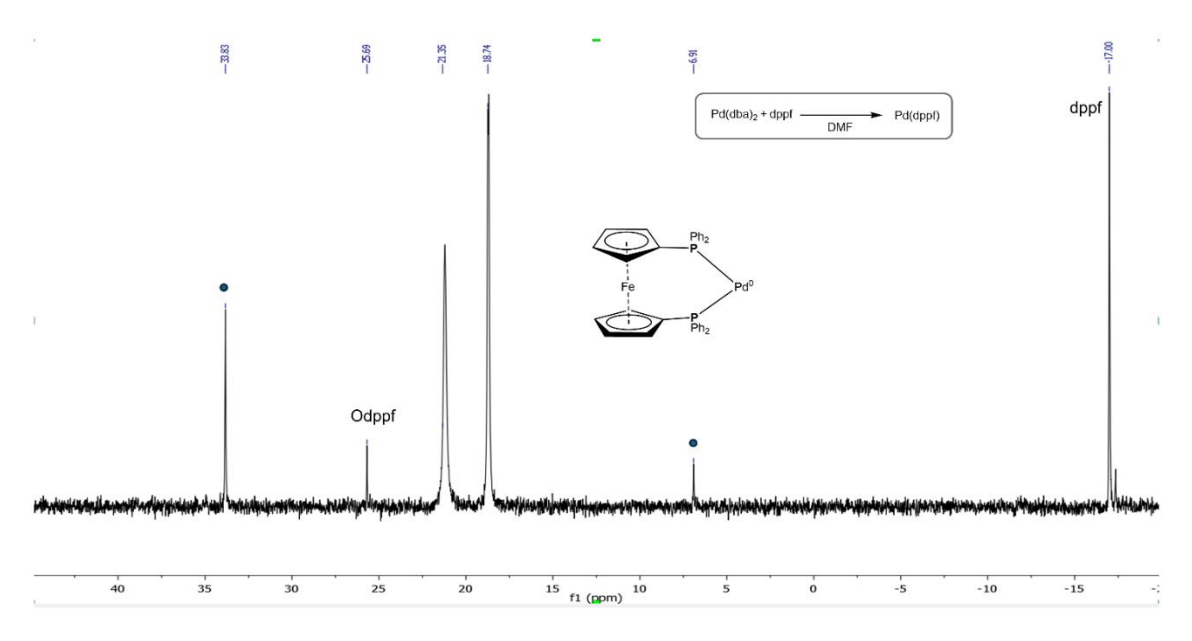
# Synthesis of palladium species with dppf

a) Entry 2, Table 17: dppf(O)

To an oven-dried 20 mL Schlenk purged under argon atmosphere,  $Pd(OAc)_2$  (1.5 mg, 0.006 mmol, 0.00177 equiv), dppf (196 mg, 0.36 mmol, 1 equiv), 1,2-dibromoethane (100  $\mu$ L, 1.15 mmol, 3.2 equiv), 10% NaOH aq (500  $\mu$ L) were added in degassed DCM (1.2 mL). The resulting mixture was refluxed with vigorous stirring for 17 h. Then, the result mixture was diluted with water (5 mL), extracted with DCM (3 x 5 mL), the combined organic layers were washed with brine and dried over Na<sub>2</sub>SO<sub>4</sub>. The solvent was removed by rotary evaporator and the crude material was purified by silica gel chromatography (DCM/EtOAc 100/0 to 50:50) to yield desired product as an orange solid (60 mg, 30% yield)[224].

<sup>31</sup>P NMR (DMF-d<sub>7</sub>): -17.43 (s); 25.95 (s)

# b) Entries 3 and 5, Table 17: Pd<sup>0</sup>(dppf) and 3NO<sub>2</sub>ArPd(dppf)I



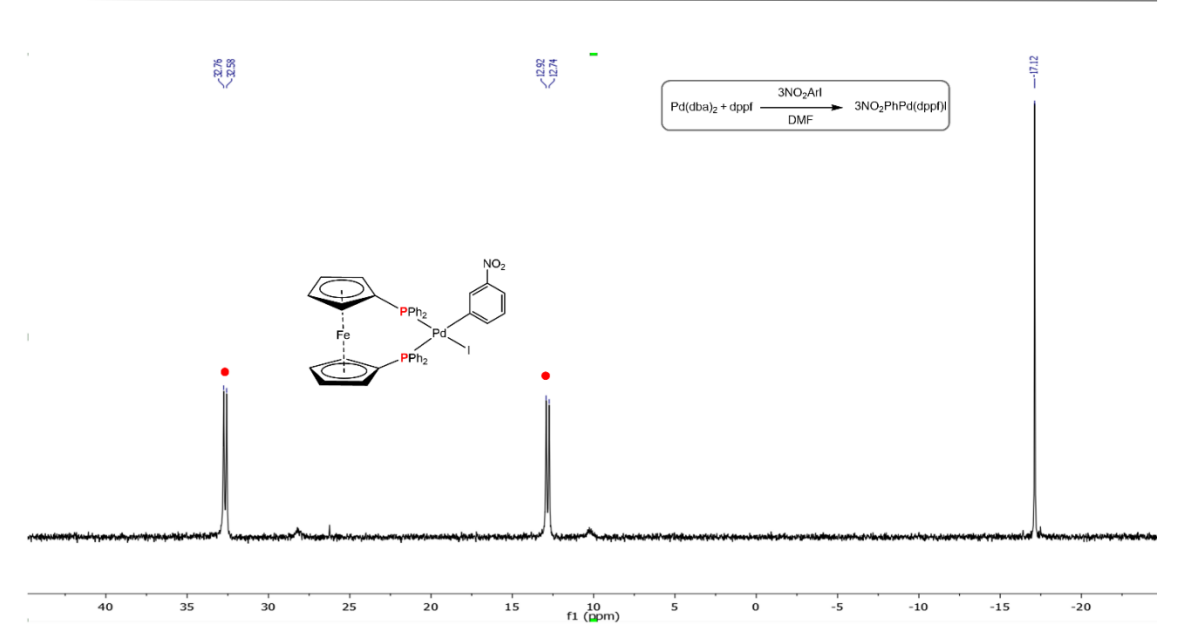


Figure 92.  $Pd(dba)_2$  (11.9 mg, 0.013 mmol, 1 equiv), dppf (7.5 mg, 0.013, 1 equiv) in DMF-d7. The peaks at 10.25, 8.95 ppm are related to the dba coordinated to the Pd compound<sup>[225,226]</sup> (top); after the addition of  $3NO_2ArI$  (16.18 mg, 0.065, 5 equiv) (bottom).

#### Pd(OAc)<sub>2</sub>

#### General Procedure 1:

To an oven-dried 20 mL Schlenk purged under argon atmosphere, the pre-catalyst Pd(OAc)<sub>2</sub> (2.91 mg, 0.013 mmol, 1 equiv) was dissolved in the degassed solvent (0.6 mL). Dppf (14.41 mg, 0.026 mmol, 2 equiv) and base (0.065 mmol, 5 equiv) were added. The reaction was stirred for 20 minutes at the desired temperature and analyzed by <sup>31</sup>P NMR analysis. To calculate the conversion of the uncompleted reduction, the triethyl phosphonoacetate (0.0065 mmol, 0.5 equiv) was added as internal standard (IS).

To further demonstrate that the formation of Pd(0) specie occurred, the 3NO<sub>2</sub>ArI (16.2 mg, 0.065 mmol, 5 equiv) was added to detect the formation of the oxidative addition (OA) complex.

Table 18. All experiments carried out to study the Pd(OAc)<sub>2</sub>dppf reduction in both DMF-d<sub>7</sub> and HEP/DMF-d<sub>7</sub><sup>a</sup>. Rows underlined in grey have already been reported Table 9.

Solvent	Base	T (°C)	Mech.	Pd(0)/Pd(II) <sup>b</sup>	P/OH°
DMF <sup>d</sup>	-	25	E	20/80	100/0
DMF	TMG	25	D	100/0	100/0
DMF	-	60	Е	100/0	100/0
DMF	TMG	60	D/E	100/0	100/0
	DMF <sup>d</sup> DMF	DMF <sup>d</sup> - DMF TMG DMF -	DMF <sup>d</sup> -         25           DMF         TMG         25           DMF         -         60	DMF <sup>d</sup> -         25         E           DMF         TMG         25         D           DMF         -         60         E	DMF <sup>d</sup> -         25         E         20/80           DMF         TMG         25         D         100/0           DMF         -         60         E         100/0

5	DMF	Cs <sub>2</sub> CO <sub>3</sub>	60	E	100/0	100/0
6	DMF	K <sub>2</sub> CO <sub>3</sub>	60	E	100/0	100/0
7	DMF/HEP <sup>e</sup>	K₂CO₃	25	Α	100/0	0/100
8	DMF/HEP	Cs <sub>2</sub> CO <sub>3</sub>	25	A/E	100/0	55/45

<sup>&</sup>lt;sup>a</sup> The reactions were carried out according to the **General Procedure 1** 

# <sup>31</sup>P NMR spectra of complete reduction as an example in both DMF and HEP/DMF a) Entry 2, Table 18:

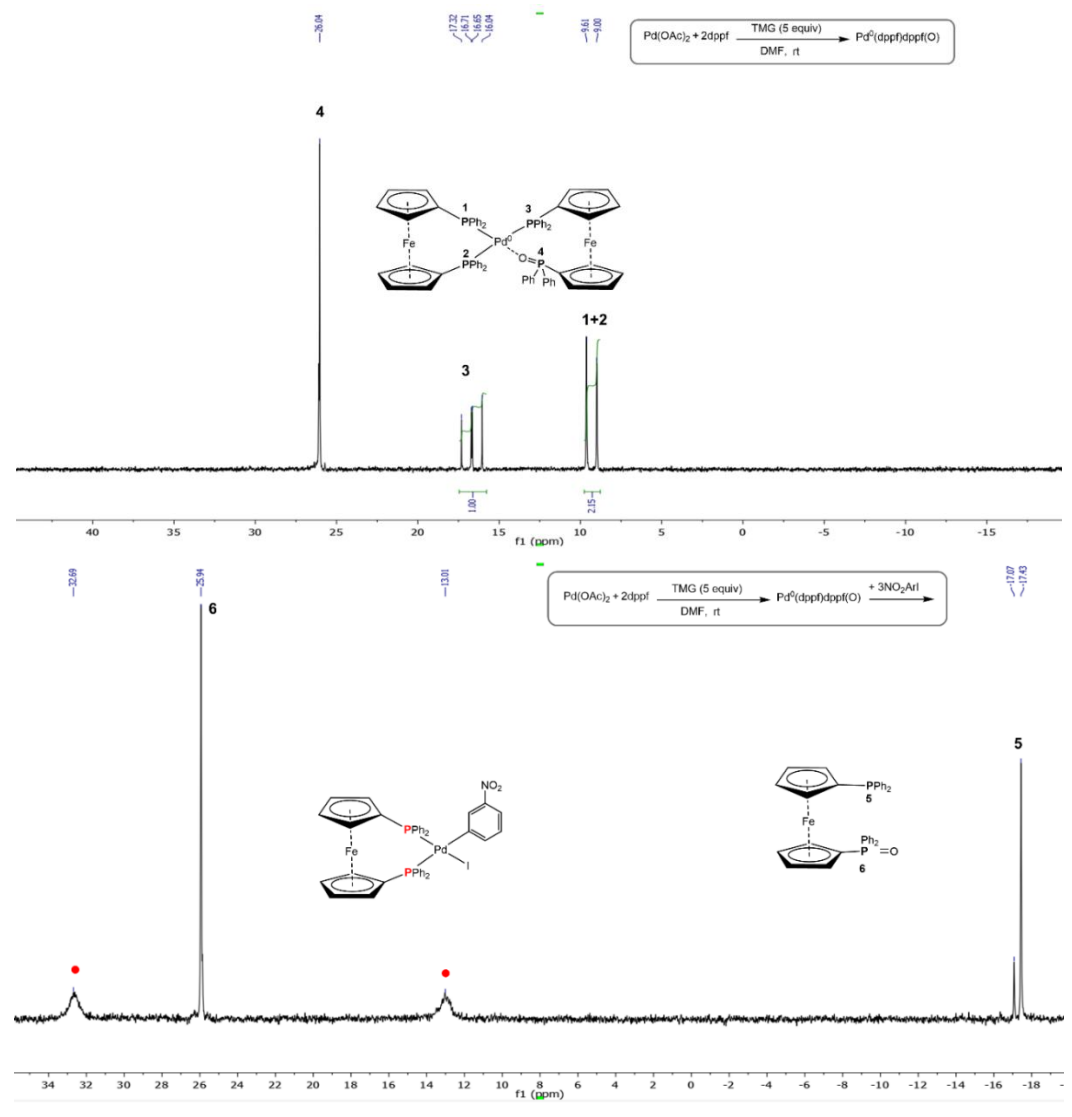


Figure 93.  $Pd(OAc)_2 + 2 dppf + Cs_2CO_3$  (5 equiv) in DMF-d<sub>7</sub> at rt for 20 min (top); after the addition of 3NO<sub>2</sub>ArI to confirm the disappearance of the Pd(0) species (bottom).

<sup>&</sup>lt;sup>b</sup> The conversion was calculated by <sup>31</sup>P NMR comparing the signals of the IS signal and Pd(OAc)<sub>2</sub>dppf

 $<sup>^{</sup>c}$ P/OH represents the ratio between the oxidation of phosphine (P) or alcohol (OH) to form Pd(0) and "nd" = not determined.

 $<sup>^{</sup>d}\,600\mu L$  of DMF-d7

 $<sup>^</sup>e$  The solvent is a mixture of HEP 200  $\mu L$  and DMF-d7  $400 \mu L$ 

## b) Entry 8, Table 18:

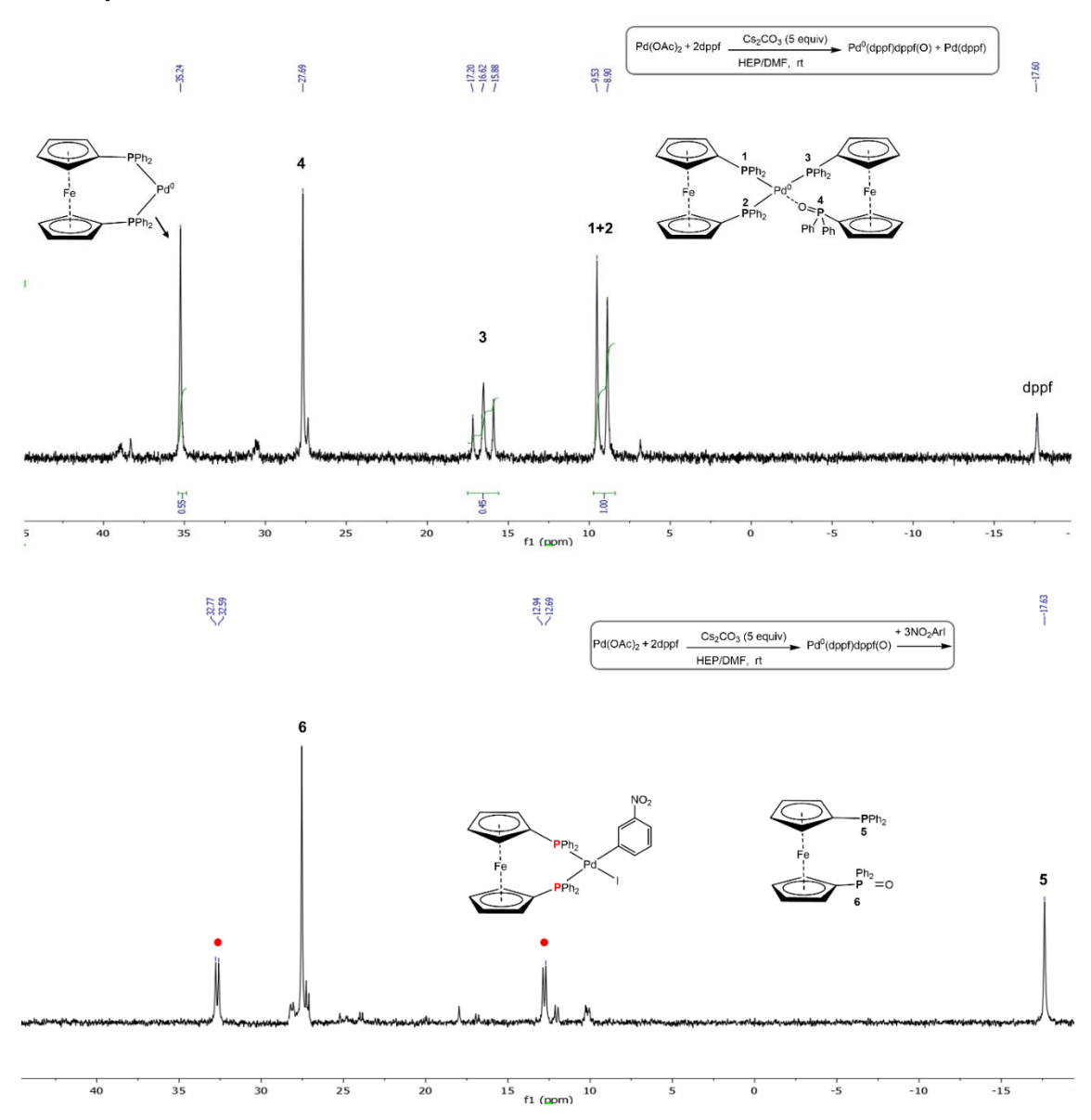


Figure 94.  $Pd(OAc)_2 + 2 dppf + Cs_2CO_3$  (5 equiv) in HEP/DMF-d<sub>7</sub> (4/2) at rt for 20 min (top); after the addition of  $3NO_2ArI$  to confirm the disappearance of the Pd(0) species (bottom).

### PdCl<sub>2</sub>

# General Procedure 2:

To an oven-dried 20 mL Schlenk purged under argon atmosphere, the pre-catalyst Pd(dppf)Cl<sub>2</sub> CH<sub>2</sub>Cl<sub>2</sub>(10.61 mg, 0.013 mmol, 1 equiv) was dissolved in the degassed solvent (0.6 mL). Dppf (7.20 mg, 0.013 mmol, 1 equiv) and base (0.065 mmol, 5 equiv) were added. The reaction was stirred for 20 minutes at the desired temperature and

analyzed by <sup>31</sup>P NMR analysis. To calculate the conversion of the uncompleted reduction, the triethyl phosphonoacetate (0.0065 mmol, 0.5 eq) was added as internal standard (IS).

Table 19. All experiments carried out to study the  $Pd(dppf)Cl_2$  reduction in both DMF-d7 and HEP/DMF-d7<sup>a</sup>. Rows underlined in grey have already been reported Table 9.

Entry	Solvent	Base	T (°C)	Mech.	Pd(0)/Pd(II) <sup>b</sup>	P/OH <sup>c</sup>
1	DMF <sup>d</sup>	DMF	25	-	0/100	-
2	DMF	TMG	25	D	100/0	100/0
3	DMF	Cs <sub>2</sub> CO <sub>3</sub>	25		39/61	100/0
4	DMF	-	60	-	0/100	-
5	DMF	Cs <sub>2</sub> CO <sub>3</sub>	60	Е	100/0	100/0
6	DMF	K₂CO₃	60	Е	100/0	100/0
7	DMF	TMG	60	E	100/0	100/0
8	DMF	TEA	80	-	0/100	-
9	DMF/HEPe	TMG	25	A/D	100/0	91/9
10	DMF/HEP	Cs <sub>2</sub> CO <sub>3</sub>	25	A/E	100/0	23/77
11	DMF/HEP	K <sub>2</sub> CO <sub>3</sub>	25	Α	100/0	0/100
12	DMF/HEP	TMG	60	D	100/0	100/0
13	DMF/HEP	Cs <sub>2</sub> CO <sub>3</sub>	60	A/E	100/0	81/19
14	DMF/HEP	K₂CO₃	60	A/E	100/0	84/16

 $<sup>^{\</sup>rm a}$  The reactions were carried out according to the  ${\bf General\ Procedure\ 2}$ 

<sup>&</sup>lt;sup>b</sup> The conversion was calculated by <sup>31</sup>P NMR comparing the signals of the IS signal and Pd(dppf)Cl<sub>2</sub>

<sup>&</sup>lt;sup>c</sup>P/OH represents the ratio between the oxidation of phosphine (P) or alcohol (OH) to form Pd(0) and "nd" = not determined.

d 600µL of DMF-d7

 $<sup>^</sup>e$  The solvent is a mixture of HEP 200  $\mu L$  and DMF-d7 400  $\mu L$ 

# <sup>31</sup>P NMR spectra of complete reduction as an example in both DMF and HEP/DMF a) Entry 2, Table 19:

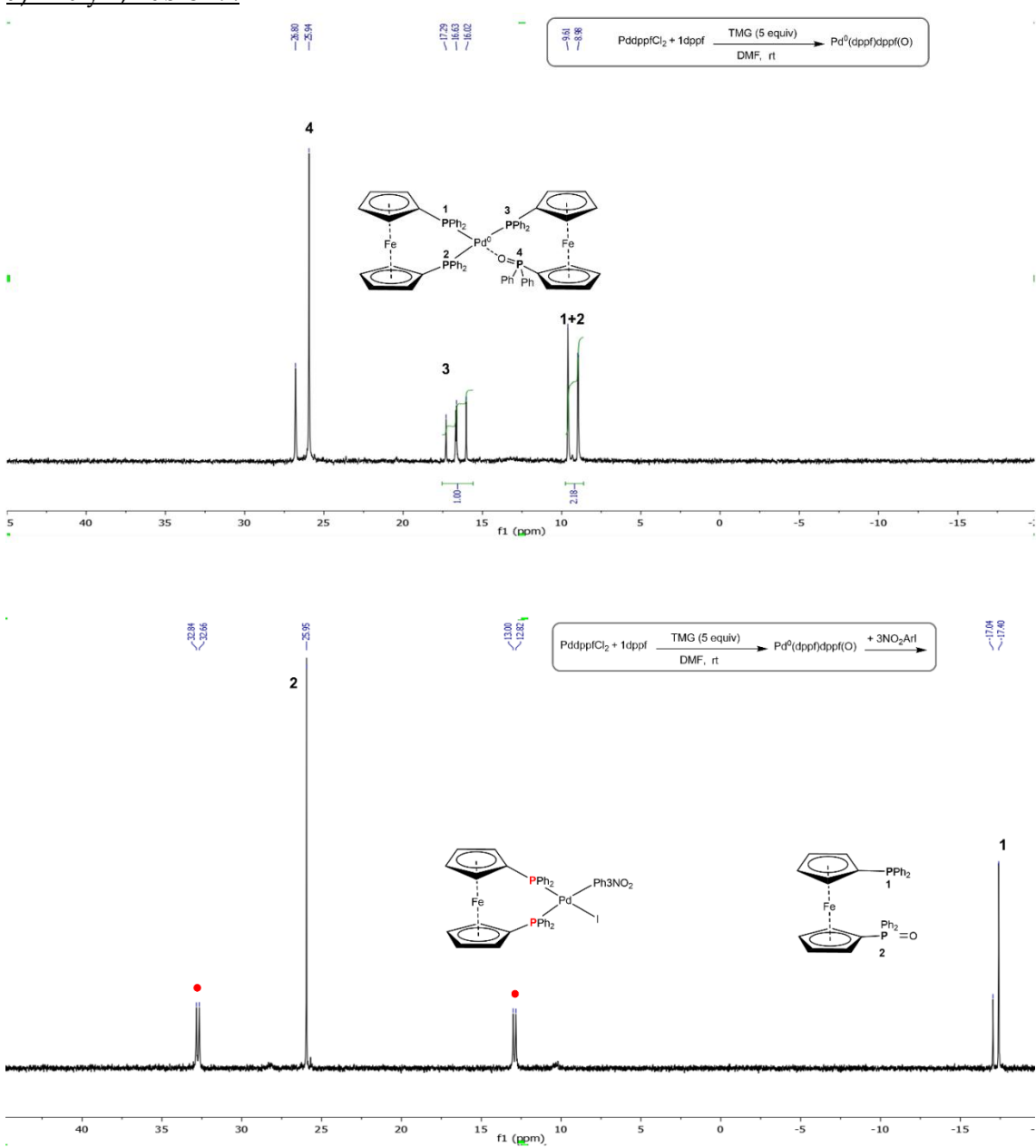


Figure 95.  $Pd(dppf)Cl_2 + 1 dppf + TMG$  (5 equiv) in DMF-d<sub>7</sub> at rt for 20 min (top); after the addition of  $3NO_2ArI$  to confirm the disappearance of the Pd(0) species (bottom).

# b) Entry 10, Table 19:

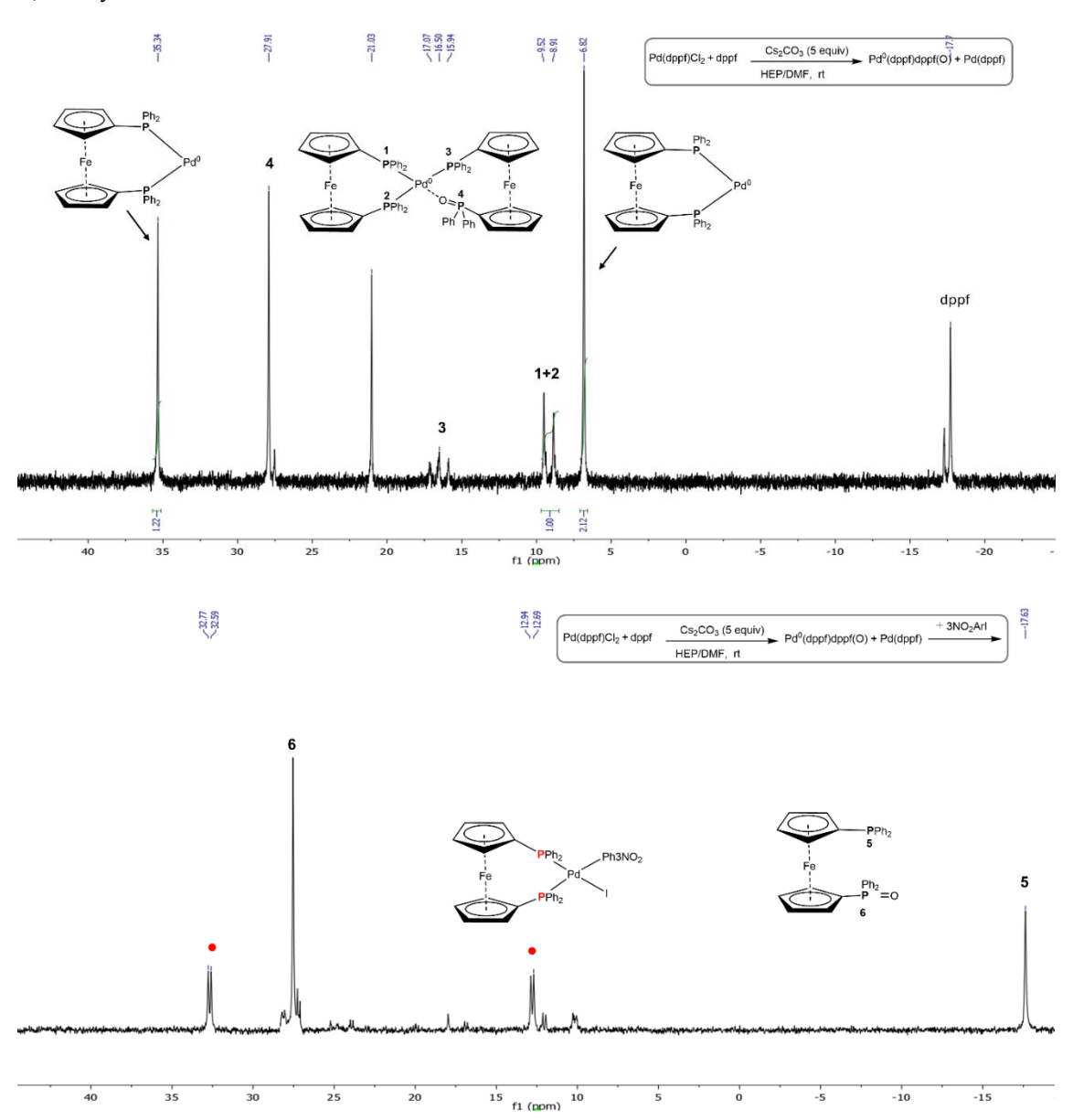


Figure 96.  $Pd(dppf)Cl_2 + 1 dppf + Cs_2CO_3$  (5 equiv) in DMF-d<sub>7</sub> at rt for 20 min (top); after the addition of  $3NO_2ArI$  to confirm the disappearance of the Pd(0) species (bottom).

# 2.2.4.4. Palladium pre-catalyst reduction with dppp

Table 20. <sup>31</sup>P NMR chemical shift in DMF-d<sub>7</sub> and HEP/DMF-d<sub>7</sub> (2:4) of palladium species with dppp.

entry	Compound	DMF-d <sub>7</sub>	HEP/DMF-d <sub>7</sub> (2:4)
1	dppp	-16.94	-17.01
2	dppp(O) <sup>a,b</sup>	-16.88; 30	-16.96; 31.71
3	Pd <sup>0</sup> (dppp) <sup>b</sup>	4.64	4.55

4	Pd(OAc) <sub>2</sub> (dppp) <sup>b</sup>	11.31	11.44
5	Pd <sup>0</sup> dppp(O)	12.37; 30.12	12.53; 31.60
6	Pd(dppp)Cl <sub>2</sub>	13.11	13.25
7	dpppO <sup>b</sup>	30.58	31.83

<sup>&</sup>lt;sup>a</sup> dppp(O) is the label for the dppp mono-oxide

#### Pd(OAc)<sub>2</sub>

#### **General Procedure 1:**

Pd(OAc)<sub>2</sub> + 2 dppp Base (5 equiv) 
$$\rightarrow$$
 Pd<sup>0</sup>(dppp)

Solvent
 $T (^{\circ}C)$ 

To an oven-dried 20 mL Schlenk purged under argon atmosphere, the pre-catalyst Pd(OAc)<sub>2</sub> (2.91 mg, 0.013 mmol, 1 equiv) was dissolved in the degassed solvent (0.6 mL). Dppp (10.71 mg, 0.026 mmol, 2 equiv) and base (0.065 mmol, 5 equiv) were added. The reaction was stirred for 20 minutes at the desired temperature and analyzed by <sup>31</sup>P NMR analysis. To calculate the conversion of the uncompleted reduction, the triethyl phosphonoacetate (0.0065 mmol, 0.5 eq) was added as internal standard (IS).

To further demonstrate that the formation of Pd(0) specie occurred, the 3NO<sub>2</sub>ArI (16.2 mg, 0.065 mmol, 5 equiv) was added to detect the formation of the oxidative addition (OA) complex.

Table 21. All experiments carried out to study the Pd(OAc)<sub>2</sub>dppp reduction in both DMF-d<sub>7</sub> and HEP/DMF-d<sub>7</sub><sup>a</sup>. Rows underlined in grey have already been reported in Table 10.

Entry	Solvent	Base	T (°C)	Mech.	Pd(0)/Pd(II)b	P/OH <sup>c</sup>
1	DMF <sup>d</sup>	-	25	E	11/89	100/0
2	DMF	TMG	25	-	0/100	-
3	DMF	Cs <sub>2</sub> CO <sub>3</sub>	25	E	23/77	100/0
4	DMF	-	60	Е	100/0	100/0
5	DMF	Cs <sub>2</sub> CO <sub>3</sub>	60	E	100/0	100/0
6	DMF	K <sub>2</sub> CO <sub>3</sub>	60	E	100/0	100/0
7	DMF/HEP <sup>e</sup>	Cs <sub>2</sub> CO <sub>3</sub>	25	A/E	100/0	nd
8	DMF/HEP	K <sub>2</sub> CO <sub>3</sub>	25	A/E	100/0	nd

b According to the literature<sup>[224]</sup>

9	DMF/HEP	Cs <sub>2</sub> CO <sub>3</sub>	60	A/E	100/0	nd
10	DMF/HEP	K <sub>2</sub> CO <sub>3</sub>	60	A/E	100/0	nd

<sup>&</sup>lt;sup>a</sup> The reactions were carried out according to the **General Procedure 1** 

# <sup>31</sup>P NMR spectra of complete reduction as an example in both DMF and HEP/DMF a) Entry 5, Table 21:

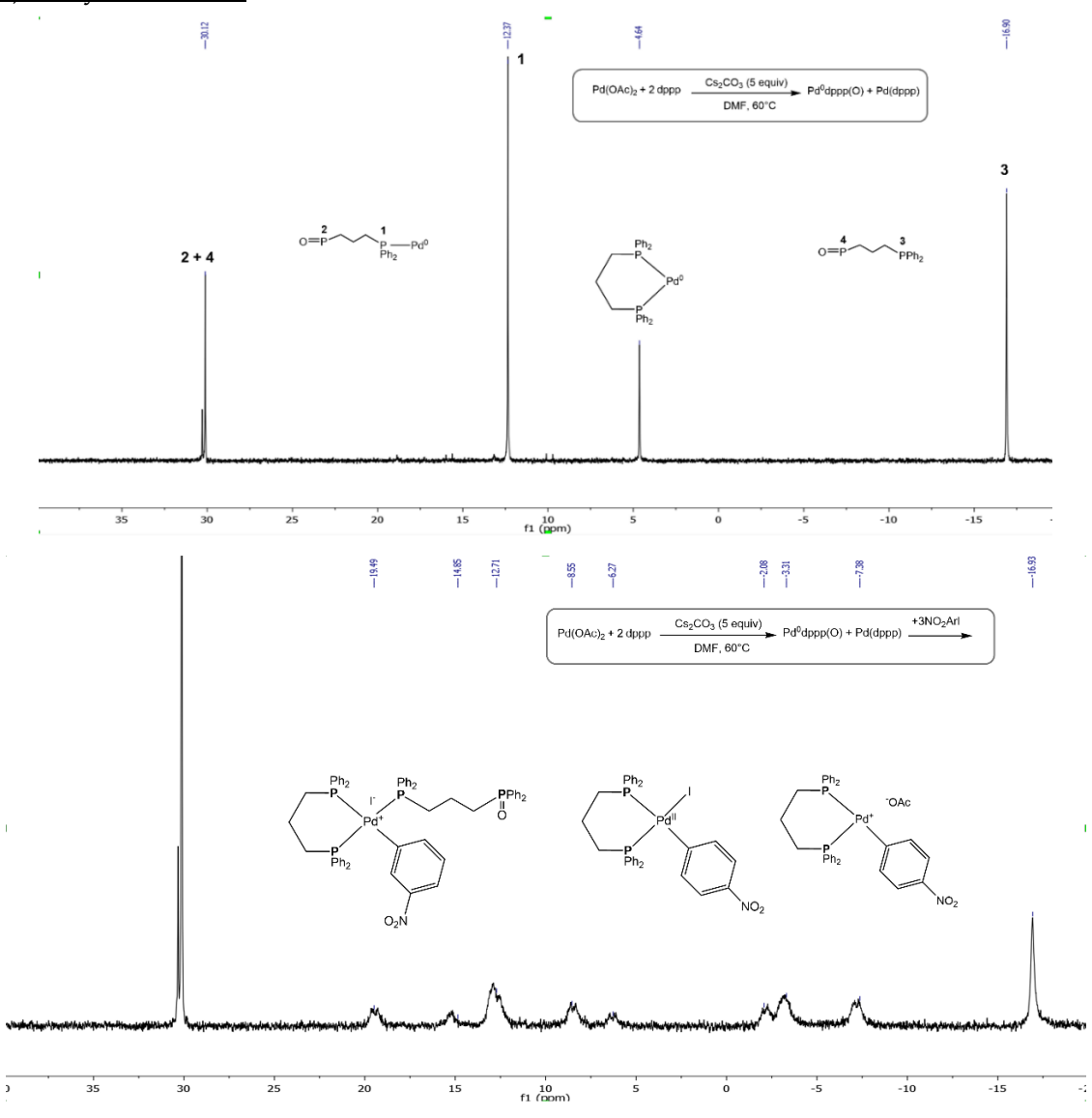


Figure 97.  $Pd(OAc)_2 + 2 dppp + Cs_2CO_3$  (5 equiv) in DMF-d<sub>7</sub> at 60°C for 20 min (top); after the addition of 3NO<sub>2</sub>ArI to confirm the disappearance of the Pd(0) species (bottom). The Pd(0) species potentially involved are shown in the first figure and all of them disappeared after the addition of the aryl halide. The possible oxidative addition complexes involved are described according to the literature<sup>[87]</sup>. Unfortunately, after the addition of the aryl halide, the spectra usually showed poor quality and broad signals.

<sup>&</sup>lt;sup>b</sup> The conversion was calculated by <sup>31</sup>P NMR comparing the signals of the IS signal and Pd(OAc)<sub>2</sub>(dppp)

<sup>&</sup>lt;sup>c</sup>P/OH represents the ratio between the oxidation of phosphine (P) or alcohol (OH) to form Pd(0) and "nd"= means not determined.

 $<sup>^</sup>d$  600 $\mu$ L of DMF-d7

 $<sup>^</sup>e$  The solvent is a mixture of HEP 200  $\mu L$  and DMF-d7 400  $\mu L$ 

## b) Entry 7, Table 21:

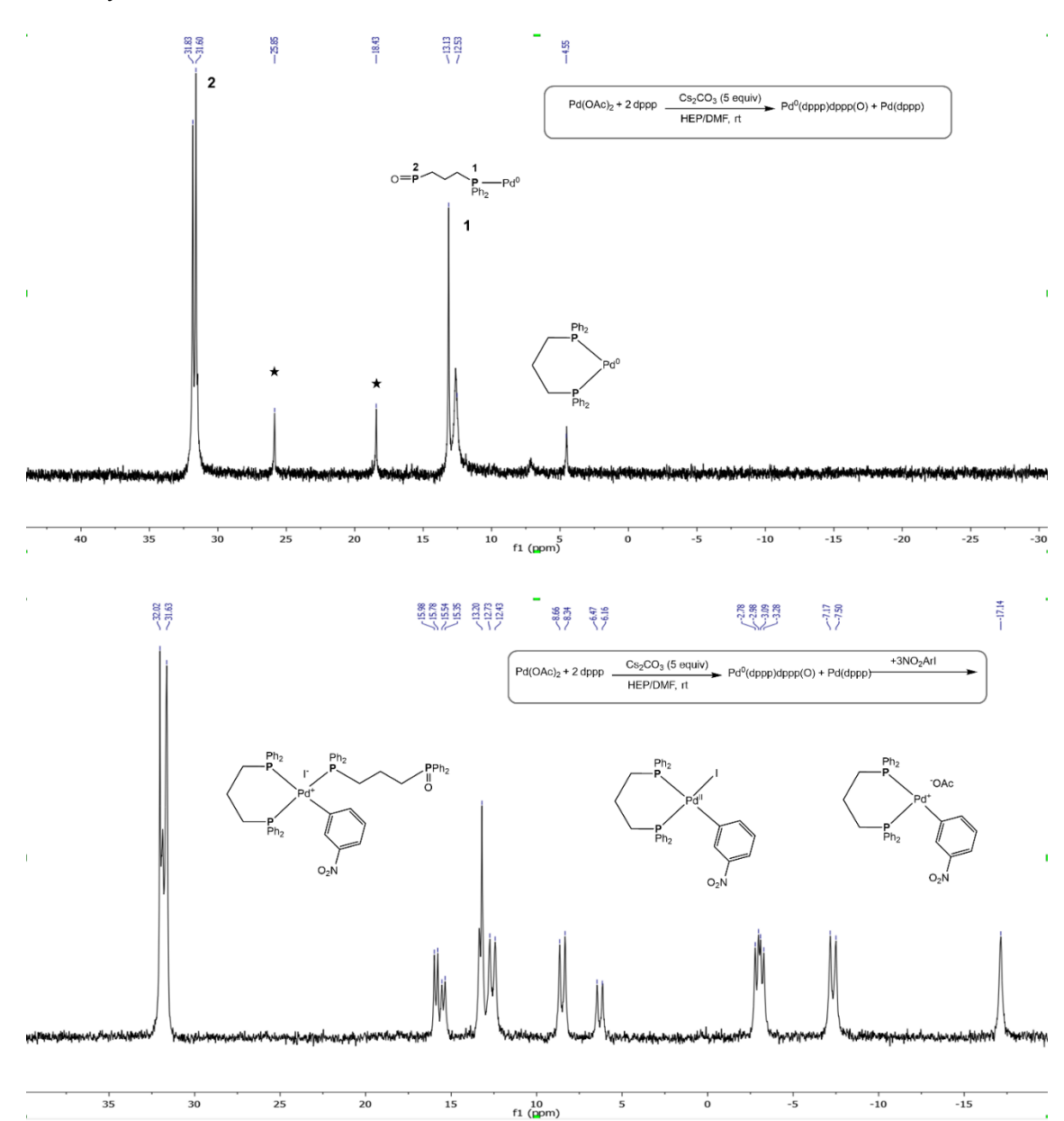


Figure 98.  $Pd(OAc)_2 + 2 dppp + Cs_2CO_3$  (5 equiv) in HEP/DMF-d<sub>7</sub> (2/4) at rt for 20 min (top); after the addition of  $3NO_2ArI$  to confirm the disappearance of the Pd(0) species (bottom). The Pd(0) species potentially involved are shown in the first figure (as the labelled peaks at 25.85 ppm and 18.43 ppm, disappeared after the addition of the aryl halide, it is reasonable to assume that these are some Pd(0) species).

The possible oxidative addition complexes involved are described according to the literature<sup>[87]</sup>. Unfortunately, after the addition of the aryl halide, the spectra usually showed poor quality and broad signals.

#### PdCl<sub>2</sub>

### General Procedure 2:

$$\begin{array}{c} \mathsf{Pd}(\mathsf{ACN})_2\mathsf{Cl}_2 + 2\mathsf{dppp} & \xrightarrow{\mathsf{Base}\ (5\ \mathsf{equiv})} & \mathsf{Pd}^0(\mathsf{dppp}) \\ \hline & \mathsf{Solvent} \\ & \mathsf{T}\ (^\circ\mathsf{C}) \end{array}$$

To an oven-dried 20 mL Schlenk purged under argon atmosphere, the pre-catalyst  $Pd(ACN)_2Cl_2$  (3.41 mg, 0.013 mmol, 1 equiv) was dissolved in the degassed solvent (0.6 mL). Dppp (10.71 mg, 0.026 mmol, 2 equiv) and base (0.065 mmol, 5 equiv) were added. The reaction was stirred for 20 minutes at the desired temperature and analyzed by  $^{31}P$  NMR analysis.

To further demonstrate that the formation of Pd(0) specie occurred, 3NO<sub>2</sub>ArI (16.2 mg, 0.065 mmol, 5 equiv) was added to detect the formation of the oxidative addition (OA) complex.

Table 22. All experiments carried out to study the Pd(dppp)Cl<sub>2</sub> reduction in both DMF-d $_7$  and HEP/DMF-d $_7$ <sup>a</sup>. Rows underlined in grey have already been reported in Table 10.

Entry	Solvent	Base	T (°C)	Mech.b	Pd(0)/Pd(II) <sup>b</sup>	P/OH <sup>c</sup>
1	DMF <sup>d</sup>	-	25	-	0/100	-
2	DMF	Cs <sub>2</sub> CO <sub>3</sub>	25	-	0/100	-
3	DMF	K <sub>2</sub> CO <sub>3</sub>	25	-	0/100	-
4	DMF	-	60	-	0/100	-
5	DMF	TMG	60	-	0/100	-
6	DMF	Cs <sub>2</sub> CO <sub>3</sub>	60	E	100/0	100/0
7	DMF	K <sub>2</sub> CO <sub>3</sub>	60	E	100/0	100/0
8	DMF/HEPd	Cs <sub>2</sub> CO <sub>3</sub>	25	Α	100/0	0/100
9	DMF/HEP	K <sub>2</sub> CO <sub>3</sub>	25	Α	55/45	0/100
10	DMF/HEP	Cs <sub>2</sub> CO <sub>3</sub>	60	A/E	100/0	nd
11	DMF/HEP	K <sub>2</sub> CO <sub>3</sub>	60	A/E	100/0	nd

<sup>&</sup>lt;sup>a</sup> The reactions were carried out according to the **General Procedure 2** 

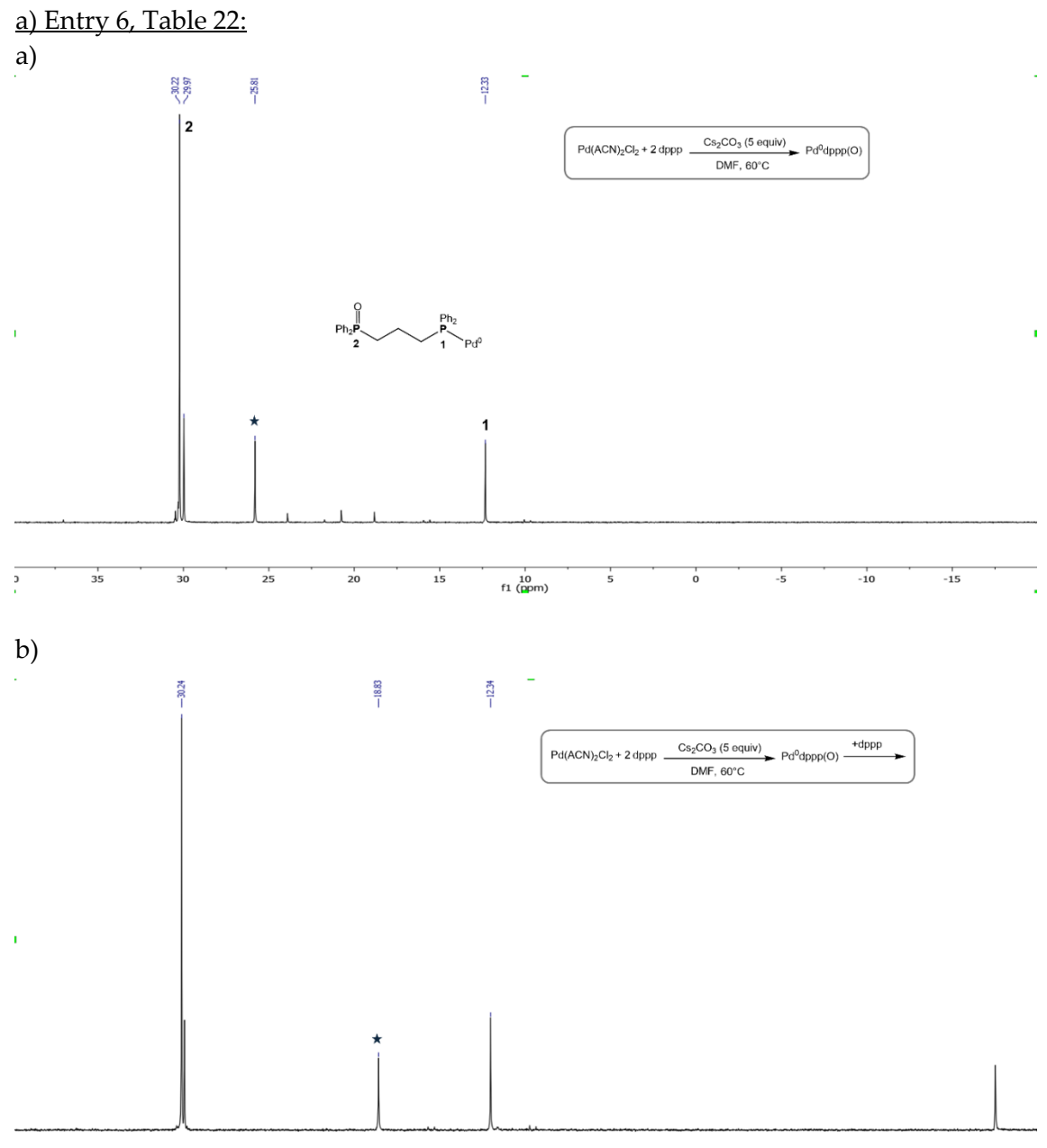
<sup>&</sup>lt;sup>b</sup> The conversion was calculated by <sup>31</sup>P NMR comparing the signals of the IS signal and Pd(dppp)Cl<sub>2</sub>

<sup>&</sup>lt;sup>c</sup>P/OH represents the ratio between the oxidation of phosphine (P) or alcohol (OH) to form Pd(0) and "nd" = not determined.

d 600µL of DMF-d7

 $<sup>^{</sup>e}$  The solvent is a mixture of HEP 200  $\mu L$  and DMF-d7 400  $\mu L$ 

<sup>31</sup>P NMR spectra of complete reduction as an example in both DMF and HEP/DMF



25

20

10 f1 (ppm)

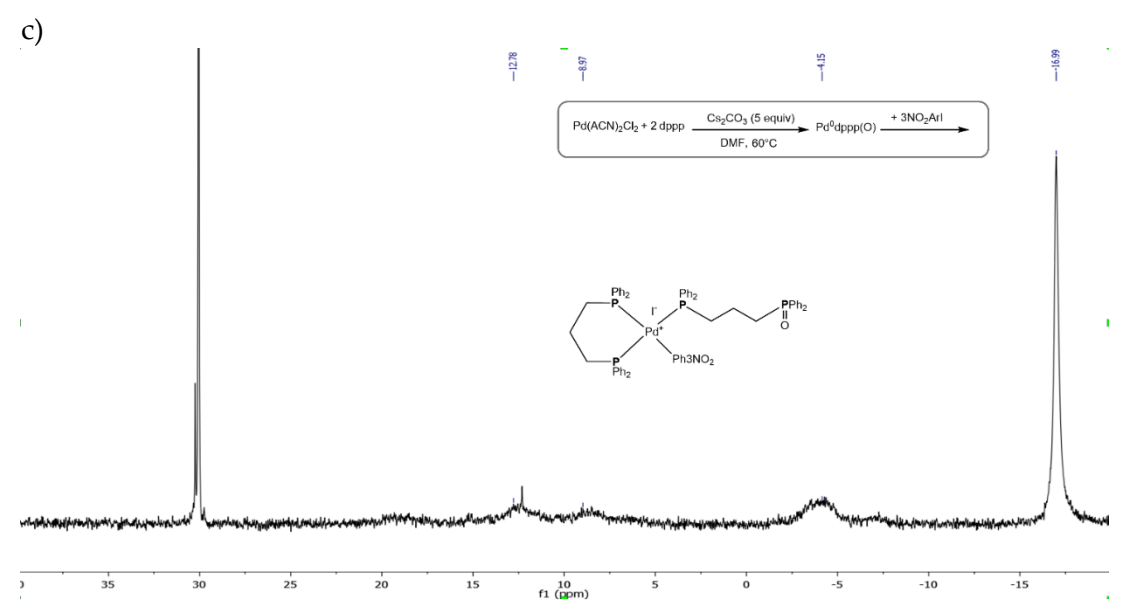
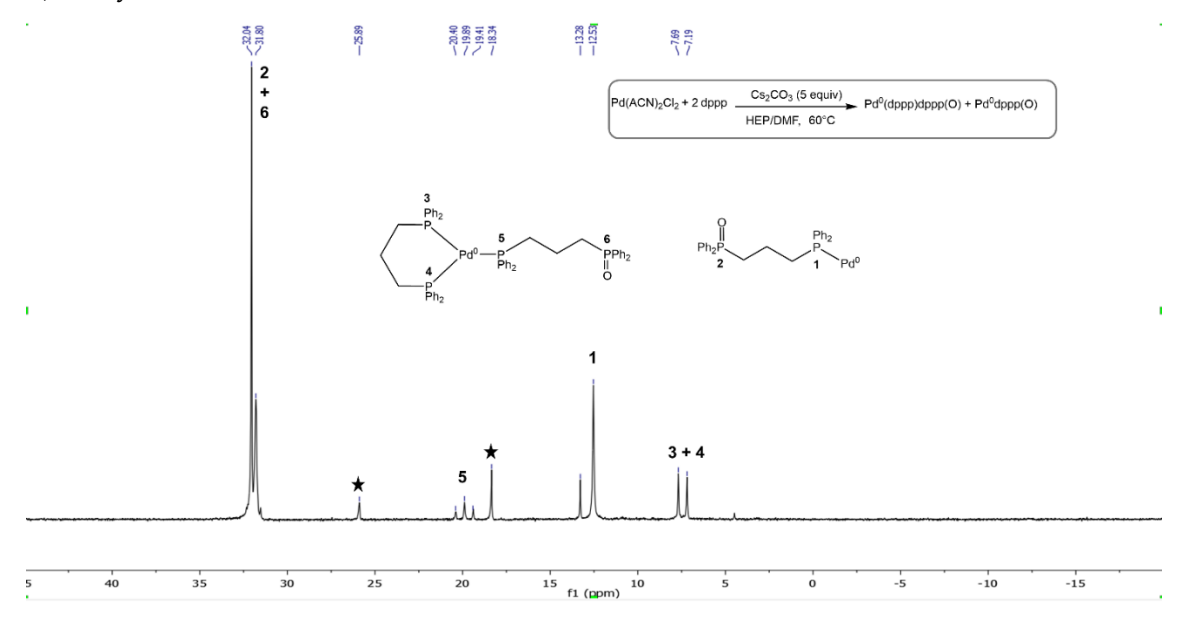


Figure 99.  $Pd(ACN)_2Cl_2 + 2 dppp + Cs_2CO_3$  (5 equiv) in DMF-d<sub>7</sub> at 60°C for 20 min (a); after the addition of 1 equiv dppp, the peak at 25.81 ppm disappeared and the peak at 18.83 ppm appeared (b); Although the resolution of the  $^{31}P$  NMR spectra is often poor after the addition of aryl halide, the Pd(0) species have clearly disappeared after the addition of the  $^{31}P$  NMR species at 25.81 ppm and 18.83 ppm are Pd(0) species in equilibrium.

# b) Entry 10, Table 22:



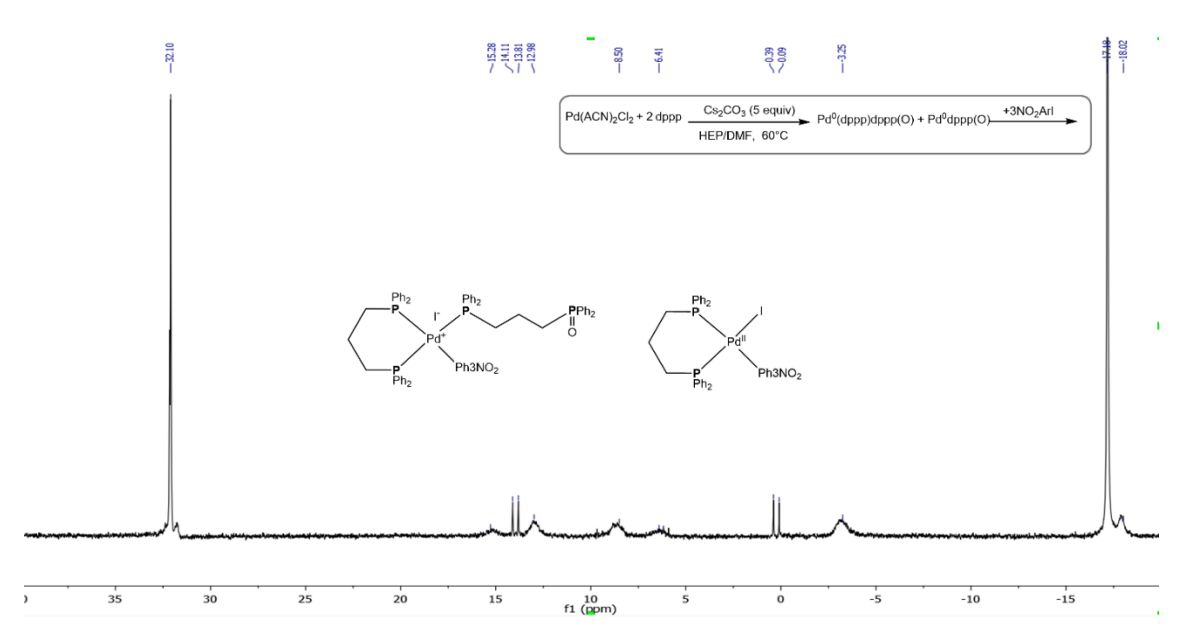


Figure 100.  $Pd(ACN)_2Cl_2 + 2 dppp + Cs_2CO_3$  (5 equiv) in HEP/DMF-d7 (2/4) at 60°C for 20 min (top); after the addition of  $3NO_2ArI$  (below). As the labelled peaks at 25.89 ppm and 18.34 ppm, disappeared after the addition of aryl halide, it is reasonable to assume that these are Pd(0) species. The possible oxidative addition complexes involved are shown, according to the literature<sup>[87]</sup>

### 2.2.4.5. Palladium pre-catalyst reduction with Xantphos

Table 23. <sup>31</sup>P NMR chemical shift in DMF-d<sub>7</sub> and HEP/DMF-d<sub>7</sub> (2:4) of palladium species with Xantphos.

entry	Compound	DMF-d <sub>7</sub>	HEP/DMF-d <sub>7</sub> (2:4)	
1	Xantphos	-17.79	-18.03	
2	Xantphos(O) <sup>a</sup> -21.83; 25		-	
3	3NO <sub>2</sub> ArPd <sup>II</sup> Xantphos(O) <sup>b</sup>	9.42; 25.02	10.22	
4	3NO <sub>2</sub> ArPdIXantphos	11.00	10.24	
5	Pd <sup>0</sup> Xantphos(O)	17.08; 41.57	17.03; 41.54	
6	Pd <sup>0</sup> Xantphos	19.39	19.18	
7	PdCl₂Xantphos	22.70	22.13	
8	OXantphos	27.56	28.60	

<sup>&</sup>lt;sup>a</sup> Xantphos(O) is the label for the Xantphos mono-oxide

As the pre-catalyst Pd(OAc)<sub>2</sub>Xantphos is not soluble in DMF-d<sub>7</sub>, we used THF-d<sub>8</sub> instead of DMF

<sup>&</sup>lt;sup>b</sup> According to the literature<sup>[219]</sup>

entry	Compound	THF-d <sub>8</sub>	HEP/ THF-d <sub>8</sub> (2:4)	
1	Xantphos(O)	-21.5; 23.16	-21.70; 28.41	
2	3NO <sub>2</sub> ArPdI(Xantphos)	10.87	10.79	
3	3NO <sub>2</sub> ArPd <sup>II</sup> Xantphos(O) <sup>b</sup>	11.62; 40.38	11.75, 40.65	
4	Pd <sup>0</sup> Xantphos	18.86	18.80	
5	Pd <sup>0</sup> Xantphos(O)	20.22; 39.53	-	
6	Pd(OAc) <sub>2</sub> Xantphos	25.51	-	
7	OXantphos	-	29	

Table 24. 31P NMR chemical shift in THF-ds and HEP/THF-ds (2:4) of palladium species with Xantphos.

# Synthesis of palladium species with Xantphos

a) Entry 2, Table 23: Xantphos(O)

To an oven-dried 20 mL Schlenk purged under argon atmosphere,  $Pd(OAc)_2$  (3.4 mg, 0.015 mmol, 0.03 equiv), Xantphos (289.3 mg, 0.5 mmol, 1 equiv), 1,2-dibromoethane (65 $\mu$ L, 0.75 mmol, 1.5 equiv), 10% NaOH aq. solution (2 mL) were added in 1.5 mL of degassed 1,2-dicloroethane (DCE).

The result mixture was allowed to stir at 20°C for 12 hours, then warmed to 50°C for 5 hours, and at 80°C for 2 hours. Then, the result mixture was diluted with water (5 mL), extracted with DCM (3 x 5 mL), the combined organic layers were washed with brine and dried over Na<sub>2</sub>SO<sub>4</sub>. The solvent was removed by rotary evaporator and the crude material was purified by silica gel chromatography (DCM/EtOAc 100/0 to 60:40) to yield desired product as a pale yellow solid (30 mg, 17% yield)<sup>[227]</sup>.

# b) Entries 4 and 6, Table 23: 3NO<sub>2</sub>ArPdI(Xantphos) and Pd<sup>0</sup>Xantphos

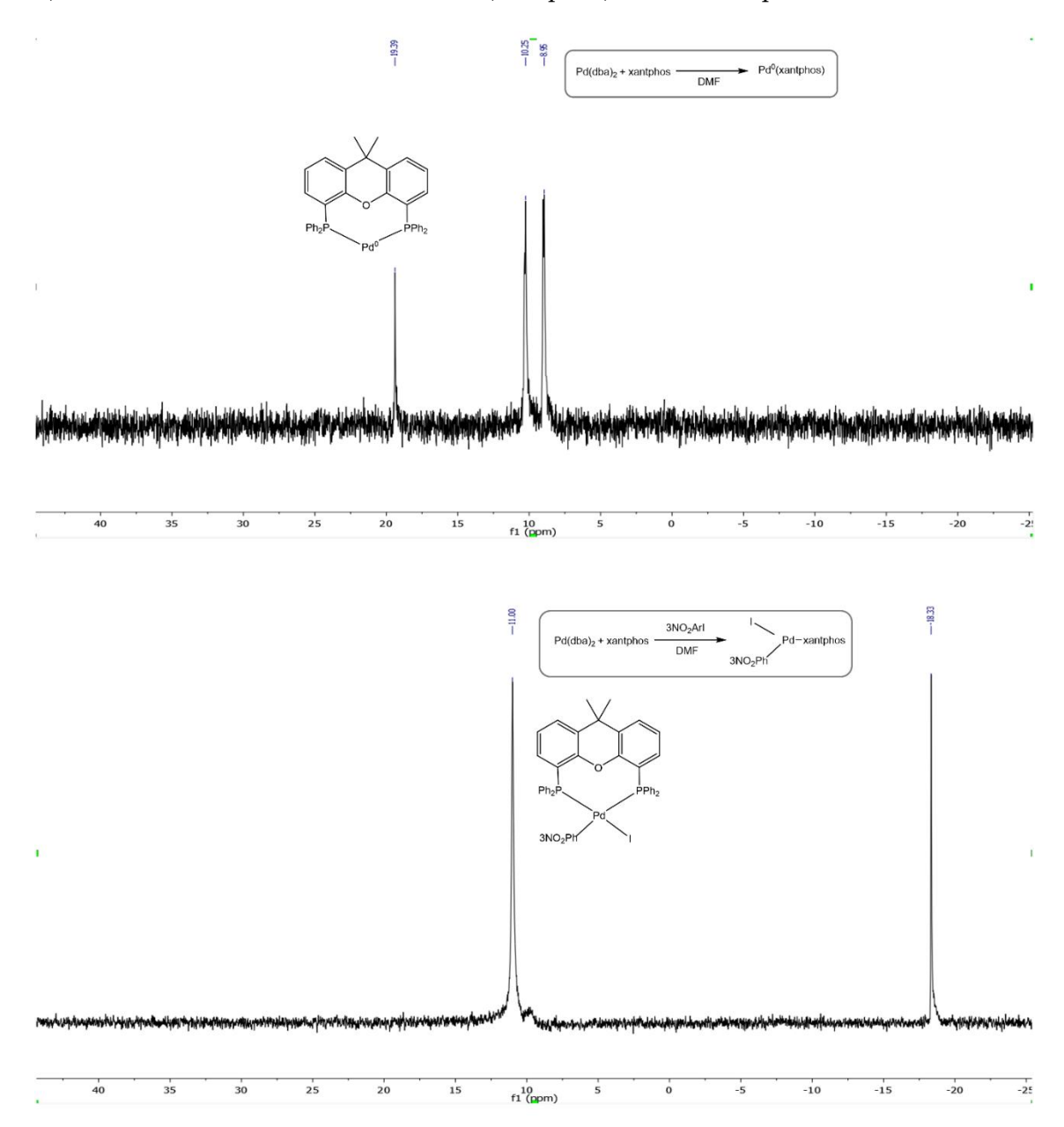


Figure 101.  $Pd(dba)_2(11.9 \text{ mg}, 0.013 \text{ mmol}, 1 \text{ equiv})$ , Xantphos (6.94 mg, 0.013, 1 equiv) in DMF-d7. The peaks at 10.25, 8.95 ppm are related to the dba coordinated to the Pd compound (top); addition of  $3NO_2ArI$  (16.18 mg, 0.065, 5 equiv) in DMF-d7 (bottom).

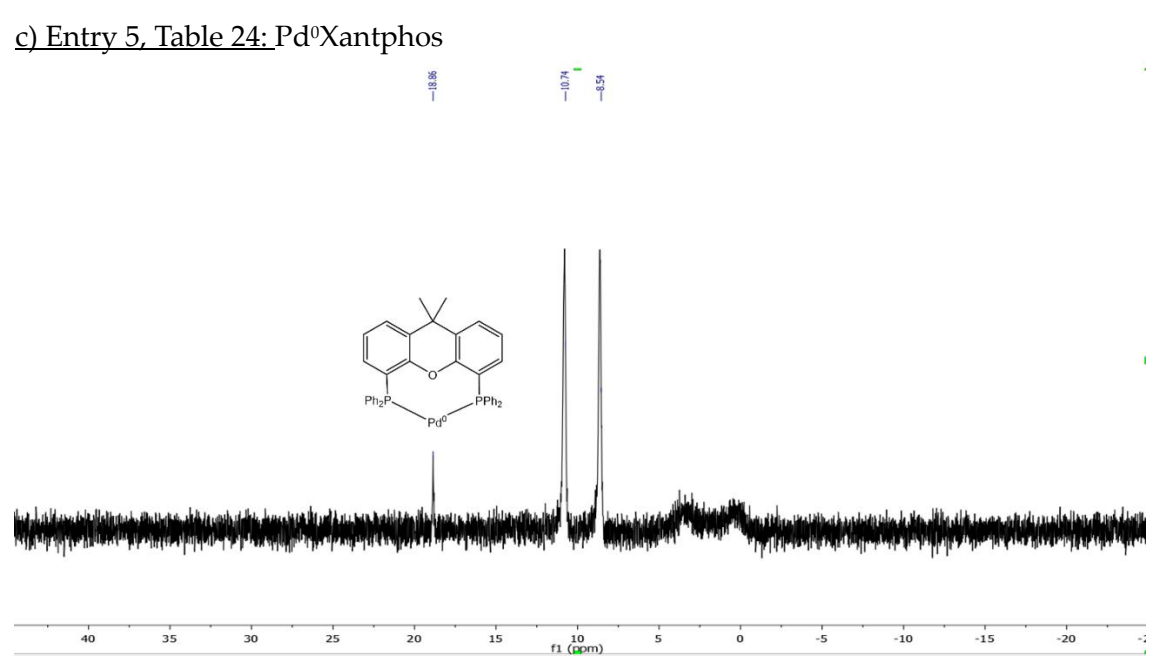


Figure 102. Pd(dba)<sub>2</sub> (11.9 mg, 0.013 mmol, 1 equiv), xantphos (6.94 mg, 0.013, 1 equiv) in THF-ds. The peaks at 10.74, 8.54 ppm are related to the dba coordinated to the Pd compound<sup>[225]</sup>.

#### • Pd(OAc)<sub>2</sub>

#### **General Procedure 1:**

To an oven-dried 20 mL Schlenk purged under argon atmosphere, the pre-catalyst Pd(OAc)<sub>2</sub> (2.91 mg, 0.013 mmol, 1 equiv) was dissolved in the degassed solvent (0.6 mL). Xantphos (7.52 mg, 0.013 mmol, 1 equiv) and base (0.065 mmol, 5 equiv) were added. The reaction was stirred for 20 minutes at the desired temperature and analysed by <sup>31</sup>P NMR analysis.

To further demonstrate that the formation of Pd(0) specie occurred, 3NO<sub>2</sub>ArI (16.2 mg, 0.065 mmol, 5 equiv) was added to detect the formation of the oxidative addition (OA) complex.

All the results have already been shown in Table 11, entries 8-14.

# <sup>31</sup>P NMR spectra of complete reduction as an example in both THF and HEP/THF Entry 9, Table 11:

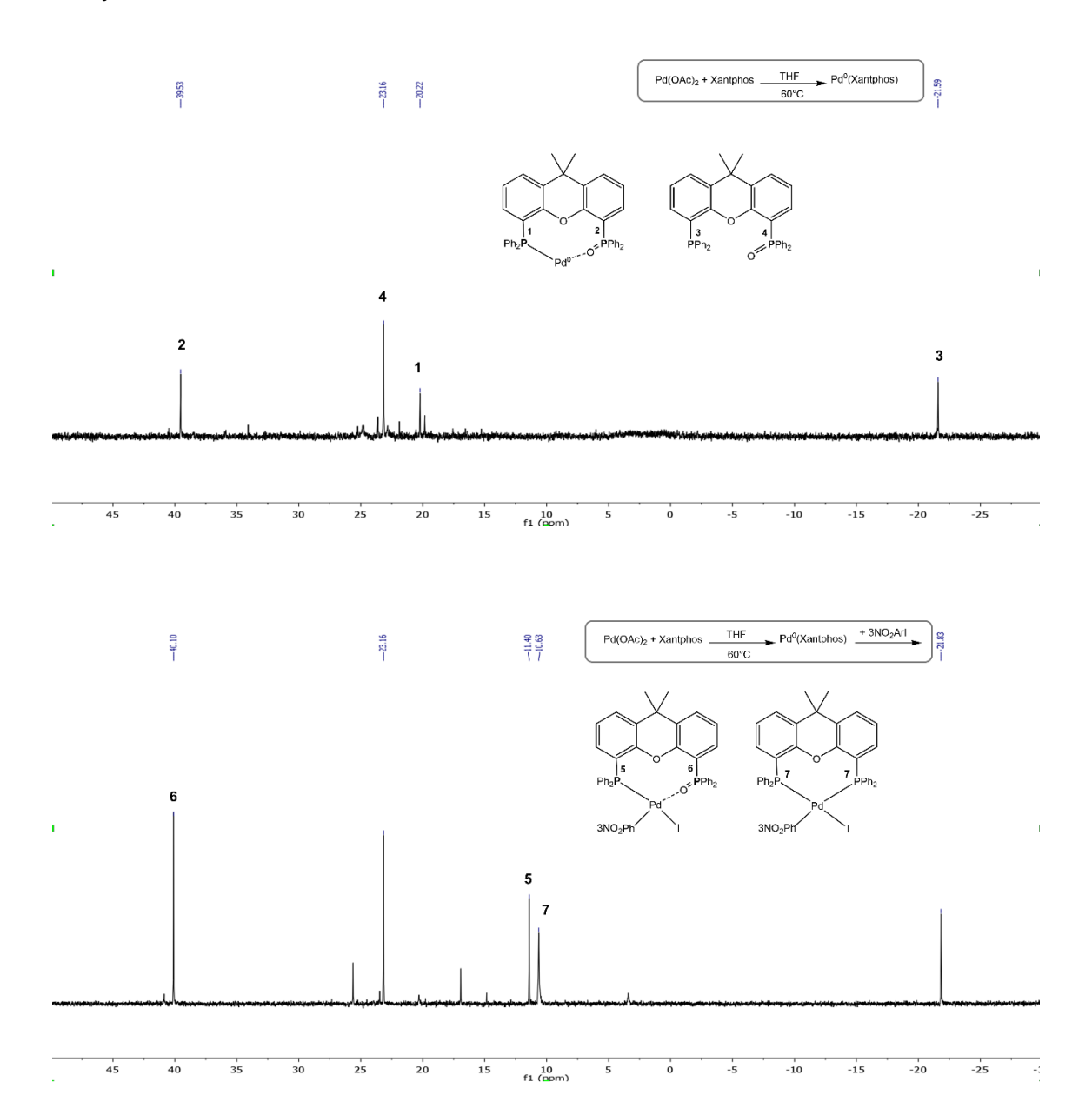


Figure 103.  $Pd(OAc)_2 + 1$  Xantphos THF-ds at 60°C for 20 min (top); after the addition of  $3NO_2ArI$  to confirm the disappearance of the Pd(0) species (bottom).

## b) Entry 14, Table 11:

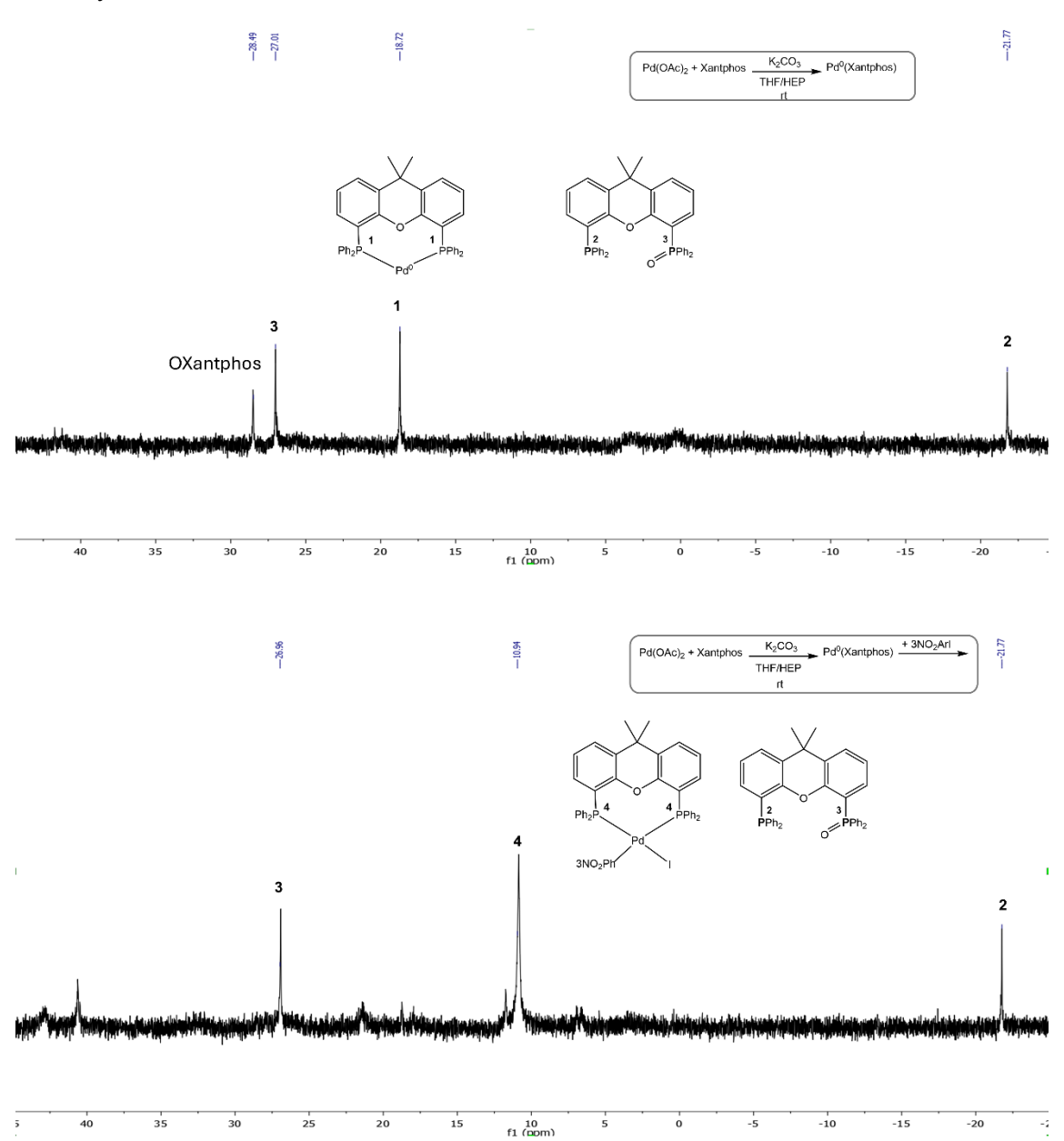


Figure 104.  $Pd(OAc)_2 + 1$  Xantphos +  $K_2CO_3$  (5 equiv) THF-ds at rt 20 min (top); after the addition of  $3NO_2ArI$  to confirm the disappearance of the Pd(0) species (bottom).

### PdCl<sub>2</sub>

# General Procedure 2:

To an oven-dried 20 mL Schlenk purged under argon atmosphere, the pre-catalyst  $Pd(ACN)_2Cl_2$  (3.37 mg, 0.013 mmol, 1 equiv) was dissolved in the degassed solvent (0.6 mL). Xantphos (7.52 mg, 0.013 mmol, 1 equiv) and base (0.065 mmol, 5 equiv) were

added. The reaction was stirred for 20 minutes at the desired temperature and analyzed by  $^{31}\mathrm{P}$  NMR analysis.

To further demonstrate that the formation of Pd(0) specie occurred, 3NO<sub>2</sub>ArI (16.2 mg, 0.065 mmol, 5 equiv) was added to detect the formation of the oxidative addition (OA) complex.

Table 25. All experiments carried out to study the  $Pd(Xantphos)Cl_2$  reduction in both DMF-d<sub>7</sub> and HEP/DMF-d<sub>7</sub><sup>a</sup>. Rows underlined in grey have already been reported in Table 11.

Entry	Solvent	Base	T (°C)	Mech.	Pd(0)/Pd(II)b	P/OH <sup>c</sup>
1	DMF <sup>d</sup>	-	60	-	0/100	-
2	DMF	TEA	80	-	0/100	-
3	DMF	TMG	60	-	0/100	-
4	DMF	Cs <sub>2</sub> CO <sub>3</sub>	60	-	0/100	-
5	DMF	K <sub>2</sub> CO <sub>3</sub>	60	-	0/100	-
6	DMF	NaOAc	60	E	100/0	100/0
7	DMF/HEP <sup>e</sup>	Cs <sub>2</sub> CO <sub>3</sub>	25	Α	100/0	0/100
8	DMF/HEP	Cs <sub>2</sub> CO <sub>3</sub>	25	Α	100/0	0/100
9	DMF/HEP	Cs <sub>2</sub> CO <sub>3</sub>	60	Α	100/0	0/100
10	DMF/HEP	K₂CO₃	60	Α	100/0	0/100

 $<sup>^{\</sup>rm a}$  The reactions were carried out according to the  ${\bf General\, Procedure\, 2}$ 

<sup>&</sup>lt;sup>b</sup> The conversion was calculated by <sup>31</sup>P NMR comparing the signals of the IS signal and Pd(Xantphos)Cl<sub>2</sub>

<sup>&</sup>lt;sup>c</sup>P/OH represents the ratio between the oxidation of phosphine (P) or alcohol (OH) to form Pd(0) and "nd" = not determined.

 $<sup>^</sup>d$  600 $\mu$ L of DMF-d7

 $<sup>^</sup>e$  The solvent is a mixture of HEP 200  $\mu L$  and DMF-d7  $400 \mu L$ 

# <sup>31</sup>P NMR spectra of complete reduction as an example in both DMF and HEP/DMF a) Entry 6, Table 25:

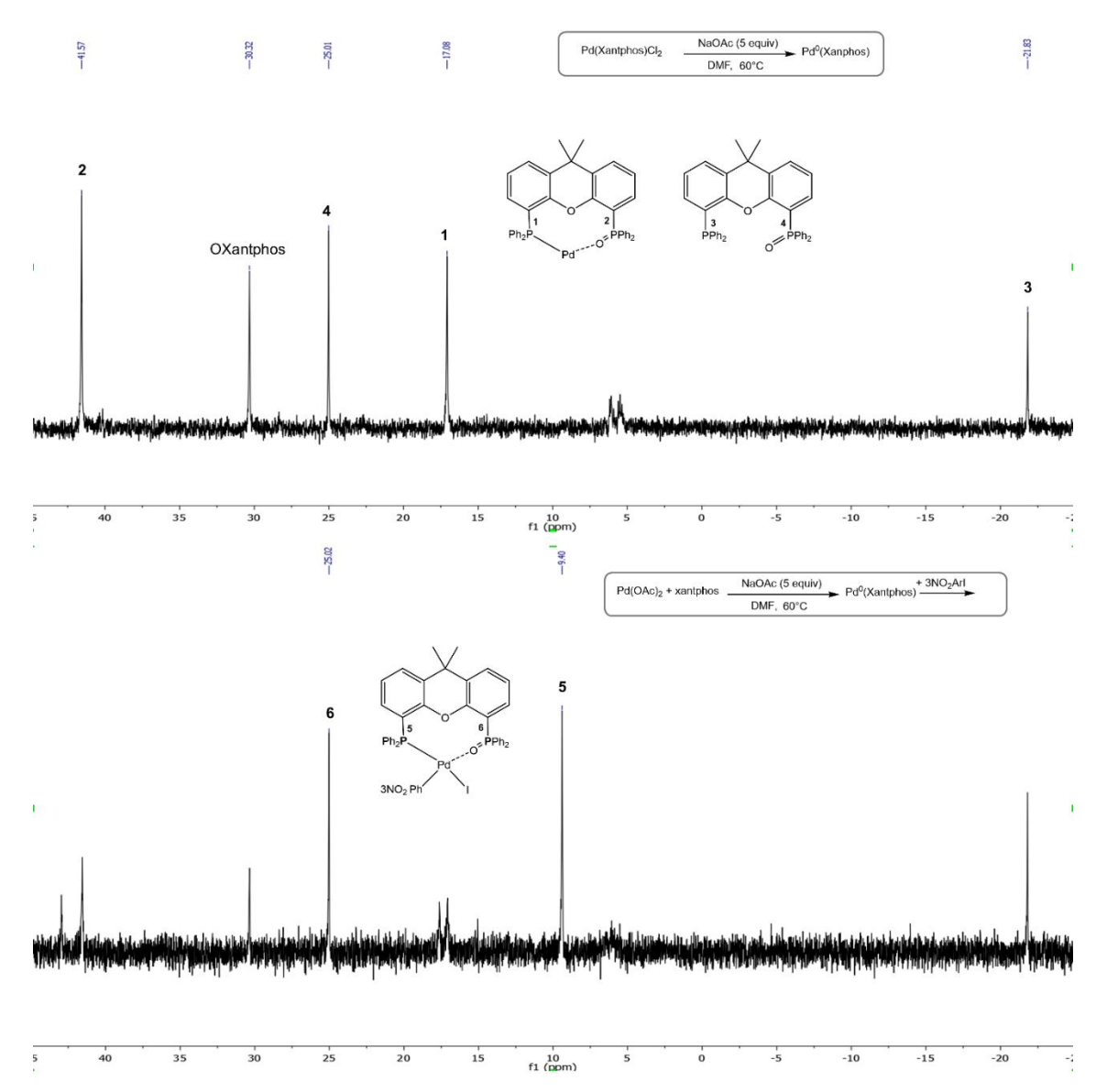


Figure 105.  $Pd(ACN)_2Cl_2 + 1$  Xantphos + NaOAc (5 equiv) DMF-d7 at 60°C in 20 min (according to the literature<sup>[219]</sup>) (top); after the addition of 3NO<sub>2</sub>ArI to confirm the disappearance of the Pd(0) species (bottom). Those are not a good quality spectra, probably due to the insolubility issue of  $Pd(OAc)_2Xanpthos$ .

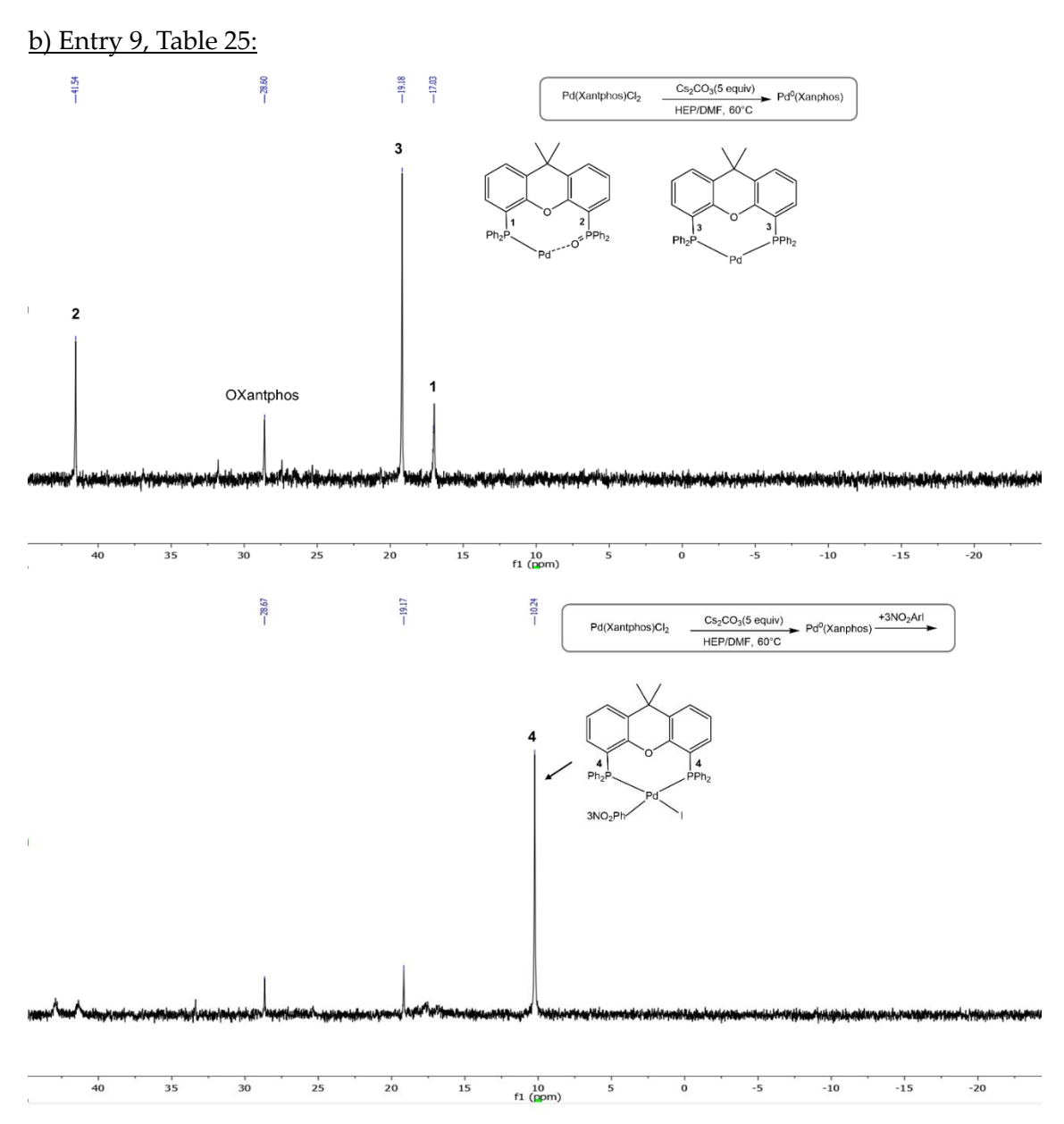


Figure 106.  $Pd(ACN)_2Cl_2 + 1$  Xantphos +  $Cs_2CO_3$  (5 equiv) HEP/DMF- $d_7$  (4/2) at 60°C in 20 min (top); after the addition of  $3NO_2ArI$  to confirm the disappearance of the Pd(0) species (bottom).

# 2.2.4.6. Palladium pre-catalyst reduction with SPhos

Table 26.  $^{31}P$  NMR chemical shift in DMF-d7 and HEP/DMF-d7 (2:4) of palladium species with SPhos

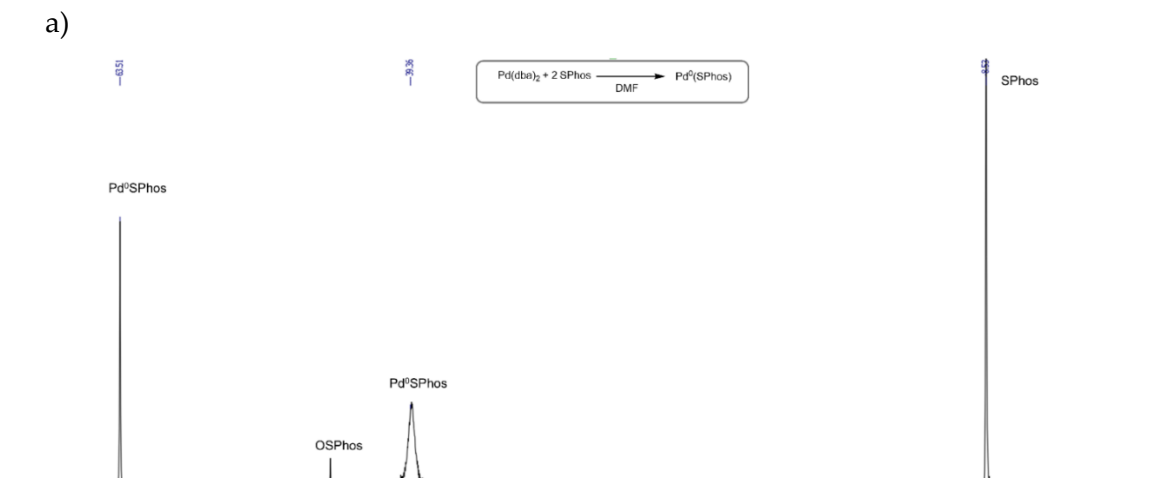
entry	Compound	DMF-d <sub>7</sub>	HEP/ DMF-d <sub>7</sub> (2:4)	
1	SPhos	-8.58	-8.73	
2	3NO <sub>2</sub> ArPd(SPhos)I	33.46	33.28	

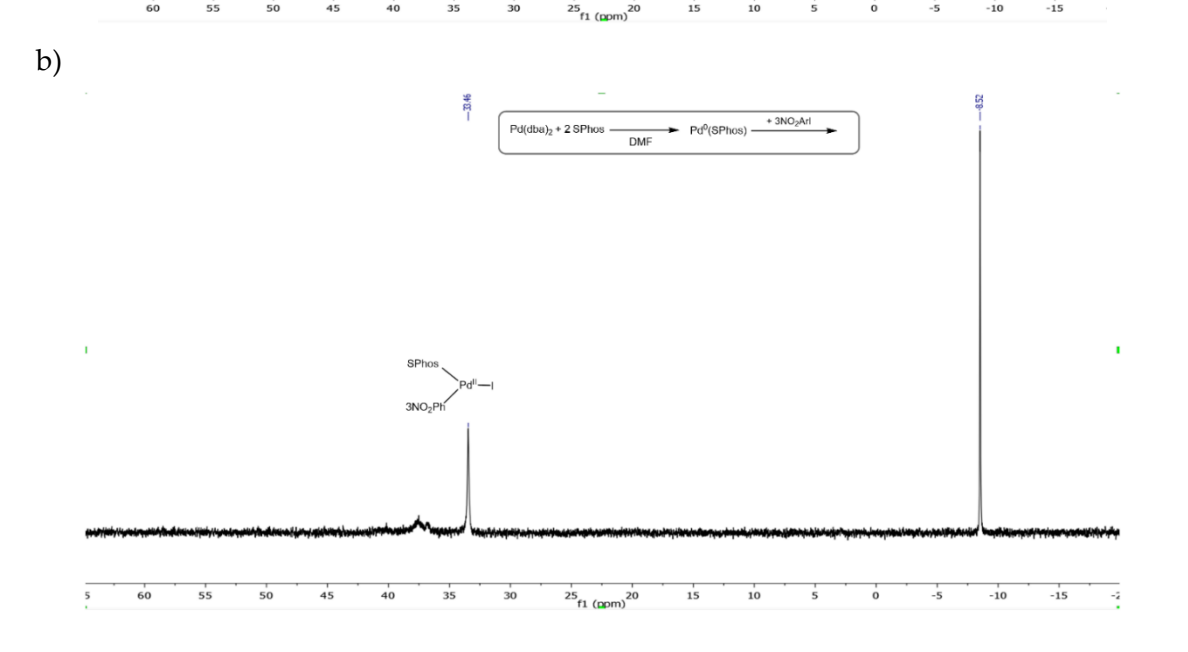
			<del>.</del>
3	Pd <sup>0</sup> (SPhos) <sup>a</sup>	39.18	39.30
4	Pd(SPhos) <sub>2</sub> Cl <sub>2</sub>	44.33	44.27
5	Pd(SPhos) <sub>2</sub> (OAc) <sub>2</sub>	46.01	48.50
6	OSPhos	46.03	48.30
7	3NO <sub>2</sub> ArPd(SPhos)(CsCO <sub>3</sub> )	51.21	48.83
8	Pd <sup>0</sup> (SPhos) <sup>a</sup>	63.50	63.30

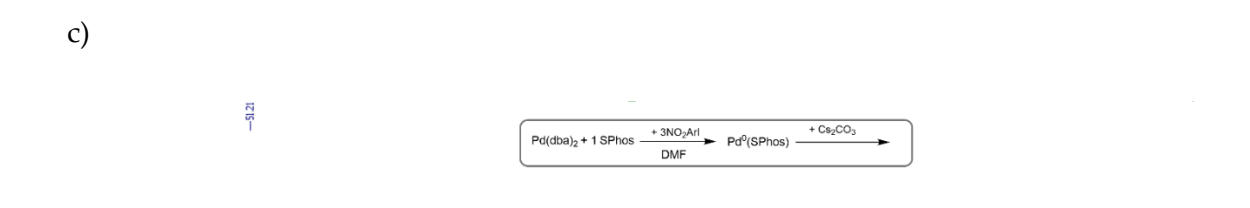
 $<sup>{}^{</sup>a}Pd^{0}\!\overline{SPhos}\ can\ exist\ in\ different\ conformations,\ according\ to\ the\ literature^{[228]}.$ 

# Synthesis of palladium species with SPhos

# <u>a) Entries 2, 7-8, Table 26:</u>







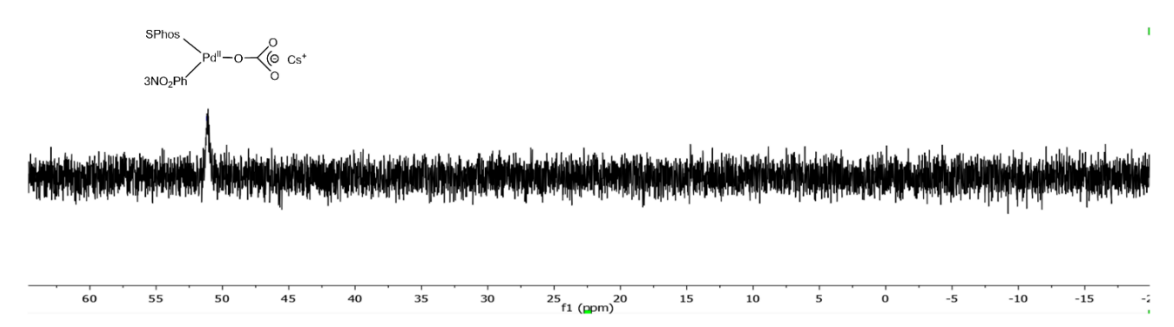


Figure 107.  $Pd(dba)_2$  (11.9 mg, 0.013 mmol, 1 equiv), SPhos (10.67 mg, 0.026, 2 equiv) in DMF-d7 (600  $\mu$ L) (a); addition of  $3NO_2ArI$  (16.17 mg, 0.065 mmol, 5 equiv) (b); After the addition of  $Cs_2CO_3$  (5 equiv), it is reasonable to assume that the species at 51.21 ppm is the one shown in the figure on the basis of the literature<sup>[229]</sup>.

#### Pd(OAc)<sub>2</sub>

### **General Procedure 1:**

To an oven-dried 20 mL Schlenk purged under argon atmosphere, the pre-catalyst Pd(OAc)<sub>2</sub> (2.91 mg, 0.013 mmol, 1 equiv) was dissolved in the degassed solvent (0.6 mL). SPhos (10.67 mg, 0.026 mmol, 2 equiv) and base (0.065 mmol, 5 equiv) were added. The reaction was stirred for 20 minutes at the desired temperature and analyzed by <sup>31</sup>P NMR analysis. To calculate the conversion of the uncompleted reduction, the triethyl phosphonoacetate (0.0065 mmol, 0.5 eq) was added as internal standard (IS).

To further demonstrate that the formation of Pd(0) specie occurred, 3NO<sub>2</sub>ArI (16.2 mg, 0.065 mmol, 5 equiv) was added to detect the formation of the oxidative addition (OA) complex.

Table 27. All experiments carried out to study the Pd(OAc)<sub>2</sub>(SPhos)<sub>2</sub> reduction in both DMF-d<sub>7</sub> and

HEP/DMF-d7<sup>a</sup>. Rows underlined in grey have already been reported in Table 12.

Entry	Solvent	Base	T (°C)	Mech.	Pd(0)/Pd(II) <sup>b</sup>	P/OH°
1	DMF <sup>d</sup>	-	25	-	0/100	-
2	DMF	TMG	25	-	0/100	-
3	DMF	Cs <sub>2</sub> CO <sub>3</sub>	25	E	71/29	100/0
4	DMF	K <sub>2</sub> CO <sub>3</sub>	25	E	54/46	100/0
5	DMF	-	60	E	29/71	100/0
6	DMF	TMG	60	E	15/85	100/0
7	DMF	Cs <sub>2</sub> CO <sub>3</sub>	60	E	100/0	100/0
8	DMF	K <sub>2</sub> CO <sub>3</sub>	60	E	100/0	100/0
9	DMF	TEA	80	E	25/75	100/0
10	DMF/HEP <sup>e</sup>	Cs <sub>2</sub> CO <sub>3</sub>	25	A/E	100/0	40/60
11	DMF/HEP	K₂CO₃	25	Α	100/0	0/100
12	DMF/HEP	TMG	60	A/E	31/69	nd

<sup>&</sup>lt;sup>a</sup> The reactions were carried out according to the **General Procedure 1** 

# <sup>31</sup>P NMR spectra of complete reduction as an example in both DMF and HEP/DMF a) Entry 8, Table 27:

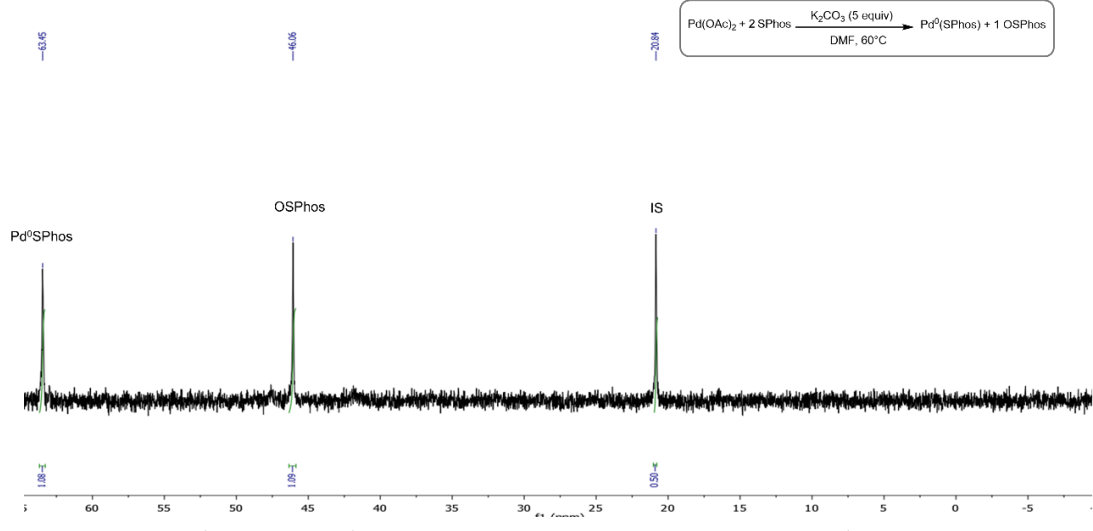


Figure 108.  $Pd(OAc)_2 + 2$  SPhos +  $K_2CO_3$  (5 equiv) + IS (0.5 equiv) in DMF-d7 at 60°C in 20 min.

<sup>&</sup>lt;sup>b</sup> The conversion was calculated by <sup>31</sup>P NMR comparing the signals of the IS signal and Pd<sup>0</sup>SPhos

 $<sup>^{</sup>c}$ P/OH represents the ratio between the oxidation of phosphine (P) or alcohol (OH) to form Pd(0) and "nd" = not determined.

 $<sup>^{</sup>d}$  600  $\mu L$  of DMF-d<sub>7</sub>

 $<sup>^</sup>e$  The solvent is a mixture of HEP 200  $\mu L$  and DMF-d7  $400 \mu L$ 

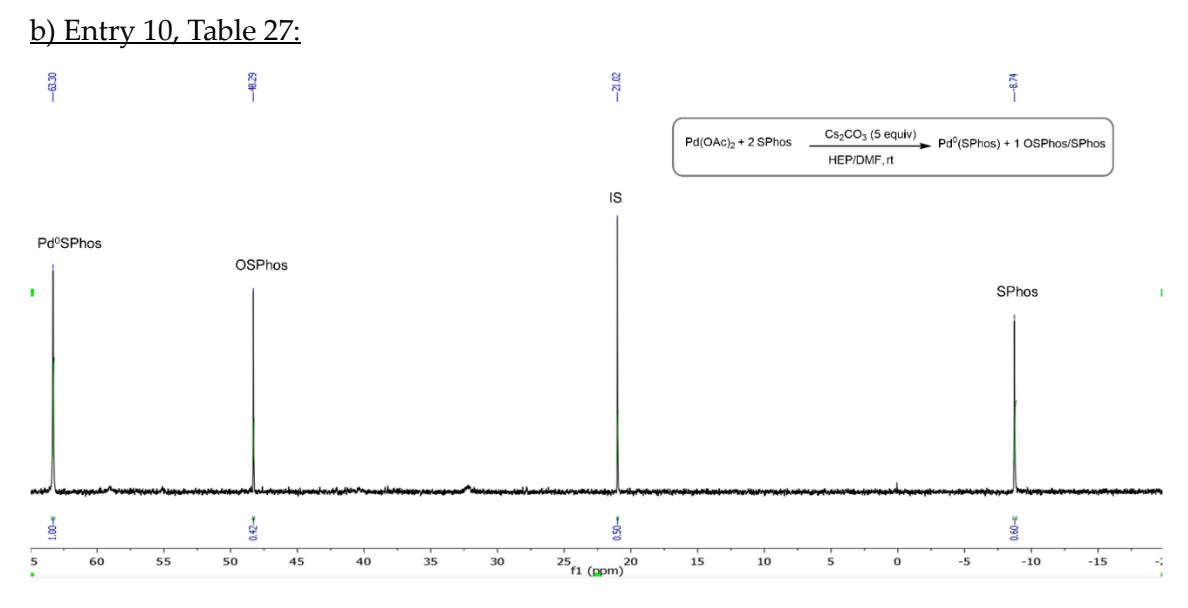


Figure 109. Pd(OAc)<sub>2</sub> + 2 SPhos + CsCO<sub>3</sub> (5 equiv) + IS (0.5 equiv) in HEP/DMF-d<sub>7</sub> (4/2) at rt in 20 min.

#### PdCl<sub>2</sub>

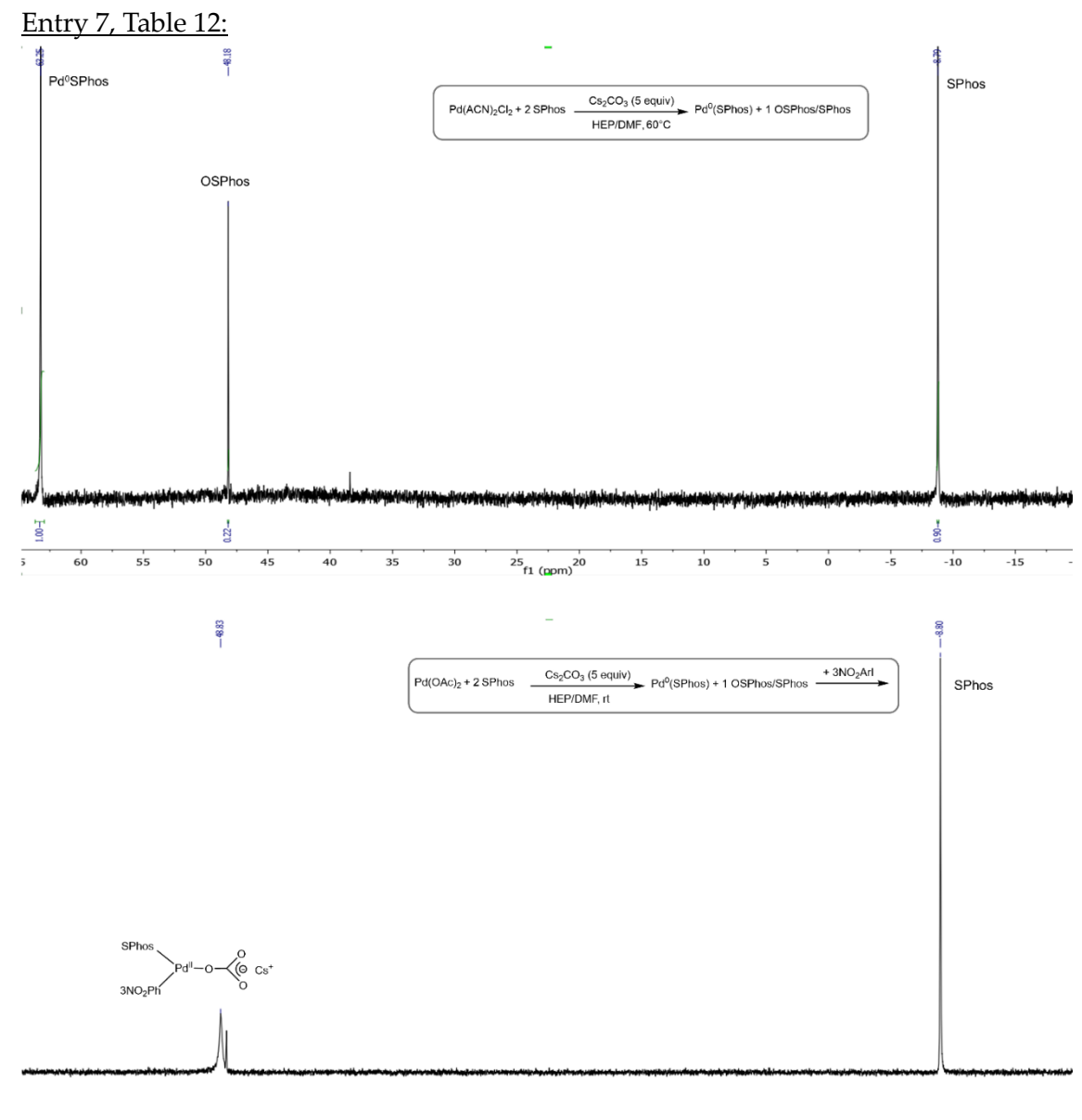
#### General Procedure 2:

$$\begin{array}{c|c} \mathsf{Pd}(\mathsf{ACN})_2\mathsf{Cl}_2 + 2 \; \mathsf{SPhos} & \underline{\qquad} & \mathsf{Base} \; (5 \; \mathsf{equiv}) \\ \hline & \mathsf{Solvent} \\ & \mathsf{T} \; (^\circ\mathsf{C}) \\ \end{array} \to \mathsf{Pd}^0\mathsf{SPhos} + 1 \; \mathsf{OSPhos/SPhos}$$

To an oven-dried 20 mL Schlenk purged under argon atmosphere, the pre-catalyst Pd(ACN)<sub>2</sub>Cl<sub>2</sub> (3.37 mg, 0.013 mmol, 1 equiv) was dissolved in the degassed solvent (0.6 mL). SPhos (10.67 mg, 0.026 mmol, 2 equiv) and base (0.065 mmol, 5 equiv) were added. The reaction was stirred for 20 minutes at the desired temperature and analyzed by <sup>31</sup>P NMR analysis. To calculate the conversion of the uncompleted reduction, the triethyl phosphonoacetate (0.0065 mmol, 0.5 equiv) was added as internal standard (IS).

To further demonstrate that the formation of Pd(0) specie occurred, 3NO<sub>2</sub>ArI (16.2 mg, 0.065 mmol, 5 equiv) was added to detect the formation of the oxidative addition (OA) complex.

All results have already been shown in Table 12, entries 1-8.



# <sup>31</sup>P NMR spectra of complete reduction as an example in both DMF and HEP/DMF

Figure 110.  $Pd(OAc)_2 + SPhos (2 equiv) + Cs_2CO_3 (5 equiv) in HEP/DMF-d_7 (4/2) at 60°C in 20 min (top); b) after the addition of <math>3NO_2ArI$ .

## 2.2.4.7. Investigation of Pd-NPs

To an oven-dried 20 mL Schlenk purged under argon atmosphere, the pre-catalyst  $PdCl_2(ddpf)$  (14.6 mg, 0.02 mmol, 1 equiv) was dissolved in degassed DMF (0.5  $\mu$ L), followed by the addition TMG (65  $\mu$ L from a stock solution of 0.66 M, 0.04 mmol, 2 equiv). After 30 min of stirring at 60°C, the solution was maintained under inert atmosphere, transferred into a falcon with silicon septum and centrifugated. The particles obtained were isolated by taking the supernatant and analysed by TEM.

The analysis showed the formation of palladium nanoparticles.

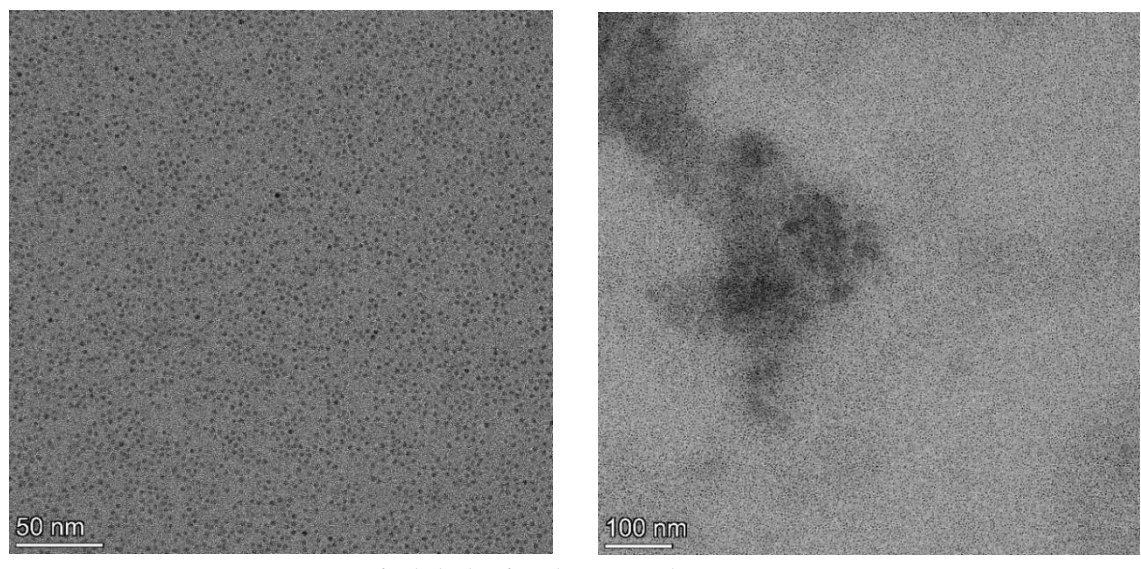
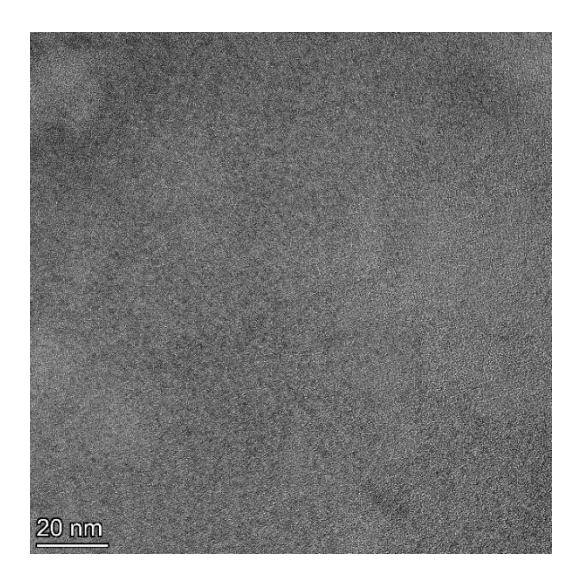
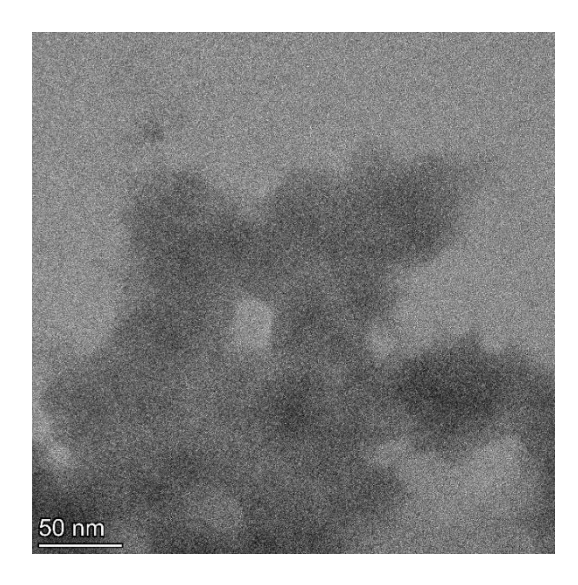


Figure 111. TEM images of PdCl<sub>2</sub>(dppf) reduction with TMG (5 equiv) in DMF at 60°C.

To an oven-dried 20 mL Schlenk purged under argon atmosphere, the pre-catalyst  $PdCl_2(ddpf)$  (14.6 mg, 0.02 mmol, 1 equiv) and dppf (11.08 mg, 0.02 mmol, 1 equiv) were dissolved in degassed DMF (0.5  $\mu$ L), followed by the addition TMG (65  $\mu$ L from a stock solution of 0.66 M, 0.04 mmol, 2 equiv). After 30 min of stirring at 60°C, the solution was maintained under inert atmosphere, transferred into a falcon with silicon septum and centrifugated. The particles obtained were isolated by taking the supernatant and analysed by TEM.

The analysis did not show the formation of palladium nanoparticles.





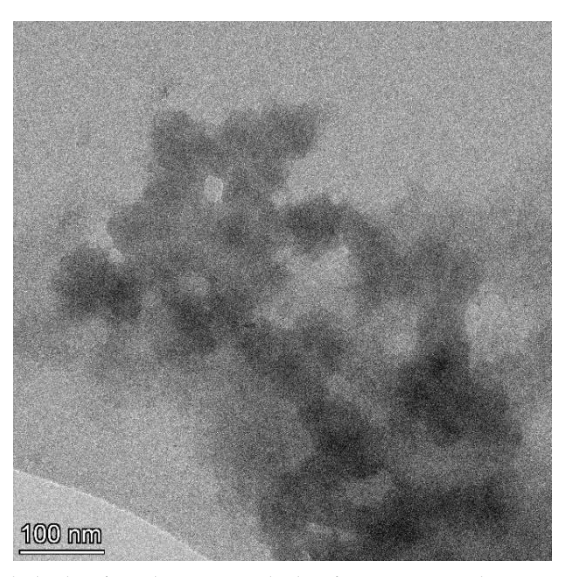


Figure 112. TEM images of PdCl<sub>2</sub>(dppf) reduction with dppf (1 equiv) and TMG (5 equiv) in DMF at 60°C.

## 2.2.4.8. Kinetic Isotope Effect (KIE)

The reaction was performed in a 20 mL Schlenk purged under argon atmosphere. Pd(ACN)<sub>2</sub>Cl<sub>2</sub> (39.37 mg, 0.152 mmol, 1 equiv), SPhos (128.80 mg, 0.304 mmol, 2 equiv) and Cs<sub>2</sub>CO<sub>3</sub> (248 mg, 0.72 mmol, 5 equiv) were dissolved in 3.2 ml MeOH/D and 1.6 ml DMF-d<sub>7</sub>. The reaction was let at room temperature and monitored by <sup>31</sup>P NMR spectroscopy at intervals of 5 minutes for 25 minutes. The triphenylphosphine oxide (0.5 equiv) was used as internal standard. (Figure 86).

## 2.2.4.9. Pd reduction with different nucleophiles

To an oven-dried 20 mL Schlenk purged under argon atmosphere, the pre-catalyst PdCl<sub>2</sub>(ACN)<sub>2</sub> (3.4 mg, 0.013 mmol, 1 equiv), the ligand SPhos (10.7 mg, 0.026 mmol, 2 equiv) and K<sub>2</sub>CO<sub>3</sub> (9.0 mg, 0.065 mmol, 5 equiv) were dissolved in degassed DMF (0.6 mL). The nucleophile (0.065 mmol, 5 equiv) of the selected reaction was then added. The reaction was stirred for 20 minutes at the desired temperature and analysed by <sup>31</sup>P NMR analysis to evaluate the formation of the Pd<sup>0</sup> complex (see results in Table 7).

## 2.2.4.10. Pd reduction with different ligands and green solvents

To an oven-dried 20 mL Schlenk purged under argon atmosphere, the pre-catalyst PdCl<sub>2</sub>(ACN)<sub>2</sub> (3.4 mg, 0.013 mmol, 1 equiv), the selected ligand (0.026 mmol, 2 equiv) and K<sub>2</sub>CO<sub>3</sub> (9.0 mg, 0.065 mmol, 5 equiv) were dissolved in the degassed solvent mixture (0.6 mL). The reaction was stirred for 20 minutes at 60°C and analysed by <sup>31</sup>P NMR analysis. To calculate the conversion of the uncompleted reduction, triphenylphosphine oxide (0.0065 mmol, 0.5 equiv) was added as internal standard (IS) (see results in Table 13).

# 2.2.4.11. Selectivity studies

To an oven-dried 20 mL Schlenk purged under argon atmosphere, the pre-catalyst PdCl<sub>2</sub>(ACN)<sub>2</sub> (3.4 mg, 0.013 mmol, 1 equiv), the ligand SPhos (10.7 mg, 0.026 mmol, 2 equiv) and K<sub>2</sub>CO<sub>3</sub> (9.0 mg, 0.065 mmol, 5 equiv) were dissolved in degassed HEP (0.6 mL). The Ph-I (0.065 mmol, 5 equiv) and the nucleophile (4MePhB(OH)<sub>2</sub> for the SM and PhC≡CH for the HC) were added to the solution. The reaction was stirred for 1h at rt and analysed by HPLC to evaluate the formation of the desired product or the side products (see Figure 84)

#### 2.2.4.12. DFT calculations

DFT calculations were conducted at CINECA, through the Italian SuperComputing Resource Allocation – ISCRA, using the Gaussian 16 software package<sup>[203]</sup>. Geometry optimizations for all reported structures were performed with the dispersion corrected B3LYP-D3 functional with a mixed basis set of LANL2DZ for Pd and 6-31G(d) (for other atoms)<sup>[230]</sup>. Frequency calculations were performed on all optimized structures to ensure that each local minimum lacked imaginary frequencies and that each transition state contained exactly one imaginary frequency. Solvation in DMF were introduced through single point calculations at optimized gas-phase geometries for all the minima and transition state using def2-TZVP for all atoms and the SMD implicit solvation model<sup>[208]</sup>. The reported Gibbs free energies were corrected considering the thermal correction computed at 298.15 K

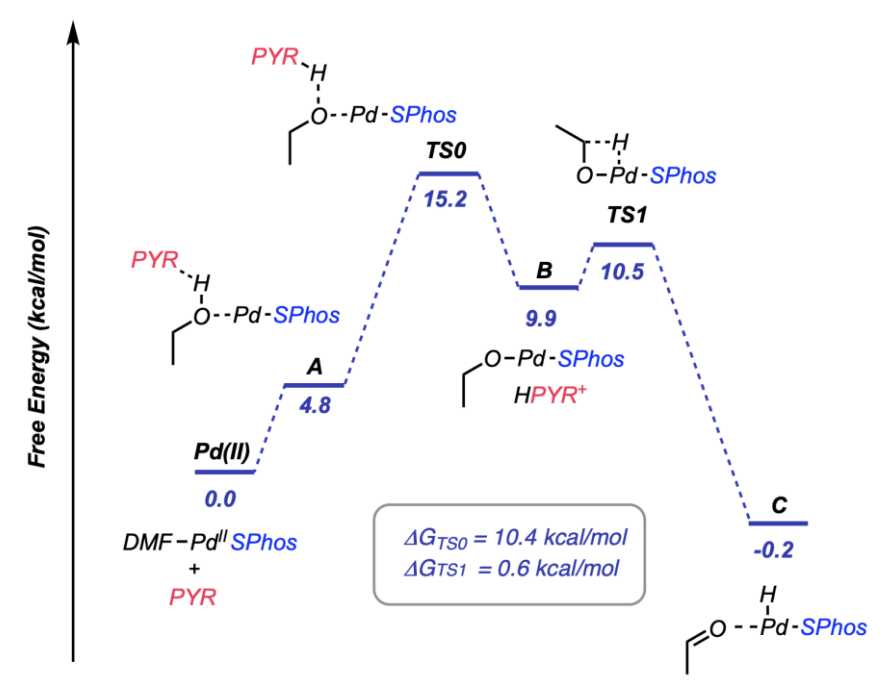


Figure 113. DFT-calculation-computed reaction profile and solution-state Gibbs free energies ( $\Delta G_{DMF}$ , kcal mol<sup>-1</sup>) B3LYP/DEF2-TZVP level of theory at 298 K for stationary points of Mechanism A with carbonate.

# 2.3. Copper-Free Heck-Cassar-Sonogashira and Suzuki-Miyaura Reactions of Aryl Chloride: a Sustainable Approach

#### 2.3.1. Introduction

As companies increasingly consider the sustainability aspects of their products and supply chains, a growing focus on the environmental impact of pharmaceutical production is stimulating innovation among chemists. In this context, metal catalysis plays an important role in making synthesis shorter and more efficient, so the development of sustainable approaches to cross-coupling reactions is becoming more and more important. The goals of green chemistry and process chemistry are very parallel, and transition metal catalysis intersects directly with these goals.

Focusing on the palladium cross-coupling reaction, the reagents aryl halides must be considered. Indeed, aryl chlorides are more attractive than the corresponding bromides, iodides and triflates from the point of view of cost and availability, but they are less reactive<sup>[67]</sup>. In addition, solvents account for the majority of waste, so more environmentally friendly alternatives need to be considered.

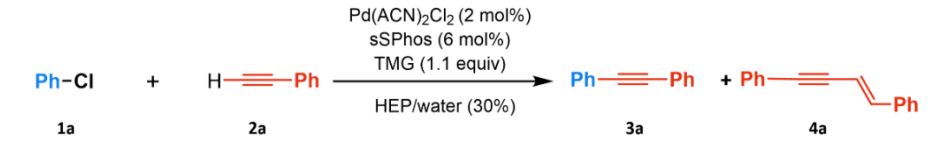
In this context, we investigated new methodologies for Suzuki-Miyaura and Heck-Cassar-Sonogashira reactions that are among the most Pd cross-coupling reactions studied and applied<sup>[188]</sup> (see *Chapter 1: General Introduction*, Figure 6). The aim was to identify flexible, reproducible and sustainable processes for HCS and SM cross-coupling reactions that allow high yields by using cheap and less reactive aryl chlorides. The process must be characterised by low metal loading, high reaction mass efficiency (RME), competitive PMI values taking into account solvent and palladium recovery, and avoidance of product metal contamination.

## 2.3.2. Results and Discussion

Sonogashira reactions with aryl iodides, bromides, and triflates with green protocols using the mixture HEP/water as solvent, have already been studied by the group<sup>[45]</sup>. Building on these, we investigated the use of sSPhos in a HEP/water solvent mixture for HCS and Suzuki-Miyaura (SM) cross-coupling reactions with aryl chlorides. HEP is non-toxic<sup>[231]</sup>, stable at elevated temperatures (flash point close to 212°C) and is already widely available as it is used in the synthesis of *N*-vinyl-pyrrolidone. As mentioned above, HEP has a very high affinity for water and with a HEP/water ratio >8/2, solvent extraction of the final product with an immiscible solvent is generally very efficient, leaving the metal in the HEP/water mixture. This feature is crucial to the protocol and is in line with the International Council for Harmonisation (ICH) Q3D guidelines for elemental impurities, which strictly limit metal content in active pharmaceutical ingredients (APIs) to ensure quality and safety<sup>[232]</sup>.

The HCS cross-coupling between phenyl halide **1a** and phenylacetylene **2a** was carried out with 2 mol% of Pd(0) catalyst, generated in situ starting from Pd(ACN)<sub>2</sub>Cl<sub>2</sub> and sSPhos, in HEP/water 70/30 and TMG as a base. These standard conditions were used to evaluate the effect of the leaving group and, for PhCl **1a**<sup>Cl</sup>, to define concentration, temperature and stoichiometry (Table 28).

Table 28. Screening for the HCS in HEP/Water/TMG system conditions<sup>a</sup>.



Entry	Conc (M)	Х	2a (equiv)	T (°C)	T (h)	AAR <sup>b</sup> (h)	Conv (%)	3a/4a
1	0.5	I	2.0	60	1	Rapid	>99	>99/1
2	0.5	Br	2.0	60	2	Rapid	>99	79/21
3	0.5	CI	2.0	60	3	Rapid	20	23/77
4	0.5	CI	2.0	70	3	Rapid	25	32/68
5	0.5	CI	2.0	80	3	Rapid	45	35/65
6	1.0	CI	1.5	60	3	4	40	42/58
7	1.0	CI	1.5	70	3	4	80	77/23
8	1.0	CI	1.05	70	8	8	>99	99/1
9	1.0	CI	1.5	80	3	3	>99	90/10
10	1.0	CI	1.05	80	4	4	>99	>99/1
11	1.0	CI	1.05	90	3	3	>99	>99/1

<sup>&</sup>lt;sup>a.</sup> All HCS couplings were carried out under nitrogen atmosphere with 2 mol% of Pd pre-catalyst and 6 mol% of sSPhos ligand, 1.1 equiv of TMG, in HEP/water 7/3. Conversion and product ratios were determined by HPLC considering the appropriate Relative Response Factor (RRF). <sup>b.</sup> AAR= Alkyne Addition Rate.

The enyne side product, (*E*)-4-[phenylbut-1-en-3-ynyl]-benzene **4a**, (see *Paragraph* 2.1.1., Figure 24b), became the main product moving from PhI **1a**<sup>I</sup> to PhBr **1a**<sup>Br</sup> and PhCl **1a**<sup>CI</sup> at 60°C (compare entries 1–3, Table 28). These results are determined by the competition between the oxidative addition of the aryl halide and the alkyne **2a**, and when the OA step is slow, as with the chlorides, the self-hydroalkynylation becomes significant. Increases in temperature and stoichiometry had no significant effect on the outcome of the reaction (entries 4-5, Table 28). Based on our previous studies on the HCS coupling<sup>[45]</sup>, we introduced the slow addition of **2a** to limit the formation of **4a** with PhCl **1a**<sup>CI</sup>. However, at 60°C, the OA of PhCl **1a** was too slow (entry 6, Table 28), but at 70°C with a longer addition rate, the selectivity towards **3a** was achieved (entry 7 vs 8, Table 28). Accordingly, complete conversion and selective formation of the bis-substituted acetylene **3a** were achieved by balancing reaction temperature and alkyne addition rate

(entries 9-11, Table 28). The temperatures of 80°C and 90°C ensured an efficient OA of PhCl **1a**<sup>Cl</sup> on the Pd(0) complex and a complete conversion into **3a** with 4 and 3 h addition rates of **2a**, respectively (entries 10 and 11, Table 28).

To have a further understanding of the competitive pathway, DFT calculations have been performed by the group using Gaussian 16 with the B3LYP hybrid functional. The differences in energy between the OA process of different aryl halides using SPhos as the ligand and the first step of the enyne formation are compared (Figure 114).

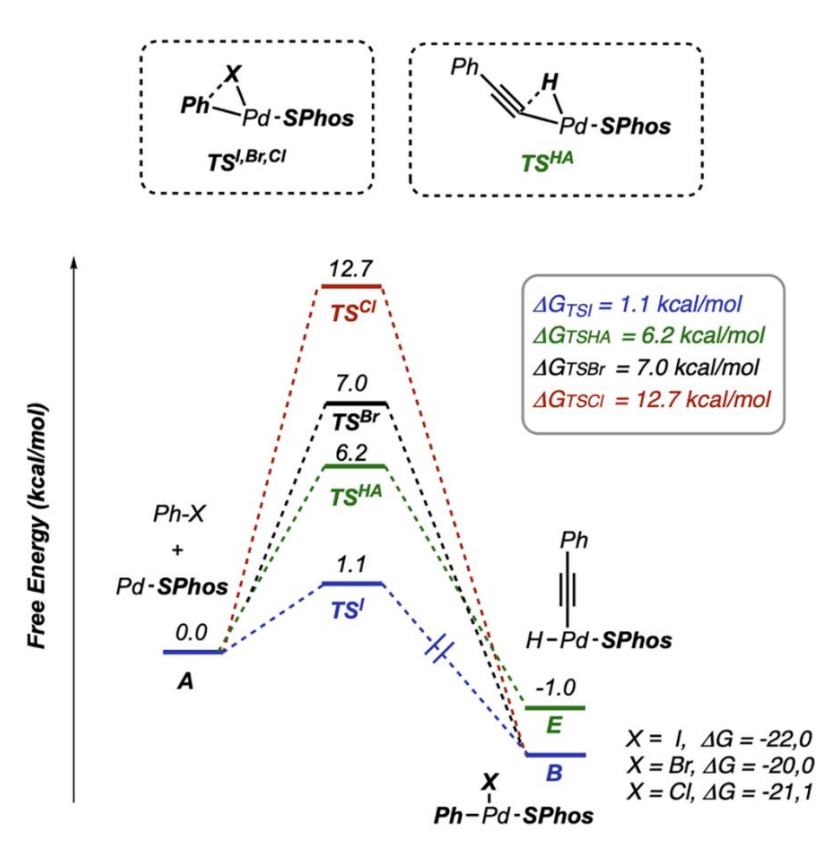
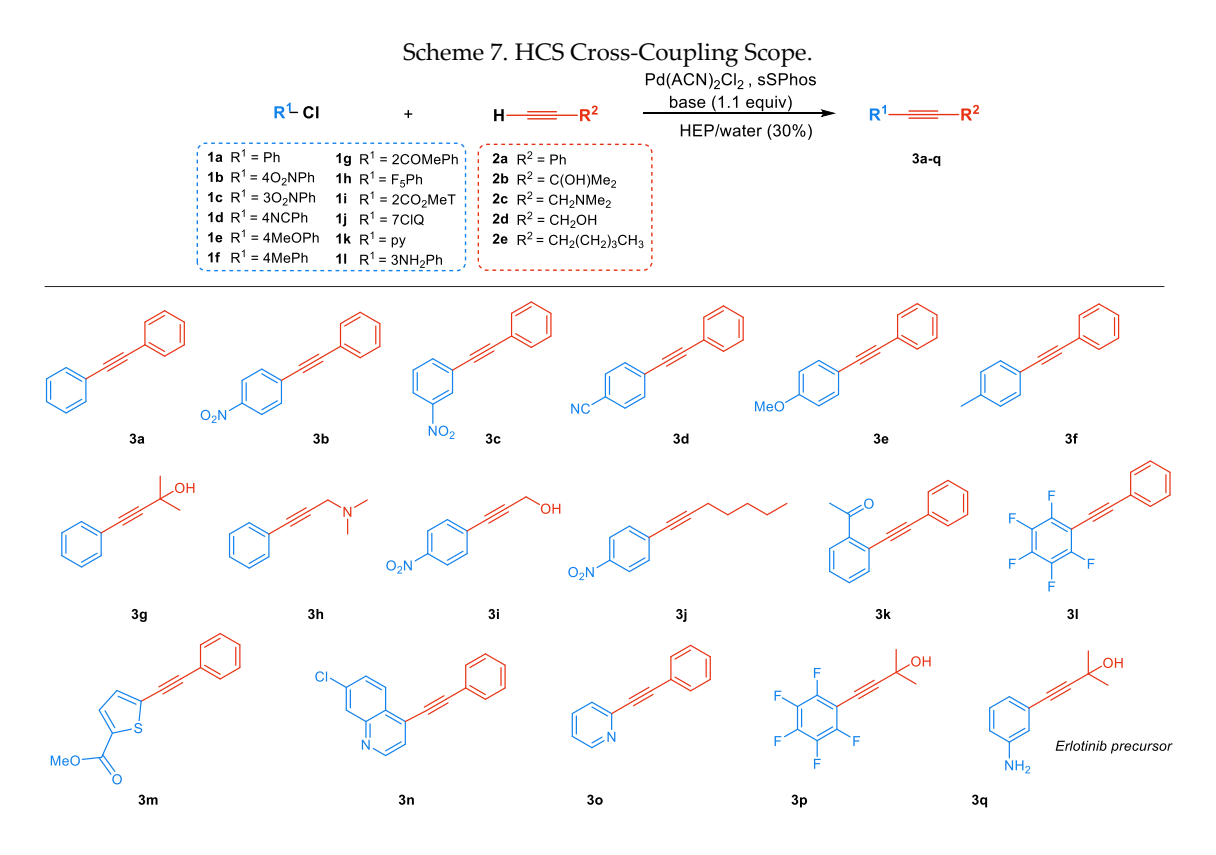


Figure 114. DFT calculations in DMF of the OA of aryl halides and the first step of the phenylacetylene insertion to give the envne byproduct 4.

The reaction coordinate was studied starting from the monoligated Pd<sup>o</sup>SPhos complex, since it is considered the active palladium species<sup>[233]</sup>, while SPhos was chosen as ligand instead of the sulfonated sSPhos to simplify the calculations. Since the experimental results showed that the enyne by-product is formed when the oxidative addition is slow, we expected the alkyne insertion to have an energy similar to that of the transition state of the oxidative addition of phenyl bromide. The Gibbs free energy barrier for the oxidative addition of the PhI 1a<sup>I</sup> is only 1.1 kcal/mol, while the phenylacetylene addition to the Pd<sup>o</sup>SPhos complex has a TS<sup>HA</sup> of 6.2 kcal/mol. This is consistent with the fact that the formation of the enyne has never been observed during reaction with aryl iodide. The energy barriers for the oxidative addition of PhBr 1a<sup>Br</sup> and PhCl 1a<sup>CI</sup> are 7.0 and 12.7 kcal, respectively, confirming the experimental results

described in Table 28. In fact, the formation of enyne 4 competed with the HCS coupling product 3 when bromides and especially chlorides are the leaving groups. The calculations were also performed without functional groups, but it is worth noting that adding an electron-withdrawing groups, such as NO<sub>2</sub>, to aryl chlorides lowers the activation energy barrier for the oxidative addition. Specifically for 4-NO<sub>2</sub>-phenyl chloride 1b, this reduces the energy barrier difference between aryl chloride and alkyne oxidative additions from 12.7 to 7.5 kcal, making the reactions more accessible (see *Experimental Section*, Figure 122).

The copper-free HCS reaction scope is described in Scheme 7. The couplings have been performed using a recycling or thermomorphic procedure (Figure 115 and Table 29) and a low Pd loading protocol in Table 30.



The aim of the study was to create a green and sustainable protocol able to ensure efficient and fast reactions under mild conditions using a low percentage of palladium catalyst. With this target, we started with the optimised conditions (entries 10-11, Table 28) to study the catalyst recycling starting from 2 mol %. After the complete conversion of aryl chloride **1a** to diphenylacetylene **3a**, we performed a simple extraction with an immiscible solvent to easily recover the final product, leaving the catalyst in the HEP/water phase. This solution was reused in the following reaction cycle by simply adding the two reagents and the TMG base. The results reported in Table 29 show that

the catalyst generated in the HEP/water/TMG system could be easily recycled up to five times, always maintaining high conversions.

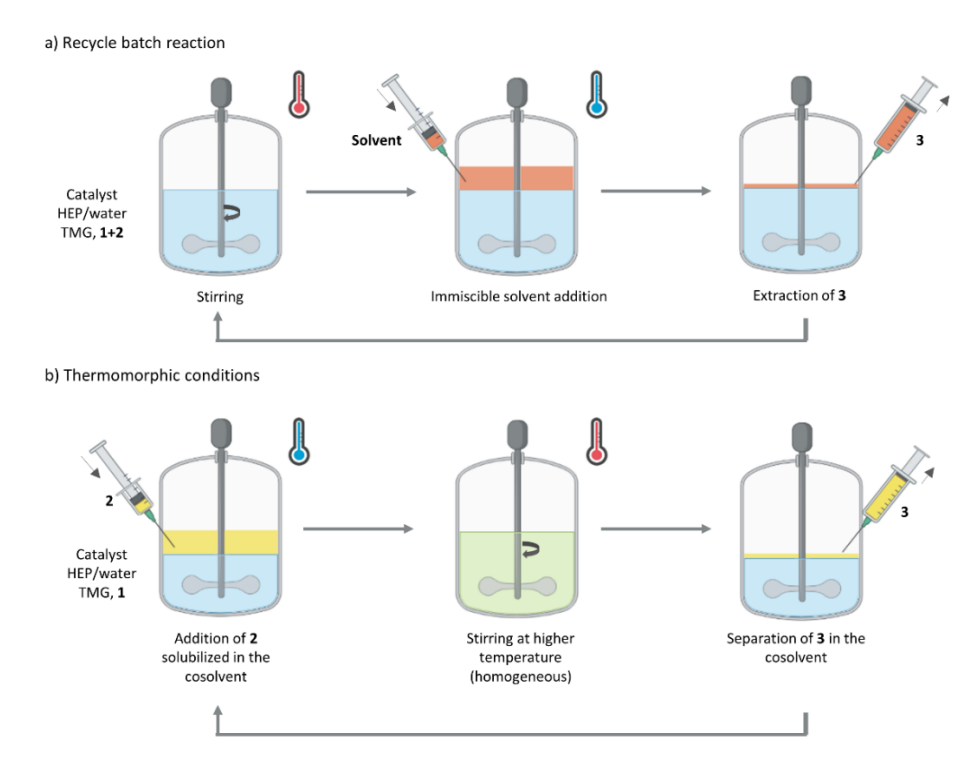


Figure 115. Batch reaction with catalyst recycling (a) and thermomorphic protocol (b).

To demonstrate the robustness of the protocol, the reaction was extended to substituted aryl chlorides and acetylenes. The mildest conditions were investigated, starting from those identified in the model reaction between 1a and 2a. While the presence of electron-withdrawing groups on the aromatic ring did not affect the reactivity (entries 2-4, Table 29), the transformation of differently substituted acetylenes and electron-donating substrates required the application of modified conditions. Even when the temperature was increased to 90°C and the acetylene addition was slowed down to 4 hours, it was still possible to obtain three recycles and maintain conversions higher than 95% and good yields (entries 5-10, Table 29). We also evaluated the effectiveness of inorganic bases and we found that Cs2CO3 is a good alternative to TMG (see entries 1 and 11, Table 29). Another interesting characteristic of the HEP/water 7/3 mixture was the possibility of carrying out the reaction under thermomorphic conditions by adding a third solvent. Indeed, by using toluene or isobutyl acetate (IBA) as cosolvents, the mixture was immiscible at room temperature and a homogeneous solution was obtained at temperatures above 80°C. Therefore, the HCS protocol was investigated using the new thermomorphic mixtures<sup>[234]</sup> of HEP/water/toluene or HEP/ water/IBA in a 7/3/5 ratio.

Table 29. HCS Reaction Scope and Catalyst Recycling<sup>a</sup>

Entry	R¹-CI	Alkyne	Alkyne (equiv)	T (°C)	Cycle time (h)	AAR	Cycles	TON	Product	Yield <sup>b</sup> (%)
1°	1a	2a	1.05	90	3	3h	5	230	3a	90
2 <sup>c</sup>	1b	2a	1.05	80	3	3h	5	235	3b	94
3°	1c	2a	1.05	80	3	3h	5	235	3c	94
4	1d	2a	1.05	80	3	3h	5	233	3d	93
5	1e	2a	1.05	90	4	4h	3	138	3e	92
6	1f	2a	1.05	90	4	4h	3	138	3f	92
7	1a	2b	1.5	90	4	4h	3	135	3g	90
8	1a	2c	1.5	90	4	4h	3	132	3h	88
9	1a	2d	1.5	90	4	4h	3	134	3i	89
10	1a	2e	1.5	90	4	4h	3	129	3j	86
11 <sup>d</sup>	1a	2a	1.05	90	3	3h	5	232	3a	92
12 <sup>e</sup>	1a	2a	1.05	90	3	3h	3	135	3a	90
13 <sup>f</sup>	1a	2a	1.05	90	3	3h	3	135	3a	92

<sup>a.</sup> All HCS couplings were carried out under nitrogen atmosphere and the cycle time correspond to the alkyne addition time. At the given time the reactions were cooled at rt, extracted with the appropriate organic solvent and the HEP/water phase containing the catalyst was recycled. <sup>b.</sup> The combined extraction solvents were distilled, and the crude was subsequently purified by flash chromatography, when necessary. <sup>c.</sup> Reaction time extended to 4h hours in the last two cycles. <sup>d.</sup> The reaction was performed using Cs<sub>2</sub>CO<sub>3</sub> instead of TMG. <sup>e.</sup> Reaction performed in a thermomorphic way through slow addition of acetylene in toluene over the course of the reaction. <sup>f.</sup> Reaction performed in a thermomorphic way through slow addition of acetylene in IBA over the course of the reaction.

A solution of **2a** in toluene or IBA was added over 3 hours and, after cooling to room temperature, **3a** was easily recovered by phase separation and the catalyst was recycled (see entries 12 and 13, Table 29 and Figure 115b). The thermomorphic procedures reported in the literature for the HCS coupling are carried out at temperature above 100°C with aryl iodides and bromides in non-sustainable solvents<sup>[235,236]</sup>.

The recycling protocol is ideal for products sensitive to temperature<sup>[45]</sup>. Indeed, when the reaction was carried out with low palladium loading, the reaction time increased consistently (see Table 30).

Table 30. Direct HCS Reaction between Aryl Chlorides **1a–l** and Alkynes 2a–e<sup>a</sup>  $Pd(ACN)_2Cl_2, sSPhos$ 

R <sup>1</sup> —CI	+	н—=	<b>=</b> − <b>R</b> <sup>2</sup>	ba	se (1.1 equi	v)	R <sup>1</sup>		-R <sup>2</sup>	$PMI \simeq 11$
K — Ci	т	- '' -	_ K	HE	EP/water (30	0%)	K		K	PMIr ≃ 4
1a-l		2	а-е		90°C, 16h			3a-q		
Entry	Conc (M)	R¹-CI	Alkyne	Alkyne (equiv)	Pd(II) (mol%)	Base	Conv <sup>b</sup> (%)	Yield (%)	TON	Product
1	1.0	1a	2a	1.05	0.4	TMG	70	65	163	3a
2	1.0	1e	2a	1.05	0.6	TMG	61	56	140	3e
3	1.0	1a	2a	1.05	0.4	Cs <sub>2</sub> CO <sub>3</sub>	>99	94	235	3a
4	1.0	1e	2a	1.05	0.6	Cs <sub>2</sub> CO <sub>3</sub>	>99	92	150	3e
5	2.5	1a	2a	1.05	0.2	Cs <sub>2</sub> CO <sub>3</sub>	>99	93	465	3a
6	2.5	1b	2a	1.05	0.2	Cs <sub>2</sub> CO <sub>3</sub>	>99	94	470	3b
7	2.5	1c	2a	1.05	0.2	Cs <sub>2</sub> CO <sub>3</sub>	>99	95	475	3c
8	2.5	1d	2a	1.05	0.2	Cs <sub>2</sub> CO <sub>3</sub>	>99	93	465	3d
9	2.5	1e	2a	1.05	0.4	Cs <sub>2</sub> CO <sub>3</sub>	>99	90	225	3e
10	2.5	1f	2a	1.05	0.4	Cs <sub>2</sub> CO <sub>3</sub>	>99	91	228	3f
11	2.5	1a	2b	1.2	0.4	Cs <sub>2</sub> CO <sub>3</sub>	>99	90	225	3g
12	2.5	1a	2c	1.2	0.4	Cs <sub>2</sub> CO <sub>3</sub>	>99	91	228	3h
13	2.5	1b	2d	1.2	0.4	Cs <sub>2</sub> CO <sub>3</sub>	>99	90	225	3i
14	2.5	1b	2e	1.2	0.4	Cs <sub>2</sub> CO <sub>3</sub>	>99	90	225	<b>3</b> j
15	2.5	1g	2a	1.5	0.4	Cs <sub>2</sub> CO <sub>3</sub>	>99	94	235	3k
16	2.5	1h	2a	1.5	0.4	Cs <sub>2</sub> CO <sub>3</sub>	>99	92	230	31
17	2.5	1i	2a	1.5	0.4	Cs <sub>2</sub> CO <sub>3</sub>	>99	93	233	3m
18	2.5	1j	2a	1.5	0.4	Cs <sub>2</sub> CO <sub>3</sub>	>99	90	225	3n
19	2.5	1k	2a	1.5	0.4	Cs <sub>2</sub> CO <sub>3</sub>	>99	91	228	30
20	2.5	1h	2b	2.0	0.4	Cs <sub>2</sub> CO <sub>3</sub>	>99	91	228	3р
21	2.5	11	2b	2.0	0.4	Cs <sub>2</sub> CO <sub>3</sub>	61	52	130	3q

<sup>&</sup>lt;sup>a.</sup>All HCS couplings were carried out under nitrogen in a HEP/water 7/3 solution, and the alkyne **2** was slowly added within the given reaction time. The reactions were cooled at rt and extracted with the appropriate organic solvent. The extraction solvent was distilled, and the crude was subsequently purified with flash chromatography when necessary b. Determined with HPLC considering the appropriate RRF.

Aryl chlorides **1a** and **1e** were chosen as model examples to assess the validity of the study. As TMG is unstable under long reaction time at high temperature<sup>[237]</sup> (entries 1 and 2, Table 30), Cs<sub>2</sub>CO<sub>3</sub> was used and complete conversions were successfully achieved (entries 3 and 4, Table 30). The process was then further optimised to reduce the required amount of Pd catalyst, improve the TON, and reduce the PMI of the protocol. Therefore, the amount of catalyst was reduced to 0.2 mol% in a 2.5 M solution,

achieving conversions above 95% for the model reaction and for those with substrates containing electron-withdrawing groups (entries 5–8, Table 30), while 0.4 mol% was required for more challenging substrates (entries 9–21, Table 30). The synthesis of erlotinib intermediate **3q** starting from 3-choloro-aniline **1l** was not competitive with respect to the industrial process that uses the corresponding bromide as the starting material<sup>[188]</sup>. The conversion was only 61% (entry 21, Table 30) and the catalyst increase did not change the activity. Based on our previous studies, the aniline moiety is able to enter the coordination sphere of the metal slowing down the reaction rate<sup>[45]</sup>.

The PMI and the PMI after recovery (PMIr) were calculated in Table 29 and Table 30 at 5 and 10 mmol scales, respectively. The recycling of the catalyst and solvent for the reactions described in Table 29 allowed us to achieve a PMI of 18. After recovery of the extraction solvent, HEP and palladium achieve a PMIr value close to 3. In the reactions reported in Table 30 at a concentration of 2.5 M with 0.2–0.4 mol% of catalyst, the PMI reached 11, while the PMIr was around 4 for all entries.

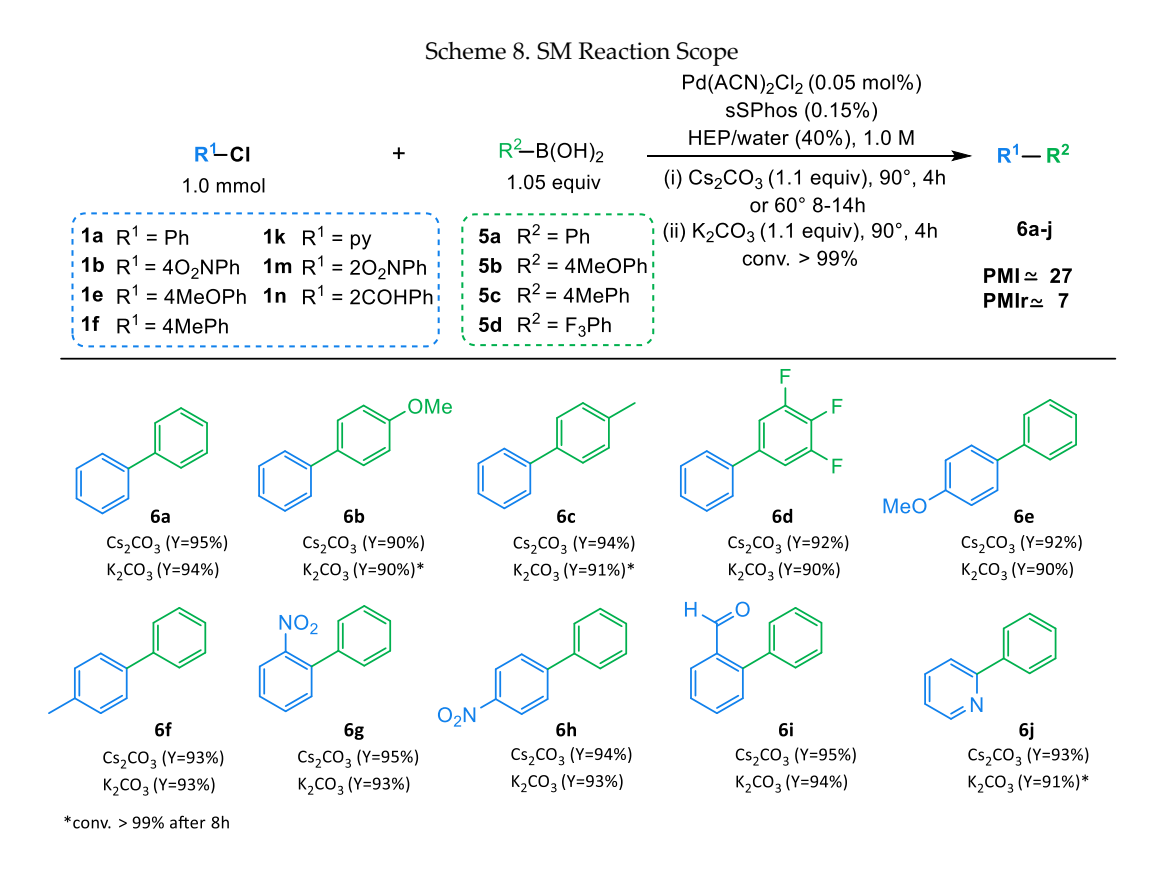
The SM reactions are, as mentioned above, the most widely used Pd cross-coupling reactions. In addition, the main advantage over other cross-coupling protocols is the use of boron compounds as coupling partners, which are readily available and give high yields and good selectivity with a wide functional group tolerance. For these reasons, we also investigated the applicability of our protocol for SM reactions. To pursue this aim, we selected to investigate the reactivity between **1a** and phenylboronic acid **5a** as a standard SM reaction in the presence of different inorganic bases and at 45°C, 60°C and 90°C (see Table 31).

Table 31. SM screening inorganic base screening.<sup>a</sup>

	Ph-CI	+ <b>Ph</b> -B(OH) <sub>2</sub>		Cl <sub>2</sub> , sSPhos .1 equiv)	→ Ph-Pl	,
	1.0 mmol	5a	HEP/wate		<b>6</b> a	
Entry	Pd (%)	5a (equiv)	Base	T (°C)	Time (h)	Conv.b (%)
1	0.1	1.2	Cs <sub>2</sub> CO <sub>3</sub>	45	16	100
2	0.2	1.05	Cs <sub>2</sub> CO <sub>3</sub>	45	16	100
3	0.2	1.05	K <sub>2</sub> CO <sub>3</sub>	45	16	100
4	0.2	1.05	Na <sub>2</sub> CO <sub>3</sub>	45	16	100
5	0.2	1.05	$K_3PO_4$	45	16	100
6	0.05	1.05	Cs <sub>2</sub> CO <sub>3</sub>	60	8	100
7	0.05	1.05	K <sub>2</sub> CO <sub>3</sub>	60	16	85
8	0.05	1.05	Na <sub>2</sub> CO <sub>3</sub>	60	16	83
9	0.05	1.05	$K_3PO_4$	60	16	76
10	0.05	1.05	Cs <sub>2</sub> CO <sub>3</sub>	90	4	100
11	0.05	1.05	K <sub>2</sub> CO <sub>3</sub>	90	4	100

<sup>&</sup>lt;sup>a</sup>All SM couplings were carried out under nitrogen in a HEP/water 6/4 solution. <sup>b</sup> Determined with HPLC considering the appropriate RRF.

The results reported in Table 31 highlight that an increasing in palladium loading or an excess of boronic acid is required to achieve complete conversions at 45°C (entries 1 and 2, Table 31). Similar data were obtained with other inorganic bases tested (entries 3-5, Table 31). Differently, a complete conversion at 60°C was only achieved with Cs<sub>2</sub>CO<sub>3</sub> using 0.05 mol% of Pd, 0.15 mol% of sSPhos, and 5% excess boronic acid (compare entries 6 vs 7–9, Table 31). Using Cs<sub>2</sub>CO<sub>3</sub> and K<sub>2</sub>CO<sub>3</sub> at 90°C, we obtained 100% conversion after 4 hours showing that they are superior compared to Na<sub>2</sub>CO<sub>3</sub> and K<sub>3</sub>PO<sub>4</sub>.



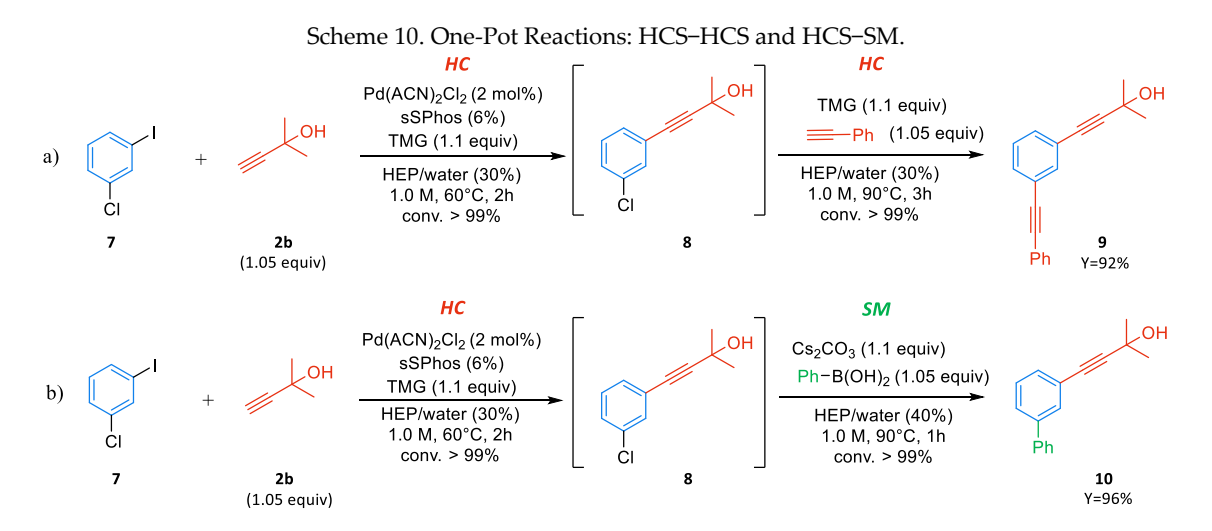
The reaction scope shown in Scheme 8 was defined using the rapid protocol at 90°C with K<sub>2</sub>CO<sub>3</sub> and at 60°C with Cs<sub>2</sub>CO<sub>3</sub>. The former ensures rapidity, while the latter requires less energy in terms of temperature, but a longer reaction time. Using these optimised reaction conditions, independently from the substitutions on the aryl chlorides and boronic acids, the conversions were always >99% with yields exceeding 90%.

The simplicity of the procedure and the high purity of the product are key aspects of this reaction protocol. The use of readily available solvents such as cyclohexane and tert-butyl acetate for extraction, followed by direct isolation by evaporation, streamlines the process making it efficient and cost effective. The high purity of the product eliminates the need for additional purification steps, saving time and resources. Such optimised procedures are important for the development of industrial synthesis, as they help to increase productivity and ensure the production of high-quality compounds. To validate this methodology, the synthesis of two fungicides containing a biaryl-motive,

such as Boscalid and Fluxapyroxad, was explored (Scheme 9). Due to the high market demand<sup>[68,238]</sup> for these products, it is important to have a low PMI and a decrease in Pd loading.

Scheme 9. General Sequence for the Industrial Synthesis of Boscalid and Fluxapyroxad.

The reaction between **1g** and **5d/5e** in HEP/water was therefore studied and carried out following a procedure similar to the one described in Scheme 8, giving complete conversions to the desired product after 6 hours. The average PMI calculated for the reactions reported in Scheme 8 was around 27 and after recovery of solvent and the metal decreased to 7. Similarly, for the SM of Boscalid and Fluxapyroxad, the PMI was around 18 and the PMIr was 5, obtaining values that are among the best results in the field. The reaction mass efficiency with the 5% excess of boronic acid is around 65–68%. However, the 5% excess of the boronic acid was used only because of the small scale. The synthesis of Boscalid and Fluxapyroxad intermediated was scaled up 10 times with an equimolecular ratio between the reagents increasing the RME of >70%.



Owing to the reaction efficiency and chemoselectivity of the described protocols, the one-pot sequences of HCS-HCS and HCS-SM reactions were carried out (Scheme 10). To achieve our goal, we chose 1-chloro-3-iodobenzene 7 as the model substrate and performed a one-pot HCS-HCS reaction in one case (Scheme 10a) and a one-pot HCS-SM in the other case (Scheme 10b), exploiting the different reactivity of the iodide leaving group towards chloride.

The reaction between 7 and alkyne **2b** with 2 mol % of palladium catalyst and TMG as a base, gave the selective product **8** with complete conversion in 2 hours at 60°C. The direct slow addition of phenylacetylene **2a** and TMG at 90°C allowed complete conversion to product **9** without any work-up. Similarly, after the formation of product **8**, the addition of phenylboronic acid **5a** and Cs<sub>2</sub>CO<sub>3</sub> at 90°C gave product **10** with 99% conversion.

## 2.3.3. Conclusion

In this study, we have reported fast and efficient protocols for HCS and SM reactions with less reactive aryl chlorides in the sustainable mixture HEP/water, giving excellent results in terms of yield, TON, RME and PMI. We have shown that the conditions must be adapted according to the typology of the chlorides and the cross-coupling, in fact the HCS cross-coupling requires the use of Cs<sub>2</sub>CO<sub>3</sub> as a base for the reaction with low palladium loading, whereas the SM can also be carried out in the presence of K<sub>2</sub>CO<sub>3</sub>.

By controlling the stoichiometry in the Heck-Cassar and Suzuki-Miyaura reactions, we were able to generate products in high yield and without purification for the SM. Eliminating the need for product purification is critical for industrial applications because it means less waste, lower environmental impact, energy efficiency and competitiveness. In particular, the SM protocol allowed the acquisition of pure products with 0.05 mol% of catalyst loading with fast and selective reactions at 90°C faster or 60°C with longer reaction times. Furthermore, by exploiting the different reactivities of aryl halides, we have shown that HC and SM reactions can be carried out in sequence, providing access to complex architectures. Two agrochemicals, Boscalid and Fluxapyroxad, were synthesised in one-pot reactions with excellent yields and PMI and RME of around 19% and 72% respectively, demonstrating the high efficiency and flexibility of the developed protocol.

## Acknowledgments:

DFT calculations for this work were performed by Dr. Tommaso Fantoni

# Published work:

The full version can be found in "C. Palladino and T. Fantoni, L. Ferrazzano, B. Muzzi, A. Ricci, A. Tolomelli, W. Cabri, ACS Sustainable Chem. Eng. 2023, 11, 15994–16004"

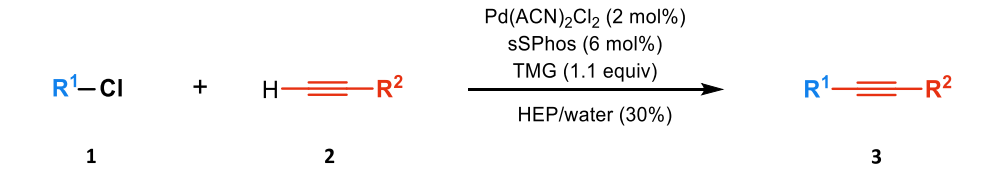
# 2.3.4. Experimental Section

#### 2.3.4.1. General Information

Commercial reagents (reagent grade, >99%) were used as received without additional purification. Solvents (cyclohexane (Cy), dichloromethane (DCM), methyl-tert-butyl ether (MTBE), N-hydroxyethylpyrrolidone (HEP), toluene, 2-methyltetrahydrofuran (2-MeTHF), isobutylacetate (IBA), isopropyl alcohol (IPA) and deuterated N,N-Dimethylformamide (DMF-d<sub>7</sub>)) are commercially available and were used after degassing. 1H NMR, 13C NMR and 31P NMR spectra were recorded with an Agilent-Technologies-Varian INOVA 400 MHz and 100 MHz instrument <sup>1</sup>H/<sup>19</sup>F/X 5 mm PFG ATB Broadband Probe, VT, single, double and triple resonance, z-axis pulsed field gradients, serves broadband probe and customized variable temperature – 5 mm Broadband probe. NMR multiplicities are abbreviated as follows: s = singlet, d = doublet, t = triplet, q = doubletquartet, spt = septet, m = multiplet, bs = broad signal. Coupling constants I are given in Hz. All <sup>1</sup>H and <sup>13</sup>C chemical shifts are calibrated to residual proto-solvents. HPLC-UV analysis was recorded with an Agilent 1260 InfinityLab instrument. Column: Zorbax® SB-C18; particle size 5 µm; pore size 100 Å; length 250 mm, internal diameter: 4.6 mm. Mobile phase A: H<sub>2</sub>O, mobile phase B: ACN. Gradient (Time(min), %B): 0, 30; 8, 80; 22, 80; 24, 10; 30, 10; flow 0.5 mL min<sup>-1</sup>column temperature 30°C; injection volume: 20 μL. NE-1010 Higher Pressure Syringe Pump used to perform slow-addition of acetylenes in the Heck-Cassar-Sonogashira cross-coupling reactions. Mass Spectrometry analysis was recorded on a QTRAP 3200 mass spectrometer in ESI+ mode. Spectrometer ICP-OES AGILENT 5110 was used to determine the concentration of Pd in the solution. Power: 1200 W; Auxiliary gas: Argon (1.0 L min<sup>-1</sup>); nebulizer gas: nitrogen (0.7 L min<sup>-1</sup>); peristaltic pump speed: 12 rpm. Samples for ICP-OES were digested with 8 mL HNO<sub>3</sub>/HCl (1:3) using a microwave digestion system held at 175 °C for 10 minutes. The volume of the digests was then made up to 50 mL with de-ionized water before analysis by ICP-OES. Calibration standards for the quantification of the digested samples were prepared in 5% HNO<sub>3</sub>. Palladium standards from Faggi Enrico and 2'-Dicyclohexylphosphino-2,6-dimethoxy-3-sulfonato-1,1'-biphenylhydrate sodium (sSPhos) from Chemieliva Pharmaceutical Co., Ltd.

## 2.3.4.2. General procedures

a) Heck-Cassar reactions with 2 mol% of catalyst<sup>[45]</sup>:



To an oven-dried 10 mL Schlenk purged under N<sub>2</sub> atmosphere, the palladium pre-catalyst Pd(ACN)<sub>2</sub>Cl<sub>2</sub> (0.02 mmol, 2 mol%, 5.2 mg), sSPhos, (0.06 mmol, 6 mol%, 30.8 mg) were dissolved in HEP and water as co-solvent in a 7/3 ratio. The other reagents were then added in the following order: TMG (126.9 mg, 138.0 μL, 1.1 mmol, 1.1 equiv) and aryl chloride (1.0 mmol, 1.0 equiv). The reaction mixture was heated to 80-90°C with an oil bath and alkyne (from 1.05 to 1.5 equiv) was added slowly with a syringe pump over the course of the reaction; the conversion was evaluated through HPLC-UV analysis at 210 nm considering the appropriate RRF (see below). At reaction completion, the mixture was extracted with an appropriate organic solvent (3x1 mL). The collected organic phases were concentrated under reduced pressure. The reaction crude was purified, when necessary, by flash chromatography.

b) Heck-Cassar reactions with 0.2-0.4 mol% of catalyst<sup>[45]</sup>:

# <u>Preparation of stock solution of the HCS catalyst:</u>

To an oven-dried 10 mL Schlenk purged under N<sub>2</sub> atmosphere, palladium pre-catalyst Pd(ACN)<sub>2</sub>Cl<sub>2</sub> (0.02 mmol, 5.2 mg) and ligand sSPhos, (0.06 mmol, 30.8 mg) were dissolved in 2 mL of HEP/water(30%) solution. The mixture was stirred for 5 min at room temperature. A yellow-orange solution was obtained for subsequent HCS reactions (stock solution is stable and can be used even after one week).

## Procedure:

To an oven-dried 10 mL Schlenk purged under  $N_2$  atmosphere, 200  $\mu$ L of the stock solution (0.2 mol% of palladium catalyst) was added along with the amount of HEP/water (30%) solution needed to achieve the desired concentration. The other reagents were then added in the following order:  $Cs_2CO_3$  (358 mg, 1.1 mmol, 1.1 equiv) and aryl chloride (1.0 mmol, 1.0 equiv). The reaction mixture was heated to 80-90°C with an oil bath and alkyne (1.05 mmol, 1.05 equiv) was added slowly with a syringe pump over the course of the reaction; the conversion was evaluated through HPLC-UV analysis at 210 nm considering the appropriate RRF (see below). At reaction completion, the mixture was extracted with an appropriate organic solvent (3x1 mL). The collected organic phases were concentrated under reduced pressure. The reaction crude was purified, when necessary, by flash chromatography.

# c) General procedure for Suzuki-Miyaura cross-coupling:

# <u>Preparation of stock solution of the SM catalyst:</u>

To an oven-dried 10 mL Schlenk purged under N<sub>2</sub> atmosphere, palladium pre-catalyst Pd(ACN)<sub>2</sub>Cl<sub>2</sub> (0.04 mmol, 10.4 mg) and ligand sSPhos, (0.12 mmol, 61.6 mg) were dissolved in 4 mL of HEP/water(40%) solution. The mixture was stirred for 5 min at room temperature. A yellow-orange solution was obtained for subsequent SM reactions (stock solution is stable and can be used even after one week).

#### Procedure:

To an oven-dried 10 mL Schlenk purged under  $N_2$  atmosphere, 50  $\mu$ L of the stock solution (0.05 mol% of palladium catalyst) was added along with the amount of HEP/water (40%) solution needed to achieve the desired concentration. The other reagents were then added in the following order: base (1.1 mmol, 1.1 equiv), aryl chloride (1.0 mmol, 1.0 equiv) and boronic acid (1.05 mmol, 1.05 equiv). The reaction mixture was heated to the desired temperature with an oil bath and maintained at this temperature under stirring; the conversion was evaluated through HPLC-UV analysis at 210 nm considering the appropriate RRF (see below). At reaction completion, the mixture was extracted with an appropriate organic solvent (3x1 mL). The collected organic phases were concentrated under reduced pressure. The product was isolated without need of purification.

# d) Recycling protocol for HCS coupling<sup>[45]</sup>:

After complete conversion of the desired reaction (monitored with HPLC-UV at 210 nm), the mixture was extracted three times under N<sub>2</sub> with an appropriate organic solvent, not miscible with the HEP/water solution (Cy, MTBE, toluene, 2-MeTHF, IBA and IPA). The organic layer was removed with a syringe, another portion of base, aryl chloride and acetylene (slowly over the curse of the reaction) were added to the HEP/water phase and another catalytic cycle was performed at 80-90°C. The conversion of the new cycle of reaction was monitored by the previously mentioned analysis. The organic phases obtained from the different cycles were combined, distilled to recover the organic solvent, and the residue purified, when necessary, by flash chromatography.

# e) Thermomorphic protocol for HCS coupling:

To an oven-dried 10 mL Schlenk purged under  $N_2$  atmosphere, palladium pre-catalyst  $Pd(ACN)_2Cl_2$  (0.02 mmol, 2 mol%, 5.2 mg), sSPhos, (0.06 mmol, 6 mol%, 30.8 mg) were dissolved in HEP and water as co-solvent. The other reagents were then added in the following order: TMG (126.9 mg, 138.0  $\mu$ L, 1.1 mmol, 1.1 equiv) and aryl chloride (1.0 mmol, 1.0 equiv). The reaction mixture was heated to 90°C with an oil bath and phenylacetylene **2a** (1.7.2 mg, 115.3  $\mu$ L, 1.05 mmol, 1.05 equiv) was added slowly with a syringe pump over the course of the reaction in 0.5 mL of toluene or IBA in a HEP/water/toluene or HEP/water/IBA 7/3/5 ratio; the conversion was evaluated through HPLC-UV analysis at 210 nm considering the appropriate RRF (see below). At reaction completion, by simply cooling the reaction mixture at room temperature, the separation of toluene (or IBA) containing the product **3a** occurred, that was simply extracted with a syringe. It was possible to recycle the catalyst and the HEP/water solution three times. The organic phases obtained from the different cycles were combined, distilled to recover the organic solvent, and the residue purified by flash chromatography.

## f) SM Scope with Cs2CO3 and K2CO3:

To an oven-dried 10 mL Schlenk purged under N<sub>2</sub> atmosphere, an aliquot of the stock solution was added along with the amount of HEP/water (40%) solution needed to achieve the desired concentration. The other reagents were then added in the following order: Cs<sub>2</sub>CO<sub>3</sub> (1.1 mmol, 357 mg, 1.1 equiv) or K<sub>2</sub>CO<sub>3</sub> (1.1 mmol, 152.1 mg, 1.1 equiv), aryl chloride **1a-1n** (1.0 mmol, 1.0 equiv) and aryl boronic acid **5a-5d** (1.05 mmol, 1.05 equiv). The reaction mixture was heated at the desired temperature with an oil bath and maintained at this temperature under stirring; the conversion was evaluated through HPLC-UV analysis at 210 nm considering the appropriate RRF (see below). At reaction completion, the mixture was extracted with an appropriate organic solvent (3x1 mL). The collected organic phases were concentrated under reduced pressure. The product was isolated without need of purification.

## g) One-pot HCS-HCS cross-coupling reactions:

To an oven-dried 10 mL Schlenk purged under  $N_2$  atmosphere, palladium pre-catalyst  $Pd(ACN)_2Cl_2$  (0.02 mmol, 2 mol%, 5.2 mg), sSPhos, (0.06 mmol, 6 mol%, 30.4 mg) were dissolved in HEP and water as co-solvent. The other reagents were then added in the following order: TMG (126.7 mg, 138.0  $\mu$ L, 1.1 mmol, 1.1 equiv), 1-chloro-3-iodobenzene 7 (238.4 mg, 123.8  $\mu$ L, 1.0 mmol, 1.0 equiv) and alkyne **2b** (92.5 mg, 106.6  $\mu$ L, 1.1 mmol, 1,1 equiv). The reaction mixture was heated to 60°C with an oil bath and the conversion

was evaluated through HPLC-UV analysis at 210 nm. After 2h, intermediate 8 was achieved with a complete conversion and a selectivity >99%. The mixture was then heated to 90°C, TMG (1.1 equiv) was directly added and phenylacetylene 2a was added slowly in 4h with a syringe pump in order to achieve product 9 with 95% of conversion. The mixture was extracted with IBA (3x5 mL). The collected organic phases were concentrated under reduced pressure. The reaction crude was purified by flash chromatography.

# h) One-pot HCS-SM cross-coupling reactions:

To an oven-dried 10 mL Schlenk purged under N<sub>2</sub> atmosphere, palladium pre-catalyst Pd(ACN)<sub>2</sub>Cl<sub>2</sub> (0.02 mmol, 2 mol%, 5.2 mg), sSPhos, (0.06 mmol, 6 mol%, 30.4 mg) were dissolved in HEP and water as co-solvent. The other reagents were then added in the following order: TMG (126.7 mg, 138.0 μL, 1.1 mmol, 1.1 equiv), 1-chloro-3-iodobenzene 7 (238.4 mg, 123.8 μL, 1.0 mmol, 1.0 equiv) and alkyne **2b** (92.5 mg, 106.6 μL, 1.1 mmol, 1,1 equiv). The reaction mixture was heated to 60°C with an oil bath and the conversion was evaluated through HPLC-UV analysis at 210 nm. After 2h, intermediate **8** was achieved with a complete conversion and a selectivity >99%. The mixture was then heated to 90°C, Cs<sub>2</sub>CO<sub>3</sub> (358.4 mg, 1.1 mmol, 1.1 equiv) and phenyl boronic acid **5a** (128.0 mg, 1.05 mmol, 1.05 equiv) were directly added to the solution. The reaction was complete in 1h giving product **10** with a complete conversion. The mixture was extracted with IBA (3x5 mL). The collected organic phases were concentrated under reduced pressure in order to achieve compound 10 without need of purification.

## 2.3.4.3. Calculation of TON, PMI and PMIr

## Turnover number (TON):

TON can be calculated by the ratio between the yield of the product at the end of the cycle, and the percentage of the mmol of catalyst divided from the number of the cycle<sup>[239]</sup>.

$$TON = \frac{average\ yield_{product}}{\%\ mmol_{catalyst}/n\ cycle}$$

## Complete Environmental Factor (cEF)[240]

The general environmental factor for an entire API process is computed by the ratio between the total mass of waste generated in the synthetic scheme and the mass of the isolated product. The simple environmental factor (sEF) neglects the solvents and water, and it is usually applied at the stage of initial research. This is the reason why, for an industrial point of view, it is better to use the complete environmental factor (cEF), that

includes all the components utilized for the entire synthesis including solvents and water:

$$cEF = \frac{\sum mass\ of\ waste}{mass\ of\ isolated\ product} = \frac{\sum mass\ of\ materials - mass\ of\ isolated\ product}{mass\ of\ isolated\ product}$$

# Process Mass Intensity (PMI)[241]

The process mass intensity (PMI) is defined as the ratio between the total mass of materials and the mass of the isolated product.

$$PMI = \frac{\sum mass\ of\ materials}{mass\ of\ isolated\ product} = cEF + 1$$

# 2.3.4.4. Recovery of HEP, and Pd in the HCS cross-coupling with 2 mol%

At the given time, the reaction was cooled at rt, extracted with cyclohexane and the HEP/water phase containing the catalyst was recycled.

After the final cycle, product 3 was again extracted with cyclohexane and the combined organic extracts were distilled and the product could be recovered without further purification. The reaction mixture, containing HEP/water, conjugated TMG acid and the catalyst complex, was treated with sodium formate (0.15 mmol, 10.0 mg) for 1h at 60°C to generate palladium black. At reaction completion, the mixture was filtered out with the aid of charcoal (30 mg) and the palladium metal was recovered. The filtrate was distilled under reduced pressure to recover HEP in 95% yield.

Table 32. Example of PMI calculation on the optimized HCS reaction on 5 mmol scale

Reagents	Single run	Single run and final	% of
Reagents	<b>(g)</b>	recovery (g) <sup>b</sup>	recovery
1a	1.12	1.12	-
2a	1.07	1.07	-
$Cs_2CO_3$	3.58	3.58	-
$Pd(ACN)_2Cl_2$	0.005	0.0005	90
sSPhos	0.03	0.03	-
HEP	3.2	0.16	95
Water	1.2	0.12	-
Sodium formate	-	0.01	-
Charcoal	-	0.06	-
Cyclohexanec	9.3	0.46	95
$3a^{d}$	1.7	1.7	-
$PMI^a$	11.1	-	-
PMI after Pd/sSPhos and HEP/water recycle	-	-	-
PMI after final recovery of Pd, HEP, Cy	-	4.4	-

<sup>a</sup>PMI calculated after 5 cycles and recycle of Pd complex and HEP/water. <sup>b</sup>PMI calculated after 5 cycles and recycle of Pd complex, HEP/water and final recovery of Pd metal, HEP and cyclohexane. <sup>c</sup>The organic phases obtained from the different cycles were combined and distilled to recover 95% of cyclohexane. It is possible to distill the cyclohexane also after each cycle. <sup>d</sup>Product 3a obtained without need of purification.

## 2.3.4.5. Recovery of HEP and Pd in the SM cross-coupling with 0.05 mol%

At the given time, the reaction was cooled at rt, extracted with cyclohexane achieving product **6a** and **6k** both with 95% yield with no need of purification. The reaction mixture, containing HEP/water, conjugated base (K<sub>2</sub>CO<sub>3</sub> or Cs<sub>2</sub>CO<sub>3</sub> acid and the catalyst complex, was treated with sodium formate (0.1 mmol, 10.0 mg) for 1h at 60°C in order to generate palladium black. At reaction completion, the mixture was filtered out with the aid of charcoal (60 mg) and the palladium metal was recovered. The filtrate was distilled under reduced pressure to recover HEP in 95% yield.

Table 33. Example of PMI calculation on the SM reaction of Scheme 8 with 10 mmol scale

Single run	Single run and final	% of
<b>(g)</b>	recovery (g) <sup>b</sup>	recovery
1.1	1.1	-
1.2	1.2	-
3.57	3.57	-
0.001	0.0001	90
0.007	0.007	-
6.8	0.34	95
4	4	-
	0.01	
-	0.01	-
-	0.06	-
23.4	1.16	95
1.47	1.47	-
27.2	-	-
-	7.7	-
	(g)  1.1 1.2 3.57 0.001 0.007 6.8 4 - 23.4 1.47	(g) recovery (g) <sup>b</sup> 1.1 1.1 1.2 1.2 3.57 3.57 0.001 0.0001 0.007 0.007 6.8 0.34 4 4 - 0.01 - 0.06 23.4 1.16 1.47 1.47 27.2 -

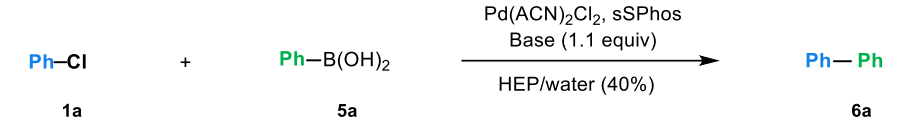
<sup>&</sup>lt;sup>a</sup>PMI calculated considering all the reagents used without recovery. <sup>b</sup>PMI calculated after final recovery of Pd metal, HEP and cyclohexane. <sup>c</sup>The organic phases obtained from the different cycles were combined and distilled to recover 95% of cyclohexane. <sup>d</sup>Product **6a** obtained without need of purification.

Table 34. Example of PMI calculation on the SM reaction of Scheme 10 with 10 mmol scale

Doggonta	Single	Single run and final	0/ of magaziani
Reagents	run (g)	recovery (mg)b	% of recovery
1g	1.1	1.1	-
5e	1.56	1.56	-
$Cs_2CO_3$	3.57	3.57	-
$Pd(ACN)_2Cl_2 \\$	0.001	0.0001	90
sSPhos	0.007	0.007	-
HEP	6.8	0.34	95
Water	4	4	-
Sodium formate	-	0.01	-
Charcoal	-	0.06	-
Cyclohexanec	23.4	1.16	95
$6k^{d}$	2.24	2.24	-
PMI <sup>a</sup>	18.0	-	-
PMI after final			
recovery of Pd,	-	5.3	-
HEP, Cy			

<sup>&</sup>lt;sup>a</sup>PMI calculated considering all the reagents used without recovery. <sup>b</sup>PMI calculated after final recovery of Pd metal, HEP and cyclohexane. <sup>c</sup>The organic phases obtained from the different cycles were combined and distilled to recover 95% of cyclohexane. <sup>d</sup>Product **6k** obtained without need of purification.

# 2.3.4.6. Base Screening in the SM coupling



To an oven-dried 10 mL Schlenk purged under  $N_2$  atmosphere, an aliquot of the stock solution was added along with the amount of HEP/water (40%) solution needed to achieve the desired concentration. The other reagents were then added in the following order: base (1.1 mmol, 1.1 equiv), chlorobenzene (50.6  $\mu$ L, 1.0 mmol, 1.0 equiv) and phenyl boronic acid (1.05 or 1.2 equiv, see the following table). The reaction mixture was heated at the desired temperature with an oil bath and maintained at this temperature under stirring; the conversion was evaluated through HPLC-UV analysis at 210 nm considering the appropriate RRF (see *paragraph* 2.3.4.9. for RRF calculation).

Table 35. Base screening in SM coupling (rows in grey have already been reported in Table 31).

Entry	Conc. (M)	Pd (mmol%)	R-B(OH) <sub>2</sub> (equiv)	Base	T (°C)	Time (h)	Conv. (%)
1	1.0	0.1	1.2	Cs <sub>2</sub> CO <sub>3</sub>	45	16	100
2	1.0	0.2	1.05	Cs <sub>2</sub> CO <sub>3</sub>	45	16	100
3	1.0	0.1	1.2	K <sub>2</sub> CO <sub>3</sub>	45	16	63
4	1.0	0.2	1.05	K <sub>2</sub> CO <sub>3</sub>	45	16	100
5	0.5	0.1	1.2	K <sub>2</sub> CO <sub>3</sub>	45	16	100
6	1.0	0.1	1.2	Na <sub>2</sub> CO <sub>3</sub>	45	16	51
7	1.0	0.2	1.05	Na <sub>2</sub> CO <sub>3</sub>	45	16	100
8	0.5	0.1	1.2	Na <sub>2</sub> CO <sub>3</sub>	45	16	76
9	1.0	0.1	1.2	K <sub>3</sub> PO <sub>4</sub>	45	16	38
10	1.0	0.2	1.05	K <sub>3</sub> PO <sub>4</sub>	45	16	100
11	0.5	0.1	1.2	K <sub>3</sub> PO <sub>4</sub>	45	16	67
12	1.0	0.05	1.05	Cs <sub>2</sub> CO <sub>3</sub>	60	8	100
13	1.0	0.05	1.05	K <sub>2</sub> CO <sub>3</sub>	60	16	85
14	0.5	0.05	1.05	K <sub>2</sub> CO <sub>3</sub>	60	16	87
15	1.0	0.05	1.05	Na <sub>2</sub> CO <sub>3</sub>	60	16	83
16	0.5	0.05	1.05	Na <sub>2</sub> CO <sub>3</sub>	60	16	85
17	1.0	0.05	1.05	K <sub>3</sub> PO <sub>4</sub>	60	16	76
18	0.5	0.05	1.05	K <sub>3</sub> PO <sub>4</sub>	60	16	79
19	1.0	0.05	1.05	Cs <sub>2</sub> CO <sub>3</sub>	90	4	100

20	1.0	0.05	1.05	K <sub>2</sub> CO <sub>3</sub>	90	4	100
21	1.0	0.05	1.05	Na <sub>2</sub> CO <sub>3</sub>	90	4	88
22	1.0	0.05	1.05	K <sub>3</sub> PO <sub>4</sub>	90	4	84

## 2.3.4.7. PdCl<sub>2</sub>(sSPhos)<sub>2</sub> reduction

To an oven-dried 20 mL Schlenk purged under nitrogen atmosphere, the pre-catalyst  $PdCl_2(ACN)_2$  (3.37 mg, 0.013 mmol, 1.0 equiv), the ligand sSPhos (13.32 mg, 0.026 mmol, 2.0 equiv) and  $Cs_2CO_3$  (21.18 mg, 0.065 mmol, 5.0 equiv) were dissolved in DMF-d7 (0.4 mL) and HEP/H2O (ratio 7:3, 0.2 mL). The reaction was stirred at 60°C and after 10 minutes the  $^{31}P$  NMR spectrum was collected (A). Chlorobenzene (6.6  $\mu$ L, 0.026 mmol, 5 equiv) was added and the reaction stirred at 60°C for 30 minutes (B). The chemical shift of ArPd(sSPhos)Cl at 44.81 ppm and the shape of the signal is in line with the chemical shift of ArPd(SPhos)Cl in toluene reported by Barder et al.  $^{[228]}$  The disappearance of the signals at 64.24 ppm and at 63.02 ppm confirmed that the reduction process occurred.

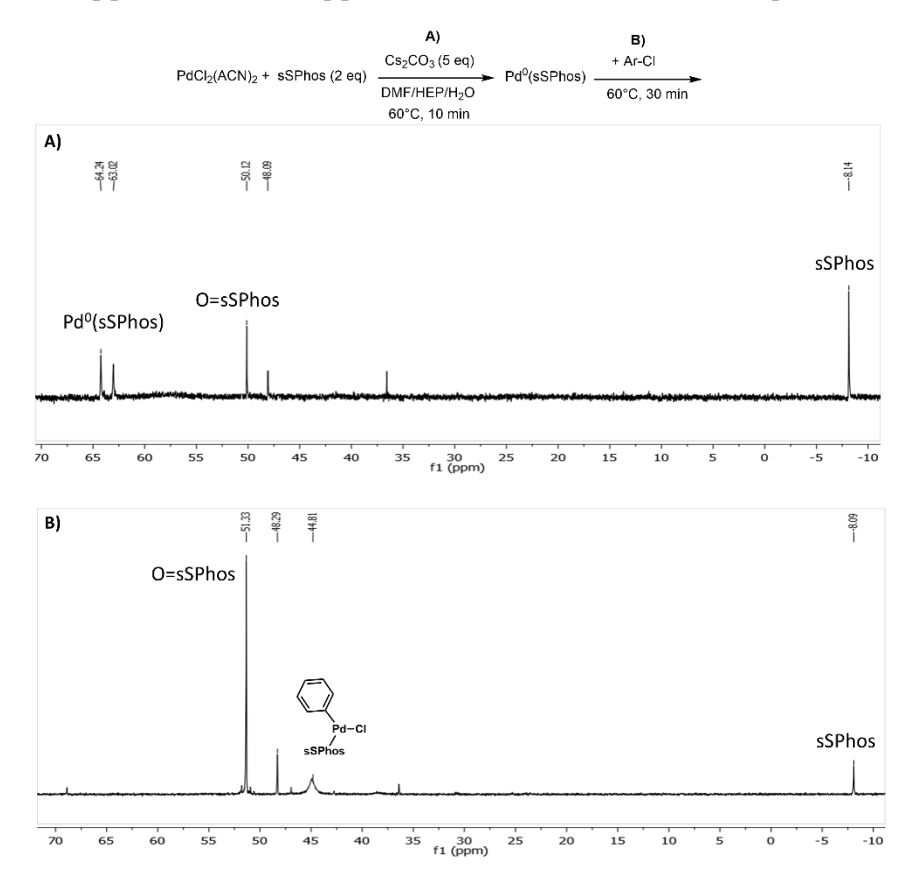


Figure 116.  $^{31}P$  NMR spectra of the reduction of  $PdCl_2(sSPhos)_2$  in DMF-d<sub>7</sub>/HEP/H<sub>2</sub>O with Cs<sub>2</sub>CO<sub>3</sub> 5 equiv at 60°C (A) and after the addition of Ar-Cl (5 equiv) (B).

As reference, the following spectra show the chemical shifts of the pre-catalyst PdCl<sub>2</sub>(sSPhos)<sub>2</sub>, the ligand sSPhos and OsSPhos:

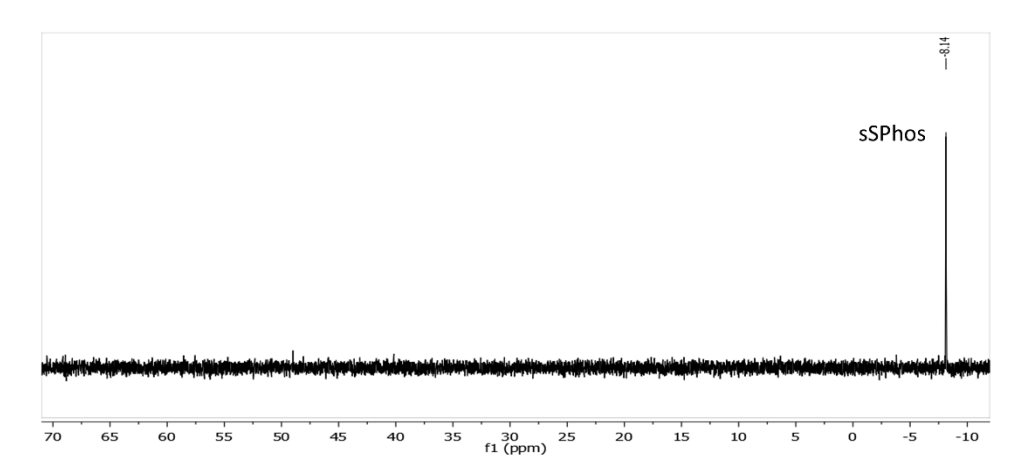


Figure 117. <sup>31</sup>P NMR spectrum of sSPhos in DMF-d<sub>7</sub>/HEP/H<sub>2</sub>O.

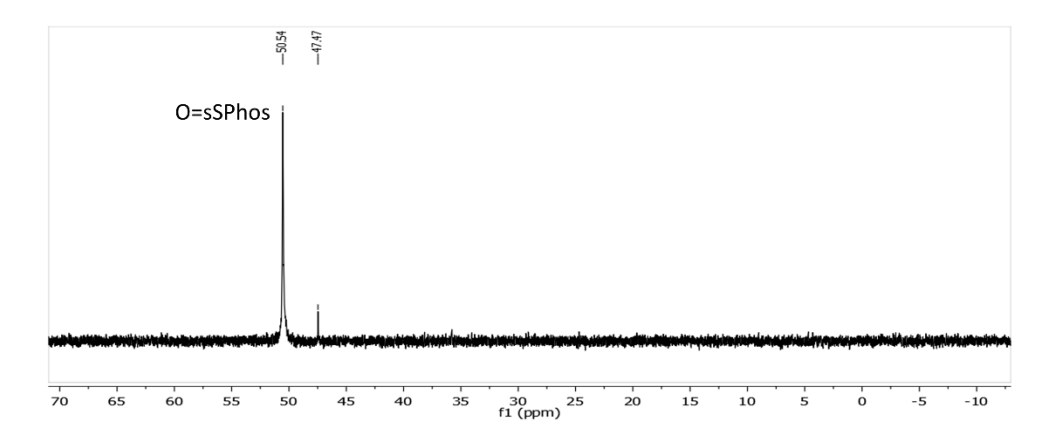


Figure 118.  $^{31}P$  NMR spectrum of OsSPhos in DMF-d<sub>7</sub>/HEP/H<sub>2</sub>O. The spectrum shows an unknown peak present also in the previous spectra

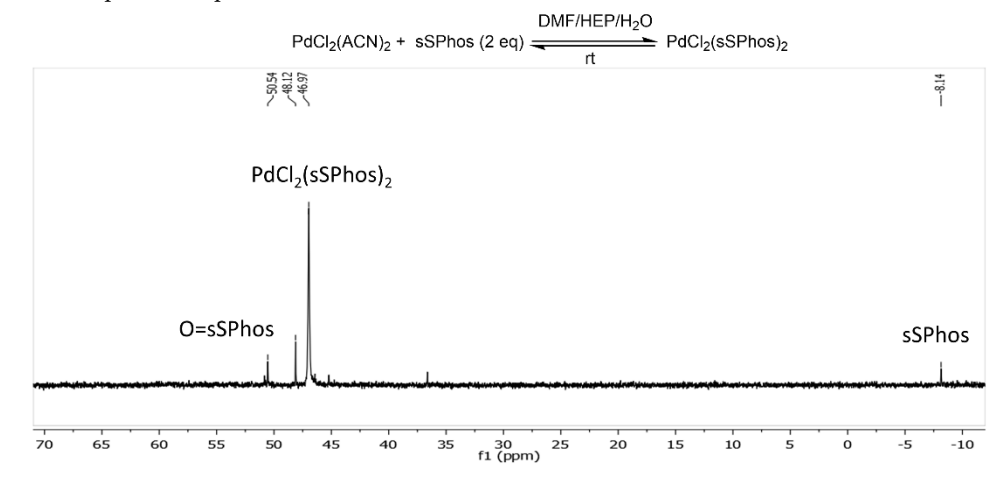


Figure 119.  $^{31}P$  NMR spectrum of PdCl<sub>2</sub>(sSPhos)<sub>2</sub> in DMF-d<sub>7</sub>/HEP/H<sub>2</sub>O. PdCl<sub>2</sub>(ACN)<sub>2</sub> (3.37 mg, 0.013 mmol, 1 equiv) and sSPhos (13.32 mg, 0.026 mmol, 2 equiv) were dissolved in DMF-d<sub>7</sub> (0.4 mL) and HEP/H<sub>2</sub>O (ratio 7:3, 0.2 mL).

**CHAPTER 2** 

# 2.3.4.8. Compound characterisation

Yields of the HCS reactions reported considering the single run of the entries in Table 30 **1,2-diphenylacetylene (3a)** 



White solid (93% yield), extraction solvent: Cy

<sup>1</sup>H NMR (400 MHz, CDCl<sub>3</sub>) δ (ppm) 7.58 – 7.56 (m, 4H), 7.39 – 7.36

(m, 6H).

<sup>13</sup>C NMR (100 MHz, CDCl<sub>3</sub>) δ (ppm) 131.27, 128.00, 127.91, 122.94, 89.04.

Anal. Calcd. for C14H10: C, 94.33; H, 5.67; found: C, 94.62; H, 5.69.

# 1-nitro-4-(phenylethynyl)benzene (3b)



Yellow solid (94% yield), extraction solvent: 'BuOAc

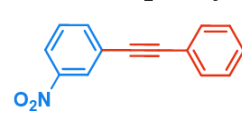
<sup>1</sup>H NMR (400 MHz, CDCl<sub>3</sub>) δ (ppm) 8.19 – 8.17 (m, 2H), 7.64 –

7.62 (m, 2H), 7.56 – 7.53 (m, 2H), 7.38 – 7.36 (m, 3H).

<sup>13</sup>C NMR (100 MHz, CDCl<sub>3</sub>) δ (ppm) 146.95, 132.27, 131.84, 130.22, 129.28, 128.57, 123.58, 122.10, 94.75, 87.59.

Anal. Calcd. for C<sub>14</sub>H<sub>9</sub>NO<sub>2</sub>: C, 75.33; H, 4.06; N, 6.27; found: C, 75.26; H, 4.06; N, 6.27.

# 1-nitro-3-(phenylethynyl)benzene (3c)



Yellow solid (95% yield), extraction solvent: <sup>t</sup>BuOAc

 $^{1}H$  NMR (400 MHz, CDCl $^{3}$ )  $\delta$  (ppm) 8.36 – 8.35 (m, 1H), 8.17 – 8,15

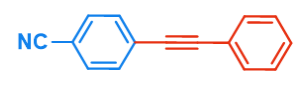
(d, 1H, J = 8.2 Hz), 7.82 - 7.80 (d, 1H, J = 7.7 Hz), 7.53 - 7.49 (m, 3H),

7.40 - 7.38 (m, 3H).

<sup>13</sup>C NMR (100 MHz, CDCl<sub>3</sub>) δ (ppm) 148.11, 137.19, 131.77, 129.35, 129.06, 128.53, 126.28, 125.10, 122.84, 122.19, 91.92, 86.91.

Anal. Calcd. for C14H9NO2: C, 75.33; H, 4.06; N, 6.27; found: C, 75.14; H, 4.06; N, 6.26.

## 4-(phenylethynyl)benzonitrile (3d)



Yellow solid (93% yield); extraction solvent: <sup>t</sup>BuOAc

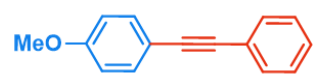
 $^{1}$ H NMR (400 MHz, CDCl<sub>3</sub>)  $\delta$  (ppm) 7.66–7.61 (m, 4H), 7.57 – 7.55

(m, 2H), 7.40 - 7.38 (m, 3H).

<sup>13</sup>C NMR (100 MHz, CDCl<sub>3</sub>) δ (ppm) 132.05, 132.02, 131.77, 129.10, 128.49, 128.23, 122.21, 118.50, 111.45, 93.76, 87.70.

Anal. Calcd. for C<sub>14</sub>H<sub>9</sub>N: C, 88.64; H, 4.46; N, 6.89; found C, 88.69; H, 4.38; N, 6.92.

# 1-methoxy-4-(phenylethynyl)benzene (3e)



White solid (90% yield), extraction solvent: <sup>t</sup>BuOAc

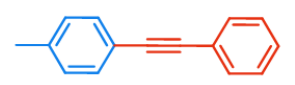
<sup>1</sup>H NMR (400 MHz, CDCl<sub>3</sub>) δ (ppm) 7.55 – 7.49 (m, 4H), 7.37 –

7.33 (m, 3H), 6.91 – 6.89 (m, 2H), 3.84 (s, 3H).

<sup>13</sup>C NMR (100 MHz, CDCl<sub>3</sub>) δ (ppm) 159.60, 133.02, 131.42, 128.28, 127.90, 123.58, 115.36, 113.98, 89.35, 88.05, 55.26.

Anal. Calcd. for C<sub>15</sub>H<sub>12</sub>O: C, 86.51; H, 5.81; found: C, 86.72; H, 5.81.

# 1-methyl-4-(phenylethynyl)benzene (3f)



White solid (91% yield), extraction solvent: Cy

<sup>1</sup>H NMR (400 MHz, CDCl<sub>3</sub>)  $\delta$  (ppm) 7.57 – 7.54 (m, 2H), 7.47 – 7.45 (d, J = 8.1 Hz, 2H), 7.38 – 7.34 (m, 3H), 7.19 – 7.17 (d, J = 7.9

Hz, 2H), 2.40 (s, 3H).

<sup>13</sup>C NMR (100 MHz, CDCl<sub>3</sub>) δ (ppm) 138.36, 131.53, 131.48, 129.09, 128.29, 128.04, 89.55, 88.71, 21.49.

Anal. Calcd. for C<sub>15</sub>H<sub>12</sub>: C, 93.79; H, 6.21; found: C, 93.57, H: 6.23.

# 2-methyl-4-phenylbut-3-yn-2-ol (3g)



Yellow oil (90% yield); extraction solvent: <sup>t</sup>BuOAc and purification by flash chromatography (Cy/EtOAc = 95/5).

 $^{1}$ H NMR (400 MHz, CDCl<sub>3</sub>)  $\delta$  (ppm) 7.44 – 7.42 (m, 2H), 7.31 – 7.29 (m, 3H), 2.53 (s, OH), 1.64 (s, 6H).

<sup>13</sup>C NMR (100 MHz, CDCl<sub>3</sub>) δ (ppm) 131.23, 127.83, 127.81, 122.37, 93.50, 81.69, 65.17, 31.08.

Anal. Calcd. for C<sub>11</sub>H<sub>12</sub>O: C, 82.46; H, 7.55; found: C, 82.78; H, 7.54.

## *N,N*-dimethyl-3-phenylprop-2-yn-1-amine (3h)



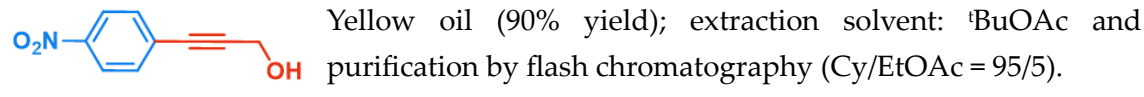
Colourless liquid (91% yield); extraction solvent: <sup>t</sup>BuOAc and purification by flash chromatography (Cy/EtOAc = 95/5).

 $^1H$  NMR (400 MHz, CDCl₃)  $\delta$  (ppm) 7.45 – 7.43 (m, 2H), 7.30 – 7.28 (m, 3H), 3.47 (s, 2H), 2.37 (s, 6H).

<sup>13</sup>C NMR (100 MHz, CDCl<sub>3</sub>) δ (ppm) 131.27, 127.82, 127.59, 122.80, 84.86, 84.13, 48.15, 43.81.

Anal. Calcd. for C11H13N: C, 82.97; H, 8.23; N, 8.80; found: C, 82.99; H, 8.22; N, 8.77.

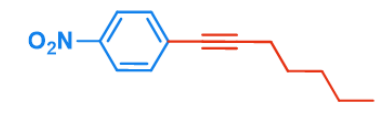
# 3-(4-nitrophenyl)prop-2-yn-1-ol (3i)



<sup>1</sup>H NMR (400 MHz, CDCl<sub>3</sub>)  $\delta$  (ppm) 8.21 – 8.18 (dd, J = 8.0, 4.0 Hz, 2H), 7.60 – 7.57 (dd, J = 8.0, 4.0 Hz, 2H), 4.55 (s, 2H).

<sup>13</sup>C NMR (100 MHz, CDCl<sub>3</sub>) δ (ppm) 147.25, 132.39, 129.41, 123.57, 92.46, 83.81, 51.49. Anal. Calcd. for C<sub>9</sub>H<sub>7</sub>NO<sub>3</sub>: C, 61.02; H, 3.98; N, 7.91; O, 27.09; found: C, 61.11; H, 3.95; N, 7.87; O, 28.1.

# 1-(hept-1-yn-1-yl)-4-nitrobenzene (3j)



Yellow oil (90% yield); extraction solvent: Cy and Purification by flash chromatography (Cy 100%).

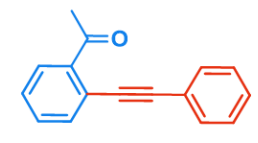
<sup>1</sup>H NMR (400 MHz, CDCl<sub>3</sub>) δ (ppm) 8.16 – 8.14 (dd,

J = 8.0, 4.0 Hz, 2H), 7.52 - 7.50 (dd, J = 8.0, 4.0 Hz, 2H), 2.46 - 2.43 (t, J = 12.0 Hz, 2H), 1.66 - 1.60 (m, 2H), 1.48 - 1.34 (m, 4H), 0.95 - 0.91 (t, J = 12.0 Hz, 3H).

<sup>13</sup>C NMR (100 MHz, CDCl<sub>3</sub>) δ (ppm) 146.53, 132.19, 131.20, 123.43, 96.79, 79.25, 31.08, 28.08, 22.16, 19.50, 13.93.

Anal. Calcd. for C<sub>13</sub>H<sub>15</sub>NO<sub>2</sub>: C, 71.87; H, 6.96; N, 6.45; O, 14.73; found: C, 71.93; H, 6.92; N, 6.50; O, 14.69.

# 1-(2-(phenylethynyl)phenyl)ethan-1-one (3k)



Yellow oil (94% yield); extraction solvent: <sup>t</sup>BuOAc and purification by flash chromatography (Cy/EtOAc = 95/5).

<sup>1</sup>H NMR (400 MHz, CDCl<sub>3</sub>) δ (ppm) 7.77 – 7.75 (d, J = 8.0 Hz, 1H), 7.64 – 7.62 (d, J = 8.0 Hz, 1H), 7.56 – 7.55 (m, 2H), 7.49 – 7.47 (t, J = 4.0 Hz, 1H), 7.42 – 7.37 (m, 4H), 2.80 (s, 3H).

<sup>13</sup>C NMR (100 MHz, CDCl<sub>3</sub>) δ (ppm) 200.35, 140.76, 133.91, 131.54, 131.34, 128.80, 128.73, 128.49, 128.31, 122.91, 121.71, 95.06, 88.53, 30.01.

Anal. Calcd. for C<sub>16</sub>H<sub>12</sub>O: C, 87.25; H, 5.49; O, 7.26; found C, 87.28; H, 5.52; O, 7.24

## 1,2,3,4,5-pentafluoro-6-(phenylethynyl)benzene (31)



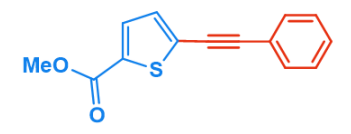
(m, 3H).

White solid (92% yield); extraction solvent: Cy and purification by flash chromatography (Cy 100%).

<sup>1</sup>H NMR (400 MHz, CDCl<sub>3</sub>) δ (ppm) 7.59 – 7.57 (m, 2H), 7.42 – 7.38

<sup>13</sup>C NMR (100 MHz, CDCl<sub>3</sub>)  $\delta$  (ppm) 147.1 (dm, J<sub>F-C</sub> = 250 Hz), 141.4 (dm, J<sub>F-C</sub> = 250 Hz), 137.6 (dm, J<sub>F-C</sub> = 250 Hz), 131.90, 129.64, 128.52, 121.55, 101.55 (m), 100.31, 73.04 (m). Anal. Calcd. for C<sub>14</sub>H<sub>5</sub>F<sub>5</sub>: C, 62.70; H, 1.88; F, 35.42; found C, 62.71; H, 1.31; F, 35.40

## methyl 5-(phenylethynyl)thiophene-2-carboxylate (3m)



Yellow solid (93% yield); Extraction solvent:  ${}^{t}BuOAc$ ; Purification by flash chromatography (Cy/EtOAc = 90/10).  ${}^{t}H$  NMR (400 MHz, CDCl<sub>3</sub>)  $\delta$  (ppm) 7.70 (d, 1H, J = 3.9 Hz), 7.55

-7.53 (m, 2H), 7.38 (m, 3H), 7.23 (d, 1H, J = 3.9 Hz), 3.91 (s, 3H).

<sup>13</sup>C NMR (100 MHz, CDCl<sub>3</sub>) δ (ppm) 162.03, 133.79, 133.32, 132.14, 131.62, 130.05, 129.06, 128.49, 122.20, 95.62, 91.99, 52.34.

Anal. Calcd. for C<sub>14</sub>H<sub>10</sub>O<sub>2</sub>S: C, 69.40; H, 4.16; O, 13.21; S, 13.23; found: C, 68.87; H, 4.01; O, 13.29; S, 13.40.

**CHAPTER 2** 

# 7-chloro-4-(phenylethynyl)quinoline (3n)



White solid (90% yield); Extraction solvent: <sup>t</sup>BuOAc; Purification by flash chromatography (Cy/EtOAc = 95/5).

<sup>1</sup>H NMR (400 MHz, CDCl<sub>3</sub>)  $\delta$  (ppm)  $\delta$  8.90 (d, J = 4.5 Hz, 1H), 8.30 (d, J = 8.9 Hz, 1H), 8.13 (d, J = 2.1 Hz, 1H), 7.71 – 7.63 (m, 2H), 7.61

-7.54 (m, 2H), 7.44 (dd, J = 5.1, 1.9 Hz, 3H).

<sup>13</sup>C NMR (100 MHz, CDCl<sub>3</sub>) δ 150.85, 148.50, 135.87, 132.00, 129.88, 129.58, 128.81, 128.65, 128.19, 127.43, 126.18, 123.64, 121.98, 99.20, 84.60.

Anal. Calcd. for C<sub>17</sub>H<sub>10</sub>ClN: C, 77.42; H, 3.82; Cl, 13.44; N, 5.31; found: C, 77.54; H, 3.76; Cl, 13.63; N, 5.22

# 2-(phenylethynyl)pyridine (30)



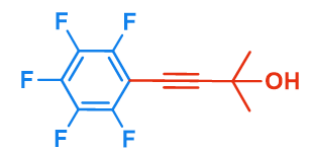
Yellow oil (91% yield); Extraction solvent: <sup>t</sup>BuOAc; Purification by flash chromatography (Cy/EtOAc = 95/5).

<sup>1</sup>H NMR (400 MHz, CDCl<sub>3</sub>)  $\delta$  (ppm)  $\delta$  7.70 – 7.67 (m, 1H), 7.61 (m, 2H), 7.54 (d, J = 8.1 Hz, 1H), 7.38, (m, 3H), 7.26 – 7.23 (m, 1H).

<sup>13</sup>C NMR (100 MHz, CDCl<sub>3</sub>) δ 150.09, 143.50, 136.17, 132.07, 128.99, 128.41, 127.18, 122.76, 122.29, 89.25, 88.62.

Anal. Calcd. for C<sub>13</sub>H<sub>9</sub>N: C, 87.12; H, 5.06; N, 7.82; found: C, 87.09; H, 5.09; N, 7.87.

## 2-methyl-4-(perfluorophenyl)but-3-yn-2-ol (3p)



Yellow solid (91% yield); Extraction solvent: <sup>1</sup>BuOAc; Purification by flash chromatography (Cy/EtOAc = 80/20).

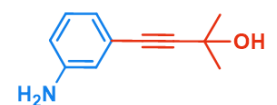
<sup>1</sup>H NMR (400 MHz, CDCl<sub>3</sub>) δ (ppm) δ 1.65 (s, 6H).

<sup>13</sup>C NMR (151 MHz, CDCl<sub>3</sub>)  $\delta$  147.11 – 145.33 (dm, J<sub>F-C</sub> = 168,0

Hz), 141.22 – 139.60 (dm, J<sub>F-C</sub> = 173,0 Hz), 137.40 – 135.76 (dm, J<sub>F-C</sub> = 164,0 Hz), 105.35, 98.61, 65.41, 64.78, 30.01.

Anal. Calcd. for C<sub>11</sub>H<sub>7</sub>F<sub>5</sub>O: C, 52.81; H, 2.82; F, 37.97; O, 6.40; found: C, 52.72; H, 2.98; F, 37.90; O, 6.54

## 4-(3-aminophenyl)-2-methylbut-3-yn-2-ol (3q)



Pale yellow solid (52%); Extraction solvent: <sup>t</sup>BuOAc; Purification by flash chromatography (Cy/EtOAc = 90/10)

<sup>1</sup>H NMR (400 MHz, CDCl<sub>3</sub>) δ (ppm) 7.08 (t, J = 7.8 Hz, 1H), 6.83 (d, J = 7.6 Hz, 1H), 6.75 (s, 1H), 6.64 (d, J = 8.0 Hz, 1H), 3.67 (s, NH<sub>2</sub>), 2.21 (s, OH), 1.61 (s, 6H). <sup>13</sup>C NMR (100 MHz, CDCl<sub>3</sub>) δ (ppm) 146.13, 129.15, 123.38, 122.03, 117.91, 115.28, 93.17, 82.26, 65.53, 31.47.

Anal. Calcd for C<sub>11</sub>H<sub>12</sub>NO: C, 75.40; H, 7.48; N, 7.99; found: C, 75.50; H, 7.43; N, 7.95;

Yields of the SM reactions reported in Scheme 8

# 1,1'-biphenyl (6a)



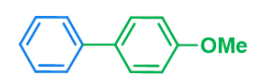
White solid (95% yield); extraction solvent: Cy

<sup>1</sup>H NMR (400 MHz, CDCl<sub>3</sub>) δ (ppm) 7.69 – 7.66 (m, 4H), 7.54 – 7.49 (m, 4H), 7.44 – 7.40 (m, 2H).

<sup>13</sup>C NMR (100 MHz, CDCl<sub>3</sub>) δ (ppm) 141.28, 128.80, 127.29, 127.21.

Anal. Calcd. for C<sub>12</sub>H<sub>10</sub>: C, 93.46; H, 6.54; found: C, 93.37; H, 6.62.

# 4-methoxy-1,1'-biphenyl (6b-6e)



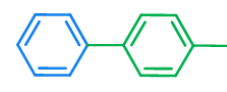
White solid (90 and 92% yield); extraction solvent: <sup>t</sup>BuOAc

<sup>1</sup>H NMR (400 MHz, CDCl<sub>3</sub>) δ (ppm) 7.58 – 7.52 (m, 4H), 7.45 – 7.41

(m, 2H), 7.33 - 7.29 (m, 1H), 7.00 - 6.98 (m, 2H), 3.87 (s, 3H). <sup>13</sup>C NMR (100 MHz, CDCl<sub>3</sub>)  $\delta$  (ppm)159.11, 140.81, 133.76, 128.68, 128.12, 126.71, 126.62, 114.17, 55.32.

Anal. Calcd. for C<sub>13</sub>H<sub>12</sub>O: C, 84.75; H, 6.57; O, 8.68; found: C, 84.77; H, 6.51; O, 8.70.

# 4-methyl-1,1'-biphenyl (6c-6f)



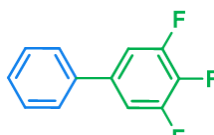
White solid (94 and 93% yield), extraction solvent: Cy<sup>1</sup>H NMR (400 MHz, CDCl<sub>3</sub>)  $\delta$  (ppm) 7.68 – 7.66 (m, 2H), 7.60 – 7.58 (m, 2H), 7.53 –

7.49 (m, 2H), 7.43 - 7.39 (m, 1H), 7.35 - 7.33 (d, J = 7.8 Hz, 2H).

<sup>13</sup>C NMR (100 MHz, CDCl<sub>3</sub>) δ (ppm) 141.22, 138.44, 137.06, 129.57, 128.79, 127.04, 127.02, 21.14.

Anal. Calcd. for C<sub>13</sub>H<sub>12</sub>: C, 92.81; H, 7.19; found: C, 92.75; H, 7.23.

# 3,4,5-trifluoro-1,1'-biphenyl (6d)



White solid (92% yield); extraction solvent: Cy

<sup>1</sup>H NMR (400 MHz, CDCl<sub>3</sub>) δ (ppm) 7.53 – 7.42 (m, 5H), 7.22 – 7.18 (m, 2H)

 $^{13}\text{C NMR}$  (100 MHz, CDCl<sub>3</sub>)  $\delta$  (ppm) 152.72 - 152.58 (dd, Jc-F = 9.9, 4.2 Hz), 150.25 - 150.11 (dd, Jc-F = 10.1, 4.4 Hz), 140.63 - 140.32 (t, Jc-F = 15.1 Hz), 138.17 - 137.43 (m), 137.45 - 137.25 (m), 129.06, 128.37, 126.81, 111.10 - 110.88 (dd, Jc-F = 16.1, 6.0 Hz).

Anal. Calcd. for C<sub>12</sub>H<sub>7</sub>F<sub>3</sub>: C, 69.23; H, 3.39; F, 27.38; found: C, 69.20; H, 3.45; F, 27.44.

# 2-nitro-1,1'-biphenyl (6g)



Yellow oil (95% yield); extraction solvent: <sup>t</sup>BuOAc

<sup>1</sup>H NMR (400 MHz, CDCl<sub>3</sub>)  $\delta$  (ppm) 7.89– 7.87 (dd, J = 8.0, 1.3 Hz, 1H), 7.65 – 7.61 (td, J = 7.6, 1.3 Hz, 1H), 7.52 – 7.44 (m, 5H), 7.38 – 7.35 (m, 2H).

<sup>13</sup>C NMR (100 MHz, CDCl<sub>3</sub>) δ (ppm) 149.32, 137.42, 136.32, 132.31, 131.97, 128.70, 128.24, 128.20, 127.91, 124.06.

Anal. Calcd. for C<sub>12</sub>H<sub>9</sub>NO<sub>2</sub>: C, 72.35; H, 4.55; N, 7.03; O, 16.06; found: C, 72.39; H, 4.52; N, 7.01; O, 16.09.

## 4-nitro-1,1'-biphenyl (6h)

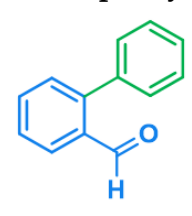
$$O_2N$$

Yellow solid (94% yield); extraction solvent: <sup>t</sup>BuOAc <sup>1</sup>H NMR (400 MHz, CDCl<sub>3</sub>) δ (ppm) 8.32 – 8.30 (m, 2H), 7.76 – 7.74 (m, 2H), 7.65 (m, 2H), 7.54 – 7.46 (m, 3H).

<sup>13</sup>C NMR (100 MHz, CDCl<sub>3</sub>) δ (ppm) 147.61, 147.07, 138.75, 129.16, 128.89, 127.80, 127.36, 124.08

Anal. Calcd. for C<sub>12</sub>H<sub>14</sub>: C, 72.35; H, 4.55; N, 7.03; O, 16.06; found: C, 72.25; H, 4.61; N, 7.07; O, 15.9.

# [1,1'-biphenyl]-2-carbaldehyde (6i)



Colorless oil (95% yield), extractions solvent: <sup>t</sup>BuOAc

 $^{1}$ H NMR (400 MHz, CDCl<sub>3</sub>)  $\delta$  (ppm) 9.88 (s, 1H), 7.94 – 7.92 (J= 8.0 Hz, d, 1H), 7.54-7.52 (m, 1H), 7.40 – 7.33 (m, 5H), 7.28-7.27 (m, 2H).

<sup>13</sup>C NMR (100 MHz, CDCl<sub>3</sub>) δ (ppm) 192.42, 145.97, 137.77, 133.74, 133.57, 130.79, 130.12, 128.45, 128.14, 127.79, 127.58

Anal. Calcd. for C<sub>13</sub>H<sub>10</sub>O, C, 85.69; H, 5.53; O, 8.78; found 85.70; H, 5.51; O, 8.76

## 2-phenylpyridine (6j)



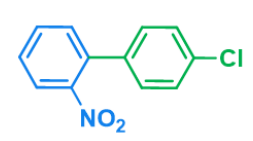
Colourless oil (93% yield). Extraction solvent: <sup>t</sup>BuOAc.

<sup>1</sup>H NMR (400 MHz, CDCl<sub>3</sub>)  $\delta$  (ppm)  $\delta$  8.71 (d, J = 3.5 Hz, 1H), 8.01 (d, J = 8.4 Hz, 2H), 7.75 (m, 2H), 7.50 – 7.42 (m, 3H), 7.23 (m, 1H).

<sup>13</sup>C NMR (100 MHz, CDCl<sub>3</sub>) δ 156.44, 148.63, 138.37, 135.70, 127.91, 127.71, 125.88, 121.05, 119.53.

Anal. Calcd. for C<sub>11</sub>H<sub>9</sub>N: C, 85.13; H, 5.85; N, 9.03; found: C, 85.16; H, 5.89; N, 9.01

## 4'-chloro-2-nitro-1,1'-biphenyl (6k)



Yellow solid (95% yield); extractions solvent: <sup>t</sup>BuOAc

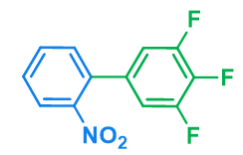
<sup>1</sup>H NMR (400 MHz, CDCl<sub>3</sub>) δ (ppm) 7.90 – 7.87 (dd, J = 8.1, 1.3 Hz, 1H), 7.65 – 7.61 (td, J = 7.6, 1.3 Hz, 1H), 7.53 – 7.49 (m, 1H), 7.43 – 7.39

(m, 3H), 7.27 - 7.25 (m, 2H).

<sup>13</sup>C NMR (100 MHz, CDCl<sub>3</sub>) δ (ppm) 149.03, 135.95, 135.15, 134.41, 132.55, 131.85, 129.30, 128.89, 128.61, 124.25.

Anal. Calcd. for C<sub>12</sub>H<sub>8</sub>ClNO<sub>2</sub>: C, 61.69; H, 3.45; Cl, 15.17; N, 5.99; O, 13.69; found: C, 61.74; H, 3.38; Cl, 15.13; N, 6.04; O, 13.74.

# 3',4',5'-trifluoro-2-nitro-1,1'-biphenyl (6l)



Yellow solid (97% yield); extractions solvent: Cy

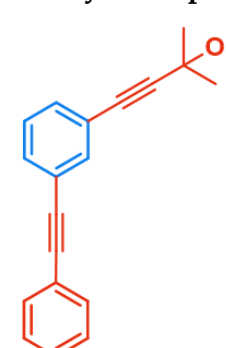
<sup>1</sup>H NMR (400 MHz, CDCl<sub>3</sub>)  $\delta$  (ppm) 7.96 – 7.93 (dd, J = 8.1, 1.3 Hz, 1H), 7.69 – 7.65 (td, J = 7.5, 1.3 Hz, 1H), 7.60 – 7.55 (dt, J = 7.8, 1.5 Hz, 1H), 7.41 – 7.39 (dd, J = 7.6, 1.5 Hz, 1H), 6.97 – 6.94 (m, 2H).

 $^{13}$ C NMR (100 MHz, CDCl<sub>3</sub>)  $\delta$  (ppm) 152.41 – 152.27 (dd, JF = 10.3, 4.2 Hz), 149.92 – 149.77 (dd, JF = 10.1, 4.4 Hz), 148.68, 141.19 – 140.89 (t, JF = 15.1 Hz), 138.68 – 138.38 (t, JF = 15.1 Hz), 133.51 – 133.46 (m), 132.79, 131.63, 129.37, 124.49, 112.68 – 112.46 (dd, JF = 16.1, 6.0 Hz).

Anal. Calcd. for C<sub>12</sub>H<sub>6</sub>F<sub>3</sub>NO<sub>2</sub>: C, 56.93; H, 2.39; F, 22.51; N, 5.53; O, 12.64; found: C, 56.98; H, 2.35; F, 22.46; N, 5.61; O, 12.60.

Yields of the one-pot reactions reported in Scheme 10

# 2-methyl-4-(3-(phenylethynyl)phenyl)but-3-yn-2-ol (9)

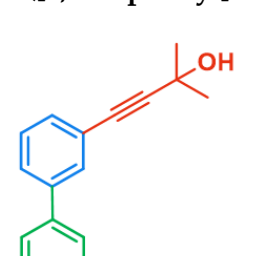


OH )Yellow oil (92% yield); extractions solvent: <sup>t</sup>BuOAc

 $^{1}$ H NMR (400 MHz, CDCl<sub>3</sub>)  $\delta$  (ppm) 7.63 (s, 1H), 7.56 – 7.53 (m, 2H), 7.49 – 7.47 (m, 1H), 7.40 – 7.30 (m, 5H), 1.65 (s, 6H).

<sup>13</sup>C NMR (100 MHz, CDCl<sub>3</sub>) δ (ppm) 134.68, 131.62, 131.29, 128.47, 128,37, 123.53, 123.08, 122.98, 94.39, 89.94, 88.47, 81.35, 65.58, 31.43. Anal. Calcd. for C<sub>19</sub>H<sub>16</sub>O: C, 87.66; H, 6.20; O, 6.15; found: C, 87.61; H, 6.29; O, 6.14.

## 4-([1,1'-biphenyl]-3-yl)-2-methylbut-3-yn-2-ol (10)



Yellow oil (96% yield); extractions solvent: <sup>t</sup>BuOAc

<sup>1</sup>H NMR (400 MHz, CDCl<sub>3</sub>) δ (ppm) 7.72 – 7.55 (m, 4H), 7.49 – 7.38 (m, 5H), 1.70 (s, 6H).

<sup>13</sup>C NMR (100 MHz, CDCl<sub>3</sub>) δ (ppm) 141.34, 140.32, 130.45, 128.89, 128.79, 127.66, 127.11, 123.30, 94.13, 82.21, 65.70, 31.57.

Anal. Calcd. for C<sub>17</sub>H<sub>16</sub>O: C, 86.40; H, 6.82; O, 6.77; found: C, 86.44; H, 6.74; O, 6.81.

## 2.3.4.9. Calculation of Relative Response Factor (RRF)

In HPLC with UV-DAD, the response of the detector is the absorbance of the compound at a fixed wavelength. Exploiting the Lambert-Beer law, it is possible to evaluate the RRF.

$$A = l \cdot c \cdot \varepsilon$$

## Where:

 $\epsilon$  is the molar attenuation coefficient or absorptivity (corresponding to the absorbance of a 1M solution).

c is expressed in molarity (mol/L).

The response factor, in analytical chemistry, is defined as the ratio between the molar concentration of a compound being analyzed and the response of the detector to that compound. In this way, the calculation of RRF is described below:

Response Factor (RF) = 
$$\frac{Peak\ Area}{Concentration\ [M]}$$

Thus, considering two substances in which one is the product (B) and the second is the reagent (A), the RRF is:

$$RF = \frac{RF_A}{RF_B} = \frac{\frac{PeakArea_A}{Concentration_A}}{\frac{PeakArea_B}{Concentration_B}} = \frac{\frac{PeakArea_A}{PeakArea_B}}{\frac{PeakArea_B}{Concentration_A}} \cdot \frac{Concentration_B}{Concentration_A}$$

Table 36. Calculation of RRF between chlorobenzene 1a and diphenylacetylene 3a at several concentrations

Concentration (M)	Chlorobenzene area (mAu)	Diphenylacetylene area (mAu)	RRF	$\Delta$ rrf
0,0025	2142.2	5633.3	2.63	
0,0005	438.7	1126.4	2.57	2.59
0,00025	256.0	658.6	2.57	-
mAU _		372		
		23:5		

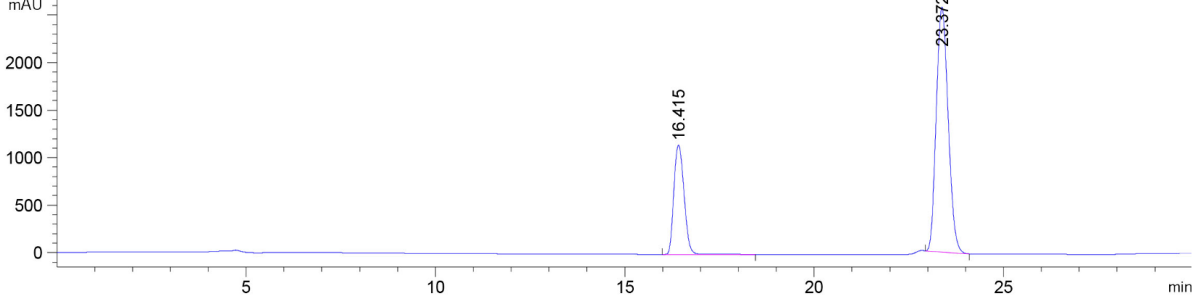


Figure 120. HPLC-UV spectrum of equimolar mixture of chlorobenzene **1a** and diphenylacetylene **3a** at 0.0025 M concentration

Table 37. Calculation of RRF between chlorobenzene 1a and biphenyl 6a at several concentrations

Concentration (M)	Chlorobenzene area (mAu)	Biphenyl area (mAu)	RRF	$\Delta_{RRF}$
0,0025	1923.8	4230.5	2.19	
0,0005	496.3	1124.2	2.26	2.23
0,00025	351.0	790.1	2.25	

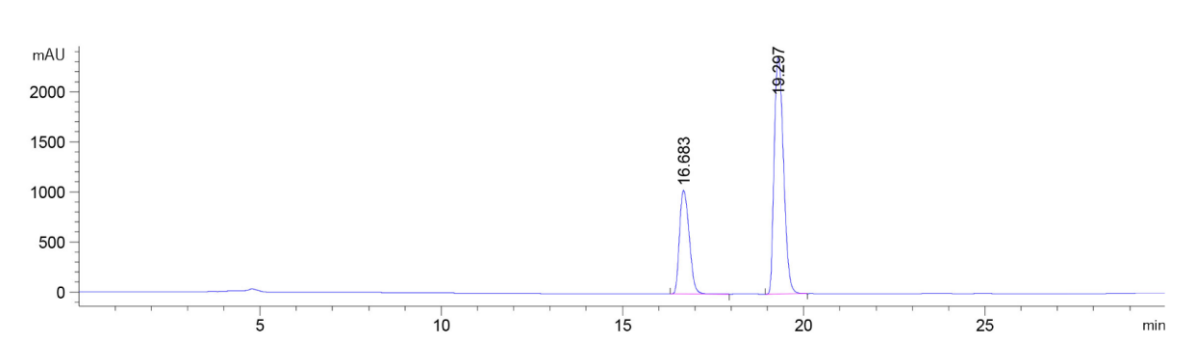


Figure S8: HPLC-UV spectrum of equimolar mixture of chlorobenzene 1a and biphenyl 6a at 0.0025 M concentration

Table 38. Calculation of RRF between diphenylacetylene 3a and 1,4-diphenyl-1-buten-3-yne 4a

Concentration (M)	Diphenylacetylene area (mAu)	1,4-diphenyl-1-buten-3-yne area (mAu)	RRF	$\Delta$ RRF
0,0025	75423.4	59859.8	1.26	
0,0005	17645.2	13573.2	1.30	- - 1.24
0,00025	7982.4	6597.0	1.21	- 1,2-7
0,000025	3426.5	2879.4	1.19	_

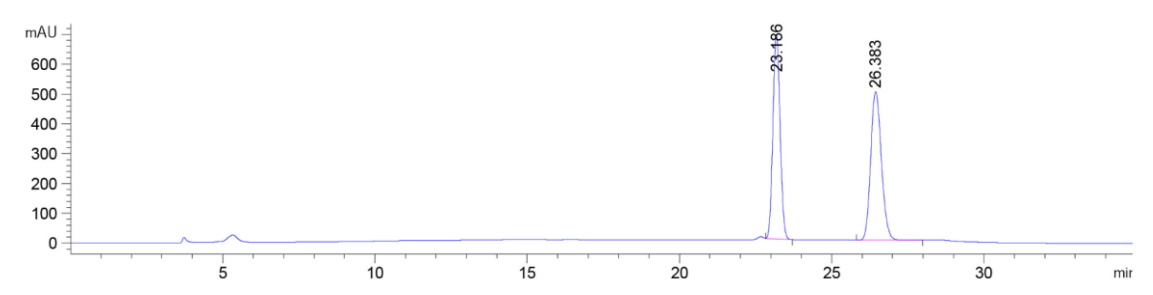


Figure 121. HPLC-UV spectrum of equimolar mixture of diphenylacetylene **3a** and 1,4-diphenyl-1-buten-3-yne **4** at 0.0005 M concentration.

## 2.3.4.10. Computational methods

DFT calculations were conducted at CINECA, through the Italian SuperComputing Resource Allocation – ISCRA, using the Gaussian 16 software package<sup>[242]</sup>. Geometry optimizations for all reported structures were performed with the dispersion corrected B3LYP-D3 functional with a mixed basis set of LANL2DZ (for Pd, I, Br, Cl) and 6-31G(d) (for other atoms).<sup>7</sup> Frequency calculations were performed on all optimized structures to ensure that each local minimum lacked imaginary frequency and that each transition state contained exactly one imaginary frequency. Solvation in DMF were introduced through single point calculations at optimized gas-phase geometries for all the minima and transition state using def2-TZVP for all atoms and the SMD implicit solvation model.<sup>[208]</sup> The reported Gibbs free energies were corrected considering the thermal correction computed at 298.15 K.

# Computed free energy profile of 4-NO2-phenyl halides

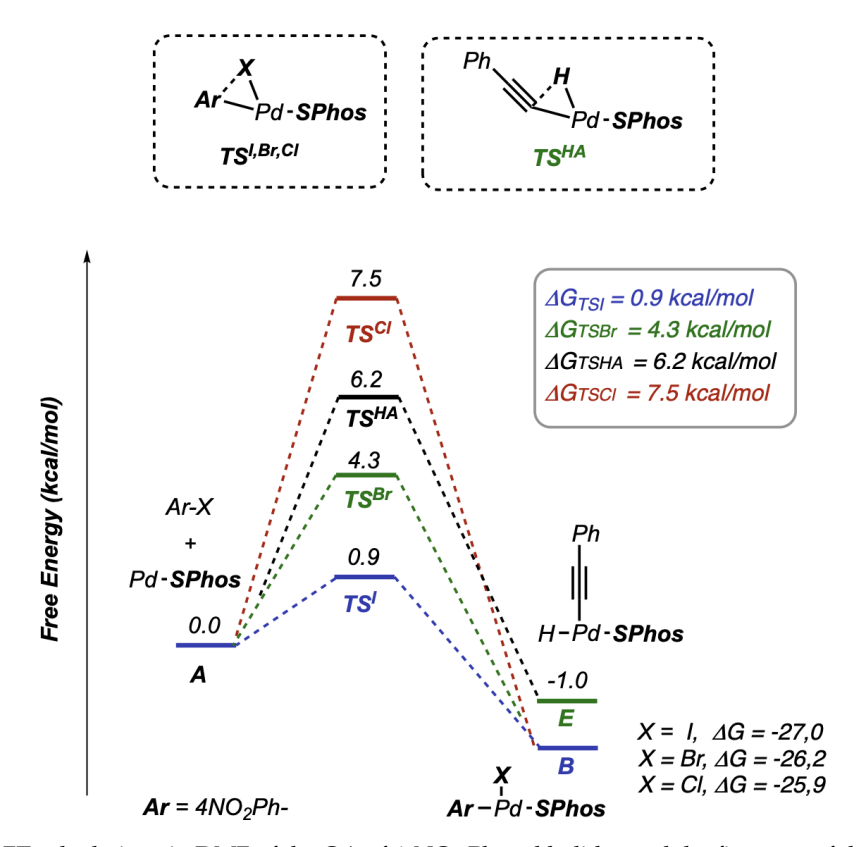


Figure 122. DFT calculations in DMF of the OA of  $4-NO_2$ -Phenyl halides and the first step of the phenylacetylene insertion to give the enyne byproduct 4.

CHAPTER 3

# **Bioactive Peptide Synthesis and Alternative Strategies**

# 3.1. T3P® as alternative coupling reagent

#### 3.1.1. Introduction

The selection of the appropriate coupling reagent is essential for the design of a protocol that is green, safe and efficient, especially in large-scale chemical production. In fact, the development of sustainable methods for amide bond formation has been highlighted by the ACS Green Chemistry Institute Pharmaceutical Roundtable (GCIPR) as one of the 10 key areas of green chemistry research<sup>[243]</sup>.

A wide range of activating reagents and additives are used in the formation of amide bonds, as different peptides often require specific conditions for optimal synthesis and there is no single preferred reagent. While various combinations of available reagents have been extensively studied for their effectiveness under different conditions, only a few can be considered as environmentally friendly approaches. Ongoing efforts are aimed at establishing comprehensive guidelines for greener and more sustainable practices<sup>[244]</sup>. However, these classification criteria have so far been based solely on the thermal stability of the reagents, with an emphasis on process safety.

Propylphosphonic anhydride (T3P®), first introduced by Wissmann and Kleiner in 1980<sup>[245]</sup>, has been recognised in the literature as an effective reagent for forming peptide bonds in solution, <sup>[246,247]</sup> as well as facilitating several other chemical transformations. T3P® offers several practical advantages over other coupling reagents: it is non-flammable, with low toxicity (LD50 in rats >2000 mg kg<sup>-1</sup>)<sup>[248,249]</sup> and its byproduct, propylphosphonic acid, can be easily removed by water washing. In peptide synthesis using T3P®, the cyclic structure of the reagent allows spontaneous reaction with the nucleophilic carboxylate of the *N*-protected amino acid, followed by rapid substitution by the amino group of a second amino acid residue (Figure 123). The

exceptional reactivity of the acylphosphate intermediate with all nucleophiles, including water, explains the frequent use of T3P® as a moisture scavenger<sup>[250]</sup>. However, this property is also a significant limitation when the reagent is used in iterative processes that require intermediate treatments with aqueous solutions.

$$PG \xrightarrow{\stackrel{}{\stackrel{}}} OH + O \xrightarrow{\stackrel{}{\stackrel{}}} O \xrightarrow{\stackrel{}{\stackrel{}}} O \xrightarrow{\stackrel{}{\stackrel{}{\stackrel{}}} O} O \xrightarrow{\stackrel{}{\stackrel{}}} O \xrightarrow{\stackrel{}{\stackrel{}}} O \xrightarrow{\stackrel{}{\stackrel{}}} O \xrightarrow{\stackrel{}{\stackrel{}} O} O \xrightarrow{\stackrel{}{\stackrel{}}} O \xrightarrow{\stackrel{}{\stackrel{}} O} O \xrightarrow{\stackrel{}{\stackrel{}}} O \xrightarrow{\stackrel{}} O \xrightarrow{\stackrel{}} O \xrightarrow{\stackrel{}{\stackrel{}}} O \xrightarrow{\stackrel{}} O \xrightarrow{\stackrel$$

Figure 123. T3P® induced peptide bond formation mechanism.

Although T3P® has been mentioned several times in the past as a peptide coupling reagent, its application has been limited to the formation of a single amide bond<sup>[251]</sup>. Albericio and co-workers<sup>[252]</sup> investigated the use of T3P® in SPPS and showed that the use of T3P® as a coupling reagent in solid phase peptide synthesis did not give the desired results, because under these conditions, T3P® only acted as an alternative to carbodiimides, requiring large excesses of OxymaPure® and diisopropylethylamine (DIPEA).

Although SPPS is currently the most widely used and reliable method, its use on an industrial scale is limited by the significant amounts of reagents and solvents required. For this reason, there has been a resurgence of interest in solution-phase peptide synthesis, and in this context, our group reported the first example of an iterative synthesis, without both isolation of intermediate oligomers and work-ups, in SolPPS with Cbz as the *N*-protecting group, using T3P® and DIPEA as coupling agents<sup>[253]</sup>. Therefore, due to the renewed interest in the homogeneous phase peptide synthesis, we decided to explore the extension of our approach to both SolPPS and PA-LPPS using *N*-Boc- and *N*-Fmoc-based protecting groups, respectively, to broaden the applicability of T3P® in the liquid phase.

#### 3.1.2. Results and Discussion

We focused our study on N-Boc and N-Fmoc protection in solution-phase peptide synthesis, building on previous research from our group. Specifically, Mattellone et al. [253] demonstrated the use of T3P® and DIPEA (1.5 equiv /3 equiv) as coupling agents

in SolPPS to combine N-Cbz protected amino acids with O $^{t}$ Bu protected amino esters within five minutes at room temperature.

First, we investigated the effectiveness of different solvents in the coupling step, and the need to consider the sensitivity of the reagent to water: aqueous work-up is necessary to remove coupling by-products, but could affect the efficiency of the coupling reagent introduced later in the synthesis, even in trace amounts. For the screening, we chose the reaction between *N*-protected phenylalanine and leucine benzyl ester (Scheme 11) as our standard coupling, measuring the conversion to dipeptide **1a,b** after ten minutes. Reactions were carried out in a nitrogen atmosphere using dry solvents. As the amino ester reactant was commercially available as a salified benzyl ester *p*-toluenesulfonate salt, one equivalent of DIPEA was always added to activate the nucleophilic amine moiety. The reaction was quenched after ten minutes by adding water and the phosphate by-products were removed by organic solvent/water extraction. The results obtained are reported in Table 39.

Scheme 11. Model reaction for T3P® induced peptide synthesis.

PG N OBN 
$$\rho$$
TsOH  $PG$  Solvent, 10 min  $\rho$ TsOH  $\rho$ TsOH

Table 39. Suitability of T3P® protocol in different solvents a.

Entry	PG	Solvent	Product	(%) Conversion <sup>b</sup>
1	Вос	DMF	1a	97
2	Fmoc	DMF	1b	>99
3	Вос	DCM	1a	>99
4	Fmoc	DCM	1b	>99
5	Вос	Anisole	1a	98
6	Fmoc	Anisole	1b	>99
7	Вос	CPME <sup>c</sup>	1a	82
8	Fmoc	CPME	1b	99
9	Вос	EtOAc	1a	97
10	Fmoc	EtOAc	1b	99
11	Вос	nPrOAc	1a	95
12	Fmoc	nPrOAc	1b	99

13	Вос	<sup>t</sup> BuOAc <sup>c</sup>	1a	85
14	Fmoc	<sup>t</sup> BuOAc	1b	>99
15	Вос	DMC	1a	92
16	Fmoc	DMC	1b	>99
17	Вос	THF	1a	96
18	Fmoc	THF	1b	>99
19	Вос	ACN	1a	93
20	Fmoc	ACN	1b	>99
21	Вос	NOP	1a	57
22	Fmoc	NOP	1b	>99

<sup>&</sup>lt;sup>a</sup>The reactions were performed with dry solvents under a nitrogen atmosphere. <sup>b</sup> Conversion calculated on the basis of the HPLC peaks area, comparing the UV signal at 220 nm of H<sub>2</sub>N-Leu-OBn with the dipeptide without an RRF correction. <sup>c</sup>The presence of undissolved material was observed.

Our investigation began with the standard reaction in DMF as a benchmark to compare the effectiveness of other organic solvents (entries 1 and 2, Table 39). We observed that after 10 minutes, conversions greater than 95% were achieved with almost all the solvents tested. Significantly lower conversions were only observed when using *N*-Boc-phenylalanine in CPME, 'BuOAc and NOP, which we attribute to solubility problems likely to affect the reaction rate. This problem was alleviated by switching to *N*-Fmoc-phenylalanine, which was fully soluble in these solvents and resulted in near complete conversions (entries 8, 14 and 22, Table 39). In addition, T3P® is known to minimise racemisation during peptide bond formation. To verify this, we evaluated the extent of racemisation in the reaction between *N*-Boc-(L)-phenylglycine and leucine methyl ester by checking for the presence of the (D)-phenylglycine dipeptide and we found that the racemic product represented approximately 0.5% of the total.

In view of an iterative oligopeptide synthesis, it is crucial to eliminate any residual moisture resulting from aqueous work-up, as water solubility in the reaction medium is a critical factor. For this reason, we performed the coupling reactions in non-anhydrous solvents, and we generally found significant decrease in yield, except when DCM was used. DCM which resulted in yields > 95% in any condition because of the low solubility of water in this solvent (below 0.24%).

The substrate scope was then extended, taking into account the requirements for the design of oligomer syntheses. The reactivity of *N*-Boc amino acids was tested in the reaction with leucine, with methyl ester chosen as the orthogonal protection in the final dipeptide. Since removal of the *N*-protecting group requires treatment with trifluoroacetic acid (TFA) followed by water washes to remove salts, we chose DCM as the solvent of choice because of its low tendency to retain moisture, as mentioned above.

The N-Fmoc protecting group is unsuitable for SolPPS, but it is commonly used in PA-LPPS, where the nucleophilic amino acid is modified as a benzylic ester. Therefore, we evaluated the reactivity of N-Fmoc protected amino acids in reactions with leucine benzyl ester. The selected results are summarised in Table 40.

Table 40. Synthesis of N-Boc/N-Fmoc dipeptides under optimized conditions <sup>a</sup>.

Entry	N-PG-Amino Acid	Amino Ester	(%) Conversion <sup>b</sup>
1	N-Boc-Leu-OH	H-Leu-OMe	98
2	N-Boc-Phe-OH	H-Leu-OMe	98
3	N-Boc-Arg(Pbf)-OH	H-Leu-OMe	99
4	N-Boc-Arg(Bn)-OH	H-Leu-OMe	96
5	N-Boc-Ser-OH	H-Leu-OMe	>99
6	N-Boc-Thr-OH	H-Leu-OMe	99
7	N-Boc-Trp-OH	H-Leu-OMe	96
8	N-Boc-Aib-OH	H-Leu-OBn	>99
9	N-Fmoc-Leu-OH	H-Leu-OBn	>99
10	N-Fmoc-Trp-OH	H-Leu-OBn	>99
11	N-Fmoc-Arg(Pbf)-OH	H-Leu-OBn	>99
12	N-Fmoc-Asp( <sup>t</sup> Bu)-OH	H-Leu-OBn	>99
13	N-Fmoc-Ser( <sup>t</sup> Bu)-OH	H-Leu-OBn	>99
14	N-Fmoc-Thr( <sup>t</sup> Bu)-OH	H-Leu-OBn	>99
15	<i>N</i> -Fmoc-Arg-OH	H-Leu-OBn	98
16	<i>N</i> -Fmoc-Aib-OH	H-Leu-OBn	99

<sup>&</sup>lt;sup>a</sup>The reactions were performed in DCM under a nitrogen atmosphere. <sup>b</sup> Conversion calculated on the basis of the HPLC peaks area, comparing the UV signal at 220 nm of the N-Boc-and N-Fmoc-amino acid with the dipeptide without an RRF correction

To verify that the exceptional speed of the T3P®-promoted coupling reaction was maintained regardless of the activated amino acid, we evaluated the conversion with all substrates after 10 min. Starting with the *N*-Boc/*C*-OMe protection strategy, we first performed couplings with *N*-Boc-Leu and *N*-Boc-Phe, which gave excellent conversions (see entries 1 and 2 in Table 40). We then explored amino acids with protected side chain functionalities, such as *N*-Boc-Arg(Pbf)-OH and *N*-Boc-Asp(Bzl)-OH. These substrates also gave satisfactory results, with almost complete conversion for the protected arginine (99%) and very good conversion for the aspartic acid derivative (96%) (entries 3 and 4, Table 40). Based on these promising results, the coupling reaction was tested on *N*-Boc amino acids bearing free functional groups in their side chains. The optimised conditions

proved effective for N-Boc-Ser-OH and N-Boc-Thr-OH, both of which have a free hydroxyl group (entries 5 and 6, Table 40). In addition, the reaction between N-Boc-Trp-OH and leucine methyl ester resulted in a 96% yield (entry 7, Table 40), suggesting that the coupling process is kinetically faster than any possible side reactions involving side chain functionalities. Complete conversion was also achieved in the reaction of N-Boc-Aib-OH, an amino acid that typically presents challenges due to the steric hindrance of its quaternary centre (entry 8, Table 40). Similarly, we tested a selection of N-Fmoc protected amino acids in coupling reactions with H-Leu-OBn, with results comparable to those obtained with N-Boc monomers. In this case, commercially available N-Fmoc-Ser('Bu)-OH and N-Fmoc-Thr('Bu)-OH were used in the screening, always giving excellent conversions (entries 13 and 14, Table 40). It is worth noting that N-Fmoc-Arg-OH, bearing the free guanidine moiety as a salt with hydrochloric acid, allowed > 99% conversion (entry 15, Table 40), thus opening the possibility of avoiding the problematic protection of the side chain with Pbf. Conversely, the protocol was unsuitable for coupling reactions involving N-Boc-Cys-OH, as it resulted in a mixture of the desired dipeptide and oxidised cysteine derivatives.

Based on the previous information, the protocol was applied to the synthesis of Leu-Enkephalin (H-Tyr-Gly-Gly-Phe-Leu-OH), a pentapeptide that is commonly prepared to test the efficacy of a method in comparison to other synthetic techniques<sup>[254]</sup>. The SolPPS was carried out with *N*-Boc protected monomers in DCM (Scheme 12). The amount of T3P® was slightly increased (2/4 ratio T3P®/DIPEA) in order to use it both as a scavenger for traces of water and as an activating reagent in the coupling. Under these conditions, the purity of the final peptide was 95% (yield 62%), an excellent value considering that the final protected peptide was isolated only by solvent evaporation and not purified by chromatography.

Although T3P®-induced coupling conditions are fully compatible with N-Fmoc amino acids, the iterative use of this protecting group in SolPPS is limited by the need to remove the water-insoluble dibenzofulvene by-product before proceeding to the next coupling step. To circumvent this problem, the T3P® coupling protocol has been applied to Fmoc chemistry using the LPPS approach, where peptide isolation is performed by precipitation to leave unwanted by-products in the mother liquors. As a proof of concept, to evaluate our methodology, we applied the standard conditions to the molecular hiving technology developed by Jitsubo and Bachem<sup>[255]</sup>, selecting a 2,5polycarbon-substituted hydrophobic benzyl alcohol (HBA) as tag<sup>[256]</sup>. The assembly of the oligopeptide involved a series of coupling reactions between N-Fmoc amino acids, and the growing peptide chain anchored to the chosen lipophilic tag. These reactions were carried out under previously optimised conditions and alternated with removal of the N-Fmoc protecting group using piperidine (Scheme 13). After each coupling step, the product was isolated by adding acetonitrile as a precipitating agent, followed by filtration of the anchored growing chain and additional washing with the same solvent. Initially, the LPPS protocol was carried out in dichloromethane (DCM) using two methods: (i) isolation of each intermediate peptide by precipitation after each coupling step, and (ii) precipitation of the peptide only after the piperidine-mediated deprotection step. Both methods achieved conversions greater than 99%.

Moreover, since the LPPS method recovers the growing peptide chain by filtration without any aqueous treatment, we considered replacing DCM with a more environmentally friendly solvent such as anisole. When the peptide sequence was synthesised using anisole, the final pentapeptide was obtained with a purity of 95.9% when purification was performed after each step, and a purity of 91.4% when precipitation was performed only after the deprotection step.

#### 3.1.3. Conclusion

In this investigation, the compatibility with *N*-Boc and *N*-Fmoc protecting groups and the suitability of different solvents were established by extending the scope of coupling to a small library of amino acids, including monomers with protection of the side chain functionalities and monomers with free active moieties in the backbone. The excellent results led to the application of this coupling reagent in the synthesis of a model pentapeptide via iterative SolPPS and LPPS. In the first approach, DCM was the best performing solvent and N-Boc-Leu-enkephalin methyl ester was isolated in excellent yield and purity. Although DCM is not a green solvent, the ability to avoid solvent evaporation at each step, while maintaining the original solution throughout the iterative sequences, is a great advantage in reducing the solvent volume and thus improving the sustainability of the process. On the other hand, the LPPS protocol produced the free Leu-enkephalin with a degree of purity comparable or even higher than those reported in the literature, both when the iterative peptide synthesis was performed in DCM and when the more sustainable anisole was used. We have shown that it is possible to carry out an iterative protocol, avoiding the isolation of intermediates and saving solvents, ensuring a simple protocol without the need for purification by chromatography. These aspects, together with the fast-coupling reactions of 10 minutes, make our approach very attractive for application on an industrial scale, where time and reagent savings and the availability of simple methods are required.

Finally, we have demonstrated that T3P® in combination with DIPEA is a useful coupling reagent in SoIPPS and LPPS and deserves to be reconsidered not only for single amide bond formation but also for an iterative protocol.

#### Published work:

The full version can be found in "A. Mattellone, D. Corbisiero, P. Cantelmi, G. Martelli, C. Palladino, A. Tolomelli, W. Cabri, *Molecules* **2023**, *28*, *7183*"

#### 3.1.4. Experimental Section

# 3.1.4.1. General Information and Analytical Methods

Unless otherwise stated, all materials, solvents, and reagents were obtained from commercial suppliers and used without further purification. High-performance liquid chromatography (HPLC) reagent-grade solvents were used. Specifically, *N*-fluorenylmethyloxycarbony (Fmoc), *N*-tert-butyloxycarbonyl (Boc) amino acids, and diisopropylethylenamine (DIPEA) were supplied by Iris Biotech, Merck, or Fluorochem. Ethyl Acetate (EtOAc), *N*,*N*-dimethylformamide (DMF), anisole, cyclopentylmethyl ether (CPME), dimethyl carbonate (DMC), *N*-octyl pyrrolidone (NOP), acetonitrile (ACN), tetrahydrofuran (THF), dichloromethane (DCM), propyl acetate (PrOAc),

tertbutyl acetate ('BuOAc), and HPLC-quality acetonitrile (ACN), hexane, and propan-2-ol ('PrOH) were purchased from Merck. Trifluoroacetic acid (TFA), triisopropyl silane (TIPS), and diisopropyl ether (DIPE)were supplied by Iris Biotech and Merck. All other chemicals were purchased from Merck and Fluorochem. Solvents and coupling reagents were individually injected into HPLC using the same analysis methods employed for the evaluation of reactions progress to establish their retention time. T3P® (50 wt. % in DCM) was supplied by Curia Global.

Thin-layer chromatography (TLC) was performed on precoated silica gel 60 F254 plates (Merck, Darmstadt, Germany), and spot detection was carried out using UV light and/or by charring with a ninhydrin solution or permanganate solution. HPLC-MS analyses were performed on an Agilent 1260 Infinity II system coupled to an ESI mass spectrometer (positive-ion mode, m/z = 100-3000 amu, fragmentor 30 V) with the following parameters: column Phenomenex Luna C18 5 µm, 250 x 4.6 mm; temperature: 35 °C; injection volume: 10 μL; UV: 220 nm; H<sub>2</sub>O + 0.08%TFA (mobile phase A) and ACN + 0.08%TFA (mobile phase B). ChemStation software (OpenLAB CDS ChemStation 35900 A/D driver, OpenLAB CDS ChemStation 490 Micro GC driver) was used for data processing. Percentage areas of integrated peaks are reported in mAu. The racemization analyses were performed using HPLC employing Daicel Chiralpack IC column. <sup>1</sup>H-NMR spectra were recorded with an INOVA 400 MHz instrument with a 5 mm probe and Bruker Avance 600 MHz. <sup>13</sup>C-NMR spectra were recorded at 101 MHz with an INOVA 400 MHz instrument and at 151 MHz with the Bruker Avance 600 MHz instrument. All chemical shifts were quoted relative to deuterated solvent signals. Chemical shifts (δ) were referenced to the corresponding solvent peaks and are reported in parts per million (ppm). Coupling constants (J) are given in Hertz. Multiplicities are abbreviated as: s (singlet), d (doublet), t (triplet), q (quartet), m (multiplet).

# 3.1.4.2. General procedure of coupling step for the solvent screening and substrate scope:

In an oven-dried Schlenk purged under a  $N_2$  atmosphere, N-Fmoc or N-Boc amino acid (0.125 mmol, 1.0 equiv) and  $H_2N$ -Leu-OMe or  $H_2N$ -Leu-OBn (0.125 mmol, 1.0 equiv) were dissolved in the desired solvent (1 mL, 0.125 M). DIPEA (0.5 mmol, 4 equiv) and  $T3P^{\$}$  (92  $\mu$ L, 50 wt. % in DCM; 0.188 mmol, 1.5 equiv) were then added at room temperature following this order. The solution was stirred at room temperature for 10 min, and the conversion was monitored by sampling the crude mixture and analysing it through HPLC-MS.

#### 3.1.4.3. Full SolPPS of Leu-Enkephalin via Boc chemistry

An oven-dried, double-neck, round-bottomed flask equipped with a stirring bar was

charged with *N*-Boc-Phe-OH (133 mg, 0.5 mmol, 1 equiv) and H-Leu-OMe hydrochloride (91 mg, 0.5 mmol, 1 equiv) in DCM (0.125 M) under a N2 atmosphere. Subsequently, DIPEA (353  $\mu$ L, 2 mmol, 4 equiv) and T3P® (50 wt. % in DCM, 365  $\mu$ L, 0.75 mmol, 1.5 equiv) were added following this order. The solution was stirred for 10 min, and the organic phase was washed once with H2O, HCl<sub>(aq)</sub> (0.01 M) and NaHCO<sub>3(aq)</sub> (0.01 M). The organic layer was dried over anhydrous Na2SO4 and was directly used in the next step, adding TFA (690  $\mu$ L, 9 mmol, 18 equiv). The solution was stirred for 2.5 h and then the organic solvent was washed twice with sat. NaHCO<sub>3(aq)</sub>. The resulting solution was dried over anhydrous Na2SO4 and directly used in further steps following the procedure mentioned above, increasing the equivalents of DIPEA and T3P® to 4 and 2 equiv, respectively. *N*-Boc-Tyr-Gly-Gly-Phe-Leu-OMe 7 was obtained as a white solid in 62% overall yield with 95% purity. Each step was monitored by HPLC-MS analysis.

# 3.1.4.4. General Procedure for the Synthesis of 2,5-Polycarbon Substituted Hydrophobic Benzyl Alcohols (HBA) Tag

An oven-dried, double-neck, 50 mL round-bottomed flask equipped with a stirring bar, 2,5-dihydroxybenzaldehyde (0.5 g, 3.6 mmol, 1 equiv), and K<sub>2</sub>CO<sub>3</sub> (3.9 g, 28.2 mmol, 7.8 equiv) was suspended in dry DMF (0.16 M), and the mixture was stirred at 110 °C. Subsequently, 1-bromodocosane (4.2 g, 10.9 mmol, 3 equiv) was added dropwise, and the mixture was stirred at the same temperature for 3 h, followed by dilution with water (22 mL). The aqueous layer was extracted with toluene (30 mL x3). The organic layer was dried over Na<sub>2</sub>SO<sub>4</sub> and concentrated in vacuo. The crude product was washed with acetonitrile at 60 °C (50 mL x3) to obtain 2,5-di(dococyloxy)benzaldehyde in 82% yield (2.1 g, 3 mmol).

 $^{1}$ H NMR (400 MHz, CDCl<sub>3</sub>)  $\delta$  (ppm): 10.47 (s, 1H), 7.31 (d, J = 3.2 Hz, 1H), 7.11 (dd, J = 9.1, 3.2 Hz, 1H), 6.92 (d, J = 9.1 Hz, 1H), 4.02 (t, J = 6.5 Hz, 2H), 3.94 (t, J = 6.6 Hz, 2H), 1.85–1.72 (m, 4H), 1.50–1.19 (m, 76H), 0.88 (t, J = 6.7 Hz, 6H).

<sup>13</sup>C NMR (101 MHz, CDCl<sub>3</sub>) δ (ppm): 189.91, 156.47, 153.18, 125.24, 124.27, 114.53, 110.97, 69.38, 68.84, 32.08, 29.86, 29.81, 29.75, 29.71, 29.54, 29.52, 29.38, 26.22, 26.15, 22.85, 22.14, 22.09, 14.27.

2,5-di(dococyloxy)benzaldehyde (2.1 g, 3 mmol, 1 equiv) was dissolved with THF (0.03 M) and 2-propanol (0.3 M), followed by the addition of NaBH<sub>4</sub> (0.2 g, 5.5 mmol, 2 equiv). The resulting reaction mixture was stirred at room temperature for 60 min, followed by dilution with brine (55 mL). The aqueous layer was extracted with THF (25 x 3 mL), dried over Na<sub>2</sub>SO<sub>4</sub>, and concentrated in vacuo. The crude product was washed with MeOH (100 mL) to obtain (2,5-bis(docosyloxy)phenyl)methanol in 97% yield (2.2 g, 2.9 mmol).

<sup>1</sup>H NMR (400 MHz, CDCl<sub>3</sub>)  $\delta$  (ppm): 6.85 (s, 1H), 6.79–6.74 (m, 2H), 4.65 (s, 2H), 3.95 (t, J = 6.6 Hz, 2H), 3.90 (t, J = 6.6 Hz, 2H), 1.76 (hept, J = 7.4 Hz, 4H), 1.48–1.11 (m, 76H), 0.88 (t, J = 6.5 Hz, 6H).

<sup>13</sup>C NMR (101 MHz, CDCl<sub>3</sub>) δ 153.19, 151.11, 130.32, 115.57, 113.96, 112.27, 68.81, 68.74, 62.62, 32.09, 29.86, 29.82, 29.77, 29.57, 29.52, 26.33, 26.21, 22.85, 14.28.

# 3.1.4.5. Full LPPS of Leu-Enkephaline via Fmoc Chemistry

Loading of the First Amino Acid on the Tag: Synthesis of H2N-Leu-Tag

To a solution of (2,5-bis(docosyloxy)phenyl)methanol (500 mg, 0.66 mmol, 1 equiv) in DCM (100 g/L), N-Fmoc-Leu-OH (582 mg, 1.7 mmol, 2.5 equiv), DIC (128  $\mu$ L, 0.8 mmol, 1.25 equiv), and DMAP (8 mg, 0.07 mmol, 0.1 equiv) were added. The resulting reaction mixture was stirred at room temperature for 1 h and was monitored using TLC (Hex:EtOAC 9:1; Rf = 0.5), followed by dilution with ACN (10 mL). The resulting precipitate was recovered by vacuum filtration and washed with ACN (5 mL x3) to obtain the N-Fmoc-Leu-Tag in 94% yield (680 mg, 0.62 mmol).

 $^{1}$ H NMR (400 MHz, CDCl<sub>3</sub>)  $\delta$  (ppm): 7.83–7.64 (m, 6H), 7.60 (d, J = 7.4 Hz, 2H), 7.40 (t, J = 7.4 Hz, 2H), 7.31 (t, J = 7.5 Hz, 2H), 6.89 (s, 1H), 6.78 (s, 2H), 5.22 (d, J = 34.5 Hz, 2H, NH), 4.51–4.34 (m, 3H), 4.23 (t, J = 7.2 Hz, 1H), 3.94–3.82 (m, 4H), 1.81–1.66 (m, 6H), 1.43–1.16 (m, 77H), 0.96–0.88 (m, 12H).

<sup>13</sup>C NMR (101 MHz, CDCl<sub>3</sub>) δ (ppm): 173.14, 156.06, 153.01, 151.15, 144.12, 143.89, 141.43, 127.79, 127.18, 125.26, 125.22, 124.88, 120.07, 120.06, 116.17, 115.05, 112.70, 69.01, 68.77, 67.11, 62.81, 52.79, 47.35, 42.09, 32.07, 29.85, 29.81, 29.77, 29.74, 29.58, 29.53, 29.51, 26.22, 26.20, 24.87, 23.00, 22.83, 22.05, 14.25.

N-Fmoc-Leu-Tag (680 mg, 0.62 mmol, 1 equiv) was solubilized with DCM or anisole (100 g/L), and piperidine (1 mL, 10.6 mmol, 16 equiv) was added. After 30 min, the reaction was monitored by TLC (Hex:EtOAC 9:1; Rf = 0.2), and the solution was diluted with ACN (10 mL). The resulting precipitates were recovered through vacuum filtration and washed with ACN (5 mL x 3) to obtain the  $H_2N$ -Leu-Tag in 99% yield (524 mg, 0.61 mmol).

 $^{1}$ H NMR (600 MHz, CDCl<sub>3</sub>)  $\delta$  (ppm): 6.88 (s, 1H), 6.81–6.74 (m, 2H), 5.17 (s, 2H), 3.92–3.88 (m, 4H), 3.51 (dd, J = 5.8, 2.7 Hz, 1H), 1.82–1.72 (m, 6H), 1.62–1.58 (m, 2H), 1.47–1.41 (m, 6H), 1.35–1.25 (m, 69H), 0.94–0.87 (m, 12H).

<sup>13</sup>C NMR (151 MHz, CDCl<sub>3</sub>) δ (ppm): 176.78, 153.01, 151.23, 125.39, 116.29, 114.84, 112.76, 69.06, 68.83, 68.76, 62.27, 53.15, 44.20, 32.08, 29.86, 29.83, 29.81, 29.77, 29.75, 29.58, 29.56, 29.54, 29.52, 26.24, 26.22, 24.91, 23.15, 22.85, 22.04, 14.27.

Elongation of the Peptide: Protocol with Precipitation after Each Step

H<sub>2</sub>N-Leu-tag was dissolved with DCM or anisole (100 g/L), and N-Fmoc-Phe-OH (1 equiv) was added, followed by the addition of DIPEA (4 equvi) and T3P® (50% in DCM; 1.5 equvi) in this order. After 5 min, the reaction was monitored through TLC (Hex:EtOAC 8:2; Rf = 0.5), and the solution was diluted with ACN (10 mL). The resulting precipitates were recovered through vacuum filtration and washed with ACN (5 mL x 3), enabling the *N*-Fmoc-Phe-Leu-Tag in 91–98% yield as a white solid.

<sup>1</sup>H NMR (400 MHz, CDCl<sub>3</sub>) δ (ppm): 7.76 (d, J = 7.6 Hz, 2H), 7.56–7.53 (m, 2H), 7.40 (t, J = 7.4 Hz, 2H), 7.31 (t, J = 7.4 Hz, 2H), 7.27–7.17 (m, 5H), 6.86 (s, 1H), 6.82–6.76 (m, 2H), 6.11 (s, NH), 5.35 (s, NH), 5.17 (s, 2H), 4.63–4.58 (m, 1H), 4.46–4.41 (m, 2H), 4.33–4.29 (m, 1H), 4.19 (t, J = 6.9 Hz, 2H), 3.92–3.87 (m, 4H), 3.11 (s, 1H), 3.03 (s, 1H), 1.79–1.11 (m, 83H), 0.90–0.85 (m, 12H). 13C NMR (101 MHz CDCl<sub>3</sub>) \_ (ppm): 172.31, 170.44, 153.00, 151.11, 143.91, 143.84, 141.43, 129.54, 128.83, 127.87, 127.22, 125.16, 124.79, 120.11, 116.23, 115.00, 112.66, 77.48, 77.16, 76.84, 69.00, 68.79, 67.21, 62.78, 47.26, 41.80, 32.08, 29.86, 29.81, 29.79, 29.76, 29.60, 29.52, 26.22, 24.84, 22.85, 22.21, 22.19, 22.17, 22.16, 22.14, 14.28.

N-Fmoc-Phe-Leu-Tag was solubilized in DCM or anisole (100 g/L), and piperidine (16 equiv) was added. The solution was stirred for 30 min (TLC: Hex:EtOAC 8:2; Rf = 0.2), followed by dilution with ACN (10 mL). The resulting precipitates were recovered by vacuum filtration and washed with ACN (10 mL x 3) to obtain the H-Phe-Leu-Tag in 98–99% yield.

 $^{1}$ H NMR (600 MHz, CDCl<sub>3</sub>)  $\delta$  (ppm): 7.70 (d, J = 8.5 Hz, NH), 7.33–7.29 (m, 2H), 7.25–7.21 (m, 2H), 6.89–6.86 (m, 1H), 6.81–6.76 (m, 2H), 5.18 (dd, J = 17.1, 12.4 Hz, 2H), 4.72–4.64 (m, 1H), 3.90 (q, J = 6.6 Hz, 4H), 3.65 (dd, J = 9.2, 4.0 Hz, 1H), 3.25 (dd, J = 13.7, 4.0 Hz, 1H), 2.73 (dd, J = 13.7, 9.2 Hz, 1H), 1.78–1.70 (m, 4H), 1.63–1.53 (m, 3H), 1.46–1.39 (m, 4H), 1.35–1.26 (m, 72H), 0.94–0.86 (m, 12H).

<sup>13</sup>C NMR (151 MHz, CDCl3) \_ (ppm): 174.11, 172.98, 153.22, 153.04, 151.12, 151.08, 137.91, 129.48, 128.84, 126.98, 125.14, 116.03, 114.88, 112.70, 69.06, 68.82, 68.76, 62.62, 62.58, 56.51, 50.66, 41.76, 40.99, 32.08, 29.86, 29.81, 29.78, 29.76, 29.60, 29.56, 29.54, 29.51, 26.32, 26.22, 26.20, 24.99, 23.03, 22.84, 22.12, 14.27.

The above procedure was repeated until H<sub>2</sub>N-Tyr(tBu)-Gly-Gly-Phe-Leu-tag was obtained.

Elongation of the Peptide: Protocol with One-Pot Coupling-Deprotection Steps

H<sub>2</sub>N-Leu-tag was dissolved with DCM or anisole (100 g/L), and N-Fmoc-Phe-OH (1 equiv) was added, followed by the addition of DIPEA (3 equiv) and T3P® (50% in DCM; 1.5 equiv) in this order. After 5 min, the reaction was completed, and piperidine (16 equiv) was added. The solution was stirred for 30 min followed by dilution with ACN (10 mL). The resulting precipitates were recovered through vacuum filtration and

washed with ACN (10 mL x 3) to obtain the *N*-Fmoc-Leu-Tag in 98–99% yield. The above procedure was repeated until  $H_2N$ -Tyr(tBu)-Gly-Gly-Phe-Leu-tag was obtained.

N-Fmoc-Gly-Gly-Phe-Leu-OTag (y = 89–94%): TLC Hex:EtOAc (1:1) Rf = 0.2.

 $^{1}$ H NMR (600 MHz, CDCl<sub>3</sub>) δ (ppm): 7.74 (d, J = 7.6 Hz, 2H), 7.60–7.57 (m, 2H), 7.38 (t, J = 7.5 Hz, 2H), 7.30–7.27 (m, 2H), 7.23–7.14 (m, 5H), 6.86 (s, 1H), 6.79–6.72 (m, 2H, NH), 5.63 (bs, NH), 5.15 (dd, J = 25.7, 12.7 Hz, 2H), 4.80 (bs, NH), 4.61–4.58 (m, 1H), 4.47–4.39 (m, 2H), 4.21–4.19 (m, 1H), 3.98–3.73 (m, 8H), 3.10–3.01 (m, 2H), 1.80–1.48 (m, 10H), 1.43–1.25 (m, 73H), 0.92–0.82 (m, 12H).

<sup>13</sup>C NMR (151 MHz, CDCl<sub>3</sub>) δ (ppm): 172.49, 170.44, 169.53, 168.33, 156.84, 153.00, 151.12, 151.09, 143.88, 143.80, 141.47, 136.39, 129.49, 128.74, 128.71, 127.89, 127.23, 127.16, 125.17, 124.89, 120.14, 116.26, 115.59, 114.92, 114.03, 113.98, 112.67, 112.30, 69.02, 68.83, 68.76, 67.38, 62.72, 62.60, 54.45, 51.24, 47.26, 44.54, 43.22, 41.61, 38.63, 38.52, 32.08, 29.86, 29.81, 29.76, 29.61, 29.57, 29.54, 29.51, 26.32, 26.21, 26.20, 24.88, 22.84, 22.13, 14.27.

## $H_2N$ -Gly-Phe-Leu-OTag (y= 92–94%): TLC Hexane: EtOAc (2:8) Rf = 0.2.

 $^{1}$ H NMR (400 MHz, 20%MeOD in CDCl<sub>3</sub>) δ (ppm): 7.09–6.99 (m, 5H), 6.77–6.63 (m, 3H), 5.03–4.94 (m, 2H), 4.48–4.45 (m, 1H), 4.38–4.35 (m, 1H), 3.82–3.62 (m, 6H), 3.51 (s, 2H), 2.95–2.91 m, 1H), 2.74 (dd, J = 13.6, 8.1 Hz, 1H), 1.69–1.38 (m, 10H), 1.36–1.04 (m, 83H), 0.75–0.65 (m, 12H).

<sup>13</sup>C NMR (151 MHz, 20%MeOD in CDCl<sub>3</sub>) δ (ppm): 172.30, 171.06, 168.82, 152.60, 150.77, 136.31, 129.00, 128.17, 126.57, 124.50, 115.99, 114.56, 112.37, 68.70, 68.52, 62.32, 60.38, 54.09, 50.77, 42.21, 40.77, 37.79, 31.67, 29.45, 29.36, 29.17, 29.11, 25.79, 24.47, 22.42, 22.37, 21.48, 13.77.

*N-Fmoc-Tyr-Gly-Gly-Phe-Leu-OTag* (y = 75–80%): TLC Hexane:EtOAc (3:7) Rf = 0.5.  $^{1}$ H NMR (400 MHz, 20%MeOD in CDCl<sub>3</sub>) δ (ppm): 7.84 (s, NH), 7.58–7.52 (m, 2H, NH), 7.46 (s, NH), 7.39–7.31 (m, 2H, NH), 7.20 (t, J = 7.4 Hz, 2H), 7.11 (t, J = 7.5 Hz, 2H), 7.05–6.98 (m, 5H), 6.92 (d, J = 8.0 Hz, 2H), 6.71–6.68 (m, 3H), 6.60 (s, 2H), 6.52 (d, J = 7.2 Hz, NH), 4.96 (q, J = 12.4 Hz, 2H), 4.47–4.35 (m, 2H), 4.19–4.13 (m, 3H), 3.96 (t, J = 7.0 Hz, 1H), 3.73–3.50 (m, 8H), 2.93 (dd, J = 14.1, 6.2 Hz, 2H), 2.79–2.71 (m, 2H), 1.59–1.36 (m, 8H), 1.25–1.07 (m, 84H), 0.71–0.66 (m, 12H).

<sup>13</sup>C NMR (151 MHz, 20%MeOD in CDCl<sub>3</sub>) δ (ppm): 172.76, 172.39,171.13, 169.95, 169.35, 156.76, 154.04, 152.76, 150.94, 143.64, 141.21, 136.43, 131.48, 129.64, 129.37, 129.20, 128.35, 127.68, 127.05, 126.75, 124.95, 124.72, 124.22, 119.87, 116.11, 114.77, 112.58, 78.67, 68.88, 68.70, 67.03, 62.46, 60.88, 56.57, 54.25, 50.99, 46.99, 42.77, 42.39, 40.90, 37.85, 37.09, 31.84, 29.61, 29.52, 29.35, 29.28, 28.59, 25.95, 24.60, 22.59, 22.54, 21.65, 13.94.

 $H_2N$ -Tyr-Gly-Phe-Leu-OTag (y = 90–96%): TLC Hexane: EtOAc (1:9) Rf = 0.2.

 $^{1}$ H NMR (400 MHz, CDCl<sub>3</sub>)  $\delta$  8.08 (s, NH), 7.37 (s, NH), 7.26–7.17 (m, 5H), 7.08 (d, J = 8.3 Hz, 2H), 6.97–6.86 (m, 3H, 2NH), 6.77 (s, 2H), 5.16 (dd, J = 22.3, 12.8 Hz, 2H), 4.76 (q, J = 7.0 Hz, 1H), 4.53 (s, 1H), 4.01–3.67 (m, 9H), 3.19–3.03 (m, 3H), 2.74–2.68 (m, 1H), 1.77–1.52 (m, 8H), 1.41–1.16 (m, 84H), 0.89–0.86 (m, 12H).

<sup>13</sup>C NMR (151 MHz, CDCl<sub>3</sub>) δ 172.49, 171.00, 169.69, 168.93, 154.51, 153.01, 151.05, 136.70, 129.83, 129.52, 128.65, 127.03, 124.92, 124.48, 116.21, 114.85, 112.66, 78.55, 69.01, 68.81, 62.67, 56.29, 54.66, 51.32, 44.43, 43.57, 43.08, 41.42, 38.42, 32.06, 29.84, 29.75, 29.60, 29.50, 28.97, 26.20, 26.18, 24.84, 22.87, 22.82, 14.25.

## Peptide Cleavage from the Tag

In an oven-dried Schlenk tube, the fully protected peptide-tag was dissolved in a cleavage cocktail (200 g/mL) composed of: 95.0% TFA, 2.5% H<sub>2</sub>O, and 2.5% TIS. The reaction mixture was stirred at room temperature for 2 h under a nitrogen atmosphere, and then DIPE ( $V_{\text{DIPE}} = 8V_{\text{TFA}}$ ) was added dropwise, inducing the formation of a white solid. After the complete addition of the solvent, the reaction mixture was cooled to 0 °C and slowly stirred for 30 min. Subsequently, the white solid was recovered by filtration. The purity of the target peptide was monitored through HPLC-MS analysis.

# 3.2. Synthesis of bioactive peptide products

#### 3.2.1. Introduction

Antibiotics have fundamentally changed the global management of infectious diseases since their discovery. They are recognised as one of the factors contributing to the increase in life expectancy in the 20th century due to the decline in mortality from infectious diseases[257]. However, widespread overuse and inappropriate use in both human and veterinary medicine and animal husbandry, have contributed significantly to the current global crisis of antibiotic resistance. This has led to an increase in resistant pathogens such as Vancomycin-resistant Enterococcus (VRE) and Methicillin-resistant Staphylococcus aureus (MRSA), exacerbated by the slow rate of new drug development[258]. As a direct consequence of the current panorama, few drugs are available in the pharmacopoeia, with the majority of antibiotics belonging to only a few chemical families (e.g. penicillins, carbapenems, cephalosporins) with similar mechanisms of action and spectra of activity. As a result, infectious diseases are a major threat to global public health, and it is estimated that microorganism infections could cause up to 10 million deaths worldwide by 2050. In recent years, the World Health Organisation (WHO) and other non-governmental organisations have called for a reversal of this situation and medicinal chemistry is challenged to identify valid alternatives to antibiotics[259].

In this context, antimicrobial peptides (AMPs) have attracted considerable interest from the scientific community. AMPs are a class of small peptides that are naturally abundant in various life forms, including mammals (a large proportion of which are human host defence peptides), amphibians, microorganisms and insects. A significant number of antimicrobial peptides have been identified for their efficacy against various types of infection, including antibacterial, antifungal, antiviral and anticancer activities. However, only a limited number of AMPs have received the FDA approval for clinical use due to their exceptionally short half-lives. Indeed, they are typically limited to intravenous use, topical treatments or, in special cases, oral administration in the form of very small tablets or capsules<sup>[260]</sup>.

AMPs are typically short chains of < 50 amino acids and the majority are cationic. They kill bacteria by disrupting their membranes (Figure 124) and/or by translocating across membranes into the cytoplasm to act on intracellular targets such as DNA, RNA and protein synthesis<sup>[261]</sup>. However, despite the existence of over 2000 naturally occurring or synthetically designed AMPs, their diverse lengths, sequences and three-dimensional structures make it difficult to correlate structure with antimicrobial activity<sup>[262]</sup>.

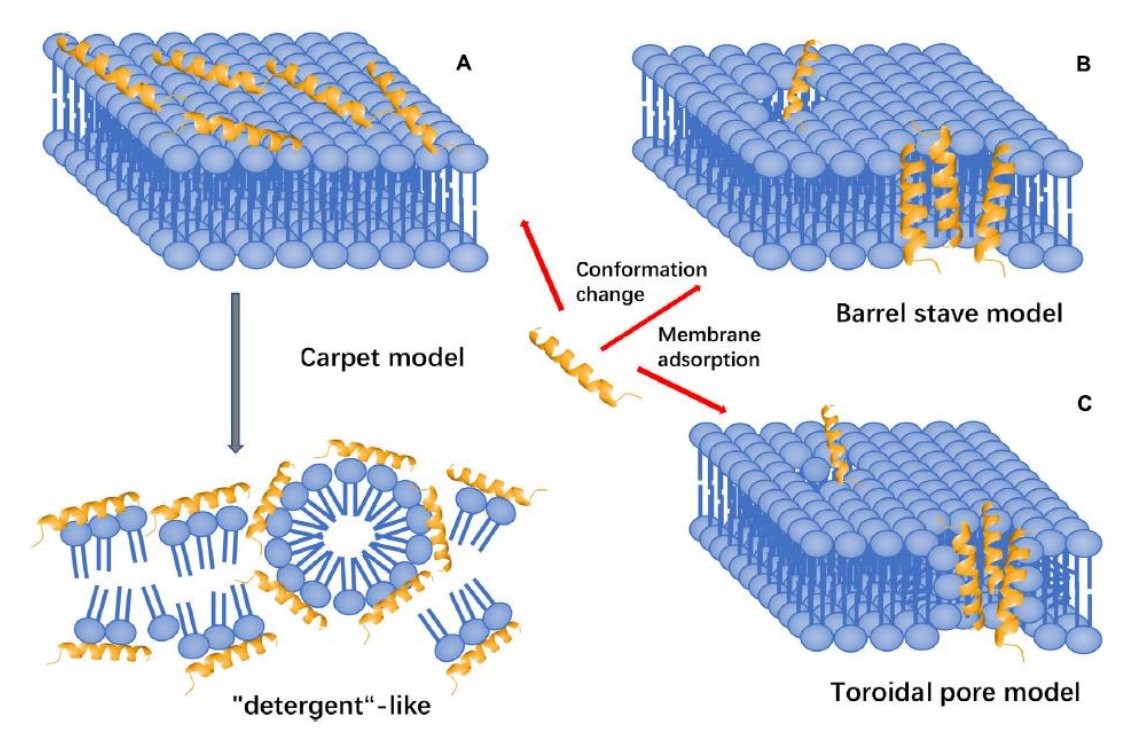


Figure 124. Antimicrobial peptide action mechanism through membrane targeting interactions (image taken from the literature<sup>[263]</sup>).

Electrostatic interactions between cationic AMPs and the negatively charged bacterial surface are key factors in determining their ability to interact with the membrane<sup>[264]</sup>. Bacteria are broadly classified into two groups, Gram-positive and Gram-

negative, based on differences in their cell envelope structures. The cytoplasmic membranes of both Gram-positive and Gram-negative bacteria are rich in negatively charged phospholipids, such as phosphatidylglycerol, cardiolipin phosphatidylserine, which attract positively charged AMPs (Figure 125). In addition, the presence of teichoic acids in the cell wall of Gram-positive bacteria and lipopolysaccharides (LPS) in the outer membrane of Gram-negative bacteria make them more electronegatively charged<sup>[265]</sup>. When AMPs come into contact with the cytoplasmic membrane, they adopt an amphipathic secondary structure (if not already formed) to facilitate the interaction. The charged regions interact with the hydrophilic head groups of the phospholipids, while the hydrophobic domains bind to the core of the lipid bilayer. AMPs have selective antibacterial activity because mammalian cell membranes are neutral, consisting mainly of zwitterionic phospholipids, making them less attractive to AMPs.

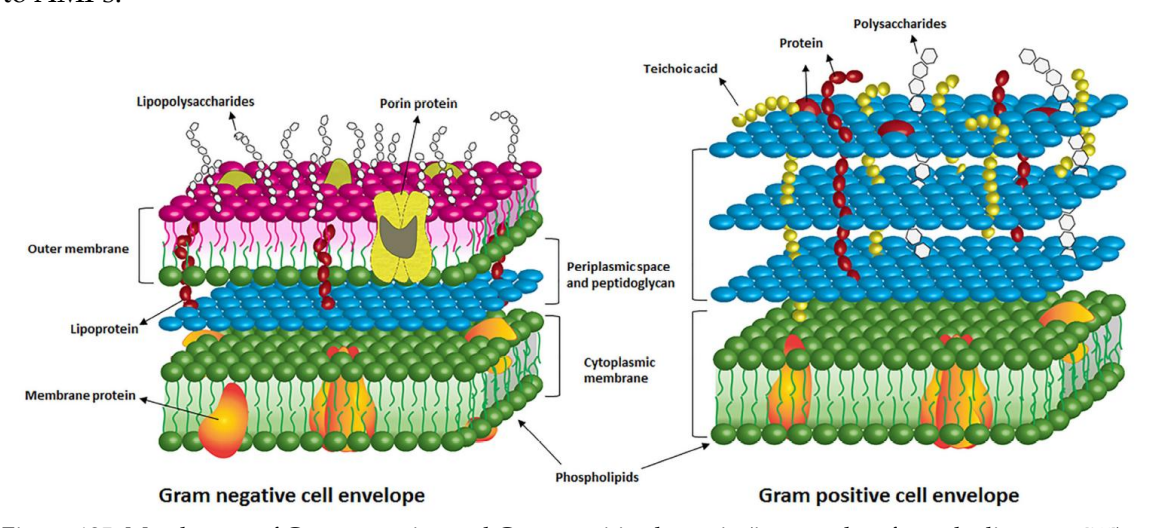


Figure 125. Membranes of Gram-negative and Gram-positive bacteria (image taken from the literature [266]).

Antibiotics may also have a detrimental effect on the gut microbiota, as their overuse appears to contribute to the development of several associated disorders<sup>[267]</sup>. Bacteria are the predominant components of the human gut microbiota, comprising over 1,000 species, the majority of which are anaerobic. The total population of these bacteria is estimated to exceed 10<sup>14</sup> cells<sup>[268]</sup>.

Most antibiotics on the market are broad-spectrum, affecting not only harmful bacteria but also beneficial ones. Disruption of the gut microbiota is the primary, but not the only consequence of antibiotic use in the gut. Other mechanisms include the direct damaging effects of antibiotics on gastrointestinal (GI) epithelial cells and the proliferation of antibiotic-resistant microorganisms. For example, clindamycin is a major risk factor for the development of *Clostridium difficile infection* (CDI), which is probably the most prominent clinical example of antibiotic-associated dysbiosis, particularly in older people. In recent years, the prevalence of CDI has risen sharply, particularly in

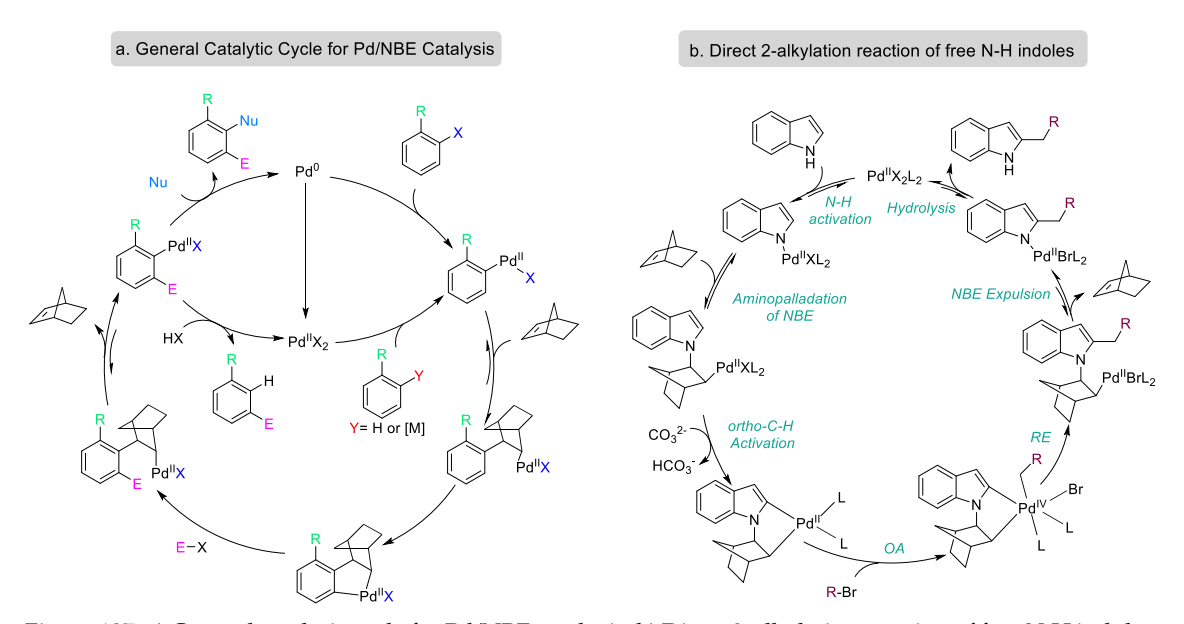
western countries[269], and it has become the leading cause of infectious diarrhoea in hospitalised patients and a major economic and public health challenge<sup>[270]</sup>. The use of βlactam antibiotic combinations, such as ampicillin and cephalosporins, has been shown to reduce the abundance of Firmicutes (mainly Lactobacilli), while promoting an increase in Bacteroidetes and Proteobacteria (particularly Enterobacteriaceae, which are often resistant to β-lactam antibiotics) and reduced microbial richness. Similarly, fluoroquinolone antibiotics have variable effects on the gut microbiota. Ciprofloxacin primarily targets Gram-negative facultative anaerobes, whereas levofloxacin also reduces populations of Gram-positive anaerobes, including beneficial bifidobacteria<sup>[267]</sup>. However, some antibiotics can also have a beneficial effect on the gut microbiota, providing a so-called 'eubiotic' effect by stimulating the growth of beneficial bacteria. For example, rifaximin (marketed as Normix® by Alfasigma) is used to treat acute and chronic intestinal infections caused by Gram-positive and Gram-negative bacteria, diarrhoeal syndromes, and pre- and post-operative prophylaxis of infectious complications in gastrointestinal surgery. Brilacidin is also being investigated for the treatment of bowel diseases, and in 2019 Innovation Pharmaceuticals announced a licensing agreement with Alfasigma S.p.A. for the development and commercialisation of brilacidin in ulcerative proctitis and ulcerative proctosigmoiditis<sup>[271]</sup>.

In this scenario, our goal was to develop an antimicrobial peptide capable of selectively targeting pathogenic bacteria and preserving the bacterial flora.

The ideal AMP should have the following characteristics: (i) high antimicrobial activity; (ii) low toxicity to mammalian membranes; (iii) short sequence to ensure higher protease stability<sup>[272]</sup> and low cost production<sup>[273]</sup>. To develop a bioactive molecule capable of discriminating pathogenic bacteria from bifidobacterial cells, we decided to modulate the lipophilic-hydrophilic balance of a short and active AMP, to generate small library of potential antimicrobial peptides with different activity and selectivity. As scaffold, we selected LTX-109, developed by Lytix Biopharma L.t.d., which is a broad-spectrum, fastacting bactericidal antimicrobial which has completed phase II trials for the treatment of impetigo in the year 2014 and uncomplicated skin and skin structure infection (uSSSI) in the year 2011[274]. LTX-109 is a synthetic tripeptide consisting of two arginines (positions 1 and 3) and a 2,5,7-triterbutilated tryptophan (Tbt), with the -COOH terminus capped by phenethylamine (Figure 126). Tryptophan (Trp), as a non-polar amino acid, is a common amino acid in AMP due to its critical role in interacting with the lipid bilayer. It has been shown that replacing Trp with Tbt increases antimicrobial activity<sup>[275]</sup>. Arginine (Arg), which is protonated at physiological pH, is essential to ensure the net positive charge of the peptide and to favour the binding between the AMP and the bacterial cytoplasmic membrane<sup>[276]</sup>.

Figure 126. LTX-109 structure

With the aim of generating a small library of novel tripeptides and investigating both their antimicrobial activity and metabolic stability, we focused on the modification of tryptophan residues at the C2 and C5 positions of the indole ring. We used palladium-catalysed reactions: the Catellani reaction for modification at the C2 position and the Sonogashira-Hagihara reaction for the C5 position. The Catellani reaction, discovered by Catellani and co-workers in 1997<sup>[277]</sup>, is a palladium-catalysed carbon-hydrogen (C-H) bond activation based on the Pd(II)-Pd(IV) catalytic cycle, where the directing group is the norbornene (NBE) which acts as a co-catalyst. It is multi-component tandem reaction involving an aryl halide, an electrophilic reagent and a terminating group (Figure 127a). In 2011, Bach and co-workers<sup>[278,279]</sup> reported the Pd/NBE catalysed direct 2-alkylation reaction of free *N*-H indoles and in 2013 they investigated the same reactivity on *N*-Boc protected tryptophan ester<sup>[280]</sup> (Figure 127b). Based on these studies, we selected the Pd/NBE catalysed reaction as the method of choice for the tryptophan functionalisation.



Figure~127.~a)~General~catalytic~cycle~for~Pd/NBE~catalysis.~b)~Direct~2-alkylation~reaction~of~free~N-H~indoles.

#### 3.2.2. Results and Discussion

The tripeptides were modified at the tryptophan residue by the addition of long and short alkyne chains and aromatic groups in order to modulate the lipophilic-hydrophilic balance and study the effect on the selectivity against pathogenic and beneficial bacteria.

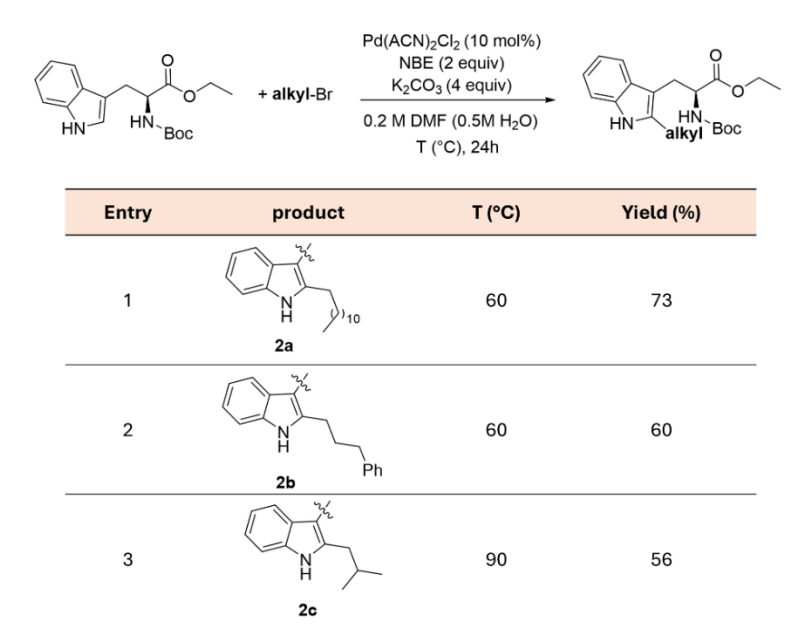
To synthesise the tripeptides with modifications at C2 and at C5 positions, the general procedures shown in Scheme 14 and Scheme 15, respectively, were followed. The synthetic scheme consists of a convergent strategy: (*i*) synthesis of modified Trp protected as ester; (*ii*) SolPPS of dipeptide (**5a-c** and **12a-b**) using T3P® and DIPEA as protocol for the coupling step; (*iii*) SolPPS of Fmoc-Arg(PBF)-OH and phenylethylamine to give intermediate **16**, after Fmoc removal; (*iv*) final coupling in SolPPS using T3P®/DIPEA and removal of the final protecting groups to give the products **7a-c** and **14a-b**.

Scheme 14. General scheme for the synthesis of compounds with modification at C2 position of Trp (7a-c).

Scheme 15. General scheme for the synthesis of compounds with modification at C5 position of Trp 14a-b.

For the synthesis of compounds **2a-c**, we took advantage of the studies of Bach and co-workers<sup>[278,280]</sup>. The Catellani reactions were carried out using PdCl<sub>2</sub>(ACN)<sub>2</sub> (10 mol%) as pre-catalyst, norbornene and K<sub>2</sub>CO<sub>3</sub> as base. The reactions were carried out in DMF, with a water concentration of 0.5 M, at 60°C (**2a** and **2b**) and 90°C for the most difficult substrate (**2c**). Indeed, according to the literature<sup>[278]</sup>, the reaction is sensitive to steric hindrance of the alkyl group for the reaction using an alkyl bromide with a secondary carbon atom adjacent to the bromide methylene group and higher temperatures are required (Table 41).

Table 41. Alkylation of Boc-NH-Trp-OEt with alkyl bromides.



To synthesise compounds **7a-b**, we started with commercially available 5-hydroxytryptophan. We first protected the amine group to avoid coordination to palladium in the Sonogashira-Hagihara reaction and then we introduced the triflate group, which acts as a leaving group (Scheme 16). We obtained a complete transformation for the synthesis of both **9a-b**.

HCI

Scheme 16. Reaction scheme of functionalization in position C5.

The biological tests were carried out in vitro by a group of biologists collaborating with the research team. The antimicrobial activities of the synthesised compounds (7a-c and 14a-b) against pathogenic and beneficial bacteria were compared with rifaximin, brilacidin (see Paragraph 3.2.1) and LTX-109 (see Table 42). The best candidate antimicrobial peptide, capable of acting selectively against Gram +/Gram - bacteria and not altering Bifidum bacteria, should have a low minimum inhibitory concentration (MIC) against the pathogen and a high MIC against the beneficial bacteria. Among the tripeptides tested, 7a (entry 4, Table 42) shown the best behaviour with a MIC = 6.25 μL/mL against S. aureus (Gram +), MIC=12.5 μL/mL against P. aeruginosa (Gram -) and MIC =  $500 \mu L/mL$  against beneficial bacteria. In contrast, 14b (entry 8, Table 42) was the worst candidate for selectivity as it has high activity against the bifidobacteria tested. Therefore, these results show that a long alkyl chain at the C2 position is beneficial to increase selectivity, whereas a long alkyl chain at the C5 position makes the tripeptide more active against beneficial bacteria.

Building on these results, we investigated the late-stage functionalisation of tryptophan. Our aim was to create a larger library of tripeptides with tryptophan modified at the C2 position to understand which type of functional group was best for our target.

		Pathogen						Beneficial												
					. aeruginosa (ATCC 27853) Gram -		Esterichia Coli (ATCC 8739)		B. longum subsp.longum (B 2356)		B. Bifidum (B 7313)		B.breve BBR8 (LMG P-17501)		B. animalis subsp.lactis (Bi1 LMG P-17502)				Lactiplantibacill us plantarum (CAB_B2)	
entry	specie	MIC range (μg/mL)	IC50 (μg/mL)	MIC range (μg/mL)	IC50 (µg/mL)	MIC (ug/ml)	MBC (μg/mL)	MIC (μg/mL)	MBC (μg/mL)	MIC (μg/mL)	MBC (μg/mL)	MIC (μg/mL)	MBC (μg/mL)	MIC (μg/mL)	MBC (μg/mL)	MIC (μg/mL)	MBC (μg/mL)	MIC (μg/mL)	MBC (μg/mL)	
1	Rifaximin	<0.0015		5.25	3.112															
2	Brilacidin	1.56	0.9135	1.56/3.125	1.544															
3	LTX-109	1.56-3.125	1.408	3.125-6.25	2.256	50	50	50	50	5	50	50	50	50	50	5	50	50	50	
4	7a	6.25	2.094	12.5	10.46	50	50	500	500	500	500	500	500	500	500	500	500	500	500	
5	7b	12.5	7.053	12.5	4.999	500	500	50	50	50	50	50	50	50	500	500	500	500	500	
6	7c	25	14.97	25	12.69	500	5000	500	500	500	500	500	500	500	500	500	500	500	500	
7	14a	6.25	3.345	12.5	6.600	500	>500	50	50	50	50	50	50	50	50	50	50	50	500	
8	14b	3.125-6.25	1.036	25	19.15	500	500	50	50	2.5	2.5	5	5	50	500	50	50	50	50	

Table 42. Biological data of 7a-c and 14a-b tested against pathogenic and beneficial bacteria<sup>a</sup>.

Metal-mediated direct C–H bond functionalisation has emerged as a viable alternative to classical cross-coupling methods, as they partially or completely eliminate, the need for substrate pre-functionalisation, which can lead to unwanted byproduct formation and lengthy synthetic operations. Particularly, tryptophan has received much attention because of its higher reactivity due to the indole ring. In 2010, Lavilla and Albericio<sup>[281]</sup> described the C2 arylation of tryptophan-containing peptides in aqueous medium using Pd(OAc)<sub>2</sub>, AgBF<sub>4</sub> to remove the iodide from the palladium AO-complex and *ortho*-nitrobenzoic acid to promote the reaction<sup>[282]</sup> (Figure 128a). In 2014 Fairlamb and co-workers reported the use of aryl boronic acid<sup>[283]</sup> and in 2015 of hypervalent aryl iodine reagents ([Ar<sub>2</sub>I]X)<sup>[284]</sup> as arylating agents. In the same period, Ackermann's group developed a metal-free strategy by using (Ar<sub>2</sub>I)OTs (Figure 128b-c). More recently they developed ruthenium (II)-catalysed C-H arylation using K<sub>3</sub>PO<sub>4</sub> as base and F<sub>5</sub>C<sub>6</sub>CO<sub>2</sub>H to ensure an efficient carboxylate-assisted C-H activation<sup>[285]</sup>, by avoiding the use of highly reactive hypervalent iodine reagents and costly silver salts (Figure 128d-e).

<sup>&</sup>lt;sup>a</sup> Experiments were carried out following the EUCAST protocol. (IC50= Half-maximal inhibitory concentration), (MBC= Minimum Bactericidal Concentration).

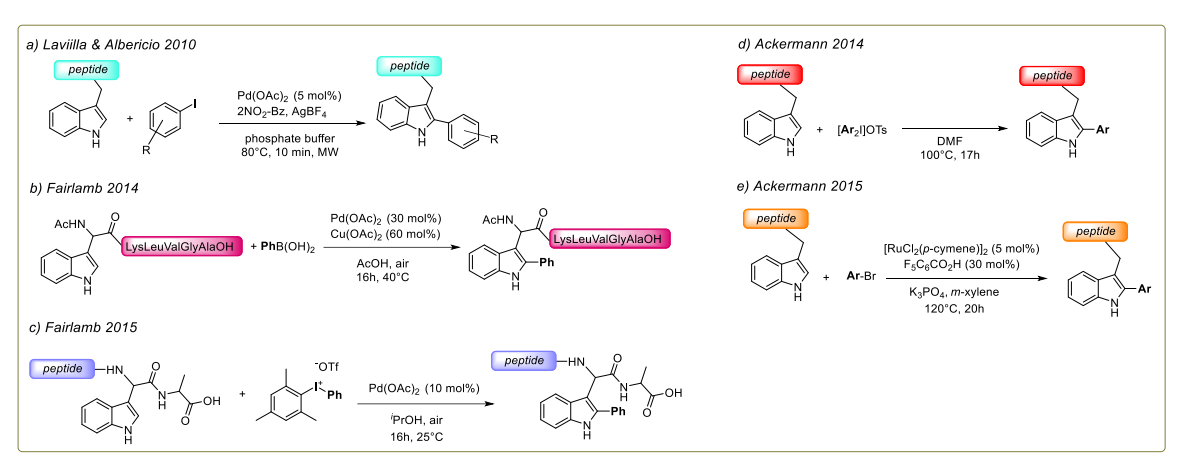


Figure 128. Key examples of C-H functionalisation of tryptophan-containing peptides.

However, late-stage modification of tryptophan-containing peptides still remains challenging. In this context, our aim was twofold: (*i*) to explore for the first time the Pd/NBE catalysed C-H activation on peptides bearing Trp, (*ii*) to rapidly expand our library of H<sub>2</sub>N-Arg-Trp-Arg-NH(CH<sub>2</sub>)<sub>2</sub>Ph modified at the C2 position.

To pursue our goal, we started our study by functionalising Boc-NH-Trp-Leu-O¹Bu in order to have a simple and non-sterically hindered dipeptide as a starting point. First, we carried out the Pd/NBE catalysed reaction on the dipeptide under the same conditions described above and we obtained lower conversions (Scheme 17). We rationalised this result with the coordination of the dipeptide with the metal, as the peptide amide bond is an excellent *N*-ligand for palladium<sup>[286,287]</sup>. In this regard, we investigated the best strategy to avoid the dipeptide acting as a ligand instead of a reagent.

Scheme 17. Comparison between the C-H functionalisation of protected Trp (1a into 2a) and of Boc-Nh-Trp-Leu-O¹Bu (1d into 2d).

We started our study by carrying out the reaction under the same conditions as for the functionalisation of Trp alone (**1a** into **2a**, Scheme 17) in presence of 1 equivalent of PPh<sub>3</sub>, with the aim of displacing the peptide from the coordination to palladium by the addition of a phosphine ligand (entry 1, Table 43). As we did not observe any change

compared to the reaction without ligands, the amount of catalyst was doubled in order to promote the reaction, but without any significant improvement (entry 2, Table 43).

Table 43. Conditions screening for C-H reaction Pd/NBE catalysed on Trp-containing dipeptides.

Entry	Pd (mmol%)	R-X	Ligand (equiv)	Solvent	Conversion (%) <sup>a</sup>
1	10%	Br	PPh <sub>3</sub> (1)	DMF/H <sub>2</sub> 0 (10:1)	6%
2	20%	Br	PPh <sub>3</sub> (1)	DMF/H <sub>2</sub> 0 (10:1)	20%
3	20%	Br	PPh <sub>3</sub> (1)	ACN/H <sub>2</sub> 0 (10:1)	0%
4	20%	I	PPh <sub>3</sub> (1)	DMF/H <sub>2</sub> 0 (10:1)	20%
5	20%	Br	PPh <sub>3</sub> (2)	DMF/H <sub>2</sub> 0 (10:1)	51%
6	20%	Br	TFP (2)	DMF/H <sub>2</sub> 0 (10:1)	44%
7	20%	Br	SPhos (2)	DMF/H <sub>2</sub> 0 (10:1)	26%
8	20%	Br	dppp (1)	DMF/H <sub>2</sub> 0 (10:1)	5%
9	10%	Br	phen	DMF/H <sub>2</sub> 0 (10:1)	3%
10	10%	Br	bipyr	DMF/H <sub>2</sub> 0 (10:1)	13%

<sup>&</sup>lt;sup>a</sup> Conversions have been calculated by using HPLC-MS.

Building on the results reported by Lautens and co-workers<sup>[288,289]</sup>, we repeated the same experiment in ACN instead of DMF, but unfortunately the reaction did not occur (entry 3, Table 43). We further demonstrated that the aryl iodide did not improve the reaction (entry 4, Table 43). Taking advantage of our study regarding the mechanistic investigation of PdCl<sub>2</sub> reduction mechanism in DMF with PPh<sub>3</sub>, K<sub>2</sub>CO<sub>3</sub> as base at 60°C (*Paragraph* 2.2.2., Table 8) we increased the ligands equivalents. Knowing that the PPh<sub>3</sub> can be partially oxidised to produce Pd<sup>0</sup>, we performed the reaction in the presence of 2 equivalents of PPh<sub>3</sub>, obtaining a conversion to 2d of 51% (entry 5, Table 43). With the aim of increasing the conversion, we evaluated the effect of various phosphines such as tri(2-furyl)phosphine (TFP), SPhos and dppp (entries 6-8, Table 43), but without any success. *N*-ligands, namely 1,10-phenantroline (phen) and 4,4'-bis(di-t-butyl)-2,2'-bipyridina (bipyr), were also investigated, but unfortunately did not help to improve the results (entries 9-10, Table 43).

This study did not provide us with a successful condition for the late-stage modification of Trp. Probably, the intermediate that precedes the OA step (Pd<sup>II</sup>-Pd<sup>IV</sup>, see Figure 127b)

is too sterically hindered, due to the presence of both NBE and dipeptide, and the ligands struggle to coordinate with palladium. Further studies are required to investigate the mechanism in detail.

# 3.2.3. Conclusion and Future Prospective

The development of pharmaceutical products capable of selectively targeting pathogenic bacteria in intestinal diseases is of great interest. In this study, we have demonstrated the synthesis of a small library of potentially antimicrobial peptides. Our aim was to functionalise the tryptophan contained in a tripeptide with the same scaffold as LTX-109, and to understand which combination of group (alkyl or aryl) and position (C2 or C5) was the most effective in achieving both a low MIC against Gram +/ Gram -bacteria and a high MIC against *Bifidobateria*. We found that H<sub>2</sub>N-Arg-Trp(2-C<sub>12</sub>H<sub>25</sub>)-Arg-NH(CH<sub>2</sub>)<sub>2</sub>Ph was the best candidate. On the basis of this result, we wanted to expand the library more rapidly by carrying out the late-stage functionalisation directly on the Trp-containing tripeptide with the Catellani reaction on the indole ring. Unfortunately, our attempts failed, probably due to the strong tripeptide-palladium coordination and the sterically hindered intermediates involved in the Pd catalytic cycle.

This project requires further investigation in order to: (*i*) use molecular modelling to understand why alkylation at the C2 position rather than the C5 position was beneficial; (*ii*) synthesise the tripeptide with Trp functionalised at both C2 and C5 positions to see if there is a positive or negative effect; (*iii*) carry out modifications at other positions of the indole ring; (*iv*) explore different approaches to carry out the latestage modification of tryptophan-containing peptides.

#### Acknowledgements:

The biological data were collected by Prof. Francesca Bonvicini (Department of Pharmacy and Biotechnology, Unibo) and Prof. Paola Mattarelli (Department of Food Science and Technology, Unibo).

Essential to the development of the project was the help of the Part Two students I supervised, Michele Ballan, Riccardo Miglioranzi and Glenn Tramontana.

#### Not published work

#### 3.2.4. Experimental Section

#### 3.2.4.1. General Information

All chemicals were purchased from commercial suppliers and were used without further purification. In particular, amino acids were supplied by Iris Biotech, Merck or Fluorochem. T3P® (50 wt. % in DCM) was supplied by Curia Global.

Thin-layer chromatography (TLC) was performed on precoated silica gel 60 F254 plates (Merck, Darmstadt, Germany), and spot detection was carried out using UV light and/or by charring with a ninhydrin solution or permanganate solution. Analytical HPLC was performed on an Agilent 1260 Infinity II system, coupled to an electrospray ionization mass spectrometer and using H<sub>2</sub>O + 0,08% TFA (mobile phase A) and CAN + 0,08% TFA (mobile phase B) as solvent at 25 °C (positive – ion mode). Agilent Zorbax – SB – C18 5  $\mu$ m, 250 x 4,6 mm was used. The injection volume was 10  $\mu$ L and the flow was 1,0 ml/min or 0,5 ml/min. ChemStation software was used for data processing. ChemStation software (OpenLAB CDS ChemStation 35900 A/D driver, OpenLAB CDS ChemStation 490 Micro GC driver) was used for data processing. Percentage areas of integrated peaks are reported in mAu. 1H-NMR spectra were recorded with an INOVA 400 MHz instrument with a 5 mm probe and Bruker Avance 600 MHz. <sup>13</sup>C-NMR spectra were recorded at 101 MHz with an INOVA 400 MHz instrument and at 151 MHz with the Bruker Avance 600 MHz instrument. All chemical shifts were quoted relative to deuterated solvent signals. Chemical shifts ( $\delta$ ) were referenced to the corresponding solvent peaks and are reported in parts per million (ppm). Coupling constants (J) are given in Hertz. Multiplicities are abbreviated as: s (singlet), d (doublet), t (triplet), q (quartet), m (multiplet).

#### 3.2.4.2. Synthesis of Boc-NH-Trp-OEt (1)

a)

In a round-bottom flask NH<sub>2</sub>-Trp-OH (2.5 g, 12.5 mmol, 1 equiv) was dissolved in EtOH (63 mL). Thionyl chloride (3.63 mL, 50 mmol, 4 equiv) was added dropwise at  $0^{\circ}$ C and, after the addition, the reaction was allowed to stir under reflux. After 6 hours, the ethanol was removed under reduced pressure and the crude was extracted with acid washes (HCl  $0.5 \text{ M} \times 3$ ) and basic washes (NaHCO<sub>3</sub> x 3). The organic phase was dried Na<sub>2</sub>SO<sub>4</sub> concentrated under reduced pressure.

<sup>1</sup>H NMR (600 MHz, CDCl<sub>3</sub>):  $\delta$ (ppm) = 8.15 (s, 1H), 7.57 (d, J = 8 Hz, 1H), 7.35 (d, J = 8 Hz, 1H), 7.19 (dt, 1H), 7.11 (dt, 1H), 7.00 (s, 1H), 5,085 (d, J = 4 Hz, 1H), 4.63 (d, J = 8 Hz, 1H), 4.13 (m, 2H), 3.29 (m, 2H), 1.43 – 1.33 (m, 9H), 1.12 (t, J = 8 Hz/4 Hz, 3H)

In a two-neck round-bottom flask, HCl·NH<sub>2</sub>-Trp-OEt (2.9 g, 12.5 mmol, 1 equiv) was dissolved in dry DCM (22 mL) under inert atmosphere and triethylamine (5.2 mL, 37.5 mmol, 3 equiv) was added. The solution was allowed to sti until the solid was completely dissolved and then, the solution was cooled at 0°C. After solubilisation of di-tert-butyl dicarbonate (Boc<sub>2</sub>O, 2.7 g, 12.5 mmol, 1 equiv) in DCM dry (22 mL), the solution was added dropwise in DCM dry. The solution was stirred at room temperature overnight. The reaction was quenched with water and the solvent was removed under vacuum. The crude was washed three times with ethyl acetate, dried with Na<sub>2</sub>SO<sub>4</sub> and concentrated under reduced pressure.

<sup>1</sup>H NMR (600 MHz, CDCl<sub>3</sub>):  $\delta$ (ppm) = 8.22 (s, 1H), 7.57 (d, J = 8 Hz, 1H), 7.35 (d, J = 8 Hz, 1H), 7.18 (t, 1H), 7.11 (t, 1H), 6.99 (s, 1H), 5.09 (d, J = 8 Hz, 1H), 4.62 (q, J = 8 Hz, 1H), 4.11 (q, J = 8 Hz, 1H), 3.29(s, 2H), 1.43 (s, 9H), 1.19(t, J=8Hz, 3H)

#### 3.2.4.3. Synthesis procedure for 3a-c

#### Catellani reaction

In a round-bottom flask Boc-Trp-OEt 1 (800 mg, 2.4 mmol, 1 equiv), norbornene (452 mg, 4.8 mmol, 2 equiv),  $K_2CO_3$  (1,33 g, 9,6 mmol, 4 equiv) were dissolved in DMF (12 mL) with  $H_2O$  (120  $\mu$ L). Then, alkyl-bromide (4 equiv) was added and finally  $Pd(ACN)_2Cl_2$  (63 mg, 0,24 mmol, 0.01 equiv) was added. The reaction was stirred at 60°C or 90°C for 24 hours. The mixture was diluted with diethyl ether and washed with water. The organic phase was dried with  $Na_2SO_4$  and concentrated under reduced pressure. The crude was purified by flash chromatography.

Purification by flash chromatography (Cy:EtOAc, 9:1). Isolated yield = 73%.

HN NMR (400 MHz, MeOD) 
$$\delta$$
(ppm) = 7.43 (d, J = 8 Hz, 1H), 7.25 (d, J=8 Hz, 2H) 7.02 (t, J=4 Hz, 1H), 6.96 (t, J=4 Hz, 1H) 4.37 (t, J = 8 Hz, 2H), 4.02 (m, 1H), 2.73 (t, J = 8 Hz, 2H), 1.71 (m, 2H), 1.41 (s, 9H),

1.44 (s, 9H), 1.34 - 1.27 (m, J = 8 Hz, 14H), 1.37 - 1.20 (m, 12H), 1.05 (t, J = 4 Hz, 3H), 0.91(t, J = 4 Hz, 3H)

Purification by flash chromatography (Cy:EtOAc, 9:1). Isolated yield = 60%.   
<sup>1</sup>H NMR (400 MHz, CDC<sub>13</sub>) 
$$\delta$$
(ppm) = 8.06 (s, 1H), 7.49 (d, J = 8 Hz, 1H), 7.32 – 7.05 (m, 9H), 5.09 (d, J = 8 Hz, 1H), 4.57 (m, 1H), 4.16 – 4.10 (m, 2H), 3.21 (d, J = 4 Hz, 2H), 2.75 (t, J = 8 Hz, 2H), 2.70 (t, J = 8 Hz, 2H), 1.99 (m, 2H), 1.42 (s, 9H), 1.12 (t, J = 8 Hz, 3H).

Purification by flash chromatography (Cy:EtOAc, 85:15). Isolated yield = 56%.

<sup>1</sup>H NMR (400 MHz, CDCl<sub>3</sub>):  $\delta$ (ppm) = 8.16 (s, 1H) 7.50 (d, J = 8Hz, 1H), 7.26 (d, J = 8Hz, 1H), 7.13 - 7.05 (t, J = 8Hz, 1H), 5.11(d, J = 8Hz, 1H), 4.61 (q, J = 8Hz, 1H), 4.10 (m, 2H), 3.24 (d, J = 8Hz, 1H), 4.10 (m, 2H), 3.24 (d, J = 8Hz, 1H), 4.61 (q, J = 8Hz, 1H), 4.10 (m, 2H), 3.24 (d, J = 8Hz, 1H), 4.10 (m, 2H), 44Hz, 2H), 2.58 (d, J = 8Hz, 2H), 1.97 (m, 1H), 1.43 (s, 9H), 1.15 (t, J = 4Hz, 3H), 0.95 (d, J = 8Hz, 6H)

# Boc removal

In a round-bottom flask, Boc-NH-Trp(2-alkyl)-OEt (1 equiv) was dissolved in DCM (0.2 M), and a solution of 2.5 equiv of triisopropyl silane (TIPS) and water 5% v/v in DCM was added. The mixture was then cooled down at 0°C and TFA (18 equiv) was added dropwise and after 1 hour the reaction was allowed to warm up at room temperature. After the completion of the reaction, monitored by TLC, the solvent was evaporated under reduced pressure and the crude material was used in the following step without further purification to obtain **3a-c** in quantitative yields.

#### 3.2.4.4. Synthetic procedure for 10a-b

#### a) Synthesis of 8

Boc-NH2-Trp(5-OH)-OEt was synthesized following the same procedure described in the Paragraph 3.2.4.2.

To an oven-dried two-neck round-bottom flask purged under nitrogen atmosphere, Boc-NH-Trp(5-OH)-Oet (750 mg, 2.15 mmol, 1 equiv) was suspended in dry DCM (5.6 mL). Pyridine (344,6  $\mu$ L, 4,3 mmol, 2 equiv) was added and the mixture was cooled at 0°C. After solubilisation of trifluoromethane sulphonic anhydride (Tf<sub>2</sub>O, 470,2  $\mu$ L, 2,8 mmol, 1.3 equiv) in DCM (5.6 mL), it was added dropwise, and the reaction was stirred at room temperature for 5 hours. Then, the reaction was quenched with HCl 1M and basic washes were carried out (NaHCO<sub>3</sub> 0.5 M x 3). The solution was dried with Na<sub>2</sub>SO<sub>4</sub> and concentrated under reduced pressure to obtain as an orange solid (y= 95%).

*Compound 8*:  $^{1}$ H NMR (400 MHz, MeOD):  $\delta$ (ppm) = 7,61 (s, 1H), 7,47 (d, J = 12 Hz, 1 H), 7,37 (s, 1H), 1,12 (d, J = 4 Hz, 1H), 7,09 (d, J = 4 Hz, 1H), 4,155 (m, 1H), 4,0 (q, J = 4 Hz, 2H), 3,130 – 3,00 (m, 2H), 1,330 – 1,23 (m, 9H), 1,090(t, J = 8 Hz, 3H).

# b) Synthesis of **9a-b**

To an oven-dried two-neck round-bottom flask purged under nitrogen atmosphere,  $Pd(ACN)_2Cl_2$  (31.0 mg, 0.12 mmol, 0.06 equiv), Sphos (122.4 mg, 0.24 mmol, 0.12 equiv), CuI (22.8 mg, 0.12 mmol, 0.06 equiv), compound 8 (980.4 mg, 2.04 mmol, 1 equiv), alkyne (1.5 equiv) and TMG (280 $\mu$ L, 2.24 mmol, 1.1 equiv) were added in degassed anisole (0.5 M). The reaction was let stirring overnight at 60°C. The crude was diluted with EtOAc and washed three times with water. The organic phase was dried with Na<sub>2</sub>SO<sub>4</sub> and concentrated under reduced pressure. The crude was purified by flash chromatography.

Purification by flash chromatography (Cy:EtOAc, 7:3). Isolated yield = 84%.

<sup>1</sup>H NMR (400 MHz, CDCl<sub>3</sub>) δ (ppm) = 8.12 (s, 1H), 7.78 (s, 1H), 7.54 (s, 1H), 7.53 (s, 1H), 7.36 – 7.31 (m, 4H), 7.04 (s, 1H), 5.09 (d, J = 8 Hz, 1H), 4.64 (m, 1H), 4.15 (m, 2H), 3.30 (m, 2H), 1.45 (s, 9H), 1.26 (t, J = 8 Hz, 3H)

Purification by flash chromatography (Cy:EtOAc, 8:2). Isolated yield = 79%.

<sup>1</sup>H NMR (400 MHz, CDCl<sub>3</sub>)  $\delta$  (ppm) = 8.12 (s, 1H), 7.62 (s, 1H), 7.23 (s, 1H), 6.69 (s, 1H), 5.09 (d, J = 8 Hz, 1H), 4.62 (m, 1H), 4.15 (m, 2H), 3.25 (m, 2H), 2.41 (t, J = 4 Hz, 2H), 1.61 (m, 2H), 1.44 (s, 9H), 5.09 (d, J = 8 Hz, 1H), 1.37 – 1.20 (m, 12H), 0.89 (t, J = 4 Hz, 3H)

# c) Synthesis of 10a-b

# Reduction of the alkyne

To an oven-dried two-neck round-bottom flask purged under nitrogen atmosphere, 9a-b (1 equiv) was dissolved in AcOEt (0.2 M). Then dry Pd/C (10% w/w) was added, and the atmosphere was switched from nitrogen to H<sub>2</sub> gas (balloon). The reaction was stirred 24h at room temperature. When the reaction was completed, the mixture was filtered through a pad of celite and washed with EtOAc. The solvent was then removed under vacuum and no further purification was required.

<sup>1</sup>H NMR (400 MHz, CDCl<sub>3</sub>)  $\delta$ (ppm) = 8.02 (s, 1H), 7.38 (s, 1H), 7,32 – 7.19 (m, 6H + CDCl<sub>3</sub>), 7.04 (d, J = 8 Hz, 1H), 6.99 (s, 1H), 5.09 (d, J = 8 Hz, 1H), 4.62 (m, 1H), 4.12 (m, 2H), 3.27 (d, J = 4 Hz, 2H), 3.04 – 2.93 (m, 4H), 1.42 (s, 9H), 1.21 (t, J = 8 Hz, 3H)

<sup>1</sup>H NMR (400 MHz, CDCl<sub>3</sub>)  $\delta$ (ppm) = 7.99 (s, 1H), 7.34 (s,1H), 7.24 (d, 1H), 7.03 (d, J = 4 Hz, 1H), 6.98 (s, 1H), 5.10 (d, J = 8 Hz, 1H), 4.63 (m, 1H), 4.13 (m, 2H), 3.27 (d, J = 4 Hz, 2H), 2.69 (t, J = 8 Hz, 2H), 1.65 (m, 2H), 1.43 (s, 9H), 1.38-1.24 (m, 14H), 1.21 (t, J = 4 Hz, 3H), 0.89 (t, J = 4 Hz, 3H)

#### Boc removal

In a round-bottom flask, Boc-NH-Trp(5-alkyl)-OEt (1 equiv) was dissolved in DCM (0.2 M), and a solution of 2.5 equiv of TIPS and water 5% v/v in DCM was added. The mixture was then cooled down at 0°C and TFA (18 equiv) was added dropwise and after 1 hour the reaction was allowed to warm up at room temperature. After the completion of the reaction, monitored by TLC, the solvent was evaporated under reduced pressure and the crude material was used in the following step without further purification to obtain 10a-b in quantitative yields.

#### 3.2.4.5. Synthesis of dipeptide 4a-c and 11a-b

To an oven-dried two-neck round-bottom flask purged under nitrogen atmosphere, 1 equiv of TFA·H<sub>2</sub>N-Trp(2-alkyl)-OEt (**3a-c**) or TFA·H<sub>2</sub>N-Trp(5-alkyl)-OEt (**10a-b**) was solubilised in DCM dry (0.2 M). Boc-Arg(PBF)-OH (1.1 equiv), DIPEA (5 equiv) and T3P® (50 wt. % in DCM, 2 equiv) were added following this order. The solution was stirred for 10 min, and the organic phase was washed once with H<sub>2</sub>O, HCl(aq) (0.01 M) and NaHCO<sub>3</sub>(aq) (0.01 M). The organic layer was dried over anhydrous Na<sub>2</sub>SO<sub>4</sub>, and the crude was purified by flash chromatography.

Purification by flash chromatography (Cy:EtOAc, 7:3). Isolated yield = 61%.

<sup>1</sup>H NMR (400 MHz, MeOD)  $\delta$ (ppm) = 7.42 (d, J = 8Hz, 1H), 7.25(d, J = 8Hz, 1H), 7.0– 6.91 (m, 2H), 5.59 (s, 1H), 4.65 (t, J = 4Hz, 1H), 4.05 – 3.85 (m, 3H), 3.25 – 3.05 (m, 4H), 2.94 (s, 2H), 2.73 (t, J = 8Hz, 1H), 2.59 (s, 3H), 2.52 (s, 3H), 2.07 (s, 3H), 1.68 (m, 2H), 1.56 – 1.20

(m, 35H), 0.94 (t, J = 8Hz, 1H), 0.89 (t, J = 4Hz, 1H).

Purification by flash chromatography (Cy:EtOAc, 8:2). Isolated yield = 58%.

<sup>1</sup>H NMR (400 MHz, MeOD)  $\delta$ (ppm) = 7.30 – 7.13 (m, 10H), 4.68(s,1H), 3.30 – 3.10 (m, 8H), 3.02 (s, 2H), 2.85 – 2.77 (m, 3H), 2.73 – 2.65 (m, 3H), 2.59(s, 2H), 2.53 (s, 2H); 2.11 (s, 2H), 1.5 – 1.20 (m, 20H).

Purification by flash chromatography (Cy:EtOAc, 7:3). Isolated yield = 64%

<sup>1</sup>H NMR (400 MHz, CDCl<sub>3</sub>)  $\delta$ (ppm) = 7.42 (dd, J = 8Hz, J = 24 2H), 7,10 – 6.99 (m, 2H), 6.72 (d, J = 8Hz, 1H), 4.75 (s, 1H), 4.12 (m, 3H), 3.29 – 3.05 (m, 3H), 2.96 (s, 2H), 2.81 (m, 1H), 2.70 – 2.50 (m, 6H), 2.60 (s, 3H), 2.53 (s, 3H), 2.11 (s, 3H), 1.50 – 1.35 (m, 12H), 1.26 (t, J = 8Hz, 3H),

0.95 (d, J = 8Hz, 3H), 0.99 (d, J = 8Hz, 3H).

Purification by flash chromatography (Cy:EtOAc, 8:2). Isolated yield = 59%

<sup>1</sup>H NMR (400 MHz, MeOD)  $\delta$ (ppm) = 7.29 (s, 1H), 7.25- 7.09 (m, 5H), 7.05 – 7.03 (m, 1H), 6.94 (m, 1H), 4.65 (s, 1H), 4.00 (s, 1H), 3.33 – 3.10 (m, 4H), 3.00 – 2.85 (m, 4H), 2.56 (s, 3H), 2.50 (s, 3H), 2.06 (s, 3H), 1.50 – 1.40 (m, 11H), 1.23 (t, J = 8Hz, 3H).

11b

Purification by flash chromatography (Cy:EtOAc, 65:35). Isolated yield = 53%

<sup>1</sup>H NMR (400 MHz, MeOD)  $\delta$ (ppm) = 8.05 (d, J = 8Hz, 1H), 7.40 (s, 1H), 7.33 (d, J = 8Hz), 7.16 (s, 1H), 7.01 (d, J = 8Hz, 1H), 4.82 (s, 1H), 4.19 – 4.11 (m, 3H), 3.38 – 3.16 (m, 5H), 3.01 (s, 2H), 3.00 – 2.85 (m, 4H), 3.01 (s, 2H), 2.75 (t, J = 8Hz 2H), 2.69 (s, 3H), 2.62 (s, 3H), 2.16 (s, 3H), 1.85 – 1.55 (m, 8H), 1.50 (s, 10H), 1.50 – 1.35 (m, 18H), 1.31 (t, J = 8Hz, 3H).

# 3.2.4.6. Synthesis of compounds 5a-c and 12a-b by removal of the ethyl ester

In a round-bottom flask, the dipeptide Boc-HN-Arg(PBF)-Trp(2-alkyl)-OEt (4a-c) or Boc-HN-Arg(PBF)-Trp(5-alkyl)-OEt (11a-b) (1 equiv) was dissolved in THF/ H<sub>2</sub>O (1:1, 0.2 M). LiOH · H<sub>2</sub>O (9 equiv) was added at 0°C and after 1 hour, the reaction was allowed to warm to room temperature and stirred overnight. The THF was evaporated under vacuum and the aqueous mixture was acidified to pH=1, diluted with EtOAc and washed with 0.1 M HCl. The organic phase was dried with Na<sub>2</sub>SO<sub>4</sub>. No further purification was carried out.

Yield= 88%.

<sup>1</sup>H NMR (400 MHz, MeOD)  $\delta$ (ppm) = 7.83 (d, J = 8Hz, 1H), 7.49 (d, J = 8Hz, 1H), 7.26 (d, J = 8Hz, 1H), 7.02 – 6.93 (m, 3H), 4.73 (t, J = 8Hz, 1H), 4.00 (s, 1H), 3.33 – 3.10 (m, 5H), 3.02 (s, 2H), 2.58 (s, 3H), 2.52 (s, 3H), 2.12 (s, 3H), 1.71 (t, J = 8Hz, 2H), 1.5 – 1.25 (m, 40H), 0.91 (t, J =

8Hz, 3H).

Yield = 91%

<sup>1</sup>H NMR (400 MHz, MeOD)  $\delta$ (ppm) = 7.24 -7.10 (m, 9H), 4.59 (s, 1H), 3.25– 3.05 (m, 7H), 3.3 – 2.92 (m, 7H), 2.97 (s, 2H), 2.78 – 2.73 (m, 3H), 2.68 – 2.62 (m, 3H), 2.57 (s, 3H), 2.50 (s, 3H), 2.07 (s, 3H), 1.5 – 1.2 (m, 20H).

Yield = 87%

<sup>1</sup>H NMR (400 MHz, MeOD)  $\delta$ (ppm) = 7.51 (d, J = 8Hz, 1H), 7.26 (d, J = 8Hz, 1H), 6.96 (m, 2H), 4.70 (s, 1H), 3.98 (s, 1H), 3.29 – 3.05 (m, 6H), 3.00 (s, 2H), 3.01 (s, 2H), 2.65 (t, J = 8Hz, 2H), 2.60 (s, 3H), 2.53 (s, 3H), 2.10 (s, 3H), 1.66 – 1.35 (m, 21H), 1.26 (t, J = 8Hz, 3H), 0,7 (d, J = 8Hz, 6H).

Yield = 90%

<sup>1</sup>H NMR (400 MHz, MeOD)  $\delta$ (ppm) = 7.38 (s,1H), 7.27 – 7.15(m, 7H), 7.08(s, 1H), 6.98 – 6.94 (m, 2H), 4.73 (s, 1H), 4.00 (s, 1H), 3.23 – 3.12 (m, 4H), 3.3 – 2.92 (m, 7H), 2.58 (s, 3H), 2.52 (s, 3H), 2.10 (s, 3H), 1.50 – 1.37 (m, 16H).

12b

Yield = 87%

<sup>1</sup>H NMR (400 MHz, CDCl<sub>3</sub>),  $\delta$ (ppm) = 7.35 – 7.25 (m, 2H), 7.21 (m, 1H), 6.97 (s, 1H), 6.93 – 6.88 (m, 1H), 4.73 (t, J = 8Hz, 1H), 4.02 (s, 1H), 3.35 – 2.95(m, 6H), 2.90 (s, 2H), 2.63 (m, 2H), 3.02 (s, 3H), 2.52 (s, 3H), 2.46 (s, 3H) 2.05 (s, 3H), 1.99 (m, 2H), 1.59 (m, 3H), 1.49 – 1.15 (m, 32H), 0.85 (m, 3H).

# 3.2.4.7. Synthesis of compound 16

#### a) Coupling

To an oven-dried two-neck round-bottom flask purged under nitrogen atmosphere, Fmoc-Arg(PBF)-OH (389.3 mg, 0.6 mmol, 1 equiv), phenethylamine (75  $\mu$ L, 0.6 mmol, 1 equiv) were dissolved in DCM dry (3.5 mL, 0.2M). DIPEA (313  $\mu$ L, 3 equiv) and T3P® (50 wt. % in DCM, 1.5 equiv) of TFA·H<sub>2</sub>N-Trp(2-alkyl)-OEt (**3a-c**) or TFA·H<sub>2</sub>N-Trp(5-alkyl)-Oet (**10a-b**) was dissolved in DCM dry (0.2 M). Boc-Arg(PBF)-OH (1.1 equiv), DIPEA (5 equiv) and T3P® (50 wt. % in DCM, 2 equiv) were added following this order. The solution was stirred for 10 min, and the organic phase was washed once with H<sub>2</sub>O, HCl(aq) (0.01 M) and NaHCO<sub>3(aq)</sub> (0.01 M). The organic layer was dried over anhydrous Na<sub>2</sub>SO<sub>4</sub>.

#### b) Fmoc Removal

In a round-bottom flask, compound **15** (1 equiv) was dissolved in EtOAc (0.2 M) and tert-butylamine (19 equiv). The reaction was allowed to stir at room temperature and monitored by TLC. After 40 minutes, the solvent was removed under reduced pressure and no further purification was carried out.

#### 3.2.4.8. Synthesis of tripeptides 6a-c and 13a-b

To an oven-dried two-neck round-bottom flask purged under nitrogen atmosphere, the dipeptides Boc-Arg(PBF)-Trp(2-akyl)-OH **5a-c** and Boc-Arg(PBF)-Trp(5-akyl)-OH **12a-b** (1 equiv) were solubilised in DCM dry (0.2 M). Compound **16** (1.1 equiv), DIPEA (3

equiv) and T3P® (50 wt. % in DCM, 1.5 equiv) were added following this order. The solution was stirred for 10 min, and the organic phase was washed once with  $H_2O$ ,  $HCl_{(aq)}$  (0.01 M) and  $NaHCO_{3(aq)}$  (0.01 M). The organic layer was dried over anhydrous  $Na_2SO_4$ , and the crude was purified by flash chromatography.

Purification by flash chromatography (DCM/MeOH = 97/3). Isolated yield = 56%  $^{1}$ H NMR (400 MHz, MeOD):  $\delta$ (ppm) = 7.43 (d, J = 8Hz, 1H), 7.27 (d, J = 8Hz, 1H), 7.17 (d, J = 8Hz, 2H), 7.09 (m, 2H), 6.99 (t, J = 8Hz, 1H), 6.93 (t, J = 8Hz, 1H), 4.1 (t, J = 4Hz, 1H), 4.17 (s, 1H), 3.78 (s, 1H), 3.30 – 2.95 (m, 8H), 2.91 (s,

4H), 2.72 (t, J = 8Hz, 2H), 2.63 (t, J = 8Hz, 2H), 2.56 (s, 6H), 2.50 (s, 6H), 2.04 (s, 6H), 1.70 - 1.45 (m, 6H), 1.38 (s, 9H), 1.35 - 1.20 (m, 24H), 0.86 (t, J = 8Hz, 3H).

2H), 1.6 – 1.2 (m, 25H).

Purification by flash chromatography (DCM/MeOH = 98/2). Isolated yield = 58%. ¹H NMR (400 MHz, MeOD):  $\delta$ (ppm) = 7.55 – 7.4 (m, 2H), 7.3 – 6.9 (m, 11H) 7.40 – 7.05 (m, 10H), 4.49 (s, 1H), 4.15 (s, 1H), 3.25 – 3.00 (m, 6H), 2.96 (s, 3H), 2.78 (m, 2H), 2.72 – 2.63 (m, 2H), 2.57 (s,4H), 2.53 (s, 4H), 2.06 (s, 6H), 2.02 – 1.96 (m,

Purification by flash chromatography (Cy:EtOAc, 6:4). Isolated yield = 41%  $^{1}$ H NMR (400 MHz, MeOD):  $\delta$ (ppm) = 7.49 (d, J = 4Hz, 1H), 7.30 (d, J = 8Hz, 1H), 7.25 – 7.20 (m, 2H), 7.17 – 7.12 (m, 2H), 7.07 – 6.95 (m, 2H), 5.58 (s, 1H), 4.54 (s,1H), 4.19 (s, 1H), 3.30- 3 (m, 6H), 2.90 (s, 3H), 2.73 – 2.60 (m, 2H), 2.60 (s, 4H), 2.09 (s, 2H), 2.73 – 2.60 (m, 2H), 2.60 (s, 4H), 2.09 (s, 2H), 2.73 – 2.60 (m, 2H), 2.60 (s, 4H), 2.09 (s, 2H), 2.73 – 2.60 (m, 2H), 2.60 (s, 4H), 2.09 (s, 2H), 2.73 – 2.60 (m, 2H), 2.60 (s, 4H), 2.09 (s, 2H), 2.73 – 2.60 (m, 2H), 2.60 (s, 4H), 2.09 (s, 2H), 2.73 – 2.60 (m, 2H), 2.60 (s, 4H), 2.09 (s, 2H), 2.73 – 2.60 (m, 2H), 2.60 (s, 4H), 2.09 (s, 2H), 2.60 (s, 2H),

4H), 2.09 - 2 (m, 1H), 1.75 - 1.20 (m, 24H), 0.95 (t, J = 8Hz, 6H).

Purification by flash chromatography (DCM/MeOH = 98/2). Isolated yield = 47%. ¹H NMR (400 MHz, MeOD):  $\delta$ (ppm) = 7.49 – 7.35 (m, 2H), 7.27 – 7.05 (m, 11H) 7.00 – 6.90 (m, 2H), 5.60 (s, 1H), 4.58 (s, 1H), 4.20 (s, 1H), 3.30 – 2.85 (m, 15H), 2.68 (t, J = 4Hz 2H), 2.59 (s,6H), 2.53 (s, 6H), 2.08 (s, 6H), 1.70 – 1.3 (m, 28H), 0.9 (m, 3H).

Purification by flash chromatography (DCM: MeOH, 96:4). Isolated yield = 65%

<sup>1</sup>H NMR (400 MHz, MeOD):  $\delta$ (ppm) = 7.78 (d, J = 8Hz, 1H), 7.62 (m, 1H) 7.40 – 7.05 (m, 10H), 6.93 (m, 1H), 4.58 (s, 1H), 4.19 (s, 1H), 3.30 – 3.00 (m, 8H), 2.96 (s, 4H), 2.8 – 2.63 (m, 4H), 2.59 (s, 6H), 2.53 (s, 6H), 2.08 (s, 6H), 1.70 – 1.2 (m, 45H), 0.9 (m, 3H).

### 3.2.4.9. Synthesis of final products 7a-c and 14 a-b

In a round-bottom flask, the cleavage cocktail TFA/H<sub>2</sub>O/TIPS (92.5:3.75:3.75) was added dropwise at 0°C to Boc-Arg(PBF)-Trp(2-akyl)-OH-Arg(Pbf)-(CH<sub>2</sub>)<sub>2</sub>Ph (6a-c) and Boc-Arg(PBF)-Trp(5-akyl)-OH-Arg(Pbf)-(CH<sub>2</sub>)<sub>2</sub>Ph (13a-b) dissolved in the minimum amount of DCM. After stirring for 30 minutes at 0°C, the reaction was allowed to stir at room temperature and monitored by TLC. Precipitation was carried out by dropwise addition of diethyl ether (Et<sub>2</sub>O) at 0°C and the resulting precipitates were recovered as white solids by vacuum filtration and washed with cold Et<sub>2</sub>O.

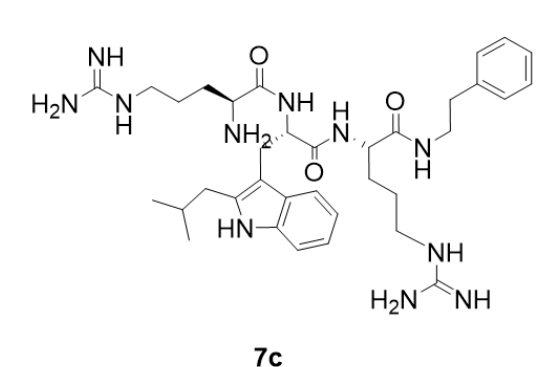
<sup>1</sup>H NMR (400 MHz, MeOD):  $\delta$ (ppm) = 7.57 (d, J = 8Hz, 1H), 7.30 – 7.23 (m, 3H), 7.18 – 7.14 (m, 3H), 7.06 – 6.99 (m, 3H), 4.64 (s, 1H), 4.23 (s, 1H), 4.06 (s, 1H), 3.30 – 2.95 (m, 8H), 2.73 (s, 2H), 2.57 (t, J = 8Hz, 2H), 2.01 (s, 2H), 1.80 – 1.40 (m, 9 H) 1.40 – 1.15 (m, 20H), 0.88 (t, J = 8Hz, 3H).

<sup>13</sup>C NMR (400 MHz, MeOD):  $\delta$ (ppm) = 174.17, 173.20, 158.67, 158.50, 140.21, 139.35, 137.10, 129.78, 129.47, 127.34, 105.87, 42.00, 36.46, 33.06, 30.77, 30.48, 23.73, 19.48, 14.49.

<sup>1</sup>H NMR (400 MHz, MeOD):  $\delta$ (ppm) = 7.58 (d, J = 8Hz, 1H), 7.30 – 6.99 (m, 14H), 4.64 (s, 1H), 4,21 (s, 1H), 4.02 (s, 1H), 3,25 – 3 (m, 8H), 2.81 (t, J = 8Hz, 2H), 2.64 (t, J = 8Hz, 2H), 2.57 (t, J = 8Hz, 2H), 1.99 (m, 4H), 1.78 – 1.46 (m, 8H).

<sup>13</sup>C NMR (400 MHz, MeOD):  $\delta$ (ppm) = 174.10, 173.18, 158.62, 143.40, 140.20, 138.86, 137.18, 129.78, 129.46, 129.42, 129.35, 127.34, 126.79, 106.16, 49.00

41.96, 36.71 36.38, 32.70, 26.81, 26.13, 19.33.



<sup>1</sup>H NMR (400 MHz, MeOD):  $\delta$ (ppm) = 7.60 (d, J = 8Hz, 1H) 7.31 – 7.25 (m, 2H), 7.20 (d, J = 8Hz, 2H), 7.08 – 6.99 (m, 2H), 4.65 (t, J = 8Hz, 1H), 4.19 (s, 1H), 3.99 (S, 1H), 3.25 – 3.01 (m, 6H), 2.66 – 2.59 (m, J = 8Hz, 3H), 2.01 (m, 2H), 1.79 – 1.4 (m, 9H), 0.97 (d, J = 8Hz, 6H).

<sup>13</sup>C NMR (400 MHz, MeOD):  $\delta$ (ppm) = 174.08, 173.16, 170.12, 158.67, 140.21, 138.41, 137.10,

129.78, 129.46, 127.35, 121.80, 119.91, 118.97, 111.73, 106.61, 53.54, 41.96, 36.38, 36.20, 30.36, 29.60, 26.14,14.95, 23, 22.90.

14a

<sup>1</sup>H NMR (600 MHz, MeOD):  $\delta$ (ppm) = 7.49 (s, 1H) 7.31 – 7.25 (m, 5,H), 7.22 – 7.15 (m, 5H), 7.08 (d, J = 8Hz, 1H), 4.73 (t, J = 2Hz, 1H), 4.25 (dd, J= 4Hz, J = 9Hz, 1H), 3.95 (t, J = 5Hz, 3H), 3.31 -3.28 (m, 2H), 3.25 - 3.21 (m, 3H), 3.00 - 2.98 (m, 3H)2H), 2.96 - 2.93 (m, 2H), 2.73 (t, J = 8Hz, 2H), 2.03-1.95 (m, 3H), 2.76 - 1.69 (m, 4H), 1.6 - 1.49 (m, 3H).

<sup>13</sup>C NMR (600 MHz, MeOD):  $\delta$ (ppm) = 174.37, 173.43, 170.17, 163.05, 162.82, 158.77, 158.66, 143.55, 140.27, 136.75, 133.86, 129.85, 129.55, 129.30, 127.48, 127.43, 126.79, 125.23, 123.78, 118.59, 112.24, 110.22, 56.46, 54.49, 53.79, 42.05, 41.92, 41.72, 40.14, 39.61, 36.42, 30.21, 29.62, 28.86, 26.04, 24.88, 24.21.

7.29 - 7.27 (m, 3H), 7.20 - 7.18 (m, 3H), 6.99 (d, J =8Hz, 1H), 4.74 (t, J = 5Hz, 1H), 4.25 (dd, J = 4Hz, J =9Hz, 1H), 3.95 (t, J = 5Hz, 3H), 3.31 - 3.05 (m, 8H), 2.71 - 2.65 (m, 4H), 1.99 - 1.95 (m, 2H), 1.80 - 1.50 (m, 10H), 1.39 - 1.29 (m, 14H), 0.9 (t, J = 12Hz, 3H). <sup>13</sup>C NMR (600 MHz, MeOD):  $\delta$ (ppm) = 174, 173, 170, 163.08, 158.46, 140.23, 136,.64, 129.84, 129.50, 128.64, 127.42, 125.01, 123.79, 118.40, 112.22, 110.05, 56.25, 54.45, 53.75, 42.01, 41.90, 41.78, 37.36, 36.40, 33.78, 33.07, 30.80, 30.76, 30.56, 30.46, 30.17, 29.65, 28.87,

<sup>1</sup>H NMR (600 MHz, MeOD):  $\delta$ (ppm) = 7.44 (s, 1H)

26.07, 24.92, 23073, 14.43.

# 3.2.4.10. Procedure for late-stage functionalisation of Boc-NH-Trp-Leu-O'Bu

To an oven-dried two-neck round-bottom flask purged under nitrogen atmosphere, PdCl<sub>2</sub> (10% or 20% mmol) and the ligand (1 or 2 equiv) were added in the solvent (0.5 M). Then, Boc-NH-Trp-Leu-O<sup>t</sup>Bu **1d** (94.7 mg, 0.2 mmol, 1 equiv), K<sub>2</sub>CO<sub>3</sub> (110.6 mg, 0.8 mmol, 4 equiv), XCH<sub>2</sub>-(CH<sub>2</sub>)<sub>10</sub>-CH<sub>3</sub> (0.8 mmol, 4 equiv), NBE (37.6 mg, 0.4 mmol, 2 equiv) were added and the reaction stirred at 60°C. After 24 hours, the reaction was quenched by the addition of water. An aliquot of the mixture was taken and diluted in 1.5 mL of ACN/H<sub>2</sub>O (5:5). The sample was then analysed by HPLC-MS to evaluate the conversion (%). The conversion was calculated from the area of the HPLC peaks by comparing the UV signal at 220 nm of **1d** with the product **2d** without RRF correction. The collected data are reported in Table 43.

An example HPLC profile is given below.

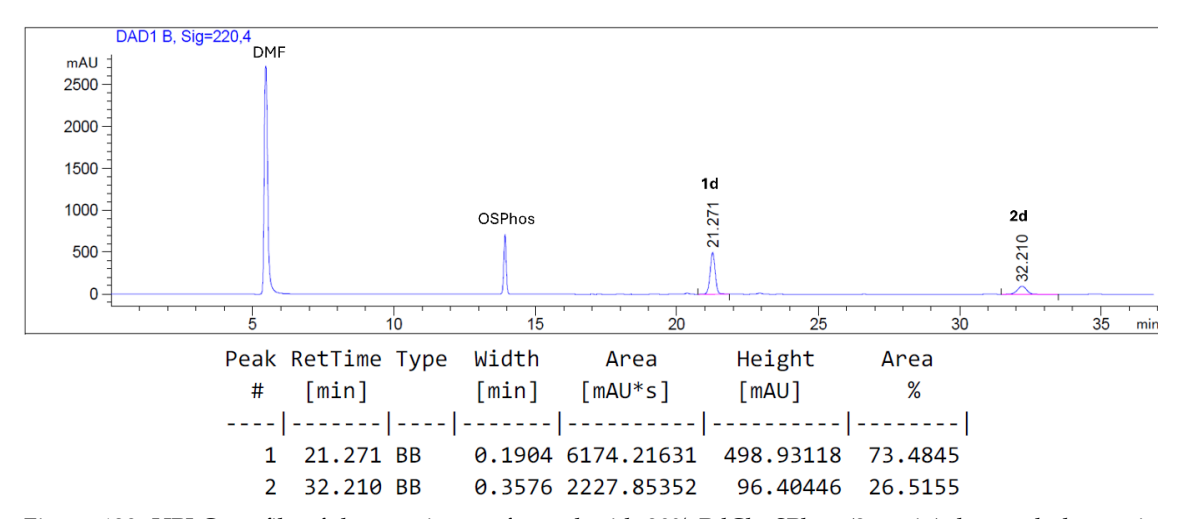


Figure 129. HPLC profile of the reaction performed with 20% PdCl<sub>2</sub>, SPhos (2 equiv), bromododecane in DMF/H<sub>2</sub>0 10:1 (0.5 M) at  $60^{\circ}$ C (see Entry 7, Table 43). HPLC method: 80%B (0 min), 80%B (22 min), 60%B (24 min), 10%B (25 min), 10%B (40 min).

# Enantioselective Nucleophilic Fluorination *via* Synergistic Phase Transfer Catalysis with KF

### 4.1. Introduction

Catalytic enantioselective fluorination has been dominated by methods using electrophilic fluorinating reagents from the development of N-fluorobenzene-sulfonimide (NFSI) and 1-chloromethyl-4-fluoro-1,4-diazoniabicyclo- [2.2.2]octane bis(tetrafluoroborates) (Selectfluor) in the 1990s<sup>[290]</sup>. Phase transfer catalysis (PTC) is one of the most successful methods applied to asymmetric electrophilic fluorinations. In 2010, Maruoka and co-workers<sup>[291]</sup> disclosed a cationic PTC for the asymmetric electrophilic fluorination of cyclic  $\beta$ -keto esters with NFSI and bis-(diarylhydroxymethyl) substituents at 3,3'-positions of the chiral binaphthyl core as phase transfer catalyst (Figure 130a). A year later, Toste and co-workers<sup>[292]</sup> reported an anionic PTC for enantioselective fluorocyclization using Selectfluor (insoluble in non-polar media) and chiral phosphate as catalyst (Figure 130b).

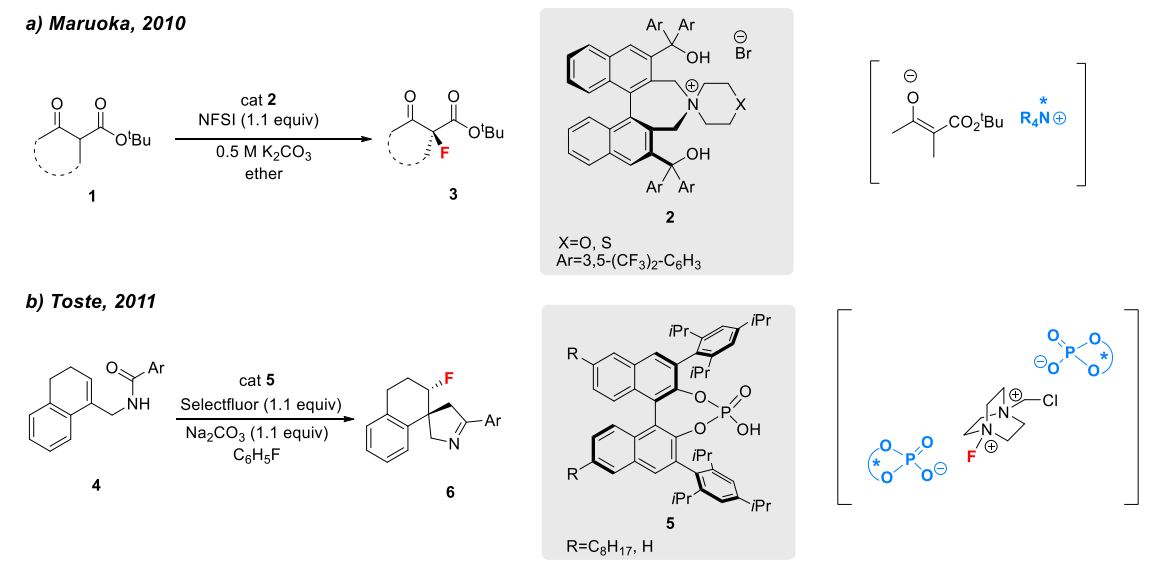


Figure 130. Asymmetric electrophilic fluorination via cationic and anionic PTC.

Alkali metal fluorides are abundant and inexpensive. However, their poor solubility in organic solvents and difficulties in dealing with the high basicity of fluoride have limited their use. Several phase transfer catalysts for nucleophilic fluorination have been investigated, with crown ethers being the most commonly used<sup>[293]</sup>. In 2018, Gouverneur and co-workers<sup>[294]</sup> reported for the first time the hydrogen-bond phase transfer catalysis (HB-PTC) for enantioselective fluorination. This strategy paved the way for the enantioselective nucleophilic fluorination using a catalytic approach. The group had previously documented the ability of diarylurea to form hydrogen-bonded complexes with F-, from tetrabutylammonium fluoride, favouring SN2 reactions over undesired E2 reactions<sup>[295]</sup>. In this work, they showed that chiral bis-urea is able to act as a solid-liquid phase transfer catalyst to obtain nucleophilic enantioselective fluorination of  $\beta$ -bromosulfides with a metal fluoride insoluble in organic media (Figure 131a). The same group also reported the synthesis of  $\beta$ -fluoroamines with KF<sup>[296]</sup> and of  $\gamma$ -fluoroamines<sup>[297]</sup> (Figure 131 b-c).

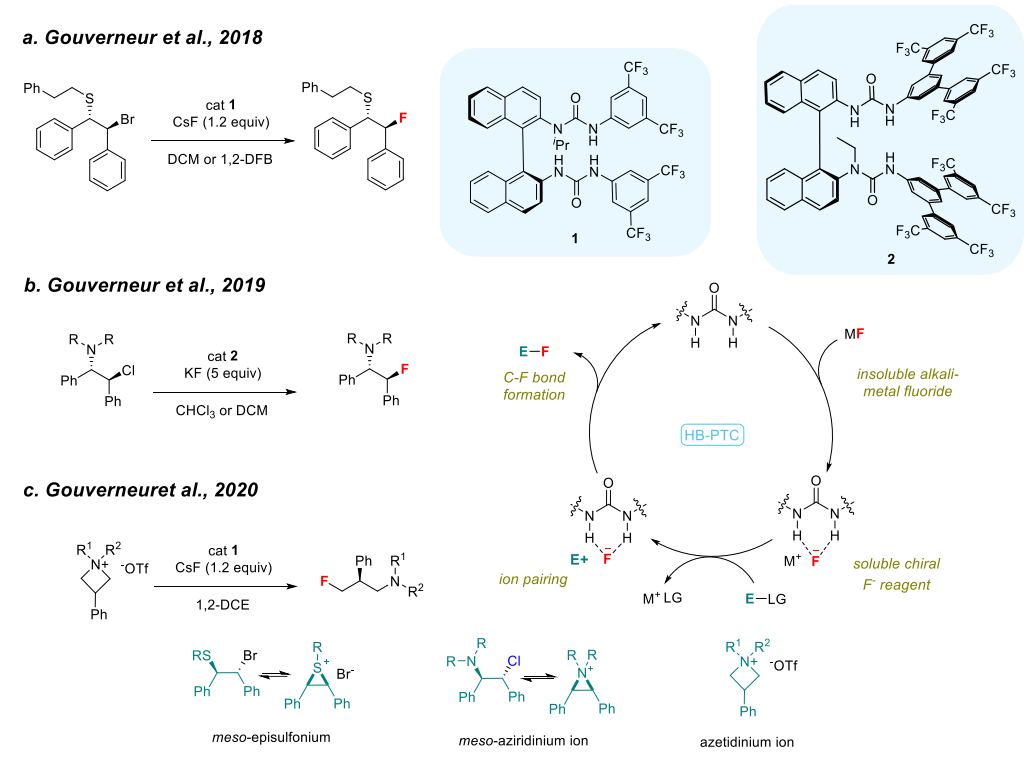


Figure 131. Enantioselective nucleophilic fluorination of charged electrophiles via HB-PTC.

The nucleophilic fluorination *via* HB-PTC described above is based on the asymmetric desymmetrisation of onium-type electrophiles generated *in situ* or preformed achiral azetidinium salts. With the aim of extending this methodology to neutral electrophiles, the Gouverneur group developed the Synergistic HB-PTC (S-HBPTC). In this case, to overcome the lack of ion pairing between the onium electrophiles and urea-fluoride complexes, an onium was employed as a co-catalyst (Scheme 18).

Scheme 18. Enantioconvergent nucleophilic substitution of benzylic bromides with KF via S-HBPTC.

They demonstrated that: (i) an apolar medium, such as p-xylene, is the best solvent for benzylic fluorination and that the fluorination occurs via an S<sub>N</sub>2-like mechanism; (ii) the bis-urea and onium salts can solubilise KF, which is completely insoluble in an apolar solvent, to form a tricoordinate hydrogen-bonded complex; (iii) tetraphenylphosphonium iodide (PPh<sub>4</sub>+I-) is the most efficient and, in particular, the onium iodide salt accelerates the reaction compared to the corresponding bromide; (iv) racemisation of the benzylic substrate occurs in the presence of both bis-urea and onium salt and that the rate of racemisation exceeds the rate of fluorination (Figure 132). The gram-scale reliability of the strategy was also demonstrated.

Figure 132. Optimised conditions of enantioselective fluorination via S-HBPTC and proposed catalytic cycle.

Chiral  $\alpha$ -halogenated carbonyl compounds are an important class of molecules with high medicinal chemistry relevance and useful building blocks in organic synthesis<sup>[298,299]</sup>. Considering the lack of synthetic approaches towards enantioenriched  $\alpha$ -fluoroketone structures, which currently rely on enamine formation and the use of expensive electrophilic fluorinating reagents (*e.g.* NFSI)<sup>[300]</sup>, we chose the  $\alpha$ -bromooketones to extend the S-HBPTC strategy to other neutral electrophiles.

In this context, during my stay at the University of Oxford in Professor Gouverneur's group, I focused on studying the catalytic asymmetric nucleophilic fluorination of  $\alpha$ -bromoketones.

# 4.2. Results and Discussion

We started this work by studying the enantioselective fluorination of the commercially available *rac*-1a under S-HBPTC with KF, PPh<sub>4</sub>+I-, and *bis*-urea 3a<sup>[294]</sup> as catalyst in different solvents (Table 44). As an inverse correlation between the dielectric constant of the solvent (ε) and the enantiomeric ratio (e.r.) was observed with benzyl bromides, we first carried out the reaction in toluene, but we observed low enantioselectivity (entry 1, Table 44). We repeated the nucleophilic substitution in more polar solvents, and we found that the acetonitrile was the best in terms of the observed enantiomeric ratio (entry 6 vs entries 1-5, Table 44).

Table 44. Solvent screening for enantioselective fluorination of  $\alpha$ -bromoketone under S-HBPTC

Entry	Solvent	3	2a (%)ª	1a (%)	e.r. <sup>b</sup>
1	Toluene	2.38	21	79	63:37
2	EtOAc	6.02	18	82	60:40
3	THF	7.58	16	84	56:44
4	DCM	8.93	17	83	60:40
5	Acetone	20.7	24	76	63:37
6	ACN	37.5	28	72	71:29

 $^{a}$ Yield determined by  $^{19}$ F NMR using 4-fluoroanisole as internal standard,  $^{b}$ e.r. was determined by HPLC analysis using a chiral stationary phase.

To improve the enantioselectivity of the substitution, we evaluated the effect of several *bis*-urea catalysts (Figure 133) on the enantiomeric ratio of **2a**. We observed that

the enantiomeric ratio was increased with the N-alkylated catalysts bearing an extended polytrifluoromethylated terphenyl  $\pi$ -system, such as (S)-3 $\mathbf{c}$  and (S)-3 $\mathbf{g}$  (entries 3-7, Table 45). As the reaction of rac-1 $\mathbf{a}$  in ACN with (S)-3 $\mathbf{c}$  afforded 2 $\mathbf{a}$  in higher yield than with (S)-3 $\mathbf{g}$ , we selected the former as the catalyst for our target.

Figure 133. Bis-urea tested as catalyst in the enantioselective fluorination of rac-1a

Table 45. Urea catalyst optimisation.

urea catalyst (10 mol%) PPh<sub>4</sub>I (10 mol%) KF (5 equiv)

Br	Br	ACN (0.25 M)	→ Br	Ē
	rac-1a	25°C, 18 h, 1200 rpm	(S)-	-2a
Entry	Catalyst	2a (%) <sup>a</sup>	1a (%)	e.r <sup>b</sup>
1	(S)-3a	28	72	71:29 ref
2	(S)-3b	24	76	77:23
3	(S)-3c	44	56	92:8
4	( <i>S</i> )-d	55	45	70:30
5	(S)-3e	19	81	87:13
6	(S)-3f	26	74	86:14
7	(S)-3g	30	70	93:7

<sup>&</sup>lt;sup>a</sup>Yield determined by <sup>19</sup>F NMR using 4-fluoroanisole as internal standard, <sup>b</sup>e.r. was determined by HPLC analysis using a chiral stationary phase.

Based on the previous results, the effect of different onium salts in promoting the formation of **2a** was investigated (Figure 134). Compared to the reference, an increase in **2a** yield was observed in the presence of tetraethylammonium iodide (entry 1 vs entry 5, Table 46). We also showed that no significant (mis)matching effect was observed when using an enantiomer of a chiral ammonium salt (Maruoka phase transfer catalysts)

(entries 7-8, Table 46). In addition, we demonstrated that in acetonitrile with (S)-3 $\mathbf{c}$ , and  $Et_4N^+I^-$  as co-catalyst, the selectivity for substitution over elimination and the rate of substrate racemisation exceeds the rate of fluorination (see *Experimental Section, Paragraph 4.4.5*).

Figure 134. Phosphonium and ammonium salt tested as co-catalyst with (*S*)-3c in the enantioselective fluorination of *rac*-1a.

Table 46. Onium salt optimisation.

Entry	Onium salt	T (°C)	2a (%)ª	1a (%)	e.r <sup>b</sup>
1	а	25	44	56	92:8 ref
2	b	25	42	58	92:8
3	С	25	39	61	91:9
4	d	25	36	64	91:9
5	е	25	60	40	92:8
6	е	60	100	0	86:14
7	f	60	100	100	86:14
8	g	60	100	0	86:14

 $<sup>^{</sup>a}$ Yield determined by  $^{19}$ F NMR using 4-fluoroanisole as internal standard,  $^{b}$ e.r. was determined by HPLC analysis using a chiral stationary phase.

Further optimisation of the reaction conditions was required to achieve higher yields and enantiomeric ratios. We found that increasing the time allowed us to improve the yield without negatively affecting the e.r. (entry 2, Table 47). Performing the reaction at 0°C was advantageous in terms of enantioselectivity (96:4 e.r.), but we obtained **2a** in 5% yield (entry 3, Table 47). Finally, the reaction at 5°C in ACN (0.5 M) gave **2a** in good yield (73%) and high enantioselectivity (95:5 e.r.) (entry 5, Table 47).

Table 47. Conditions optimisation.

entry	mmol/ml	T (°C)	Time (h)	2a (%) <sup>a</sup>	1a (%)	e.r. <sup>b</sup>
1	0.25 M	25	18	60	40	92:8 ref
2	0.25 M	25	63	91	9	92:8
3	0.25 M	0	63	5	95	96:4
4	0.25 M	5	96	43	57	95:5
5	0.5 M	5	96	73	27	95:5
6	0.125 M	5	63	22	78	95:5

 $^{a}$ Yield determined by  $^{19}$ F NMR using 4-fluoroanisole as internal standard,  $^{b}$ e.r. was determined by HPLC analysis using a chiral stationary phase.

With the optimal reaction conditions established, the scope of the reaction was investigated (Scheme 19). Variation of the electronic substitution in the para position of the phenyl ring affected the reactivity compared to the model reaction (rac-1a into 2a). Substrates bearing electron withdrawing groups (EWG) underwent fluorination with higher yields (2b-2d), while reactivity and enantioselectivity were maintained when chloride and fluoride were in the para position instead of bromide (2e-2f). The reaction of substrates with electron donating groups (EDG) or without any functional group, was carried out at 25°C to obtain high yields and good e.r. (2g-2i). The elongation of the alkyl chain further emphasised the selectivity for substitution over elimination, as no side product formation was observed (2j). Fluorination of  $\alpha$ -bromoketones bearing a thiophene motif was also carried out, giving products 2k and 2l in a good yield and enantiomeric ratio. Ketones containing a naphthalene ring (2m-2o) were fluorinated with great yield (>93%) and high enantioselectivity at 25°C (up to 98:2 e.r.). Finally, 2p, which is a starting reagent for bioactive molecules (e.g. Azaperone), was synthesised in a good yield and e.r.

Scheme 19. Substrate Scope.

<sup>a</sup>Performed at 25°C, <sup>b</sup>Performed at 40°C

With these conditions in hand, we also tried to apply this strategy to the synthesis of  $\alpha$ -fluorinated amides and esters, but without success due to their lower reactivity compared to the ketones (Scheme 20). There is a need to further investigate the applicability of S-HBPTC to these carbonyl compounds.

Scheme 20. Failed substrates.

# 4.3. Conclusion

The catalytic enantioselective nucleophilic fluorination of racemic  $\alpha$ -bromoketones via S-HBPTC has been reported for the first time and is based on the use of KF as the fluoride source instead of expensive reagents.

The new catalytic strategy relies on a *bis*-urea catalyst and an onium salt cocatalyst working together as a solid-liquid phase transfer to enable enantioselective nucleophilic fluorination with a metal fluoride insoluble in organic media. The nature of both catalyst and co-catalyst, as well as the type of solvent, must be adapted to the specific requirements of different electrophiles. The reaction takes place under mild conditions and with KF, which is an ideal fluoride source in terms of safety, availability and cost. In addition, the method is easy to use as it can be performed in an open vessel and there is no need for dry solvents or pre-treatment of the KF.

This study has shown that Synergistic HB-PTC, previously applied to racemic benzylic bromides, can be extended to other neutral electrophiles, such as  $\alpha$ -bromoketones, to synthesise molecules of high medicinal chemistry interest.

### Acknowledgment:

This work was developed at the University of Oxford in Professor Véronique Gouverneur's group.

I would like to thank Véronique for accepting me into her wonderful group for six months and for her support, and Claire Dooley for working with me very hard.

### Published work:

The full version can be found in "C. Dooley, F. Ibba, B. B. Botlik, **C. Palladino**, C. A. Goult, Y. Gao, A. Lister, R. S. Paton, G. C. Lloyd-Jones, V. Gouverneur, *Nature Catalysis 8*, 107–115 (2025)"

# 4.4. Experimental Section

### 4.4.1. General Information

Unless stated reagents were purchased from commercial suppliers and used without further purification. Unless stated solvents were used without drying or degassing, all reactions that required anhydrous conditions were performed in flamed-dried glassware under an inert atmosphere of nitrogen and solvents from stills were used. CsF (99.9% trace metal basis from Sigma-Aldrich) was ground prior to reactions and used without pre-drying. KF (99.99% trace metal basis from Alfa Aesar) was ground prior to reactions and used without pre-drying. Reactions were monitored by thin layer chromatography (TLC) supplied by Merck (Kieselgel 60 F<sub>254</sub> plates). Visualisation of reaction on TLC was accomplished by irradiation with UV light at 254 nm and/or cerium ammonium molybdate (CAM) stain and/or permanganate stain. Flash column chromatography (FCC) was performed on Merck silica gel (60, particle size 0.040-0.062 mm). Optical rotations were measured on an Autopol L 2000 (Schmidt-Haensh) at 589 nm, 25 °C. Data

are reported as  $[\alpha]^D$  25 °C concentration (c in g/100 mL), and solvent. High resolution mass spectra (HRMS, m/z) were recorded on a Thermo Exactive mass spectrometer equipped with Waters Acquity liquid chromatography system using the heated electrospray (HESI-II) probe for positive electrospray ionization (ESI+) or atmospheric pressure chemical ionization (APCI) or on an Agilent 7200 Q-TOF spectrometer equipped with a direct insertion probe supplied by Scientific Instrument Manufacturer (SIM) GmbH using electron ionization (EI - 20eV). Some compounds were found to be unstable under a variety of MS ionization methods (CI, EI, ESI, GC-MS) and therefore no HRMS could be obtained for them; this is stated for the relevant compounds. Infrared spectra were recorder as the neat compound or in liquid solution using a Bruker tensor 27 FT-IR spectrometer, absorptions are reported in wavenumber (cm<sup>-1</sup>) Melting points of solids were measured on a Griffin apparatus and are uncorrected. All enantiomeric ratios (e.r.) were determined by HPLC analysis on a Shimadzu i-Prominence LC-2030 (PDA detector), employing a chiral stationary phase, post purification and compared to traces of the racemic mixtures, which were independently prepared. All NMR spectra were recorded on Bruker AVIIIHD 400, AVIIIHD 500, AVII 500 or AVIII HD 600. Deuterated solvents were purchased from Sigma-Aldrich and used without purification. NMR spectra are recorded at 298 K, unless otherwise specified. NMR spectra are referenced to the residual solvent peak for <sup>1</sup>H and <sup>13</sup>C spectra, while <sup>19</sup>F NMR spectra are referenced relative to CFCl<sub>3</sub> in CDCl<sub>3</sub>. Coupling constants, J, are reported in Hz to the nearest 0.1 Hz. Unless otherwise stated, <sup>13</sup>C spectra are <sup>1</sup>H decoupled. The following abbreviations are used to describe peak multiplicities: s = singlet, d = doublet, t = triplet, q= quartet, sext = sextet, sept = septet, m = multiplet). Determination of absolute stereochemistry by comparison of the optical rotation value and chromatographic data for compound 2a with reported literature values.[301]

### 4.4.2. Optimisation of reaction conditions

### a) Screening of the Solvent

General procedure: In a 1.75 mL screw-capped vial equipped with a magnetic stirring bar were added, 2-bromo-1-(4-bromophenyl)propan-1-one *rac-***1a** (14.5 mg, 0.05 mmol, 1 equiv), pre-ground potassium fluoride (14.5 mg, 5 equiv.), (*S*)-**3a** (4.2 mg, 0.005 mmol, 0.1 equiv.), PPh<sub>4</sub>+I- (2.3 mg, 0.005 mmol, 0.1 equiv) and the selected solvent (0.25 M). The vial was sealed, and the reaction was stirred at 1200 rpm for 18 h at 25°C. The crude reaction was filtered over celite and the solvent removed under reduced pressure. Samples were dissolved in CDCl<sub>3</sub> and analysed by <sup>1</sup>H and <sup>19</sup>F NMR using 4-fluoroanisole as an internal standard. e.r. was determined by HPLC analysis using a chiral stationary phase (see Table 44).

# b) Screening of the bis-urea catalyst

General procedure: In a 1.75 mL screw-capped vial equipped with a magnetic stirring bar were added, 2-bromo-1-(4-bromophenyl)propan-1-one (14.5 mg, 0.05 mmol, 1 equiv,), pre-ground potassium fluoride (14.5 mg, 5 equiv.), the selected urea catalyst (0.005 mmol, 0.1 equiv PPh<sub>4</sub>+I- (2.3 mg, 0.005 mmol, 0.1 equiv), and ACN (0.25 M). The vial was sealed, and reaction was stirred at 1200 rpm for 18 h at 25°C. The crude reaction was filtered over celite and the solvent removed under reduced pressure. Samples were dissolved in CDCl<sub>3</sub> and analysed by <sup>1</sup>H and <sup>19</sup>F NMR using 4-fluoroanisole as an internal standard. e.r. was determined by HPLC analysis using a chiral stationary phase. (see Figure 133, Table 45). Urea catalysts have already been synthesised by the group in accordance with the procedure in the literature<sup>[294,296,302]</sup>.

### c) Screening of the onium salt

General procedure: In a 1.75 mL screw-capped vial equipped with a magnetic stirring bar were added, 2-bromo-1-(4-bromophenyl)propan-1-one (14.5 mg, 0.05 mmol, 1 equiv,), pre-ground potassium fluoride (14.5 mg, 5 equiv.), (*S*)-3c (7 mg, 0.005 mmol, 0.1 equiv.), the selected co-catalyst (0.005 mmol, 0.1 equiv) and ACN (0.25 M). The vial was sealed, and reaction was stirred at 1200 rpm for 18 h at 25°C or 60°C. The crude reaction was filtered over celite and the solvent removed under reduced pressure. Samples were dissolved in CDCl<sub>3</sub> and analysed by ¹H and ¹9F NMR using 4-fluoroanisole as an internal standard. e.r. was determined by HPLC analysis using a chiral stationary phase (see Figure 134, Table 46).

## 4.4.3. Control experiments

In a 1.75 mL screw-capped vial equipped with a magnetic stirring bar were added, 2-bromo-1-(4-bromophenyl)propan-1-one (14.5 mg, 0.05 mmol, 1 equiv,), pre-ground potassium or cesium fluoride (5 equiv.), (S)-3c (7 mg, 0.005 mmol, 0.1 equiv.) if present, Et<sub>4</sub>N+I- (1.3 mg, 0.005 mmol, 0.1 equiv) if present and ACN (0.25 M). The vial was sealed, and reaction was stirred at 1200 rpm at 25°C or 60°C for 18h. The crude reaction was filtered over celite and the solvent removed under reduced pressure. Samples were

dissolved in CDCl<sub>3</sub> and analysed by <sup>1</sup>H and <sup>19</sup>F NMR using 4-fluoroanisole as an internal standard. e.r. was determined by HPLC analysis using a chiral stationary phase.

Table 48.	Control	experiments.

Entry	T (°C)	Urea (mol%)	MF	NEt <sub>4</sub> +I-	2a(%) <sup>a</sup>	1a (%)	e.r. <sup>b</sup>
1	25	10	KF	10	60	40	92:8
2	25	0	KF	0	0	100	nd
3	25	10	KF	0	30	70	92:8
4	25	0	KF	10	5	95	55:45
5	60	10	KF	10	100	0	86:14
6	60	10	KF	0	100	0	86:14
7	60	0	KF	10	48	52	50:50
8	25	10	CsF	0	100	1	50:50
9	25	0	CsF	0	50	50	50:50

<sup>&</sup>lt;sup>a</sup>Yield determined by <sup>19</sup>F NMR using 4-fluoroanisole as internal standard, <sup>b</sup>e.r. was determined by HPLC analysis using a chiral stationary phase.

# 4.4.4. Time course experiments

Table 49. Time course experiments.

Entry	Time (h)	2a ee <sup>b</sup>	2a yield (%) <sup>a</sup>	1a ee <sup>b</sup>
1	1	84	6.1	0
2	2	86	9.5	1
3	4	83	15	4
4	6	84	18.8	4
5	8	83	25.7	6
6	24	84	65.2	12

General conditions: **1a** (0.05 mmol), (*S*)-**3c** (10 mol%), Et<sub>4</sub>N<sup>+</sup>I<sup>-</sup> and KF (5 equiv.) in 200  $\mu$ L of ACN stirred at 1200 rpm <sup>a</sup>Determined by <sup>1</sup>H and/or <sup>19</sup>F NMR using 4-fluoroanisole as internal standard, <sup>b</sup>e.e. was determined by HPLC analysis using a chiral stationary phase.

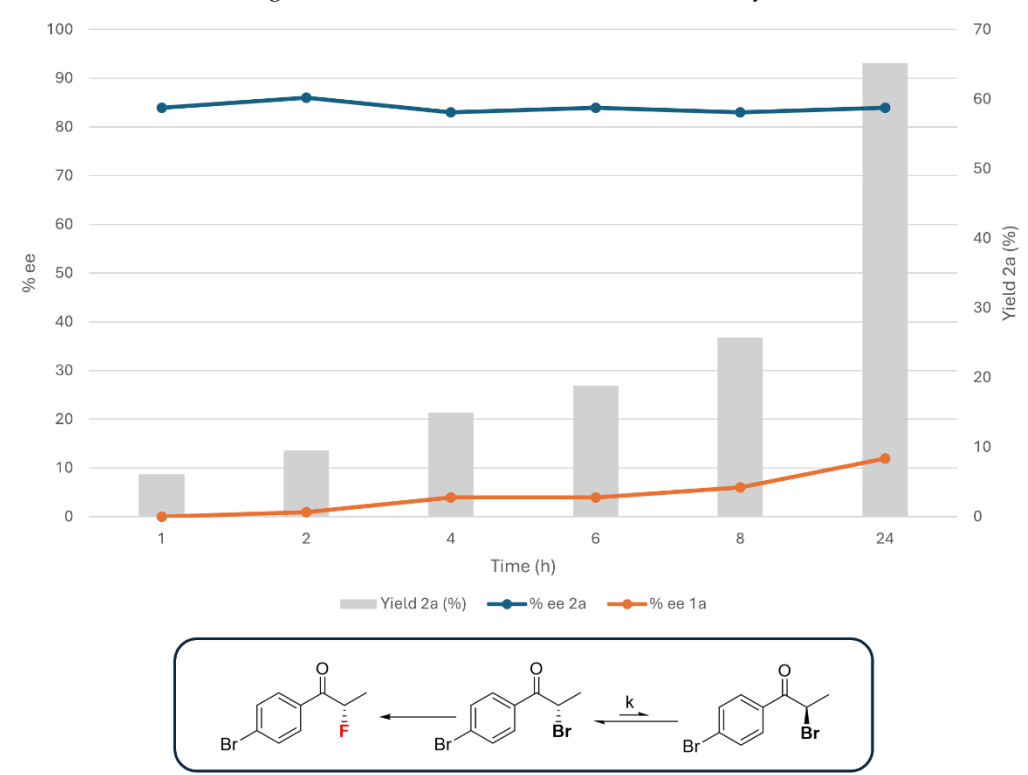


Chart 1. Monitoring of the enantiomeric excess of 1a and 2a and yield of 2a over time.

# 4.4.5. Substrate synthesis and Characterisation

### General Procedure A

$$\begin{array}{c|c}
O & Br_2 & O \\
R_1 & DCM, rt & R_1 & Br
\end{array}$$

According to the procedure described in the literature<sup>[303]</sup>, bromine (2.5 mmol, 1 equiv) was added dropwise under inert atmosphere to a solution of ketone (1 equiv) in dry DCM (0.1 M) at  $0^{\circ}$ C. The solution was stirred at room temperature for 18 h and then a saturated aqueous solution of Na<sub>2</sub>S<sub>2</sub>O<sub>3</sub> was slowly added.

The aqueous layer was extracted with DCM ( $20 \, \text{mL} \, \text{x} \, 3$ ), the collected organic layers were dried over anhydrous Na<sub>2</sub>SO<sub>4</sub> and concentrated under reduced pressure. Finally, the crude was purified by FCC.

Ketones precursors *rac-***1a** (CAS: 2114-00-3), *rac-***1e** (CAS: 345-94-8), *rac-***1f** (CAS: 877-37-2), *rac-***1g** (CAS: 100679-76-3), *rac-***1h** (CAS: 1451-82-7), *rac-***1i** (CAS 21086-33-9) were commercially available.

# 2-bromo-1-(4-nitrophenyl)propan-1-one (rac-1b)

The compound *rac-***1b** was prepared according to the general procedure A. The product was isolated by FCC (eluent: pentane/DCM, 60/40) as a yellow solid in 86% yield.

 $^{1}$ H NMR (400 MHz, CDCl<sub>3</sub>)  $\delta$  = 8.37 – 8.29 (m, 2H), 8.22 – 8.14 (m, 2H), 5.26 (q, J = 6.6 Hz, 1H), 1.94 (d, J = 6.6 Hz, 3H).8.35-8.31 (m,

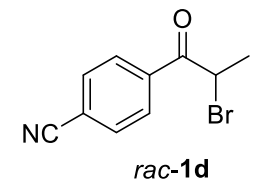
2H);  ${}^{13}$ C NMR (101 MHz, CDCl<sub>3</sub>)  $\delta$  = 191.66, 150.52, 138.79, 130.00, 123.90, 41.41, 19.77; HRMS (EI) m/z calculated for C<sub>16</sub>H<sub>16</sub>BrO (M)<sup>+</sup> 303.0379, found 303.0377.

## 2-bromo-1-(4-(trifluoromethyl)phenyl)propan-1-one (rac-1c)

The compound *rac-***1c** was prepared according to the general procedure A. The product was isolated by FCC (eluent: pentane/DCM, 70/30) as a white solid in 91% yield. Spectroscopic data are in accordance with those in literature<sup>[304]</sup>.

rac-1c  $^{1}$ H NMR (400 MHz, CDCl<sub>3</sub>) δ = 8.17-8.09 (m, 2H), 7.79 – 7.72 (m, 2H), 5.26 (q, J = 6.6 Hz, 1H), 1.93 (d, J = 6.6 Hz, 3H);  $^{19}$ F NMR (376 MHz, CDCl<sub>3</sub>) δ= -63.24;  $^{13}$ C NMR (101 MHz, CDCl<sub>3</sub>) δ = 192.28, 136.88, 134.87 (q, J=32.8 Hz) 129.29, 125.80 (q J = 3.7 Hz), 123.47, (q, J = 272.8 Hz), 41.34, 19.87.

## 4-(2-bromopropanoyl)benzonitrile (rac-1d)

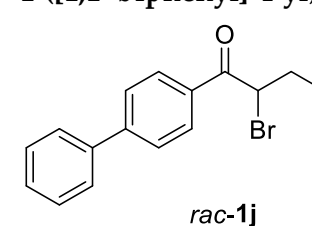


The compound *rac-***1d** was prepared according to the general procedure A. The product was isolated by FCC (eluent: Pentane/DCM, 60/40) as a white solid in 85% yield.

 $^{1}$ H NMR (400 MHz, CDCl<sub>3</sub>)  $\delta$  = 8.15 – 8.08 (m, 2H), 7.81 – 7.78 (m, 2H), 5.23 (q, J = 6.6 Hz, 1H), 1.92 (dd, J = 6.5, 1.7 Hz, 3H);  $^{13}$ C NMR

 $(101 \text{ MHz}, \text{CDCl}_3) \delta = 191.86, 137.25, 132.54, 129.35, 117.76, 116.85, 41.20, 19.78.$ 

### 1-([1,1'-biphenyl]-4-yl)-2-bromobutan-1-one (*rac*-1j)



The compound *rac-***1j** was prepared according to the general procedure A. The product was isolated by FCC (eluent: Pentane/DCM, 80/20) as a pale-yellow solid in 87% yield.

<sup>1</sup>H NMR (400 MHz, CDCl<sub>3</sub>)  $\delta$  = 8.12 – 8.09 (m, 2H), 7.73 – 7.70 (m, 2H), 7.65 – 7.62 (m, 2H), 7.51 – 7.39 (m, 2H), 7.48 – 7.37 (m,

1H), 5.11 (dd, J = 7.7, 6.4 Hz, 1H), 2.34 – 2.12 (m, 2H), 1.11 (t, J = 7.3 Hz, 3H);  $^{13}$ C NMR (101 MHz, CDCl<sub>3</sub>)  $\delta$ = 192.82, 146.39, 139.69, 133.19, 129.48, 129.01, 128.42, 127.42, 127.31, 49.15, 26.96, 12.24.; HRMS (EI) m/z calculated for C<sub>16</sub>H<sub>16</sub>BrO (M)<sup>+</sup> 303.0379, found 303.0377.

# 2-bromo-1-(thiophen-2-yl)propan-1-one (rac-1k)

The compound *rac-***1k** was prepared according to the general procedure A. The product was obtained as a brownish solid without further purification (y=97%). Spectroscopic data are in accordance with those in literature[305].

rac-1k <sup>1</sup>H NMR (400 MHz, CDCl<sub>3</sub>) 7.84 (dd, J = 3.8, 1.1 Hz, 1H), 7.70 (dd, J = 4.9, 1.1 Hz, 1H), 7.16 (dd, J = 4.9, 3.9 Hz, 1H), 5.14 (q, J = 6.7 Hz, 1H), 1.90 (d, J = 6.7 Hz, 3H); <sup>13</sup>C NMR (101 MHz, CDCl3)  $\delta$ = 186.84, 140.90, 134.89, 133.09, 128.31, 42.45, 20.36; HRMS (EI) m/z calculated for C<sub>7</sub>H<sub>8</sub>BrOS (M)<sup>+</sup> 218.9474, found 218.9473.

# 2-bromo-1-(6-(dimethylamino)naphthalen-2-yl)propan-1-one (rac-1m)

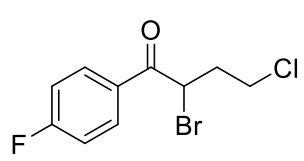
rac-1m

The compound *rac-***1m** was prepared according to the general procedure A. The product was isolated by FCC (eluent: Pentane/Et<sub>2</sub>O, 90/10) as a yellow solid in 78% yield.

<sup>1</sup>H NMR (400 MHz, CDCl<sub>3</sub>)  $\delta$  = 8.47 (d, J = 1.9 Hz, 1H), 8.35 (d, J = 9.0 Hz, 1H), 8.10 (dd, J = 9.0, 1.8 Hz, 1H), 7.90 (d, J = 8.8 Hz,

1H), 7.47 (d, J = 23.2 Hz, 1H), 5.43 (q, J = 6.6 Hz, 1H), 3.00 (s, 6H), 1.96 (d, J = 6.6 Hz, 3H); <sup>13</sup>C NMR (101 MHz, CDCl<sub>3</sub>)  $\delta$  = 191.79, 135.06, 129.63, 129.19, 126.46, 124.99, 119.99, 114.77, 43.28, 42.75, 40.57, 19.17.

### 2-bromo-4-chloro-1-(4-fluorophenyl)butan-1-one (rac-1p)



rac-1p

The compound rac-1p was prepared according to the general procedure A. The product was isolated by FCC (eluent: Pentane/DCM, 90/10) as a white solid in 73% yield.

<sup>1</sup>H NMR (400 MHz, CDCl<sub>3</sub>) 8.12 - 8.03 (m, 2H), 7.23 - 7.13 (m, 2H), 5.43 (dd, J = 8.1, 5.8 Hz, 1H), 3.88 - 3.71 (m, 2H), 2.65 - 2.48

(m, 2H); <sup>19</sup>F NMR (376 MHz, CDCl<sub>3</sub>)  $\delta$ = -103.16 – -103.24 (m); <sup>13</sup>C NMR (101 MHz, CDCl<sub>3</sub>)  $\delta = 190.96$ , 166.20 (d, J = 256.8 Hz), 131.77 (d, J = 9.5 Hz), 130.38 (d, J = 3.0 Hz), 116.11 (d, I = 22.0 Hz), 43.50, 42.35, 35.65.

### General Procedure B

1B) Following the procedure described in the literature [306], the aldehyde (2.5 mmol, 1 equiv) was dissolved in dry THF (0.1 M) under an inert atmosphere, followed by the Grignard addition at -10°C. The reaction was stirred at room temperature and monitored by TLC. When the aldehyde was fully consumed, the reaction was quenched with saturated NH $_4$ Cl solution. The aqueous layer was extracted with Et $_2$ O (15 mL x 3) and the collected organic phase was washed with brine and dried with MgSO $_4$ . The solvent was removed under vacuum.

2B) To obtain the desired  $\alpha$ -bromo ketone, the corresponding alcohol synthesised in the previous step, was dissolved in 1,4-dioxane (0.125 M). NBS (2 equiv) was added and the reaction was stirred at 60°C. The reaction was monitored by TLC and quenched with a slowly added saturated aqueous solution of Na<sub>2</sub>S<sub>2</sub>O<sub>3</sub>.

The aqueous layer was extracted with  $Et_2O$  (15 mL x 3), the collected organic layers were washed with brine and dried with MgSO<sub>4</sub>. The solvent was removed under vacuum and the crude was purified by FCC.

## 1-(5-phenylthiophen-2-yl)propan-1-ol (rac-4l)

SOH

rac-4I

The compound *rac-***41** was prepared according to the procedure 1B as a pale-yellow solid.

 $^{1}$ H NMR (600 MHz, CDCl<sub>3</sub>)  $\delta$  = 7.55 – 7.43 (m, 2H), 7.34 – 7.23 (m, 2H), 7.20 – 7.14 (m, 1H), 7.08 (d, J = 3.6 Hz, 1H), 6.85 (dd, J = 3.6, 0.7 Hz, 1H), 4.74 (t, J = 6.6 Hz, 1H), 2.05 (bs, 1H), 1.92 – 1.73 (m,

2H), 0.92 (t, J = 7.4 Hz, 3H);  $^{13}$ C NMR (151 MHz, CDCl<sub>3</sub>)  $\delta$  = 147.00, 142.42, 133.40, 127.84, 126.40, 124.65, 123.74, 121.48, 70.92, 31.06, 9.13.

# 1-(4-fluoronaphthalen-1-yl)propan-1-ol (rac-4n)

но

rac-4n

The compound *rac-***4n** was prepared according to the procedure 1B as a white solid.

<sup>1</sup>H NMR (600 MHz, CDCl<sub>3</sub>)  $\delta$  = 8.16 – 8.13 (m, 2H), 7.59 – 7.54 (m, 3H), 7.13 (dd, J = 10.2, 8.0 Hz, 1H), 5.35 (dd, J = 7.6, 5.1 Hz, 1H), 2.04 – 1.89 (m, 2H), 1.02 (t, J = 7.4 Hz, 3H); <sup>19</sup>F NMR (565 MHz, CDCl<sub>3</sub>)  $\delta$  = -124 (m); <sup>13</sup>C NMR (151 MHz, CDCl<sub>3</sub>)  $\delta$  = 157.27 (d, J = 251.5 Hz), 134.99 (d, J = 4.4 Hz), 130.80 (d, J = 4.4 Hz), 125.85, 124.81 (d, J = 2.8 Hz), 122.89 (d, J = 16.0 Hz), 122.27 (d,

J = 2.8 Hz), 121.94 (d, J = 8.3 Hz), 120.27 (d, J = 6.1 Hz), 107.72 (d, J = 19.8 Hz), 71.32, 30.11, 9.46.

### 1-(naphthalen-1-yl)propan-1-ol (rac-4o)

но

rac-**4o** 

The compound *rac-***4o** was prepared according to the procedure 1B as a colourless oil. Spectroscopic data are in accordance with those in literature<sup>[307]</sup>.

<sup>1</sup>H NMR (400 MHz, CDCl<sub>3</sub>)  $\delta$  = 8.17 – 8.08 (m, 1H), 7.93 – 7.84 (m, 1H), 7.79 (dt, J = 8.2, 1.1 Hz, 1H), 7.64 (dt, J = 7.1, 1.0 Hz, 1H), 7.57 – 7.43 (m, 3H), 5.40 (td, J = 6.0, 2.1 Hz, 1H), 2.05 – 2.02 (m, 1H), 2.03 – 1.87 (m, 2H), 1.04 (t, J = 7.4

Hz, 3H);  $^{13}$ C NMR (101 MHz, CDCl3)  $\delta$  = 140.4, 134.0, 130.6, 129.0, 128.0, 126.1, 125.6, 125.5, 123.4, 123.0, 72.7, 31.2, 10.7.

# 2-bromo-1-(5-phenylthiophen-2-yl)propan-1-one (rac-1l)

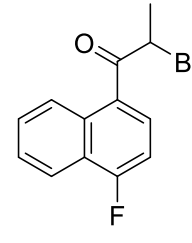
rac-1I

The compound *rac-***1l** was prepared according to the procedure 2B from *rac-***4l**. The product was isolated by FCC (eluent: Pentane/DCM, 70/30) as a yellow solid in 71% yield.

 $^{1}$ H NMR (400 MHz, CDCl<sub>3</sub>)  $\delta$  = 7.81 (d, J = 4.0 Hz, 1H), 7.69 – 7.63 (m, 2H), 7.48 – 7.36 (m, 3H), 7.35 (d, J = 4.1 Hz, 1H), 5.15 (q, J =

6.7 Hz, 1H), 1.91 (d, J = 6.7 Hz, 3H);  $^{13}$ C NMR (101 MHz, CDCl<sub>3</sub>)  $\delta$  = 186.62, 154.01; HRMS (EI) m/z calculated for C<sub>13</sub>H<sub>12</sub>BrOS (M)<sup>+</sup> 294.9787, found 294.9785.

### 2-bromo-1-(4-fluoronaphthalen-1-yl)propan-1-one (rac-1n)



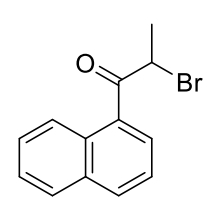
rac-1n

The compound *rac-***1n** was prepared according to the procedure 2B from *rac-***4n**. The product was isolated by FCC (eluent: Pentane/DCM, 70/30) as a white solid in 86% yield.

 $^{1}$ H NMR (600 MHz, CDCl<sub>3</sub>) δ = 8.58 (m, 1H), 8.21 – 8.15 (m, 1H), 7.91 (dd, J = 8.1, 5.2 Hz, 1H), 7.69 (ddd, J = 8.5, 6.8, 1.4 Hz, 1H), 7.63 (ddd, J = 8.1, 6.8, 1.1 Hz, 1H), 7.17 (dd, J = 9.7, 8.1 Hz, 1H), 5.36 (q, J = 6.6 Hz, 1H), 1.97 (d, J = 6.6 Hz, 3H);  $^{19}$ F NMR (565 MHz, CDCl<sub>3</sub>) δ = - 131.46

(m);  $^{13}$ C NMR (151 MHz, CDCl<sub>3</sub>)  $\delta$  = 195.34, 161.46 (d, J = 260.7 Hz), 133.08 (d, J = 5.5 Hz), 129.62 (d, J = 4.5 Hz), 129.28, 128.09 (d, J = 10.0 Hz), 127.11 (d, J = 2.2 Hz), 125.89 (d, J = 2.7 Hz), 124.25 (d, J = 15.9 Hz), 120.87 (d, J = 6.3 Hz), 108.13 (d, J = 21.3 Hz), 45.04, 20.51; HRMS (EI) m/z calculated for  $C_{13}H_{11}BrFO$  (M)+ 280.9972, found 280.9969.

### 2-bromo-1-(naphthalen-1-yl)propan-1-one (rac-1o)



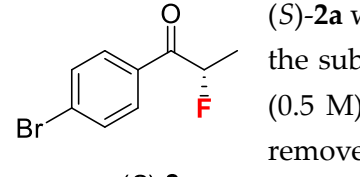
The compound *rac-***1o** was prepared according to the procedure 2B from *rac-***4o**. The product was isolated by FCC (eluent: Pentane/DCM, 80/20) as a white solid in 84% yield. Spectroscopic data are in accordance with those in literature<sup>[308]</sup>

<sup>1</sup>H NMR (400 MHz, CDCl<sub>3</sub>)  $\delta$  = 8.44 (dq, J = 8.6, 0.9 Hz, 1H), 8.02 (dt, J rac-1o = 8.2, 1.1 Hz, 1H), 7.93 – 7.83 (m, 2H), 7.67 – 7.46 (m, 3H), 5.37 (q, J = 6.7 Hz, 1H), 1.98 (d, J = 6.7 Hz, 3H); <sup>13</sup>C NMR (101 MHz, CDCl<sub>3</sub>)  $\delta$  = 196.68, 133.95, 133.84, 133.16, 130.90, 128.47, 128.16, 126.73, 126.68, 125.64, 124.21, 45.59, 20.51; HRMS (EI) m/z calculated for C<sub>13</sub>H<sub>12</sub>BrO (M)<sup>+</sup> 263.0066, found 263.0065.

# 4.4.6. General procedure for enantioselective fluorination and Characterisation

The selected substrate (0.4 mmol, 1 equiv), pre-ground potassium fluoride (116 mg, 2 mmol, 5 equiv), (S)-3c (56 mg, 0.04 mmol, 0.1 equiv), Et<sub>4</sub>N<sup>+</sup>I<sup>-</sup> (11 mg, 0.04 mmol, 0.1 equiv) and ACN (0.25-0.5 M) were added sequentially to a 7 mL screw-capped vial equipped with a magnetic stirring rod. The vial was sealed, and the reaction was stirred at 1200 rpm at the appropriate temperature for 96 h. The crude reaction was filtered over celite, solvent removed under reduced pressure and purified by FCC to give the product.

# (S)-1-(4-bromophenyl)-2-fluoropropan-1-one (2a)



(S)-**2a** 

highly volatile).

(*S*)-**2a** was prepared according to the *General Procedure* starting from the substrate *rac*-**1a** (117 mg). The reaction was let stirring in ACN (0.5 M) at 5°C at 1200 rpm for 96 h. After filtration over celite to remove KF, the product was isolated by FCC (eluent: Pentane/DCM, 70/30) as a colourless oil in 65% yield, 60 mg, 95:5 e.r. (the product is

<sup>1</sup>H NMR (600 MHz, CDCl<sub>3</sub>)  $\delta$  = 7.90 – 7.82 (m, 2H), 7.67 – 7.60 (m, 2H), 5.62 (dq, J = 48.5, 6.8 Hz, 1H), 1.66 (dd, J = 24.1, 6.8 Hz, 3H); <sup>19</sup>F NMR (565 MHz, CDCl<sub>3</sub>)  $\delta$  = -180.50 (m); <sup>13</sup>C NMR (151 MHz, CDCl<sub>3</sub>)  $\delta$  = 196.3 (d,  $J_{\text{C-F}}$  = 20.4 Hz), 132.9 (d,  $J_{\text{C-F}}$  = 2.2 Hz), 132.2, 130.7 (d,  $J_{\text{C-F}}$  = 5.0 Hz), 129.3, 90.8 (d,  $J_{\text{C-F}}$  = 180.5 Hz), 18.3 (d,  $J_{\text{C-F}}$  = 22.6 Hz);

HRMS (EI) m/z calculated for  $C_9H_9BrFO$  (M)<sup>+</sup> 230.9815, found 230.9815; HPLC separation: DAICEL CHIRALPAK® ID-3, Heptane: IPA = 99.2:0.8 mL/min;  $t_1$  = 5.0 (major),  $t_2$ = 25.4 (minor).

### (S)-2-fluoro-1-(4-nitrophenyl)propan-1-one (2b)



(*S*)-**2b** was prepared according to the *General Procedure* starting from the substrate *rac*-**1b** (103 mg). The reaction was let stirring in ACN (0.5M) at 5°C at 1200 rpm for 96 h. After filtration over celite to remove KF, the product was isolated by FCC (eluent: Pentane/DCM,

70/30) as a yellow solid in 91% yield, 72 mg, 91:9 e.r.

<sup>1</sup>H NMR (600 MHz, CDCl<sub>3</sub>) δ = 8.36 – 8.31 (m, 2H), 8.19 – 8.14 (m, 2H), 5.64 (dq, J = 48.3, 6.8 Hz, 1H), 1.70 (dd, J = 24.1, 6.8 Hz, 3H); <sup>19</sup>F NMR (565 MHz, CDCl<sub>3</sub>) δ = - 181.73 (m); <sup>13</sup>C NMR (151 MHz, CDCl<sub>3</sub>) δ = 195.98 (d, J = 21.6 Hz), 150.55, 138.68 (d, J = 2.2 Hz), 130.26 (d, J = 5.0 Hz), 123.82, 91.03 (d, J = 180.9 Hz), 17.90 (d, J = 22.5 Hz); HPLC separation: DAICEL CHIRALPAK® ID-3, Heptane: IPA = 99.2:0.8 mL/min; t<sub>1</sub> = 15.7(major), t<sub>2</sub>= 22.8 (minor).

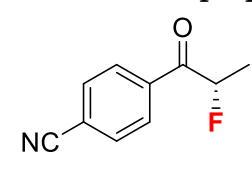
# (S)-2-fluoro-1-(4-(trifluoromethyl)phenyl)propan-1-one (2c)

(S)-2c

(*S*)-**2c** was prepared according to the *General Procedure* starting from the substrate *rac*-**1c** (112 mg). The reaction was let stirring in ACN (0.5 M) at 5°C at 1200 rpm for 96 h. After filtration over celite to remove KF, the product was isolated by FCC (eluent: Pentane/DCM, 70/30) as a white solid in 78% yield, 69 mg, 92:8 e.r.

<sup>1</sup>H NMR (600 MHz, CDCl<sub>3</sub>) δ = 8.10 (m, 2H), 7.79 – 7.72 (m, 2H), 5.66 (dq, J = 48.4, 6.8 Hz, 1H), 1.68 (dd, J = 24.1, 6.8 Hz, 3H); <sup>19</sup>F NMR (565 MHz, CDCl<sub>3</sub>) δ = -63.32 (s), -180.72,(m); <sup>13</sup>C NMR (151 MHz, CDCl<sub>3</sub>) δ = 196.32 (d, J = 20.9 Hz), 136.81, 134.92 (q, J = 32.8 Hz), 129.46 (d, J = 4.4 Hz), 125.72 (q, J = 3.9 Hz), 123.45 (q, J = 272.7 Hz), 90.77 (d, J = 180.6 Hz), 18.02 (d, J = 22.4 Hz); HPLC separation: DAICEL CHIRALPAK® ID-3, Heptane: IPA = 99.5:0.5 mL/min; t<sub>1</sub> = 4.0 (major), t<sub>2</sub> = 4.6 (minor).

# (S)-4-(2-fluoropropanoyl)benzonitrile (2d)

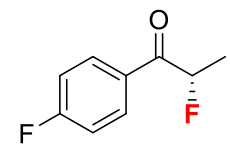


(S)-**2d** 

(*S*)-2d was prepared according to the *General Procedure* starting from the substrate *rac*-1d (95 mg). The reaction was let stirring in ACN (0.5 M) at 5°C at 1200 rpm for 96 h. After filtration over celite to remove KF, the product was isolated by FCC (eluent: Pentane/DCM, 70/30) as a white solid in 86% yield, 61 mg, 93:7 e.r.

<sup>1</sup>H NMR (600 MHz, CDCl<sub>3</sub>)  $\delta$  = 8.11 – 8.05 (m, 2H), 7.81 – 7.75 (m, 2H), 5.63 (dq, J = 48.3, 6.8 Hz, 1H), 1.67 (dd, J = 24.1, 6.8 Hz, 3H); ); <sup>19</sup>F NMR (565 MHz, CDCl<sub>3</sub>)  $\delta$  = -180.54 (m); <sup>13</sup>C NMR (151 MHz, CDCl<sub>3</sub>)  $\delta$  = 196.08 (d, J = 21.4 Hz), 137.16 (d, J = 2.2 Hz), 132.48, 129.57 (d, J = 4.6 Hz), 117.34 (d, J = 123.3 Hz), 90.90 (d, J = 180.9 Hz), 17.93 (d, J = 22.3 Hz); HPLC separation: DAICEL CHIRALPAK® ID-3, Heptane: IPA = 99.2:0.8 mL/min; t<sub>1</sub> = 20.6 (major), t<sub>2</sub>= 25.4 (minor).

# (S)-2-fluoro-1-(4-fluorophenyl)propan-1-one (2e)



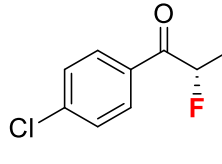
volatile).

(S)-**2e** 

(*S*)-**2e** was prepared according to the *General Procedure* starting from the substrate *rac*-**1e** (92 mg). The reaction was let stirring in ACN (0.5 M) at 5°C at 1200 rpm for 96 h. After filtration over celite to remove KF, the product was isolated by FCC (eluent: Pentane/DCM, 70/30) as a white solid in 55% yield, 37 mg, 96:4 e.r. (the product is highly

<sup>1</sup>H NMR (600 MHz, CDCl<sub>3</sub>)  $\delta$  = 8.08 – 8.01 (m, 2H), 7.20 – 7.12 (m, 2H), 5.63 (dq, J = 48.6, 6.8 Hz, 1H), 1.66 (dd, J = 24.1, 6.8 Hz, 3H); <sup>19</sup>F NMR (565 MHz, CDCl<sub>3</sub>)  $\delta$  = -103.55 (m), -180.17 (m); <sup>13</sup>C NMR (151 MHz, CDCl<sub>3</sub>)  $\delta$  = 194.40 (d, J = 20.0 Hz), 165.02 (d, J = 256.1 Hz), 130.84 (dd, J = 9.4, 4.6 Hz), 129.41 (t, J = 2.7 Hz), 114.91 (d, J = 22.0 Hz), 89.59 (d, J = 180.3 Hz), 17.22 (d, J = 22.6 Hz); HRMS (EI) m/z calculated for C<sub>9</sub>H<sub>9</sub>F<sub>2</sub>O (M)<sup>+</sup> 171.0616, found 171.0617; HPLC separation: DAICEL CHIRALPAK® ID-3, Heptane: IPA = 99.8:0.2 mL/min; t<sub>1</sub> = 8.2 (major), t<sub>2</sub>= 10.0 (minor).

### (S)-1-(4-chlorophenyl)-2-fluoropropan-1-one (2f)



volatile).

(S)-**2f** 

(*S*)-**2f** was prepared according to the *General Procedure* starting from the substrate *rac*-**1f** (99 mg). The reaction was let stirring in ACN (0.5 M) at 5°C at 1200 rpm for 96 h. After filtration over celite to remove KF, the product was isolated by FCC (eluent: Pentane/DCM, 70/30) as a white solid 68% yield, 48 mg, 95:5 e.r. (the product is highly

 $^1H$  NMR (600 MHz, CDCl<sub>3</sub>)  $\delta$  = 7.97 – 7.91 (m, 2H), 7.49 – 7.43 (m, 2H), 5.63 (dq, J = 48.6, 6.8 Hz, 1H), 1.66 (dd, J = 24.1, 6.8 Hz, 3H);  $^{19}F$  NMR (565 MHz, CDCl<sub>3</sub>)  $\delta$  = -180.46 (m);  $^{13}C$  NMR (151 MHz, CDCl<sub>3</sub>)  $\delta$  = 195.87 (d, J = 20.3 Hz), 140.32, 132.33 (d, J = 2.4 Hz), 130.51 (d, J = 4.4 Hz), 129.08, 90.61 (d, J = 180.5 Hz), 18.21 (d, J = 22.6 Hz); HRMS (ESI+) m/z calculated for C9H9ClFO (M+H)+187.0321, found 187.0554.

### (S)-2-fluoro-1-phenylpropan-1-one (2g)



(S)-**2g** 

volatile).

(*S*)-**2g** was prepared according to the *General Procedure* starting from the substrate *rac*-**1g** (85 mg). The reaction was let stirring in ACN (0.5 M) at 25°C at 1200 rpm for 96 h. After filtration over celite to remove KF, the product was isolated by FCC (eluent: Pentane/DCM, 80/20) as a colourless oil 91% yield, 55 mg, 90:10 e.r. ((the product is highly

 $^{1}$ H NMR (600 MHz, CDCl<sub>3</sub>) δ = 8.00 – 7.95 (m, 2H), 7.62 – 7.58 (m, 1H), 7.52 – 7.46 (m, 2H), 5.71 (dq, J = 48.6, 6.8 Hz, 1H), 1.67 (dd, J = 24.0, 6.8 Hz, 3H);  $^{19}$ F NMR (565 MHz, CDCl<sub>3</sub>) δ = -181.41 (m);  $^{13}$ C NMR (151 MHz, CDCl<sub>3</sub>) δ =196.92 (d, J = 19.4 Hz), 137.78, 128.96 (d, J = 3.8 Hz), 128.73, 90.28 (d, J = 180.2 Hz), 18.37 (d, J = 22.6 Hz); HRMS (EI) m/z

calculated for C<sub>9</sub>H<sub>9</sub>FO (M)<sup>+</sup> 153.0710, found 153.0711 00; HPLC separation: DAICEL CHIRALPAK® ID-3, Heptane: IPA = 99.2:0.8 mL/min;  $t_1$  = 4.7 (major),  $t_2$ = 5.3 (minor).

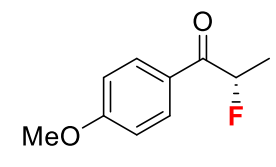
### (S)-2-fluoro-1-(p-tolyl)propan-1-one (2h)

(S)-**2h** 

(*S*)-**2h** was prepared according to the *General Procedure* starting from the substrate *rac*-**1h** (91 mg). The reaction was let stirring in ACN (0.5 M) at 25°C at 1200 rpm for 96 h. After filtration over celite to remove KF, the product was isolated by FCC (eluent: Pentane/DCM, 80/20) as a colourless oil 83% yield, 55 mg, 92:8 e.r. <sup>1</sup>H NMR (600

MHz, CDCl<sub>3</sub>)  $\delta$  = 7.88 (d, J = 8.1 Hz, 2H), 7.31 – 7.26 (m, 2H), 5.69 (dq, J = 48.7, 6.8 Hz, 1H), 2.43 (s, 3H), 1.66 (dd, J = 24.0, 6.8 Hz, 3H); <sup>19</sup>F NMR (565 MHz, CDCl<sub>3</sub>)  $\delta$  = -181.32 (m); <sup>13</sup>C NMR (151 MHz, CDCl<sub>3</sub>)  $\delta$  = 196.6 (d,  $J_{C-F}$  = 19.3 Hz), 144.9, 131.6, 129.6, 129.2 (d,  $J_{C-F}$  = 3.9 Hz), 90.4 (d,  $J_{C-F}$  = 179.9 Hz), 21.9, 18.6 (d,  $J_{C-F}$  = 23.1 Hz); HRMS (EI) m/z calculated for C<sub>10</sub>H<sub>12</sub>FO (M)<sup>+</sup> 167.0867, found 167.0867; HPLC separation: DAICEL CHIRALPAK® ID-3, Heptane: IPA = 99.2:0.8 mL/min; t<sub>1</sub> = 5.9 (major), t<sub>2</sub>= 6.6 (minor).

# (S)-2-fluoro-1-(4-methoxyphenyl)propan-1-one (2i)

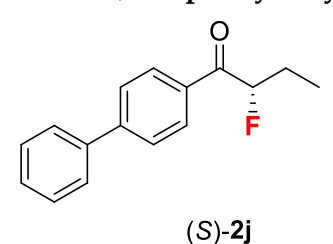


(S)-**2i** 

(*S*)-**2i** was prepared according to the *General Procedure* starting from the substrate *rac*-**1i** (97 mg). The reaction was let stirring in ACN (0.5 M) at 25°C at 1200 rpm for 96 h. After filtration over celite to remove KF, the product was isolated by FCC (eluent: Pentane/DCM, 70/30) as a white solid 90% yield, 65 mg, 92:8 e.r.

<sup>1</sup>H NMR (600 MHz, CDCl<sub>3</sub>) δ = 8.03 – 7.95 (m, 2H), 7.01 – 6.90 (m, 2H), 5.65 (dq, J = 48.8, 6.8 Hz, 1H), 3.88 (s, 3H), 1.65 (dd, J = 24.2, 6.8 Hz, 3H). <sup>19</sup>F NMR (565 MHz, CDCl<sub>3</sub>) δ = -180.44 (m); <sup>13</sup>C NMR (151 MHz, CDCl<sub>3</sub>) δ = 195.30 (d, J = 19.6 Hz), 163.99, 131.40 (d, J = 4.0 Hz), 126.93, 113.95, 90.35 (d, J = 179.6 Hz), 55.53, 18.53 (d, J = 22.7 Hz); HRMS (EI) m/z calculated for C<sub>10</sub>H<sub>12</sub>FO<sub>2</sub> (M)<sup>+</sup> 183.0816, found 183.0816; HPLC separation: DAICEL CHIRALPAK® ID-3, Heptane: IPA = 99.5:0.5 mL/min; t<sub>1</sub> = 21.2 (major), t<sub>2</sub>= 23.7 (minor).

### (S)-1-([1,1'-biphenyl]-4-yl)-2-fluorobutan-1-one (2j)



(*S*)-2**j** was prepared according to the *General Procedure* starting from the substrate *rac*-1**j** (121 mg). The reaction was let stirring in ACN (0.5 M) at 40°C at 1200 rpm for 96 h. After filtration over celite to remove KF, the product was isolated by FCC (eluent: Pentane/DCM, 80/20) as a white solid, 83% yield, 80 mg, 92:8 e.r.

<sup>1</sup>H NMR (600 MHz, CDCl<sub>3</sub>)  $\delta$  = 8.08 – 8.04 (m, 2H), 7.73 – 7.68 (m, 2H), 7.65 – 7.62 (m, 2H), 7.51 – 7.45 (m, 2H), 7.45 – 7.39 (m, 1H), 5.54 (ddd, J = 49.3, 7.8, 4.5 Hz, 1H), 2.16 – 1.96 (m, 2H), 1.11 (t, J = 7.4 Hz, 3H). <sup>19</sup>F NMR (565 MHz, CDCl<sub>3</sub>)  $\delta$  = -190.52 (m); <sup>13</sup>C NMR

(151 MHz, CDCl<sub>3</sub>)  $\delta$  = 196.41 (d, J = 19.7 Hz), 146.42, 139.68, 133.09 (d, J = 1.4 Hz), 129.51 (d, J = 3.9 Hz), 129.01, 128.43, 127.32 (d, J = 6.6 Hz), 95.00 (d, J = 183.6 Hz), 26.19 (d, J = 21.5 Hz), 9.14 (d, J = 4.5 Hz); HRMS (EI) m/z calculated for C<sub>16</sub>H<sub>16</sub>FO (M)<sup>+</sup> 243.1180, found 243.1180; HPLC separation: DAICEL CHIRALPAK® ID-3, Heptane: IPA = 99.2:0.8 mL/min; t<sub>1</sub> = 16 (major), t<sub>2</sub>= 19.2 (minor).

# (S)-2-fluoro-1-(thiophen-2-yl)propan-1-one (2k)

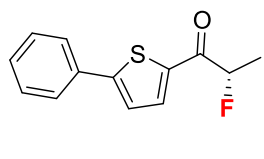


(S)-2k

(*S*)-**2k** was prepared according to the *General Procedure* starting from the substrate *rac*-**1k** (87.6 mg). The reaction was let stirring in ACN (0.5 M) at 25°C at 1200 rpm for 96 h. After filtration over celite to remove KF, the product was isolated by FCC (eluent: Pentane/DCM, 80/20) as a pale-yellow oil, 60% yield, 38 mg, 88:12 e.r.

<sup>1</sup>H NMR (600 MHz, CDCl<sub>3</sub>) δ = 7.97 (dt, J = 3.9, 1.3 Hz, 1H), 7.74 (dd, J = 4.9, 1.1 Hz, 1H), 7.18 (dd, J = 4.9, 3.9 Hz, 1H), 5.43 (dq, J = 49.1, 6.8 Hz, 1H), 1.68 (dd, J = 24.3, 6.8 Hz, 3H); <sup>19</sup>F NMR (565 MHz, CDCl<sub>3</sub>) δ = -179.39 (m); <sup>13</sup>C NMR (151 MHz, CDCl<sub>3</sub>) δ = 190.63 (d, J = 22.0 Hz), 139.98 (d, J = 3.3 Hz), 135.08 (d, J = 2.3 Hz), 134.23 (d, J = 8.6 Hz), 128.40 (d, J = 2.0 Hz), 91.83 (d, J = 182.3 Hz), 18.82 (d, J = 22.5 Hz); HRMS (EI) m/z calculated for C<sub>7</sub>H<sub>8</sub>FOS (M)<sup>+</sup> 159.0274, found 159.0274; HPLC separation: DAICEL CHIRALPAK® ID-3, Heptane: IPA = 99.2:0.8 mL/min; t<sub>1</sub> = 6.4 (major), t<sub>2</sub>= 7.6 (minor).

# (S)-2-fluoro-1-(5-phenylthiophen-2-yl)propan-1-one (2l)



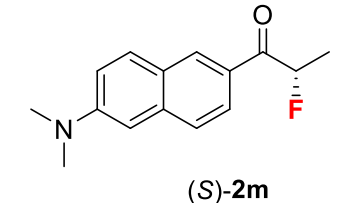
(S)-**2I** 

(*S*)-21 was prepared according to the *General Procedure* starting from the substrate *rac*-11 (118 mg). The reaction was let stirring in ACN (0.5 M) at 25°C at 1200 rpm for 96 h. After filtration over celite to remove KF, the product was isolated by FCC (eluent: Pentane/DCM, 80/20) as a yellow solid, 70% yield, 65.5 mg, 88:12

e.r.

 $^{1}$ H NMR (600 MHz, CDCl<sub>3</sub>)  $\delta$  =7.94 (dd, J = 4.1, 1.5 Hz, 1H), 7.71 – 7.65 (m, 2H), 7.47 – 7.35 (m, 4H), 5.44 (dq, J = 49.1, 6.8 Hz, 1H), 1.70 (dd, J = 24.4, 6.8 Hz, 3H);  $^{19}$ F NMR (565 MHz, CDCl<sub>3</sub>)  $\delta$  = -179.28 (m);  $^{13}$ C NMR (151 MHz, CDCl<sub>3</sub>)  $\delta$  = 190.39 (d, J = 22.0 Hz), 154.09 (d, J = 2.5 Hz), 138.59 (d, J = 3.8 Hz), 135.37 (d, J = 9.0 Hz), 133.08, 129.33, 129.18, 126.43, 124.28 (d, J = 2.0 Hz), 91.94 (d, J = 182.3 Hz), 18.91 (d, J = 22.5 Hz); HRMS (EI) m/z calculated for C<sub>13</sub>H<sub>12</sub>FOS (M)+ 235.0587, found 235.0587; HPLC separation: DAICEL CHIRALPAK® IB-3, Heptane: IPA = 99:1 mL/min; t<sub>1</sub> = 5.8 (major), t<sub>2</sub>= 7.1 (minor).

# (S)-1-(6-(dimethylamino)naphthalen-2-yl)-2-fluoropropan-1-one (2m)

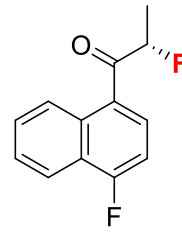


(S)-2m was prepared according to the General Procedure starting from the substrate *rac-***1m** (122 mg). The reaction was let stirring in ACN (0.5 M) at 25°C at 1200 rpm for 96 h. After filtration over celite to remove KF, the product was isolated by FCC (eluent: Pentane/DCM, 70/30) as a yellow solid, 93%

yield, 91 mg, 91:9 e.r.

<sup>1</sup>H NMR (600 MHz, CDCl<sub>3</sub>)  $\delta$  = 8.48 (d, J = 1.7 Hz, 1H), 8.36 (d, J = 9.0 Hz, 1H), 8.07 (dd, J = 9.0, 1.8 Hz, 1H), 7.91 (d, J = 8.8 Hz, 1H), 7.45 (d, J = 8.8 Hz, 1H), 5.83 (dq, J = 48.7, 6.8 Hz, 1Hz)1H), 3.01 (s, 6H), 1.75 (dd, J = 24.1, 6.8 Hz, 3H); <sup>19</sup>F NMR (565 MHz, CDCl<sub>3</sub>)  $\delta = -180.47$ , <sup>13</sup>C NMR (151 MHz, CDCl<sub>3</sub>)  $\delta$  = 196.32 (d, J = 19.4 Hz), 152.53, 136.17, 131.04 (d, J = 5.4 Hz), 130.21, 129.82 (d, J = 38.2 Hz), 127.40, 125.86 (d, J = 2.7 Hz), 121.01, 115.72, 90.59 (d, J = 2.7 Hz), 121.01, 115.72, 115.7= 180.3 Hz), 44.25, 18.52 (d, J = 23.0 Hz); HRMS (EI) m/z calculated for C<sub>15</sub>H<sub>17</sub>FNO (M)<sup>+</sup> 246.1289, found 246.1285; HPLC separation: DAICEL CHIRALPAK® ID-3, Heptane: IPA = 99:1 mL/min;  $t_1 = 9.4 \text{ (major)}$ ,  $t_2 = 11.7 \text{ (minor)}$ .

### (S)-2-fluoro-1-(4-fluoronaphthalen-1-yl)propan-1-one (2n)



(S)-2n was prepared according to the General Procedure starting from the substrate rac-1n (112 mg). The reaction was let stirring in ACN (0.5 M) at 25°C at 1200 rpm for 96h. After filtration over celite to remove KF, the product was isolated by FCC (eluent: Pentane/DCM, 80/20) as a white solid, 97% yield, 85 mg, 96:4 e.r.

(S)-2n

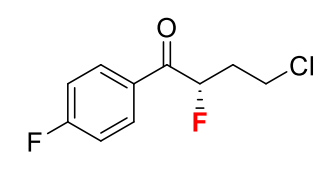
<sup>1</sup>H NMR (600 MHz, CDCl<sub>3</sub>)  $\delta$  = 8.59 (ddt, J = 8.7, 1.9, 0.9 Hz, 1H), 8.20 – 8.15 (m, 1H), 7.90 (ddd, J = 8.1, 5.4, 1.4 Hz, 1H), 7.68 (ddd, J = 8.5, 6.9, 1.4 Hz, 1H), 7.63 (ddd, J = 8.1, 6.8, 1.1 Hz, 1H), 7.18 (dd, J = 9.7, 8.1 Hz, 1H), 5.74 (dq, J = 48.8,

6.9 Hz, 1H), 1.68 (dd, J = 23.6, 6.8 Hz, 3H);  $^{19}$ F NMR (565 MHz, CDCl<sub>3</sub>)  $\delta$  = -178.71 (m), -113.26 (m);  ${}^{13}$ C NMR (151 MHz, CDCl<sub>3</sub>)  $\delta$  = 199.44 (d, J = 20.3 Hz), 161.50 (d, J = 260.8 Hz), 132.84 (d, J = 5.5 Hz), 129.52 (dd, J = 10.1, 5.7 Hz), 129.31, 128.42 (d, J = 4.4 Hz), 127.07 (d, J = 2.1 Hz), 125.57 (d, J = 2.6 Hz), 124.27 (d, J = 15.6 Hz), 120.93 (d, J = 6.4 Hz), 108.17 (d, J = 6.4 Hz), 108.17 (d, J = 6.4 Hz) = 21.0 Hz), 90.66 (d, J = 182.7 Hz), 18.29 (d, J = 22.6 Hz); HRMS (EI) m/z calculated for C<sub>13</sub>H<sub>11</sub>F<sub>2</sub>O (M)<sup>+</sup> 221.0773, found 221.0772; HPLC separation: DAICEL CHIRALPAK® IF-3, Heptane: IPA = 99.2:0.8 mL/min;  $t_1 = 7.0$  (major),  $t_2 = 8.9$  (minor).

# (S)-2-fluoro-1-(naphthalen-1-yl)propan-1-one (20)

**(S)-20** was prepared according to the *General Procedure* starting from the substrate *rac-***10** (105 mg). The reaction was let stirring in ACN (0.5 M) at 25°C at 1200 rpm for 96 h. After filtration over celite to remove KF, the product was isolated by FCC (eluent: Pentane/DCM, 80/20) as a white solid, 96% yield, 77 mg, 98:2 e.r.

# (S)-4-chloro-2-fluoro-1-(4-fluorophenyl)butan-1-one (2p)



(S)-**2p** 

(*S*)-2**p** was prepared according to the *General Procedure* starting from the substrate *rac*-1**p** (112 mg). The reaction was let stirring in ACN (0.5 M) at 40°C at 1200 rpm for 96 h. After filtration over celite to remove KF, the product was isolated by FCC (eluent: Pentane/DCM, 80/20) as a white solid, 78% yield, 68 mg, 84:16 e.r.

<sup>1</sup>H NMR (600 MHz, CDCl<sub>3</sub>)  $\delta$  = 8.04 (m, 2H), 7.20 – 7.15 (m, 2H), 5.90 – 5.78 (m, 1H), 3.84 – 3.74 (m, 2H), 2.46 – 2.34 (m, 2H); <sup>19</sup>F NMR (565 MHz, CDCl<sub>3</sub>)  $\delta$  = -182.82 (m); -191.94 (m); <sup>13</sup>C NMR (151 MHz, CDCl<sub>3</sub>)  $\delta$  = 193.94 (d, J = 18.8 Hz), 166.23 (d, J = 256.9 Hz), 131.82 (dd, J = 9.5, 4.1 Hz), 130.39, 116.12 (d, J = 22.0 Hz), 89.94 (d, J = 183.3 Hz), 39.96 (d, J = 3.8 Hz), 35.10 (d, J = 21.4 Hz); HRMS (EI) m/z calculated for C<sub>10</sub>H<sub>10</sub>ClF<sub>2</sub>O (M)+ 219.0383, found 219.0382, HPLC separation: DAICEL CHIRALPAK® ID-3, Heptane: IPA = 99.2:0.8 mL/min; t<sub>1</sub> = 6.8 (major), t<sub>2</sub>= 9.8 (minor).

# **References:**

- [1] B. G. de la Torre, F. Albericio, *Molecules* **2024**, *29*, 585.
- [2] J. Rayadurgam, S. Sana, M. Sasikumar, Q. Gu, Org. Chem. Front. 2021, 8, 384–414.
- [3] J. Magano, J. R. Dunetz, Chem. Rev. 2011, 111, 2177–2250.
- [4] D. L. Hughes, Organic Process Research & Development 2016, 20, 1855–1869.
- [5] B. S. Takale, F.-Y. Kong, R. R. Thakore, *Organics* **2022**, *3*, 1–21.
- [6] S. Frigoli, C. Fuganti, L. Malpezzi, S. Serra, Org. Process Res. Dev. 2005, 9, 646-650.
- [7] A. Caporale, S. Tartaggia, A. Castellin, O. D. Lucchi, *Beilstein J. Org. Chem.* **2014**, *10*, 384–393.
- [8] C. Torborg, M. Beller, Advanced Synthesis & Catalysis 2009, 351, 3027–3043.
- [9] W. Cabri, P. Cantelmi, D. Corbisiero, T. Fantoni, L. Ferrazzano, G. Martelli, A. Mattellone, A. Tolomelli, *Front. Mol. Biosci.* **2021**, *8*.
- [10] T. Willemse, W. Schepens, H. W. T. van Vlijmen, B. U. W. Maes, S. Ballet, *Catalysts* **2017**, 7, 74.
- [11] T. Liu, J. X. Qiao, M. A. Poss, J.-Q. Yu, Angew Chem Int Ed Engl 2017, 56, 10924–10927.
- [12]H. Ali, S. Ait-Mohand, S. Gosselin, J. E. van Lier, B. Guérin, *The Journal of Organic Chemistry* **2011**, *76*, 1887–1890.
- [13] E. V. Vinogradova, C. Zhang, A. M. Spokoyny, B. L. Pentelute, S. L. Buchwald, *Nature* **2015**, *526*, 687–691.
- [14] A. J. Rojas, J. M. Wolfe, H. H. Dhanjee, I. Buslov, N. L. Truex, R. Y. Liu, W. Massefski, B. L. Pentelute, S. L. Buchwald, *Chem. Sci.* **2022**, *13*, 11891–11895.
- [15] Z. Li, Q. Ruan, Y. Jiang, Q. Wang, G. Yin, J. Feng, J. Zhang, *Journal of Medicinal Chemistry* **2024**, *67*, 21644–21670.
- [16] M. Zhou, Z. Feng, X. Zhang, Chem. Commun. 2023, 59, 1434–1448.
- [17]H.-Y. Zhao, Z. Feng, Z. Luo, X. Zhang, *Angewandte Chemie International Edition* **2016**, *55*, 10401–10405.
- [18] C. W. Kee, O. Tack, F. Guibbal, T. C. Wilson, P. G. Isenegger, M. Imiołek, S. Verhoog, M. Tilby, G. Boscutti, S. Ashworth, J. Chupin, R. Kashani, A. W. J. Poh, J. K. Sosabowski, S. Macholl, C. Plisson, B. Cornelissen, M. C. Willis, J. Passchier, B. G. Davis, V. Gouverneur, *Journal of the American Chemical Society* 2020, 142, 1180–1185.
- [19] F. Roschangar, R. A. Sheldon, C. H. Senanayake, *Green Chem.* 2015, 17, 752–768.
- [20] P. J. Dunn, K. K. Hii, M. J. Krische, M. T. Williams, Sustainable Catalysis: Challenges and Practices for the Pharmaceutical and Fine Chemical Industries, 2013.
- [21] C. C. Johansson Seechurn, M. O. Kitching, T. J. Colacot, V. Snieckus, *Angewandte Chemie International Edition* **2012**, *51*, 5062–5085.
- [22] E. Negishi, Angewandte Chemie International Edition 2011, 50, 6738–6764.
- [23] A. Suzuki, Angewandte Chemie International Edition 2011, 50, 6722–6737.
- [24] R. F. Heck, J. P. Nolley, J. Org. Chem. 1972, 37, 2320–2322.
- [25] P. T. Anastas, J. C. Warner, *Green Chemistry, Theory and Practice*, Oxford University Press: New York, 1998., **1998**.
- [26] J. D. Hayler, D. K. Leahy, E. M. Simmons, *Organometallics* **2019**, *38*, 36–46.
- [27] Https://Tradingeconomics.Com/Commodity/Palladium.
- [28] Https://Matthey.Com/Products-and-Markets/Pgms-and-Circularity/Pgm-Markets/Palladium.
- [29] S. Tang, M. Takeda, Y. Nakao, T. Hiyama, Chem. Commun. 2011, 47, 307–309.
- [30] J. Diccianni, O. Lin, T. Diao, Acc Chem Res 2020, 53, 906–919.
- [31] V. B. Phapale, D. J. Cárdenas, Chem. Soc. Rev. 2009, 38, 1598–1607.
- [32] S. Thapa, B. Shrestha, S. K. Gurung, R. Giri, Org. Biomol. Chem. 2015, 13, 4816–4827.
- [33]G. Evano, N. Blanchard, M. Toumi, *Chemical Reviews* **2008**, *108*, 3054–3131.
- [34] P. Karna, Z. Finfrock, J. Li, Y. Hu, D.-S. Yang, *The Journal of Physical Chemistry C* **2023**, 127, 5791–5799.

- [35]G. Cahiez, A. Moyeux, Chemical Reviews 2010, 110, 1435–1462.
- [36] C. Gosmini, J.-M. Bégouin, A. Moncomble, Chem. Commun. 2008, 3221–3233.
- [37] X. Luo, D. Yang, X. He, S. Wang, D. Zhang, J. Xu, C.-W. Pao, J.-L. Chen, J.-F. Lee, H. Cong, Y. Lan, H. Alhumade, J. Cossy, R. Bai, Y.-H. Chen, H. Yi, A. Lei, *Nat Commun* 2023, 14, 4638.
- [38] M. U. Luescher, F. Gallou, B. H. Lipshutz, Chemical Science 2024, 15, 9016–9025.
- [39] V. M. Chernyshev, V. P. Ananikov, ACS Catal. 2022, 12, 1180–1200.
- [40] K. S. Egorova, V. P. Ananikov, *Angewandte Chemie International Edition* **2016**, *55*, 12150–12162.
- [41] T. Djekić, A. G. J. van der Ham, A. B. de Haan, *Journal of Chromatography A* **2007**, *1142*, 32–38.
- [42] Q. Yao, E. P. Kinney, Z. Yang, J. Org. Chem. 2003, 68, 7528–7531.
- [43]B. S. Takale, R. R. Thakore, S. Handa, F. Gallou, J. Reilly, B. H. Lipshutz, *Chem. Sci.* **2019**, *10*, 8825–8831.
- [44] M. Cortes-Clerget, N. Akporji, J. Zhou, F. Gao, P. Guo, M. Parmentier, F. Gallou, J.-Y. Berthon, B. H. Lipshutz, *Nat Commun* **2019**, *10*, 2169.
- [45]T. Fantoni, S. Bernardoni, A. Mattellone, G. Martelli, L. Ferrazzano, P. Cantelmi, D. Corbisiero, A. Tolomelli, W. Cabri, F. Vacondio, F. Ferlenghi, M. Mor, A. Ricci, *ChemSusChem* **2021**, *14*, 2591–2600.
- [46] D. J. C. Constable, A. D. Curzons, V. L. Cunningham, *Green Chem.* **2002**, *4*, 521–527.
- [47] Https://Echa.Europa.Eu/Substances-Restricted-under-Reach.
- [48] Https://Eur-Lex.Europa.Eu/Legal-Content/EN/TXT/?uri=CELEX%3A32021R2030&qid=1629107278018.
- [49] Https://Echa.Europa.Eu/Registry-of-Restriction-Intentions.
- [50] M. C. Bryan, P. J. Dunn, D. Entwistle, F. Gallou, S. G. Koenig, J. D. Hayler, M. R. Hickey, S. Hughes, M. E. Kopach, G. Moine, P. Richardson, F. Roschangar, A. Steven, F. J. Weiberth, *Green Chem.* 2018, 20, 5082–5103.
- [51] C. M. Alder, J. D. Hayler, R. K. Henderson, A. M. Redman, L. Shukla, L. E. Shuster, H. F. Sneddon, *Green Chem.* **2016**, *18*, 3879–3890.
- [52] J. Sherwood, J. H. Clark, I. J. S. Fairlamb, J. M. Slattery, *Green Chemistry* **2019**, *21*, 2164–2213.
- [53] R. A. Sheldon, *Green Chem.* **2005**, *7*, 267–278.
- [54] G. Strappaveccia, L. Luciani, E. Bartollini, A. Marrocchi, F. Pizzo, L. Vaccaro, *Green Chem.* **2015**, *17*, 1071–1076.
- [55] K. L. Wilson, A. R. Kennedy, J. Murray, B. Greatrex, C. Jamieson, A. J. B. Watson, *Beilstein Journal of Organic Chemistry* **2016**, *12*, 2005–2011.
- [56] G. Dilauro, A. Francesca Quivelli, P. Vitale, V. Capriati, F. M. Perna, *Angewandte Chemie International Edition* **2019**, *58*, 1799–1802.
- [57] K. Yoneto, A. Ghanem, W. I. Higuchi, K. D. Peck, S. Kevin Li, *Journal of Pharmaceutical Sciences* **1995**, *84*, 312–317.
- [58] L. Ferrazzano, G. Martelli, T. Fantoni, A. Daka, D. Corbisiero, A. Viola, A. Ricci, W. Cabri, A. Tolomelli, *Org. Lett.* **2020**, *22*, 3969–3973.
- [59] A. P. Abbott, G. Capper, D. L. Davies, R. K. Rasheed, V. Tambyrajah, *Chem. Commun.* **2003**, 70–71.
- [60]F. M. Perna, P. Vitale, V. Capriati, Current Opinion in Green and Sustainable Chemistry **2020**, 21, 27–33.
- [61] L. Cicco, G. Dilauro, F. M. Perna, P. Vitale, V. Capriati, *Org. Biomol. Chem.* **2021**, *19*, 2558–2577.
- [62]G. Dilauro, S. M. García, D. Tagarelli, P. Vitale, F. M. Perna, V. Capriati, *ChemSusChem* **2018**, *11*, 3495–3501.
- [63] F. Messa, G. Dilauro, F. M. Perna, P. Vitale, V. Capriati, A. Salomone, *ChemCatChem* **2020**, *12*, 1979–1984.

- [64] G. Dilauro, C. S. Azzollini, P. Vitale, A. Salomone, F. M. Perna, V. Capriati, *Angewandte Chemie International Edition* **2021**, *60*, 10632–10636.
- [65]X. Marset, A. Khoshnood, L. Sotorríos, E. Gómez-Bengoa, D. A. Alonso, D. J. Ramón, *ChemCatChem* **2017**, *9*, 1269–1275.
- [66] V. V. Grushin, H. Alper, Chem. Rev. 1994, 94, 1047–1062.
- [67] A. F. Littke, G. C. Fu, Angew. Chem. Int. Ed. 2002, 41, 4176–4211.
- [68] P. Orecchia, D. S. Petkova, R. Goetz, F. Rominger, A. S. K. Hashmi, T. Schaub, *Green Chem.* **2021**, *23*, 8169–8180.
- [69]B. S. Takale, R. R. Thakore, R. Mallarapu, F. Gallou, B. H. Lipshutz, *Org. Process Res. Dev.* **2020**, *24*, 101–105.
- [70]H. Peng, Y.-Q. Chen, S.-L. Mao, Y.-X. Pi, Y. Chen, Z.-Y. Lian, T. Meng, S.-H. Liu, G.-A. Yu, *Organic & Biomolecular Chemistry* **2014**, *12*, 6944–6952.
- [71]R. A. Sheldon, *Chem. Ind* **1992**, 903–906.
- [72] A. F. Littke, C. Dai, G. C. Fu, J. Am. Chem. Soc. 2000, 122, 4020–4028.
- [73] U. Christmann, R. Vilar, Angewandte Chemie International Edition 2005, 44, 366–374.
- [74] B. T. Ingoglia, C. C. Wagen, S. L. Buchwald, *Tetrahedron* **2019**, *75*, 4199–4211.
- [75] R. Martin, S. L. Buchwald, Acc. Chem. Res. 2008, 41, 1461–1473.
- [76] J. P. Stambuli, R. Kuwano, J. F. Hartwig, *Angewandte Chemie International Edition* **2002**, 41, 4746–4748.
- [77] T. J. Colacot, *Platinum Metals Review* **2009**, *53*, 183–188.
- [78] M. Aufiero, T. Sperger, A. S.-K. Tsang, F. Schoenebeck, *Angewandte Chemie International Edition* **2015**, *54*, 10322–10326.
- [79]M. Aufiero, T. Scattolin, F. Proutière, F. Schoenebeck, *Organometallics* **2015**, *34*, 5191–5195.
- [80] K. L. Barnett, J. R. Howard, C. J. Treager, A. T. Shipley, R. M. Stullich, F. Qu, D. L. Gerlach, K. H. Shaughnessy, *Organometallics* **2018**, *37*, 1410–1424.
- [81] M. R. Biscoe, B. P. Fors, S. L. Buchwald, *Journal of the American Chemical Society* **2008**, 130, 6686–6687.
- [82] T. Kinzel, Y. Zhang, S. L. Buchwald, *Journal of the American Chemical Society* **2010**, *132*, 14073–14075.
- [83] N. C. Bruno, N. Niljianskul, S. L. Buchwald, *The Journal of Organic Chemistry* **2014**, 79, 4161–4166.
- [84] C. J. O'Brien, E. A. B. Kantchev, C. Valente, N. Hadei, G. A. Chass, A. Lough, A. C. Hopkinson, M. G. Organ, *Chemistry A European Journal* **2006**, *12*, 4743–4748.
- [85] S. J. Firsan, V. Sivakumar, T. J. Colacot, Chemical Reviews 2022, 122, 16983–17027.
- [86] C. Amatore, A. Jutand, M. A. M'Barki, Organometallics 1992, 11, 3009–3013.
- [87] C. Amatore, A. Jutand, A. Thuilliez, Organometallics 2001, 20, 3241–3249.
- [88] F. Sirindil, R. Pertschi, E. Naulin, D. Hatey, J.-M. Weibel, P. Pale, A. Blanc, *ACS Omega* **2022**, *7*, 1186–1196.
- [89] M. Muttenthaler, G. F. King, D. J. Adams, P. F. Alewood, *Nat Rev Drug Discov* **2021**, *20*, 309–325
- [90] Https://Www.Mordorintelligence.Com/Industry-Reports/Peptide-Therapeutics-Market. /13rd November 2024.
- [91]M. Muttenthaler, G. F. King, D. J. Adams, P. F. Alewood, *Nat Rev Drug Discov* **2021**, *20*, 309–325.
- [92] R. B. Merrifield, Journal of the American Chemical Society 1963, 85, 2149–2154.
- [93] S. G. Koenig, C. Bee, A. Borovika, C. Briddell, J. Colberg, G. R. Humphrey, M. E. Kopach, I. Martinez, S. Nambiar, S. V. Plummer, S. D. Ribe, F. Roschangar, J. P. Scott, H. F. Sneddon, *ACS Sustainable Chemistry & Engineering* **2019**, *7*, 16937–16951.
- [94] V. Declerck, P. Nun, J. Martinez, F. Lamaty, *Angewandte Chemie International Edition* **2009**, *48*, 9318–9321.
- [95] J. Bonnamour, T.-X. Métro, J. Martinez, F. Lamaty, Green Chem. 2013, 15, 1116–1120.

- [96] S. Rizzo, A. Toplak, M. Macis, L. Ferrazzano, A. Ricci, A. Tolomelli, W. Cabri, ACS Sustainable Chemistry & Engineering 2024, 12, 16791–16799.
- [97] Y. E. Jad, G. A. Acosta, S. N. Khattab, B. G. de la Torre, T. Govender, H. G. Kruger, A. El-Faham, F. Albericio, *Org. Biomol. Chem.* **2015**, *13*, 2393–2398.
- [98] Y. E. Jad, G. A. Acosta, S. N. Khattab, B. G. de la Torre, T. Govender, H. G. Kruger, A. El-Faham, F. Albericio, *Amino Acids* **2016**, *48*, 419–426.
- [99]Y. E. Jad, T. Govender, H. G. Kruger, A. El-Faham, B. G. de la Torre, F. Albericio, *Organic Process Research & Development* **2017**, *21*, 365–369.
- [100] A. Kumar, A. Sharma, B. G. de la Torre, F. Albericio, *Green Chemistry Letters and Reviews* **2021**, *14*, 545–550.
- [101] J. Pawlas, J. H. Rasmussen, ChemSusChem 2021, 14, 3231–3236.
- [102] Https://Www.Syensqo.Com/En/Brands/Rhodiasolv-Polarclean.
- [103] J. Lopez, S. Pletscher, A. Aemissegger, C. Bucher, F. Gallou, *Organic Process Research & Development* **2018**, *22*, 494–503.
- [104] G. Martelli, P. Cantelmi, A. Tolomelli, D. Corbisiero, A. Mattellone, A. Ricci, T. Fantoni, W. Cabri, F. Vacondio, F. Ferlenghi, M. Mor, L. Ferrazzano, *Green Chem.* 2021, 23, 4095–4106.
- [105] L. Ferrazzano, D. Corbisiero, G. Martelli, A. Tolomelli, A. Viola, A. Ricci, W. Cabri, *ACS Sustainable Chemistry & Engineering* **2019**, 7, 12867–12877.
- [106] L. A. Carpino, G. Y. Han, Journal of the American Chemical Society 1970, 92, 5748–5749.
- [107] L. Ferrazzano, M. Catani, A. Cavazzini, G. Martelli, D. Corbisiero, P. Cantelmi, T. Fantoni, A. Mattellone, C. D. Luca, S. Felletti, W. Cabri, A. Tolomelli, *Green Chem.* **2022**, 24, 975–1020.
- [108] A. El-Faham, F. Albericio, *Peptide Science* **2020**, *112*, e24164.
- [109] J. D. Wade, M. N. Mathieu, M. Macris, G. W. Tregear, *Letters in Peptide Science* **2000**, 7, 107–112.
- [110] O. Seitz, F. Bergmann, D. Heindl, *Angewandte Chemie International Edition* **1999**, *38*, 2203–2206.
- [111] J. Hachmann, M. Lebl, Journal of Combinatorial Chemistry 2006, 8, 149–149.
- [112] P. H. G. Egelund, S. Jadhav, V. Martin, H. Johansson Castro, F. Richner, S. T. Le Quement, F. Dettner, C. Lechner, R. Schoenleber, D. Sejer Pedersen, *ACS Sustainable Chemistry & Engineering* **2021**, *9*, 14202–14215.
- [113] I. Guryanov, A. Orlandin, A. Viola, B. Biondi, F. Formaggio, A. Ricci, W. Cabri, *Organic Process Research & Development* **2020**, *24*, 274–278.
- [114] G. Martelli, P. Cantelmi, C. Palladino, A. Mattellone, D. Corbisiero, T. Fantoni, A. Tolomelli, M. Macis, A. Ricci, W. Cabri, L. Ferrazzano, *Green Chem.* **2021**, *23*, 8096–8107.
- [115] F. Albericio, A. El-Faham, Organic Process Research & Development 2018, 22, 760–772.
- [116] A. El-Faham, F. Albericio, Organic Letters 2007, 9, 4475–4477.
- [117] W. König, R. Geiger, Chemische Berichte **1970**, 103, 788–798.
- [118] L. A. Carpino, Journal of the American Chemical Society 1993, 115, 4397–4398.
- [119] K. J. McKnelly, W. Sokol, J. S. Nowick, J Org Chem 2020, 85, 1764–1768.
- [120] R. Subirós-Funosas, R. Prohens, R. Barbas, A. El-Faham, F. Albericio, *Chemistry* **2009**, *15*, 9394–9403.
- [121] P. Cherkupally, G. A. Acosta, L. Nieto-Rodriguez, J. Spengler, H. Rodriguez, S. N. Khattab, A. El-Faham, M. Shamis, Y. Luxembourg, R. Prohens, R. Subiros-Funosas, F. Albericio, *European Journal of Organic Chemistry* **2013**, *2013*, 6372–6378.
- [122] R. Subirós-Funosas, A. El-Faham, F. Albericio, Org. Biomol. Chem. 2010, 8, 3665–3673.
- [123] Y. E. Jad, S. N. Khattab, B. G. de la Torre, T. Govender, H. G. Kruger, A. El-Faham, F. Albericio, *Org. Biomol. Chem.* **2014**, *12*, 8379–8385.
- [124] A. El-Faham, F. Albericio, Journal of Peptide Science 2010, 16, 6–9.

- [125] A. El-Faham, R. S. Funosas, R. Prohens, F. Albericio, *Chemistry A European Journal* **2009**, *15*, 9404–9416.
- [126] A. D. McFarland, J. Y. Buser, M. C. Embry, C. B. Held, S. P. Kolis, *Organic Process Research & Development* **2019**, *23*, 2099–2105.
- [127] S. R. Manne, O. Luna, G. A. Acosta, M. Royo, A. El-Faham, G. Orosz, B. G. de la Torre, F. Albericio, *Organic Letters* **2021**, *23*, 6900–6904.
- [128] A. Isidro-Llobet, M. N. Kenworthy, S. Mukherjee, M. E. Kopach, K. Wegner, F. Gallou, A. G. Smith, F. Roschangar, *The Journal of Organic Chemistry* **2019**, *84*, 4615–4628.
- [129] D. B. Harper, D. O'Hagan, C. D. Murphy, *The Handbook of Environmental Chemistry*, (Springer, Heidelberg, Germany, Germany, **2003**.
- [130] Y. Yu, A. Liu, G. Dhawan, H. Mei, W. Zhang, K. Izawa, V. A. Soloshonok, J. Han, *Chinese Chemical Letters* **2021**, *32*, 3342–3354.
- [131] J. He, Z. Li, G. Dhawan, W. Zhang, A. E. Sorochinsky, G. Butler, V. A. Soloshonok, J. Han, *Chinese Chemical Letters* **2023**, *34*, 107578.
- [132] N. Wang, H. Mei, G. Dhawan, W. Zhang, J. Han, V. A. Soloshonok, *Molecules* 2023, 28.
- [133] S. Ali, A. A. Bolinger, J. Zhou, Curr Top Med Chem 2024, 24, 843–849.
- [134] A. Mullard, Nat Rev Drug Discov 2024, 23, 88–95.
- [135] Novel Drug Approvals for 2024, Https://Www.Fda.Gov/Drugs/Novel-Drug-Approvals-Fda/Novel-Drug-Approvals-2024.
- [136] M. Inoue, Y. Sumii, N. Shibata, ACS Omega 2020, 5, 10633–10640.
- [137] J. J. Petkowski, S. Seager, W. Bains, Sci Rep 2024, 14, 15575.
- [138] K. Zhao, D. S. Lim, T. Funaki, J. T. Welch, Bioorganic & Medicinal Chemistry 2003, 11, 207–215.
- [139] K. Müller, C. Faeh, F. Diederich, Science 2007, 317, 1881–1886.
- [140] M. B. van Niel, I. Collins, M. S. Beer, H. B. Broughton, S. K. F. Cheng, S. C. Goodacre, A. Heald, K. L. Locker, A. M. MacLeod, D. Morrison, C. R. Moyes, D. O'Connor, A. Pike, M. Rowley, M. G. N. Russell, B. Sohal, J. A. Stanton, S. Thomas, H. Verrier, A. P. Watt, J. L. Castro, *Journal of Medicinal Chemistry* 1999, 42, 2087–2104.
- [141] J. A. Olsen, D. W. Banner, P. Seiler, B. Wagner, T. Tschopp, U. Obst-Sander, M. Kansy, K. Müller, F. Diederich, *ChemBioChem* **2004**, *5*, 666–675.
- [142] J. A. Olsen, D. W. Banner, P. Seiler, U. Obst Sander, A. D'Arcy, M. Stihle, K. Müller, F. Diederich, *Angew Chem Int Ed Engl* **2003**, *42*, 2507–2511.
- [143] R. Paulini, K. Müller, F. Diederich, Angew Chem Int Ed Engl 2005, 44, 1788–1805.
- [144] A. Harsanyi, G. Sandford, *Green Chem.* **2015**, *17*, 2081–2086.
- [145] J. Aigueperse, P. Mollard, D. Devilliers, M. Chemla, R. Faron, R. Romano, J. P. Cuer, in *Ullmann's Encyclopedia of Industrial Chemistry*, John Wiley & Sons, Ltd, **2000**.
- [146] C. W. Scheele, Kongl. Vetenskaps Akademiens Handlingar (Transactions of the Royal Swedish Academy of Sciences), Royal Swedish Academy Of Sciences, 1771.
- [147] S. Caron, Organic Process Research & Development 2020, 24, 470–480.
- [148] J. C. Bertolini, *J Emerg Med* **1992**, *10*, 163–168.
- [149] L. Kearney, *Reuters* **2019**.
- [150] S. Yakubov, B. Dauth, W. J. Stockerl, W. da Silva, R. M. Gschwind, J. P. Barham, ChemSusChem, 2024, 17, e202401057.
- [151] G. W. Bluck, N. B. Carter, S. C. Smith, M. D. Turnbull, *Journal of Fluorine Chemistry* **2004**, *125*, 1873–1877.
- [152] H. Guyon, D. Cahard, in *Fluorination* (Eds.: J. Hu, T. Umemoto), Springer, Singapore, **2020**, pp. 529–551.
- [153] T. Umemoto, S. Fukami, G. Tomizawa, K. Harasawa, K. Kawada, K. Tomita, *Journal of the American Chemical Society* **1990**, *112*, 8563–8575.
- [154] D. Meyer, H. Jangra, F. Walther, H. Zipse, P. Renaud, Nat Commun 2018, 9, 4888.
- [155] T. Umemoto, Y. Yang, G. B. Hammond, *Beilstein Journal of Organic Chemistry* **2021**, 17, 1752–1813.
- [156] Q. Gu, E. Vessally, *RSC Adv.* **2020**, *10*, 16756–16768.

- [157] A. F. Shields, J. R. Grierson, B. M. Dohmen, H.-J. Machulla, J. C. Stayanoff, J. M. Lawhorn-Crews, J. E. Obradovich, O. Muzik, T. J. Mangner, *Nat Med* **1998**, *4*, 1334–1336.
- [158] J. Ford, S. Ortalli, V. Gouverneur, *Angewandte Chemie International Edition* **2024**, *63*, e202404957.
- [159] T. Gendron, G. Destro, N. J. W. Straathof, J. B. I. Sap, F. Guibbal, C. Vriamont, C. Caygill, J. R. Atack, A. J. Watkins, C. Marshall, R. Hueting, C. Warnier, V. Gouverneur, M. Tredwell, *EJNMMI Radiopharmacy and Chemistry* 2022, 7, 5.
- [160] J. Ajenjo, G. Destro, B. Cornelissen, V. Gouverneur, *EJNMMI Radiopharmacy and Chemistry* **2021**, *6*, 33.
- [161] H. Teare, E. G. Robins, E. Årstad, S. K. Luthra, V. Gouverneur, *Chem. Commun.* **2007**, 2330–2332.
- [162] H. Teare, E. G. Robins, A. Kirjavainen, S. Forsback, G. Sandford, O. Solin, S. K. Luthra, V. Gouverneur, *Angew Chem Int Ed Engl* **2010**, *49*, 6821–6824.
- [163] J. Becaud, L. Mu, M. Karramkam, P. A. Schubiger, S. M. Ametamey, K. Graham, T. Stellfeld, L. Lehmann, S. Borkowski, D. Berndorff, L. Dinkelborg, A. Srinivasan, R. Smits, B. Koksch, *Bioconjugate Chemistry* 2009, 20, 2254–2261.
- [164] Z. Gao, V. Gouverneur, B. G. Davis, *Journal of the American Chemical Society* **2013**, 135, 13612–13615.
- [165] M. B. Nodwell, H. Yang, M. Čolović, Z. Yuan, H. Merkens, R. E. Martin, F. Bénard, P. Schaffer, R. Britton, *Journal of the American Chemical Society* **2017**, *139*, 3595–3598.
- [166] G. Yuan, F. Wang, N. A. Stephenson, L. Wang, B. H. Rotstein, N. Vasdev, P. Tang, S. H. Liang, Chem. Commun. 2017, 53, 126–129.
- [167] S. Verhoog, C. W. Kee, Y. Wang, T. Khotavivattana, T. C. Wilson, V. Kersemans, S. Smart, M. Tredwell, B. G. Davis, V. Gouverneur, *Journal of the American Chemical Society* 2018, 140, 1572–1575.
- [168] C. Patel, E. André-Joyaux, J. A. Leitch, X. M. De Irujo-Labalde, F. Ibba, J. Struijs, M. A. Ellwanger, R. Paton, D. L. Browne, G. Pupo, S. Aldridge, M. A. Hayward, V. Gouverneur, *Science* 2023, 381, 302–306.
- [169] A. G. Myers, M. E. Fraley, N. J. Tom, S. B. Cohen, D. J. Madar, *Chemistry & Biology* **1995**, *2*, 33–43.
- [170] P. A. Donets, G. V. Latyshev, N. V. Lukashev, I. P. Beletskaya, Russ Chem Bull 2007, 56, 504–508.
- [171] H. A. Dieck, F. R. Heck, Journal of Organometallic Chemistry 1975, 93, 259–263.
- [172] L. Cassar, Journal of Organometallic Chemistry 1975, 93, 253–257.
- [173] K. Sonogashira, Y. Tohda, N. Hagihara, Tetrahedron Letters, 1975, 16, 4467-4470.
- [174] P. Siemsen, R. C. Livingston, F. Diederich, Angew. Chem. Int. Ed. 2000, 39, 2632–2657.
- [175] T. Ljungdahl, K. Pettersson, B. Albinsson, J. Mårtensson, J. Org. Chem. **2006**, 71, 1677–1687.
- [176] R. Chinchilla, C. Nájera, *Chem. Soc. Rev.* **2011**, *40*, 5084.
- [177] O. Rivada-Wheelaghan, A. Comas-Vives, R. R. Fayzullin, A. Lledós, J. R. Khusnutdinova, *Chemistry A European J* **2020**, *26*, 12168–12179.
- [178] X. Wang, Y. Song, J. Qu, Y. Luo, Organometallics 2017, 36, 1042–1048.
- [179] B. C. Barnard, *Platinum Metals Review* **2008**, *52*, 38–45.
- [180] M. Karak, L. C. A. Barbosa, G. C. Hargaden, RSC Adv. 2014, 4, 53442–53466.
- [181] A. M. Thomas, A. Sujatha, G. Anilkumar, RSC Adv. **2014**, 4, 21688–21698.
- [182] A. Streitwieser, D. M. E. Reuben, J. Am. Chem. Soc. 1971, 93, 1794–1795.
- [183] M. I. Terekhova, E. S. Petrov, S. F. Vasilevskii, V. F. Ivanov, M. S. Shvartsberg, *Russ Chem Bull* **1984**, *33*, 850–852.
- [184] A. Soheili, J. Albaneze-Walker, J. A. Murry, P. G. Dormer, D. L. Hughes, *Org. Lett.* **2003**, *5*, 4191–4194.
- [185] T. Ljungdahl, T. Bennur, A. Dallas, H. Emtenäs, J. Mårtensson, *Organometallics* **2008**, 27, 2490–2498.

- [186] M. García-Melchor, M. C. Pacheco, C. Nájera, A. Lledós, G. Ujaque, *ACS Catal.* **2012**, 2, 135–144.
- [187] M. Gazvoda, M. Virant, B. Pinter, J. Košmrlj, *Nat Commun* **2018**, *9*, 4814.
- [188] T. Fantoni, A. Tolomelli, W. Cabri, Catalysis Today 2022, 397–399, 265–271.
- [189] W. Cabri, Oldani, E., Process for the Industrial Preparation of Aminoacetylenes.
- [190] J. E. Taylor, S. D. Bull, J. M. J. Williams, Chem. Soc. Rev. 2012, 41, 2109.
- [191] D. D. Hennings, T. Iwama, V. H. Rawal, *Org. Lett.* **1999**, *1*, 1205–1208.
- [192] A. Jutand, A. Mosleh, J. Org. Chem. 1997, 62, 261–274.
- [193] A. Ivančič, J. Košmrlj, M. Gazvoda, Commun Chem 2023, 6, 51.
- [194] P. Fitton, E.A. Rick, J. Org. Chem, 1971, 2, 587-591.
- [195] O. L. Kaliya, O. N. Temkin, G. S. Kirchenkova, E. M. Smirnova, Ya. M. Kimel'fel'd, R. M. Flid, Russ Chem Bull 1969, 18, 2690–2691.
- [196] A. Jutand, S. Négri, A. Principaud, European Journal of Inorganic Chemistry 2005, 2005, 631–635.
- [197] A. Jutand, A. Mosleh, Organometallics 1995, 14, 1810–1817.
- [198] S. A. Kondrashova, F. M. Polyancev, S. K. Latypov, *Molecules* **2022**, *27*, 2668.
- [199] M. Ahlquist, P. Fristrup, D. Tanner, P.-O. Norrby, *Organometallics* **2006**, *25*, 2066–2073.
- [200] F. Schoenebeck, K. N. Houk, J. Am. Chem. Soc. 2010, 132, 2496–2497.
- [201] T. Zhou, P.-P. Xie, C.-L. Ji, X. Hong, M. Szostak, Org. Lett. 2020, 22, 6434–6440.
- [202] L. M. Alcazar-Roman, J. F. Hartwig, *Organometallics* **2002**, *21*, 491–502.
- [203] Gaussian 16 Rev. A. 03 (Wallingford, CT, 2016)
- [204] J. P. Perdew, K. Burke, M. Ernzerhof, Phys. Rev. Lett. 1997, 78, 1396–1396.
- [205] C. Adamo, V. Barone, The Journal of Chemical Physics 1999, 110, 6158–6170.
- [206] "Effect of the damping function in dispersion corrected density functional theory Grimme 2011 Journal of Computational Chemistry Wiley Online Library"
- [207] F. Weigend, R. Ahlrichs, *Phys. Chem. Chem. Phys.* **2005**, *7*, 3297–3305.
- [208] A. V. Marenich, C. J. Cramer, D. G. Truhlar, J. Phys. Chem. B 2009, 113, 6378–6396.
- [209] S. S. Zalesskiy, V. P. Ananikov, *Organometallics* **2012**, *31*, 2302–2309.
- [210] K. S. Iyer, K. B. Dismuke Rodriguez, R. M. Lammert, J. R. Yirak, J. M. Saunders, R. D. Kavthe, D. H. Aue, B. H. Lipshutz, *Angewandte Chemie International Edition* **2024**, *63*, e202411295.
- [211] N. C. Bruno, S. L. Buchwald. US8981086 (23 October 2014).
- [212] A. M. Trzeciak, A. W. Augustyniak, Coordination Chemistry Reviews 2019, 384, 1–20.
- [213] L. J. Higham, D. W. Allen, J. C. Tebby, *Organophosphorus Chemistry*, Royal Society Of Chemistry, **2022**.
- [214] P. C. J. Kamer, P. W. N. M. van Leeuwen, J. N. H. Reek, *Accounts of Chemical Research* **2001**, *34*, 895–904.
- [215] T. E. Barder, S. D. Walker, J. R. Martinelli, S. L. Buchwald, *Journal of the American Chemical Society* **2005**, *127*, 4685–4696.
- [216] T. Ikawa, T. E. Barder, M. R. Biscoe, S. L. Buchwald, *Journal of the American Chemical Society* **2007**, *129*, 13001–13007.
- [217] P. R. Melvin, D. Balcells, N. Hazari, A. Nova, ACS Catalysis 2015, 5, 5596–5606.
- [218] S. Subongkoj, S. Lange, W. Chen, J. Xiao, *Journal of Molecular Catalysis A: Chemical* **2003**, *196*, 125–129.
- [219] Y. Ji, R. E. Plata, C. S. Regens, M. Hay, M. Schmidt, T. Razler, Y. Qiu, P. Geng, Y. Hsiao, T. Rosner, M. D. Eastgate, D. G. Blackmond, J. Am. Chem. Soc. 2015, 137, 13272–13281.
- [220] D. S. Surry, S. L. Buchwald, Chem. Sci. 2010, 2, 27-50.
- [221] J. Struwe, L. Ackermann, F. Gallou, Chem Catalysis 2023, 3, 100485.
- [222] E. B. Landstrom, S. Handa, D. H. Aue, F. Gallou, B. H. Lipshutz, *Green Chem.* **2018**, *20*, 3436–3443.

- [223] N. Akporji, R. R. Thakore, M. Cortes-Clerget, J. Andersen, E. Landstrom, D. H. Aue, F. Gallou, B. H. Lipshutz, *Chemical Science* **2020**, *11*, 5205–5212.
- [224] V. V. Grushin, Organometallics **2001**, 20, 3950–3961.
- [225] C. Amatore, G. Broeker, A. Jutand, F. Khalil, J. Am. Chem. Soc. 1997, 119, 5176–5185.
- [226] X. Moreau, J. M. Campagne, G. Meyer, A. Jutand, Eur J Org Chem 2005, 2005, 3749–3760.
- [227] J. I. Murray, L. Zhang, A. Simon, M. V. Silva Elipe, C. S. Wei, S. Caille, A. T. Parsons, Org. Process Res. Dev. 2023, 27, 198–205.
- [228] T. E. Barder, M. R. Biscoe, S. L. Buchwald, Organometallics 2007, 26, 2183–2192.
- [229] D. Ortiz, M. Blug, X.-F. Le Goff, P. Le Floch, N. Mézailles, P. Maître, *Organometallics* **2012**, *31*, 5975–5978.
- [230] G. He, G. Lu, Z. Guo, P. Liu, G. Chen, *Nature Chemistry* **2016**, *8*, 1131–1136.
- [231] "Substance Information ECHA," can be found under https://echa.europa.eu/substance-information/-/substanceinfo/100.020.328.
- [232] International Conference of Harmonization Guideline Q3D.
- [233] S. Wagschal, L. A. Perego, A. Simon, A. Franco-Espejo, C. Tocqueville, J. Albaneze-Walker, A. Jutand, L. Grimaud, *Chemistry A European Journal* **2019**, *25*, 6980–6987.
- [234] W. Keim, Green Chem. 2003, 5, 105–111.
- [235] E. Tessema, Y.-W. Fan, C.-F. Chiu, V. Elakkat, H. A. Rahayu, C.-R. Shen, K. C. Shanthakumar, P. Zhang, N. Lu, *Tetrahedron* **2022**, *122*, 132961.
- [236] N. Lu, Y.-C. Chen, W.-S. Chen, T.-L. Chen, S.-J. Wu, *Journal of Organometallic Chemistry* **2009**, *694*, 278–284.
- [237] C. A. Jr. Lewis, R. Wolfenden, J. Am. Chem. Soc. 2014, 136, 130–136.
- [238] K. Eicken, H. Rang, A. Harreus, N. Goetz, E. Ammermann, G. Lorenz, S. Strathmann, 1997, DE19531813.
- [239] J. Hagen, Industrial Catalysis: A Practical Approach, John Wiley & Sons, 2015.
- [240] E. S. Degtyareva, E. V. Borkovskaya, V. P. Ananikov, ACS Sustainable Chem. Eng. 2019, 7, 9680–9689.
- [241] A. P. Dicks, A. Hent, *Green Chemistry Metrics: A Guide to Determining and Evaluating Process Greenness*, Springer International Publishing, Cham., **2015**.
- [242] Gaussian 16 Rev. A.03 (Wallingford, CT, 2016).
- [243] M.-G. Braun, A. Díaz-Rodríguez, L. Diorazio, Z. Fei, K. Fraunhoffer, J. Hayler, M. Hickey, M. McLaws, P. Richardson, G.-D. Roiban, A. T. Parsons, A. Steven, J. Terrett, T. White, J. Yin, *Organic Process Research & Development* 2019, 23, 1118–1133.
- [244] A. Isidro-Llobet, M. N. Kenworthy, S. Mukherjee, M. E. Kopach, K. Wegner, F. Gallou, A. G. Smith, F. Roschangar, *J Org Chem* **2019**, *84*, 4615–4628.
- [245] K. Weissermel, H.-J. Kleiner, M. Finke, U.-H. Felcht, *Angewandte Chemie International Edition in English* **1981**, *20*, 223–233.
- [246] A. L. L. García, Synlett **2007**, 2007, 1328–1329.
- [247] J. Klose, M. Bienert, C. Mollenkopf, D. Wehle, C. Zhang, L. A. Carpino, P. Henklein, *Chem. Commun.* **1999**, 1847–1848.
- [248] Https://Echa.Europa.Eu/Substance-Information/-/Substanceinfo/100.102.078.
- [249] A. A. Waghmare, R. M. Hindupur, H. N. Pati, *Review Journal of Chemistry* **2014**, *4*, 53–131.
- [250] Basavaprabhu, T. M. Vishwanatha, N. R. Panguluri, V. V. Sureshbabu, *Synthesis* **2013**, 45, 1569–1601.
- [251] J. R. Dunetz, Y. Xiang, A. Baldwin, J. Ringling, Organic Letters 2011, 13, 5048–5051.
- [252] O. Al Musaimi, R. Wisdom, P. Talbiersky, B. G. De La Torre, F. Albericio, *ChemistrySelect* **2021**, *6*, 2649–2657.
- [253] A. Mattellone, D. Corbisiero, L. Ferrazzano, P. Cantelmi, G. Martelli, C. Palladino, A. Tolomelli, W. Cabri, *Green Chem.* **2023**, *25*, 2563–2571.
- [254] K. M. Sivanandaiah, V. V. S. Babu, C. Renukeshwar, *International Journal of Peptide and Protein Research* **1992**, *39*, 201–206.

- [255] Y. Okada, H. Suzuki, T. Nakae, S. Fujita, H. Abe, K. Nagano, T. Yamada, N. Ebata, S. Kim, K. Chiba, *The Journal of Organic Chemistry* **2013**, *78*, 320–327.
- [256] H. Wakamatsu, Y. Okada, M. Sugai, S. R. Hussaini, K. Chiba, *Asian Journal of Organic Chemistry* **2017**, *6*, 1584–1588.
- [257] W. A. Adedeji, Annals of Ibadan Postgraduate Medicine 2016, 14, 56.
- [258] V. L. Simpkin, M. J. Renwick, R. Kelly, E. Mossialos, *J Antibiot* **2017**, *70*, 1087–1096.
- [259] S. A. H. Abdel Monaim, Y. E. Jad, A. El-Faham, B. G. de la Torre, F. Albericio, *Bioorg Med Chem* 2018, 26, 2788–2796.
- [260] F. Asif, S. U. Zaman, Md. K. H. Arnab, M. Hasan, Md. M. Islam, *The Microbe* **2024**, *2*, 100051.
- [261] R. E. W. Hancock, H.-G. Sahl, Nat Biotechnol 2006, 24, 1551–1557.
- [262] J. Li, J.-J. Koh, S. Liu, R. Lakshminarayanan, C. S. Verma, R. W. Beuerman, *Frontiers in Neuroscience* **2017**, *11*, 73.
- [263] Y. Huan, Q. Kong, H. Mou, H. Yi, Front. Microbiol. 2020, 11.
- [264] A. Giuliani, G. Pirri, S. Nicoletto, Open Life Sciences 2007, 2, 1–33.
- [265] M. Mahlapuu, J. Håkansson, L. Ringstad, C. Björn, Front Cell Infect Microbiol 2016, 6, 194.
- [266] Y. Li, X. Xia, W. Hou, H. Lv, J. Liu, X. Li, International Journal of Nanomedicine 2023, 18, 1109.
- [267] G. Ianiro, H. Tilg, A. Gasbarrini, Gut 2016, 65, 1906–1915.
- [268] F. Sommer, F. Bäckhed, *Nature Reviews Microbiology* **2013**, 11, 227–238.
- [269] F. C. Lessa, Y. Mu, W. M. Bamberg, Z. G. Beldavs, G. K. Dumyati, J. R. Dunn, M. M. Farley, S. M. Holzbauer, J. I. Meek, E. C. Phipps, L. E. Wilson, L. G. Winston, J. A. Cohen, B. M. Limbago, S. K. Fridkin, D. N. Gerding, L. C. McDonald, *New England Journal of Medicine* 2015, 372, 825–834.
- [270] S. M. McGlone, R. R. Bailey, S. M. Zimmer, M. J. Popovich, Y. Tian, P. Ufberg, R. R. Muder, B. Y. Lee, *Clinical Microbiology and Infection* **2012**, *18*, 282–289.
- [271] Https://Www.Alfasigma.Com/Products/Brilacidin-License-Agreement-with-Innovation-Pharmaceuticals.
- [272] J. Svenson, W. Stensen, B.-O. Brandsdal, B. E. Haug, J. Monrad, J. S. Svendsen, *Biochemistry* **2008**, *47*, 3777–3788.
- [273] J. Li, J.-J. Koh, S. Liu, R. Lakshminarayanan, C. S. Verma, R. W. Beuerman, *Front. Neurosci.* **2017**, *11*, DOI 10.3389/fnins.2017.00073.
- [274] M. S. Butler, M. A. Blaskovich, M. A. Cooper, *J Antibiot* **2017**, *70*, 3–24.
- [275] J. Svenson, W. Stensen, B.-O. Brandsdal, B. E. Haug, J. Monrad, J. S. Svendsen, *Biochemistry* **2008**, *47*, 3777–3788.
- [276] S.-H. Kim, D. Semenya, D. Castagnolo, European Journal of Medicinal Chemistry 2021, 216, 113293.
- [277] M. Catellani, F. Frignani, A. Rangoni, *ChemInform* **1997**, 28.
- [278] L. Jiao, T. Bach, Journal of the American Chemical Society 2011, 133, 12990–12993.
- [279] L. Jiao, E. Herdtweck, T. Bach, *Journal of the American Chemical Society* **2012**, *134*, 14563–14572.
- [280] H. K. Potukuchi, T. Bach, *The Journal of Organic Chemistry* **2013**, 78, 12263–12267.
- [281] J. Ruiz-Rodríguez, F. Albericio, R. Lavilla, *Chemistry A European Journal* **2010**, *16*, 1124–1127.
- [282] N. Lebrasseur, I. Larrosa, *Journal of the American Chemical Society* **2008**, *130*, 2926–2927.
- [283] T. J. Williams, A. J. Reay, A. C. Whitwood, I. J. S. Fairlamb, *Chem. Commun.* **2014**, *50*, 3052–3054.
- [284] A. J. Reay, T. J. Williams, I. J. S. Fairlamb, *Organic & Biomolecular Chemistry* **2015**, *13*, 8298–8309.
- [285] L. Ackermann, Chemical Reviews **2011**, 111, 1315–1345.

- [286] W. Gong, G. Zhang, T. Liu, R. Giri, J.-Q. Yu, *Journal of the American Chemical Society* **2014**, *136*, 16940–16946.
- [287] A. S. Barahdia, K. L. Thakare, L. Kaur, R. Jain, *Advanced Synthesis & Catalysis* **2024**, 366, 2844–2858.
- [288] M. Lautens, S. Piguel, Angewandte Chemie International Edition 2000, 39, 1045–1046.
- [289] S. Pache, M. Lautens, *Organic Letters* **2003**, *5*, 4827–4830.
- [290] X. Yang, T. Wu, R. J. Phipps, F. D. Toste, Chemical Reviews 2015, 115, 826–870.
- [291] X. Wang, Q. Lan, S. Shirakawa, K. Maruoka, Chem. Commun. 2010, 46, 321-323.
- [292] V. Rauniyar, A. D. Lackner, G. L. Hamilton, F. D. Toste, *Science* **2011**, *334*, 1681–1684.
- [293] V. H. Jadhav, H. J. Jeong, W. Choi, D. W. Kim, *Chemical Engineering Journal* **2015**, 270, 36–40.
- [294] G. Pupo, F. Ibba, D. M. H. Ascough, A. C. Vicini, P. Ricci, K. E. Christensen, L. Pfeifer, J. R. Morphy, J. M. Brown, R. S. Paton, V. Gouverneur, *Science* **2018**, *360*, 638–642.
- [295] L. Pfeifer, K. M. Engle, G. W. Pidgeon, H. A. Sparkes, A. L. Thompson, J. M. Brown, V. Gouverneur, *Journal of the American Chemical Society* **2016**, *138*, 13314–13325.
- [296] G. Pupo, A. C. Vicini, D. M. H. Ascough, F. Ibba, K. E. Christensen, A. L. Thompson, J. M. Brown, R. S. Paton, V. Gouverneur, *Journal of the American Chemical Society* 2019, 141, 2878–2883.
- [297] G. Roagna, D. M. H. Ascough, F. Ibba, A. C. Vicini, A. Fontana, K. E. Christensen, A. Peschiulli, D. Oehlrich, A. Misale, A. A. Trabanco, R. S. Paton, G. Pupo, V. Gouverneur, *Journal of the American Chemical Society* **2020**, *142*, 14045–14051.
- [298] H. Ibrahim, A. Togni, Chem. Commun. 2004, 1147–1155.
- [299] W. Chung, C. D. Vanderwal, *Angewandte Chemie International Edition* **2016**, *55*, 4396–4434.
- [300] P. Kwiatkowski, T. D. Beeson, J. C. Conrad, D. W. C. MacMillan, *Journal of the American Chemical Society* **2011**, *133*, 1738–1741.
- [301] Y.-S. Xu, Y. Tang, H.-J. Feng, J.-T. Liu, R. P. Hsung, *Organic Letters* **2015**, *17*, 572–575.
- [302] A. C. Vicini, G. Pupo, F. Ibba, V. Gouverneur, Nat Protoc 2021, 16, 5559–5591.
- [303] Z. Li, B. Wang, C. Zhang, W. Y. Lo, L. Yang, J. Sun, *Journal of the American Chemical Society* **2024**, *146*, 2779–2788.
- [304] M. Yus, C. Nájera, F. Foubelo, J. M. Sansano, *Chemical Reviews* **2023**, *123*, 11817–11893.
- [305] Y.-F. Zhang, X.-Y. Dong, J.-T. Cheng, N.-Y. Yang, L.-L. Wang, F.-L. Wang, C. Luan, J. Liu, Z.-L. Li, Q.-S. Gu, X.-Y. Liu, *Journal of the American Chemical Society* **2021**, *143*, 15413–15419.
- [306] M. Zhu, W. Wei, D. Yang, H. Cui, H. Cui, X. Sun, H. Wang, Org. Biomol. Chem. 2016, 14, 10998–11001.
- [307] K. Tanaka, M. Tomihama, K. Yamamoto, N. Matsubara, T. Harada, *The Journal of Organic Chemistry* **2018**, *83*, 6127–6132.
- [308] Patent ASTERAND UK WO 2005/12263, 2005, A1.

Borsa di dottorato del Programma Operativo Nazionale Ricerca e Innovazione 2014-2020 (CCI 2014IT16M2OP005), risorse FSE REACT-EU, Azione IV.4 "Dottorati e contratti di ricerca su tematiche dell'innovazione" e Azione IV.5 "Dottorati su tematiche Green."

Codice CUP J35F21003060006

### Acknowledgments

I would like to thank my **professors Walter Cabri** and **Alessandra Tolomelli** for having me in their research group. Professor Alessandra has had me in her lab since my undergraduate degree and has made me feel comfortable in this environment, giving me great support from the beginning. Professor Walter was the best supervisor I could have ever asked for my PhD, he asked as much from me as he gave back.

I would like to thank all the people who have been part of this group. Special thanks to the former members Giulia, Paolo and Ama: Giulia was my first guide in the lab, she taught me how to plan my daily work in a fast and effective way. She was also incredibly supportive, and she was a friend. During my PhD, it was really important to me to have Paolo in the fume hood next to mine: he made me laugh when I needed to, he was supportive both chemically and emotionally, and he made me feel calmer. Ama was too many things (also because she is too much!!!) and I don't have enough space to list what Ama meant to me. First of all, she was (and still is) a true and sincere friend, it was like having a sister in the lab. Another special thank you goes to Tommi, who was always there to make me happy with his incredible sense of humour. He has always believed in me, and he taught me to believe in myself more. We have worked hard together, and we have shared as many difficulties as we have achieved goals. I will never find a better colleague than him (T&K forever).

I would like to thank all the wonderful people I have met along the way. Especially **Vale and Robi**, who were my safe haven during the hard days and my "chocolate partners in crime". **Nunzio**, who, despite making the worst first impression ever, became an important friend and Temptation Island-watching buddy. Finally, **Ema**, who has been incredibly supportive and an amazing friend. He has always been able to turn on the light for me, reminding me that "Happiness can be found even in the darkest of times, if one only remembers to turn on the light" (Albus Dumbledore).

I would like to thank all my friends I met at university, especially **Sara and Lucia**, because without them I wouldn't be here. Climbing a mountain is hard, but we proved that it is easier and more fun to do it together. They always had the ability to make the hardest days easier, to get me excited about cooking together (even though I am not a good cook), and make me happy.

I would like to thank **Prof. Véronique** for being so kind to me and for hosting me in her wonderful research group at the University of Oxford. Not only have I learnt a lot, but I have also met special people and true friends. Thank you, **Claire**, for working hard with me and teaching me so much, your support has been precious to me. Thank you, **Artemis**, for being so kind and supportive to me from the beginning. Thank you to all the other people who have made me feel like a member of their group from the beginning. Special thanks to **Gabi** (and **Emil**), **Thomas H.**, **Chris**, **Job**, **Thomas S.**, **Columbus**, **Nicolas** and **Caleb** for our nights in the pub, for our Sunday Roast at the Chester Arms, for inviting me to the formal dinners, for being good students of Italian body language, for sharing chocolate with me (:P) and much more... but most of all for being (while I was there, but still now) FRIENDS.

I would also like to thank my English family, Clare, Brian, Connie (+ Joseph), Jack and Alice, who welcomed me with love and kindness and made me feel like a member of their family.

I would also like to thank all my friends from outside the university, as their support and friendship has been (and hopefully will continue to be) a very strong source of energy and happiness. Special thanks to **Bariga**, **Sister**, **Regina**, **Cate**, **Marti**, **Paolo**, **Rocco**, **Claretta**, **Dario**, **Ali** & **Dalla**.

I would like to thank my boyfriend, **Fede**, for always being by my side. With his love, he replenished my energy when it was running low. He has always helped me find the best solution to my problems, found time and space for me and, in the darkest days, he was able to help me find the colours among the shades of grey.

Infine, ringrazio la mia **Famiglia** perché ovviamente senza il loro supporto (sia economico che morale) non sarei arrivata fino qui. In particolare, ringrazio i miei genitori perché sono sempre stati i miei fans numero 1, per avermi insegnato che per raggiungere un importante traguardo bisogna faticare e tenere duro, per avermi lasciato la libertà di quale strada intraprendere senza mai forzarmi, per avermi sempre ascoltata, per aver saputo portare pazienza più volte e per avermi sempre fatto sentire la cosa più preziosa che avessero. Ringrazio i miei nonni per avermi sempre viziata e coccolata e per avermi cresciuta con così tanto amore (un amore che riesco a percepire tutt'ora anche da chi qui non c'è più).